UNIVERSITY OF SOUTHAMPTON

THE SENSITIVITY ANALYSIS OF A SUSPENSION SEAT DYNAMIC MODEL

THOMAS PETER GUNSTON

DOCTOR OF PHILOSOPHY

INSTITUTE OF SOUND AND VIBRATION RESEARCH,
FACULTY OF ENGINEERING AND APPLIED SCIENCE

NOVEMBER 2002

UNIVERSITY OF SOUTHAMPTON

ABSTRACT

FACULTY OF ENGINEERING AND APPLIED SCIENCE

INSTITUTE OF SOUND AND VIBRATION RESEARCH

Doctor of Philosophy

THE SENSITIVITY ANALYSIS OF A SUSPENSION SEAT DYNAMIC MODEL

by Thomas Peter Gunston

The key objectives of this thesis were to develop a general non-linear theoretical model of a suspension seat and to use this model to quantify the effect of the seat component parts on the performance of a conventional suspension seat design using a relevant range of frequencies and magnitudes.

Wheeled off-road vehicles are capable of subjecting the operator to substantial amounts of whole-body vibration. Suspension seats are often fitted to this type of vehicle to reduce the vibration transmitted to the operator. Unfortunately, the need to limit the relative movement between the operator and the vehicle controls requires the seat stroke to be limited, usually using rubber buffers. The impacts as the suspension contacts these end-stops can result in more vibration on the seat surface than on the cab floor.

Non-linear simulation studies are potentially useful for investigating the performance of complex systems, but previous suspension seat simulations were tested over a limited range of conditions. This thesis describes the development of a non-linear theoretical model of a specific suspension seat and investigates the model performance in response to a systematic range of input frequencies, magnitudes and durations of realistic test motions.

Test motions were derived from cab floor vibration measurements from three off-road machines (an agricultural tractor, a forestry forwarder and an earthmover) in situations that commonly led to seat suspension end-stop impact events. The motions were observed to result in similar occurrence of end-stop impacts in the laboratory as observed in the field with the three vehicle seats. Laboratory tests also identified that the accepted procedure for measuring seat surface vibration can result in artefactual measurements on suspension seats if the occupant loses contact with the seat surface.

A general theoretical suspension seat model was developed using a non-linear lumped parameter approach. The dynamics of the component parts of the three seats were measured and a non-linear parameter optimisation process was developed to estimate the friction from the dynamic behaviour of the complete seat. The results of this process gave confidence in the performance of the model of the earthmover seat. .The performance of the earthmover seat model was quantified by comparison with 673 laboratory measurements of the seat performance using the anthropodynamic dummy as the seat load. The model was found to predict the seat transmissibility (using the VDV-based SEAT value) to within 15% of the measured value in 81% of the tests.

A systematic parametric sensitivity analysis of the earthmover seat model predicted the effect of each component on the overall seat performance. The sensitivity analysis was conducted over a range of frequencies, magnitudes and durations of input motion. Approximately 40,000 evaluations were made and summaries were provided showing how each component affected the seat transmissibility and time domain performance.

Acknowledgements

This majority of the work described in this thesis was carried out as part of the European Union TESTOPS EC Standards Measurements and Testing programme - project no. SMT4-CT97-21. I am grateful for the assistance of everyone involved in this project and especially Chris Howard and his team at Kab Seating Ltd.

Thank you to my supervisor, Professor Griffin, for giving me space to try things my way and offering gentle guidance when I began to flounder. I very much appreciate the support and encouragement I have received throughout the past few years.

Thank you also to all the staff at the Human Factors Research Unit for being helpful and useful people, especially Dr Lewis for his knowledge and experience and Gary Parker for helping assemble my experiments very effectively at very short notice.

Finally, thank you to my wife for all her patience and support and for working against all odds to keep me sane and balanced.

Contents

CHAPTER 3: APPARATUS AND EXPERIMENTAL METHODS

1 Introduction

1.1 Objective of the thesis

The first objective of this thesis was to develop a theoretical model capable of simulating the dynamic performance of production suspension seats in response to input motions with a range of frequencies, magnitudes and waveform shapes representative of those observed in the field on wheeled off-road vehicles. The second objective of the thesis was to use this model to understand and quantify the influence of the individual seat components on the seat performance over this range of test conditions. A sensitivity analysis of this type will aid the understanding of the effect of each seat component on suspension seat dynamic behaviour. No previous study has conducted a systematic sensitivity analysis in both the frequency and magnitude domains.

1.2 General introduction

Wheeled off-road vehicles are capable of producing high levels of whole-body vibration at low frequencies (predominantly less than 5 Hz). In order for the seat to usefully attenuate the vibration transmitted from the vehicle floor to the operator, the seat resonance frequency must be sufficiently below the predominant frequencies of vibration on the floor of a particular vehicle. The resonance frequency of a foam

Figure 1-1 A suspension seat

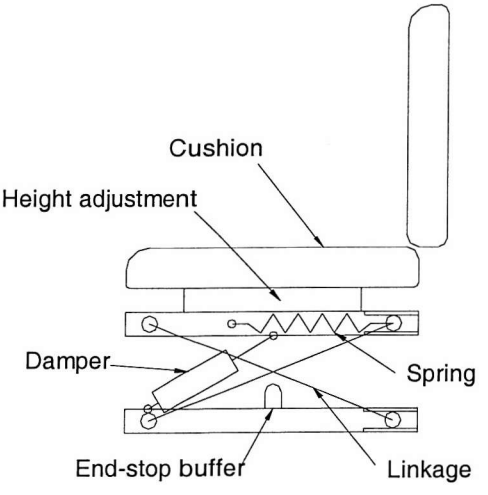

Figure 1-2 Schematic of a suspension seat

cushion seat is typically in the 3 to 6 Hz region and therefore tends to amplify the vibration of wheeled off-road vehicles rather than attenuate it.

One method of reducing the vibration exposure of wheeled off-road vehicle operators is to use a suspension seat (Figure 1-1 and Figure 1-2). A mechanical suspension mechanism between the seat cushion and the vehicle floor allows the first resonance frequency of the seat to occur at a lower frequency than is possible with a foam cushion seat. However, the dynamic characteristics of a seat must be matched to the characteristics of the vehicle. As a general approximation, larger vehicles exhibit lower frequency vibration and a seat with a low resonance frequency and a comparatively long suspension stroke (~100mm) is typical. Smaller vehicles exhibit higher frequency vibration and usually have less space in the cab so a more compact seat is usually used. A seat must fit into the available space, reduce the vibration, provide a comfortable working environment and be cost effective.

The work in this thesis involved co-operation with three major European suspension seat manufacturers who operate in competitive a global market. In such a market there is considerable financial pressure not to over design the product. A dynamically acceptable seat produced for a lower cost could be a useful product in a market where a dynamically more effective but more expensive seat would be less attractive to the customer. However, suspension seats are highly non-linear and when in use are exposed to a wide range of vibration magnitudes.

Accurate and well-quantified theoretical models could aid in understanding the relationships between the suspension components and the seat performance leading to improvements in seat design and better matching of seats to vehicles. Such a model should be able to demonstrate the quantitative effect of a component on the performance of a specific production seat in response to a given motion, in order to determine what modifications to the component would benefit the seat performance or what performance loss would be tolerable if a cheaper component were to be substituted.

Evaluating the effect of each seat component on the overall seat performance in a laboratory situation would be time consuming and difficult. As an example, the act of dismantling a seat to modify one component may affect the seat performance in other ways, perhaps by altering the friction due to a different torque on a mounting bolt, resulting in a meaningless or biased result for the component of interest. A theoretical simulation provides a controlled platform for investigating the influence of individual seat components.

1.3 Content of the thesis

The thesis consists of the following sections:

Chapter 1 Introduction

A general background to the research as described above and the present section summarising the content of each chapter.

Chapter 2 Review of literature

The second chapter consists of a review of relevant work in the area of suspension seat simulation, including sections on human response to vibration, suspension seat dynamics, theoretical modelling methods and the dynamic properties of seat components.

Chapter 3 Apparatus and experimental methods

The third chapter contains descriptions of the laboratory test apparatus, the data analysis techniques and the three suspension seats used during the thesis.

Chapter 4 Definition of suitable test motions

The objective of the fourth chapter was to determine suitable input motions for use with the model and for testing suspension seats in the laboratory. Measurements of the vibration at the base of the seat in the field on three off-road wheeled machines; an agricultural tractor, a forestry forwarder and a backhoe-loader earthmoving machine were used. The machines were tested in the field in situations that the operators indicated were likely to result in the seat suspension exceeding the available travel and impacting the end-stop buffers. The field motions were examined and idealised motions were defined for use in laboratory tests and as inputs to the model and the seat responses with these motions were compared with the seat motions recorded in the field. The earthmoving machine results also permitted a limited investigation into the effect of wearing a seat belt on the occurrence of end-stop impacts.

Chapter 5 Laboratory seat tests

The first objective of this chapter was to compare the response of the vehicle seats in controlled laboratory situations when using three different loading conditions, an inert mass, twelve human subjects and an anthropodynamic dummy designed to simulate the dynamic response of the seated human body, in order to determine if a dynamic model for the seat load would be required. The second objective of this chapter was to provide measurements of the performance of each of the seats over a range of

frequencies and magnitudes for comparison with the theoretical model developed in later chapters. The use of the idealised motions allowed the seat performance to be characterised in the laboratory using motions relevant to the usual operating conditions of the seats, but with precisely defined time and frequency domain characteristics.

Chapter 6 Seat component measurements

The objective of chapter 6 was to quantify the dynamic characteristics of the components of each of the three suspension seats in sufficient detail to allow a theoretical model of each seat to be developed. The seat cushion and the suspension damper in particular were identified as having strongly non-linear dynamic behaviour. These components were therefore examined in some detail to allow the potential for more complex models for these components to be developed than used in studies up to the present time.

Chapter 7 The Model structure

Chapter 7 describes the mathematical and computational structure of the non-linear suspension seat model developed for this thesis. Suitable operating parameters for the non-linear equation solving routine were determined and the expected error due to the approximations inherent in these routines was quantified.

Chapter 8 Suspension damping parameter optimisation

Chapter 8 involved the use of a non-linear parameter optimisation process to estimate the seat suspension damping characteristics from the measured performance of the complete seat. This process was necessary as the measurements of the suspension damper friction forces described in Chapter 6 were substantially different when measured on two sets of test apparatus before and after the laboratory tests conducted in Chapter 5. The actual friction force present during the laboratory tests was therefore not known so it was necessary to determine this for each seat by some other method.

Chapter 9 The model performance

Chapter 9 quantified the performance of the model in response to the test motions obtained in the laboratory in the work described in Chapter 5. A total of 673 conditions were compared, the distribution of the error between the measured and predicted results was determined. Test conditions that produced errors in the upper quartile of the distribution were examined in more detail and explanations for some of these differences were proposed.

Chapter 10 Cushion non-linearities

The objective of Chapter 10 was to quantify the effect of including in the model the change in the stiffness and damping of the cushion with cushion compression in order to determine if a more complex cushion model would result in better predictions of the seat-load system performance.

Chapter 11 Parametric sensitivity analysis

The work described in Chapter 11 quantified the influence of each of the seat component parameters on the predicted vibration isolation performance of the seat over the range of test conditions used in Chapters 5 and 9.

Chapter 12 Conclusions

Chapter 12 summarised the findings of the thesis and suggested further research that might be performed.

2 Review of literature

2.1 Introduction

This literature review considers the effect of vibration on the seated human body, the dynamics of the seated human body, the vibration found in off-road vehicles, the characteristics of suspension seats, methods of testing seats in the laboratory, the methods used to simulate suspension seating and mathematical methods relevant to non-linear simulation and optimisation.

The objectives of the review were to identify suitable methods for evaluating the performance of suspension seats and to identify the state of the art of suspension seat simulations. Suspension seat modelling was considered in terms of the methods of assessing the seat component parts, the mathematical techniques for simulating the complete seats, the forms on input applied to the models, the methods of assessing the performance of the models with respect to the physical systems and the extent to which these models were used to advance the understanding of suspension seat behaviour.

2.2 Seated human vibration, perception and health

2.2.1 Vibration characteristics

2.2.1.1 Vibration frequency

The effect of frequency on the discomfort experienced by a seated human subject has been investigated by a number of authors and variations in perceived discomfort with frequency were found.

Ziegenruecker and Magid (1959) and Magid *et al.* (1960) used sinusoids with peak accelerations exceeding 15 ms^{-2} to investigate the tolerance of human subjects to vibration. Further research in terms of equivalent comfort contours was reviewed by Griffin (1990, section 3.3.2) and some examples of the equivalent comfort contours are shown in Figure 2-1. Most contours show a decreasing acceleration (corresponding to an increase in sensitivity) between 2 and 6 Hz and then a decrease in sensitivity from 10 Hz.

The use of a frequency weighting filter derived from the equivalent comfort contours allows a time history to be simply adjusted for the variable sensitivity of the human body to different frequencies of vibration. Standardised frequency weightings for vertical seated vibration were defined in ISO2631 (1974, 1985 and 1997) and BS6841 (1987). The ISO2631 weighting appeared to have been initially influenced by the research of Ziegenruecker and Magid (1959) and Magid *et al.* (1960) investigating the human tolerance limit to vibration, while the BS6841 'W_b' weighting was based on more recent research as described by Griffin *et al.* (1982), Corbridge and Griffin (1986) and others, in terms of equivalent comfort contours. The two weighting curves are shown in Figure 2-2.

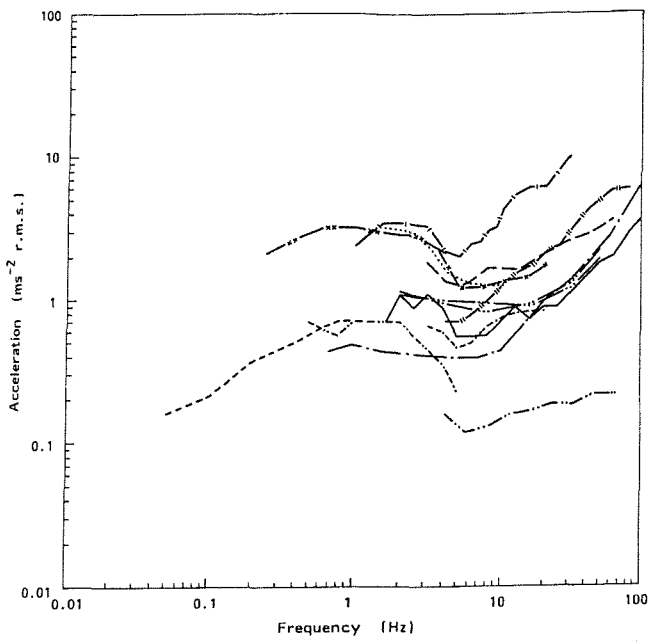

Figure 2-1 Equivalent comfort contours for seated, vertical vibration, From Griffin (1990). One contour is shown for Miwa (1967), Shoenberger and Harris (1971), Yokenawa and Miwa (1972), Dupuis *et al.* (1972), Jones and Saunders (1972), Shoenberger (1975), Griffin (1976), Griffin *et al.* (1982), Parsons *et al.* (1982), Oborne and Boarer (1982), Donati *et al.* (1983), Corbridge and Griffin (1986) and Howarth and Griffin (1988).

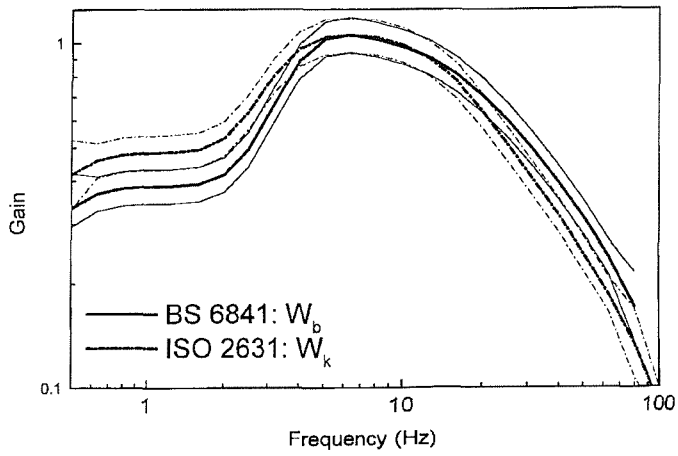

Figure 2-2 The W_b and W_k weighting curves for vertical vibration under the seated human body

These frequency weightings can be implemented as filters which can be applied to measured vibration time histories in order to produce a 'weighted' time history that

emphasises the frequencies to which the body is most sensitive. Some industrial sources appear to assume that that W_k was developed as a weighting for use when assessing health risk whereas W_b is for use when assessing discomfort, but this is not the case. Both weighting curves were developed from measures of discomfort in various forms, weather as a tolerance as used by Magid *et al.*, or an equivalent discomfort as used by Griffin and others.

The work involved in this thesis is expected to involve vibrations that are uncomfortable but not intolerable. The W_b weighting curve will therefore be used throughout the thesis to account for the discomfort caused by different frequency components within the vibrations.

2.2.1.2 Vibration direction

The principal axes of vibration for seated subjects are defined in BS6841 (1987) as shown in Figure 2-3. A summary of the equivalent comfort contours for lateral seated vibration is shown in Figure 2-4 and Figure 2-5 from Griffin (1990), but the research presented in this thesis was restricted to vertical vibration (*z* in Figure 2-3).

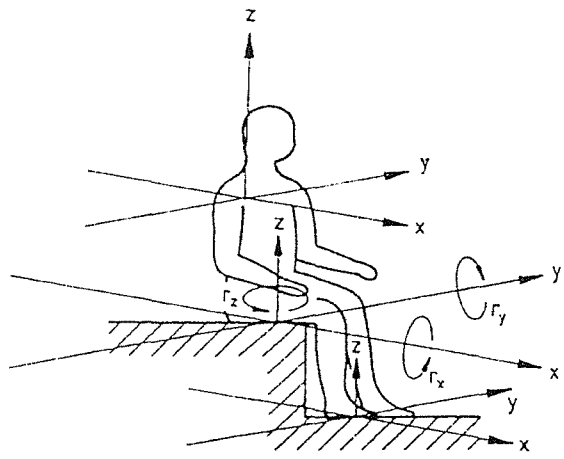

Figure 2-3 Principal basicentric axes for a seated person (BS6841,1987)

This thesis was restricted to vertical vibration only for two reasons. Firstly the seat suspensions used in the majority of off-road vehicles currently in use are restricted to the vertical axis only. Secondly, the inclusion of additional axes of vibration was considered too ambitious given the non-linearity of the seat-person system and the range of vibration magnitudes for which the system was expected to be subjected. The expansion of a seat-load model to include additional axes, with or without secondary, horizontal suspension mechanisms, was identified as an interesting avenue for further work.

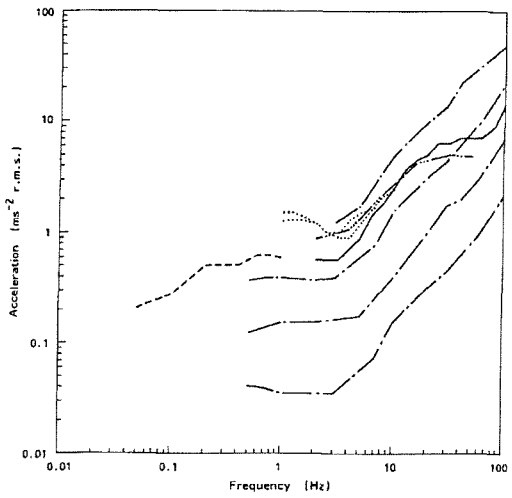

Figure 2-4 Equivalent comfort contours for fore-and-aft vibration of seated subjects from Griffin (1990). Results are shown for studies by Miwa (1967), Yonekawa and Miwa (1972), Griffin *et al.* (1982), Parsons *et al.* (1982) and Donati *et al.* (1983).

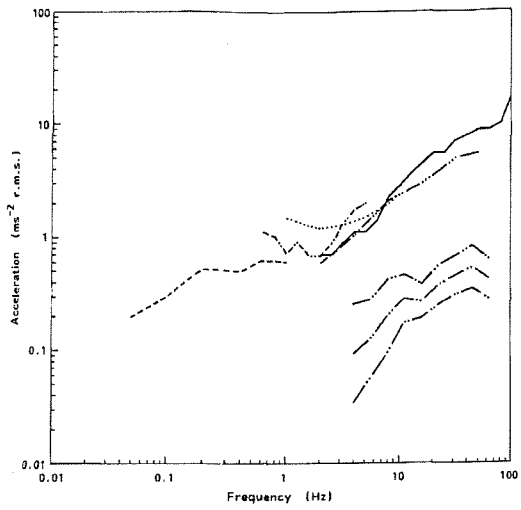

Figure 2-5 Equivalent comfort contours for lateral vibration of seated subjects from Griffin (1990). Results are shown for studies by Yonekawa and Miwa (1972), Griffin *et al.* (1982), Parsons *et al.* (1982), Donati *et al.* (1983), Corbridge and Griffin (1986) and Howarth and Griffin (1988).

2.2.1.3 Vibration magnitude

Stevens, (1975) suggested the power law shown in Equation 2-1 to relate the psychophysical vibration magnitude, ψ, to the measured vibration magnitude, φ using a constant k and an exponent n. Griffin (1990, section 3.2.1) reviewed some of the research conducted to determine a suitable value for the exponent n and observed that most results for seated vertical vibration were close to unity in the region from 2 to 80 Hz as shown in Table 2-1. A doubling in measured vibration magnitude might therefore be expected to correspond to a doubling in the subjective discomfort due to the vibration. The methods of assessing vibration discomfort in this thesis followed this assumption.

$$\psi = k\varphi^{n} \qquad \text{Equation 2-1}$$

Table 3.2 Growth functions for whole-body vibration (i.e. exponents from Stevens' power law)[a]

Frequency (Hz)	Study										
	Miwa (1968a)		Shoenberger and Harris (1971)	Shoenberger (1975)	Jones and Saunders (1974)		Clarke and Oborne (1975a)	Leatherwood and Dempsey (1976)		Howarth and Griffin (1988a)	
	$< 1\ m\ s^{-2}$	$> 1\ m\ s^{-2}$			Male	Female		Discomfort	Intensity	z-axis	y-axis
0.25				1.34							
0.4				1.47							
0.63				1.47							
1.0				1.48							
1.6				1.47							
2.0								1.35	1.12		
2.5				1.35							
3.0							1.08				
3.5			0.95								
4.0				1.43						1.21	0.68
5.0	0.6	0.46	1.04		0.88	0.95	1.08	1.43	1.20	1.04	0.85
5.6											
7.0			0.86				0.94				
8.0					0.94	0.95		1.20	1.20	1.09	0.93
9.0			0.97								
10/11			0.98		0.96	0.93		1.30	1.10		
14/15			0.91					1.40	1.15		
16/17					0.94	0.93		1.10	1.12	1.14	1.99
20	0.6	0.46	0.87		0.93	0.90	0.90	1.12	1.02		
22/23								1.13	1.15	1.47	1.75
26								1.10	1.00		
29/30					0.91	0.92	0.78	1.14	1.20		
31.5										1.35	1.76
40					0.90	0.99					
44.5										1.28	1.57
50							0.82				
60	0.6	0.46									
63										1.29	1.69
80					0.90	0.94					

[a] In addition, at 10 Hz, Fothergill and Griffin (1977c) obtained 1.13 using magnitude estimation and 1.75 using magnitude production. Hiramatsu and Griffin (1984), at 8 Hz obtained 0.96 over durations from 2 to 50 s. Clarke and Oborne (1975a) have reported values obtained by fractionation methods.

Table 2-1 Summary of exponents to Steven's power law (Griffin, 1990)

2.2.1.4 Vibration duration

The root-mean-square (r.m.s.) was suggested in early standards as a method of summarising the relationship between comfort and vibration, implying that discomfort varies with vibration duration according to the equation $a^2.t = constant$.

Studies by Griffin and Whitham (1977, 1980) indicated that subjective response could be better matched to vibration magnitude by a root-mean-quad relationship, especially in the cases of signals with high crest factors. A shock is perceived as more uncomfortable than a more prolonged period of low-level vibration with the same r.m.s. level. These studies led to the development of the vibration dose value (VDV) to give a simple measure of experienced vibration level. The VDV is defined in Equation 2-2, where $a_w(t)$ is the frequency-weighted acceleration.

$$VDV = \left[\int a_w^4(t)dt\right]^{1/4} \qquad \text{Equation 2-2}$$

Raising the acceleration to the fourth power rather than squaring it gives more emphasis to a short duration, high magnitude motion compared with a longer duration lower magnitude motion.

2.2.2 Vibration and health

2.2.2.1 Occupation and health

A range of responses have been reported relating to situations involving whole-body vibration. These effects were reviewed by Griffin (1990, section 5.2) and included increases in heart rate, blood pressure and oxygen intake (Guingard 1965, 1985), effects on the postural control of muscles (Goodwin *et al.,* 1972, Eklund, 1969), electromyographic activity in the back muscles (Seidel, 1988, Robertson and Griffin, 1989), disturbance of vision and hearing loss. Whole-body vibration has also been related to lower back pain or damage to the vertebral disks (Seidel and Heide, 1986).

Kelsey and Hardy (1975) found a high correlation between the operation of trucks and the occurrence of low back pain and herniated disks. Sandover (1981) reported that vehicle operators typically report between two and four times the number of lower back problems and disabilities reported by the normal population. Rosegger and Rosegger (1960) found that 71.3% of tractor drivers suffered from pathological spine deformations and a high incidence of stomach problems and Dupuis and Christ (1966) and Christ and Dupuis (1968, two papers) indicated that tractor driver as an occupation was associated with damage to the lower back.

However, the association of back problems with a particular occupation also associated with high magnitudes of vibration does not of itself link the vibration to the back problems. Reviews of epidemiological studies were conducted by Seidel and Heide (1986), Hulsof and van Zanten (1987) and Kjellberg *et al.* (1994) and criticised the lack of vibration measurements and the epidemiological standards used in published surveys of vibration and health.

Bovenzi and Hulsoff (1998) have conducted a review of recent studies on vibration and health attempting to relate vibration exposure and back pain. Stayner (2001) and Pope *et al.* (1995) have also summarised the literature in this area. Among the studies reviewed were Bovenzi and Betta (1994) who observed increasing back pain with increasing driving hours and Boshuizen *et al.* (1992) observed that younger fork-lift drivers had a greater prevalence of back pain than a reference population.

Research has also been directed to identifying the form of damage caused by exposure to vibration. Sandover (1981) proposed that fatigue failures in the vertebral endplates are the dominant form of damage that lead to whole-body vibration related diseases of the spine and subsequent research by Hasson *et al.,* (1987) and

Brinckmann *et al.* (1988) noted that failures in conditions of repeated compression occurred at lower magnitudes than for a single force loading. Further research by Brinckmann *et al.* (1994, 1998) quantified the occurrence of such injuries in work-forces exposed to whole-body vibration.

It is difficult to prove a link between low and moderate vibration and the occurrence of lower back pain or damage, as the pain or damage develops over time rather than immediately (Bovenzi and Betta, 1994). Seidel *et al.* (1998) described a technique for evaluating whole-body vibration based on the likelihood of failure of the inter-vertebral disks estimated from the spinal loading, the number of cycles of vibration and the strength of the vertebral disks. The effect of posture on the predicted spinal loading was investigated and a bending forward posture was found to result in lower predicted loads than a driving posture.

In situations involving very high magnitudes of motion, it is possible for the back to be damaged as a direct and immediate consequence of the motion, as in the case of aircraft ejector seats. Edwards (1997) found that greater weight was more likely to lead to a severe injury during ejection and greater than average height was more likely to lead to a back injury. This suggests that taller and/or heavier off-road machine operators may be more at risk from severe end-stop impact events.

However, research is still in progress to link whole-body vibration with injury and in particular spinal injury. While there is suggestion from a number of studies that people in occupations that involve whole-body vibration have a greater prevalence of some forms of injury to the spine or pain in the back, the link between vibration and injury is still unclear and the injury mechanisms have not been conclusively proved.

It is interesting to note that the subjects tested by Ziegenruecker and Magid (1959) and Magid *et al.* (1960) indicated a variety of reasons for stopping the test including chest pain, head symptoms and general discomfort, but did not identify back pain. The test motions were sinusoidal motions with peak amplitudes in excess of 15 ms^{-2}.

2.2.2.2 Posture

Griffin (1975) demonstrated large differences in vibration transmissibility through the body due to differences in seated posture and several studies have linked body transmissibility with operator visual and motor performance (Guignard and Irving 1960, Griffin and Lewis 1978, Lewis and Griffin, 1978). However, Oborne *et al.* (1981) reported that transmissibility had only a small effect on comfort. The study by Bovenzi

and Betta (1994) identified posture as a contributing factor leading to lower back pain in a population of tractor drivers and found that posture and vibration were independent contributors.

A clearly identified postural problem with the drivers of agricultural tractors and forklifts is the tendency of the driver to operate the vehicle while looking backwards. Saint-Eve and Donati (1992) noted that forklift drivers often operate in reverse due to the poor forward visibility offered by the mast, forks and load. Donati *et al.* (1982) observed that during some tasks tractor drivers can spend around 50% of the time looking backwards in order to monitor a load or attachment and may twist in the seat more than 15 times a minute.

2.2.2.3 Shocks

There is no clean-cut division between 'vibration' and 'shock. Broadly speaking, a shock is a short duration high amplitude movement whereas a vibration is a longer duration event of more consistent amplitude. It has been suggested that occasional shocks may have a greater affect on the well-being of a vehicle operator than more uniform low-level vibration (Allen, 1977, Sandover, 1988, Kjellberg and Wikstrom, 1985). Attempts have been made to define general methods to assess the severity of a measured shock but the complexity of the subject implies that no single method will be applicable to all situations. Two suggested methods for assessing the severity of shocks are the dynamic response index (DRI) and the VDV.

The dynamic response index (DRI) assumes the response of the body can be approximated to the response of a single degree of freedom system. A shock time history is input into a damped single degree-of-freedom model of the body and the peak stress on the spine is assumed to be approximated by the peak displacement of the model. This approach was proposed by Payne (1965) and Payne and Band (1971). The DRI has been used extensively in assessing the damage caused by aircraft pilot ejections, but a study by Anton (1986) found poor correlation between occurrence of injury and DRI for 4 out of 5 ejector seats used for 223 ejections.

The VDV is also capable of assessing shock-like motions. This measure accounts for both the time and magnitude of a shock and can cope simply with compound shocks and shocks within longer term lower amplitude vibrations. The VDV was developed from measures of subjective discomfort. A tentative daily exposure VDV of 15 $ms^{-1.75}$

has been suggested (BS 6841, 1987) on the assumption that health risk due to vibration has the same frequency, magnitude and time dependence as comfort.

2.3 Off-road vehicle vibration and the need for suspension seating

2.3.1 The benefit of suspension seating

Off-road machines with pneumatic tyres are known to produce narrow-band vibration on the cab floor with energy in the frequency range from 1 to 5 Hz (Marsh 1965, Chisholm, 1970) as illustrated in Figure 2-6 from Marsh (1965). Off-road vehicles usually have no primary suspension, although some are fitted with front suspensions. Only a few, of which the JCB Fastrac is the most widely used, have full primary vehicle suspensions allowing higher road speeds under current legislation. The vibration at the cab floor is therefore caused on the majority of off-road vehicles by the oscillation of the vehicle mass on the pneumatic tyres resulting in a lightly damped, narrow-band vibration.

The main resonance frequency of a cushion seat-human subject system has been reported by Patten *et al.* (1998), Griffin (1978), Corbridge *et al.* (1989) and many others as being between 2 and 5 Hz. A foam cushion seat in an off-road vehicle will therefore act as a vibration amplifier rather than an isolator as reported by Griffin (1978) and Payne and Band (1971).

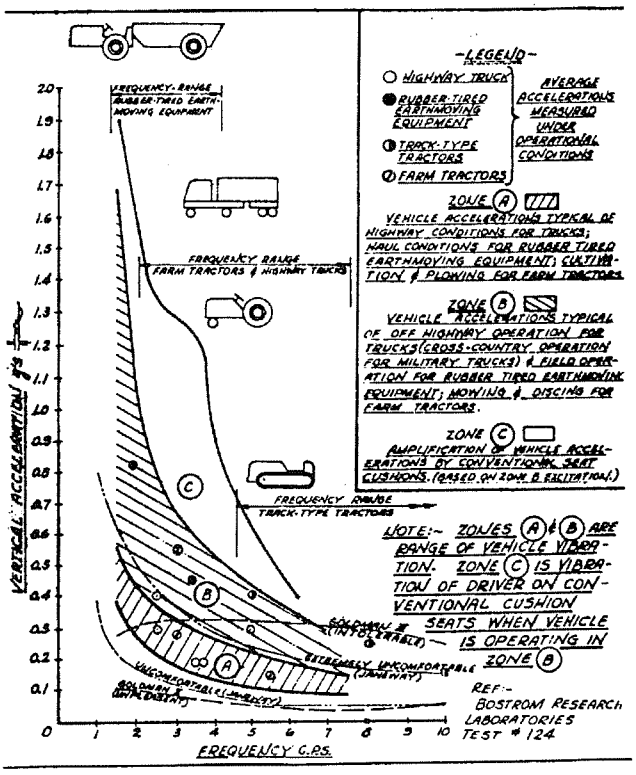

Figure 2-6 The vibration environment on commercial and military vehicles (Marsh, 1965)

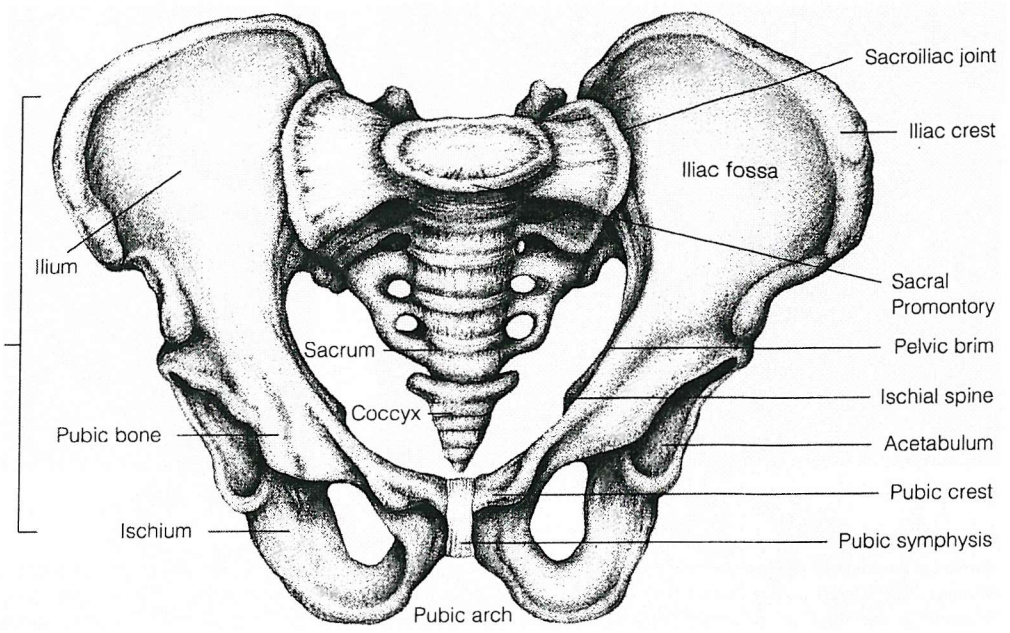

Figure 2-7 The ischial tuberosities are the thickened underneath surfaces of the ischium (Marieb, 1995).

The seat surface is a compromise between dynamic performance and static comfort. The human body when seated on a hard, flat surface is supported on the iscial tuberosities (Figure 2-7). This results in an uncomfortable concentration of pressure. Some form of contoured or compliant surface is necessary to distribute this pressure over a wider area (Umehara *et al.* 1971, Hertzberg, 1972). The balance between static and dynamic comfort was investigated by Ebe and Griffin (2000a, 2000b). Wu *et al.* (1996) found that the ischial pressure and the total contact area showed maximum variation around the resonance frequency of the human-seat system using a foam cushion seat (2.5 to 3 Hz). The maximum ischial pressure and total contact area were found to increase with increasing vibration magnitude. However, Gyi and Porter (1999) investigated the relationship between pressure distribution and perceived discomfort but found no clear trends.

Given that some form of compliant surface is necessary to provide static comfort for a range of different operator physiques and that it is not currently possible to manufacture foam capable of reducing the driver-cushion resonance frequency below 2 Hz, it is necessary to reduce the resonance frequency by some other means. An additional, mechanical seat suspension using coil springs or air springs has become a common solution.

2.3.2 Laboratory suspension seat evaluation

Seat performance is usually expressed in terms of the amount of vibration transmitted from the seat base to the vehicle operator. Automotive seats have been demonstrated to have some non-linearities with the frequency and magnitude of the peak transmissibility decreasing with increasing magnitude. However, it has been suggested that this may be due to the non-linearity of the human on the seat (Fairley and Griffin, 1986). A linear transfer function may be sufficient to describe the cushion vibration transmission characteristics. This approach cannot be used so easily with a more highly non-linear suspension seat as the seat produces a substantially different response for different input magnitudes as illustrated in Figure 2-8.

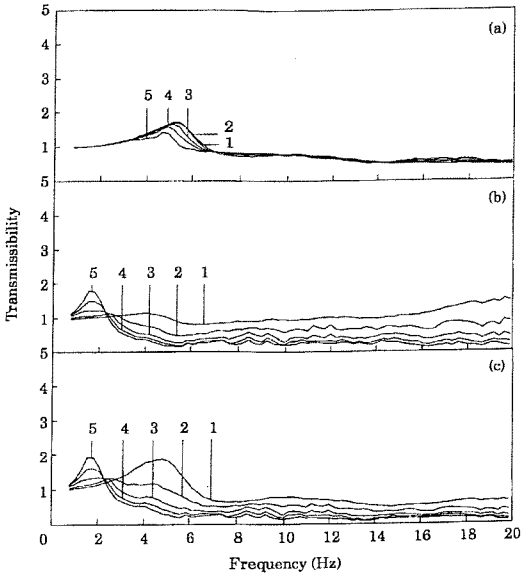

Figure 2-8 The effect of varying input vibration magnitude on the transmissibility of a suspension seat showing the transmissibility of the cushion (top), the suspension and the complete seat (bottom). Increasing numbers indicate r.m.s. acceleration magnitudes increasing from 0.35 to 1.75 ms^{-2} in equal steps. (Wu and Griffin, 1996).

A simple summary method of describing the performance of any seat to a particular motion is the SEAT value, pronounced see-at, first suggested by Griffin (1978). This measure is the ratio of the 'amount' of vibration at the seat surface (typically an r.m.s. acceleration or VDV) to the amount of vibration at the seat base, expressed as a percentage as shown in Equation 2-3 where a_s is the weighted vibration on the seat surface and a_p is the weighted acceleration on the platform under the seat. This measure has been adopted for use in current national and international standards.

$$SEAT = \frac{a_s}{a_p} x100\% \qquad \text{Equation 2-3}$$

where a_s is the frequency-weighted acceleration at the seat surface and a_P is the frequency-weighted acceleration at the seat base.

Evaluating suspension seats using field tests is expensive and time consuming. A vehicle and a suitable test track are required. An artificial, durable test track is a major investment in order to obtain a single test condition. Even with such a track the variability between vehicles, or with the same vehicle with different tyres, fuel loads or weather conditions could affect the test results. Conditions can be more closely controlled by using a shaker in the laboratory to test the performance of a seat. The input motion can be varied in a controlled manner, but a suitable input motion must be defined to ensure that the seat is adequately tested.

Stayner and Bean (1971) obtained representative test motions by reproducing in the laboratory the vertical acceleration measured in a tractor on a test track. Stayner (1971) emphasised the need to use realistic testing conditions due to the highly non-linear behaviour of suspension seating. The European standard EEC/78/764 (1978, including revisions up to 1997) was developed using this philosophy and uses a recorded cab floor vibration as the test input.

More recent international standards for suspension seat testing (e.g. ISO7096, 1982 and 2000) used a filtered random motion with a frequency content representative of that found on the cab floor of a particular type of off-road vehicle. This form of test motion has a noticeably different amplitude distribution with time as compared to the EEC/78/764 test signal. The EEC/78/764 motion involves periods of relatively high magnitude motion interspersed with lower amplitude regions as compared to the random amplitude-time distributions of the ISO signals. Both forms of test signal are relatively long in duration (between 60 and 300 seconds).

The test motions described above have a defined magnitude for which the seat is required to provide a specified amount of vibration isolation. A test using a fixed input magnitude does not account for the fact that the vehicle-seat-driver system includes an adaptive feedback element. If provided with an especially good seat the driver is likely in some circumstances to increase the vehicle speed in order to more quickly complete the task at hand, resulting in greater vibration on the vehicle floor. Wu and Griffin (1996) suggested a test method whereby an input stimulus would be applied to the seat base at progressively increasing magnitude so quantifying the seat performance in terms of the change in transmissibility with magnitude instead of the transmissibility at a single magnitude.

2.3.3 Vibration observed in the field

Given the large numbers of off-road vehicles in use worldwide, there are comparatively few published accounts of vehicle vibration characteristics. It is assumed that in the majority of cases where vehicle vibrations are quantified there are commercial interests involved that prevent or discourage publication.

The study by Malchaire *et al.* (1995) took 480 measurements of vibration on fork-lift trucks. The study suggested that vibration exposure is mostly influenced by the roughness of the track, the vehicle speed and the quality of the seat. An earlier study by Marsh (1965) published typical vibration characteristics for a range of vehicles and current standards (e.g. ISO7096:2000, EN13490:2001, ISO 5007:1990) provide typical vehicle vibration characteristics for specific vehicles, but do not provide information on how these motions were determined as typical.

Other studies involving off-road vehicles have tended to use summary measures of the vibration (VDV or r.m.s.) and have been more concerned with the effect of the vibration on the operator rather than the characteristics of the vibration of the vehicle. Sorainen *et al.* (1999) investigated the vibration on nine agricultural tractors and found that the '8-hour fatigue decreased proficiency boundary' as described in ISO 2631-1 (1985) was exceeded in all cases and instantaneous accelerations of two or three times the mean level were observed. Stayner and Bean (1971), Stiles (1994) and Lines *et al.* (1995) conducted two surveys of the vibration exposure of tractor drivers and indicated that the vibration exposure of tractor drivers had not changed substantially in the time between the two surveys.

2.3.4 Discussion of the vehicle vibration

It is usually frequency domain characteristics and the summary magnitude of off-road vehicle vibrations which are reported. The 'typical' vibration characteristics of the standardised classes of vehicle, at least in the vertical axis, are well known. The time and amplitude domain characteristics of the vehicle vibration are less well known. The characteristics of the cab floor motions that lead to seat end-stop impact events in particular have not been investigated.

The use of cab suspensions (Lines *et al.* 1989) and partial or full vehicle suspensions on new vehicles will change the vibration characteristics on the cab floor. The present standardised methods for evaluating the suitability of a seat for such a vehicle will no longer be applicable as the standard vibration test signals will no longer be relevant.

A further deficiency with the present seat test standards is that only a single magnitude of motion is tested. The seat in the field will be subjected to a wide range of magnitudes and in some circumstances will experience suspension over-travel (or end-stop impact) situations. The performance of the seat during these severe motions may be of greater importance than the performance at lower magnitudes.

2.4 An introduction to suspension seating

A separate suspension mechanism between the seat cushion and the vehicle floor can be adjusted to have a resonance frequency below the predominant frequencies of vibration on the floor of a particular vehicle, so reducing the vibration transmitted to the operator in vehicles where vibration occurs in a frequency range that would be amplified by a foam cushion seat. A suspension seat can be reduced to a number of components, each having some effect on the dynamic response of the whole.

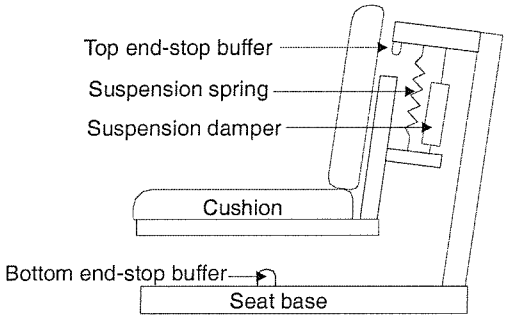

Figure 2-9 Schematic of a behind-seat suspension

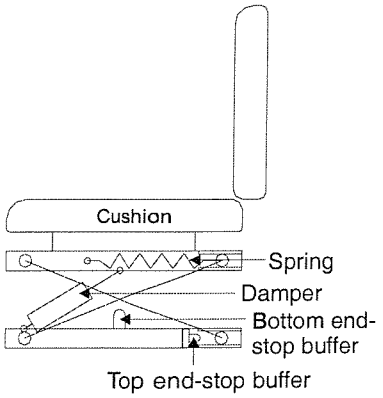

Figure 2-10 Schematic of an under-seat suspension

Figure 2-9 and Figure 2-10 show schematics of two common suspension seat configurations. The performance of the component parts in both systems is essentially the same. Stiffness is provided by a spring, usually steel coil springs, torsion springs or air springs. The spring is selected so that the resonance frequency of the seat-driver system is sufficiently low to isolate the frequencies of vibration expected in the vehicle. Seat suspensions are usually limited to a maximum of 100 mm of vertical travel by rubber end-stop buffers to prevent excessive relative displacement between

the driver and the controls. The spring is preloaded so that the mean suspension displacement is close to the centre of the travel.

Stiles (1994) reported that 45% of suspension seats involved in a survey of agricultural tractors caused greater vibration on the seat surface than on the vehicle floor. Impacts with the end-stop buffers were suspected as one possible cause of this poor performance. Oil-filled damper units are used in current suspension seat designs to reduce the relative motion across the suspension in order to reduce the likelihood of end-stop impact events.

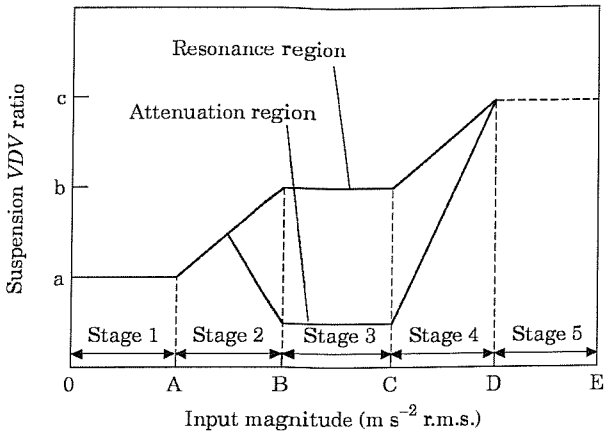

Figure 2-11 The variation of the vibration isolation performance of a suspension seat varying with input magnitude for an input frequency close to the suspension resonance frequency and for an input frequency sufficiently high for the seat to provide attenuation (Wu and Griffin, 1996)

Wu and Griffin (1996) identified five stages of suspension seat behaviour varying with input magnitude as shown in Figure 2-11. At low magnitudes, stage 1 describes a seat with the suspension mechanism friction-locked and immobile. As the amplitude increases, stage 2 describes a seat suspension breaking away from friction. Stage 3 is the quasi-linear region with the seat suspension using most of the available stroke but not impacting the end-stops. Stage 4 involves end-stop impacts and stage 5 involves severe impacts with the seat repeatedly striking the top and bottom buffers in turn.

2.5 Suspension seat component parts

2.5.1 The linkage

The linkage mechanism restricts the mass of the seat to move over a limited stroke, usually in one axis only. The linkage provides the framework to which the spring, damper and seat are attached and may be arranged with the suspension behind or below the seat as described above.

Most suspension mechanisms are designed to limit seat movement to the vertical direction only. Lowe (1972) mentions that fore-and-aft movement of more than 10 mm on a nominally vertical suspension system is liable to cause complaint from drivers

and that lateral movement can lead to a subjective sense of insecurity. The use of an X-mechanism (Figure 2-10) was recommended from a stability point of view, and this form of mechanism is used on the majority of seats in current production where the suspension is fitted under the seat.

Zach (1971) provided information on the development of a 'knee hinge' design with whereby the seat rotates about an effective pivot point at the drivers knee (Figure 2-12). This allows a long stroke for the purposes of isolation performance while minimising the 'leg pumping' effect caused by high relative displacements at the front of the seat. This form of mechanism has not been widely adopted for commercial use, possibly due in part to the non-vertical components introduced by the suspension mechanism and the complexity (and therefore cost) of the adjustable oil and gas suspension system.

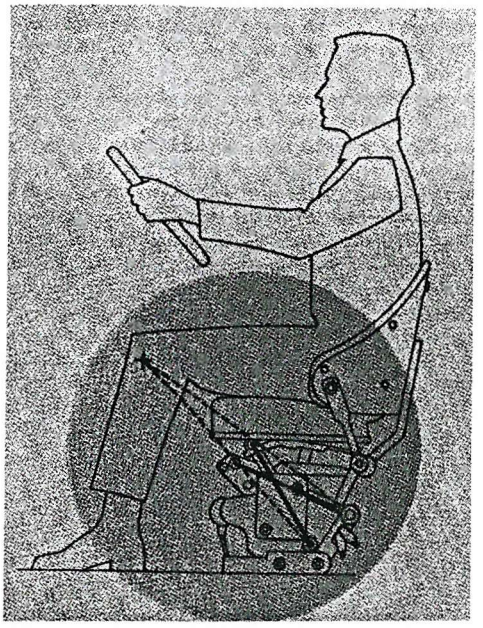

Figure 2-12 Schematic of a knee-hinge suspension (Zach 1971).

2.5.2 The suspended mass

The mass of the moving part of the suspension seat is relatively small compared to the mass of the driver. This mass consists of the moving parts of the suspension, the seat pan and some accounting for the cushions and backrest. A simulation study by Rakheja *et al.* (1994) indicated that increasing the suspension mass can improve the isolation performance of a suspension seat. However, an increase in the mass of the seat results in higher shipping costs for seat manufacturers. Seat designs with water tanks on the suspension to increase the mass without increasing the shipping costs have been investigated by some manufacturers but have not progressed past the prototype stage.

2.5.3 The suspension stroke

The vertical stroke of the suspension is constrained by two main factors. Vertical space in vehicle cabs is limited, especially in older vehicles that were not originally designed to be fitted with suspension seats or in small vehicles such as fork-lift trucks. The compact seats fitted in such cases typically have a stroke length of 30 mm (INRS, 1992) and often have no damper fitted (Comite de pilotage charge de la mise au point

de guides par le choix de sieges suspendus de chariots elevateurs, 1992) relying on friction to provide the necessary damping.

The second factor limiting the suspension stroke is that excessive displacements of the driver relative to the controls may be uncomfortable. The stroke must be long enough to provide useful vibration isolation without reaching the end of the suspension travel. Lowe (1972) suggested that 100 mm was a good compromise stroke length, giving acceptable isolation and allowing some leeway for inaccurate adjustment of the seat while not causing too much displacement relative to the controls. This value appears to be generally accepted and operating displacements up to this value are usually welcomed due to the increased isolation achieved. However, Boileau and Rakheja (1990) report the case of a seat that gave good vibration isolation performance but was unsatisfactory to the driver due to the high but non-limiting relative displacement between the seat surface and the vehicle. No studies have looked at the effect of mounting some of the vehicle controls onto the seat suspension to avoid the need for the driver to experience relative motion across the arms and legs.

2.5.4 Lateral and rotational movement

Some seats have suspension systems designed to isolate vibration in the fore-and-aft and lateral vibration. Corbridge (1984) has shown that fore-and-aft isolation can improve the ride in the fore-and-aft direction by about 40%. Griffin (1990) suggested that fore-and aft suspensions can suffer end-stop impact problems due to their low frequency and limited travel and that the relative motion can impair the precision of hand and foot movements. Fore-and-aft isolators are fitted to some current production seats, often for use in agricultural tractors, but there are no published reports of the effectiveness of these suspensions.

2.5.5 Seat adjustment

Suspension seats should have the facility to conveniently adjust to suit different builds and weights of driver. Boileau and Rakheja (1990) mention that fore-and-aft adjustment of ±75 mm is typical and that air suspension seats have an available vertical travel of ±75 mm. The same study stressed that the means for adjusting the vertical height of the seat and the means for adjusting the spring tension to suit the driver weight should be clearly separate. Confusion of these controls may lead to poor

vibration isolation and the possibility of more end-stop impacts due to incorrect weight settings positioning the suspension close to one of the end-stops.

Donati and Patel (1999) conducted a study involving twelve forklift truck drivers to investigate seat adjustment ranges. This study also found that drivers had little understanding of the importance of the weight adjustment control. Perkio-Makela and Riihimaki (1997) investigated the seat adjustment of 100 forestry tractor drivers. Pain, stiffness, fatigue and low back pain at the end of a shift were reported to have decreased for most drivers after the seat was adjusted by a technician as compared to the driver's usual settings.

2.5.6 Friction

The joints of the linkage mechanism lead to a dry friction damping component in the system. Investigating friction in a controlled manner is challenging as it is not possible to manufacture a 'frictionless' reference system and it is difficult to control the system friction in a systematic manner. Stayner and Bean (1971) conducted a laboratory study and did not find a direct relationship between friction and transmissibility, but the figures obtained suggest that higher friction led to poorer seat performance. Lowe (1972) stressed that due to the low spring rate required for a suspension seat, a relatively small frictional force can cause a significant loss of seat performance based on that author's experience of manufacturing production seats. The effect of friction in 'locking up' the suspension at low vibration magnitudes has been noted by many authors (e.g. Wu and Griffin, 1995; Fairley, 1990).

More recent computer simulations of suspension seating have included friction elements allowing more detailed investigations into the effect of friction on the system behaviour. Boileau and Rakheja (1990) noted that friction acts as additional damping to help reduce the peak transmissibility at the suspension resonance frequency, but that too much friction deteriorates the seat performance in the isolation region. Gouw *et al.* (1990) found that an increased load on the seat while testing with an indenter led to a higher measured friction. Fairley (1990) found that the overall seat damping increased with decreasing mass loading and assumed this was due to less inertia force being available to overcome a constant friction force. Rakheja *et al.* (1994) conducted a simulation study of a suspension seat and noted that a reduction in friction can improve the performance of a seat for some input signals. The model used in the study also showed the locking up of the suspension at low vibration magnitudes.

While many of the studies above have provided evidence that friction adversely affects the performance of a suspension seat, only the simulation study by Rakheja *et al.* (1994) attempted to quantify the influence of the friction magnitude on the seat performance. This study indicated that increased friction was detrimental to the seat performance and that for the seat under investigation a halving of the friction force would be expected to result in a reduction in the acceleration power spectral density on the seat surface of approximately 25%. The investigation used one magnitude of random motion defined as for Class II agricultural tractors by SAE J1386 (1986).

The variation of suspension seat friction force with time has not been widely investigated. Stayner (1972) mentioned that running-in a seat reduced the friction, but operation over rough conditions for 200 hours resulted in an increase in friction leading to a reduction in isolation efficiency.

2.5.7 The spring and the driver weight adjustment control

The suspension seat spring must be able to support the mass of the seat and the driver such that the resonance frequency of this system is sufficiently below the lowest frequency of vibration expected at the seat. Rakheja *et al.* (1987) reported that driver masses might be expected to range between 50 kg and 100 kg and that 75% to 82% of the driver mass is supported by the seat. Other studies have used values within this range suggesting an extreme seat loading range from 37.5 kg to 82 kg. Lowe (1972) suggested $5/7^{th}$ of driver mass (approximately 71%) but noted that the loading on the seat depends on the layout of the controls and that a seat loading capacity corresponding to driver weights from 45 to 110 kg is satisfactory in practice.

Steel, rubber or air springs are generally used in suspension seating. Leaf springs were used in some early designs but are not capable of the displacements required by modern seats (although some modern leaf-sprung seats using laminates of different materials may be under development). Torsion bars and coil springs have been used in several seat designs. Air springs are popular for their ease of adjustment, especially in vehicles equipped with air lines where the driver weight adjustment can be automatic or servo controlled (Boileau and Rakheja, 1990), but are more expensive than steel coil springs.

2.5.8 The damper

The damper is included in the design to limit the amplification of vibration at frequencies near the resonance frequency of the seat-driver system and to reduce the relative motion of the seat suspension when exposed to high magnitude motions, so reducing the likelihood and severity of end-stop impacts. However, the vibration isolation performance of the suspension at higher frequencies is poorer with high damping. Oil-filled dampers involving a piston with an orifice moving through the oil are the most common form of suspension seat damper. Some have driver-accessible controls to allow the orifice to be varied by means of a lever attached to the seat, so varying the amount of damping provided.

An orifice damper of this form theoretically exhibits a damping force proportional to the square of the velocity, but systems exist with different damping depending on the direction of travel of the seat relative to the cab floor. Dampers may exhibit changes in gradient due to the presence of bleed and blow-off valves or non-linear behaviour of

the fluid passing through the damper orifice. The dynamic properties of the oil can lead to other dynamic characteristics. The compressibility of the oil/gas solution introduces a stiffness component and changes in oil temperature cause changes in the oil viscosity. Other effects include friction due to the oil seals and flexing of the cylinder walls. Some past models of seat and automotive suspensions included the damping as a linear force-velocity characteristic, but this approach has generally been abandoned as too simplistic to produce reliable results.

A detailed model for a suspension damper was proposed by Lang (1977) but required over 80 parameters. Less complicated models (Rakheja *et al.*, 1994; Ranganathan and Sriram, 1994) have used two-slope or three-slope models to account for the fact that the force-velocity characteristic of a suspension damper is often not linear. Both of these models included a Coulomb friction component in parallel with the non-linear viscous component.

Methods exist to model the damper force as a surface in terms of velocity and displacement as described by Worden and Tomlinson (1992). The surfaces obtained using this method were relevant for single frequency excitation and were therefore referred to as an 'isofrequent map'. This method has limited use in automotive suspension modelling as it is better suited to sinusoidal rather than broadband input motions. A refinement of this method by Duym (1997) using acceleration and velocity instead of displacement and velocity showed improved results for broadband excitations.

As the damper is dissipating energy from the vibrating system, an increase in temperature is to be expected. Fairley (1990) noted a slight decrease in suspension damping with time which was attributed to an increase in temperature of the damper used in the seat under test and present standards (ISO 10326-1, 1992) stress the need to monitor the temperature of the damper when running in a seat prior to testing to prevent overheating. Oil viscosity is known to change with temperature and the energy dissipated within the oil during relatively high amplitude motion can cause the oil temperature to rise. Most models assume constant temperature operation. Surace *et al.* (1992) characterised the temperature dependence of an automotive suspension damper in terms of isofrequent mappings, but this resulted in the damper behaviour being described in terms of a number of different maps.

Recent investigations into characterising dampers have used higher order frequency response functions (HFRFs). This is a frequency domain method that characterises

the non-linear components of a system from the higher frequency components produced in response to inputs consisting of one or more sinusoids. The output from the system is represented as the sum of terms of a Volterra series (Volterra, 1959) and the terms of the series are Fourier transformed to obtain the HFRFs. A description of the methods for characterising an automotive damper using HFRFs is given by Cafferty and Tomlinson (1997). However, the approach was found to be limited by non-linear behaviour of the actuator and was not found to provide useful information beyond that obtained from the more conventional polynomial curve-fitting methods.

Equipment is commercially available to obtain force-velocity and friction values from damper units. These devices generally consist of an actuator to exercise the damper over a known displacement with a sinusoidal motion. The friction component can be estimated from a low frequency motion and the force-velocity characteristic from higher velocity motions.

An alternative method was suggested by Feeny and Liang (1996). The method is a combination of the logarithmic decrement method initially described by Rayleigh (1877) for viscous damping and the alternative version described by Lorentz (1924) for Coulomb damping. Equations were presented to obtain a viscous and a damping coefficient from the decay of a suspended mass subject to an impulse. Suspension seats are generally close to overdamped so this method could not be applied to the seat suspension directly. A test apparatus incorporating the damper into a system with a greater mass and a stiffer spring might sufficiently reduce the relative system damping to allow this method to be applied.

2.5.9 Active and semi-active damper control

The development of active or semi-active suspensions with controllable damping is an attractive proposition as such systems could achieve low amplitudes near the seat resonance without reducing the seat isolation performance at high frequencies. Barak (1992) reviewed the differences between passive, semi-active and active suspensions as applied to vehicle primary suspension systems. Active systems were identified as less reliable and more expensive as they require a closed loop control system with sensor devices and a powered actuator to provide the required force to minimise the movement of the isolated part. Passive systems were identified as unpowered systems providing vibration isolation by storing and dissipating energy in mechanical

components. Semi-active systems observed to generally involve a controllable damper which is varied according to a closed-loop control policy.

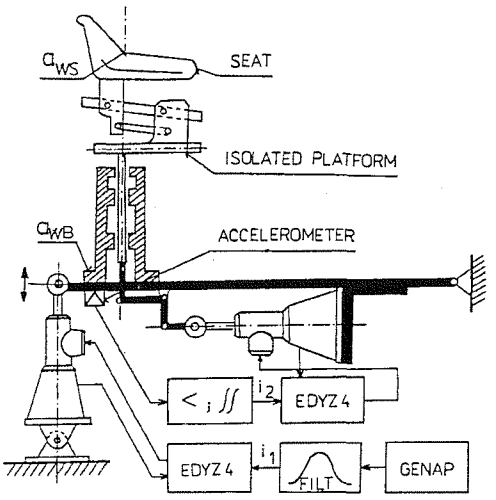

Figure 2-13 Schematic of combined passive and active seat suspension system (Stein and Ballo, 1991)

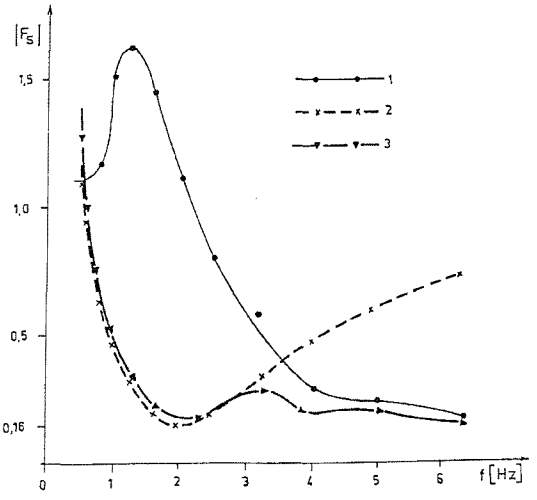

Figure 2-14 The transmissibility of the passive/active seat (line 3) compared with the passive (line 1) and active (line 2) suspensions acting alone (Stein and Ballo, 1991).

Suggs *et al.* (1970) developed a hydraulic active seat suspension unit to replace a seat suspension shown in Figure 2-13. The unit achieved 65 to 75 percent attenuation of acceleration in the 1.5 to 8 Hz frequency range. The components used in this system would be considerably more expensive than those required for a passive system. Stein and Ballo (1991) also tested an active hydraulic vibration isolation system in series with a passive seat suspension and obtained the improvements in response (Figure 2-13 and Figure 2-14). The main disadvantages of this system were the size, cost and power requirements of the hydraulic actuator.

Stein *et al.* (1992) tested an active suspension system controlling the pressure of an air spring seat suspension. The preliminary results using this system showed the ability to tune the seat isolation frequency to within a narrow boundary, but that performance at higher frequencies tended to be poorer than the passive system. The pneumatic design was developed further (Stein, 1995a, 1995b, 1995c, 1997). Electronic 'sky hook' damping was introduced as the hydraulic damper originally employed on the seat which was hampering the performance of the active control. The performance of the active vibration isolation system as compared with the pseudo-passive 'sky hook' seat showed an improvement in the SEAT values of

greater than a factor of two when using agricultural tractor and earthmover motions as defined in ISO 5007 (1990) and ISO 7096 (1982). The system schematic and the results for different control methods are shown in Figure 2-15 and Figure 2-16 The author noted that the main disadvantage of the active pneumatic isolation system was the complexity as compared with passive systems and the cost of the transducers. This latter problem was addressed by Stein (1998a, 1998b) by using a pressure control valve in place of the flow control valve used previously, enabling one of the transducers to be dispensed with and simplifying the control circuitry.

Other researchers have investigated the performance of semi-active suspension systems with on-off control policies, frequently using electro-rheological dampers (e.g Krasnicki, 1981; Nell and Steyn, 1994; Rakheja and Sankar, 1995; Wu *et al.*, 1994). Semi-active suspensions use a spring and damper combination but with some control method to modify the system response, usually a variable damper. Power is usually required to operate the control equipment, but an actuator and power supply sufficiently powerful to drive the entire seat is not needed. On - off control is normally simpler to implement than a continuous method. Electro-rheological fluids change their properties when a voltage is applied across them, allowing the properties of the damper to be changed quickly. Wu and Griffin (1997) developed such a system for use in a suspension seat with the specific intention of reducing the occurrence of end-stop impacts. The apparatus used for testing the system is shown in Figure 2-17. The system proved effective in reducing impacts without severely reducing the isolation

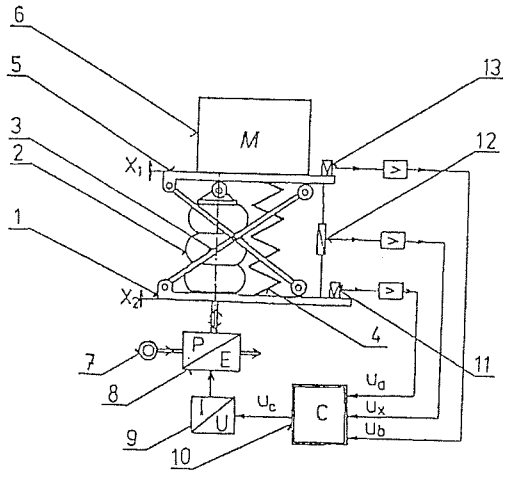

Figure 2-15 Schematic of the pneumatic active suspension (Stein, 1997).

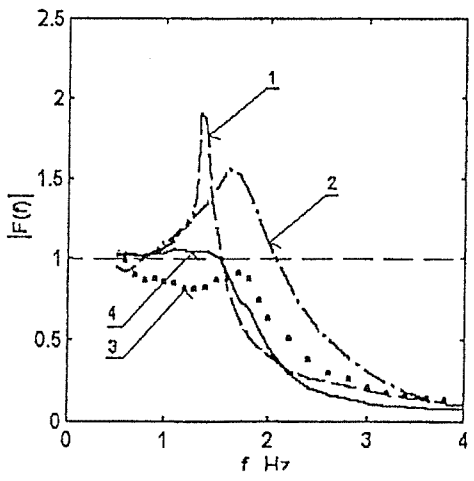

Figure 2-16 Transmissibility of the pneumatic active suspension using four control arrangements: 1-'sky cloud', 2-'sky-hook', 3-'sky-cloud' and 'sky hook', 4-limted 'sky-cloud' and 'sky-hook' (Stein, 1997).

performance of the seat.

Yao *et al.* (1995) investigated the properties of Electro-rheological fluid for application to vibration control. Morishata and Mitsui (1991) and Petek (1992) both investigated using electro-rheological fluid in a controllable shock-absorber. The performance of moving plate and sliding plate electro-rheological damper designs were compared by Yao *et al.* (1997). Low voltages produced predominantly viscous damping, while higher voltages resulted in predominantly coulomb damping. The moving plate design was found to be more effective for vibration control.

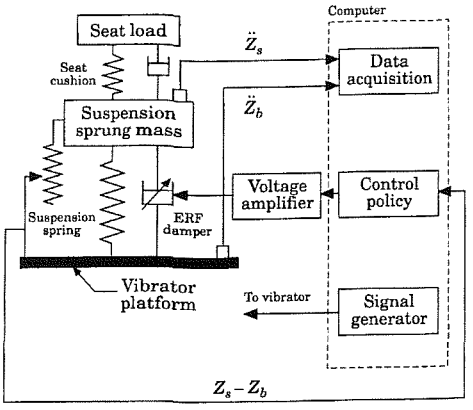

Figure 2-17 Semi-active seat suspension (Wu and Griffin, 1997)

Karnopp (1979) noted that active suspension systems are more complex, more expensive and less reliable to implement than conventional passive systems. The Lear Motion Master system is the only active seat system currently commercially available and it appears that any systems must be low-cost if they are to be adopted by seat manufacturers for large-scale markets.

2.5.10 End-stop buffers

A seat suspension is normally displacement limited by rubber buffers to reduce the accelerations caused by end-stop impacts. Suspension seat end-stop buffers are usually manufactured of moulded carbon-filled vulcanised rubber. Vulcanisation involves the addition of sulphur atoms to the heated rubber elastomer. These atoms form cross-links between the elastomer chains, resulting in improvements in elasticity, strength and resistance to degradation (Callister, 1994). Unvulcanised rubber is soft and tacky. Increasing quantities of sulphur result in harder and less extensible vulcanised rubber. The addition of carbon black increases the strength and durability of the rubber.

Wu and Griffin (1995) used a simulation with a rubber buffer simulated as a two stage spring and a linear damper to investigate the effect of end-stop buffer characteristics on seat performance. This study indicated that the buffer force-displacement characteristic had a significant effect on the severity of end-stop impacts and that an ideal buffer would have an approximately linear force-displacement characteristic. A higher damping coefficient than that of rubber was found to be preferable in reducing

the severity of impacts. However, this study and a laboratory study with a theoretical seat model (Wu and Griffin, 1995) used the vibration transmitted through the suspension rather than the vibration experienced by the vehicle operator.

Other models of suspension seating have used linear springs as the end-stop stiffness. No studies on suspension seats have used more specific dynamic models for rubber blocks such as the Maxwell model consisting of spring and damper elements in series as described by Dove *et al.* (1977) or the triboelastic model consisting of a large number of friction elements connected by springs as described by Turner (1988).

Stiles (1994) reported that 45% of suspension seats investigated in a field survey increased the vibration to the driver and suggested that a possible reason was the occurrence of end-stop impacts. A suspension seat has the potential to exert shocks in an upward or downward direction as the seat impacts with the bottom or top end-stop in overtravel situations. Howarth and Griffin (1991) found no difference between the discomfort caused by 'up' and 'down' shocks of identical vibration dose value and Wu and Griffin (1998) proposed that top and bottom end-stop impacts would cause similar discomfort. This conflicts with the opinions of seat manufacturers who generally consider the bottom end-stop to be of greater importance and comments from researchers involved in field trials that have observed drivers offsetting the seat towards the top of the stroke to avoid the bottom end-stop. The time histories shown by Wu and Griffin do indeed show shocks of similar peak acceleration at the top and the bottom stop (Figure 2-18), but these time histories were recorded on the suspension mechanism, not the seat load. The seat load is naturally limited to the downwards acceleration, with the load lifting off the seat if the seat acceleration exceeds this value. End-stop impact situations involving the driver leaving the seat therefore involve different waveform characteristics at the bottom and the top end-stop, so the results of Howarth and Griffin (1991) regarding the relative comfort of upwards and downwards

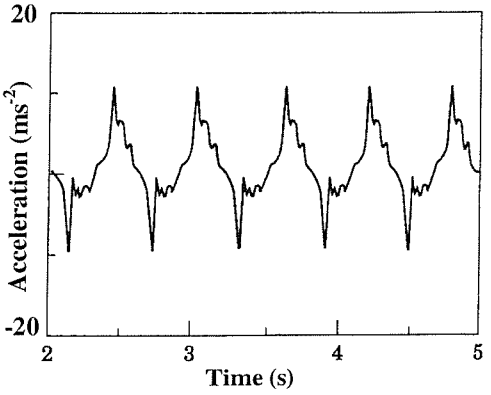

Figure 2-18 Time histories of the acceleration at the top of a seat suspension showing top stop (downward acceleration) and bottom stop (upward acceleration) impacts (Wu and Griffin, 1998)

shocks cannot be applied directly to all magnitudes of suspension seat end-stop impact.

2.5.11 Cushion

Open-celled polyurethane foams as used in seat cushions were described by Hilyard (1982) as consisting of a viscoelastic elastomeric matrix (Figure 2-19) with a fluid (air) trapped within the matrix. A compressed foam exhibits damping as the air is displaced through the foam (pneumatic damping) as well as viscous damping due to the compression of the matrix. As the frequency increases, the air ceases to be displaced and compresses instead. The damping of a foam cushion therefore rises with increasing frequency, passes through a maximum and then decreases, while the stiffness increases to an equilibrium value. A theoretical model based on this approach was described by Gent and Rusch (1966) and improved upon by Hilyard and Kanakkanatt (1970) with the inclusion of viscoelastic properties of the polymer matrix.

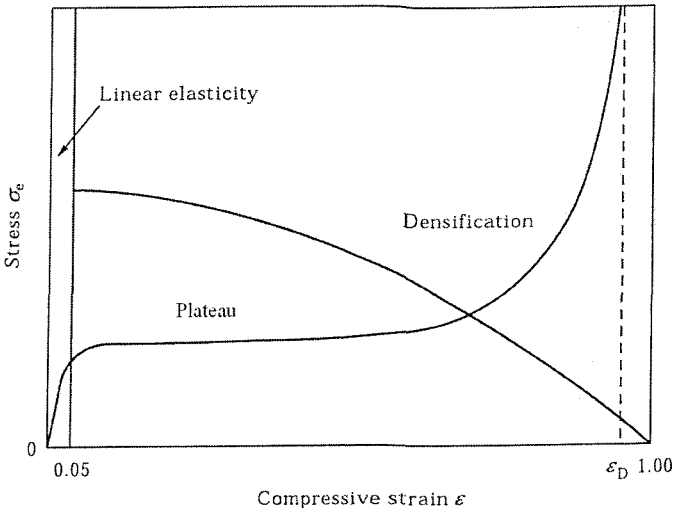

Figure 2-20 Stress-strain curve for open cell foam (Patten *et al.*, 1998)

The stiffness of a polymer matrix under compression is also non-linear. The stress-strain curve for a possible foam cushion is shown in Figure 2-20 (from Patten *et al.*, 1998). This initially illustrates the matrix bending and displaying linear elastic properties, then the cell structure begins to buckle and the stiffness stops increasing and finally the matrix becomes completely collapsed and all the air expelled or trapped causing the stiffness to increase rapidly.

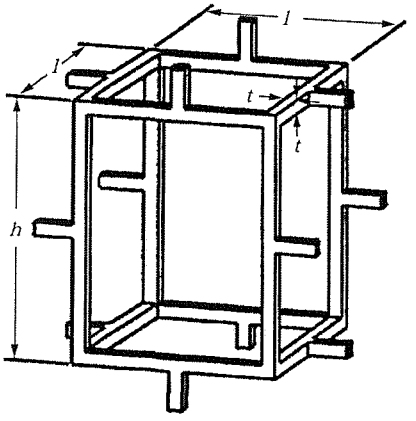

Figure 2-19 A square prism mold for open cell foam (Gibson and Ashby, 1988)

Patten *et al.* (1998) described a theoretical model to simulate the dynamic properties of a

foam cushion including the non-linear damping effects. The following equation to predict the acceleration, $\ddot{x}$, of a mass, M, on a foam seat cushion was taken from the equations provided by Patten, Sha and Mo (1998):

$$\ddot{x}_1 = \frac{-E_f \dfrac{aA}{(cH + d_1|z|)^{p_1}} z - \dfrac{32\mu AH}{3d\zeta}\dot{z} - \dfrac{\rho A}{3K_b\zeta^2}|\dot{z}|\dot{z}}{M} \qquad \text{Equation 2-4}$$

where z and $\dot{z}$ are the relative displacement and velocity respectively between the load and the base of the cushion, E_f is the Young's modulus of the foam, A is the cushion area, H is the cushion height, K_b is a surface factor relating the foam cell size to the available area through which air can flow, ζ is the relative density of the foam, ρ and μ are respectively the density and viscosity of air and the remaining coefficients describe a curve fit to the measured cushion stress-strain relationship as follows:

$$\sigma = E_f \frac{a}{(c + d_1\varepsilon)^{p_1}}\varepsilon \qquad \text{Equation 2-5}$$

where σ is the stress, ε is the strain and the other coefficients are as above.

The disadvantage of this method is that knowledge of the physical properties of the foam cell structure are required and these values are not easy to obtain without specialist equipment. Other researchers have investigated methods of modeling seat cushions from measurements of the dynamics of the complete cushion without requiring knowledge of the cell structure of the foam as described in the following paragraphs.

Hilyard *et al.* (1983) simulated the response of a foam cushion seat and driver system in an earthmoving machine using linear parameters for the seat cushion. The force-deflection characteristic was measured at velocities from 83μms^{-1} to 3.3 mms^{-1} with the loading force cycling between 294N and 981N. The stiffness was derived from the gradient

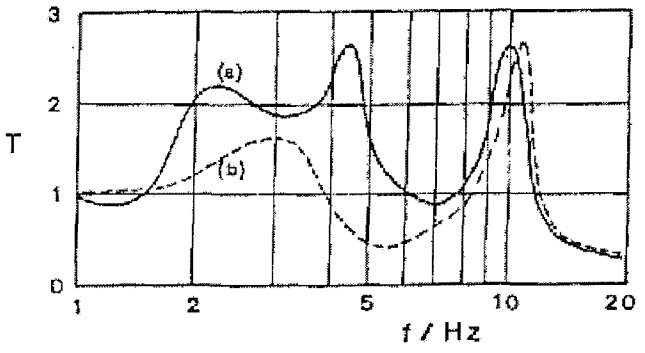

Figure 2-21 Measured (curve a) and predicted (curve b) seat transmissibilities for a foam cushion seat in a JCB 3CX earthmoving machine (Hilyard *et al.*, 1983).

of the force deflection characteristic and the damping coefficient was equated to the ratio of energy dissipated to energy stored during each cycle. The predicted seat transmissibility from Hilyard *et al.* (1983) using the two degree-of-freedom model for the human body from Payne and Band (1971) as compared to a human subject are shown in Figure 2-21.

A more recent study by Kinkelaar and Cavender (1998) provided some background to the technologies used to manufacture automotive foams and correlated the dynamic performance of the seat cushion when loaded with a rigid mass with other methods of assessing foam characteristics such as the ball rebound test. Correlations were found but were dependant on the type of foam technology used.

Fairley and Griffin (1986) developed a method for predicting seat transmissibility from separate measurements of the seat impedance and the impedance of the human subject. This method was investigated further by Wei and Griffin (1998). The cushion was exposed to a 100 second random motion with a constant acceleration power spectral density between 1 and 30 Hz with preloads of between 300N and 800N. The stiffness and damping coefficients were determined by curve fitting to the real and imaginary parts of the measured dynamic stiffness of the cushion. The coefficients of a two

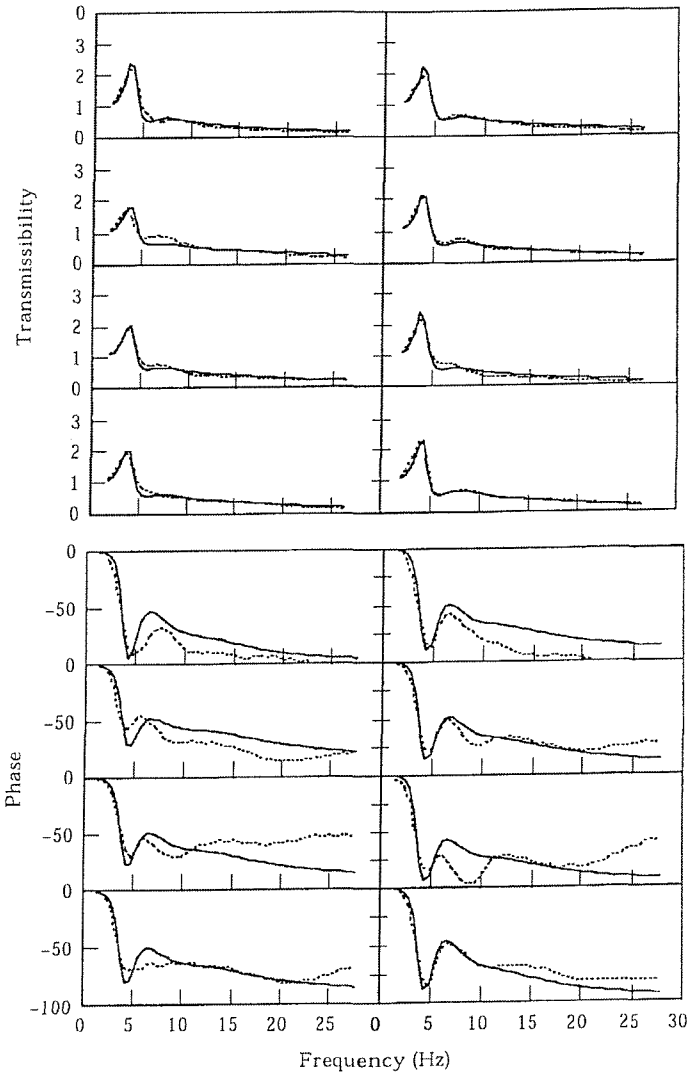

Figure 2-22 Measured (solid line) and predicted (dotted line) seat transmissibility and phase for eight male subjects (Wei and Griffin, 1998)

degree-of-freedom system representing the human body were fitted to the measured apparent mass of the human subjects. The combined cushion and body models were used to predict the response of the body on the seat. The results obtained can be seen in Figure 2-22.

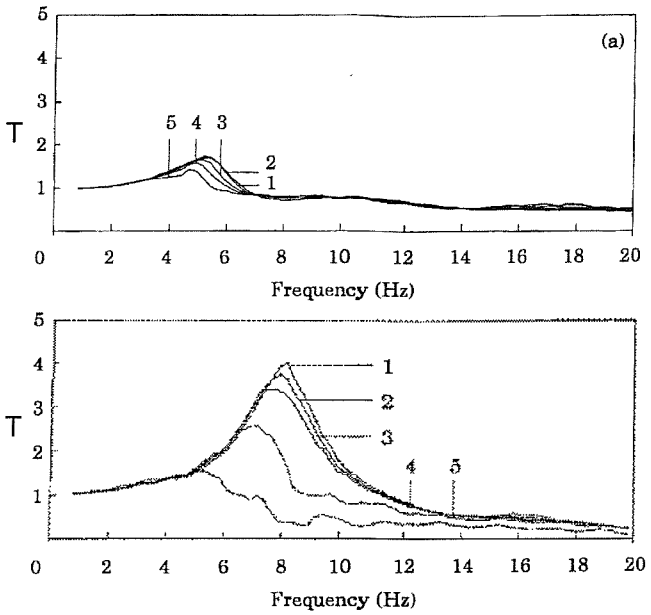

Figure 2-23 The transmissibility of a cushion on a suspension seat loaded with a human subject (upper graph) and a rigid mass (lower graph) for five increasing magnitudes of vibration numbered 1 to 5 (Wu and Griffin, 1996).

The results obtained by Wei and Griffin (1998) demonstrated that predictions of the seat transmissibility could be obtained using a linear cushion model with coefficients obtained from dynamic measurements using a preload similar to that of the intended seat loading.

The frequency and peak transmissibility of a seat cushion have been observed to be greater when the cushion is loaded with a rigid mass compared with a human subject as illustrated in Figure 2-23 taken from Wu and Griffin (1996). Vibration tests at frequencies greater than 4 Hz gave different cushion transfer functions with this cushion when a simple mass was used as the seat load in place of the impedance of the human body. Some variation in this frequency might be expected for other cushions with different physical properties.

The suspension seat model described by Rakheja *et al.* (1994) used a linear seat cushion. The stiffness value was taken as the gradient to the force-deflection characteristic obtained using the Society of Automotive Engineers (SAE) recommended method (SAE, 1980) on the assumption that the stiffness would be relatively constant for small displacement amplitudes. The SAE method involves the compression and release of the cushion using a circular indenter at a rate equivalent to 3.7Ns^{-1} with a peak loading force of 1334N. The damping coefficient was estimated from the energy dissipated per cycle of vibration using sinusoidal excitation at frequencies from 1 to 8 Hz.

All of the above models assumed that the relative motions across the cushion are small. This assumption is likely to be reasonable for automotive seats and for suspension seat motions up to the occurrence of end-stop impacts. No previous study has demonstrated a cushion model for use in suspension seat end-stop impact situations.

Payne (1969) noted that thinner cushions were better for reducing the shocks experienced on aircraft ejector seats. Thick cushions were found to compress during the start of the ejection process and then rapidly stiffen so imparting a rapid increase of force to the pilot. A thinner cushion coupled the pilot more closely to the seat structure and so led to a more gradual acceleration. This finding may not be directly applicable to suspension seating as an ejector seat exerts a relatively prolonged upwards force on the pilot, while the motion of an off-road vehicle is oscillatory resulting in less sustained peak accelerations due to the seat suspension end-stop impacts.

Huston *et al.* (1998) investigated the use of air-filled cushions to reduce the vibration transmitted to the operators of industrial trucks. The investigation found that the air cushions were found to reduce the vibration for some subjects at some frequencies and suggested that a more 'tuned' air cushion (different air sac size, duct size between air sacs, sac shape, etc.) could be an inexpensive method of reducing the vibration transmitted to the driver.

2.5.12 Backrest and armrests

The backrest and armrests have not yet featured on models of suspension seating. Both have the potential to alter the dynamic response of the driver by transmitting vibration around the cushion.

2.6 The dynamics of the driver

2.6.1 The apparent mass of the seated human body

A study of the apparent masses of sixty men, women and children was conducted by Fairley and Griffin (1989). The apparent masses of all the subjects were remarkably similar when normalised with respect to sitting weight (Figure 2-24 and Figure 2-25). However, there was statistically significant correlation between apparent mass and some body characteristics (such as weight and age). The study also noted that relative movement between the feet and the seat was found to affect the apparent mass at frequencies below resonance, particularly near zero-frequency (Figure 2-26).

The resonance frequency generally increased with the use of a backrest, an erect posture and, in particular, increased muscle tension; but there was considerable inter-subject variability in the changes (Figure 2-27). The magnitude of the vibration was observed to have a consistent effect: the resonance frequency decreased from about 6 to 4 Hz when the magnitude of the vibration was increased from 0.25 to 2.0 ms^{-2} r.m.s (Figure 2-28). This change in the human apparent mass with vibration amplitude was investigated by Mansfield (1997), who suggested amplitude-dependent parameters for single degree-of-freedom human body model in order to reproduce this form of behaviour.

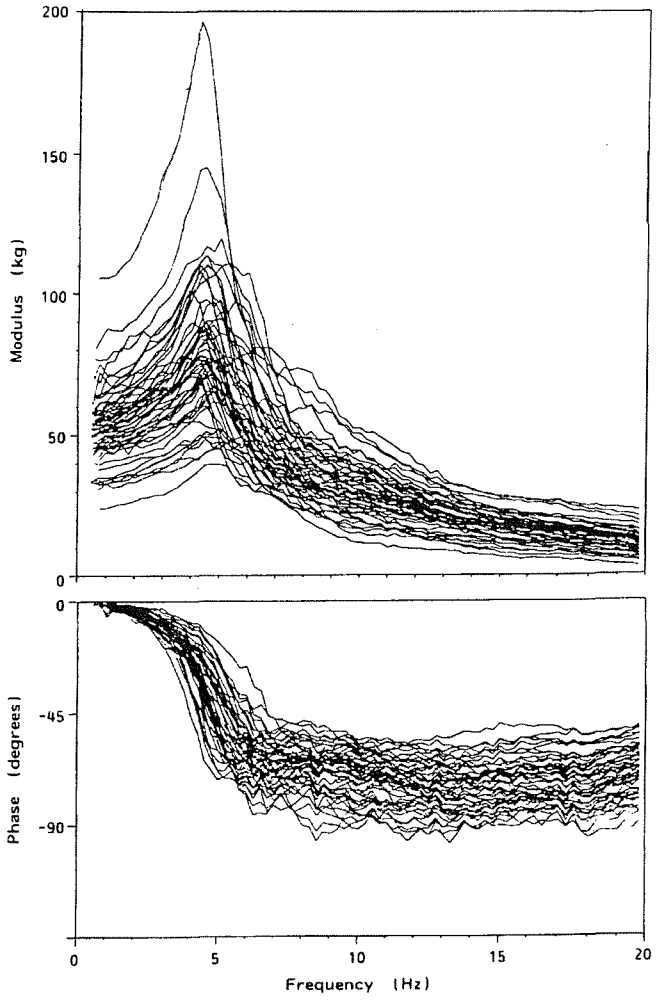

Figure 2-24 Absolute apparent masses of 60 people (Fairley and Griffin, 1989)

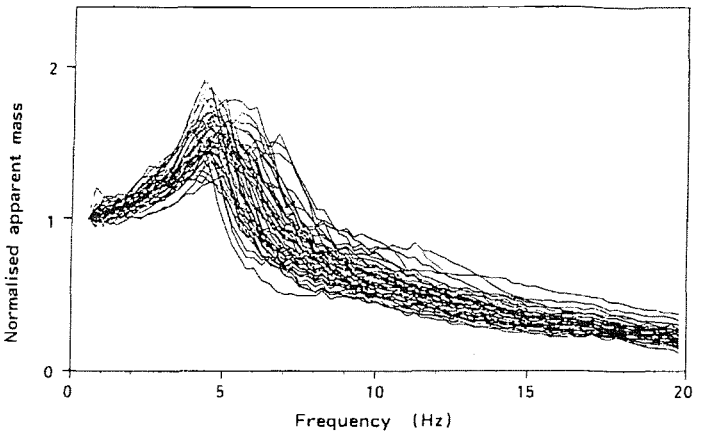

Figure 2-25 Normalised apparent masses of 60 people (Fairley and Griffin, 1989)

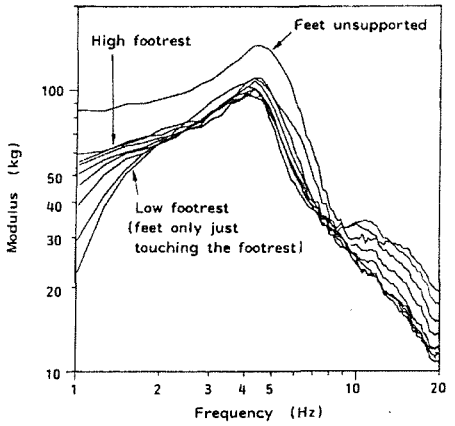

Figure 2-26 Effect of footrest height on apparent mass of one person (Fairley and Griffin, 1989)

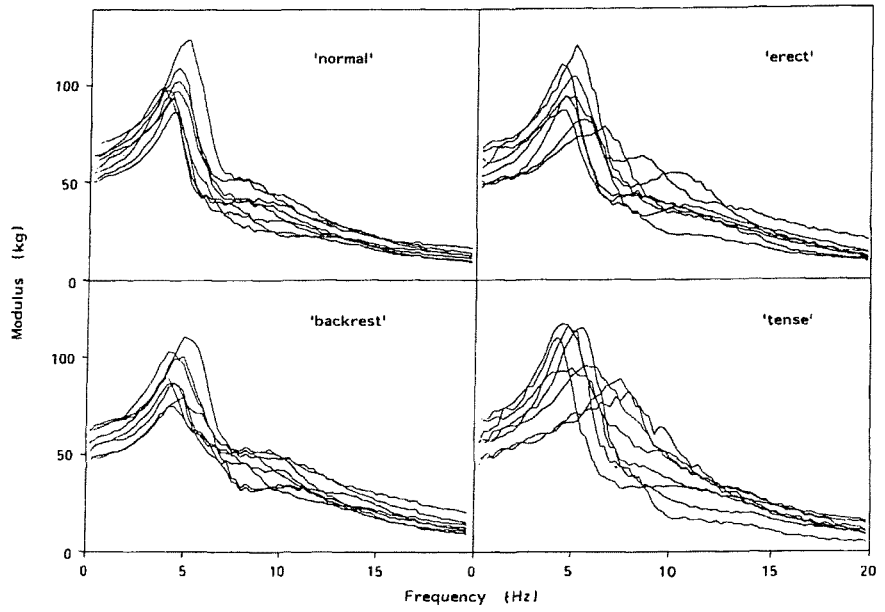

Figure 2-27, Effect of posture and backrest on the apparent mass of eight subjects (Fairley and Griffin, 1989)

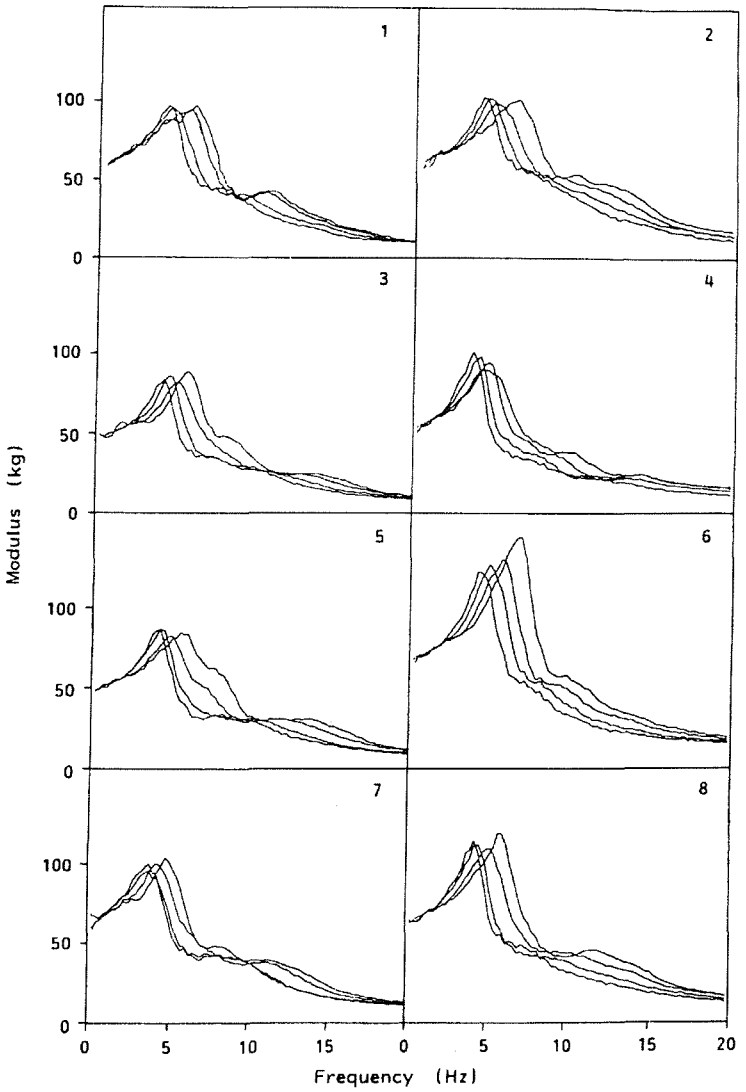

Figure 2-28 Effect of vibration magnitude (0.25, 0.5, 1.0 and 2.0 ms^{-2} r.m.s. acceleration) on the apparent mass of eight people. The resonance frequency consistently decreased with increasing magnitude (Fairley and Griffin, 1989)

Boileau *et al.* (1998) reviewed some of the reported sets of measurements of the impedance and apparent mass of the seated human body obtained in similar test situations. The studies considered are shown in Table 2-2 and the apparent masses obtained are shown in Figure 2-29.

Table 2-2 Studies reporting measurements of the apparent mass of the seated human body in response to vertical vibration (Boileau *et al.*, 1998)

Characterization of the data sets considered for mechanical impedance and apparent mass

	Subjects		Excitation			
Reference	Number	Mass (kg)	Type	Level ($m\,s^{-2}$ r.m.s.)	Freq. range (Hz)	Reported function
Fairley and Griffin (1983)	1	63	Random Gaussian	1·0	0·25–20	Apparent mass magnitude and phase
Hinz and Seidel (1983)	4	56–83	Sinusoidal	1·5	2–12	Mean apparent mass magnitude and phase
Hinz and Seidel (1983)	4	56–83	Sinusoidal	3·0	2–12	Mean apparent mass magnitude and phase
Holmlund *et al.* (1995)	30	54–93 mean 70	Sinusoidal	0·5	2–100	Mean normalized mechanical impedance magnitude and phase
Suggs *et al.* (1969)	11	58–90	Sinusoidal	2·54‡	1·75–10	Mean mechanical impedance magnitude and phase
Donati & Bonthoux (1983)	15	49–74	Sine sweep	1·6	1–10	Mean mechanical impedance magnitude and phase
Donati & Bonthoux (1983)	15	49–74	Broad band random	1·6	1–10	Mean mechanical impedance magnitude and phase
Sandover (1982)	6	52·7–87·2	Random	1·0	1–25	Individual apparent mass magnitude and phase
Fairley and Griffin (1986)	8	57–85	Random	1·0	0·5–20	Individual apparent mass magnitude and phase
Seidel (1996)	11	60–70	Random (off-road machinery)	<1·4	0·5–20	Mean mechanical impedance magnitude
Seidel (1996)	14	70–80	Random (off-road machinery)	<1·4	0·5–20	Mean mechanical impedance magnitude
ISO CD 5982 (1993)	39	51–93·8	Sinusoidal	1·0–2·0†	0·5–31·5	Mean mechanical impedance magnitude and phase
Boileau *et al.* (1997)	6	69·6–80·9 mean 75·4	Sinusoidal sweep	1·0–2·0	0·5–10	Mean mechanical impedance magnitude and phase
Boileau *et al.* (1997)	6	69·6–80·9 mean 75·4	Random White noise	1·0–2·0	0·5–10	Mean mechanical impedance magnitude and phase

† $m\,s^{-2}$; ‡ mm peak-to-peak.

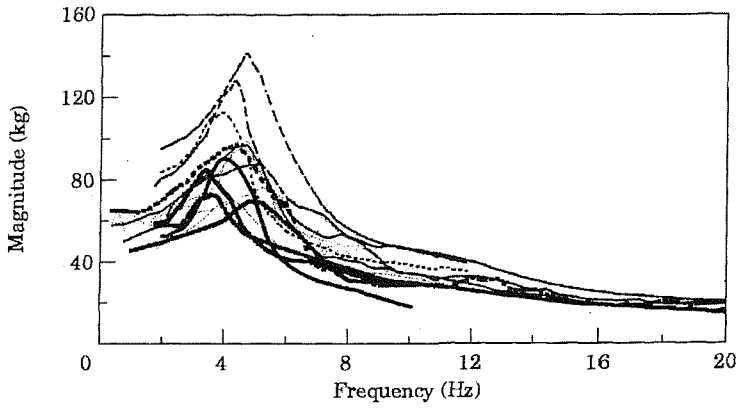

Figure 2-29 The apparent mass of the seated human body subjected to vertical vibration (Boileau *et al.*, 1998). The studies are summarised in Table 2-2.

Sandover and Dupuis (1987) suggested that the main 5 Hz resonance was due to a flexing of the spine rather than a vertical compression. This was supported by Hinz *et al.* (1988) who found that a 4.5 Hz flexation of the spine led to an up and down motion of the body. Kitazaki and Griffin (1997, 1998) investigated the resonance modes of the seated human body. Eight modes of vibration were observed below 10 Hz. A 5 Hz vertical whole-body mode was identified as due to axial and shear motions of the

buttock tissue in combination with bending of the upper spine. A second mode close to this first mode was identified as due to bending of the lower spine and a pitching of the head. The second principal mode at around 8 Hz corresponded to a pitching motion of the pelvis. A more slouched posture was found to decrease the natural frequency of the body. It was suggested that the risk of injury may be primarily due to the bending of the spine and that simple body models that do not reproduce the complex body motions will not be able to adequately predict the forces that lead to injuries. Matsumoto and Griffin (1998) conducted an experimental study to investigate the transmission of vibration through the seated human body using accelerometers attached to the surface of the body adjacent to spinal vertebrae. This study also observed that bending of the spine was more dominant than axial motion at resonances close to 5 Hz. The 5 Hz resonance observed in the human body apparent mass was hypothesised to consist of a bending mode of the spine, a rocking mode of the thoracic spine, a mode involving axial and shear deformation of the tissue beneath the pelvis and a pitch mode of the pelvis.

2.6.2 Legs and footrest motion

Fairley (1988) investigated the effect of the legs on the apparent mass of the body and found that including the effect of legs improved the predictions of the response of a suspension seat-driver system when using a linear approach for moderate vibration levels. The stiffness due to the legs arose from contact between the thighs and the seat, while the damping appeared to be due to musculo-skeletal structure.

2.6.3 Theoretical lumped parameter models of the body

The first seated human body lumped parameter models were single degree-of-freedom systems as described by Latham (1957), Payne (1965) and Coerman and Wittwer (1960), who suggested a mechanical analogue to the human body shown in Figure 2-30. In this report and a later paper (Coerman, 1962), a single degree-of-freedom system was shown to give a reasonable approximation to the response of the body. In the second paper, differences in the response of the body were

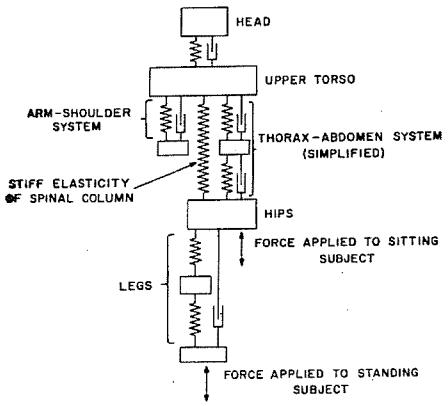

Figure 2-30 Model of the human body (Coerman and Wittwer, 1960)

noted with different postures and attempts were made to measure the relative displacements of parts of the body.

More degrees of freedom were suggested by successive studies including a four degree-of-freedom arrangement proposed by Payne and Band (1971). More recent models include a five degree-of freedom system from Smith (2000) and a four degree-of-freedom system proposed by Boileau and Rakheja (1999).

Many human body models have been developed for other applications, including the two dimensional model of an automotive seat and the pelvis and spine up to L3 developed by Sinha *et al.* (1996) for use in impact response situations and the seated human body model developed by van Deursen *et al.* (2000) to simulate the response to rotational motion, using the ADAMS android rigid body package. However, the research in this thesis was restricted to vertical seated motion in normal vehicle operating situations.

2.6.4 Anthropodynamic dummies

Anthropodynamic dummies are physical analogues of the dynamic characteristics of the human body. The use of dummies can reduce the need for exposing people to vibration for testing purposes, eliminate variation due to changes in posture and avoid the practical problems of having suitable test subjects on hand when required. The following list summarises some of the anthropodynamic dummies developed up to the present time.

- Suggs *et al.* (1969) developed a two degree-of-freedom dummy to simulate human seated response. The performance of the dummy was observed to be closer to that of seated human subjects at low frequencies as compared with higher frequencies.
- Tomlinson and Kyle (1970) developed a mechanical dummy to mimic the response of the human body, as they considered an inert mass to be a dynamically unsuitable load when testing seating. One and two degree-of-freedom models were constructed and the performance agreed well with human subjects. It was reported that high suspension seat friction resulted in poorer predictions.
- Mansfield and Griffin (1996) reported the performance of a single degree-of-freedom dummy in measuring the transmissibility of car seats in the region of resonance.

- Lewis and Griffin (2000) reported the performance of an active dummy with the potential for simulating body non-linearities and different human body impedances. This active dummy involved an electro-dynamic actuator in place of a damper.

2.6.5 Inert seat loads

Alternatives to human subjects have been used for laboratory seat testing. Wu and Griffin (1998), Fairley (1990) and Rakheja *et al.* (1994) were specifically interested in the performance of the seat and so used a simple mass load to remove the variability associated with a human subject load. The magnitude of the phase shift of the apparent mass is only approximately 15° at 3 Hz, so an inert mass would appear reasonable for vibration tests at this frequency and below. However, the non-linearities inherent in suspension seats might introduce some higher frequency components.

The variation in suspension seat performance with magnitude was investigated by Wu and Griffin (1996) using sinusoidal input motions. Measurements were made with sand ballast and with one human subject on one seat. The study suggested that a 56 kg sand bag tended to produce SEAT values greater than those with a 75 kg subject. The study also suggested that a composite mass (such as a sand bag) would be more suitable than a rigid load for severe top stop impacts as this would be less likely to leave the seat than a rigid load.

2.7 Theoretical suspension seat models

2.7.1 Introduction

Investigating the response of seating generally involves exposing a person to vibration in order to test the seat realistically. The use of models can reduce the need to expose subjects to vibration for testing purposes and allow the effect of different aspects of the seat construction on the overall seat performance to be investigated in response to different vibrations. A further benefit of theoretical modelling is that the development of a model can provide insights into the behaviour of the real system.

Theoretical models of suspension seats and seated humans have been developed by a number of researchers and are reviewed chronologically in the following sections.

2.7.2 Rakheja and Sankar (1983)

The authors of this study described a seat suspension model including vertical lateral, fore-and-aft and roll vibration isolators. The full equations describing the model were given and schematics of the suspension models were shown as reproduced in Figure 2-31 to Figure 2-33.

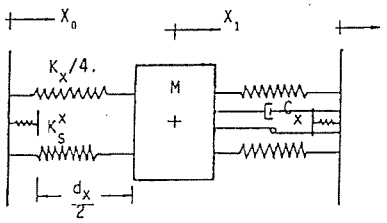

Figure 2-31 Fore-and-aft suspension model (Rakheja and Sankar, 1983)

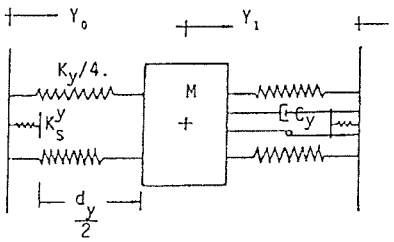

Figure 2-33 Lateral suspension model (Rakheja and Sankar, 1983)

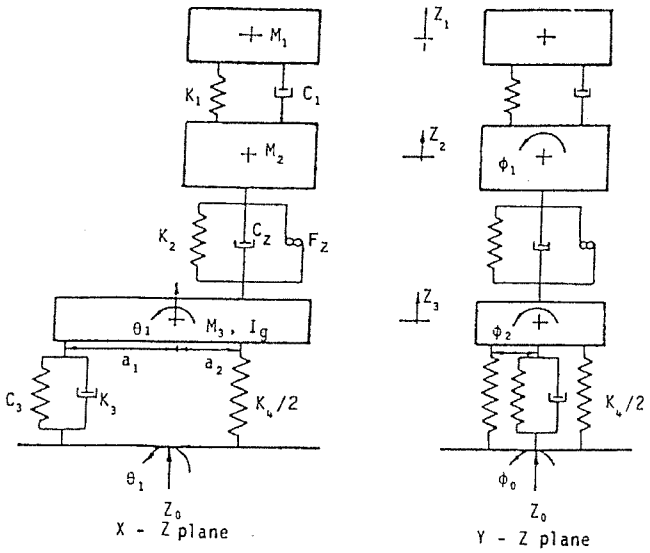

Figure 2-32 Vertical, roll and pitch suspension model (Rakheja and Sankar, 1983)

The suspension damping was included as a velocity squared characteristic. The suspension stiffness was assumed to be linear. Travel limiting stops were included as linear stiffnesses. Friction was included as a constant force opposing the motion for relative suspension velocities greater than a coefficient Δv. For lower suspension velocities the friction force was considered viscous with a force inversely proportional to Δv such that as the velocity approaches zero the force approaches infinity.

The model was linearised to allow analysis to be performed in the frequency domain using an energy dissipation approach. This approach evaluates the relative motion across each component as a function of frequency and determines an equivalent linear coefficient for the non-linear suspension components such as the frictional damping. The linearised results as compared with numerical integration results are shown in Figure 2-34.

The linearised model was used to optimise the seat dynamic performance in response to measured agricultural tractor motions using a Hooke and Jeeves pattern search routine as reported by Himmelblau (1972). The optimal seat vibration was compared with the ISO 2631 (1974) 4-hour exposure time fatigue-decreased proficiency limit. It was found that the bounce, longitudinal, pitch and roll vibrations could be attenuated by the optimal seat, but that lateral vibration isolation would require a very low natural frequency isolator to attenuate the 1.2 Hz vibration found in this axis. The proposed roll isolator was found to assist in the attenuation of vibration in the roll, pitch and bounce modes. The model coefficients used in the vertical (bounce) suspension were based on the measured performance of an existing seat.

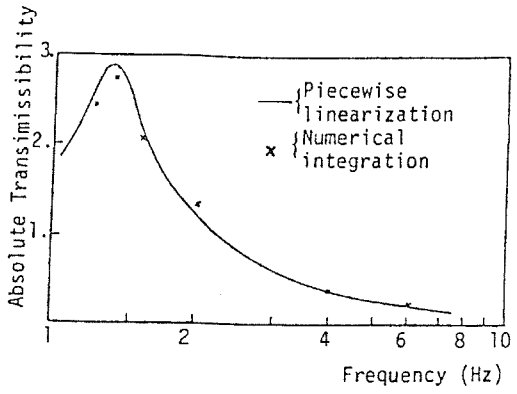

Figure 2-34 Comparison of the numerical integration and linearised model response for vertical vibration (Rakheja and Sankar, 1983)

It was not clear from the paper which coefficients had been used for this optimal seat although the range of permissible values for some coefficients was given. The value of Δv in particular was not clear.

This study was intended as a feasibility study to determine if such a multi-axial suspension seat would be beneficial. It was therefore not possible to compare the model performance with laboratory or field results due to the lack of a suitable test seat. A parametric investigation was mentioned but no results were reported.

2.7.3 Rakheja and Sankar (1984)

This study used a seat model identical to that reported in Rakheja and Sankar (1983) and coupled this with a cab suspension consisting of four corner mounts and fore-and-aft and lateral isolators consisting of linear stiffness and damping elements (Figure 2-40). The coefficients of the model were determined by the Hooke and Jeeves algorithm as in the previous study.

Various combinations of seat and cab suspension were investigated in response to measurements of an agricultural tractor on the 100m test track described by Matthews (1973) and were evaluated in the frequency domain in comparison with the ISO 4-hour fatigue deficiency (ISO 2631:1985) It was concluded that a cab suspension could provide useful vibration isolation in all five modes (vertical, lateral, fore-and-aft, roll, pitch). Improved vertical isolation could be achieved by adding a vertical seat suspension but the addition of lateral and roll seat isolators was found to worsen the vibration in these axes due to interaction between the seat and cab suspensions. The parameter values of the optimal suspensions were reported and constrained to within what were considered to be practically achievable ranges.

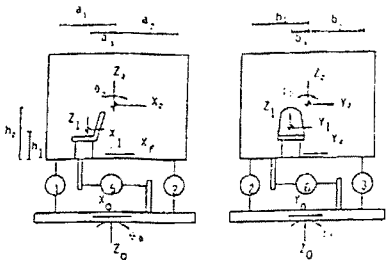

Figure 2-35 Longitudinal and lateral cab suspension model schematics (Rakheja and Sankar, 1984)

A parametric investigation was reported although no values were given. It was stated that stiffer cab mounts led to poorer bounce but better lateral vibration isolation and that the longitudinal isolator had little effect on lateral, vertical or roll response.

2.7.4 Rakheja *et al.* (1987)

This report initially described an eleven degree-of-freedom linear model of a tractor-semi trailer system using a linear vertical suspension seat (Figure 2-36). The paper then went on to consider the suspension seat model in more detail. The geometric differences between parallelogram and x-linkage suspensions were included along with the non-near effects of end-stop buffers (linear stiffness), coulomb friction, velocity squared damping and the damper geometry. No equations were given for the model, but a schematic of the model structure was shown (Figure 2-37).

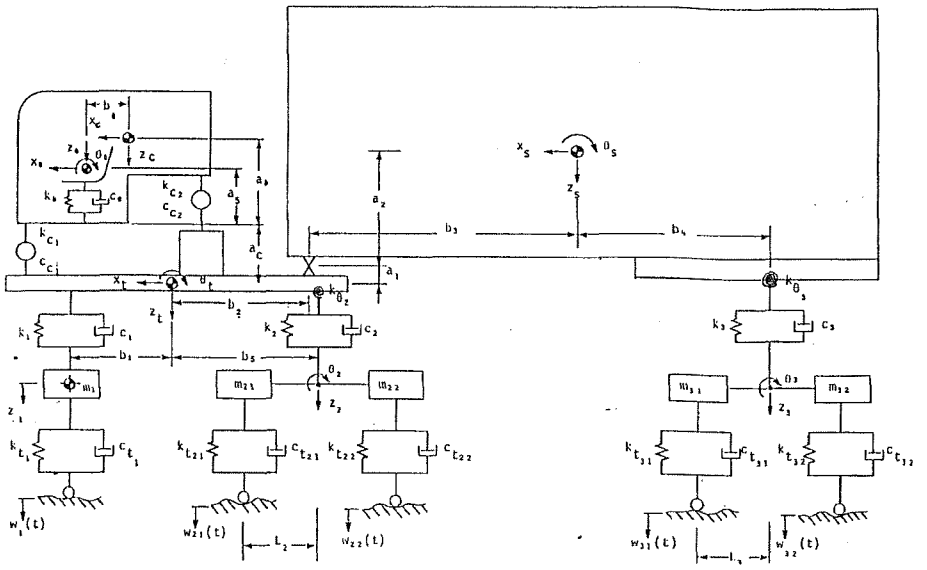

Figure 2-36 The linear seat/tractor/semitrailer model (Rakheja *et al.*, 1987)

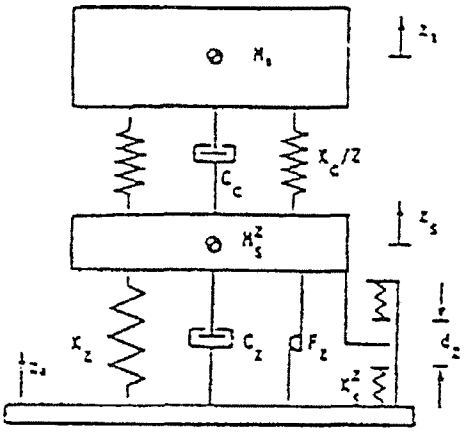

Figure 2-37 The non-linear seat model schematic (Rakheja *et al.*, 1987)

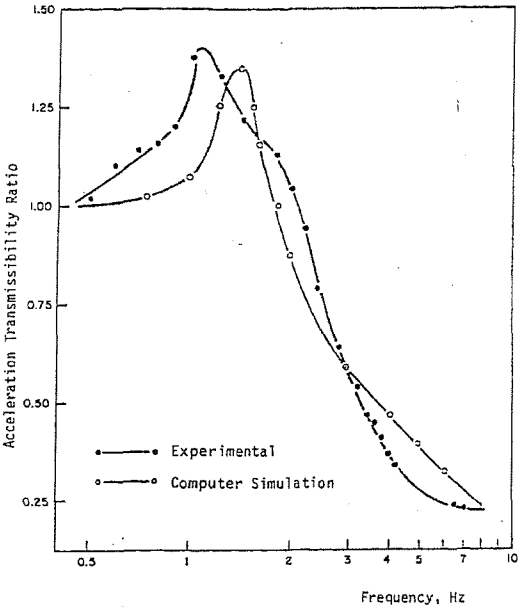

Figure 2-38 Comparison of the experimental and theoretical seat transmissibilities for one seat (Rakheja *et al.*, 1987)

This is the first paper to compare the performance of the seat model with laboratory measurements of the modelled seat. The model was subjected to a constant displacement swept sine up to 8 Hz (assumed to be from 0.5 to 8 Hz from the results presented) at 'peak' displacements of 6.35 mm and 12.7 mm (assumed to be the

amplitude not the peak to peak displacement). The test seats were loaded with a 'manikin', which appeared from the photograph of the apparatus to be of the type used for automobile crash testing. Results were shown for one of the three seats tested, reproduced in Figure 2-38.

A parametric sensitivity analysis was conducted and the performance of three seats, one with an x-linkage and two with a parallelogram linkage was discussed and two results were presented. The effect of friction on the performance of one of the parallelogram seats (Figure 2-39) showed the friction force acting to reduce the resonance peak at the expense of higher frequency performance. The second result showed that the suspension viscous (orifice) damping had a strong effect on the seat transmissibility (Figure 2-40 for the other parallelogram seat). It was also noted that the mean ride position on one of the parallelogram seats affected the pitch response of a lighter driver and the vertical response of a heavier driver.

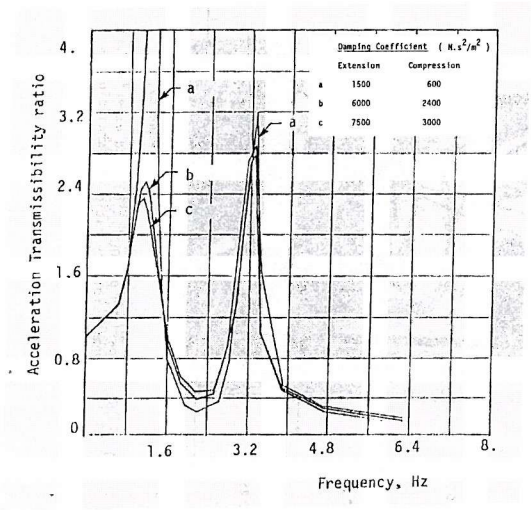

Figure 2-39 The effect of the suspension damping on the acceleration transmissibility of one seat (Rakheja *et al.*, 1987)

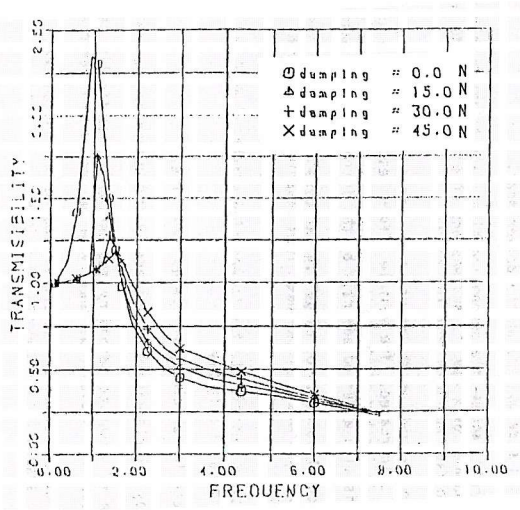

Figure 2-40 The effect of the suspension friction on the displacement transmissibility of one seat (Rakheja *et al.*, 1987)

2.7.5 Fairley (1990)

Fairley (1990) predicted the behaviour of an air-sprung suspension seat using the apparent mass. The apparent mass of the suspension unit was calculated from the transfer function of the seat. This was combined with the apparent mass of the body and legs to predict the behaviour of the complete seat - person system (Figure 2-41). This technique assumes an ideal massless spring-damper combination for the

suspension unit and calculates the linear system equivalent to the real seat for a particular magnitude and frequency. Predictions made from measurements at three magnitudes of vibration gave good agreement with measured data as shown in Figure 2-42. Neglecting the effect of the legs caused the seat transmissibility at resonance to be underestimated, but the cushion was found to have little effect for the particular seat tested.

A sensitivity analysis of the effect of the vibration duration and magnitude, the load on the seat and the height adjustment mechanism on the linearised stiffness and damping of the seat suspension was carried out. These results are shown in Figure 2-43 to Figure 2-46.

This linear, frequency domain method cannot be expected to provide a model of the seat that will be effective for any input motion, but it has the advantage that it does not require detailed measurements of all aspects of the seat behaviour. The apparent mass of the seat could be measured using an input signal of interest and combined with the apparent mass of a typical person to give an estimate of the seat performance when exposed to that motion.

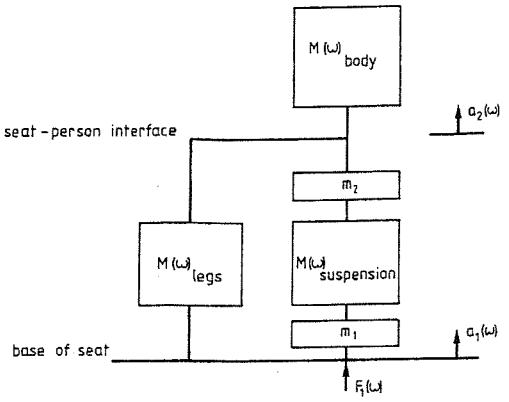

Figure 2-41 The apparent mass model of the seat-person system (Fairley, 1990)

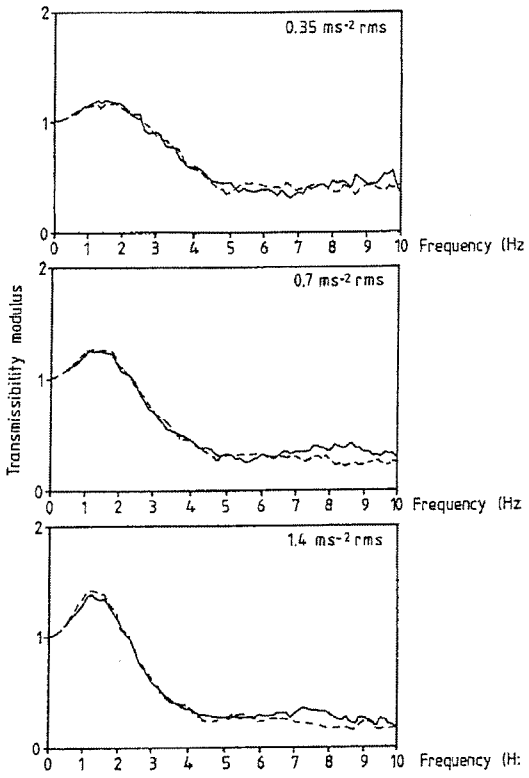

Figure 2-42 The measured (solid line) and predicted (dotted line) transmissibilities of the seat loaded with a person for three vibration magnitudes (Fairley, 1990)

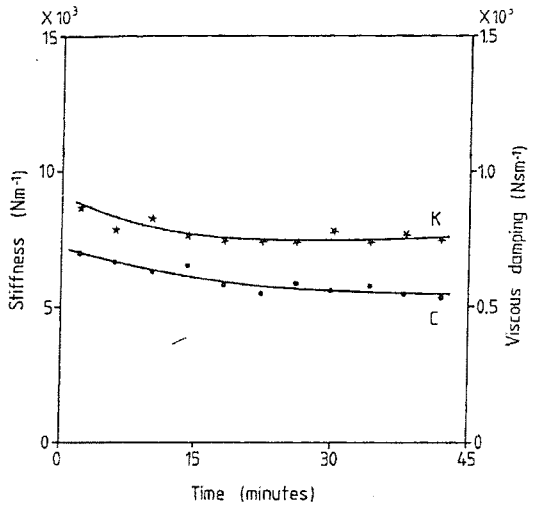

Figure 2-43 The effect of vibration duration on the linearised seat stiffness and damping (Fairley 1990)

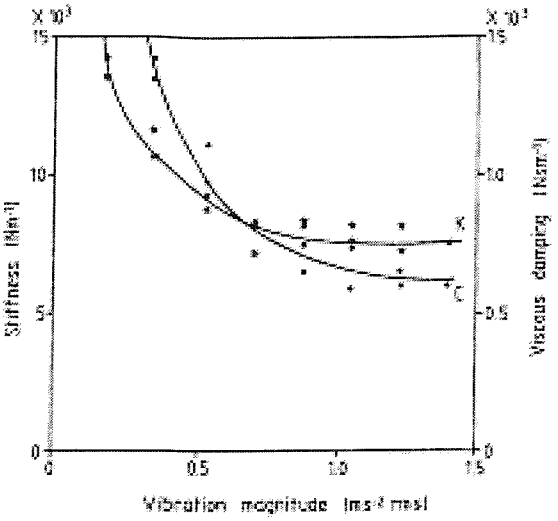

Figure 2-44 The effect of vibration magnitude on the linearised seat stiffness and damping (Fairley 1990)

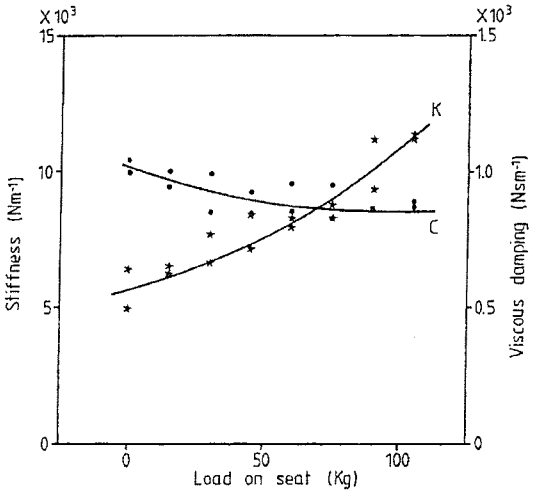

Figure 2-45 The effect of the seat load on the linearised seat stiffness and damping (Fairley, 1990)

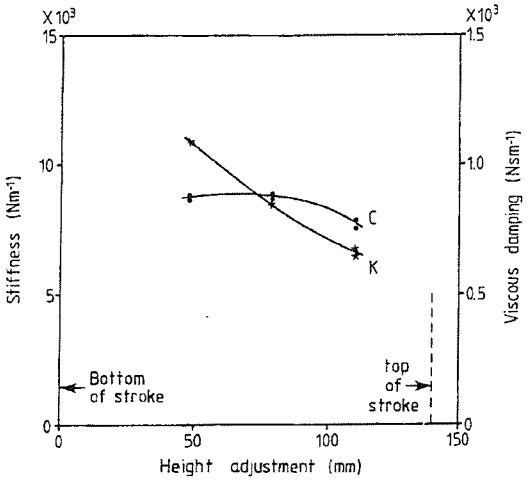

Figure 2-46 The effect of the suspension height adjustment on the linearised seat stiffness and damping (Fairley, 1990)

2.7.6 Gouw *et al.* (1990)

The vertical suspension seat described by this paper (Figure 2-47) showed a difference in mathematical content as compared to the original model described by Rakheja and Sankar (1983) in that the friction was modelled as a simple constant force opposing the motion without the additional viscous element for low velocities.

The model was also simplified by restricting the motion to the vertical axis only, excluding the horizontal and rotational suspension elements.

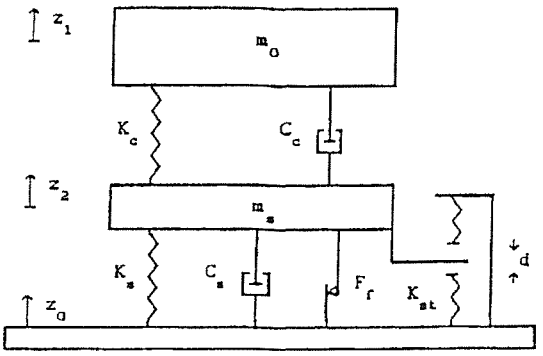

Figure 2-47 Schematic of the seat-load model used by Gouw *et al.* (1990)

The methods used to determine the coefficients were described. The cushion was modelled as a linear spring and damper system with the stiffness derived from a force-deflection measurements and the damping from the energy loss during sinusoidal motions. The suspension stiffness was modelled as a linear spring with the stiffness taken from the measured force-deflection characteristic of the suspension. The Coulomb friction force was also extracted from the suspension force-deflection measurement. The damper used a velocity squared damping characteristic which was 'determined analytically'.

One comparison between the measured and predicted transmissibilities was shown (Figure 2-48). The excitation of 2.5 cm peak-to-peak would not be expected to result in end-stop impacts on this seat, which had a stroke in excess of 80 mm, but it appeared that the lowest frequencies resulted in friction-locked seat behaviour.

A parametric sensitivity analysis was reported and the effects of changes in the cushion stiffness, suspension damping, suspension coulomb friction and suspension spring rate on the seat performance were shown in the frequency domain (Figure 2-49 to Figure 2-53). The discussion of these figures suggested that a medium-high friction might be desirable as this reduces the resonance peak at the expense of reducing the effective travel of the seat. It was also

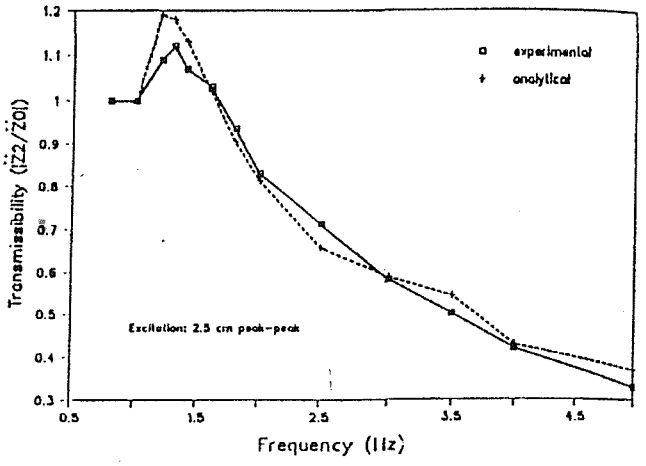

Figure 2-48 The measured (solid line) and predicted (dotted line) transmissibility of a suspension seat (Gouw *et al.*, 1990)

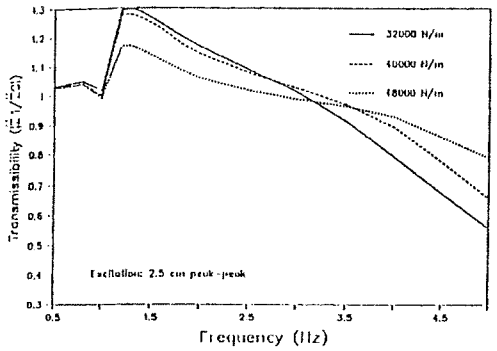

Figure 2-49 The effect of cushion stiffness on the acceleration transmissibility of the seat (Gouw *et al.* 1990)

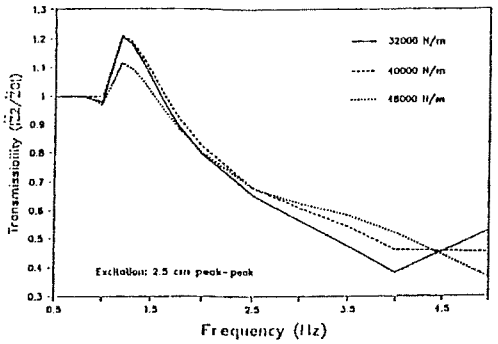

Figure 2-50 The effect of cushion stiffness on the acceleration transmissibility of the suspension (Gouw *et al.* 1990)

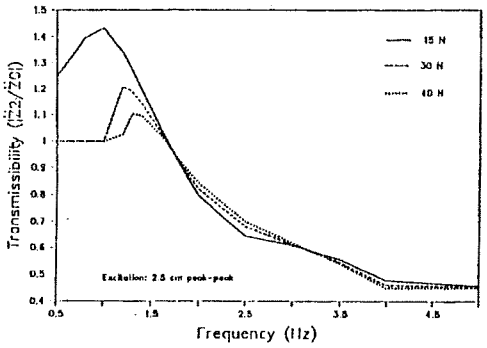

Figure 2-51 The effect of Coulomb friction on the acceleration transmissibility of the seat (Gouw *et al.* 1990)

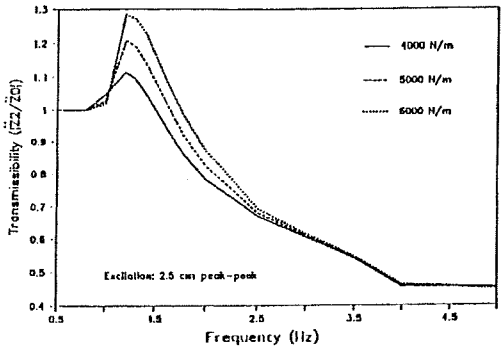

Figure 2-52 The effect of the suspension spring rate on the acceleration transmissibility of the seat (Gouw *et al.* 1990)

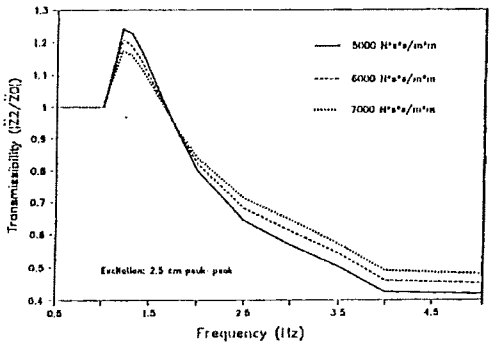

Figure 2-53 The effect of the suspension damping on the acceleration transmissibility of the seat (Gouw *et al.* 1990)

suggested that light damping was desirable to improve the seat performance but that this could lead to occasional end-stop impacts.

A damper with bleed and blow-off control was recommended to improve the seat performance. However, such a damper was described by these authors in later papers as having a greater force-velocity coefficient at low magnitudes and a lower

coefficient at high magnitudes. This would result in a reduction in the damping at high magnitudes where damping would be desirable to prevent end-stop impacts and greater damping at low magnitudes were minimal damping would be beneficial to reduce the transmitted vibration.

2.7.7 Boileu *et al.* (1993)

This paper reported a non-linear vertical seat suspension as shown in Figure 2-54. The model used a rigid seat load and was therefore considered applicable for motions below 2 Hz. The input motion was determined by filtering a half-sine shock through a linear vehicle model including rotational components.

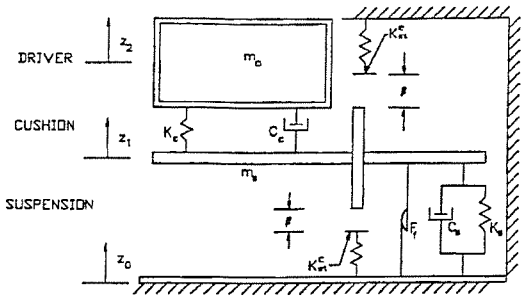

Figure 2-54 The seat-load model used by Boileau *et al.* (1993)

The model included linear coefficients for the suspension spring, end-stop buffers and the cushion. The damper was described by a two-stage force-velocity coefficient and a 15N coulomb friction force was included. The seat coefficients were those measured during the study by Rakheja *et al.* (1994).

Time histories were shown comparing the measured and simulated results including end-stop impact occurrence. The general waveform shape was similar in both cases (Figure 2-55). The r.m.s. and r.m.q. acceleration measured on the seat was compared with that predicted by the model for moderate vibration magnitudes as shown in Figure 2-56 and Figure 2-57, but comparisons between the model and the measured results for more severe conditions including end-stop impacts were not provided.

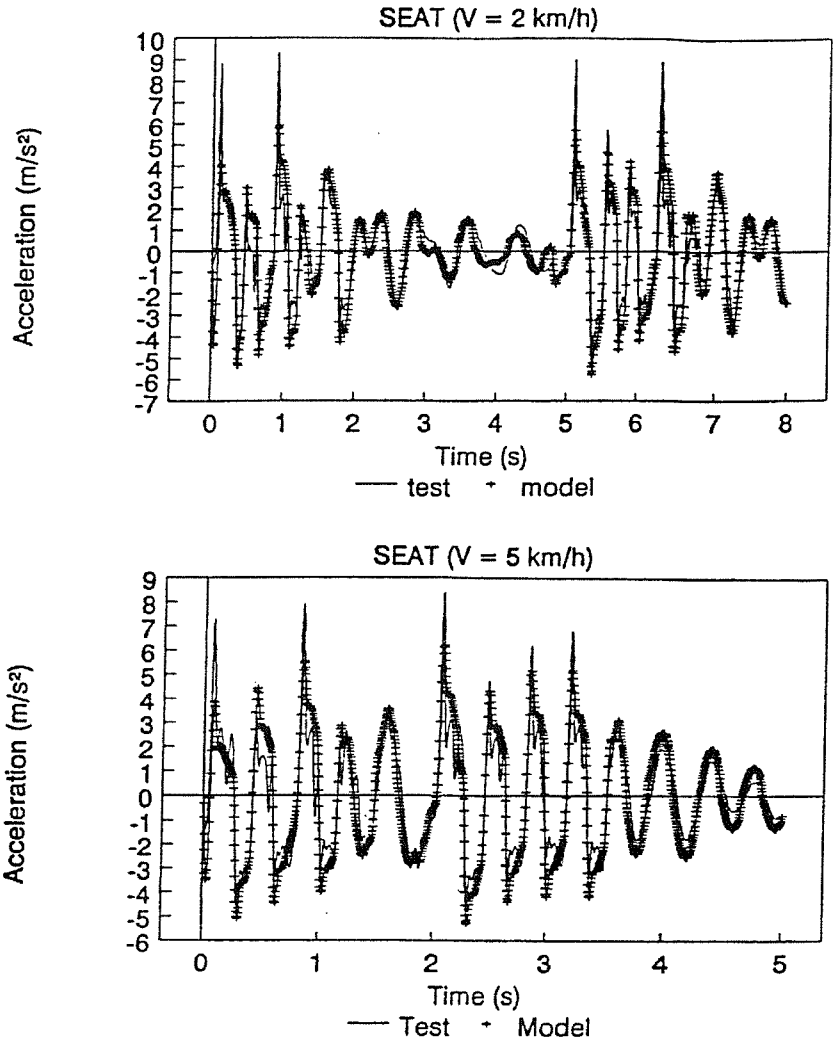

Figure 2-55 The accleration of the mass on the seat measured (solid line) and predicted (+ symbols) for vehicle speeds of 2 and 5kmh^{-1} (Boileau *et al.*, 1993)

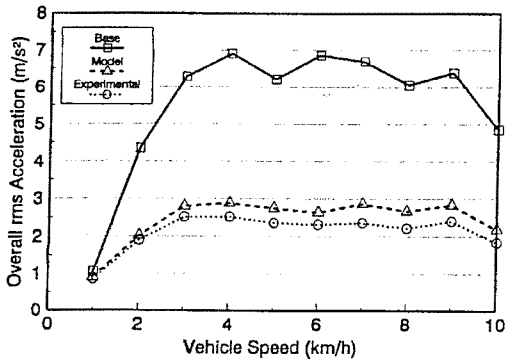

Figure 2-56 The predicted and measured root-mean-square acceleration in response to the base motion shown as the solid line (Boileau *et al.*, 1993)

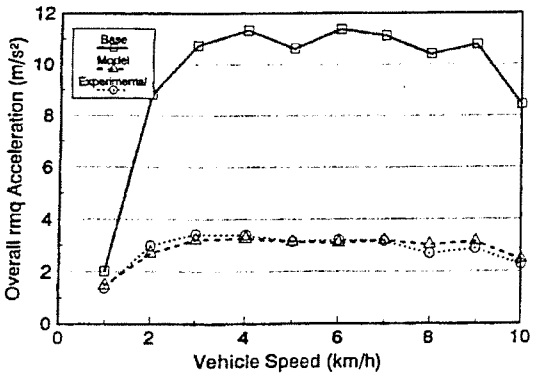

Figure 2-57 The predicted and measured root-mean-quad acceleration in response to the base motion shown as the solid line (Boileau *et al.*, 1993)

A parametric sensitivity analysis was conducted showing the influence of the suspension spring and damper on the seat performance. Two input motions and five parameter values were used, one for a moderate magnitude and one in a condition where end-stop impacts occurred.

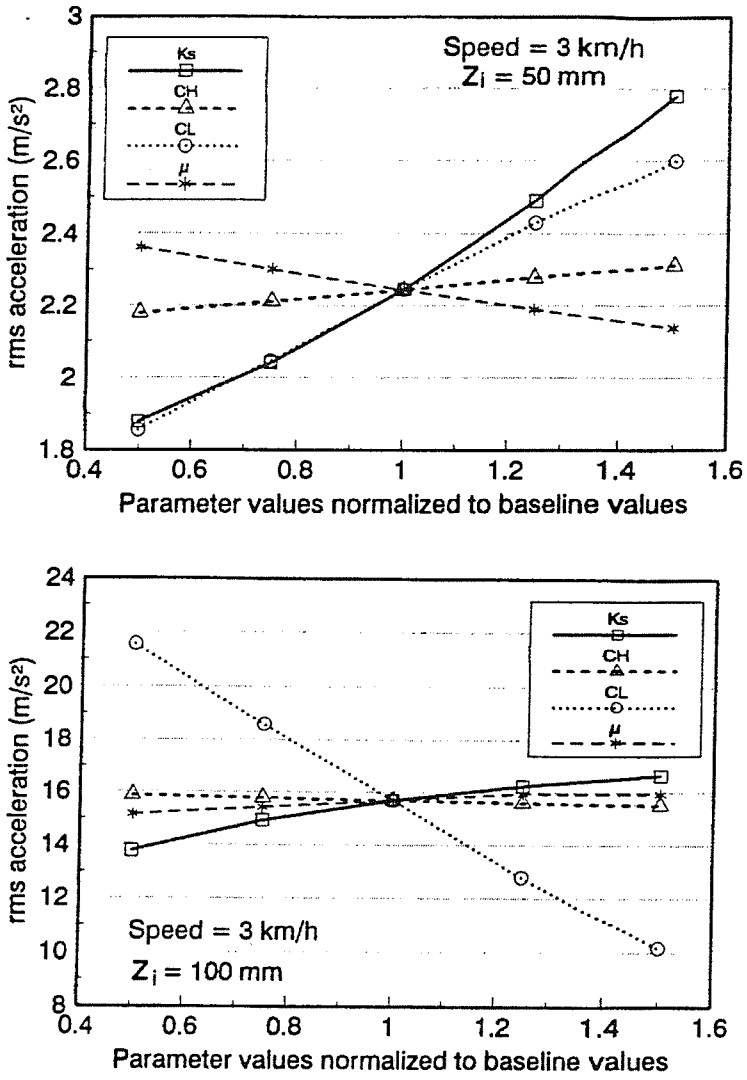

Figure 2-58 The effect of the suspension stiffness (K_s), the suspension damping coefficient at low and high velocities (C_L and C_H) and the ratio of the suspended seat mass to the load mass on the seat response to the simulated vehicle passing over a bump of 50 mm (top graph) and 100 mm (bottom graph), from Boileau *et al.* (1993).

2.7.8 Rakheja *et al.* (1994)

This paper describes a suspension seat model incorporating the bleed and blow-off damping system mentioned in the previous study. The model used one and two degree-of-freedom systems to simulate the dynamics of the human body (Figure 2-59) as well as the rigid mass used in previous studies.

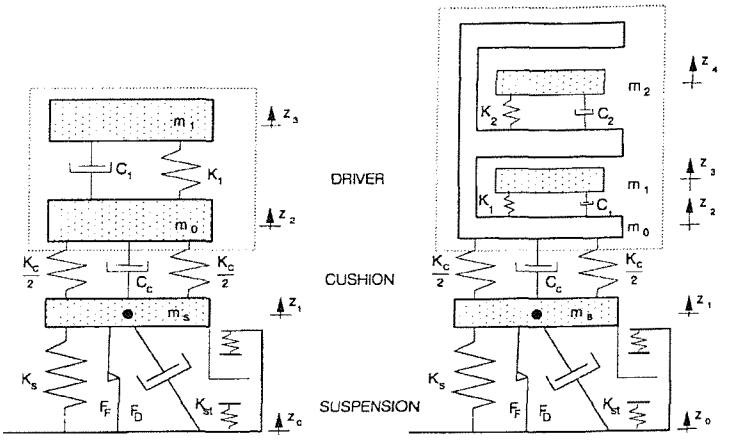

Figure 2-59 Seat-driver models incorporating one and two degree-of-freedom human body models (Rakheja *et al.*, 1994)

Some of the parameter values used in the model were reported and the methods used to determine the coefficient values were described in some detail. The damper characteristics were taken from the data provided by the damper manufacturer. The cushion stiffness was taken as a tangent to the measured force-deflection characteristic at a representative loading. A comparatively low value for the cushion damping was taken as it was assumed that off-road vehicle vibration results in high velocities and that cushion damping at high velocities is comparatively low. The suspension stiffness was taken from the suspension force-deflection characteristic and the friction was estimated from the

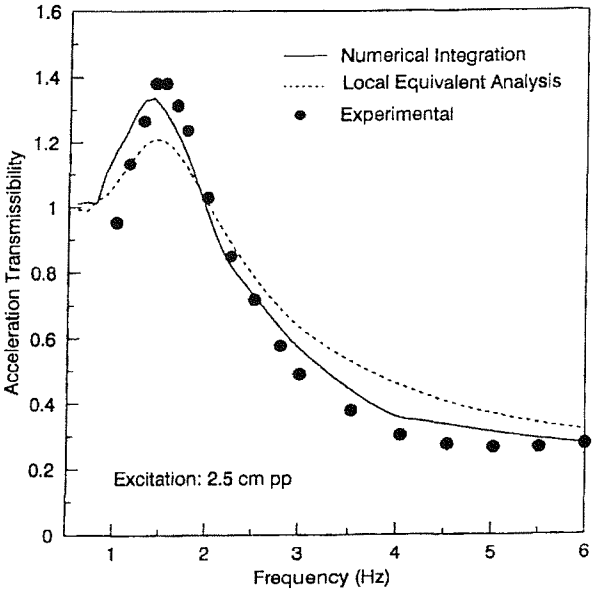

Figure 2-60 The measured and predicted transmissibility of the suspension seat modelled by Rakheja *et al.* (1994)

inertia force corresponding to suspension breakaway during dynamic testing. More details on this potentially useful method of measuring the seat friction were not available as the internal report containing the information could not be located.

The model was linearised to allow analysis to be performed in the frequency domain by the energy similarity technique used in the earlier studies. The performance of the non-linear model, solved by numerical integration and the linearised model were compared with measured seat performance at frequencies from 1 to 6 Hz using a 25 mm peak-to-peak sinusoidal motion (Figure 2-60). The non-linear model would be expected to be more accurate than the linearised model and can be seen to be within approximately 15% of the measured data over most frequencies. Greater differences can be seen at low frequencies where friction was more dominant. The seat showed a peak transmissibility at resonance of 1.4 and the suspension stroke was 75 mm, so it may be assumed that the seat did not strike the buffers during this comparison test.

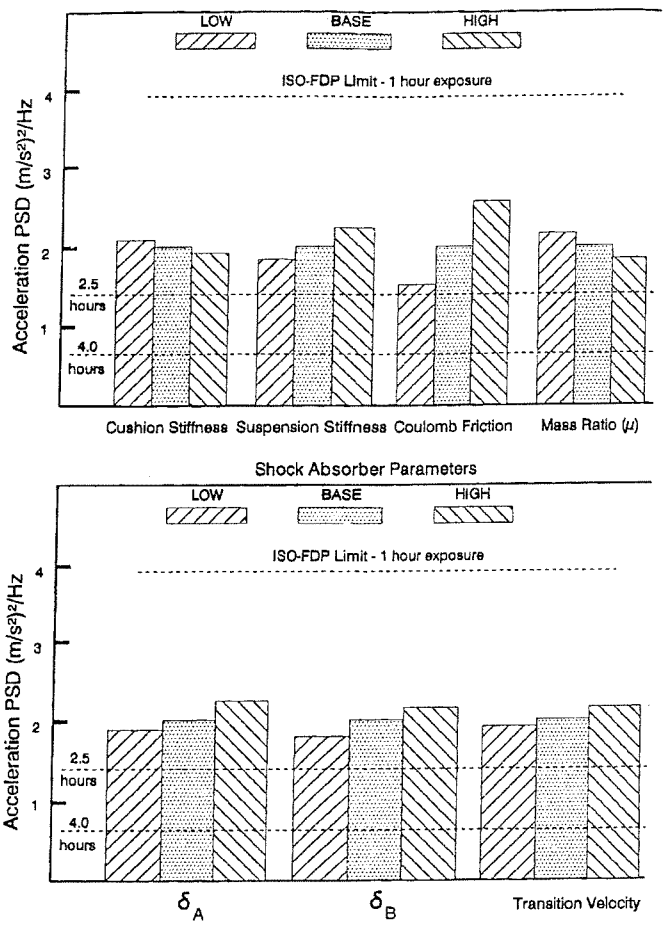

Figure 2-61 The influence on the peak PSD in response to the ISO7096:1984 Class II input motion of the cushion stiffness, the cushion damping, the Coulomb friction, the ratio of the suspended seat mass to the load mass, the low and high velocity damping coefficients (δ_A and δ_B) and the transition velocity (Rakheja *et al.*, 1994)

The performance of the seat when subjected to standard ISO test motions for off-road vehicles was evaluated in comparison with the ISO2631(1985) 1, 2.5 and 4 hour fatigue-decreased proficiency limits. A parametric sensitivity analysis was performed to investigate the effect of the cushion stiffness, suspension damping, coulomb friction, load mass and damper characteristics on the seat performance using the

peak PSD on the seat surface as the performance criteria (Figure 2-61). Tables of values for the low, base and high values were provided, but the system for selecting these values was not clear.

2.7.9 Ranganathan and Sriram (1994)

This paper included the equations for the vertical suspension seat model by Rakheja *et al.* (1994). The structure of a software package incorporating this model for use by manufacturers was described with figures showing the interface and example results. No dynamic investigations were performed. This paper was more of a product summary than a research report and took the important step of attempting to get the tools developed from research onto the desks of the engineers that would benefit from them.

2.7.10 Lewis (1994)

This study used a linear single degree-of-freedom system (Figure 2-62) to simulate the seat-load system. The variation in seat performance with magnitude was shown and the model stiffness and damping coefficients were fitted to the measured frequency domain response

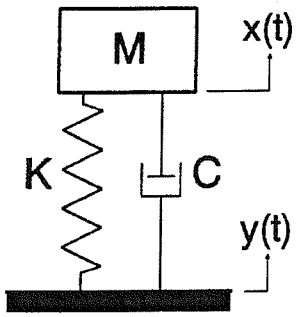

Figure 2-62 The simple linear model used by Lewis (1994)

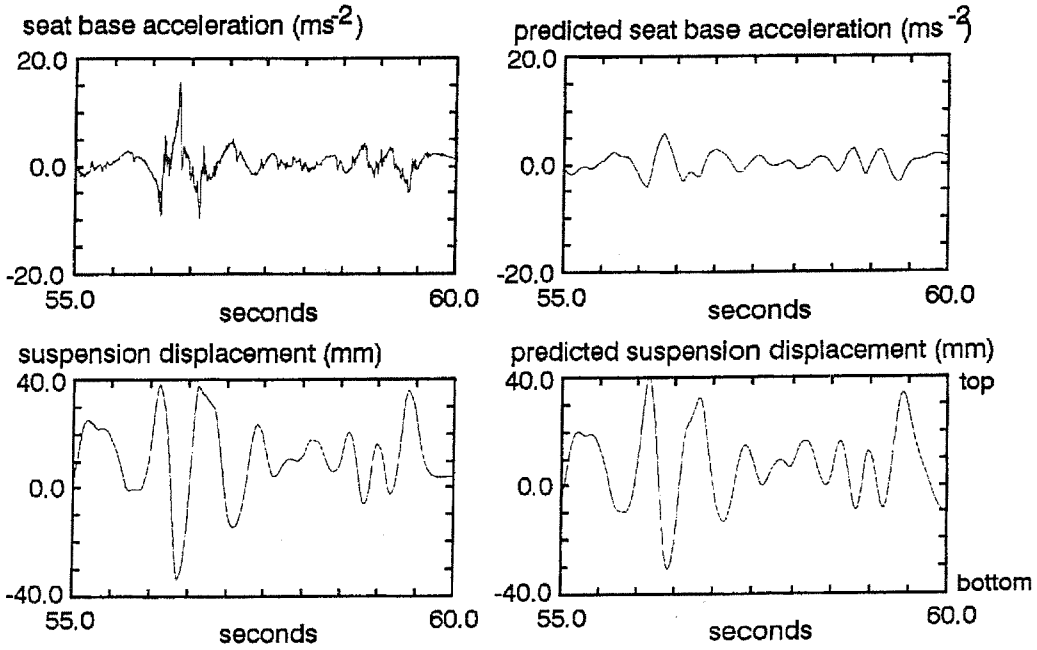

Figure 2-63 The measured and predicted accelerations at the base of the seat cushion (above the suspension) and suspension displacements using a simple, single degree-of-freedom seat model (Lewis, 1994)

for a particular magnitude.

The comparison between the linear model and the measured seat performance for one test condition was shown (Figure 2-63). This approach was intended to predict the suspension displacement in order to anticipate the occurrence of end-stop impacts, rather than to predict the dynamics of the system once end-stop impacts began to occur.

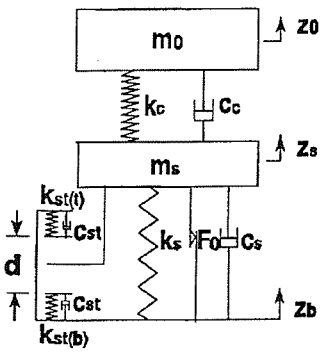

Figure 2-64 Schematic of the seat model from Wu and Griffin (1995)

2.7.11 Wu and Griffin (1995)

This non-linear vertical suspension seat model referred directly to previous studies by Rakheja and associates, but was developed independently. The model (Figure 2-64) differed from the Rakheja *et al.* (1994) model by using a linear suspension damper but including a two-stage stiffness for the end-stop buffers. A rigid load was used on the seat surface.

The coefficient values and the methods of obtaining them were reported. The suspension stiffness and coulomb friction were determined from quasi-static force-deflection measurements of the suspension mechanism. The cushion stiffness and damping were determined from dynamic measurements of the seat cushion and extracting linear coefficients at the cushion resonance frequency (3.7 Hz) using the following equation from Fairley and Griffin (1986).

$$S(\omega)=\frac{F(\omega)}{-\omega^{a}(\omega)}=k(\omega)+jc(\omega)\omega \qquad \text{Equation 2-6}$$

where ω is the angular frequency, F is the force transmitted by the cushion, a is the acceleration applied to the cushion and k and c are the linear stiffness and damping coefficients.

The comparison of predicted and measured performance was shown in the time domain using a test condition including end-stop impacts (Figure 2-65). It was reported that the model did not adequately reproduce the locking up of the suspension at low magnitudes but results were not shown.

A parametric sensitivity analysis was conducted in the amplitude domain to investigate the effect of the suspension damper and the buffer stiffness and damping on the end-stop impact performance of the seat. The results are shown in Figure 2-66 to Figure 2-70.

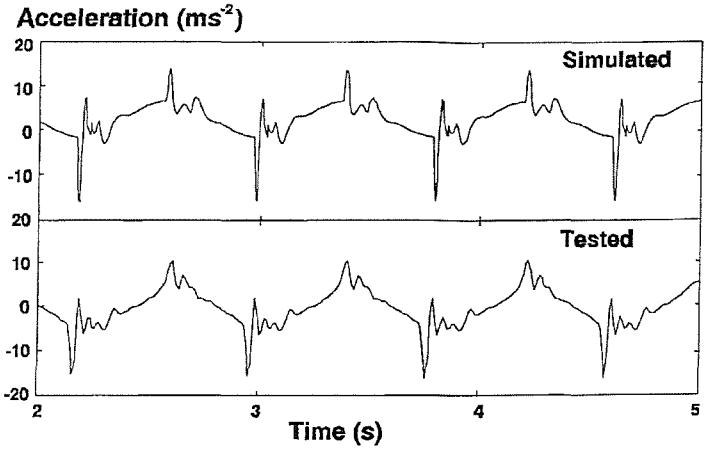

Figure 2-65 The mesured and predicted acceleration at the top of the suspension (Wu and Griffin, 1995)

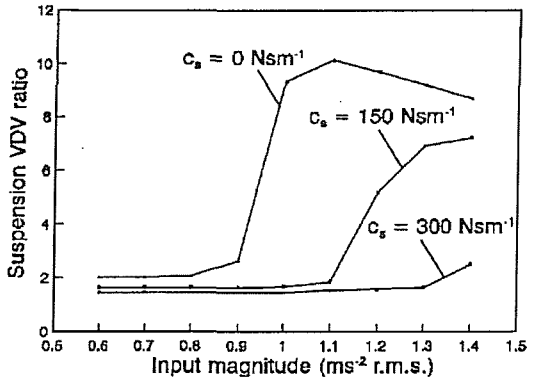

Figure 2-66 The effect of suspension damping on the seat suspension performance (Wu and Griffin, 1995)

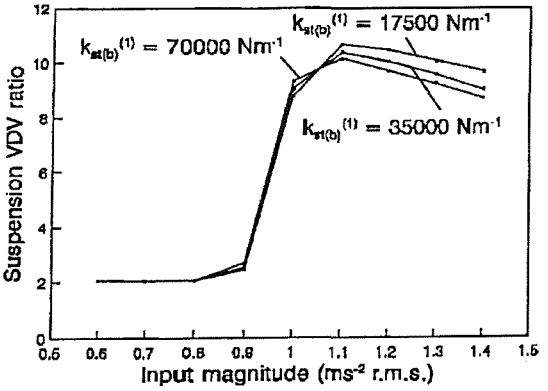

Figure 2-67 The effect of the bottom buffer stiffness on the seat suspension performance (Wu and Griffin, 1995)

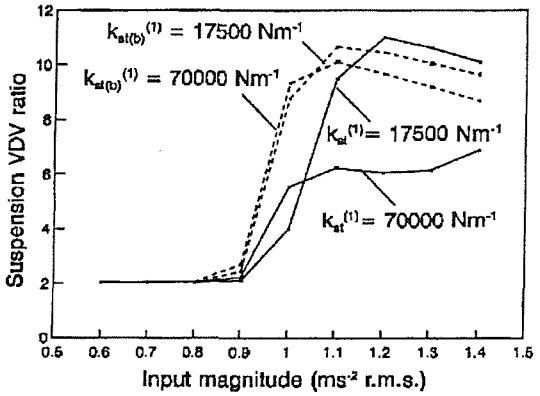

Figure 2-68 The effect of buffer stiffness on the seat suspension performance (Wu and Griffin, 1995)

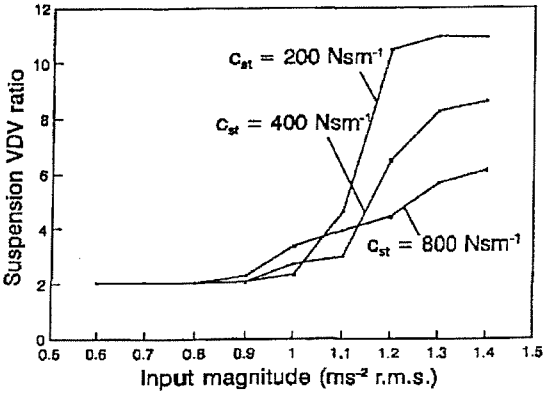

Figure 2-69 the effect of buffer damping (no buffer stiffness) on the seat performance (Wu and Griffin, 1995)

The study showed substantial reductions in vibration by including top end-stop buffers, but considered the vibration transmitted through the suspension, not the vibration experienced by the load.

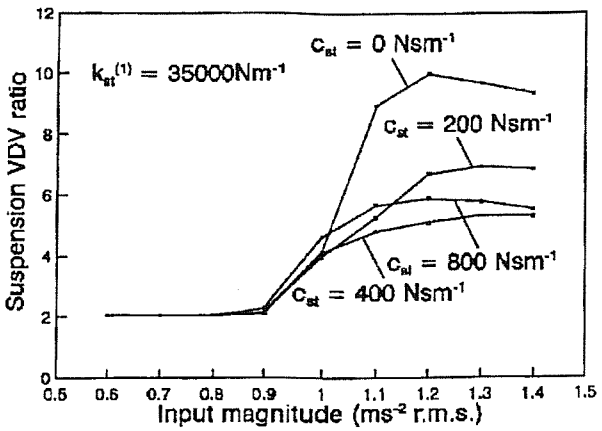

Figure 2-70 The effect of buffer damping (with stiffness) on the seat performance (Wu and Griffin, 1995)

2.7.12 Discussion

The suspension seat modelling field is dominated by a small number of researchers. The original non-linear suspension seat model as described by Rakheja and Sankar (1983) has been refined by subsequent authors, but the most recent models still use the same lumped parameter approach. Suspension seating lends itself well to this form of analysis as the seat can be naturally dismantled into component parts with distinct dynamic characteristics.

Efforts have been made to linearise the suspension seat models to allow the analysis to be conducted in the frequency domain. However, the work of Wu and Griffin (1996) has shown the importance of understanding the performance of suspension seats in the amplitude domain. Investigations of suspension seat performance in the amplitude domain will require a non-linear model.

The performance of the models as compared to measured laboratory or field results was initially not reported as the first models were intended as theoretical feasibility studies only. Subsequent studies showed the performance of the model as compared with measured results using one or two magnitudes in the frequency domain. The study by Boileau *et al.* (1993) performed the most comprehensive comparisons with measured results and compared both the time histories and the r.m.s. and r.m.q acceleration at the seat load for several vehicle speeds. This study used the model described by Rakheja *et al.* (1994).

The coulomb friction forces used in previous models, where reported, were substantially lower than the forces measured in the later chapters of this thesis. It is not clear if this was by coincidence, or if the seats were adjusted or chosen to minimise the friction before the models were developed. A low friction force might be expected to lead to a more linear seat for low to moderate magnitudes and so make

the simulations less complex for studies primarily concerned with moderate or high magnitude seat performance.

The parametric sensitivity analyses carried out using suspension seat models have allowed general effects to be identified. However, it is difficult to obtain a complete picture of the relative effect of each parameter due to the restricted range of test conditions and the lack of a systematic method for selecting the parameter ranges. The most systematic parametric analysis was that of Boileau *et al.* (1993) which used consistent variations for each parameter around baseline values and only Boileau *et al.* (1993) and Wu and Griffin (1995) conducted any parametric sensitivity analysis in the amplitude domain.

No investigation has conducted a parametric sensitivity analysis investigating seat performance in both the frequency and amplitude domains using a model quantified against experimental results. Such a study would be able to evaluate more completely than previously the relative importance of each suspension component on the overall seat performance.

2.8 Numerical methods

It became apparent during the course of the thesis that non-linear parameter optimisation techniques would be required. A parameter optimisation process allows a set of parameters to be obtained that result a minimum error in the model output. This process can be visualised as trying to locate the lowest point on an unknown surface defined by some function.

Optimisation methods can be loosely divided into gradient and non-gradient methods. Gradient methods use derivatives of the function to be minimised in order to locate a minimum. The function must usually be smooth (no discontinuities) and it is possible for a gradient method to become trapped in local minima.

Difficulties with optimisation are converging to the solution within a reasonable number of iterations (where 'reasonable' generally relates to the amount of processing power available), identifying when a solution has been reached and converging to the global solution and not a local minimum value.

The Nelder and Mead (1965) Simplex downhill search is probably the most widely used method. This method is recognised as versatile and robust, but can be trapped into a local minimum. A refinement of this method was described by Box (1965) including constraints on the parameters.

An alternative approach to optimisation uses genetic algorithms. These are functions used in machine learning applications and describe a Darwinesque evolutionary process. A number of 'parent' parameter sets are 'bred' together by exchanging parameters to form 'children'. The child sets that result in the lowest error are selected as the 'fittest' and are bred together to form the next generation. This process was described in detail by Holland (1975), Goldberg (1989) and others.

Comparisons of genetic algorithms with more conventional optimisation processes (e.g. Jansson *et al.*, 1995; Seo, 2001) indicated that genetic algorithms were more computationally intensive and slower to converge to the global minimum, but capable of minimising more complex, discontinuous functions.

The choice of optimisation method is highly dependant on the characteristics of the function to be solved. A more cautious method involves more evaluations of the function in order to increase the chance of finding the global minimum while faster methods have a greater chance of converging to a local rather than the global minimum. Global optimisation processes have been applied to automotive suspension engineering to the extent that products with active or semi-active suspensions have now reached the market, but the application of control engineering to seating dynamics is less advanced. Chen and Griffin (1989) used a non-linear least squares optimisation process to predict the transmissibility of an automotive seat, but the only known instance of a global optimisation process being applied to a seat suspension is the Nelder-Mead Simplex method used by Rebelle (2000) to obtain the coefficients for a seat suspension described in terms of a Bouc-Wen equation.

Non-linear optimisation routines are often developed for a specific application. The topography of the 'surface' describing the effect of changes of the component parts of a suspension seat model on the model accuracy was unknown at the start of this project, but was not expected to be simple due to the presence of non-linear component parts. It was therefore accepted that it may be necessary to modify an existing procedure or develop a new procedure in order to obtain useful results.

2.9 Conclusions

2.9.1 Vibration evaluation

Vibration has been shown to have an adverse effect on the health of vehicle operators, resulting in the development of lower back pain. Vibration also results in driver discomfort. Methods exist for evaluating the severity of vibration on the seated

human body and these methods have in many cases been standardised on a national and international scale. It is not the intention of this thesis to directly address the affect of vibration on the human body, so the standardised methods of quantifying the effect of vibration on the seated body will be used. Due to the high crest-factor, shock-like motions that are expected to occur in seat end-stop situations, the vibration dose value will be used as the preferred quantification method throughout this thesis.

2.9.2 Vehicle vibration

The nature of the vehicle-seat-operator system whereby the driver has control of the vibration level has not been addressed in the literature. A fixed magnitude vibration tests is not sufficient to evaluate the performance of a suspension seat. The performance of a seat in response to high magnitude motions which may result in considerable discomfort is of particular interest. The time-domain characteristics of the vehicle floor vibration in the field have not been widely reported and the characteristics of the vehicle motions that result in seat end-stop impacts are not known.

2.9.3 Suspension seat simulation

A number of models have been developed to simulate suspension seat performance. However, no study has attempted to map the influence of the seat components in the frequency and magnitude domains, or quantify the model performance at both low and high magnitudes. A model used to investigate suspension seat performance in such detail should be quantified against laboratory measurements using a range of frequencies and magnitudes of motion resulting in seat performance from being friction-locked at low magnitudes up to end-stop impacts at high magnitudes. It is not possible to 'validate' a non-linear theoretical model, but it is possible to build confidence in the performance of a model by testing it over a range of conditions. The most challenging (i.e. most non-linear) conditions for a suspension seat are expected to be at low magnitudes with high friction and at high magnitudes in end-stop impact situations. Previous modelling studies have reported few test results using these conditions.

2.9.4 Seat component modelling

There is scope to improve on the current methods for simulating some of the components used within suspension seat models. The cushion and suspension damper in particular have complex non-linear dynamic behaviour and merit further

attention. The form of model used to represent the driver also needs to be addressed. The focus of the thesis is the performance of the seat, so a consistent, repeatable load would be preferable to human subjects if such a load can be shown to give results similar to those obtained with subjects.

2.9.5 Application to the thesis

Standardised methods exist for measuring vibration on seats and for estimating the discomfort of the seat occupant due to vibration of the seat surface. It is beyond the scope of this thesis to comment on the effect of vibration on the comfort or health of the human body so these standardised methods will be used wherever possible.

The mechanical impedance or apparent mass of the seated human body has also been investigated by a number of authors. The dynamics of the human body are of great interest when assessing the performance of seats, but this thesis will focus primarily on the physical properties of the seat. The influence of driver dynamics on suspension seat performance will where possible be left as a subject of further research.

Specific characteristics (e.g. tyre stiffness, suspension characteristics, weight distribution) of the off-road vehicles in which suspension seats are used are also outside the scope of the thesis, but the motion of the cab floor of the vehicle when in a relevant operating environment needs to be known. Many existing test standards use band limited motions which may exclude aspects of the vehicle motion that affect a non-linear seat model, so measurements on relevant vehicles will be made.

Authors working in the automotive field have investigated the measurement and modelling of suspension seat components. The assessment of seat cushion dynamics and the performance of suspension dampers are both of great interest to the automotive design industry. Techniques developed for car seats and suspension could be adapted for use in measuring suspension seats.

The literature shows a number of non-linear suspension seat models have been developed over the past twenty years, but that detailed investigations to build confidence in these models over a range of test conditions have not been reported. Sensitivity analyses have been carried out for some seat components but there has been no systematic attempt to build a comprehensive picture of the effect of each component on the seat performance with varying frequency and magnitude of test motion. This will be the main objective of this thesis.

3 Apparatus and experimental methods

3.1 Introduction

This chapter describes the experimental equipment used for the laboratory experiments conducted at the Human Factors Research Unit at the Institute of Sound and Vibration Research. This chapter presents the performance of the shakers, transducers, data acquisition and analysis systems, statistical methods, safety and ethics procedures and describes the three test seats used during this thesis.

3.2 Data acquisition and analysis

During experiments, data were output to the shaker, acquired from the transducers and summarily analysed to monitor the vibration exposure of subjects using an *HVLab* data acquisition and analysis system (January 1999 and April 2000 versions).

The *HVLab* software was a Forth-based application running under DOS on an IBM-PC. The system controlled an *Advantech* PCL-818 data acquisition card capable of 2 channels of digital to analogue output and 16 channels of analogue to digital input. A *Techfilter* TF-16 programmable filter card also controlled from the software applied an anti-aliasing filter to each of the acquired signals before digitisation by the PCL-818. The generation of the test motions and the majority of the data analysis were performed using *Matlab 5.3. Microsoft Excel 2000* was used to summarise and display some data and *SPSS v10* was used to conduct statistical analysis of results. A schematic of the data acquisition system is shown in Figure 3-1.

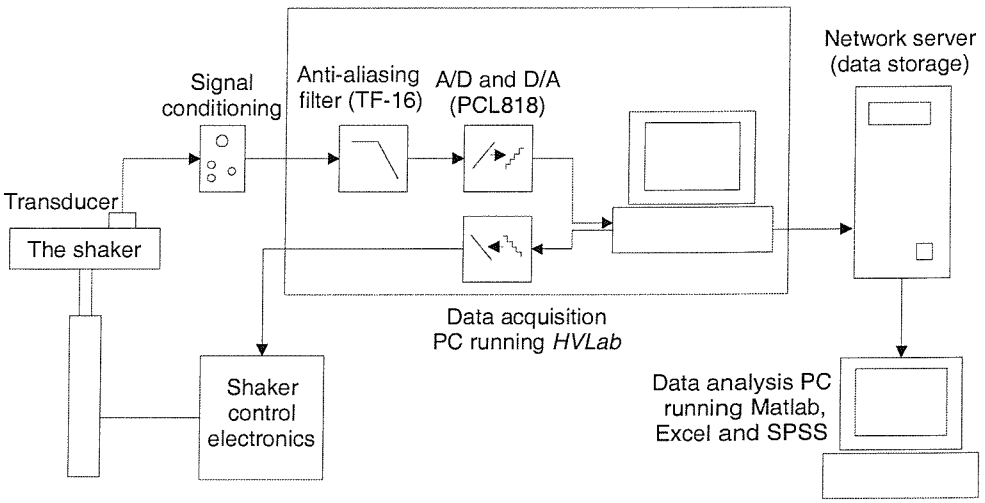

Figure 3-1 A schematic of the data acquisition system showing the signal path

3.3 Shakers

3.3.1 "The VP85"

The test rig used to measure some of the dynamic properties of the seat components used a *Derritron VP85* electro-dynamic shaker, referred to throughout this thesis as the VP85 (Figure 3-2). This device was driven from a 1 kW amplifier and was quoted as capable of accelerations up to 55 g, peak-to-peak displacements of up to 25.4 mm and a frequency range of 1.5 Hz to 3700 Hz. It was found to be possible to conduct experiments at frequencies between 1 and 10 Hz by equalising the input motion to correct for the roll-off in the shaker performance at low frequencies (see Section 3.3.3).

Figure 3-2 A VP85 electro-dynamic shaker

3.3.2 "The 1-metre vertical"

A schematic of the Human Factors Research Unit 1-metre vertical shaker is shown in Figure 3-4 and a photograph of the 1500 x 900 mm shaker platform is shown in Figure 3-3. The shaker was manufactured by *Servotest* and is capable of 10 kN dynamic force, 8.8 kN preload force, 1 metre peak-to-peak displacement, 10 ms^{-2} peak acceleration and frequencies from 0.05 Hz to 50 Hz.

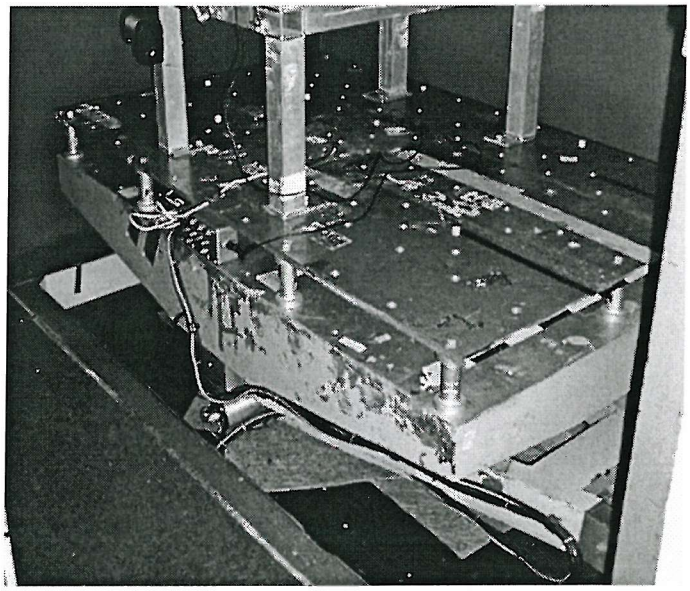

Figure 3-3 The platform of the 1m vertical shaker

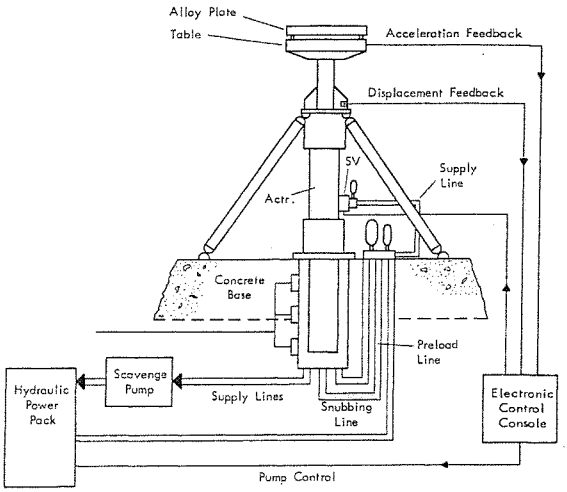

Figure 3-4 Schematic of the 1-metre vertical electro-hydraulic shaker (from Corbridge et al, 1990)

3.3.3 Equalisation

The *HVLab* software included a facility to compensate for the response of a shaker and the associated control circuitry. A random motion with a frequency content similar to that of the desired motion was output to the shaker and the platform motion was acquired using a calibrated accelerometer. The transfer function between the output and acquired signal was used to generate a filter describing the response of the shaker system and the inverse of this filter was applied to the desired motion in order to produce a compensated output signal. Outputting this signal to the shaker would result in the desired motion being reproduced on the shaker platform if the shaker system was linear. The effect of non-linearities was reduced by running the compensation procedure with all the experimental apparatus in place on the platform and using a random motion of similar mean amplitude to that of the

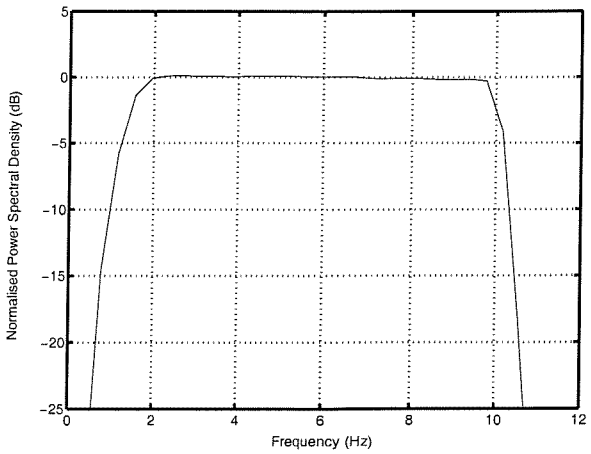

Figure 3-5 The PSD of the displacement on the VP85 shaker platform using a constant displacement amplitude (2 mm peak-to-peak) chirp function swept from 1 Hz to 10 Hz over 120 seconds. The displacement was estimated from numerical integration of the acceleration recorded on the shaker platform. The resolution of the PSD is 0.39 Hz.

desired motion. The power spectral density (PSD) of an equalised motion recorded on the VP85 is shown in Figure 3-5.

3.4 Transducers

3.4.1 Accelerometers

Accelerations were measured in the laboratory using Entran EGCSY-240D-10 piezo-resistive accelerometers (Figure 3-6) unless stated otherwise. These devices had a sensitivity of between 8 and 15 mV/g at 30 Hz and an operating range of ±10g over a temperature range from –40 to 120°C. The devices had a damping coefficient of 0.58 and resonance frequencies between 450 and 480 Hz. The frequency responses varied by less than ±0.5 dB from 0 to 250 Hz.

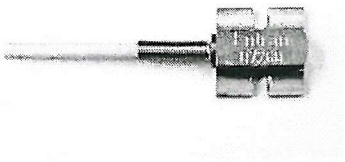

Figure 3-6 An Entran EGSY-240-D accelerometer

The accelerometers were calibrated before each experiment using the rollover method as described in ISO5347-5 (1993). The transmissibility between the accelerometers used in each experiment was inspected to ensure that the variation in response over the frequency range of interest was less than 5%.

The signal conditioning and power supply for the accelerometers was either an *HVLab* 16-channel signal conditioning box or an HFRU single channel accelerometer amplifier. Both devices were manufactured within the Human Factors Research Unit and include the power supply, pre-amplifier and DC offset correction controls required by the EGCSY-240D-10 accelerometers.

3.4.2 SAE pad

The vertical acceleration between the seat surface and a human subject was measured using a semi-rigid disk, referred to as an SAE pad from the original specification developed by the Society of Automotive Engineers. The SAE pad used during this thesis complied with ISO 10326 (1992) and is shown in Figure 3-7. The pad was 190 mm in diameter with a maximum thickness

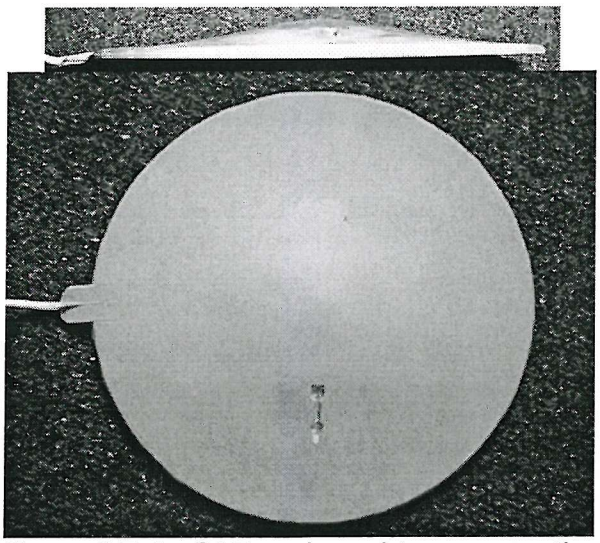

Figure 3-7 An SAE pad used to measure the seat surface acceleration

of 15 mm and contained an Entran EGSY-240D-10 accelerometer oriented to measure the acceleration perpendicular to the plane of the disk. The suggested positioning for the disk on the seat surface from ISO10326 (1992) is shown in Figure 3-8. The subject seated on the pad was requested to position the pad so that the bulge on the upper surface was between the ischial tuberosities. The pad was not secured to the seat or to the subject.

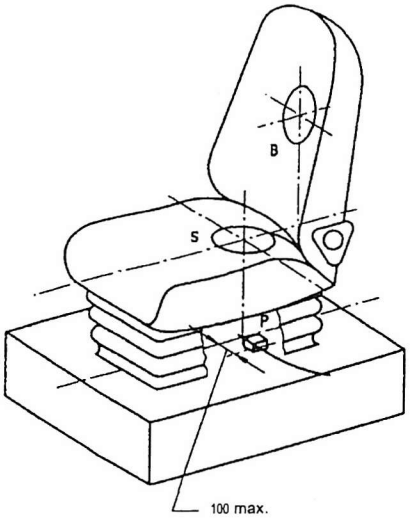

Figure 3-8 The location for accelerometers on the platform (P), the seat surface (S) and the backrest (B) as specified by ISO 10326 (1992). The SAE pad used for human subject tests in this thesis was positioned on the seat surface as shown in this figure.

3.4.3 Force cell

Measurements of force were made using a Kistler 9321A force cell (Figure 3-9) connected to a Kistler 5007 charge amplifier. The charge amplifier was equipped with three time constants to correct for any low frequency drift in the signal from the transducer. The 'short' and 'long' settings were used during this project. As used with the 9321A force cell, the 'short' time constant was approximately 0.5 seconds and the 'long' time constant was greater than 15 minutes.

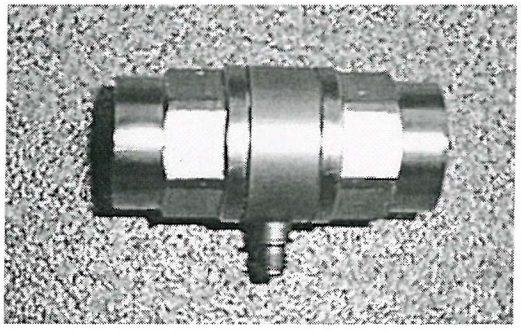

Figure 3-9 A Kistler 9321A force cell

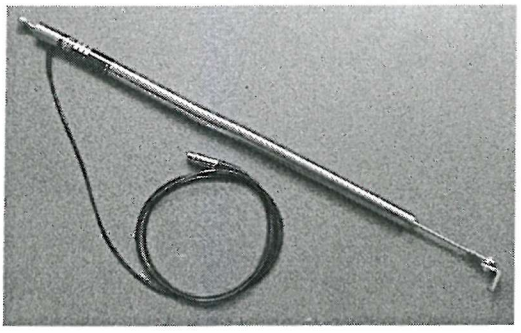

Figure 3-10 An RDP DCT4000C LVDT

3.4.4 Linear variable differential transformer

Displacements were measured using an RDP DCT4000C linear variable differential transformer (LVDT) as shown in Figure 3-10. This device had an operating stroke of 200 mm and included an internal amplifier to allow the device to accept a +12V DC power supply and output a voltage directly proportional to the displacement. No signal conditioning was required except for an attenuator to reduce the ±5V output voltage

range of the device to the same order of magnitude as the accelerometers, but the device was usually connected via an accelerometer amplifier to allow a DC offset to be introduced. This DC offset was used to correct for any difference between the mid point (0V output) of the LVDT and the reference (0 mm) displacement for the experiment, for instance the mid point of the suspension stroke.

3.5 The test seats

All three seats used during this thesis were current production models intended for use in off-road vehicles.

3.5.1 The earthmover seat

The earthmover seat (Figure 3-11) was a mechanical (steel sprung) suspension seat specified for use in earthmoving machinery. The seat suspension had two parallel steel coil springs mounted horizontally in the upper part of the suspension linkage to provide the suspension stiffness. The spring preload was manually adjusted using a calibrated control at the front of the suspension mechanism to account for the operator weight by adjusting the ride position of the suspension to the centre of the available suspension travel. An oil and gas damper was mounted at an angle between the upper and lower parts of the suspension towards the rear of the mechanism. The manufacturer indicated that the damper was at the 'lighter' end (i.e. lower force-velocity gradient) of the range of dampers available for this seat.

The two bottom end-stop buffers were wedge-shaped and mounted on either side of the bottom of the suspension mechanism, contacting part of the top part of the mechanism when the mechanism was compressed. The two top buffers were

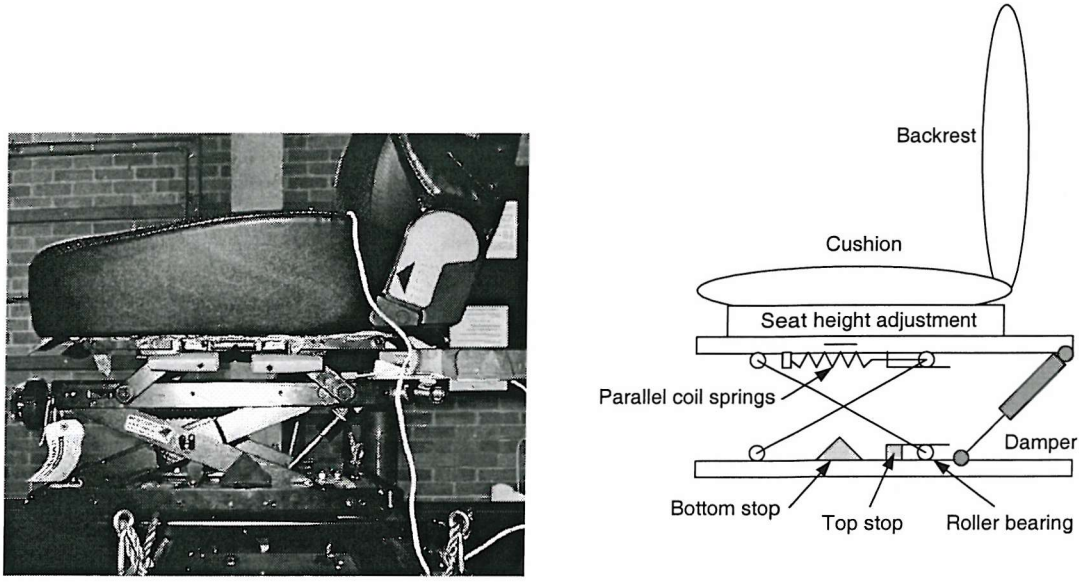

Figure 3-11 Photograph and schematic of the earthmover seat suspension

mounted in the runners of the suspension linkage, acting horizontally against the roller bearings. The end-stop buffer locations are shown in Figure 3-12.

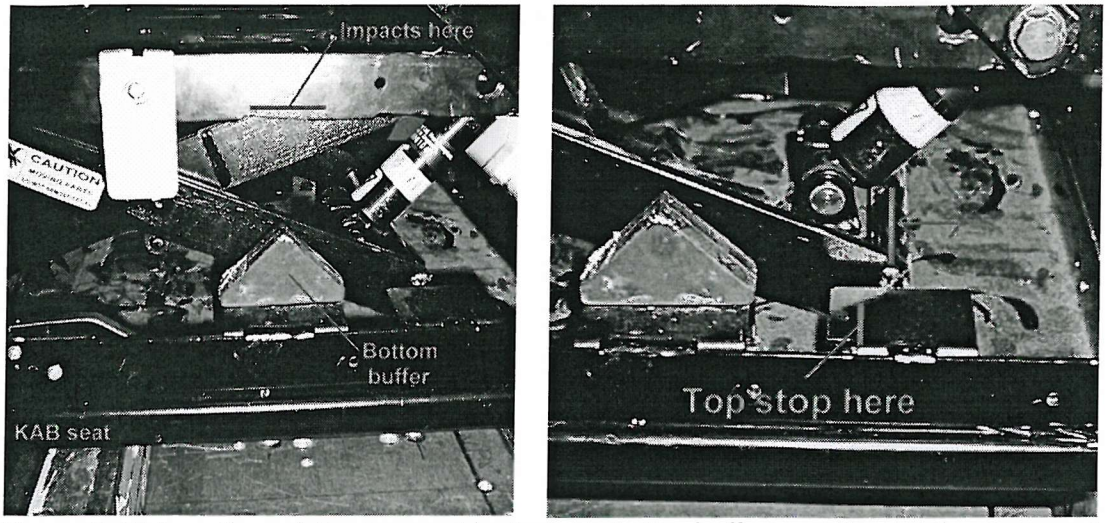

Figure 3-12 Location of the top and bottom end-stop buffers on the earthmover seat suspension

3.5.2 The forestry forwarder seat

The forwarder seat is shown in Figure 3-13. This seat used a cloth covered foam cushion and had an air spring in place of the steel coil springs used in the earthmover seat. An oil damper was mounted at an angle between the top and bottom parts of the under-seat suspension mechanism.

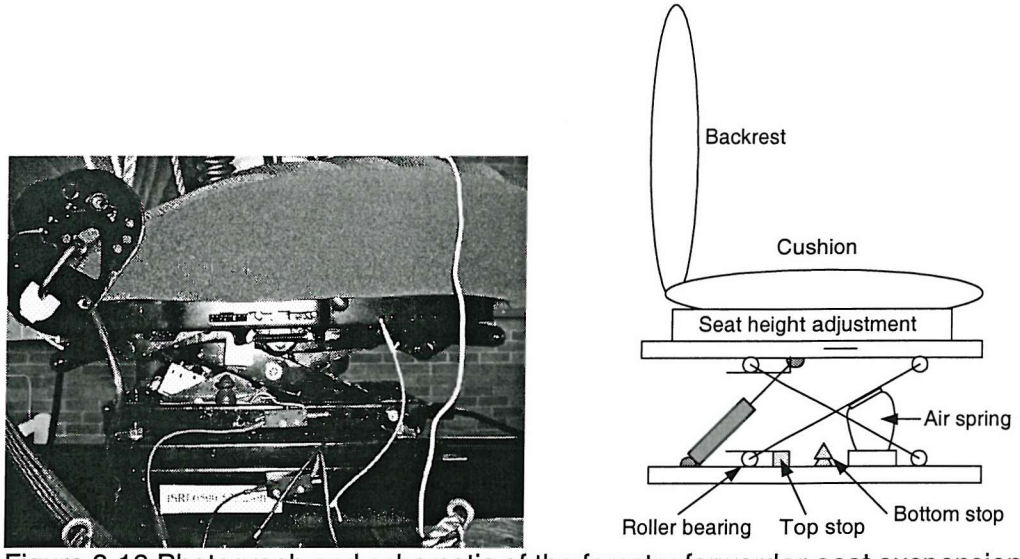

Figure 3-13 Photograph and schematic of the forestry forwarder seat suspension

The end-stop buffers were positioned in a similar manner to the earthmover seat, with two bottom buffers acting vertically against the top part of the suspension mechanism and two top buffers acting horizontally against the suspension linkage roller bearings.

The seat as shipped commercially was equipped with a self-levelling mechanism that automatically adjusted the air pressure in the spring according to the weight of the

driver. The air pressure was reduced when the suspension was close to the top of the available travel and increased when close to the bottom. The seat was therefore constantly seeking a central mean ride position. However, tests showed that this system became unstable when using some repeated sinusoidal input motions that cause end-stop impacts. As the seat contacted the bottom stop, the stiff but lightly damped rubber buffer accelerated the suspension upward. This rapid acceleration caused the seat to spend more time near the top of the travel than near the bottom where the impact occurred so the adjustment mechanism reduced the air pressure lowering the mean ride position and causing a more severe bottom stop impact. The self-levelling mechanism hence caused the mean ride position to move towards the impact rather than away from it. The mechanism was disabled for the laboratory tests using this seat by supplying air directly to the spring and manually adjusting the pressure to adjust the suspension to the desired ride position before starting the dynamic tests.

3.5.3 The agricultural tractor seat

The agricultural tractor seat (Figure 3-14) used an air sprung mechanism with an integrated height adjustment. The seat height was set by the operator by adjusting the pressure in the air spring. This adjustment was linked to a levelling device that ensured there was sufficient suspension stroke above and below the chosen ride position and a belt-operated device limited the upward travel to an approximately constant distance above the chosen ride position. The travel from the chosen ride position to the bottom stop therefore varied according to the seat height setting. In order to obtain repeatable results the belt mechanism was disabled and the seat was manually adjusted to a central mean ride position. The distance to both end-stop buffers therefore remained constant for all seat loads but the available suspension stroke was greater than as supplied commercially.

The oil damper was mounted at an angle as with the other seats but was equipped with a valve to adjust the damping force. The seat was tested at the lowest damper setting. The seat was also equipped with a separate fore-and aft suspension mechanism which was disabled for all tests.

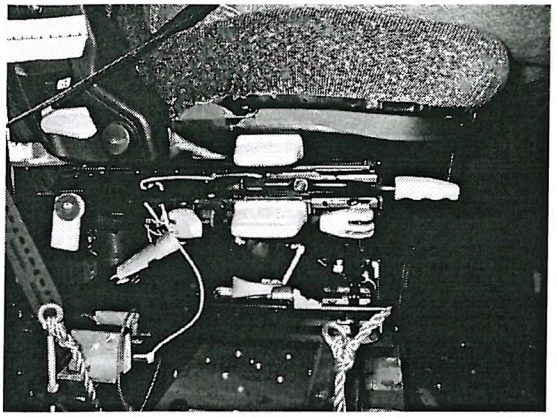

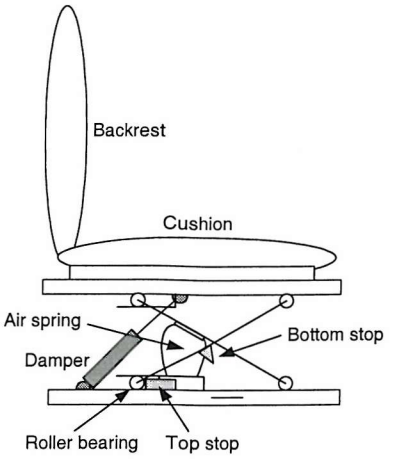

Figure 3-14 Photograph and schematic of the agricultural tractor seat suspension

The end-stop buffers were mounted in a slightly different manner on this seat. The two bottom-stop buffers were attached to the suspension mechanism linkage arms on either side of the seat and contacted the base of the suspension mechanism and a single top stop buffer was positioned to contact the centre of one of the linkage cross-pieces (Figure 3-15).

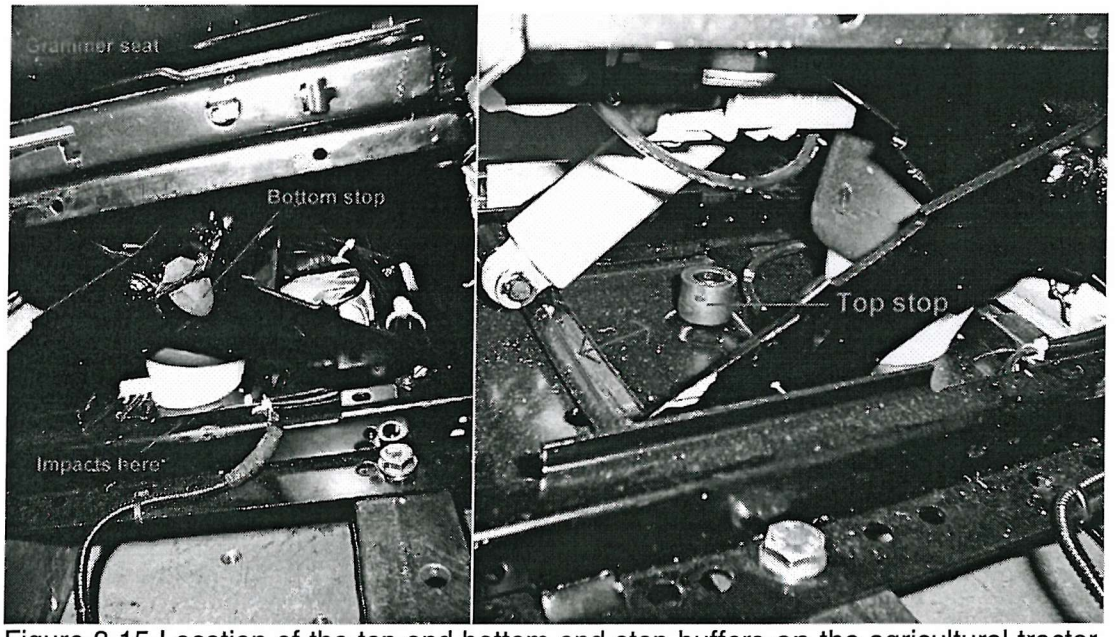

Figure 3-15 Location of the top and bottom end-stop buffers on the agricultural tractor seat suspension

3.6 Calculation of the transmission of vibration

3.6.1 Overview

A number of different measures of vibration transmission were used during this project. The following definitions and descriptions are taken from Griffin (1990), Bies and Hansen (1996) and Ifeachor and Jervis (1993).

3.6.2 Spectrum estimation, transfer functions and transmissibility

The linear transfer function ($H(\omega)$) between two points can be estimated from the power spectral density (PSD) and the cross spectral density (CSD) for the two locations:

$$H(\omega)=\frac{G_{xy}}{G_{xx}} \qquad \text{Equation 3-1}$$

where ω is the angular frequency in radians, G_{xy} is the cross spectral density between the two locations and G_{xx} is the power spectral density of x.

$$G_{xx}(\omega)=X(\omega)X^{*}(\omega) \qquad \text{Equation 3-2}$$

$$G_{xy}(\omega)=Y(\omega)X^{*}(\omega) \qquad \text{Equation 3-3}$$

where X and Y are the Fourier transforms of the motions $x(t)$ and $y(t)$ in the time domain at the two points as shown below and X^{*} is the complex conjugate of X.

$$X(\omega)=\int_{-\infty}^{\infty} x(t)e^{-j\omega t}dt \qquad \text{Equation 3-4}$$

$$Y(\omega)=\int_{-\infty}^{\infty} y(t)e^{-j\omega t}dt \qquad \text{Equation 3-5}$$

Due to the finite duration and digitally sampled nature of measured signals it is not possible to evaluate the transfer function exactly. Throughout this project transfer functions were estimated using Welch's modified periodogram method as implemented in Matlab 5.3 unless stated otherwise.

Using Welch's method, each digital time history was divided into a number of overlapping sections. Each section was detrended, Hanning windowed and then zero padded, usually to 2048 datapoints. The PSD and CSD were estimated by averaging the discrete Fourier transforms (DFTs) of all the overlapping sections and the transfer function was calculated from the estimated PSD and CSD. The discrete Fourier transforms of each zero-padded section of digital time histories x and y (both padded to a time length T and N datapoints) were evaluated using a fast Fourier transform (FFT) algorithm. The discrete Fourier transforms of x and y are:

$$X(\omega)=\sum_{n=0}^{N-1} x(nT)e^{-j\omega nT}T \qquad \text{Equation 3-6}$$

$$Y(\omega)=\sum_{n=0}^{N-1} y(nT)e^{-j\omega nT}T \qquad \text{Equation 3-7}$$

The estimated PSD and CSD were evaluated using:

$$G_{xx}(\omega)=\frac{1}{q}\sum_{n=1}^{q}X_n(\omega)X_n^*(\omega)$$ Equation 3-8

$$G_{xy}(\omega)=\frac{1}{q}\sum_{n=1}^{q}Y_n(\omega)X_n^*(\omega)$$ Equation 3-9

where the spectra were estimated from q overlapping sections and the transfer function was calculates as in the ideal case by:

$$H(\omega)=\frac{G_{xy}}{G_{xx}}$$ Equation 3-10

The transmissibility between x and y (T_{xy}) is defined as the magnitude of the transfer function:

$$T_{xy}(\omega)=|H(\omega)|$$ Equation 3-11

The coherence (C_{xy}) of the transfer function is a measure of linear agreement and is calculated from the PSD and CSD by:

$$C_{xy}=\frac{|G_{xy}|^2}{G_{xx}G_{yy}}$$ Equation 3-12

3.6.3 The SEAT value and the vibration dose value

The Seat Effective Amplitude Transmission value (SEAT, pronounced see-at) is a non-dimensional measure of the vibration isolation performance of a seat. There are several alternative methods of calculating this value depending on the characteristics of the system and the input motion. The method most suited to transient input motions and highly non-linear seat behaviour is the vibration dose value (VDV) method. This method was used throughout the project.

The SEAT value calculated in this manner makes no assumptions of linearity. The calculation is intended to relate the motion to the perceived discomfort and involves a 4^{th} power sum and a weighing filter emphasising frequencies in the region of 5 Hz. The SEAT value was calculated as follows:

1. The digitally sampled acceleration time histories were obtained for two locations, usually the seat base and the load on the seat surface, either acquired from accelerometers or predicted by simulations.
2. The time histories were normalised to remove any DC offset. This was simplified for most of the experiments described in this thesis by starting the data acquisition 0.5 seconds before the motion and subtracting the mean of the acquired time history between 0.1 and 0.4 seconds. The more common

method of subtracting the mean of the complete signal was not suitable for the transient motions used during this project.

3. The vibration dose value (VDV) of each time history was calculated according to:

$$VDV = \left[\int a_w{}^4(t)dt\right]^{1/4} \qquad \text{Equation 3-13}$$

where a_w is the frequency-weighted acceleration.

The VDV calculation involves a frequency weighting to account for the sensitivity of the human body to different frequencies of vibration The 'W$_b$' filter for seated, vertical vibration specified in BS6841 (1987) was used throughout this project unless otherwise stated.

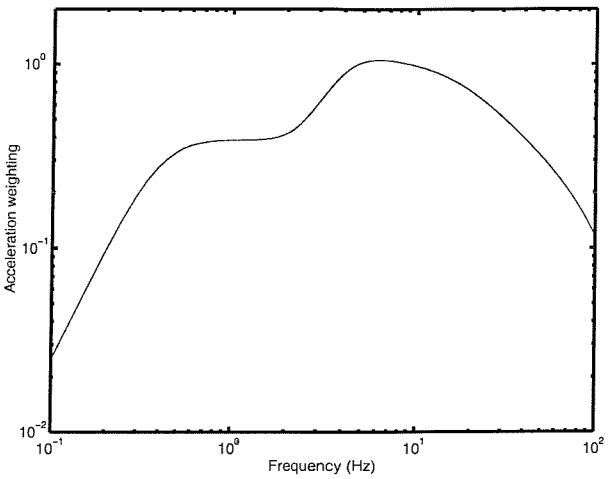

Figure 3-16 The W$_b$ frequency weighting specified in BS6841.

The weighting emphasises the importance of frequencies around 5 Hz as shown in Figure 3-16. Throughout this project an implementation of W$_b$ including all phase effects was used.

4. Finally, the SEAT value was calculated from the VDV by:

$$SEAT(\%) = \frac{VDV_{seat\_load}}{VDV_{seat\_base}} \times 100 \qquad \text{Equation 3-14}$$

3.7 Statistical methods

3.7.1 Overview

The following statistical methods were used during this project. The definitions were taken from Barlow (1989), Siegel (1956) and from the *SPSS v10* documentation. The majority of statistical methods were 'distribution-free' or 'non-parametric' methods. These methods use the rank order of the data and in some cases the difference in value rather than the absolute value. This was not because the absolute values of the

data were not of interest but because it was not always valid to make assumptions about the distribution of the data. Parametric methods require normally distributed data.

3.7.2 The mean and the median

The average value of a distribution was evaluated during this project using the median and the mean. The mean (Equation 3-15) assumes a normal distribution and estimates the value at the centre of this distribution. The median selects the measured value closest to the centre of the distribution with half the data above and half the data below and makes no assumption of the distribution.

$$\bar{x} = \frac{1}{N}\sum_{i-1}^{N} x_i \qquad \text{Equation 3-15}$$

3.7.3 Skewness

The skewness is a measurement of the relative lengths of the tails of a distribution. A non-zero skewness indicates that the distribution has a longer tail in one direction. A criteria for normality is the ratio of the standard error of the skewness to the respective value of the skewness being less than 2 (Brown, 1997). This indicates a significantly skewed distribution at the 5% probability level.

The skewness is defined as:

$$\gamma = \frac{1}{N\sigma^3}\sum_{i}(x_i - \bar{x})^3 \qquad \text{Equation 3-16}$$

Where x_i is the i^{th} value of a sample with mean $\bar{x}$ and the standard deviation σ is defined by:

$$\sigma = \sqrt{\overline{x^2} - \bar{x}^2} \qquad \text{Equation 3-17}$$

where $\overline{x^2}$ indicates the mean of the squared values of the sample x and $\bar{x}^2$ indicates the square of the mean of sample x.

3.7.4 Spearman's correlation coefficient

The correlation between two factors was investigated using Spearman's correlation coefficient, also known as Spearman's Rho. The coefficient can take values from -1 to 1. A value of zero indicates no correlation, a value of one indicates a perfect positive correlation and a value of -1 indicates a perfect negative correlation. The symbol ρ will be used to indicate the correlation coefficient throughout the text.

$$\rho = 1 - \frac{6\sum_{i-1}^{N} D_i^2}{N^3 - N} \qquad \text{Equation 3-18 Spearman's correlation coefficient}$$

where D is the difference between each pair of x_i and y_i with the data ranked in order. The significance p of the coefficient is given by

$$p = \rho\sqrt{\frac{N-2}{1-\rho^2}} \qquad \text{Equation 3-19}$$

3.7.5 The Mann-Whitney U-test

This test hypothesises that two sets of independent data are different and is also known as the rank sum test and Wilcoxon's test. This test can be used with samples of differing sizes

The values from each sample are arranged in a sequence of increasing value. The test determines if the values from both samples are evenly distributed within the sequence (e.g. *xxyxyyxyyxxyxyy*). If the median values are substantially different then the values from one sample will tend to favour one end of the sequence or the other (e.g. *xxxxxxxyyxyyyyy*) and a significant difference will be indicated.

The significance of the difference is given by:

$$p = \frac{U_x \pm 0.5 - m(N+1)/2}{\sqrt{mn(N+1)/12}} \qquad \text{Equation 3-20}$$

where U_x is the sum of the ranks positions of the values from the first (x) sample and m and n are the number of values within the x and y samples respectively.

3.7.6 The Wilcoxon's matched-pairs signed ranks test

In situations where the individual values for two samples are related, for instance when the same set of test conditions have been used for both samples, Wilcoxon's matched-pairs signed ranks test should be used. This test will be referred to throughout the text as Wilcoxon's matched-pairs signed ranks test or Wilcoxon's test.

This test involves ranking the differences between each pair of related samples in order without regard for sign. Differences of zero are dropped from the analysis. Tied differences are assigned an equal, average rank, but the ranking for the next difference is increased by the number of tied ranks (example from Siegel: if three pairs returned differences of +1, +1 and -1 then all would be assigned a rank of 2 as (1+2+3)/3=2. The next difference would be assigned a rank of 4). The test statistic T^+ is the sum of the ranks of the positive differences. The significance of the difference is given by:

$$p = \frac{T^{+} - N(N+1)/4}{N(N+1)(2N+1)/24 - 1/2\sum_{j=1}^{g} t_j (t_j - 1)(t_j + 1)}$$ Equation 3-21

where g is the number of groupings with different tied ranks, t_j is the number of tied ranks in grouping j and N is the total number of values in the sample with zero tied differences excluded.

3.8 Safety and ethics procedures

All experiments involving human subjects conducted during this thesis were approved by the Institute of Sound and Vibration Research Human Experimentation Safety and Ethics Committee. All subjects were volunteers and were screened using a health questionnaire (Appendix 1). A signed consent form was obtained from each subject before each test. The vibration exposure of each subject was monitored and details of the vibration exposure of all subjects were logged. In no case was a subject exposed to a daily VDV greater than 15 $ms^{-1.75}$ which is the daily limit suggested in section A6 of BS6841 (1987). Subjects were provided with a loose-fitting seat belt and an emergency stop button when seated on the shaker and it was made clear to each subject that they may stop the experiment at any time without providing a reason.

4 The definition of suitable input motions for testing suspension seat end-stop impact performance

4.1 Introduction

The objective of this chapter was to define suitable input motions for the testing of suspension seats in the laboratory with particular application to end-stop impact situations. The motions were intended to be representative of the vehicle cab floor motions in situations that might be expected to cause seat suspension end-stop impacts during normal vehicle operation while being as simple as possible to define and reproduce in the laboratory. Acceleration time histories provided by field test laboratories from field trials conducted on three types of off-road vehicle were examined for end-stop impacts. The vehicle motions had been recorded as each vehicle traversed obstacles identified by vehicle operators as likely to cause end-stop impacts during typical vehicle operation. Test motions were proposed after examination of the measured cab floor and seat motions, and tests were conducted in the laboratory to determine if the proposed motions resulted in similar seat behaviour to that observed in the field.

4.2 Summary of field trial conditions

4.2.1 Vehicles

Field tests were carried out using a JCB 3CX back-hoe loader earthmover (Figure 4-1, a Valmet 840 S-2 eight-wheeled forestry forwarder (Figure 4-2) and a Setyr 9105 agricultural tractor (Figure 4-3). The earthmover was tested by Kab Seating Ltd, of Northampton, UK, the forestry forwarder was tested by the National Institute for Working Life in Umeå, Sweden and the agricultural tractor was tested by Bundesansalt für Landtechnik of Wieselburg, Austria, on behalf of Grammer AG of Kümmersbruk, Germany.

Figure 4-1 The earthmover

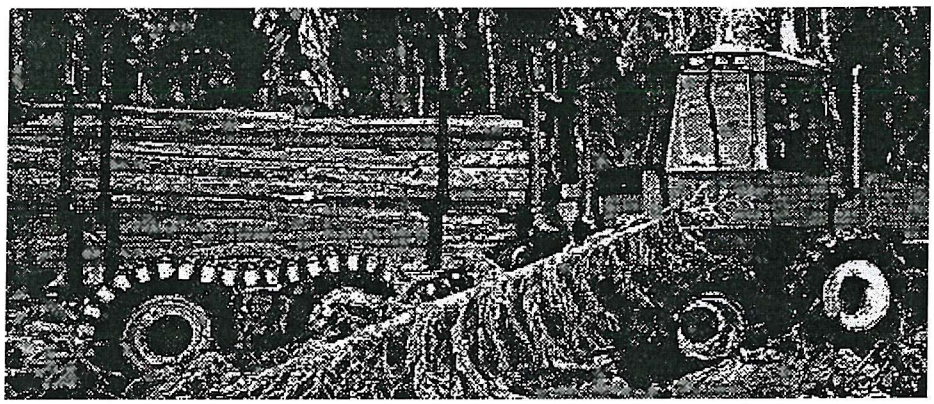

Figure 4-2 The forestry forwarder

Figure 4-3 The agricultural tractor

4.2.2 Test conditions

4.2.2.1 Overview

Discussions between the test laboratories and vehicle operators for all three test vehicles indicated that end-stop impacts were most noticeable when the vehicle traversed a single, severe obstacle. However, the nature of the 'typical' obstacle varied depending on the operating environment of the vehicle.

4.2.2.2 The agricultural tractor test track

The agricultural tractor was tested on a rough natural forest road without gravel or metal. The sections of track chosen were considered to be typical of well-travelled forest or farm tracks. Tests were carried out over several sections of road using two drivers of 56 kg and 98 kg and one seat with two seat suspension damper settings. The vehicle was travelling at what the driver considered to be a high speed leading to end-stop impacts as the vehicle traversed potholes and ruts in the track.

4.2.2.3 The earthmover test track

The earthmover was tested on a Macadam track representative of a quarry track. A track of this type is constructed of layers of material but does not have a tarmac surface. Small ditches usually cross these tracks at intervals to allow rainwater run-off and these can cause vehicle vibration leading to seat end-stop impacts if the vehicle is travelling at speed. This situation was identified from the experience of the vehicle operators and test engineers as a common cause of seat suspension end-stop impacts. The test runs were conducted over a section of Macadam track with a single obstacle approximately 0.5 m across. The vehicle was tested with two drivers (66 kg and 90 kg) with and without a restraining lap belt. The vehicle traversed the obstacle at constant speeds from 1 ms^{-1} to 2.7 ms^{-1}.

4.2.2.4 The forestry forwarder test track

Forestry forwarders operate in an off-road environment where obstacles such as rocks and tree-stumps are to be expected. Discussions with vehicle operators indicated that end-stop impacts would be expected when the vehicle climbs up or falls off an obstacle such as a tree stump or large rock. Repeatable field measurements were not possible as the heavy (15,000 kg) forwarder could significantly alter the nature of the terrain. Instead, an artificial obstacle was constructed of more durable materials to (see Figure 4-4). The forwarder was tested with two drivers close to the 25^{th} and 75^{th} percentile static masses for European males. The vehicle traversed the

obstacle at constant speeds from 0.56 ms^{-1} to 1.53 ms^{-1} increasing in steps of 0.14 ms^{-1}.

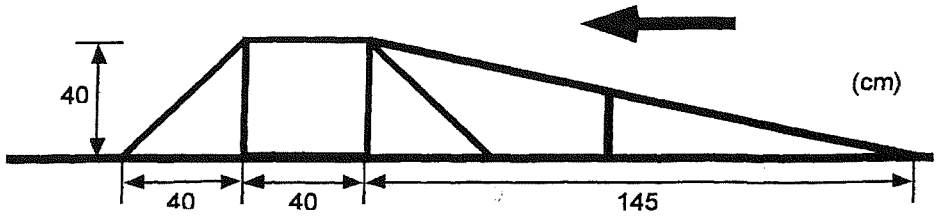

Figure 4-4 Obstacle used to test the forwarder

4.3 Data acquisition

The following channels of data were acquired during all field trials

- The acceleration on the cab floor under the seat
- The acceleration at the top of the seat suspension
- The acceleration at the top of the cushion
- Contact with the end-stop buffers, detected using microswitches

The displacement of the suspension mechanism relative to the cab floor was also acquired for the majority of trials, measured using linear variable differential transformers. The agricultural tractor data were acquired at 100 samples per second, the forwarder data at 400 samples per second and the earthmover data at 1000 samples per second.

4.4 Examination of field data

4.4.1 Time synchronisation for averaging time domain data

The earthmover and forwarder trials involved repeated runs over the same test obstacle so it was possible to average the time histories obtained at the same vehicle speed. It was necessary to adjust the time offset of the signals to ensure that the time at which the vehicle encountered the obstacle was synchronised before averaging the data. The vehicle floor acceleration time histories for each vehicle speed were cross-correlated against a reference time history selected at random and the time lag corresponding to the peak of the cross-correlation function was used to align each time history with the reference.

4.4.2 Power spectral density estimates

The power spectral density estimates were based on a single Fourier transform of the time histories due to the transient nature of the signals. The data were zero-padded to

a give a sample length of 4096 data points and the resulting spectra are shown normalised to the peak value.

4.4.3 The seat base motion analysis

4.4.3.1 Agricultural tractor

Examples of the time histories obtained using the agricultural tractor on the forestry road are shown in Figure 4-5. It was possible to identify sections of high magnitude floor motion which caused seat suspension end-stop impacts. Figure 4-5A shows a short duration floor motion causing a top end-stop impact then a bottom stop impact. Figure 4-5B shows a motion with several top stop impacts and Figure 4-5 shows a severe floor motion involving many top and bottom stop impacts. The greater number of top stop impacts may be due to the seat configuration. The height adjustment mechanism on the seat used in these tests was an integral part of the seat suspension and operated in conjunction with a system for limiting the upwards travel according to the seat height setting. Using this system, the available upwards travel remains fairly constant with different seat height settings, but the available downwards travel varies so it is possible for the correctly adjusted seat to have a mean ride position closer to the top buffer than the bottom buffer.

The spectra of samples 2 and 3 (Figure 4-5D) suggest that there may be two lightly damped vehicle modes at around 2.3 Hz and 2.5 Hz. The spectra from sample 1 is based on a very small sample of data and provides little information beyond suggesting at least one mode in the vicinity of 2.5 Hz.

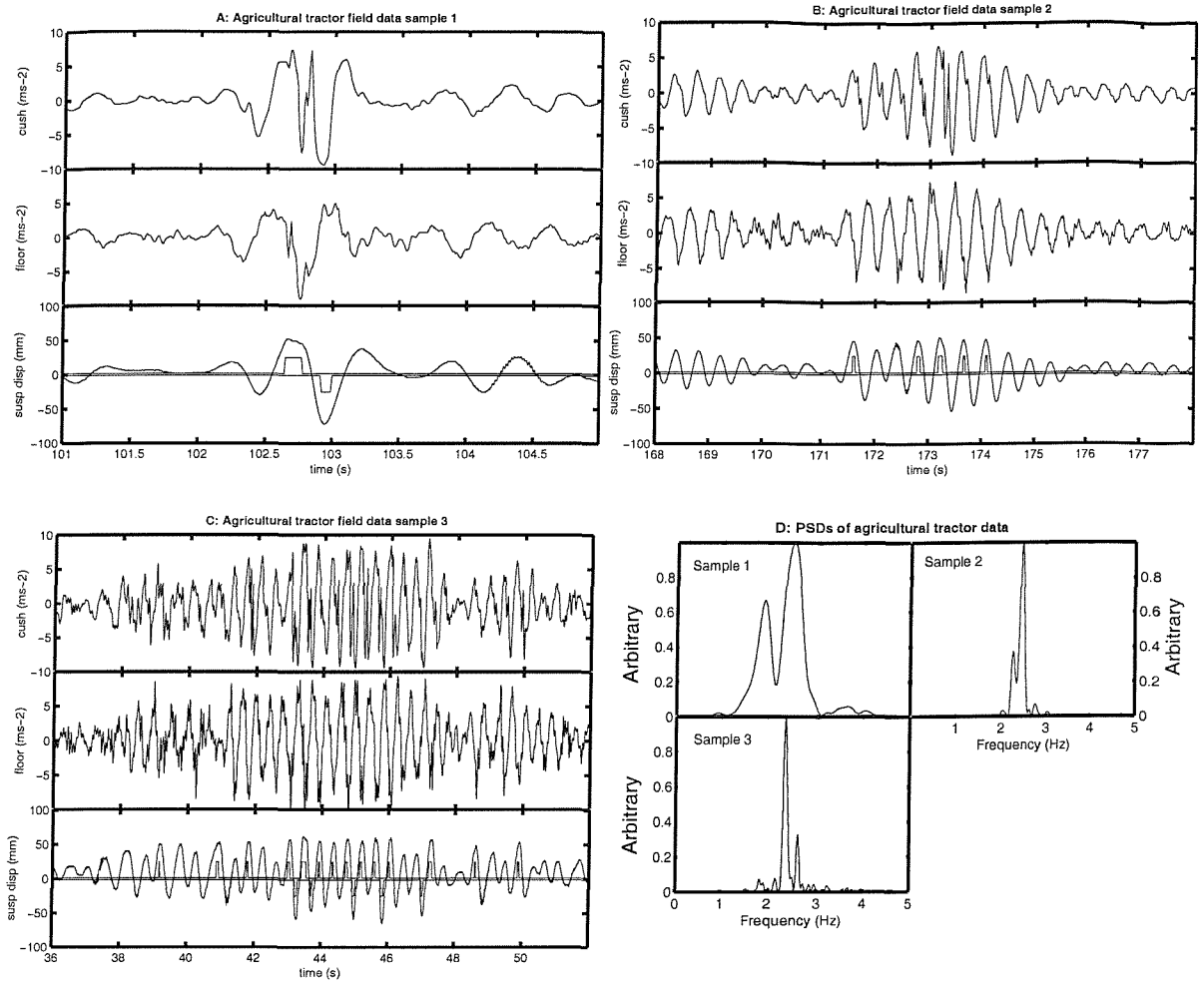

Figure 4-5 Agricultural tractor seat motions measured in the field (note the different time scales and durations). The top graphs of A, B and C show the acceleration on the seat cushion. The middle graphs show the acceleration on the cab floor. The lower graphs show the displacement of the seat suspension relative to the cab floor and the output signals from switches detecting contact with the end-stop buffers. D shows the power spectral densities of the data shown in A, B and C.

The variety of terrain encountered during the agricultural tractor field trials provided an indication of the range of waveform shapes which might be encountered using off-road vehicles in the field. The cab floor motions that caused end-stop impacts were narrow-band and might be considered as 'events' which rise from and decay back to a lower amplitude. The rise of the amplitude envelope of the motion varies considerably between events but in many cases an exponential decay was discernable (Figure 4-5B from 38 seconds and (Figure 4-5C from 47 seconds and from 49 seconds). This is assumed to be the free response of the vehicle mass on the tyres. The event duration also varied considerably from the 1.5 second event shown in (Figure 4-5A to the long event of around 7 seconds duration shown in (Figure 4-5C between the times marked as 41 to 48 seconds).

4.4.3.2 Earthmover

Figure 4-6 shows data obtained using the earthmover at three speeds over the Macadam track. The data shown are the mean of four test runs using a lightly damped seat, one run with each driver with and without a seat belt. The vehicle initially contacted the obstacle at the point marked (I). The seat struck the top stop (II), severely contacted the bottom stop (III) then the top stop (IV). It was estimated from the vehicle speed and wheelbase that the vehicle rear wheels struck the obstacle at around (V). This reduced the seat displacement magnitude. Several top and bottom impacts occurred after this but were not as severe as the initial impacts.

The spectra (Figure 4-6D) seem to show a vehicle mode close to 2.5 Hz at all speeds, another at around 2.1 Hz at vehicle speeds of 2.3 ms^{-1} and 2.7 ms^{-1} (Figure 4-6B and 3C) and a third mode at 1.3 Hz at 2 ms^{-1} (Figure 4-6A). Examination of the zero crossing times of the cab floor acceleration time histories suggests that the 2.1 Hz motion is responsible for the more severe end-stop impacts. The 2.5 Hz motion becomes more apparent at lower magnitudes later in the motion. The peaks visible in the spectra may be caused by amplitude-dependant non-linearities in the vehicle-tyre system or different vehicle vibration modes.

The seat movement, as shown by the relative displacement during the initial part of the motion (between I and V), is similar at all speeds and all the cab floor acceleration data show an exponentially decaying amplitude envelope (Figure 3A, 3B and 3C).

The acceleration waveform recorded on the cushion differs between top and bottom impacts. A severe bottom-stop impact causes a peak in the waveform as the cushion and the bottom buffer are compressed. A severe top-stop impact causes a negative peak closely followed by a positive peak as the driver parts company with the seat and returns. This was positively identified later from laboratory tests described in Chapter 5 as an artefact of the measurement method. During a severe top-stop impact, the waveform shows the acceleration experienced by the SAE pad, not necessarily that experienced by the cushion or the driver.

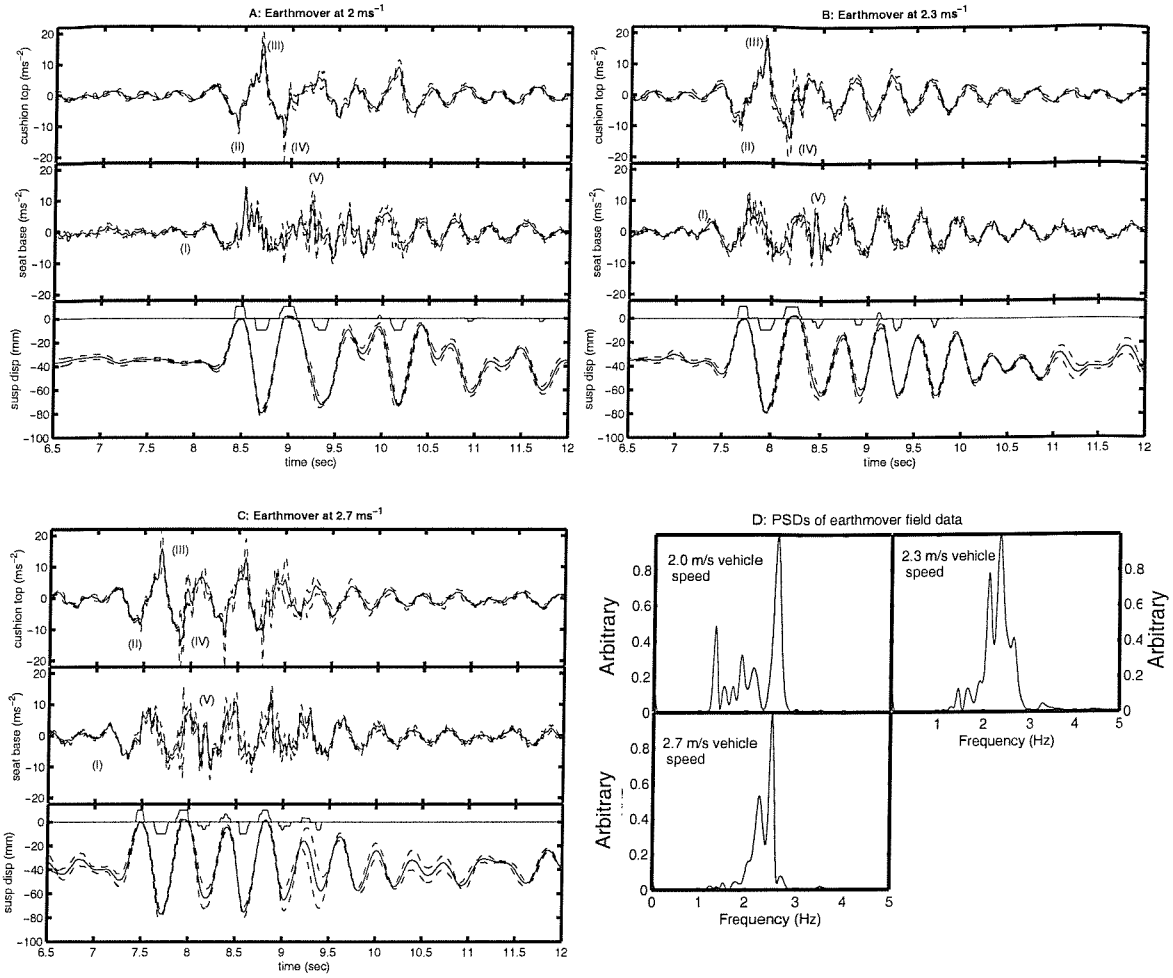

Figure 4-6 Mean of four earthmover seat motions measured in the field. The top graphs of A, B and C show the acceleration on the seat cushion. The middle graphs show the acceleration on the cab floor. The lower graphs show the displacement of the seat suspension relative to the cab floor and the output signals from switches detecting contact with the end-stop buffers. In all cases the dashed lines indicate ±1 standard deviation. Graph D shows the power spectral densities of the data shown in A, B and C.

4.4.3.3 Forestry Forwarder

Figure 4-7 shows data obtained using the forestry forwarder at three speeds over the test obstacle. The data were obtained using two drivers of 55 kg and 94 kg and a relatively light seat suspension damper. Figure 4-7A is the average of 5 runs, Figure 4-7B the average of 7 runs and Figure 4-7C the average of 3 runs. Each graph shows a transient event (I) as the first pair of wheels passed over the obstacle sometimes leading to a bottom stop end-stop impact (II). The second event (III) was caused by the second pair of wheels. This motion also caused bottom stop end-stop impacts (IV). These were particularly severe with the vehicle travelling at the highest speed of 1.39 ms^{-1} (Figure 4-7C). The motion caused by the first of the two pairs of trailing

wheels is also visible on graph C. The trailing wheels caused lower magnitude cab floor accelerations than the leading pairs.

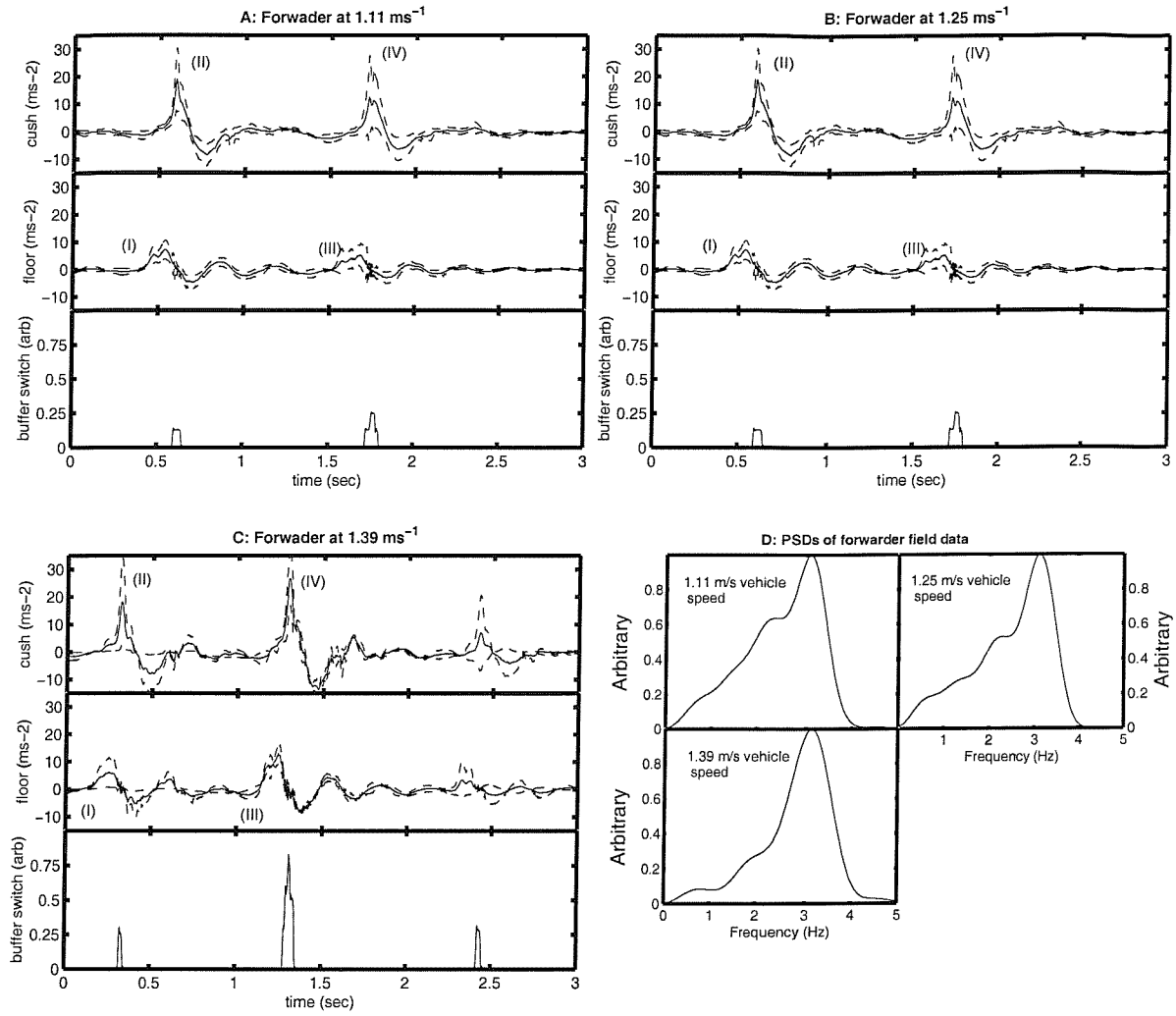

Figure 4-7 Mean forestry forwarder seat motions measured in the field. The top graphs of A, B and C show the acceleration on the seat cushion. The middle graphs show the acceleration on the cab floor. The lower graphs show the displacement of the seat suspension relative to the cab floor and the output signals from switches detecting contact with the end-stop buffers. In all cases the dashed lines indicate ±1 standard deviation. Graph D shows the power spectral densities of the data shown in A, B and C.

4.4.4 End-stop impact occurrence data using the earthmover seat

The earthmover field trials used microswitches to detect contact with either the top or bottom end-stop buffers and involved test runs with and without seat belts and with different driver weights. It was therefore possible to investigate the effect of these factors on the occurrence of end-stop impacts, while recognizing that the results were obtained with a single specific combination of terrain, vehicle and seat.

Figure 4-8 compares the effect on the number of end-stop impacts of wearing a lap belt. Both drivers and top and bottom stops are considered separately. Statistical treatment was not used as there was only a single test run for each condition, but there does not appear to be a large difference between runs with a seat belt and runs without.

Figure 4-9 compares the effect of driver weight on the number of end-stop impacts (with and without seat belt) recorded at each stop. At the top stop for four out of the seven speeds the heavier driver experienced a greater number of end stop impacts, while at the bottom stop for three out of the seven speeds the lighter driver experienced more impacts. In only two cases is the difference greater than 2.0 recorded impact events. It is possible that the seat was not adjusted to the same mid-ride position for both drivers although efforts were made to ensure that consistent seat adjustment settings were used and that the mid-ride positions were close to the mid point of the seat free travel. It was tentatively assumed that driver weight does not have a large effect on the occurrence of end-stop impacts pending further information.

Figure 4-10 compares the number of end-stop impacts recorded at each buffer for all conditions (both drivers with and without seat belt). At all vehicle speeds apart from 1 ms^{-1} (the slowest, no impacts recorded) and 2.7 ms^{-1} (the fastest), there are more bottom stop impacts recorded than top stop impacts at all except the highest vehicle speed. There are a number of possible reasons for this asymmetry including the characteristics of the motion at the seat base, non-linearity of the seat components, the seat adjustment or non-linearities due to the vehicle operator.

Figure 4-11 shows the total recorded end-stop impacts with increasing vehicle speed. The number of impacts recorded shows a sequential and almost linear rise with increasing vehicle speed.

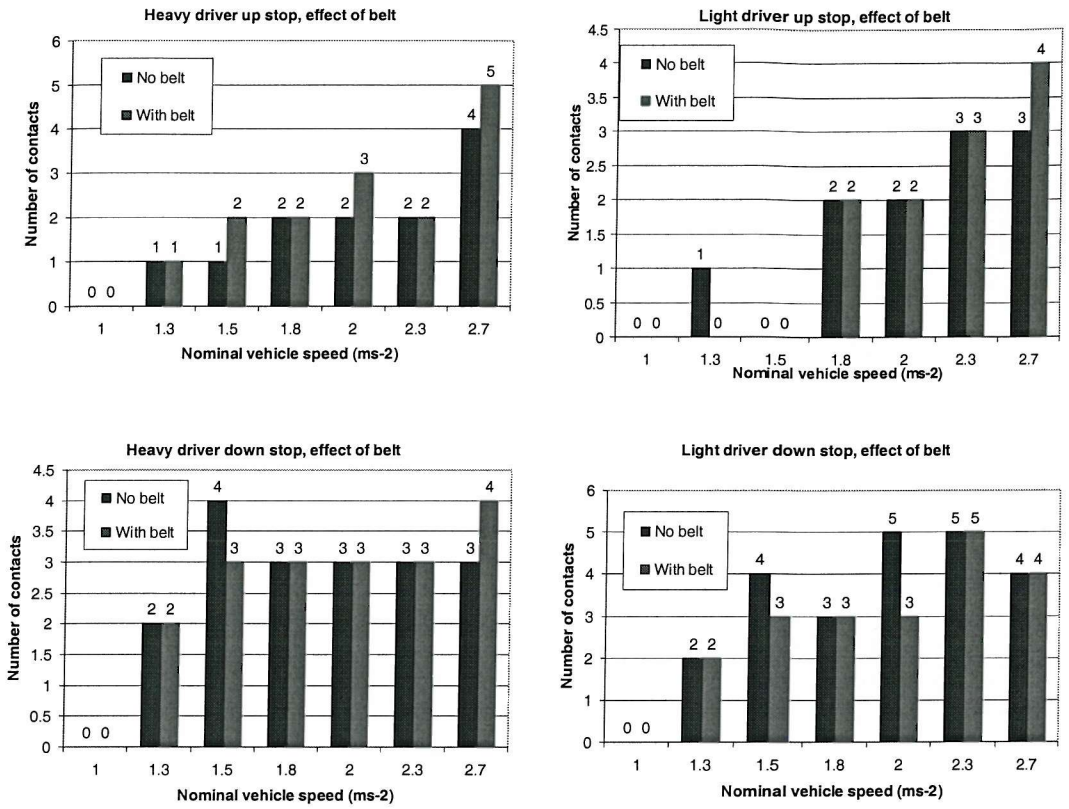

Figure 4-8 Effect of wearing a seat belt on the occurrence of end-stop impacts. The drivers and top (up) and bottom (down) end stops are considered separately.

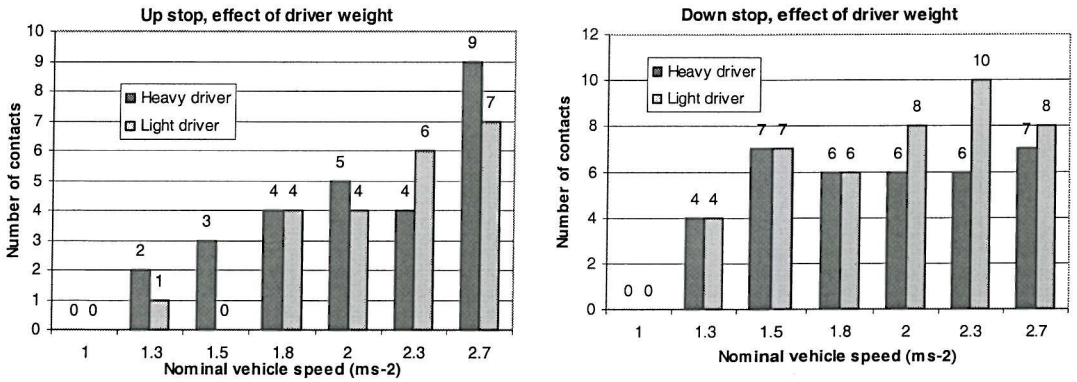

Figure 4-9 Effect of driver weight on the occurrence of end-stop impacts. Top and bottom stops considered separately.

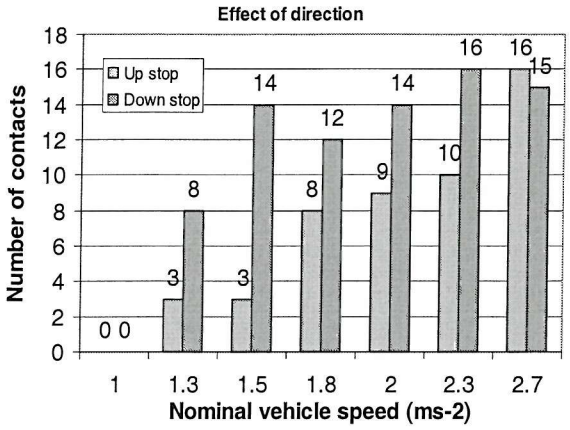

Figure 4-10 Comparison of the number of end-stop impacts recorded at the top (up) and bottom (down) buffers. Both drivers weights with and without seat belts included.

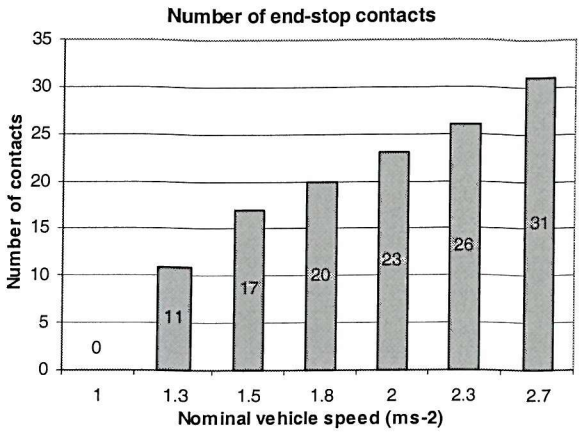

Figure 4-11 Total number of end-stop impacts recorded at both stops with both drivers with and without seat belt.

4.4.4.1 Summary of the earthmover end-stop impact occurrence data

The following observations were made from the limited amount of data available:

- The occurrence of end-stop impacts was not strongly affected by the wearing of a seat belt.
- The occurrence of end-stop impacts may be affected by the weight of the driver, but this effect is not obvious from the data available.
- More impacts occurred at the bottom stop than at the top stop at most speeds.
- The total number of end-stop impacts increased sequentially with increasing vehicle speed.

4.5 Requirements of a standard cab floor motion

There are a number of required and desirable features of an input motion for testing suspension seats in the laboratory for end-stop impact performance.

4.5.1 Means of definition

An input motion may be defined as a mathematical function of time, as a mathematical function of frequency, or point by point as a time history.

The use of filtered random motions defined in terms of filter functions in the frequency domain is not desirable for this test. A short test for a non-linear system requires a repeatable time history.

Defining the motion as a time history would require that the time history can be supplied to test laboratories in a useable format. This would allow the use of complex motions such as digitised field measurements. Supplying the data on paper (as in 78/764/EEC, 1999) is possible, but requires each laboratory to manually enter the data values. Supplying the time history as a standardised electronic format is a more convenient alternative but the electronic form of the input signal must be made available, requiring additional administration.

Defining the motion as a function of time allows a test laboratory to exactly generate the input motions. However, a complex input motion is likely to require a complex equation.

4.5.2 Shaker performance

Suspension seat test stimuli in some current standards have peak displacements of approximately 55 mm (ISO 7096:2000 Class 1) and peak accelerations of approximately 8 ms^{-2} (ISO 5007:1990 Class 1). Test laboratories have equipment capable of reproducing these motions.

Electro-hydraulic shakers are driven using displacement or acceleration waveforms, but any given shaker may not be configured to accept both. It is therefore desirable to define an input signal in terms of acceleration and displacement to ensure that it can always be input directly.

4.5.3 Realism

The cab floor motion 'events' that caused seat suspension end-stop impacts in the field appear to be similar on repeated runs over a single obstacle. However, the tractor data suggest that considerable variation in amplitude envelope might be expected in operational conditions.

Interaction between motions caused by consecutive pairs of wheels only appeared to be an issue with the earthmover motions. The tractor motions do not show obvious effects of two pairs of wheels and the forwarder motions due to each pair of wheels are well separated. The most severe end-stop impacts occurred during the initial part of the earthmover floor motion. The later part of the motion during and after the vibration as the second pair of wheels contacted the obstacle is therefore of less importance.

Analysis of the field data suggests that a suitable signal would be narrow-band, or sinusoidal, close to the main vehicle resonance frequency. A signal might be between 1 and 7 seconds in duration, depending on the vehicle and terrain and modulated by a suitable rising and falling envelope to fit vehicle motions which can lead to severe end-stop impacts. The falling envelope as seen on the field data was often an exponential decay. However, end-stop impacts did not occur during this part of the motion so it does not appear to be essential to reproduce this part of the motion exactly at the expense of other factors.

4.6 A possible input motion

An input motion is suggested using the following equation:

$$\frac{d^2x(t)}{dt^2} = -A \cdot \sin(2 \cdot \pi \cdot f \cdot t) \cdot \sin\left(\frac{\pi \cdot f \cdot t}{n}\right) \qquad \text{Equation 4-1}$$

over the range $t=0$ to $t=n/f$ where A is the peak acceleration, f is the frequency of the sinusoid in Hz, n is the number of cycles of the sinusoid within the envelope and t is time.

The motion consists of a sinusoid of a specified number of cycles modulated by a half-sine envelope and an exact equation can be obtained for the equivalent displacement waveform. The number of cycles should be chosen as $n=m+0.5$ where m is a positive integer (e.g. n=1.5, 2.5, 3.5...). If this condition is satisfied, the displacement, velocity and acceleration waveforms will start and end at zero, as shown in the following equations. The motion can therefore be reproduced repeatedly on a shaker without the need to include high pass 'washout' filters or reset the shaker platform position after each motion.

The displacement can be obtained from integrating the acceleration twice with respect to time:

$$x(t) = -\iint \sin(2\pi ft)\sin\left(\frac{\pi ft}{n}\right) dtdt \qquad \text{Equation 4-2}$$

Using the trigonometric identity $2\sin A \sin B = \cos(A-B) - \cos(A+B)$, the displacement becomes:

$$x(t) = -\iint \frac{1}{2}\left[\cos\left(2\pi ft - \frac{\pi ft}{n}\right) - \cos\left(2\pi ft + \frac{\pi ft}{n}\right)\right] dtdt \qquad \text{Equation 4-3}$$

$$\therefore x(t) = -\frac{1}{2}\iint\left[\cos\left(\pi ft\left(2-\frac{1}{n}\right)\right)-\cos\left(\pi ft\left(2+\frac{1}{n}\right)\right)\right]dtdt \qquad \text{Equation 4-4}$$

$$\therefore x(t) = -\frac{1}{2}\int\left[\frac{\sin\left(\pi ft\left(2-\frac{1}{n}\right)\right)}{\pi f\left(2-\frac{1}{n}\right)}-\frac{\sin\left(\pi ft\left(2+\frac{1}{n}\right)\right)}{\pi f\left(2+\frac{1}{n}\right)}+C\right]dt \qquad \text{Equation 4-5}$$

$$\therefore x(t) = -\frac{1}{2}\left[-\frac{\cos\left(\pi ft\left(2-\frac{1}{n}\right)\right)}{\left(\pi f\left(2-\frac{1}{n}\right)\right)^2}+\frac{\cos\left(\pi ft\left(2+\frac{1}{n}\right)\right)}{\left(\pi f\left(2+\frac{1}{n}\right)\right)^2}\right]+Ct+D \qquad \text{Equation 4-6}$$

Substituting for an initial condition of *x(t)=0* at *t=0* gives a value for C of zero and a value for D of:

$$D = \frac{1}{2\left(\pi f\left(2-\frac{1}{n}\right)\right)^2}-\frac{1}{2\left(\pi f\left(2+\frac{1}{n}\right)\right)^2} \qquad \text{Equation 4-7}$$

This constant can be included within the displacement equation:

$$\therefore x(t) = -\frac{1}{2}\left[\frac{\cos\left(\pi ft\left(2+\frac{1}{n}\right)\right)-1}{\left(\pi f\left(2+\frac{1}{n}\right)\right)^2}-\frac{\cos\left(\pi ft\left(2-\frac{1}{n}\right)\right)-1}{\left(\pi f\left(2-\frac{1}{n}\right)\right)^2}\right] \qquad \text{Equation 4-8}$$

At $t=n/f$, the numerator cosine functions become $\cos(2\pi n \pm \pi)$ which are equal to 1 if a half-integer value of n is used. This gives a value of zero for the displacement at this time.

Three test motions were used in the laboratory, with values for n of 1.5, 4.5 and 11.5. These values were chosen to give similar waveform shapes as observed for the forwarder, earthmover and agricultural tractor field trials respectively and to give a range of input durations for use in the remainder of the thesis ranging from a short, shock-like motion to a more steady state motion. The three motions are shown in terms of acceleration and displacement in Figure 4-12.

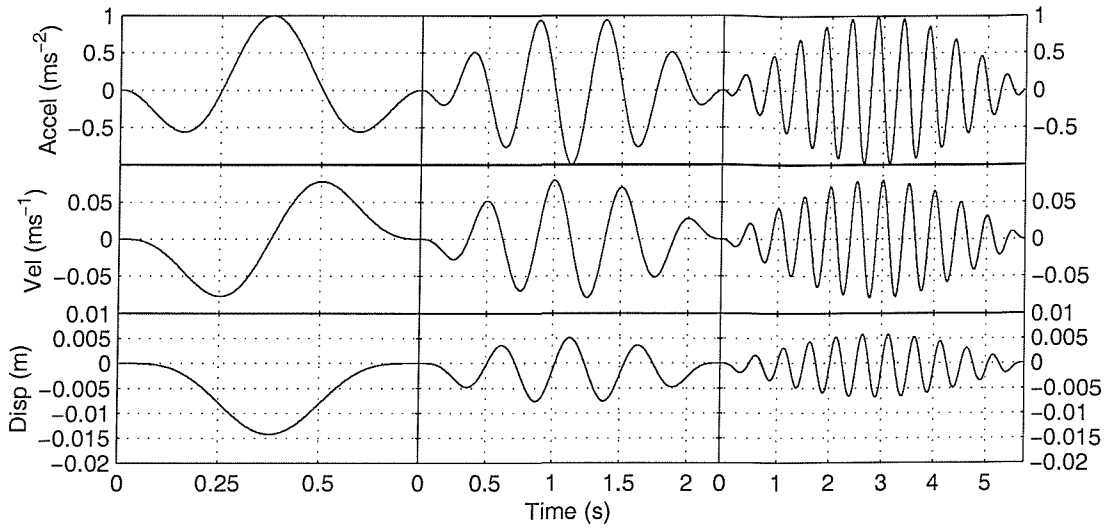

Figure 4-12 The time histories of the 1.5, 4.5 and 11.5 cycle duration input motions shown in terms of acceleration, velocity and displacement with an arbitrary 1 ms^{-2} peak acceleration at 2 Hz.

4.7 Comparison of laboratory and field data

Motions were generated using Equation 4-1 and reproduced in the laboratory using the 1m vertical shaker. The seats were the units that had been used in the vehicles the field trials and accelerometers were positioned at the seat base and on the seat surface with an LVDT to measure the seat suspension displacement. The data shown are from tests using a 78 kg 1.78m subject.

Figure 4-13A compares a 2.5 Hz 11.5 cycle motion with sample 2 from the agricultural tractor field trials. The laboratory motion is of a slightly higher frequency that the field data and a severe top stop impact at around t=5.5 seconds does not occur in the laboratory due to differences in the automatic stroke length adjustment featured on this model of seat which was disabled during the laboratory tests. The waveforms are otherwise similar.

Figure 4-13B compares a 2 Hz 4.5 cycle motion with data from the earthmover at 2.3 ms^{-1}. The waveforms are similar up to the point where the rear wheels contacted the obstacle and acted to reduce the amplitude of the field data (t = 8.4 seconds). Local maxima and minima occur at the same times in the laboratory and the field and the waveform shapes around the severe bottom and top buffer impacts are similar.

Figure 4-13C compares a 3.15 Hz 1.5 cycle motion with data from the forestry forwarder field trials shown in Figure 4-7C. The severe bottom stop impact observed in the field is reproduced well in the laboratory.

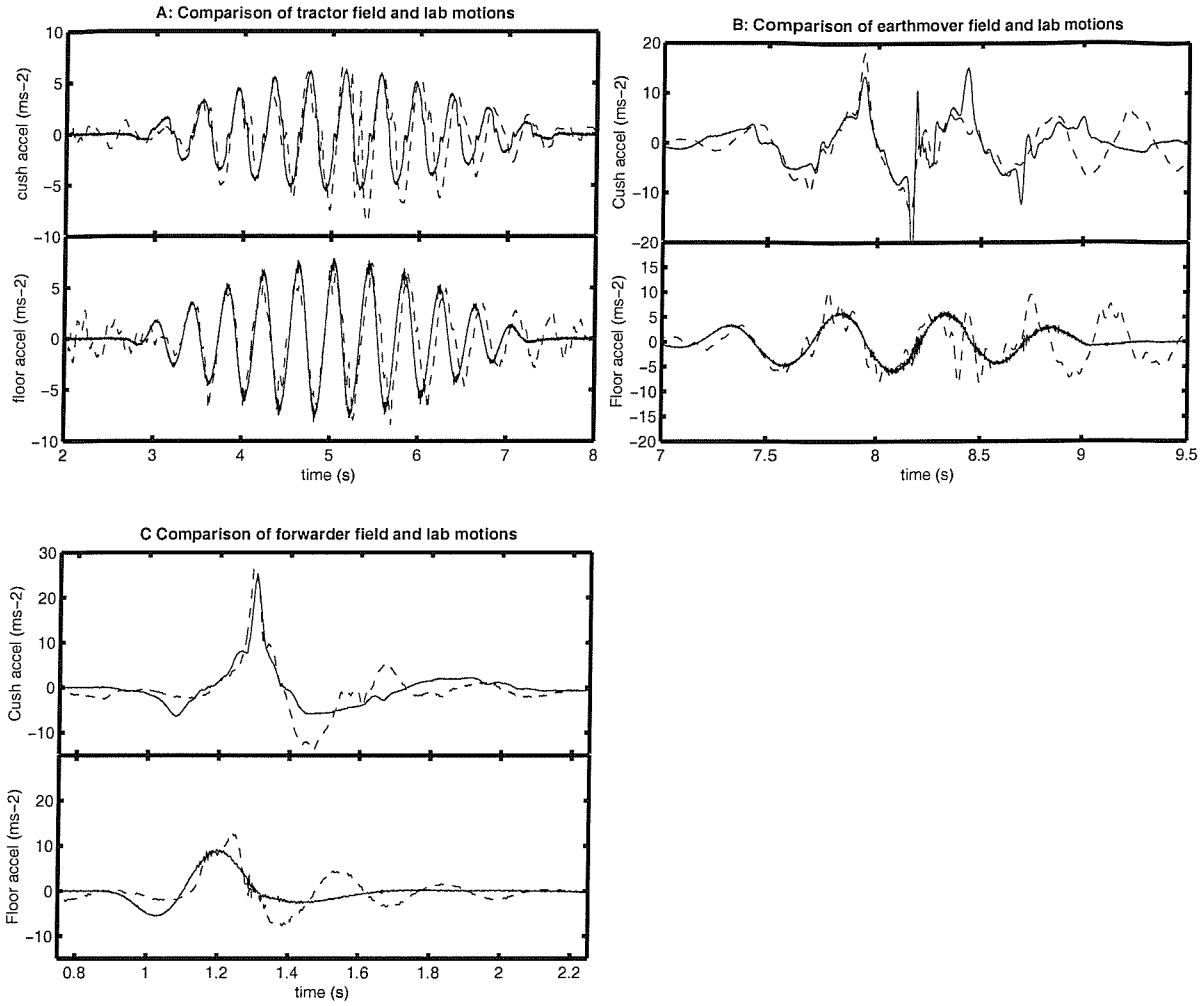

Figure 4-13 Comparison of laboratory and field measurements. The field data are shown as dotted lines, the laboratory data as solid lines.

4.8 Conclusions

This study was based on data obtained using a small sample of vehicles and terrains. However, it was possible to make some observations that may be generally applicable.

The cab floor motions which caused end-stop impacts were narrow-band and 'events' could be identified where the amplitude envelope of the acceleration time history was higher than adjacent sections. Events of between 1 and 7 seconds were observed in field data. The rise of the envelope varied from several cycles seen in some examples of the agricultural tractor data to within one cycle of motion for the forwarder. An exponential decay envelope was often seen in the cab floor motions of all three

vehicles. It may be that the rise was influenced primarily by the terrain, with an area of rough ground causing the relatively slow rise seen on the tractor and a sudden drop causing the rapid rise seen on the forwarder. The envelope decay may have been primarily influenced by the free response of the vehicle mass on the tyres and end-stop impacts were not usually found to occur during this section of the motion. Results from one vehicle suggested that the occurrence of end-stop impacts was not strongly affected by the driver weight or by the wearing of a lap belt.

The test motions do not include higher frequency components which might be caused by other sources of vehicle vibration besides the oscillation of the vehicle on the tyres, such as the engine attached implements such as excavating buckets, spray booms, etc. These higher frequency motions are more easily isolated by suspension seats and were not observed to be responsible for the large seat displacements that might lead to end-stop impacts. A benefit of using a simple signal as the input to a non-linear system is that visual examination of the resulting time histories produced by the system can provide useful clues to the details of the system behaviour. Visual examination of the motions produced in response to a band-limited pseudo-random or other multi-frequency motion would be less informative than visual examination of the system response to a simple, sinusoidal input.

The suggested motions are simple to generate and capable of producing similar seat behaviour in the laboratory as seen in the field. Three motions are suggested as possible input motions for testing three types of vehicle. However, it would be beneficial to investigate more field data in order to specify suitable motions for a wider range of vehicles and terrain. The three durations of motion used in this experiment were all considered realistic while providing a range of test conditions from a shock-like input (1.5 cycles) as might be caused by the vehicle falling off the edge of an obstacle to a more steady state (11.5 cycle) input representative of a vehicle on a rough track.

5 Suspension seat performance with three loading methods

5.1 Introduction

The first objective of this chapter was to compare the performance of suspension seats using three different loading conditions over a realistic range of frequencies and magnitudes of input vibration. The three loading conditions were human subjects, an anthropodynamic dummy designed to simulate the apparent mass of a seated human and a semi-rigid mass consisting of bags of lead shot within a rigid shell. It was hypothesised that the seat performance would be independent of the type of load used and that the seat performance would depend on the mass of the subjects.

The second objective for this chapter was to obtain a comprehensive and systematic set of laboratory data for later comparison with the mathematical model.

5.2 Method

5.2.1 Overview

A series of tests was carried out on three seats using the three input motions defined in Chapter 4 (1.5 cycle, 4.5 cycle and 11.5 cycle windowed sinusoids shown in Figure 5-1) with three loading conditions, a semi-rigid mass, an anthropodynamic dummy and twelve human subjects. The seats were tested at five frequencies from 1.25 Hz to 3.15 Hz. The lowest frequency was lower than would be expected on the cab floor of a wheeled off-road vehicle and the highest frequency would not be expected to cause end-stop impacts on an off-road vehicle suspension seat within the range of motions that can be safely reproduced in the laboratory. The inputs were reproduced using the 1m vertical stroke electo-hydraulic shaker, described in Chapter 3, at magnitudes that resulted in W_b-weighted VDVs at the seat base of between 0.5 and 4 $ms^{-1.75}$.

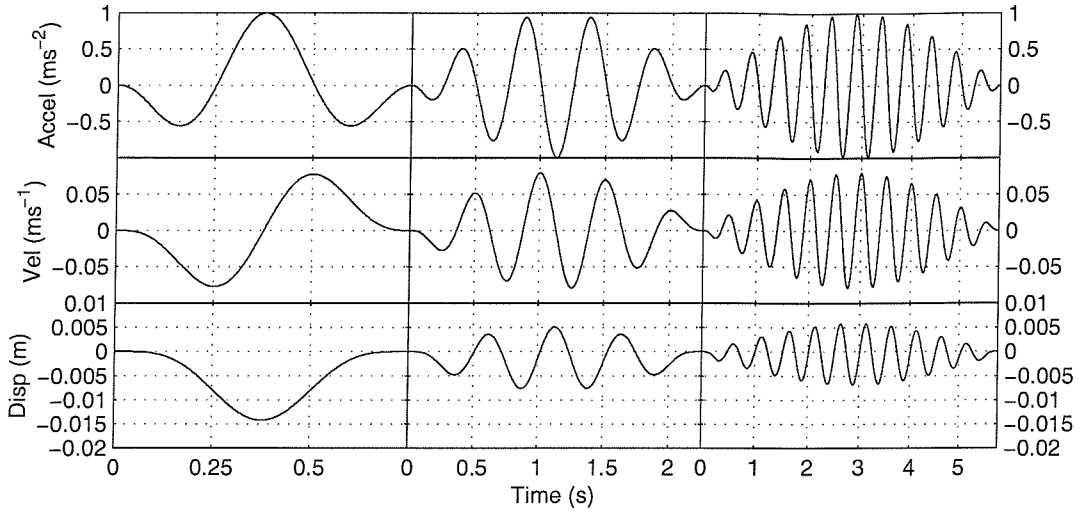

Figure 5-1 The time histories of the 1.5, 4.5 and 11.5 cycle duration input motions shown in terms of acceleration, velocity and displacement with an arbitrary 1 ms^{-2} peak acceleration at 2 Hz.

5.2.2 Loading conditions

5.2.2.1 Human Subjects

Antropometric data for the 12 human subjects that took part in this experiment are shown in Table 5-1. Subjects were selected to provide a mass distribution centred close to the 77 kg equivalent static mass of the anthropodynamic dummy. No other selection criteria were used except for the safety and ethics procedures relating to human subject testing as described in Chapter 3.

Table 5-1 Human subject anthropometric data

Subject number	1	2	3	4	5	6	7	8	9	10	11	12	mean
Sex (m/f)	f	m	f	m	f	m	f	m	m	m	m	m	-
Mass (kg)	68	70	58	87	70	78	56	98	81	88	82	76	76
Stature (m)	1.68	1.71	1.65	1.83	1.65	1.81	1.70	1.83	1.78	1.90	1.80	1.81	1.77
Age (years)	26	43	24	32	24	28	19	51	31	23	63	27	33

5.2.2.2 The anthropodynamic dummy

Anthropodynamic dummies are mechanical devices intended to simulate some aspect of the dynamic response of the human body. The specific device used in this thesis was designed to simulate the impedance of the seated human body at the point of contact with the seat cushion when exposed to vertical vibration. This device allows seat testing to be performed without the need to expose human subjects to vibration and avoids the associated inter- and intra-subject variability issues. This is of particular interest to

suspension seat testing as the magnitudes of vibration found on suspension seats can easily exceed the suggested maximum daily vibration dose value of 15 $ms^{1.75}$ (BS6841, 1987).

The specific device used in this experiments for this chapter of the thesis was described by Lewis (1998) and is shown photographically and schematically in Figure 5-2. This device was developed from an initial prototype described by Mansfield and Griffin (1996). The device contacted the seat cushion using a SIT-BAR indenter (Whitham and Griffin, 1977). A second SIT-BAR was used to contact the backrest. This backrest indenter was attached to the backrest and articulated to allow the dummy to move freely in the vertical direction.

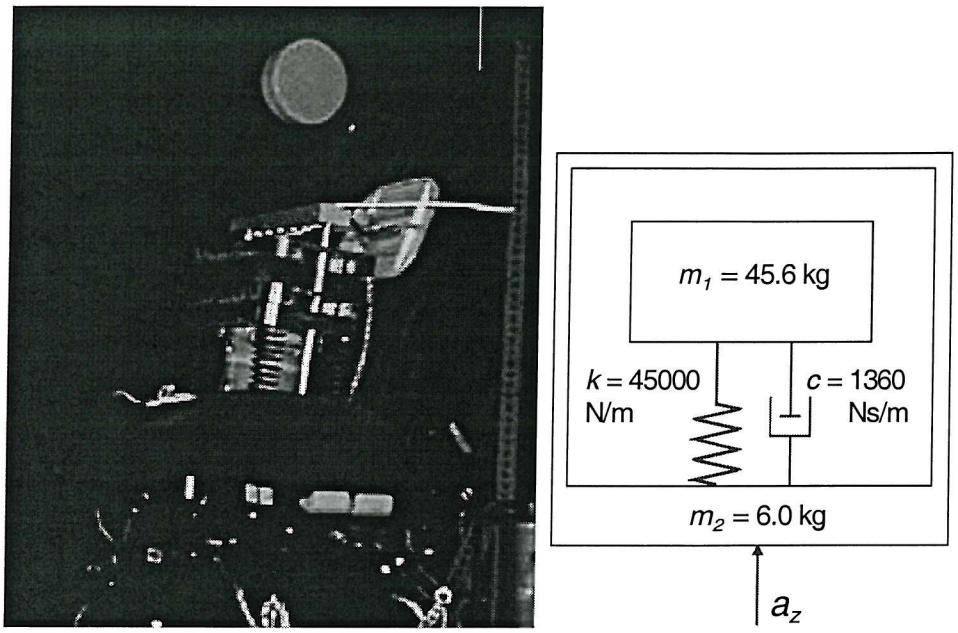

Figure 5-2 Photograph and schematic of the anthropodynamic dummy described by Lewis (1998). The schematic is taken from that publication. Note that the dummy configuration as used in the thesis had a case mass of 10 kg and an upper mass of 46 kg.

The apparent mass of the theoretical anthropodynamic dummy system as compared with the normalised apparent masses of 60 subjects (measured by Fairley and Griffin, 1989) is shown in Figure 5-3. The measured response of the dummy is shown in Figure 5-4. The anthropodynamic dummy was used in this configuration for the tests described in this chapter.

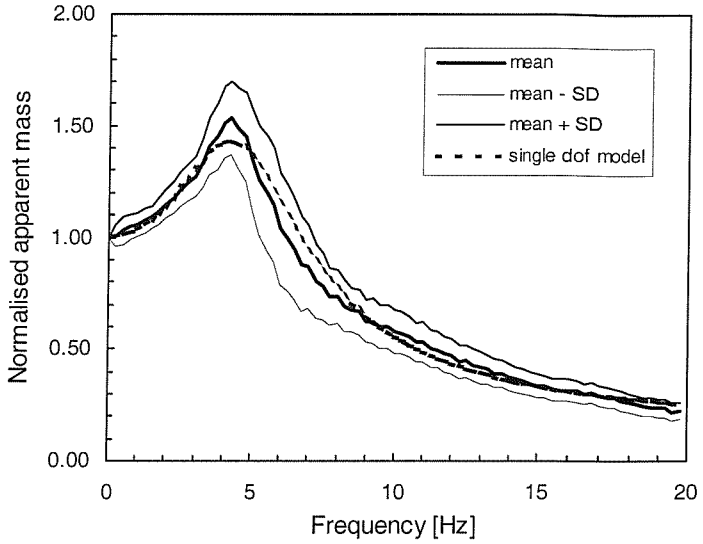

Figure 5-3 The normalised apparent mass of a single degree-of-freedom mechanical system compared to the mean apparent mass of sixty seated human subjects ± 1 standard deviation (from Lewis, 1998, after Fairley and Griffin, 1989).

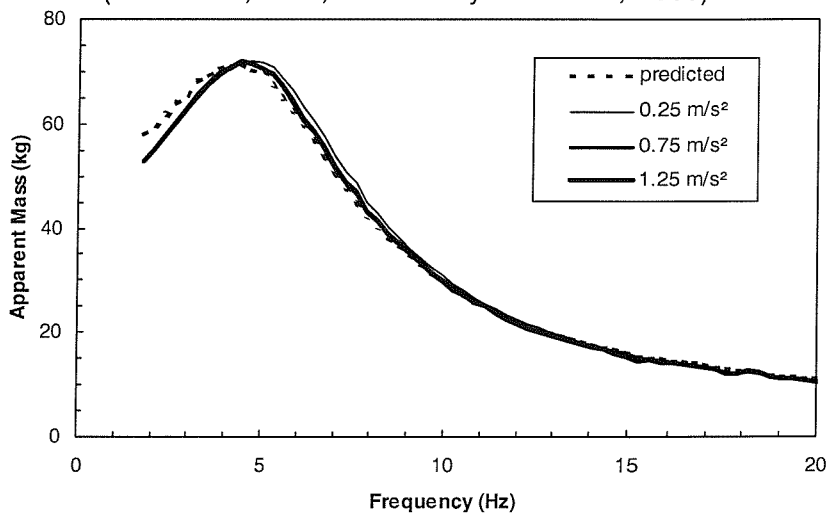

Figure 5-4 The measured apparent mass of the anthropodynamic dummy at three magnitudes of vibration (from Lewis, 1998)

The centre of mass of the dummy was located on the seat surface 40 mm forwards of the seat index point (SIP). This point is defined by ISO 5353 (1999) and is shown in Figure 5-5. The dummy rested against the backrest using an articulated indenter to allow the dummy to move unimpeded in the vertical direction. The backrest indenter plate was fastened by adhesive tape to the backrest so that the indenter could compress the

backrest foam but not lift free of the foam or move translationally across the backrest surface.

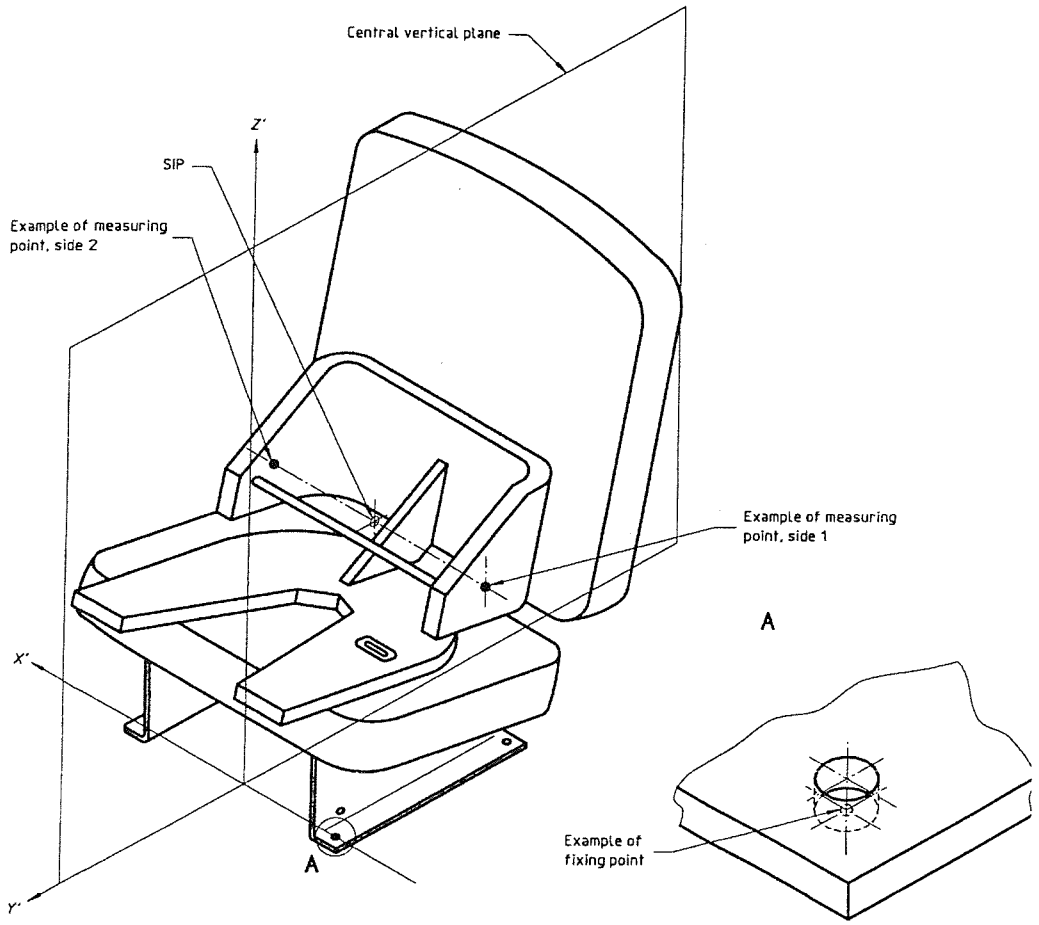

Figure 5-5 The seat index point (SIP) as defined by ISO 5353(1999). The dimensions of the device shown on the seat surface are defined by the standard.

5.2.2.3 The semi-rigid mass

The semi-rigid mass consisted of the H-point measurement device described in ISO 5353 (1978) without additional leg or masses. This device was ballasted with lead shot in 10 kg bags up to a total mass of 54 kg, statically equivalent to a 76 kg human if 71% of the body mass is supported on the seat (Lowe, 1972). The upper part of the device designed to contact a backrest was fixed at an angle 10° forward of the vertical, out of contact with the backrest of the test seats. The centre of mass of the device was 40 mm forwards of the

seat index point. The ballasted H-point device was positioned on the seat surface with approximately 5 mm clearance between the load and the seat backrest, avoiding any shear-like interaction between the mass and the backrest. Figure 5-6 shows the semi-rigid mass positioned on one of the test seats.

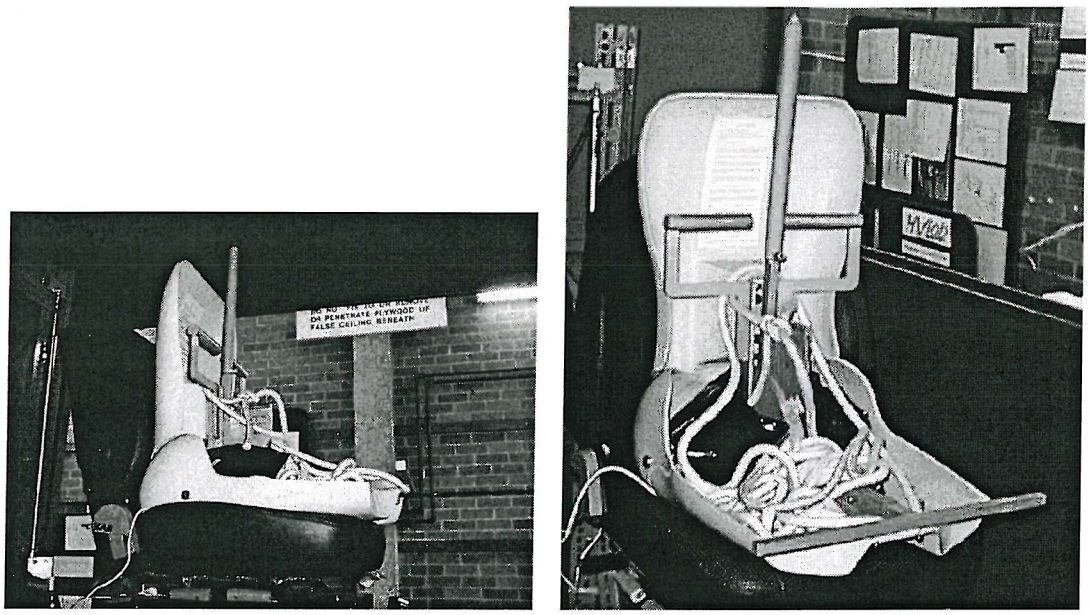

Figure 5-6 Views of the H-point device shell ballasted with lead shot bags.

5.2.3 Data acquisition

Data were acquired at 1000 samples per second via a 330 Hz anti-aliasing filter using an *HVLab* data acquisition and analysis system. Data were acquired from 0.5 seconds before the start of the motion to 1 second after the end of the motion. The following channels were acquired:

1. The vertical acceleration at the interface between the seat cushion and the seat load.
2. The vertical acceleration at the top of the seat suspension mechanism, underneath the cushion.
3. The vertical acceleration at the base of the seat.
4. The relative vertical displacement between the shaker platform and the top of the suspension mechanism using the LVDT described in Chapter 3.

The vibration experienced by the subjects was measured according to ISO10326-1 (1992) using a semi-rigid disk containing an accelerometer positioned between the seat cushion and the ischial tuberosities. The vertical vibration on the semi-rigid mass was measured using the disk containing an accelerometer securely attached to the underside of the mass, vertically in line with the SIP. The vertical vibration on the dummy was measured using an accelerometer attached to the upper surface of the seat indenter plate. The accelerometer attached to the base plate of the dummy was in the order of 20 mm forward of the SIP. The base plate rotation of the dummy was locked once the dummy had been positioned on the seat so the accelerometer position was not expected to affect the results in comparison with the other loading conditions.

The acceleration at the base of the seat was measured using an accelerometer positioned within 10 cm of the SIP as projected vertically onto the shaker platform surface.

The relative displacement between the suspension mass and the shaker platform was measured using the LVDT described in Chapter 3. The LVDT was mounted vertically on the shaker platform with the sensing rod connected to a horizontal L-section aluminium bar attached to the upper part of the seat suspension mechanism.

Methods of detecting the contact between the suspension and the end-stop buffers using microswitches or foil contact switches were found to be unreliable. Foil contact switches placed between the end-stop buffer and the suspension mechanism did not survive the experiments and the sensing arms of microswitches positioned so as to detect a light impact did not survive a series of severe impacts. End-stop buffer contact was instead deduced from the measurement of the relative displacement of the suspension.

Figure 5-7 shows schematically the locations of the transducers when testing with the anthropodynamic dummy.

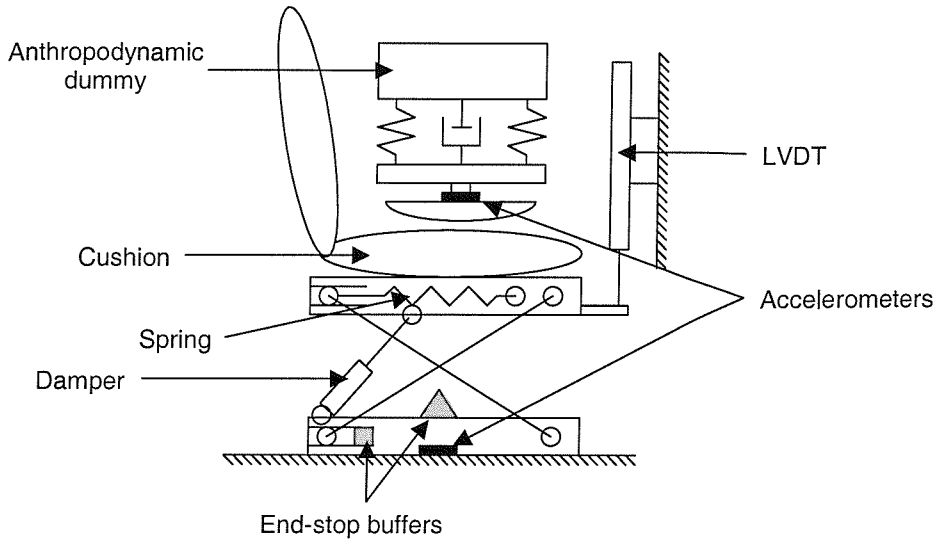

Figure 5-7 Transducer locations

5.2.4 Experimental procedure.

The seat was mounted on the shaker with a footrest positioned to comply with the recommendations of the agricultural tractor seat test standard 78/764/EEC (1999). One seat was mounted on the shaker at a time. Subjects were instructed to maintain a relaxed posture while seated with their feet on the footrest and their hands in their laps holding an emergency stop button (see Figure 5-8). A seat belt was provided with fixing points on the shaker platform. The belt was fitted so as not to interfere with the motion of the subject even in the case of severe top stop impacts. The VDV experienced by the subjects was monitored throughout the experiment to ensure that the exposures did not approach the suggested action level of 15 $ms^{-1.75}$ (BS6841, 1987). Each subject was tested once for each combination of seat, waveform, frequency and magnitude. The tests with the dummy and the semi-rigid mass were repeated five times for each test condition.

The seat suspension preload was adjusted so that the suspension was at a point 10 mm below the mid point of the free travel between the end-stop buffers using a ±1 mm 4 Hz sinusoid to 'buzz' the suspension in order to cause the seat to break away from friction. This position was estimated to be close to the mid point of the total available travel as the lower bump stop on all three seats was thicker and softer than the top stop. The subject, dummy or mass occupied the seat for 3 minutes before the test commenced, inclusive of the time taken to adjust the suspension preload in order to allow the cushion to become accustomed to the load (see Chapter 6 for measurements of the time constant of one of the test cushions). The test motions were output to the shaker with a pause of approximately 5 seconds between each motion.

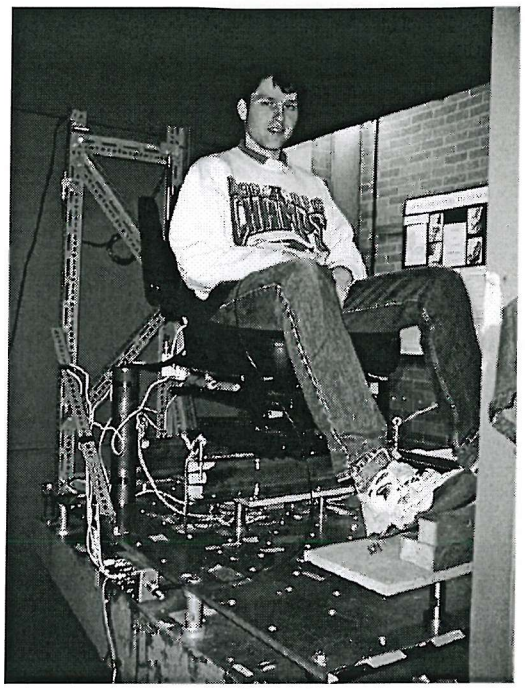

Figure 5-8 A subject on the earthmover seat

The presentation of seat, waveform and frequency to the subject was randomised. Each session consisted of tests on a randomly chosen seat. All three waveforms were tested during the session in a randomly chosen order. For each waveform the order of presentation of the five frequencies was also randomised. The amplitudes were presented in sequentially increasing order for the reasons described below. The range of test conditions is illustrated schematically in Figure 5-9.

The combinations of frequency, amplitude, signal, seat and load that would cause severe impacts could not be identified before the experiment began as the exact dynamic response of the seats was not known. The safety of the human subjects was essential so the experimental procedure was designed to carefully control the vibration exposure of each subject. The input motions for each frequency and waveform were generated at sixteen equally spaced magnitudes with a W_b-weighted vibration dose value from 0.5 $ms^{-1.75}$ up to 4.0 $ms^{-1.75}$. The cumulative VDV for the subject during each session was calculated after each motion and the tests at for a particular frequency were discontinued

once the cumulative VDV for that frequency exceeded 5 $ms^{-1.75}$. A total VDV for a session in excess of 9.8 $ms^{-1.75}$ was expected, this being the fourth power sum of fifteen 5 $ms^{-1.75}$ exposures resulting from tests with 5 frequencies and 3 waveforms. This is substantially less than the recommended maximum daily dose of 15 $ms^{-1.75}$ which corresponds to fifteen exposures of 7.6 $ms^{-1.75}$. The overall cumulative VDV for the session was also monitored to ensure that it did not approach 15 $ms^{-1.75}$.

The above approach resulted in fewer than 16 magnitudes of vibration being tested at some frequencies for safety reasons.

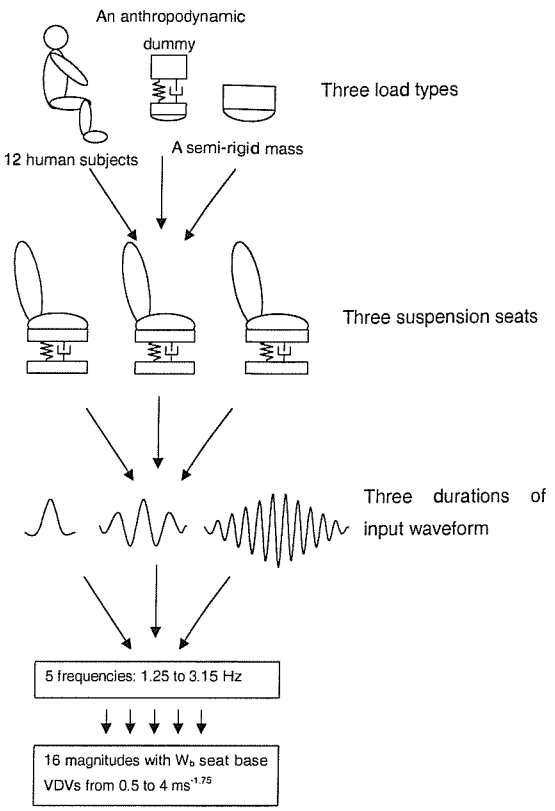

Figure 5-9 Schematic showing the range of test conditions

5.2.5 Data analysis

5.2.5.1 The SEAT value

The results obtained for all frequencies and magnitudes for each combination of seat, input waveform and load were expressed in terms of the difference in SEAT value obtained between the subjects and the dummy and the subjects and the semi-rigid mass. The SEAT value is defined as:

$$SEAT(\%) = \frac{VDV_{seat\_load}}{VDV_{seat\_base}}$$

with the vibration dose value (VDV) defined by

$$VDV = \left[\int a_w{}^4(t)dt\right]^{1/4}$$

where a_w is the BS 6841 (1987) W_b-weighted acceleration.

5.2.5.2 *Grouping by suspension seat 'stage'*

Due to the non-linear behaviour of the suspension seat-load system, a direct comparison of results between different frequencies or magnitudes was not possible. Efforts were made to divide the data into relevant groups within which the system behaviour was sufficiently similar for comparisons to be made.

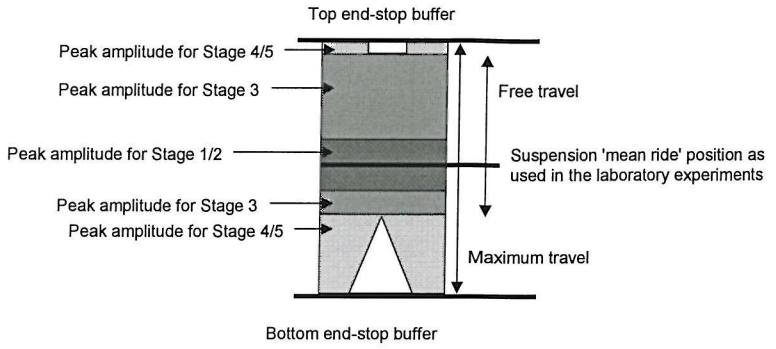

Figure 5-10 The amplitudes of seat suspension motion used to classify seat motion

The results for each test were grouped in terms of the stages of suspension seat performance in the amplitude domain suggested by Wu and Griffin (1996) and described in Chapter 2 and summarised in Table 5-2. For this study, these five stages were compacted into three, defined as follows and illustrated in Figure 5-10:

Table 5-2 A method of characterising suspension seat behaviour with changing input magnitude, summarised from Wu and Griffin (1996)

Stage 1	Low magnitudes with the seat suspension friction locked
Stage 2	'Breaking away' from friction
Stage 3	Moving relatively freely but not contacting the end-stop buffers
Stage 4	Mild to moderate end-stop impacts
Stage 5	Severe end-stop impacts

- Low magnitude seat motions with the suspension moving over less than ±15 mm. This arbitrary value represents about half of the free travel of the seat with the shortest stroke. The suspension friction is unrelated to the stroke of the seat so the same ±15 mm was used as the low magnitude region for all three seats. This region was intended to encompass stages 1 and 2 where the seat was friction locked or breaking away from friction.
- Medium magnitude seat motions with the peak suspension displacement greater than ±15 mm but without contact with the end-stop buffers. This was intended to encompass stage 3 where the seat was moving comparatively freely.
- High magnitude seat motions with the seat contacting the end-stop buffers on one or more occasions, corresponding to stages 4 and 5.

Each seat was considered separately but the results from the three waveform durations were grouped together.

5.2.6 Selection of data

5.2.6.1 Overview

Not all of the acquired data were found to be useful. Data were disregarded either due to electrical noise contamination (Section 5.2.6.2), severe impacts (Section 5.2.6.3) or to reduce bias caused by the lack of heavy subject data at high magnitudes (Section 5.2.6.4). Approximately 8000 tests were conducted during this experiment with each test producing 6 channels of acquired data. Each time history was visually inspected to check weather the data were acceptable.

5.2.6.2 Electrical noise

Due to an electrical problem caused by electrical noise from another piece of apparatus it was expected that some data would be discarded. The noise spikes were of less than 1 ms duration and contaminated approximately three percent of the acquired data with the spikes occurring on all channels simultaneously. Where possible the contaminated data were repaired. Each time history was examined visually and where the spike was in a relatively non-transient part of the motion (i.e. not coincidental with an end-stop impact or a friction jolt) the section of data including the spike was replaced. The time history was low pass filtered at 20 Hz using a zero-phase filter and the relevant section from this filtered time history was used to replace the contaminated section of the unfiltered data without introducing any discontinuity.

If the noise contamination was too severe to be corrected, or coincided with transient data, the measurement was discarded.

5.2.6.3 'Impact' noise

The impact noise occurred during severe top-stop impacts. It was not anticipated before the experiment began that difficulties would occur in the measurement of top-stop impacts. Preliminary tests had been made using the anthropodynamic dummy and these tests had not resulted in misleading measurements.

The data obtained during severe end-stop impacts, in particular top-stop impacts, was sometimes not useful due to interaction between the load and the transducer. The severe top-stop impacts could cause the load or the subject to be thrown clear of the seat surface. In the case of human subjects, once the subject was clear of the seat surface

there was no longer any force holding the transducer against the ischial tuberosities so some separation tended to occur. When the subject returned to the seat surface, the impact between the subject and the transducer could result in a misleading transient

Time histories obtained with the dummy and with one subject of similar equivalent mass (subject 8, 78 kg) are shown in Figure 5-11. The majority of the waveforms, in particular the peaks due to contact with the bottom stop (at 1.7 and 2.2 seconds), are similar. There is a difference in waveform shape in the vicinity of the relatively severe top stop impacts at 1.9 seconds, with the subject showing a greater magnitude of the transient event than the dummy.

Examination of the time histories obtained with all subjects indicated that the top stop transient tended to be of greater magnitude with heavier subjects. In the case of subject 7 (95 kg), the portion of the waveform from 1.8 to 2 seconds was responsible for an increase in VDV from 3 to 5 $ms^{-1.75}$.

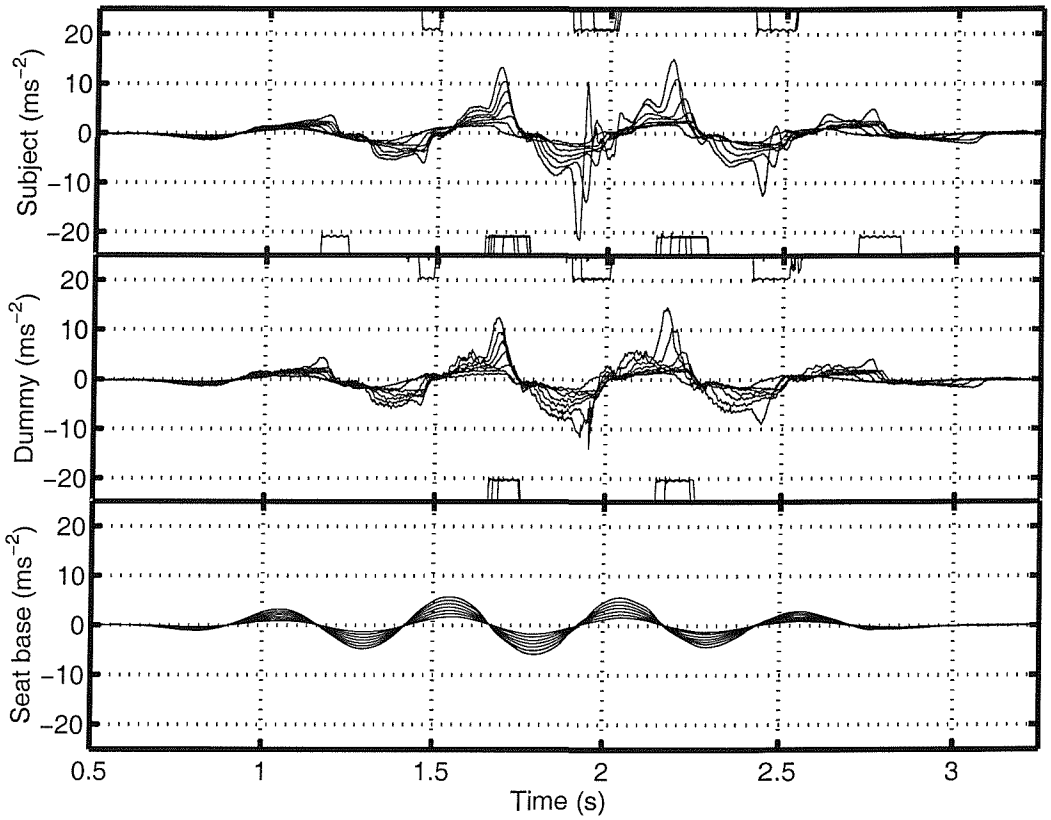

Figure 5-11 Acceleration on the SAE pad with a 78 kg subject (top graph), on the dummy cushion indenter plate (middle graph) and at the base of the seat (bottom graph) at 7 magnitudes of input motion. Also shown are the signals from microswitches detecting seat suspension top and bottom end-stop buffer contacts.

A better experimental arrangement would have been to secure the semi-rigid disk in some way to the subject. Ideally the transducer would be attached rigidly to the skeleton but this is impractical. The accepted procedure for taking measurements with human subjects on seats as described in ISO10326 (1992) specified that the semi-rigid disk should be loose between the subject and the seat, but this does not appear to be sufficient for measurements involving top-stop impacts. Any seat load time history acquired during this experiment showing the distinctive transient caused by an impact between the subject and the transducer was discarded as misleading. The SEAT values for human subjects used in this thesis are therefore for situations that do not involve severe top end-stop impacts.

For tests with the mass and the dummy, the transducer was attached directly to the structure of the device. This arrangement apparently produced more appropriate results in severe impact situations, but some severe impacts could cause the component parts of the semi-rigid mass to separate or the dummy to exceed its available stroke. In these situations an impact could occur within the load and was detected by the load accelerometer as a short burst of high amplitude wide-band acceleration. Any measurement showing this effect was also discarded.

5.2.6.4 Data missing due to safety limitations

Finally, the safe operation of the experiment as described in Section 5.2.4 required the tests to be halted before results were obtained for all 16 magnitudes of vibration for each condition if the cumulative vibration dose value experienced by a subject was too high. Heavier subjects tended to reach the safety cut-off level at a lower magnitude than lighter subjects. This resulted in incomplete sets of data at the higher magnitude due to the absence of results from the heavier subjects. It was expected that subject mass would correlate with the SEAT value at some magnitudes, so these incomplete datasets were expected to become increasingly biased as the number of measurements decreased leaving a set of subjects with a lower mean mass.

The median SEAT values were calculated from a minimum of 3 measurements with the semi-rigid mass or the dummy and a minimum of 10 measurements with subjects. If insufficient measurements were present then a mean SEAT value was not calculated.

5.3 Results

5.3.1 Overview

The results are displayed in terms of the SEAT value and relative suspension displacement in Appendix 2 and the results are discussed in the following sections. An example showing the results obtained with the 4.5 cycle test motion using the earthmover seat shown in Figure 5-12. The SEAT value calculated from the VDV measured at the load and the VDV at the base of the seat for each of the five test frequencies is shown in the left hand column and the peak suspension displacement (upwards and downwards) is shown in the right hand column.

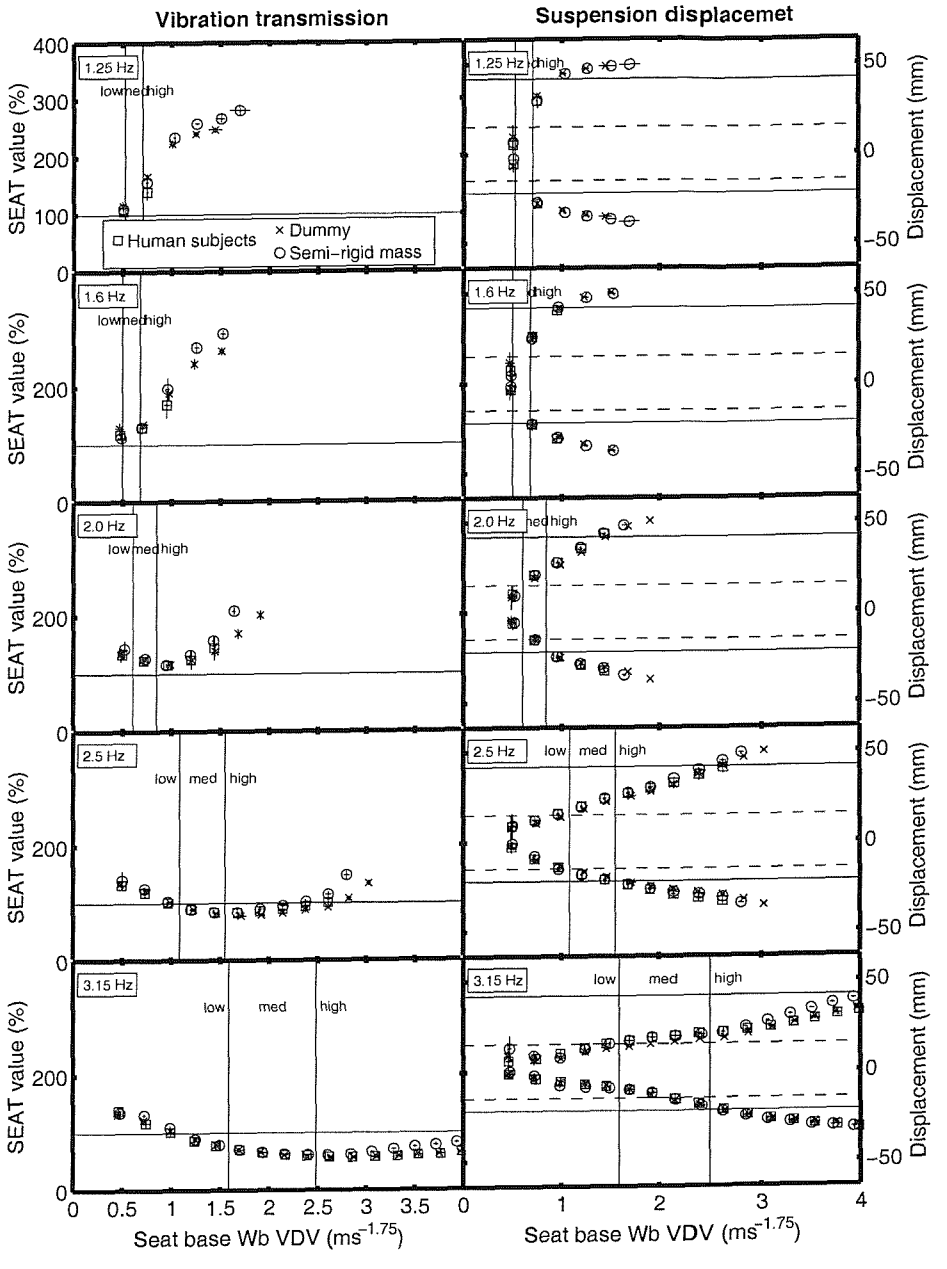

Figure 5-12 Mean SEAT values obtained with 12 subjects and 5 repeat tests with the anthropodynamic dummy and the semi-rigid mass for the earthmover seat with the 4.5 cycle input motion. The error bars indicate the inter-quartile range in the x and y axes.

5.3.2 The relationship between SEAT value and subject mass

5.3.2.1 Spearman's correlations

Spearman's Rho was used to test for a correlation between the subject mass and the SEAT value for each test condition. A heavier subject results in a lower resonance frequency for the system and so it was expected that there would be a negative correlation between SEAT value and subject mass for stage 3 motions (greater than 30 mm peak-to-peak suspension motion without end-stop impacts) at higher frequencies with the heavy subjects benefiting from better vibration isolation. It was also expected that there would be a positive correlation for situations involving end-stop impacts as better vibration isolation implies a greater relative displacement across the suspension mechanism causing end-stop impacts at lower magnitudes compared to lighter subjects. The results are shown in Appendix 3.

The obvious trends were for significant positive correlations at low frequencies where 49% of a total of 43 tests for all seats and test conditions at 1.25 Hz showed significant positive correlations (Spearman, $p<0.05$). At higher frequencies the opposite was found. At 3.15 Hz, 71% out of a total of 129 for all seats and test conditions showed significant negative correlations between SEAT value and subject mass (Spearman, $p<0.05$). The negative correlations at high frequencies corresponded to conditions where the heavier subjects would be expected to cause greater vibration isolation by lowering the resonance frequency of the seat-load system. The positive correlations at low frequencies may be due to the heavier subjects causing greater movement of the suspension with the seat-load system being exited at a frequency close to resonance, or may be due to the heavier subjects suffering more severe end-stop impacts. Of a total of 21 significant positive correlations at 1.25 Hz (Spearman, $p<0.05$), 57% occurred in situations without impacts and 43% in situations with impacts.

There was no statistically significant evidence for a transition from a negative correlation to a positive correlation with increasing input vibration magnitude for any one combination of seat, waveform or frequency. This situation might be expected as the seat-load system moves from isolating the vibration with the heaviest subjects benefiting most, to end-stop impact situations with the heavier subjects experiencing the most severe impacts. There were non-significant trends pointing to this effect. The forestry forwarder seat with the 11.5 cycle motion at 2 Hz showed significant ($p<0.05$) negative correlations before the occurrence of end-stop impacts and a non-significant positive correlation ($p=0.072$) with

end-stop impacts. However, there were also circumstances involving end-stop impacts showing a significant negative correlation between SEAT value and subject mass (the earthmover seat with the 4.5 cycle motion at 2 Hz).

5.3.2.2 Skewed distributions

A preliminary examination of the distribution of the SEAT values obtained with the twelve subjects for some test conditions showed one or two outlying values and a more closely bunched main group. This effect occurred in test conditions where some of the subjects were just experiencing end-stop impacts while other subjects were not. This effect was investigated further by evaluating the skewness of all results to identify conditions that showed a strongly skewed distribution and examining these test conditions in more detail.

A criterion for a skewed distribution has been suggested as where the absolute value for the skewness is less than twice the corresponding standard error (Brown, 1997). Of the 377 test conditions with human subjects, 90.7% were not classed as skewed using this criterion and 5.0% showed a value for the skewness up to three times the corresponding standard error so were classified as weakly skewed. The remaining 4.2% (16 test conditions) showed a strongly skewed distribution. These conditions were observed to corresponded to three situations:

Situation one: The agricultural tractor seat in end-stop impact situations (end-stop impacts only occurred on this seat with the shortest, 1.5 cycle test motion). Twelve out of fifteen test conditions showed skewed distributions. Examination of the SEAT values obtained for individual subjects showed the heaviest subject with a substantially higher SEAT value as shown in Figure 5-13.

Examination of the time histories corresponding to this result indicated that only the heaviest subjects were impacting the end-stop buffer and that the data did not appear to be faulty. Example time histories for three subjects, the two heaviest (subject 8, 98 kg and subject 10, 88 kg) and one close to the mean subject mass (subject 7, 76 kg) are shown in Figure 5-14. Although the heaviest subject shows a severe impact, an impact is also visible for the 88 kg subject.

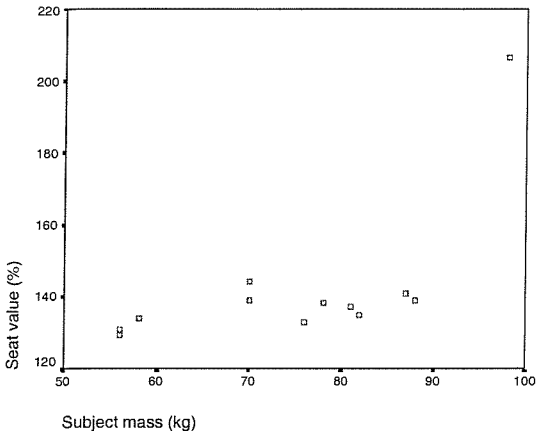

Figure 5-13 Scatterplot of subject mass and SEAT value for the agricultural tractor seat with the short (1.5 cycle) input motion in an end-stop impact situation (1.25 Hz with a seat base VDV of 1.9 $ms^{-1.75}$)

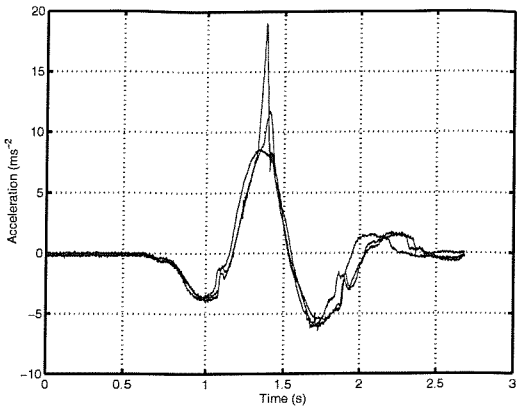

Figure 5-14 Time histories recorded at the subjects for subject 8 (98 kg), subject 10 (88 kg) and subject 7 (76 kg) for the agricultural seat with the 1.5 cycle input motion at 1.25 Hz with a seat base VDV of 1.67 $ms^{-1.75}$. The highest peak accelerations correspond to the highest subject mass.

Situation two: The forwarder seat at the transition between medium (no impact) and high (end-stop impact) situations. Of the 112 test conditions with human subjects using the forwarder seat, 10 were found to skewed. Of these 10 conditions, 8 occurred within one input magnitude of the transition between medium and high magnitude situations. The strongest effects (highest skewness and kurtosis) were at 1.25 Hz and 2.0 Hz with the 11.5 cycle waveform, but weak non-normal behaviour was observed with all three waveforms. These two most severe conditions are shown in Figure 5-15 and Figure 5-16. It can be seen that the SEAT value due to one subject is substantially different from the remainder.

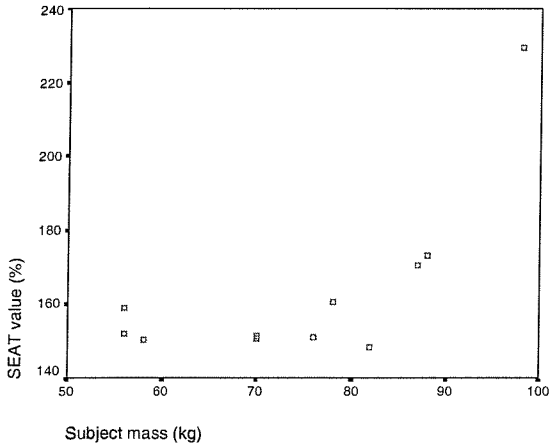

Figure 5-15 Scatterplot of subject mass and SEAT value for the forwarder seat with the long (11.5 cycle) input motion at the transition between medium and high magnitude seat behaviour (1.25 Hz with a seat base VDV of 0.97 $ms^{-1.75}$)

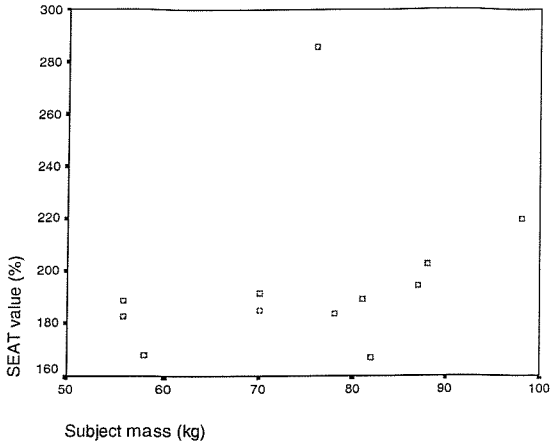

Figure 5-16 Scatterplot of subject mass and SEAT value for the forwarder seat with the long (11.5 cycle) input motion at the transition between medium and high magnitude seat behaviour (2.0 Hz with a seat base VDV of 1.43 $ms^{-1.75}$)

Situation three: The earthmover seat at low frequencies and magnitudes. The long (11.5 cycle) waveform showed skewed behaviour at 1.25 Hz and 1.6 Hz and the medium (4.5 cycle) input waveform at 1.25 Hz for the lowest input magnitude. The results at 1.25 Hz for both waveforms are shown in Figure 5-17 and Figure 5-18. It can be seen that again one or two subjects returned a SEAT value substantially different from the remainder of the group.

The time histories corresponding to these two conditions are shown in Figure 5-19. The situations with more suspension displacement correspond to the greater SEAT values. The skewed distribution in these situations appears to be due to one or two subjects causing the seat suspension to break away from friction more (or less) than the remainder of the group.

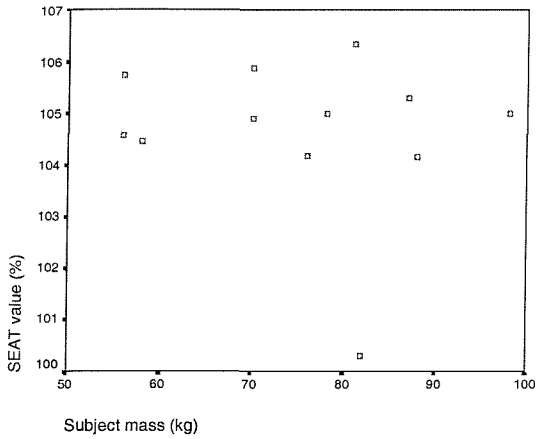

Figure 5-17 Scatterplot of subject mass and SEAT value for the earthmover seat with the long (11.5 cycle) input motion at the lowest magnitude at 1.25 Hz (seat base VDV of 0.5 $ms^{-1.75}$)

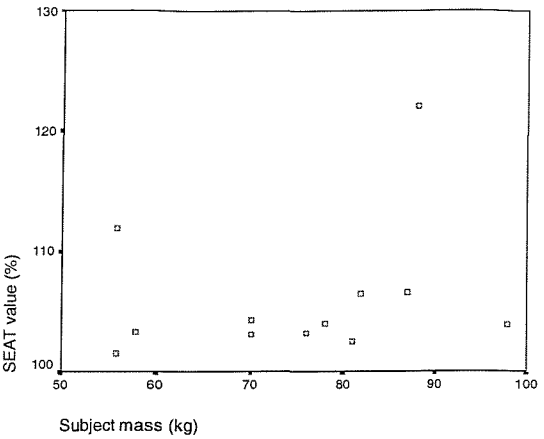

Figure 5-18 Scatterplot of subject mass and SEAT value for the earthmover seat with the medium (4.5 cycle) input motion at the lowest magnitude at 1.25 Hz (seat base VDV of 0.5 $ms^{-1.75}$)

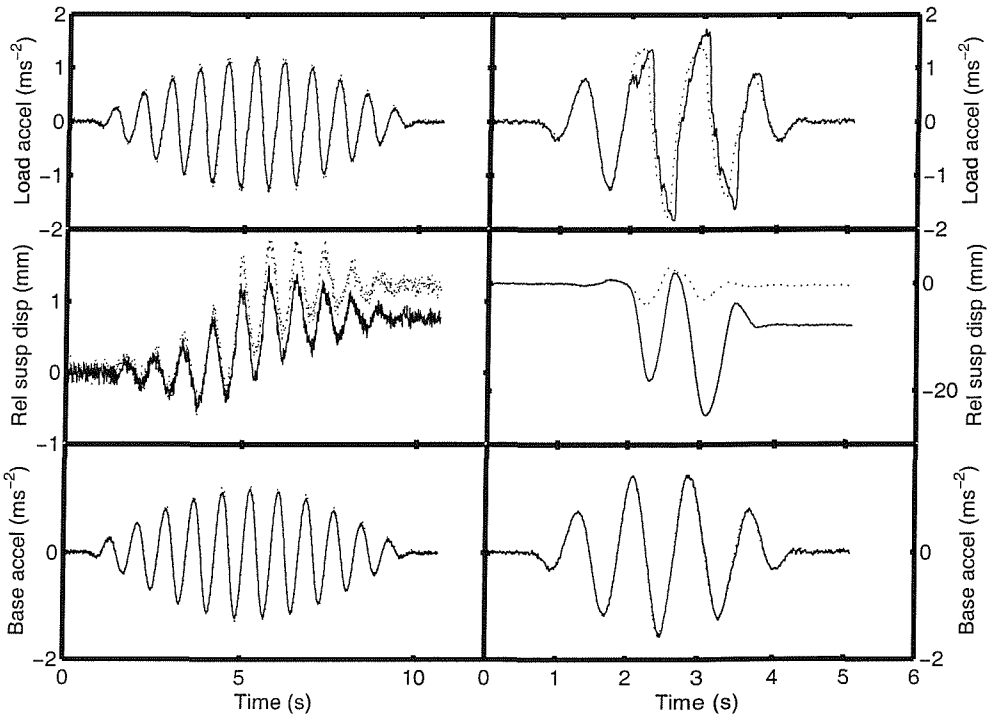

Figure 5-19 Time histories corresponding to the most extreme outliers from Figure 5-17 and Figure 5-18 (Subject 11, 82 kg and subject 10, 88 kg, respectively) as solid lines compared with results from a subject more representative of the remainder of the group (subject 12, 76 kg) shown with dotted lines.

5.3.3 The differences in SEAT value between the loading conditions grouped in terms of magnitude

The difference in SEAT value for each test condition (seat, waveform, frequency and magnitude) was explored initially using a Mann-Whitney U test. These results, shown in Appendix 4, give a detailed analysis of which individual test conditions showed statistically significant differences between loading methods. Due to the narrow distributions observed for many test conditions, there are statistically significant differences between loading conditions in many situations. It should be noted that a statistically significant difference does not directly indicate a large difference.

The difference between the SEAT values obtained with the human subjects and those obtained with the other two loading conditions are summarised in Table 5-3. The median SEAT values obtained with each loading condition were compared using Wilcoxon's matched-pairs signed ranks test (the results with each load for each test condition were averaged and these averages were compared within each magnitude group). It can be seen that although there were significant differences, none of the groups (low, medium or high magnitude) showed a consistent trend across all three seats for the alternative loads to under- or over-estimate the SEAT value compared with the subjects.

Table 5-3 The median difference in SEAT value between the subjects and the other two loading conditions. Positive values indicate that the alternative loads showed greater SEAT values than the subjects.

Seat	Magnitude	Median difference in SEAT value between the subjects and the dummy.	Median difference in SEAT value between the subjects and the semi-rigid mass.
Agricultural tractor	**Low (stage 1/2)**	+2.6**	+2.2**
	Medium (stage 3)	-5.9**	-3.1**
	High (stage 4/5)	-9.5**	-6.1**
Forestry forwarder	**Low (stage 1/2)**	-6.0**	-1.7
	Medium (stage 3)	-11.4**	+1.7
	High (stage 4/5)	-8.8	+17.2**
Earthmover	**Low (stage 1/2)**	+3.2**	+0.5
	Medium (stage 3)	+2.7**	+3.0**
	High (stage 4/5)	+7.0	+18.0**

**indicates that the difference is significant at $p<0.01$ (Wilcoxon)

5.3.4 The variability of the SEAT values obtained with each loading condition

The range of SEAT values obtained for each test condition with each loading method is summarised in Table 5-4. The subjects were statistically compared with the other two loading conditions using Wilcoxon's test by comparing the median ranges obtained for each test condition across each magnitude group.

It can be seen that for most situations the alternative loads returned significantly smaller ranges of SEAT values for each test condition compared to the human subjects. It can also be seen that the variation obtained with the dummy and the semi-rigid mass was not significantly different for the majority of groups and that for the three test groups where there was a significant difference, two showed a smaller range with the dummy and one showed a smaller range with the mass.

Table 5-4 Summary of the variation in SEAT value for the three loading conditions expressed in terms of the median range, where the range of SEAT values is the maximum SEAT value minus the minimum SEAT value for a single test condition.

Seat	Magnitude	Subjects	Dummy	Semi-rigid mass	Subjects vs. Dummy	Subjects vs. Mass	Dummy vs. Mass
Agricultural tractor	Low (stage 1/2)	23.7	11.1	12.6	**	**	-
	Medium (stage 3)	22.8	11.4	7.2	**	**	**
	High (stage 4/5)	78.4	19.4	26.5	**	**	**
Forestry forwarder	Low (stage 1/2)	7.4	3.0	2.5	**	**	-
	Medium (stage 3)	12.5	3.4	8.3	**	**	**
	High (stage 4/5)	35.4	22.3	20.8	**	**	-
Earthmover	Low (stage 1/2)	4.5	5.2	4.9	-	-	-
	Medium (stage 3)	3.9	2.4	3.1	**	-	-
	High (stage 4/5)	11.6	6.2	7.4	**	**	-

**indicates that the difference was significant at $p<0.01$ (Wilcoxon)

5.4 Discussion and Conclusions

Heavier subjects showed poorer seat performance compared to lighter subjects at frequencies close to the main resonance frequency of the seat-subject system. The heavier subjects showed better seat performance at higher frequencies where the seat was acting as a vibration isolator.

The median difference in SEAT value between the subjects and the dummy was less than 12% for all groups of data, but some larger differences were observed for individual test conditions. There were no consistent trends in the tendency to over-estimate or under-estimate the SEAT value when all results for a particular seat, test waveform, or frequency were considered together.

The median difference in SEAT value between the semi-rigid mass and the subjects was comparable to that obtained with the dummy in most situations, with median differences between the mass and the subjects of less than 7% across all test conditions. Again there was little consistency in the tendency to over-estimate or under-estimate the SEAT value. However, at high magnitudes the semi-rigid mass overestimated the SEAT value by an average of 17% with the forwarder seat and 18% with the earthmover seat. The agricultural tractor seat did not show this effect, but there were fewer high magnitude results available for this seat (12 comparisons as opposed to 45 with the forestry forwarder seat and 49 with the earthmover seat). The indications are that the semi-rigid mass will result in an over-estimate of the SEAT values as compared to human subject for a test condition resulting in high magnitude seat behaviour using this type of input motion. In other test conditions either the dummy or the semi-rigid mass would be expected to give a reasonable estimate of the SEAT value.

The anthropodynamic dummy and the semi-rigid mass both showed significantly less variation in SEAT value than the human subjects. The variability obtained with the dummy was similar to that obtained with the semi-rigid mass.

Finally, a revision of the existing methods of measuring suspension seat acceleration with human subjects may be necessary, precisely specifying some manner of attaching the transducer to the subject to reduce the effect spurious top-stop impact transients. The time histories recorded with the subjects and the mass suffered distortion during top stop impacts due to impacts between the load and the transducer and there were indications

that the semi-rigid mass tended to overestimate the SEAT value at high magnitudes. The time histories obtained with the dummy will therefore be used for comparison with the model during the remainder of this project.

6 Measurement of seat component parameters

6.1 Introduction

This chapter describes the experiments that were conducted to quantify the dynamic characteristics of the seat components. Each seat was considered in terms of the following components:

- The cushion
- The suspended mass, including the cushion and backrest and the moving parts of the suspension mechanism
- The suspension spring
- The friction in the linkage mechanism
- The suspension damper, including the geometry of the fixing points
- The end-stop buffers including the geometry of the parts of the suspension linkage that contacted the buffers

All measurements were conducted on the assumption that motion of the seat base and the load would be non-rotational and confined to the vertical direction (z-axis). The intention was to quantify the dynamic properties of each seat component in terms relating to displacement, velocity or acceleration in the time domain.

Details of the shakers, transducers and data acquisition systems used in these tests can be found in Chapter 3.

6.2 The cushion

6.2.1 Introduction

The methods described by Fairley and Griffin (1986) and developed by Wei and Griffin (1998) were used to obtain linear coefficients for the suspension seat cushions. This dynamic method of determining the damping coefficients is linearly equivalent to the method of estimating the damping from the hysteresis curve from one cycle of sinusoidal vibration as used by Hilyard (1982), Rakheja *et al.* (1994) and others. The dynamic method of determining the stiffness accounts for in-phase dynamic effects present in the cushion that are not apparent from quasi-static measurements.

The "quasi-static" stiffnesses of the cushions were also measured for comparison with the dynamic measurements.

6.2.2 The low velocity ("quasi-static") cushion force-deflection characteristic

6.2.2.1 Method

Each cushion was detached from the suspension mechanism and was compressed manually by an indenter at a constant velocity of 1.5 mms^{-1} until the compressive force exceeded 2 kN and then released at the same rate. The force applied to the cushion by the indenter and the displacement of the indenter were both recorded. Three repeat measurements were made on each cushion and one cushion was tested at three velocities to confirm that the cushion characteristics were relatively insensitive to velocity for the test conditions used.

6.2.2.2 Apparatus

Measurements were made on each of the seat cushions using an indenter rig (Figure 6-1). This rig had a steel box section frame mounted over the VP85 electro-dynamic shaker. The shaker was not used during these tests and the top plate of the shaker was clamped to the shaker body to ensure that the compliance of the shaker suspension did not affect results.

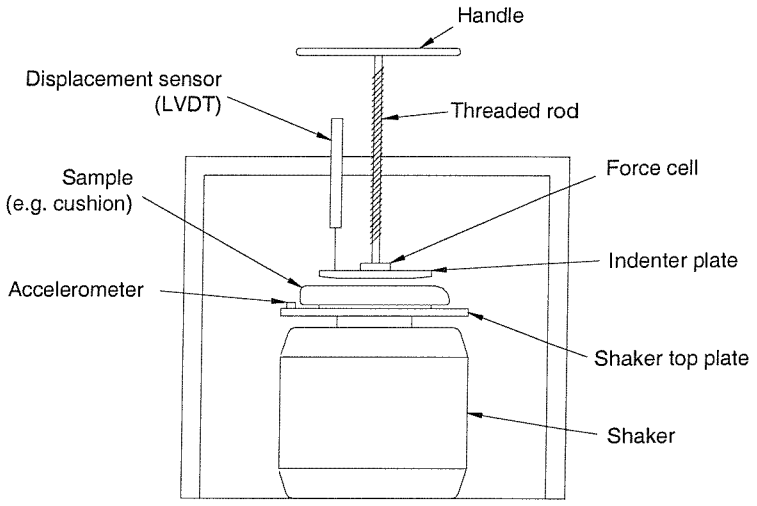

Figure 6-1 Structure of the indenter rig used for quasi-static cushion force-deflection tests

A force was applied to the cushion via an indenter plate attached to a threaded rod passing through a bearing on the frame. The indenter plate was a 25 cm radius disk as shown in Figure 6-2. The indenter vertical displacement was adjusted by rotation of the handle. Figure 6-3 illustrates the displacement of the indenter for one test.

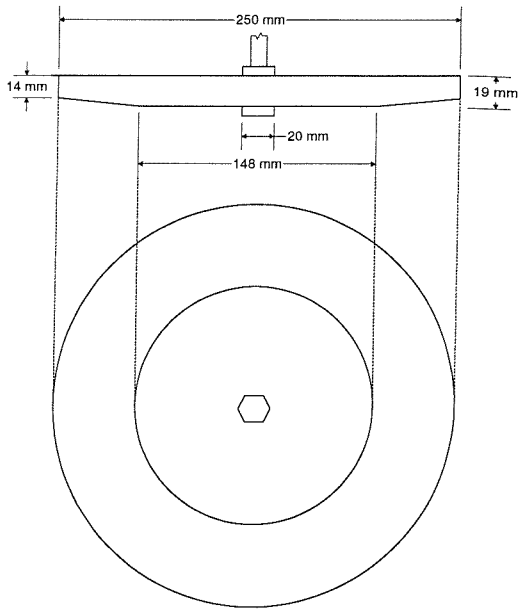

Figure 6-2 Geometry of the indenter plate

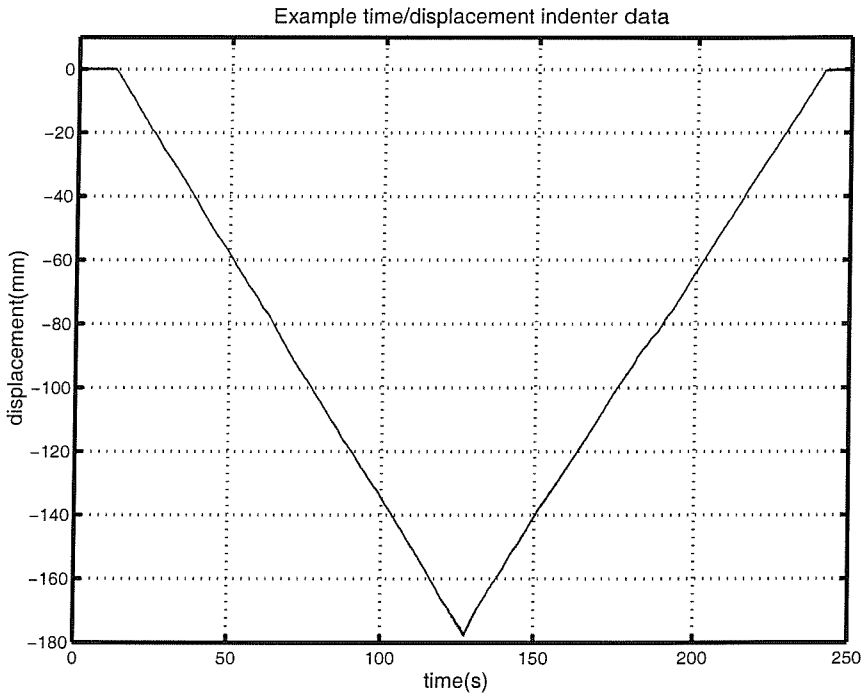

Figure 6-3 Example time/displacement data for a single quasi-static cushion indenter test

The displacement of the indenter plate was monitored using the LVDT and the applied force was measured using the Kistler force cell (Both described in Chapter 3). The vertical force at the indenter plate and the displacement of the indenter plate were acquired digitally using an *HVLab* data acquisition system at 200 samples per second via a 66 Hz low pass analogue anti-aliasing filter. The acquired displacement and

force time histories were digitally filtered using a 5 Hz 8-pole zero phase low pass Butterworth filter to remove high frequency noise. The filtered force and displacement vectors were plotted against each other with the origin of both axes adjusted to the point at which the indenter contacted the cushion causing the acquired force to increase.

6.2.2.3 Results

Figure 6-4 shows the force deflection characteristic of the earthmover seat cushion tested at compression rates of 0.75 mms^{-1}, 1.5 mms^{-1} and 3 mms^{-1}. Two measurements are shown for each compression rate. The results at all compression rates were similar.

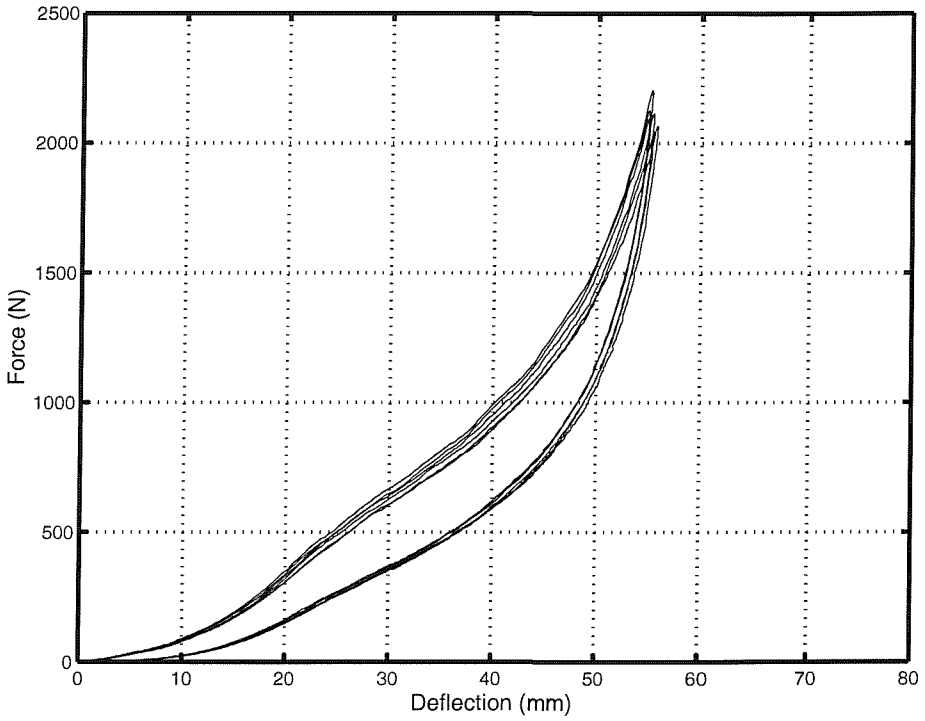

Figure 6-4 Quasi-static force-deflection charachterisitc of the earthmover seat cushion tested at 0.75 mms^{-1}, 1.5 mms^{-1} and 3 mms^{-1} showing 2 repeat measurements at each compression rate

Figure 6-5 to Figure 6-7 show the measured quasi-static force-deflection characteristics of the earthmover, forwarder and agricultural tractor seat cushions respectively at a compression rate of 1.5 mms^{-1}.

An 8^{th} order polynomial (see below) was fitted to the mean of the compression and extension curves for each of the cushions. The polynomial was constrained to zero at

zero displacement. The compression and extension curves were averaged to obtain a lossless estimate, shown as the solid line on Figure 6-5 to Figure 6-7. The curve-fit is shown as the dashed line and was usually indistinguishable from the lossless curve. The coefficients are listed in Table 6-1.

$$f(x) = a_1 x^8 + a_2 x^7 + a_3 x^6 + a_4 x^5 + a_5 x^4 + a_6 x^3 + a_7 x^2 + a_8 x$$

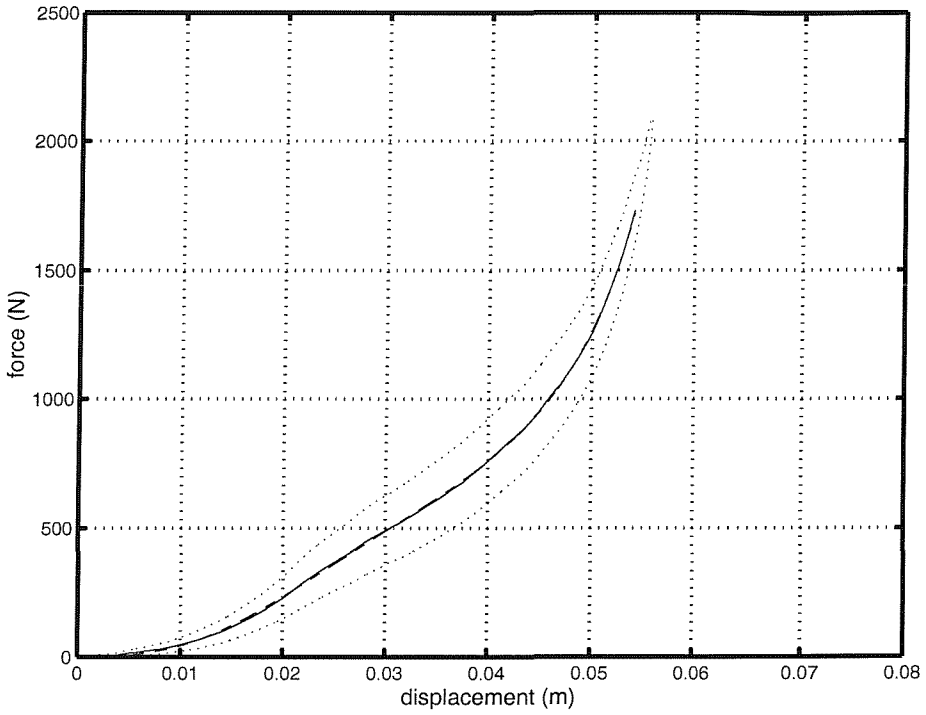

Figure 6-5 Quasi-static force-deflection characteristic of the earthmover seat cushion tested at 1.5 mms^{-1}, showing measured (dotted), averaged (solid) and curve-fit (dashed) data.

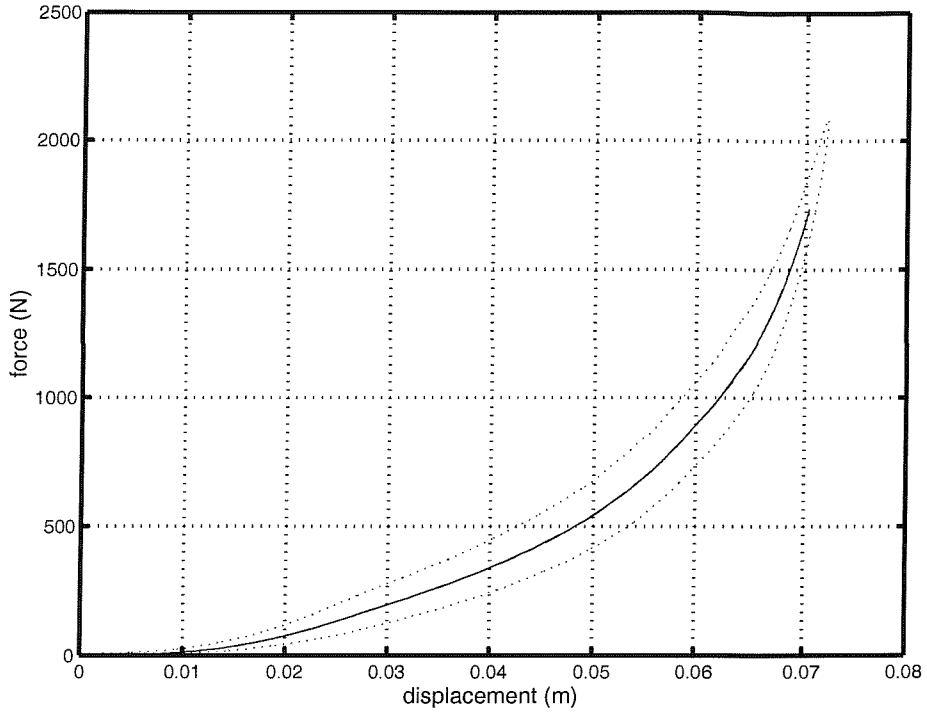

Figure 6-6 Quasi-static force-deflection characteristic of the forwarder seat cushion tested at 1.5 mms^{-1}, showing measured (dotted), averaged (solid) and curve-fit (dashed) data.

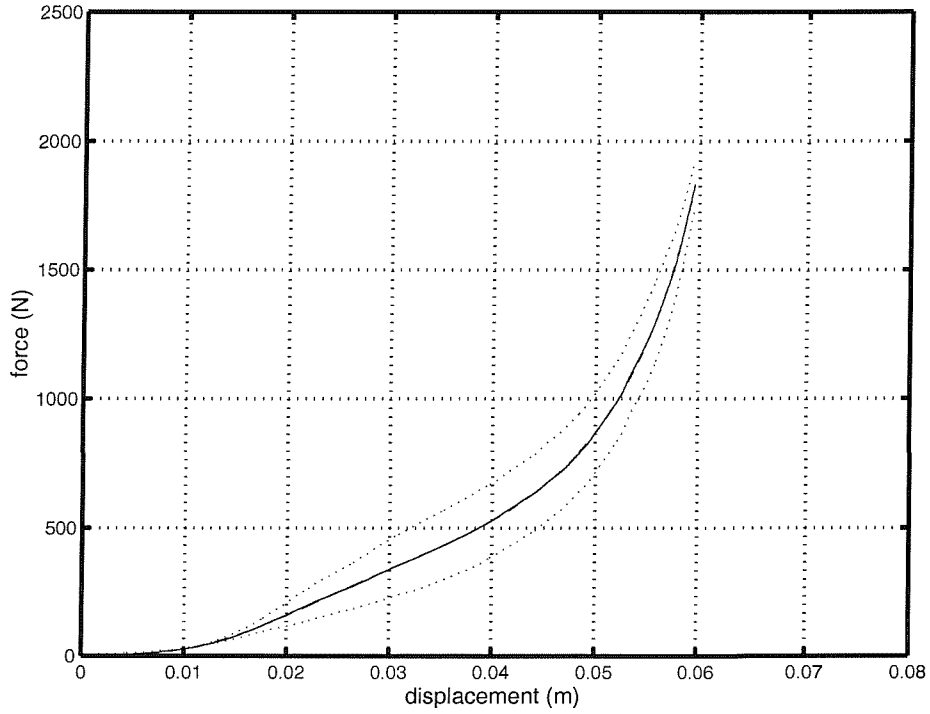

Figure 6-7 Quasi-static force-deflection characteristic of the agricultural tractor seat cushion tested at 1.5 mms^{-1}, showing measured (dotted), averaged (solid) and curve-fit (dashed) data.

Table 6-1 Quasi-static cushion force-deflection polynomial curve fit coefficients

	Earthmover seat	Forwarder seat	Agricultural tractor seat
a_1	6.36×10^{14}	1.47×10^{14}	4.78×10^{14}
a_2	-1.14×10^{14}	-3.47×10^{13}	-9.43×10^{13}
a_3	7.83×10^{12}	3.21×10^{12}	7.20×10^{12}
a_4	-2.32×10^{11}	-1.40×10^{11}	-2.50×10^{11}
a_5	1.56×10^{9}	2.66×10^{9}	3.09×10^{9}
a_6	4.77×10^{7}	-7.43×10^{6}	1.75×10^{7}
a_7	-7.22×10^{4}	-7.26×10^{4}	-1.09×10^{5}
a_8	-1.32×10^{2}	1.07×10^{3}	5.32×10^{2}

The measured lossless force-deflection characteristic was differentiated numerically in order to obtain an estimate for the cushion stiffness as shown in Figure 6-8 to Figure 6-10. The polynomial curve fit function was differentiated exactly and is shown as the dashed line.

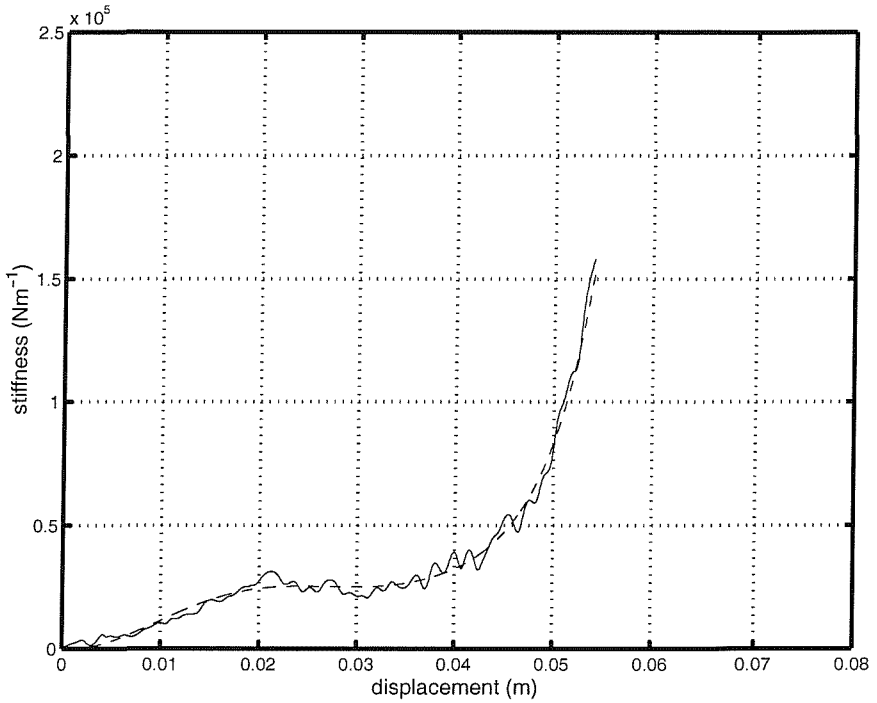

Figure 6-8 Cushion stiffness varying with overall cushion compression displacement estimated from the differentiated mean force-deflection characteristic of the earthmover seat cushion.

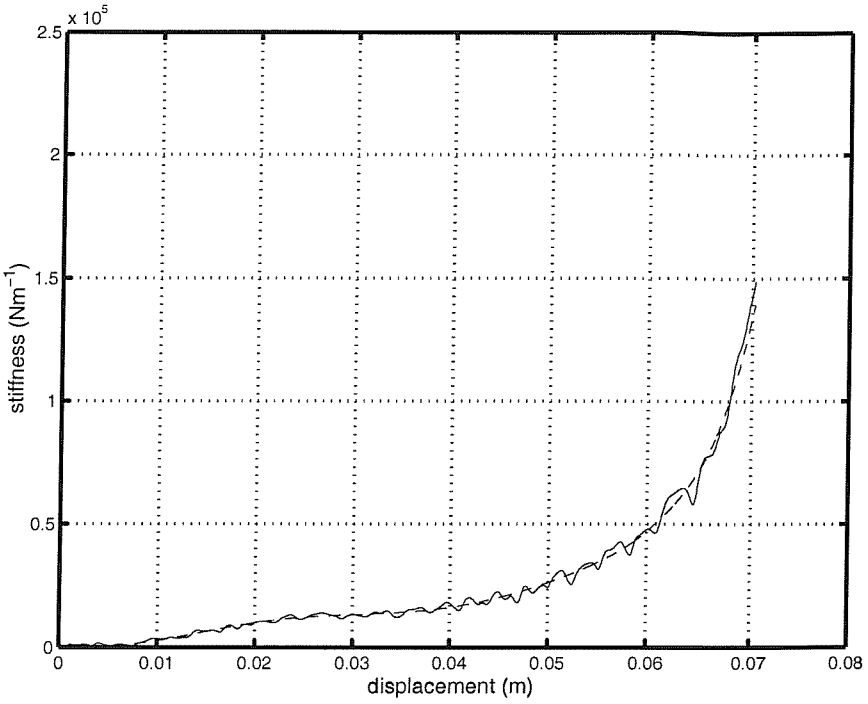

Figure 6-9 Cushion stiffness varying with overall cushion compression displacement estimated from the differentiated mean force-deflection characteristic of the forwarder seat cushion.

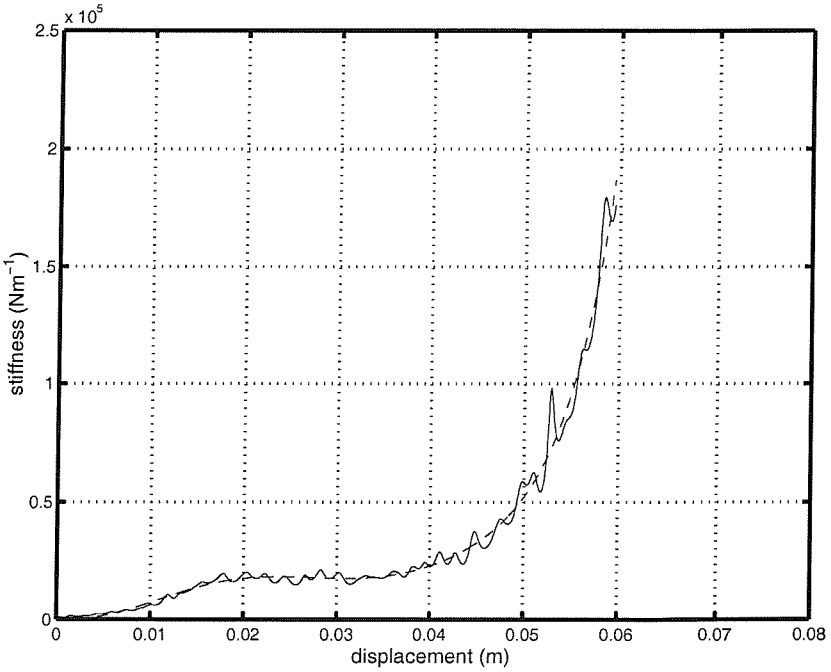

Figure 6-10 Cushion stiffness varying with overall cushion compression displacement estimated from the differentiated mean force-deflection characteristic of the agricultural tractor seat cushion.

6.2.2.4 Summary of quasi-static measurements

The cushions were found to have stiffnesses in the constant stiffness region (results are at 30 mm compression) of 25.0 kNm^{-1}, 13.3 kNm^{-1} and 17.3 kNm^{-1} for the earthmover, forwarder and agricultural tractor seat respectively using this measurement method. All three cushions clearly showed the quasi-linear, constant stiffness and exponentially increasing stiffness stages as described in Chapter 2 Section 2.5.11. The forwarder seat cushion showed a less pronounced constant stiffness region as compared with the other two cushions.

6.2.3 Dynamic cushion measurements

6.2.3.1 Theory

Assuming that the cushion can be approximated to a parallel linear spring and damper arrangement, the stiffness and damping coefficients for an angular frequency, ω, can be calculated as follows (adapted from Wei and Griffin, 1998)

$$F(\omega) = k \cdot x(\omega) + c \cdot \dot{x}(\omega) \qquad \text{Equation 6-1}$$

$$\therefore F(\omega) = \left(-\frac{k}{\omega^2} - \frac{j \cdot c}{\omega} \right) \cdot \ddot{x}(\omega) \qquad \text{Equation 6-2}$$

where k is the cushion stiffness, c is the cushion damping, x is the motion across the cushion and ω is the angular frequency.

Using the apparent mass, a complex quantity defined as the force transmitted through the cushion divided by the acceleration,

$$M(\omega) = \frac{F(\omega)}{\ddot{x}(\omega)} \qquad \text{Equation 6-3}$$

$$M(\omega) = -\frac{k}{\omega^2} - \frac{j \cdot c}{\omega} \qquad \text{Equation 6-4}$$

Gives the linear cushion stiffness and damping in terms of the apparent mass as:

$$k = -\mathrm{Re}(M(\omega)) \cdot \omega^2 \qquad \text{Equation 6-5}$$

$$c = -\mathrm{Im}(M(\omega)) \cdot \omega \qquad \text{Equation 6-6}$$

A measure of the apparent mass of the cushion therefore allows the linear stiffness and damping to be estimated.

6.2.3.2 Preloading method

It is known that some dynamic characteristics of open-cell foam cushions have time constants in excess of a minute. In order to develop a suitable preloading method, these long time constant effects must be allowed for.

Before beginning the measurements, the agricultural tractor seat cushion was compressed over approximately 5 seconds to preloads of 380N, 580N and 765N in turn with a 30 minute interval between each test. The static compression displacement was kept constant for a 5 minute period. The agricultural tractor seat cushion was chosen as preliminary tests showed that this cushion took the longest to approach an equilibrium condition. The variation in the force exerted by the cushion on the indenter plate over this period was measured and is shown in Figure 6-11 to Figure 6-13.

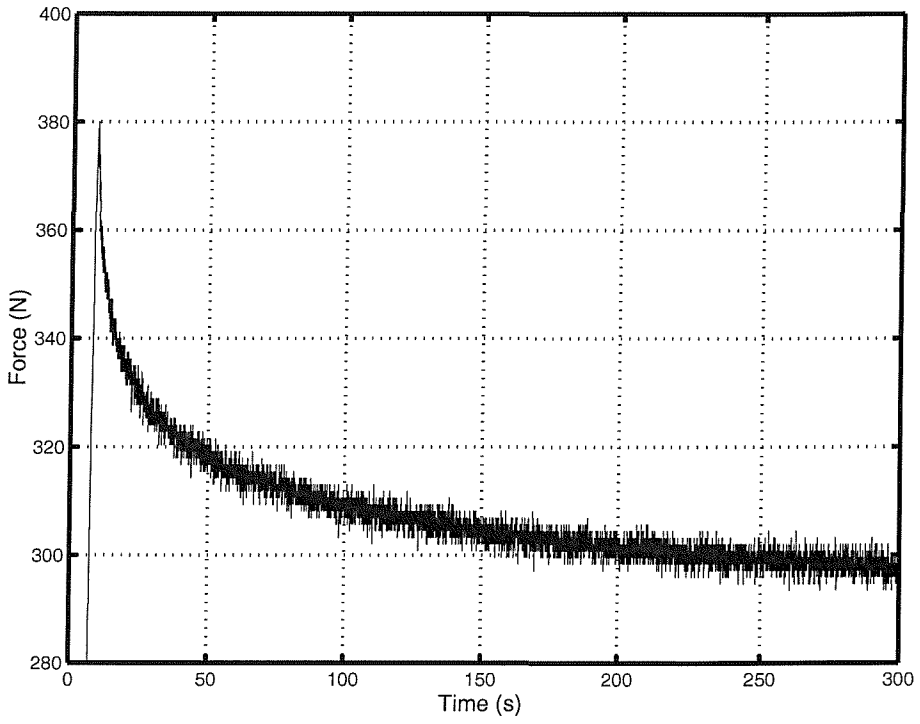

Figure 6-11 Change in force over 5 minutes of constant displacement compression of the agricultural tractor seat cushion starting at 380N

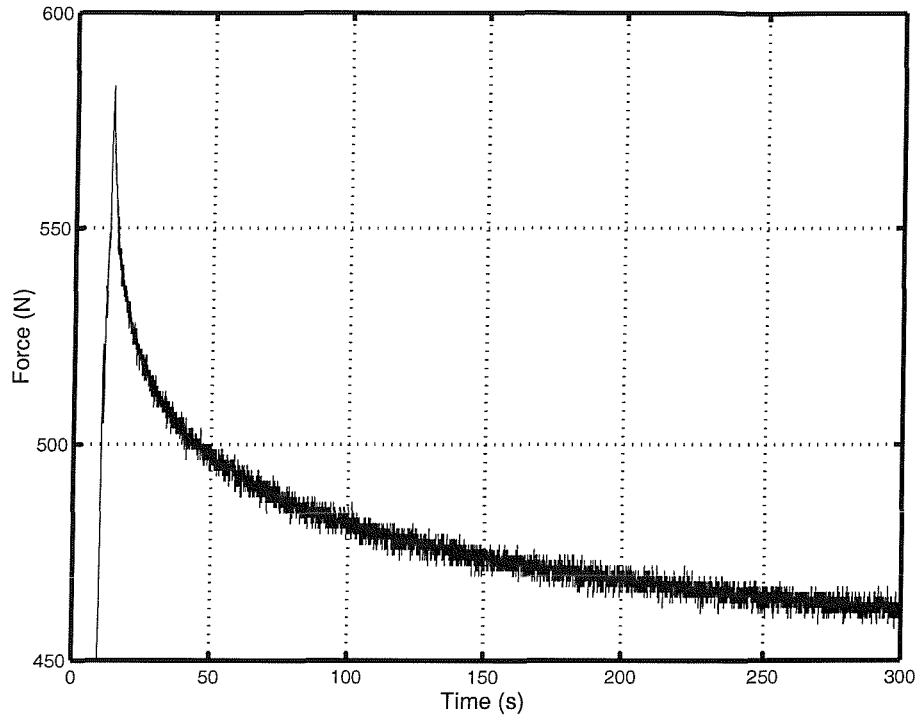

Figure 6-12 Change in force over 5 minutes of constant displacement compression of the agricultural tractor seat cushion starting at 580N

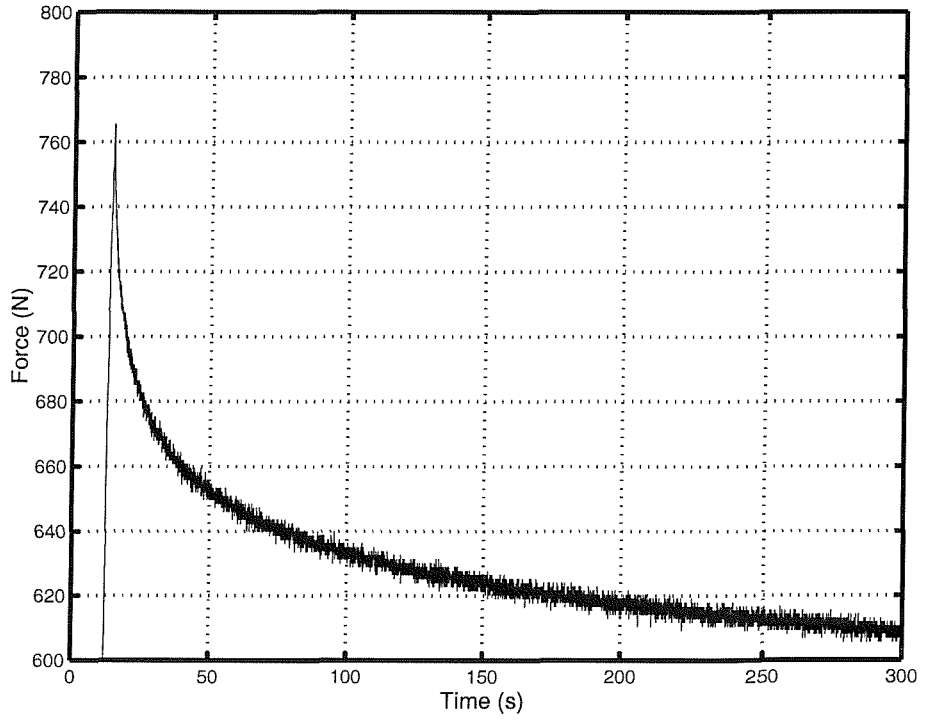

Figure 6-13 Change in force over 5 minutes of constant displacement compression of the agricultural tractor seat cushion starting at 765N

In all three cases, a reduction in cushion force of around 25 % was observed over the 5-minute period (27%, 25% and 25% in order of increasing starting force). However, a reduction of approximately 20% occurred in the first minute (20%, 19%, 19%), while the last minute showed a change of less than 1% in all cases. It was concluded that a 5 minute settling time would be sufficient. As a result of these tests, a simple procedure for obtaining a stable preload was developed:

1. Begin with the indenter plate clear of the cushion and the force cell charge amplifier set to a range of at least ±1500 N and set to the 'long time constant' setting (minimum time constant quoted as 16 minutes 40 seconds)
2. Compress the cushion to a preload of approximately 25% greater than that desired.
3. Allow the cushion to 'settle' for 5 minutes.
4. Check the preload is within 5% of the desired value. If not, adjust the indenter displacement until an acceptable force measurement is obtained.
5. Wait for 1 minute.
6. Iterate steps 4 and 5 as necessary, observing that the charge amplifier time constant will start to affect results after around 10 minutes from the start of this process.
7. Switch the charge amplifier to the 'short time constant' setting (quoted maximum time constant of 50 seconds) and a smaller range (selected according to the input signal magnitude and cushion compression, both of which increased the transmitted force).
8. Proceed with the test.

6.2.3.3 Test method

Each cushion was tested with preload forces of 100 N, 300 N, 500 N, 700 N and 900 N. A motion was applied to the base of the cushion and the force and acceleration were acquired. Two input waveforms were used:

- Constant displacement amplitude swept sine wave swept from 1 Hz to 10 Hz over 100 seconds at a constant rate of change of frequency, with an additional 5 seconds of linear ramp up or down on each end. Peak-to-peak amplitudes of 2 mm and 4 mm were used.

- Uniformly distributed random motion with a constant acceleration spectrum characteristic, bandpass filtered at 1 Hz and 10 Hz using 6 pole Butterworth filters. The higher magnitude used the same waveform as the low magnitude motion with a gain of 2.0.

The input motions were reproduced at two magnitudes as shown in Table 6-2. These values are the mean values on the shaker platform for all measurements. The acquired data were filtered using a 30 Hz 8 pole low pass Butterworth filter to attenuate the predominantly 50 Hz noise present on the acquired acceleration signals.

Table 6-2 Mean r.m.s. acceleration measured on the shaker platform. Errors are ± 1 standard deviation.

	Low	**High**
Random	0.169 ± 0.036 ms^{-2}	0.285 ± 0.030 ms^{-2}
Sinusoidal	0.658 ± 0.012 ms^{-2}	1.294 ± 0.015 ms^{-2}
Nominal amplitude	2 mm peak-to-peak	4 mm peak-to-peak

The acceleration at the shaker plate and the force transmitted through the cushion were acquired at 200 samples per second via a 66 Hz low pass analogue anti-aliasing filter using an *HVLab* data acquisition system.

6.2.3.4 Methods for calculating the apparent mass

The apparent mass is defined as the ratio of the applied force to the acceleration measured at the point of application of the force and can be calculated from the transfer function between the acceleration and the force. The methods used to estimate the apparent mass were different for the two input motions used as discussed in the following paragraphs.

The apparent mass for the tests using the random motion was estimated using Welch's averaged periodogram method as described in Chapter 3. This method is not suitable for use with a swept sine time history. The process of dividing the sinusoid into sections can introduce unwanted artefacts. Instead, a single 'raw' transfer function estimate was obtained by taking the PSD or CSD of the complete time histories and using the cross-spectral density method to calculate the transfer function. The transfer function was then smoothed using a 10-point moving average.

6.2.3.5 Apparatus

The test rig was as described in Section 6.2.2.2. The shaker platform was free to move and the indenter was clamped in place before vibration was applied.

The vertical force at the indenter plate and the acceleration on the indenter plate were acquired digitally using an *HVLab* data acquisition system at 200 samples per second via a 66 Hz low pass analogue anti-aliasing filter.

6.2.3.6 Results

Figure 6-14 to Figure 6-16 show the linear stiffness and damping estimates for the three seat cushions using both high magnitude input signals. The coherence refers to the random motion and is consistently high across the frequency range from 1 to 10 Hz for all seats. The coherence for the low magnitude input motions was also consistently high.

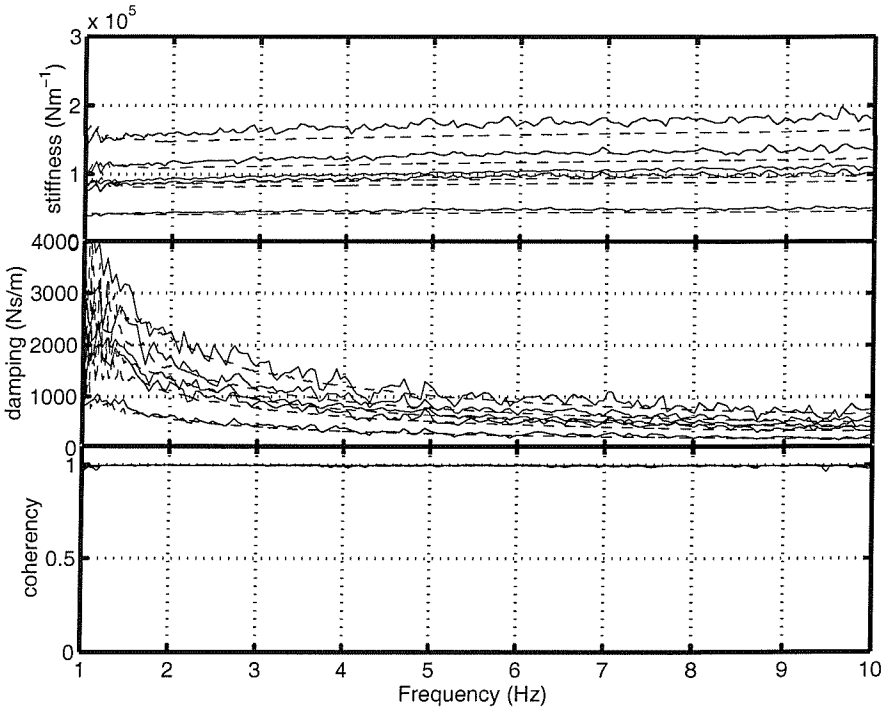

Figure 6-14 Estimated linear dynamic stiffness and damping with 5 preloads increasing linearly from 100 N to 900 N and with random (solid) and sinusoidal (dashed) input waveforms using the earthmover seat cushion. Stiffness and damping both increase with increasing preload.

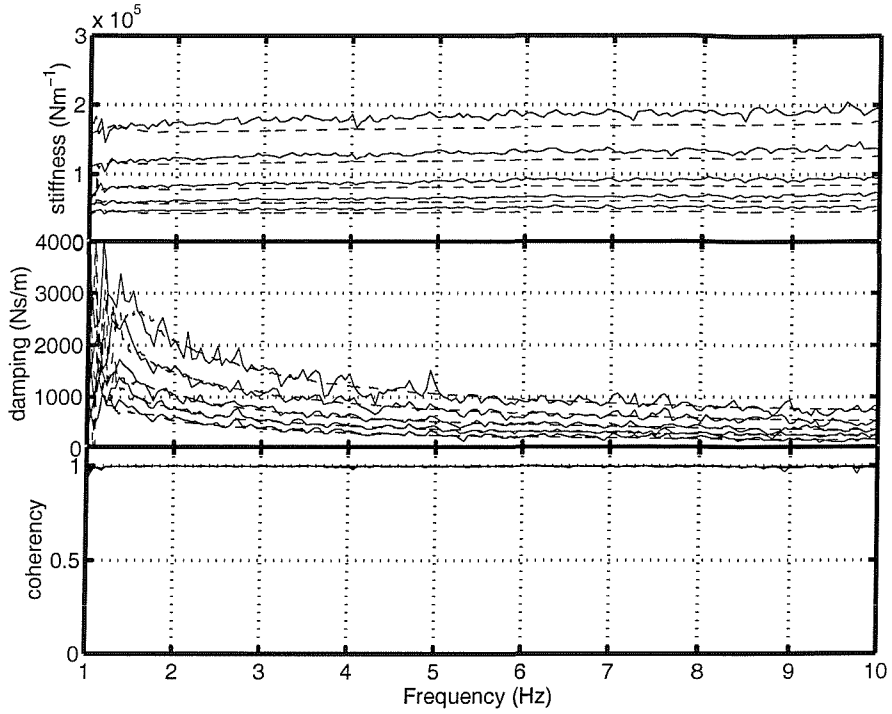

Figure 6-15 Estimated linear dynamic stiffness and damping with 5 preloads increasing linearly from 100 N to 900 N and with random (solid) and sinusoidal (dashed) input waveforms using the forwarder seat cushion. Stiffness and damping both increase with increasing preload.

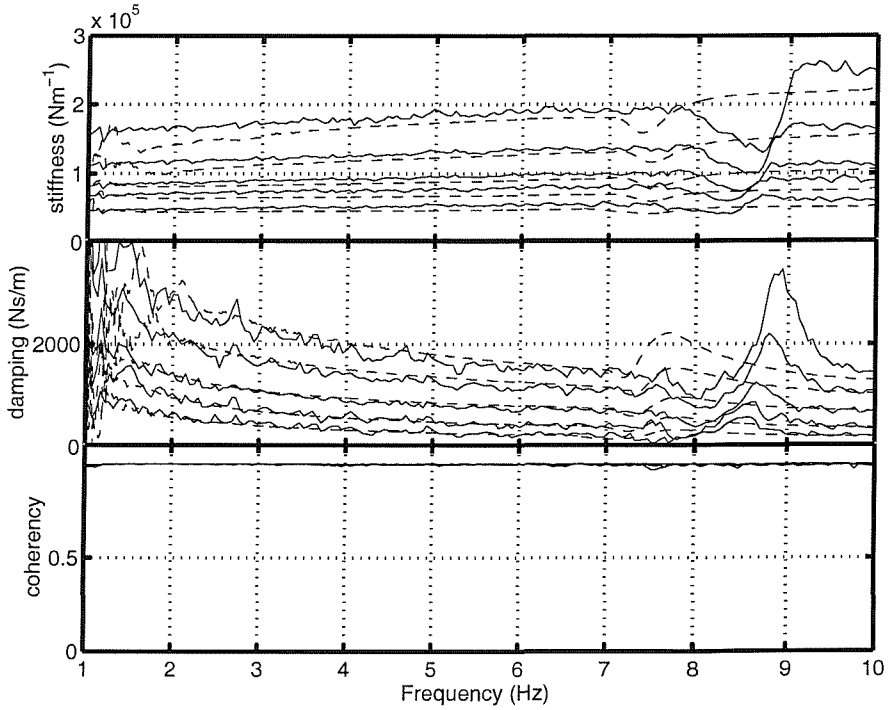

Figure 6-16 Estimated linear dynamic stiffness and damping with 5 preloads increasing linearly from 100 N to 900 N and with random (solid) and sinusoidal (dashed) input waveforms using the agricultural tractor seat cushion. Stiffness and damping both increase with increasing preload.

The artefact visible on the results for the agricultural tractor seat between 7 and 9.5 Hz was probably due to a resonance of the backrest that was visible during measurements. The difference between the swept sine and random results in this region may have been due to the backrest being at a slightly different angle for the two tests. Apart from this feature, all the data show smooth and gradual changes across the frequency range. The following features are apparent from studying the results for all three seats:

- Both the cushion stiffness and damping increase with increasing preload at all frequencies.
- The 'swept sinusoid' method gives slightly lower estimates for the cushion stiffness than the 'random' method at any preload and frequency. The magnitudes of the input motions are shown in Table 6-2 and it can be send that the r.m.s. acceleration magnitude of the sinusoidal motion is substantially higher than the random motion.
- The stiffness estimates using both methods increase with increasing frequency. Stiffness estimates for a given preload were found to increase by between 10% and 20% from 1 to 10 Hz.
- The damping estimates were similar using both sinusoidal and random inputs.
- The damping estimates decreased exponentially with increasing frequency, approaching a non-zero asymptote.

The effect of vibration amplitude on the linear estimates is shown in Figure 6-17 to Figure 6-22.

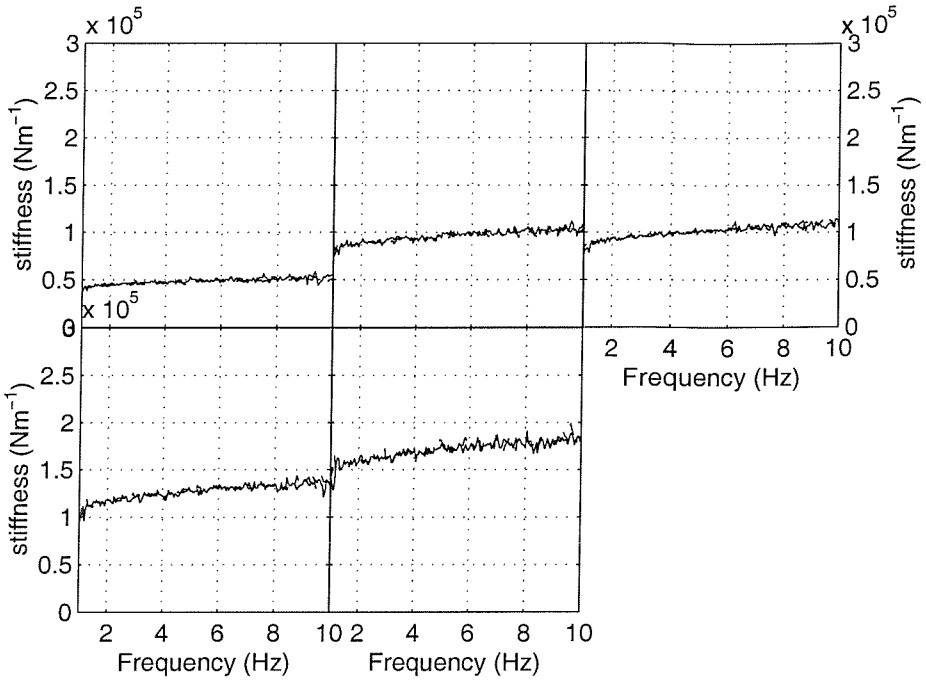

Figure 6-17 Estimated cushion linear dynamic stiffness at 5 preloads and both magnitudes (low-solid, high-dashed) using the random input motion with the earthmover seat cushion

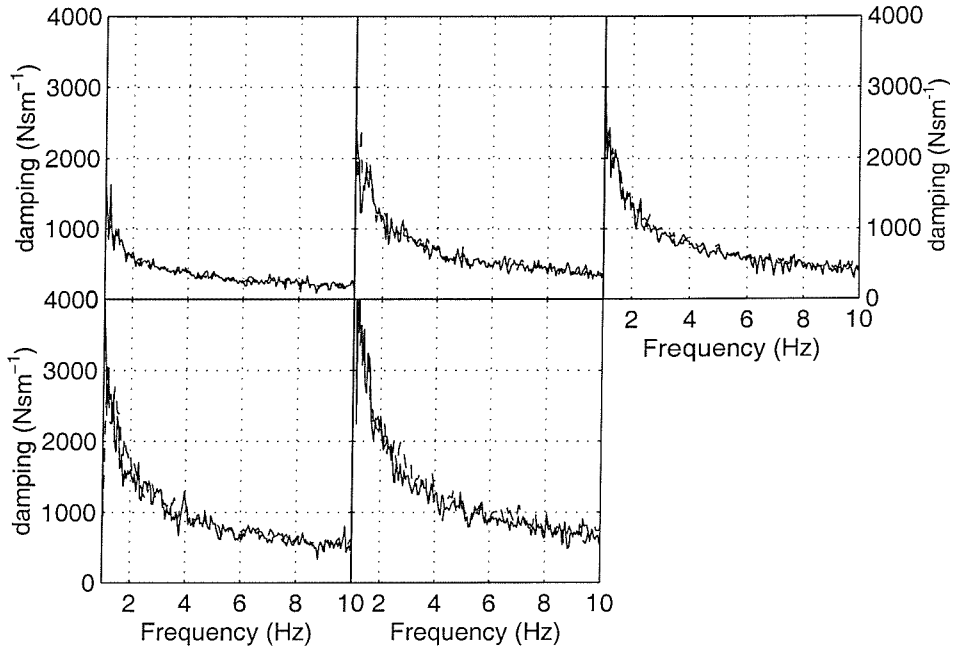

Figure 6-18 Estimated cushion linear dynamic damping at 5 preloads and both magnitudes (low-solid, high-dashed) using the random input motion with the earthmover seat cushion.

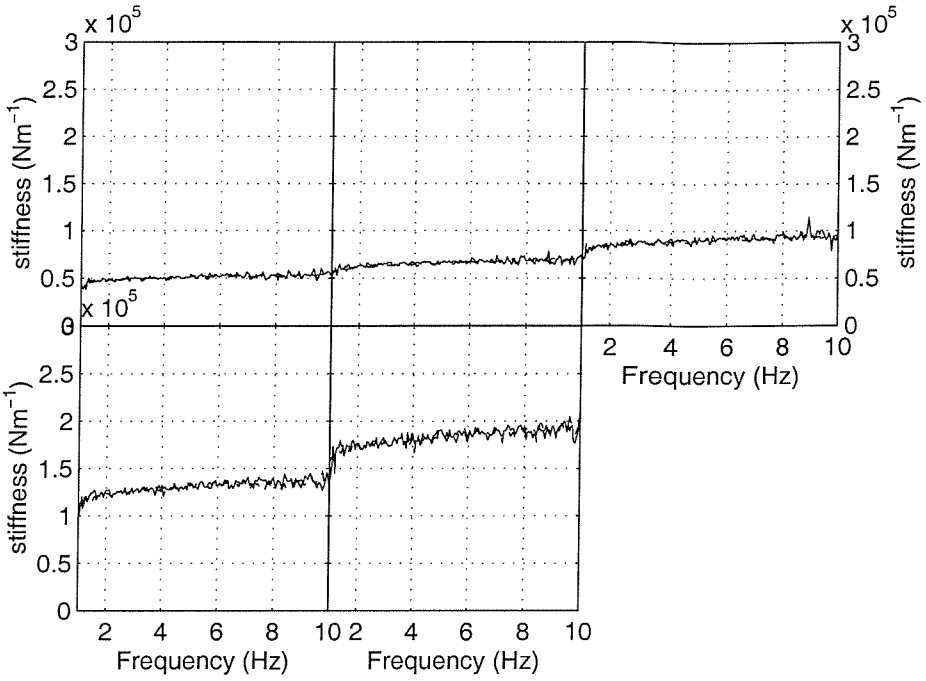

Figure 6-19 Estimated cushion linear dynamic stiffness at 5 preloads and both magnitudes (low-solid, high-dashed) using the random input motion with the forwarder seat cushion

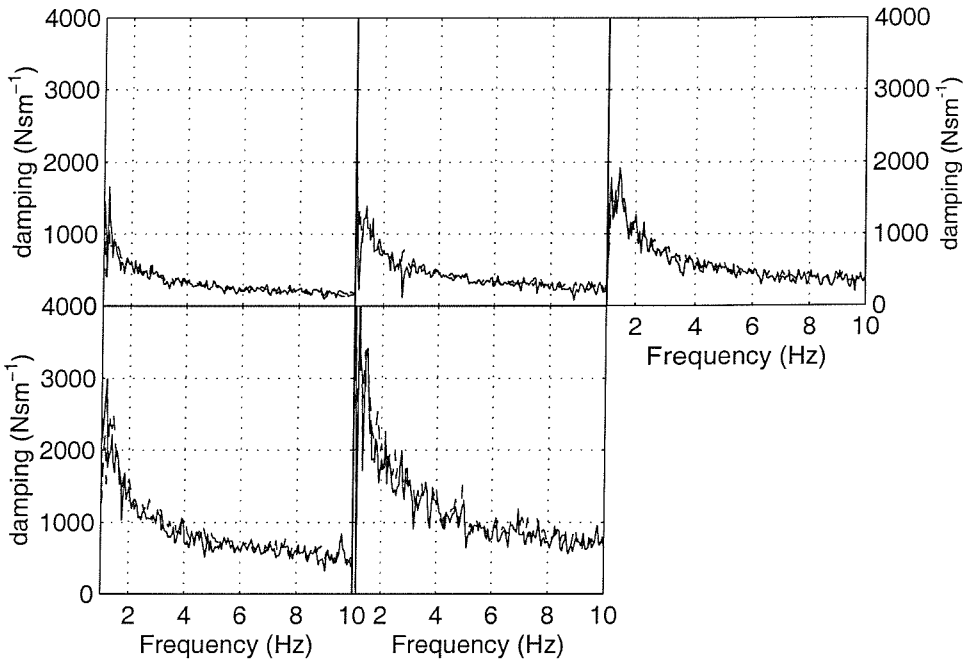

Figure 6-20 Estimated cushion linear dynamic damping at 5 preloads and both magnitudes (low-solid, high-dashed) using the random input motion with the forwarder seat cushion.

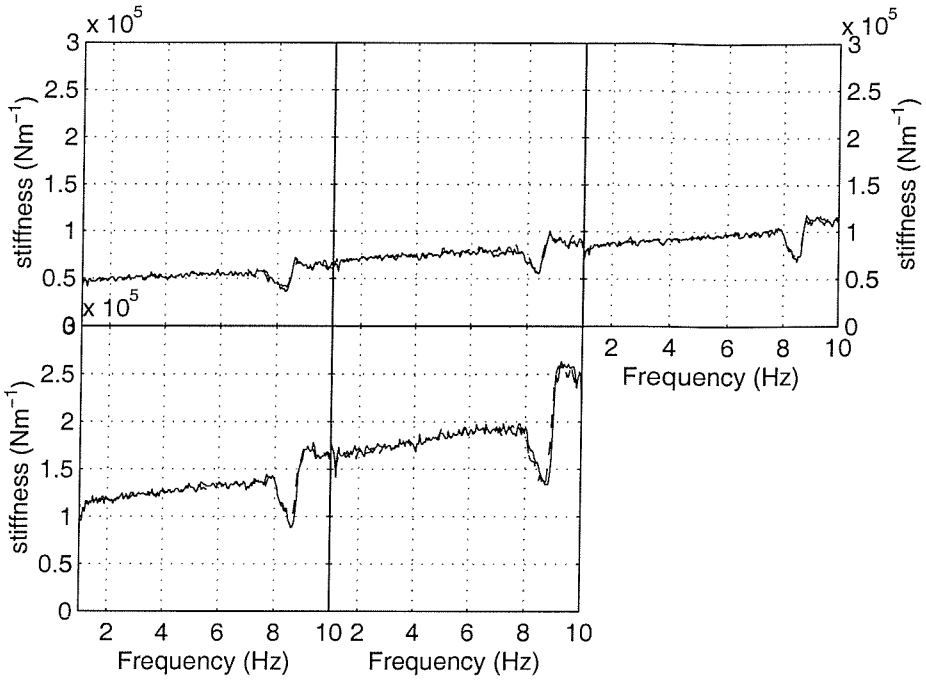

Figure 6-21 Estimated cushion linear dynamic stiffness at 5 preloads and both magnitudes (low-solid, high-dashed) using the random input motion with the agricultural tractor seat cushion

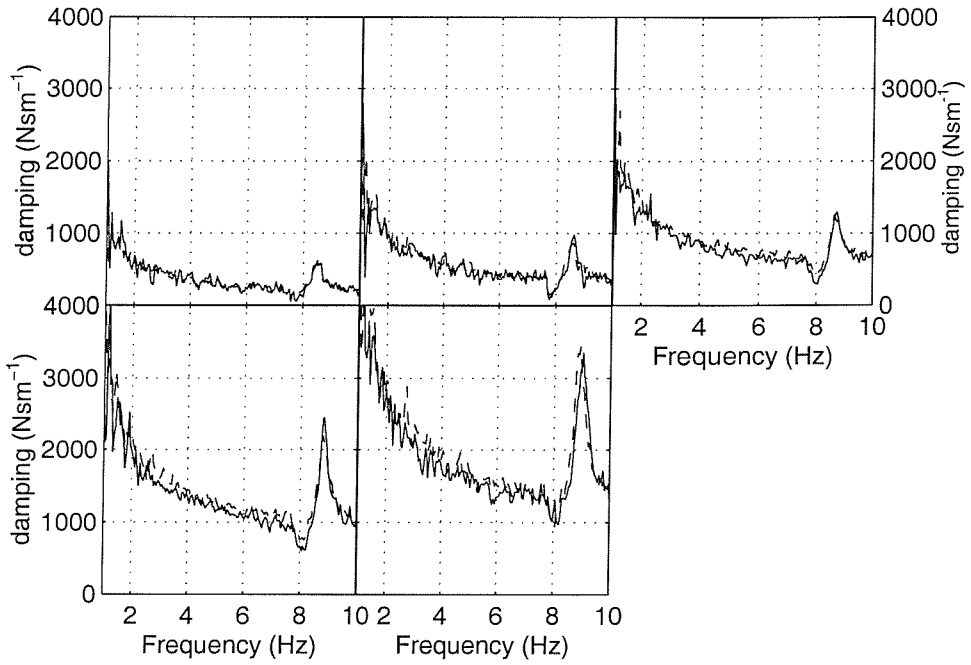

Figure 6-22 Estimated cushion linear dynamic damping at 5 preloads and both magnitudes (low-solid, high-dashed) using the random input motion with the agricultural tractor seat cushion.

6.2.3.7 The dynamic cushion damping

6.2.3.7.1 Overview

The damping estimates were almost identical for both waveforms and both amplitudes of motion and showed an exponential decrease with increasing frequency. This could be represented by a displacement-proportional component in the overall damping force. The asymptote towards which the damping estimate decayed at high frequencies (and therefore low displacements) would be the velocity-proportional viscous component. However, this explanation does not seem to agree with other models for the behaviour of foam that suggest that foam damping should be described by a viscous and a velocity squared term (Patten *et al*, 1998).

6.2.3.7.2 Extraction of displacement- and velocity-proportional damping coefficients

Separate coefficients for the displacement- proportional and velocity-proportional damping can be extracted using the following procedure. If it is assumed that the damping force consists of a velocity and a displacement proportional component, the damping force might assumed to be

$$F = c_v \dot{x} + c_d x$$

Where c_v is the viscous damping coefficient and c_d is the displacement proportional component. If all elements of the damping force are in phase then the damping force becomes:

$$F = \left(c_v + \frac{c_d}{\omega} \right) \dot{x}$$

This would show a decay towards an asymptote as seen in the data. Multiplying through by the angular frequency (ω) gives converts the damping force from constant velocity to constant displacement, with the form

$$F = c_v \omega + c_d$$

Therefore, the gradient of the damping force in the frequency domain expressed in terms of constant displacement gives the velocity-proportional damping force and the zero intercept gives the displacement proportional damping force.

These values were extracted from the data by applying a least-squares straight line fit to the measured constant displacement magnitude damping force for frequencies at which with coherence was above 0.95. The data from the high magnitude random input tests are shown in Figure 6-23 to Figure 6-25 and the damping values are summarised in Table 6-3.

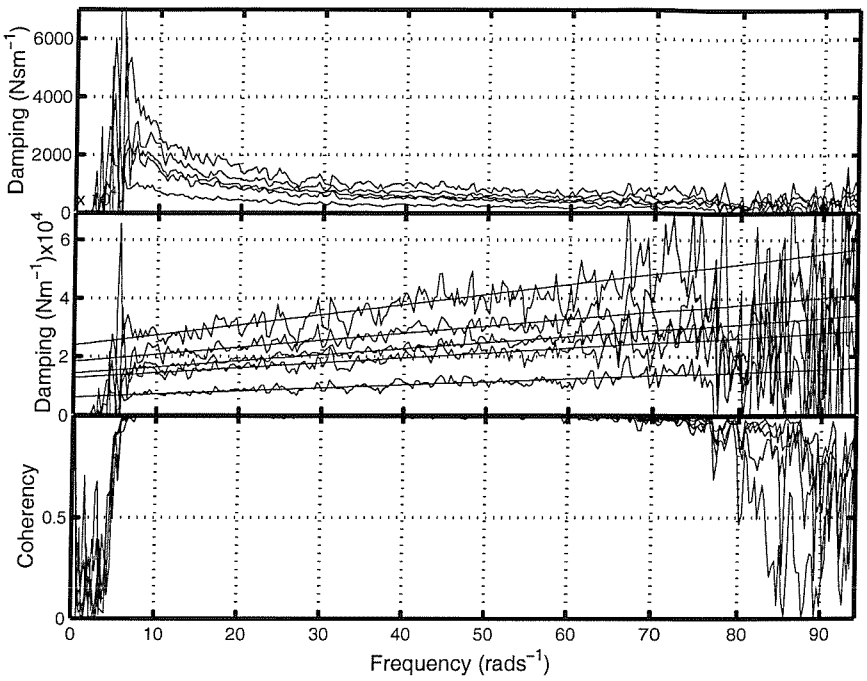

Figure 6-23 Linear damping coefficient estimates for the earthmover seat cushion expressed in terms of velocity- and displacement-proportional coefficients. Data are shown for all five preloads and the high magnitude input. The line fits used to estimate the damping coefficients are also shown.

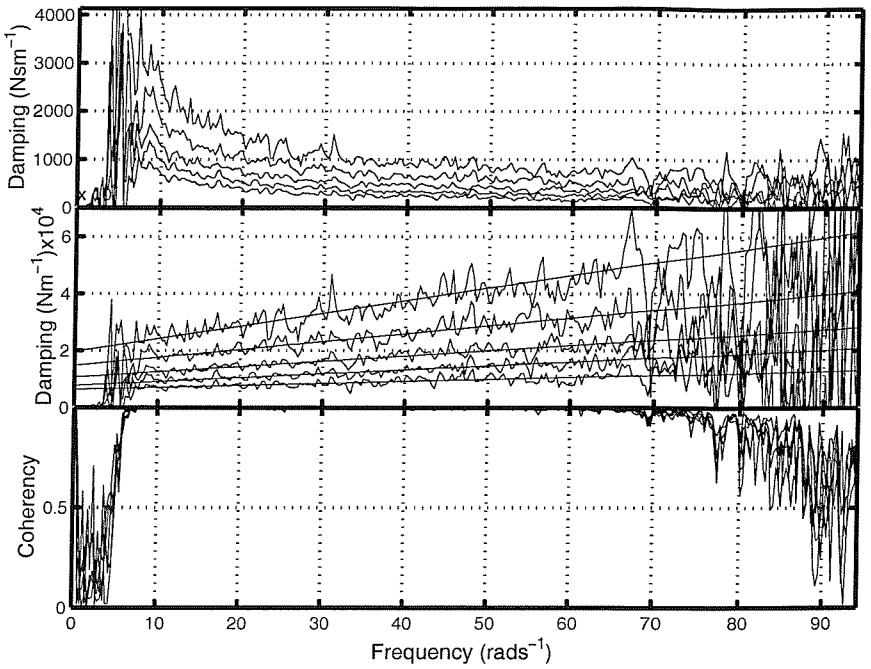

Figure 6-24 Linear damping coefficient estimates for the forwarder seat cushion expressed in terms of velocity- and displacement-proportional coefficients. Data are shown for all five preloads and the high magnitude input. The line fits used to estimate the damping coefficients are also shown.

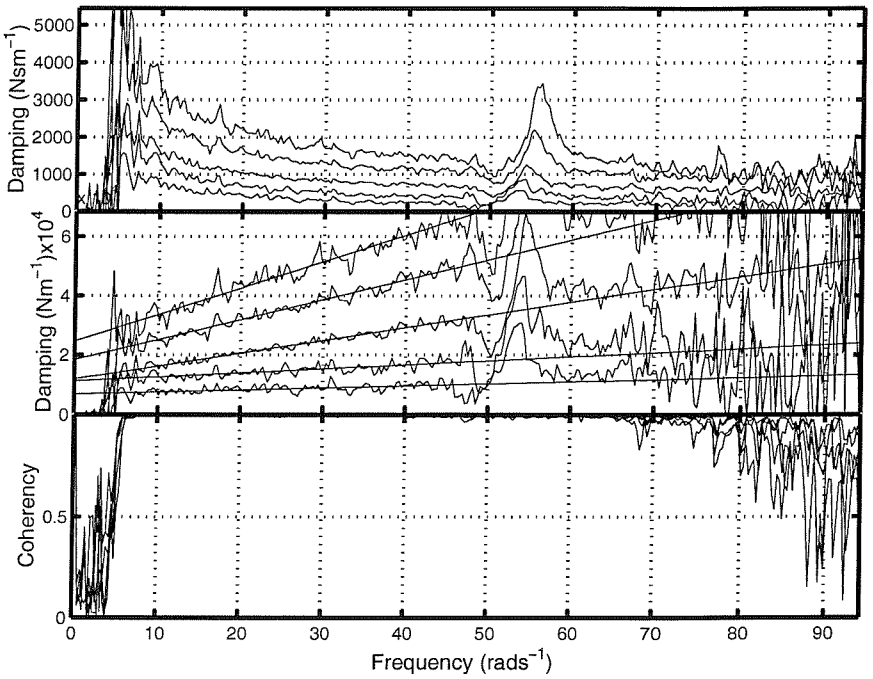

Figure 6-25 Linear damping coefficient estimates for the agricultural tractor seat cushion expressed in terms of velocity- and displacement-proportional coefficients. Data are shown for all five preloads and the high magnitude input. The line fits used to estimate the damping coefficients are also shown.

Table 6-3 Estimated velocity- and displacement-proportional damping coefficients using the medium magnitude random input

Preload (N)	Tractor seat		Forwarder seat		Earthmover seat	
	$\propto \dot{x}$ (Nsm^{-1})	$\propto x$ (Nm^{-1})	$\propto \dot{x}$ (Nsm^{-1})	$\propto x$ (Nm^{-1})	$\propto \dot{x}$ (Nsm^{-1})	$\propto x$ (Nm^{-1})
100	68	6918	72	6304	95	6533
300	129	11365	120	8336	159	13186
500	430	11949	203	10067	208	14619
700	678	18131	282	14941	238	18650
900	891	24634	406	20764	306	24643

6.2.3.7.3 The variation in dynamic damping with cushion compression

The estimated damping values for all cushions and all input magnitudes using the random input are shown in Figure 6-26 and Figure 6-27. As mentioned, the damping forces were similar with all magnitudes of random and sinusoidal motion.

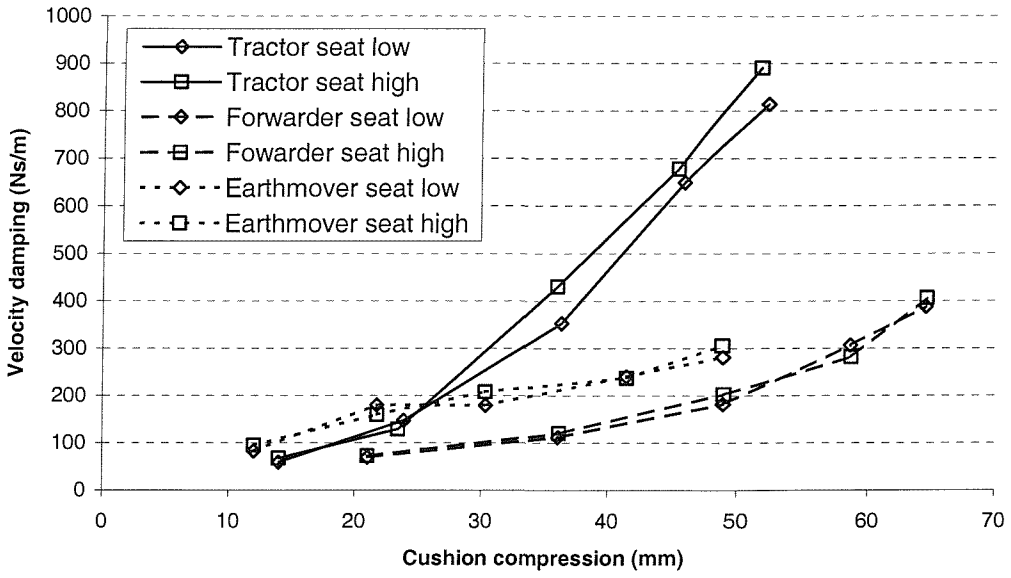

Figure 6-26 Estimated velocity-proportional dynamic damping coefficients for all cushions and magnitudes of random input motion

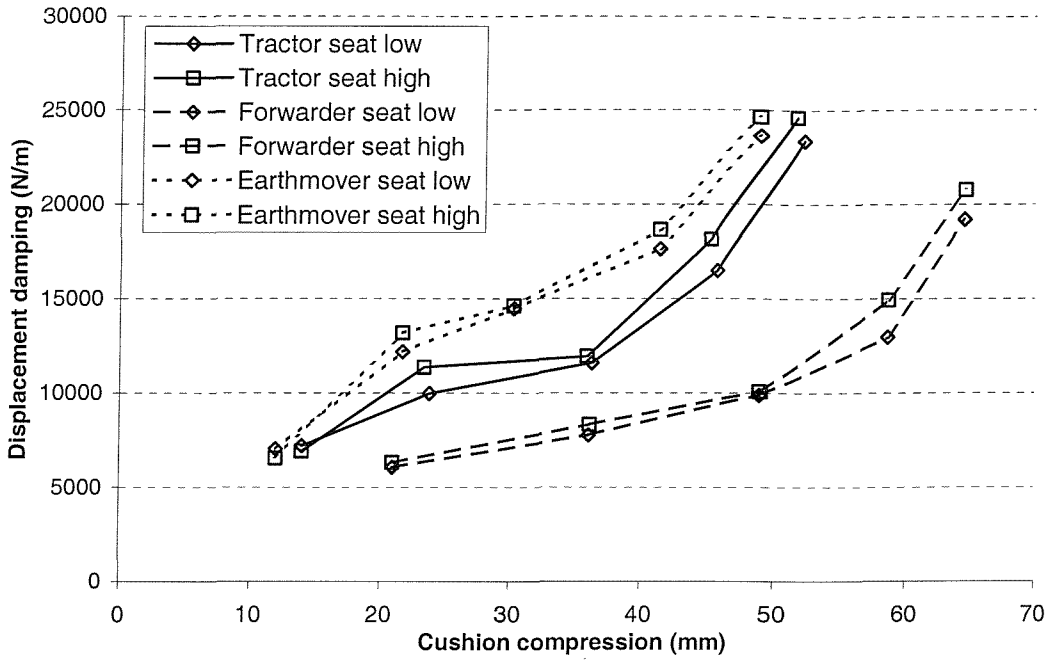

Figure 6-27 Estimated displacement-proportional dynamic damping coefficients for all cushions and all magnitudes of random input motion

The variation in damping coefficient with cushion compression can be expressed in terms of polynomial curve fit coefficients. Figure 6-28 shows the dynamic velocity-proportional damping coefficients for the high magnitude random motion varying with the compression of the cushion due to the preload. The figures also show a least-squares 3rd order polynomial fit to the data, extrapolated for high preloads and confined to zero at zero preload. The curve fit equation was:

$$c_v(x) = a_1 x^3 + a_2 x^2 + a_3 x \qquad \text{Equation 6-7}$$

where a_1, a_2 and a_3 are the curve fit coefficients and c_v is the velocity-proportional damping coefficient varying with cushion compression x. The curve fit coefficients are shown in Table 6-4.

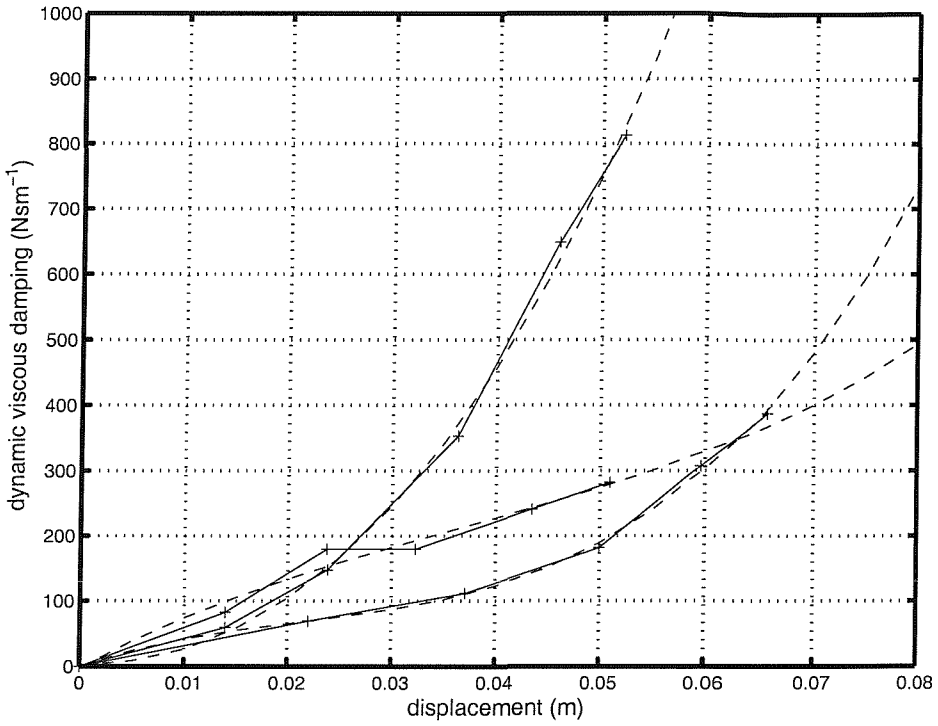

Figure 6-28 Cushion velocity-proportional dynamic damping coefficients mesured with the high magnitude random motion and fitted with a 3rd-order polynomial (dashed line). Coefficients are for the forwarder, earthmover and agricultural tractor seat cushions in order of increasing damping at 0.04 m compression.

Table 6-4 Cushion viscous damping 3rd order polynomial curve fit coefficients to dynamic measurements

	Earthmover seat	Forwarder seat	Tractor seat
a_1	1.07 x 10^6	2.72 x 10^6	1.49 x 10^6
a_2	-1.18 x 10^5	-1.73 x 10^5	2.25 x 10^5
a_3	8.74 x 10^3	5.63 x 10^3	1.26

Figure 6-29 shows the change in displacement-proportional damping with cushion compression. A 4th order polynomial was fitted to the dynamic displacement-proportional damping coefficients according to the following equation. The figure shows the curve fit function extrapolated for high preloads and restricted to zero at zero compression.

$$c_d(x) = b_1x^4 + b_2x^3 + b_3x^2 + b_4x \qquad \text{Equation 6-8}$$

where b_1, b_2, b_3 and b_4 are the curve fit coefficients and c_d is the displacement-proportional damping coefficient varying with cushion compression x. The curve fit coefficients are shown in Table 6-5.

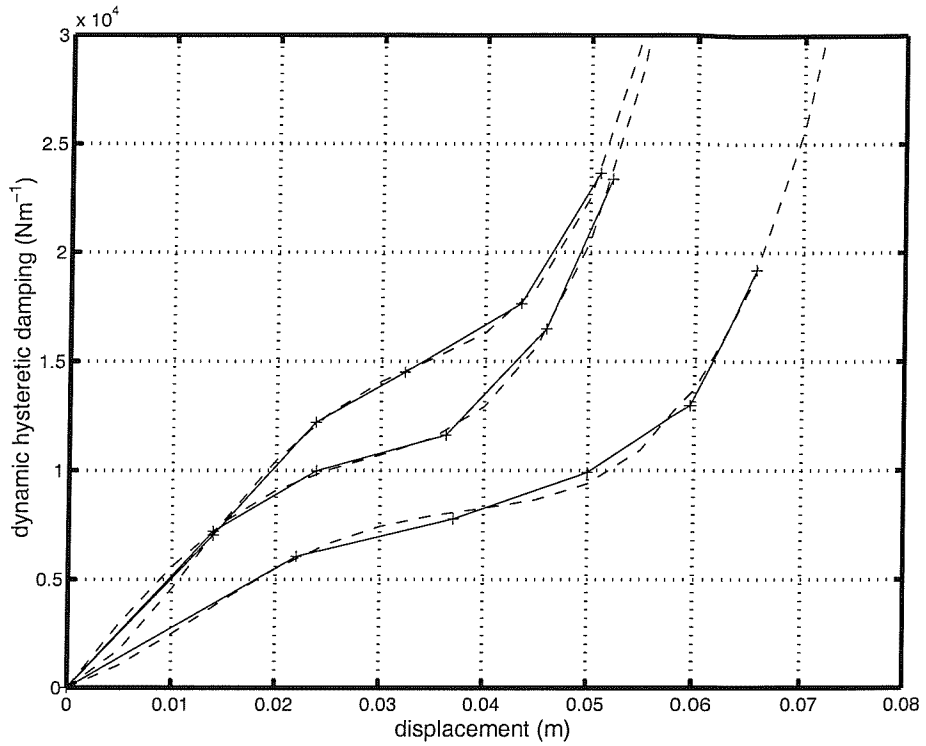

Figure 6-29 Cushion displacement-proportional dynamic damping coefficients mesured with the medium magnitude radom motion and fitted with a 4th-order polynomial (dashed line). Coefficients are for the forwarder, agricultural tractor and earthmover seat cushions in order of increasing damping at 0.04 m compression.

Table 6-5 Cushion hysteretic damping 4th order polynomial curve fit coefficients to dynamic measurements

	Earthmover seat	Forwarder seat	Tractor seat
b_1	2.22×10^{10}	6.17×10^{9}	9.43×10^{9}
b_2	-1.93×10^{9}	-6.29×10^{8}	-5.29×10^{8}
b_3	4.65×10^{7}	1.71×10^{7}	-1.19×10^{6}
b_4	2.50×10^{5}	1.34×10^{5}	6.14×10^{5}

6.2.3.7.4 An overall damping coefficient

Previous investigations (Wei and Griffin, 1998) used a single coefficient to represent the damping by taking a mean value over a range of frequencies. These studies were concerned with seat cushion simulation for automotive applications where the input motion has energy at frequencies up to 20 Hz. Unfortunately at the low frequencies (2 to 3 Hz) found on the cab floor of the off-road vehicles used for this thesis the damping shows a distinct frequency dependence as can be seen in Figure 6-14 to Figure 6-16.

An overall damping coefficient for each cushion was obtained by taking the value at 2 Hz, which was the median frequency used in the laboratory experiments described in Chapter 5. These coefficients are shown in Table 6-6.

Table 6-6 Estimated coefficient for the overall cushion damping at 2 Hz using the medium magnitude random input and a 500 N preload

Preload (N)	**Tractor seat** (Nsm^{-1})	**Forwarder seat** (Nsm^{-1})	**Earthmover seat** (Nsm^{-1})
100	619	574	615
300	1033	783	1208
500	1381	1004	1371
700	2121	1471	1722
900	2851	2058	2267

6.2.3.8 The dynamic cushion stiffness

The dynamic stiffness coefficient for each cushion was defined using the same conditions as used to define the dynamic damping coefficient. The stiffness coefficient was the value obtained at 2 Hz using the high magnitude random motion (see Figure 6-17, Figure 6-19 and Figure 6-21).

The variation in cushion stiffness coefficient with increasing cushion compression for all cushions and random input magnitudes are shown in Figure 6-30. The values corresponding to the medium magnitude input are shown in Table 6-7.

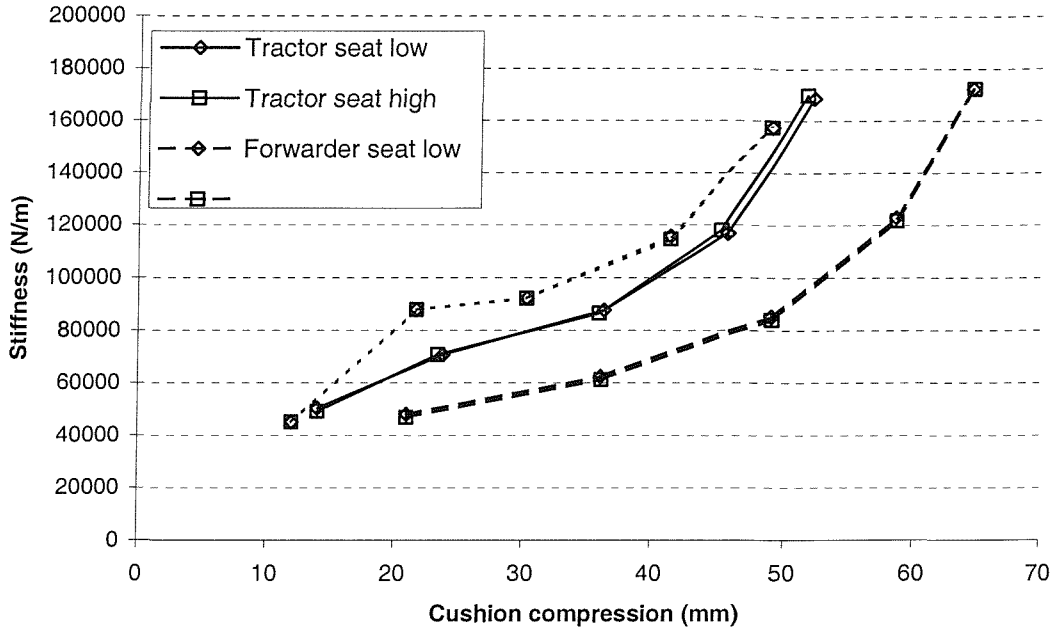

Figure 6-30 Estimated linear dynamic stiffness values for all cushions and all magnitudes of random input motion

Table 6-7 Estimated cushion dynamic stiffness using the medium magnitude random input motion

Preload (N)	**Cushion stiffness (kNm^{-1})**		
	Tractor seat	**Forwarder seat**	**Earthmover seat**
100	49.2	46.8	45.0
300	70.8	61.2	87.9
500	86.4	84.0	92.1
700	118.1	121.7	114.6
900	179.0	172.3	157.5

The variation in dynamic cushion stiffness with preload can be defined using polynomial curve fit coefficients. Figure 6-31 to Figure 6-33 show the dynamic cushion stiffness as a function of cushion compression. The quasi-static stiffnesses are also shown for comparison. The dashed lines show the 8th order polynomial function fitted to the low velocity stiffness coefficients (see Section 6.2.2.3) and a 4th order polynomial least squares fit applied to the dynamic stiffness coefficients according to:

$$k(x) = d_1x^4 + d_2x^3 + d_3x^2 + d_4x \qquad \text{Equation 6-9}$$

where d_1, d_2, d_3 and d_4 are the curve fit coefficients and k is the dynamic stiffness coefficient varying with cushion compression x. The polynomial functions were restricted to zero at zero compression and are summarised in Table 6-8.

It can be seen that the cushion stiffness determined dynamically was approximately 4 times the value determined using the quasi-static test for all three seats. The trends for changes in stiffness with cushion compression are similar using both measurement methods. The differences in stiffness coefficient magnitude may have been caused by the different behaviour of the air trapped within the foam structure as described by Hilyard (1982).

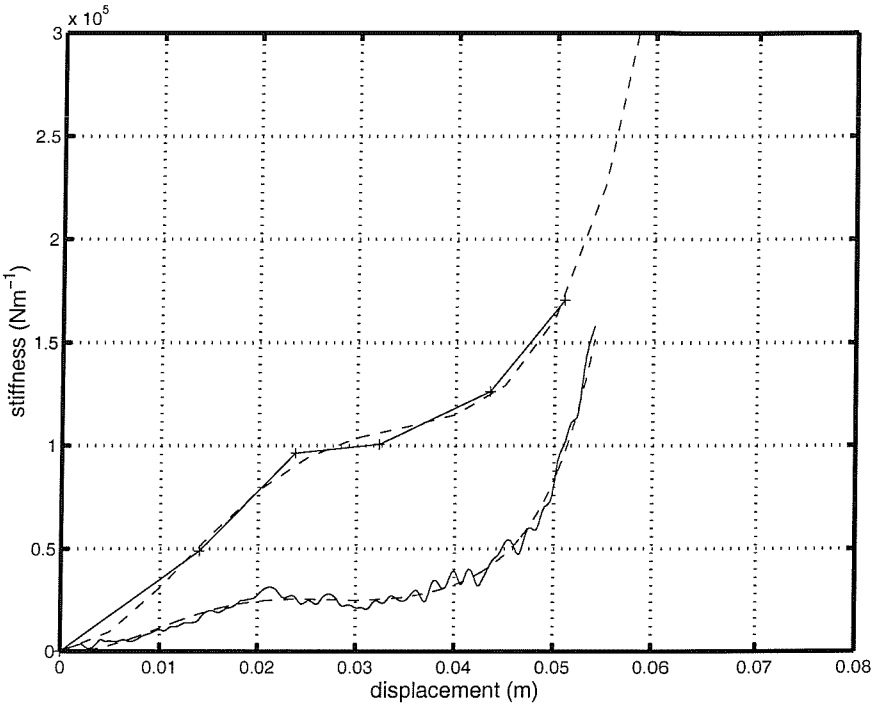

Figure 6-31 Earthmover seat cushion stiffness with cushion compression displacement estimated from quasi-static (lower curve) and dynamic measurements. The dashed lines are polynomial fits to the data (quasi-static: 8th order, dynamic: 4th order)

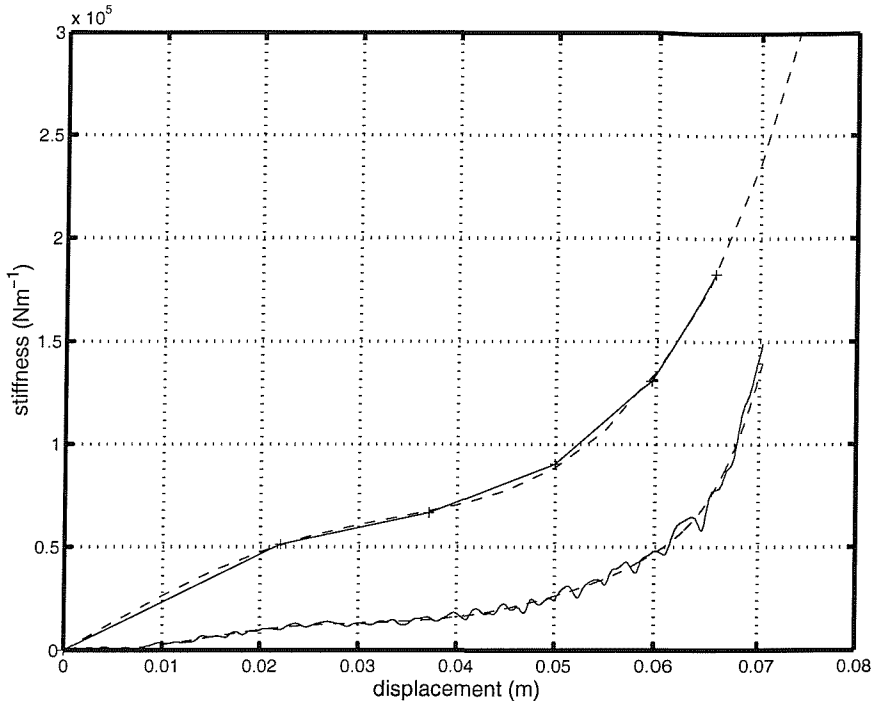

Figure 6-32 Forwarder seat cushion stiffness with cushion compression displacement estimated from quasi-static (lower curve) and dynamic measurements. The dashed lines are polynomial fits to the data (quasi-static: 8th order, dynamic: 4th order)

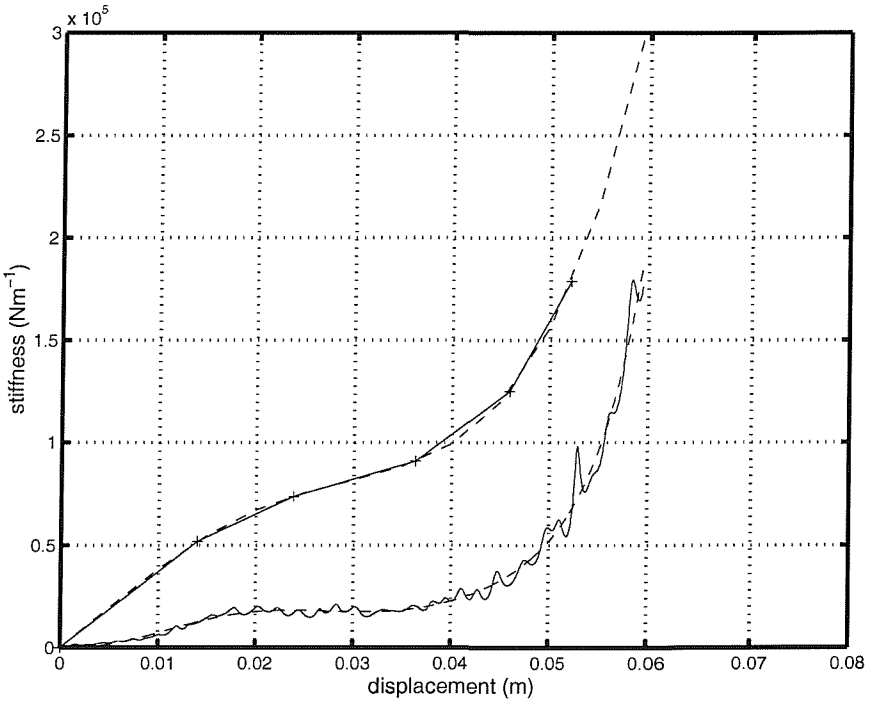

Figure 6-33 Agricultural tractor seat cushion stiffness with cushion compression displacement estimated from quasi-static (lower curve) and dynamic measurements. The dashed lines are polynomial fits to the data (quasi-static: 8th order, dynamic: 4th order)

Table 6-8 Cushion stiffness 4th order polynomial curve fit coefficients to the dynamic stiffness coefficients using the medium magnitude random input motion.

	Earthmover seat	Forwarder seat	Tractor seat
d_1	1.80×10^{11}	3.10×10^{10}	8.35×10^{10}
d_2	-1.96×10^{10}	-2.33×10^{9}	-5.60×10^{9}
d_3	4.58×10^{8}	2.20×10^{7}	5.89×10^{7}
d_4	7.69×10^{4}	2.63×10^{6}	3.74×10^{6}

6.2.4 Summary of the cushion

The cushion measurements conducted during this study indicated that:

1. The dynamic cushion stiffness and damping increased with increasing preload.
2. The dynamic cushion stiffness increased in a linear manner by between 10 and 20% over the frequency range from 1 to 10 Hz.
3. The dynamic damping decreased exponentially towards a non-zero asymptote with increasing frequency.
4. The random and sinusoidal input motions resulted in similar dynamic stiffness and damping coefficients.
5. The input magnitude was found to have little effect on the dynamic stiffness and damping coefficients.
6. The dynamic stiffness was in the order of a factor of 4 greater that the static stiffness for all cushions and all compressions but showed the same trends with increasing compression.
7. The displacement-proportional dynamic damping coefficients showed similar trends to the stiffness coefficients with increasing preload.

Coefficients have been determined to describe the following dynamic properties of the three seat cushions involved in this project:

1. The static stiffness varying with cushion compression.
2. The dynamic stiffness varying with cushion compression determined at 2 Hz.
3. The component of the damping force proportional to the velocity across the cushion varying with cushion compression.

4. The component of the damping force proportional to the displacement across the cushion varying with cushion compression.
5. The overall damping force varying with cushion compression determined at 2 Hz.

6.3 The suspended mass

6.3.1 Introduction

The suspended mass included the mass of the cushion, the backrest, the seat pan, any seat attachments (armrests, headrests, seat belt anchorages, etc.) and the moving parts of the suspension mechanism. By treating the individual masses of these components as a single lumped mass the dynamic behaviour of the suspension and the cushion could be considered in terms of massless elements, considerably reducing the complexity of the model.

6.3.2 Method and results

The moving mass of the suspension mechanism was estimated for each seat using the following technique:

1. The cushion or seat pan and backrest assembly were removed from the suspension and weighed separately.
2. The dampers were disconnected to reduce the friction and weighed separately.
3. The coil springs were removed from the earthmover seat and weighed separately. The springs were mounted in the upper part of the suspension on this seat and therefore contributed to the suspended mass. The exhaust valves to the air springs on the other two seats, effectively removing the suspension stiffness to zero.
4. A spring balance was attached to the centre of the top suspension mechanism of each seat and the suspension was lifted using the balance to a point close to the centre of the free travel.
5. The force required causing the suspension to break away from friction upwards and downwards at this point was measured.
6. The mean of the upward and downward force was taken to be the weight of the moving mass of the suspension mechanism. It was assumed that the friction force was equal in the upward and downward

directions. The masses of any removed components were added to this to give an estimate for the total suspended mass.

The results are shown in Table 6-9.

Table 6-9 Suspension moving mass (kg)

	Tractor	Forwarder	Earthmover
Moving mass	36 kg	21 kg	27 kg

6.4 The suspension spring and the linkage friction

6.4.1 Introduction

The suspension stiffness and the linkage friction were determined from the quasi-static force-deflection characteristic of the suspension mechanism. The indenter rig as used to test the cushions in Section 6.2.2 was used.

The suspension damper was removed from the suspension to be tested separately and the seat assembly (the cushion, backrest, armrests, etc.) was removed to prevent the compliance of the cushion from affecting the results.

6.4.2 Pre-loading conditions

The suspension mechanisms were tested with seat loading forces of 370N, 550N and 740N. The weights of any parts of the cushion and backrest assembly that had been removed were added to each of these preloads.

In order to adjust the seat to this preload, the mechanisms were compressed using the indenter until the suspension reached a point 10 mm below the centre of the free travel. The suspension spring mechanism was adjusted until the measured force corresponded to the desired preload. The spring was adjusted either by altering the preload on the coil springs on the earthmover seat or altering the pressure in the air springs for the forwarder and agricultural tractor seats.

Once the suspension preload was adjusted the suspension was released before beginning measurements. Any self-levelling devices present on the air suspension seats were disabled so that the quantity of air in the spring did not vary during the measurements.

6.4.3 Measurement method

The quasi-static force-deflection characteristics of suspension mechanisms were measured by compressing and releasing the mechanism at a velocity of 1.5 mm per second. Each suspension unit was placed on the shaker top plate and the plate was

secured so that the compliance of the shaker would not influence the results. The VP85 shaker was not used for these measurements.

The indenter plate was positioned so as to be not quite in contact with the top of the suspension. The point of application of the indenter force was positioned close to the centre of the mechanism top plate. The suspension was compressed at 1.5 mm per second until a force of approximately 2000N was recorded. The indenter was then moved back up to the starting position at the same rate with no pause between compressing and releasing the mechanism. The displacement of the indenter plate and the force applied to the test item were acquired at 200 samples per second using an *HVLab* data acquisition system via a 66 Hz anti-aliasing filter. Each measurement was repeated three times.

6.4.4 Results

The quasi-static force-deflection characteristics of the three suspension mechanisms are shown in Figure 6-34 to Figure 6-36.

The initial rise visible in all the plots was due to the top end-stop buffer. The force-deflection plots then reach an approximately linear region due to the suspension spring. The rapid rise at high displacements was due to the bottom end-stop buffer. The losses were due to friction in the linkage mechanism opposing the motion.

The behaviour of the steel coil spring mechanism (the earthmover seat, Figure 6-34) was noticeably more linear than the air sprung mechanisms of the other seats (Figure 6-35 and Figure 6-36). The force-deflection gradients (and therefore spring rates) of the air sprung mechanisms tended to increase as the mechanism becomes more compressed. The difference between the compression and extension forces at any displacement, indicative of the friction force, tended to decrease with greater compression of the air sprung mechanisms.

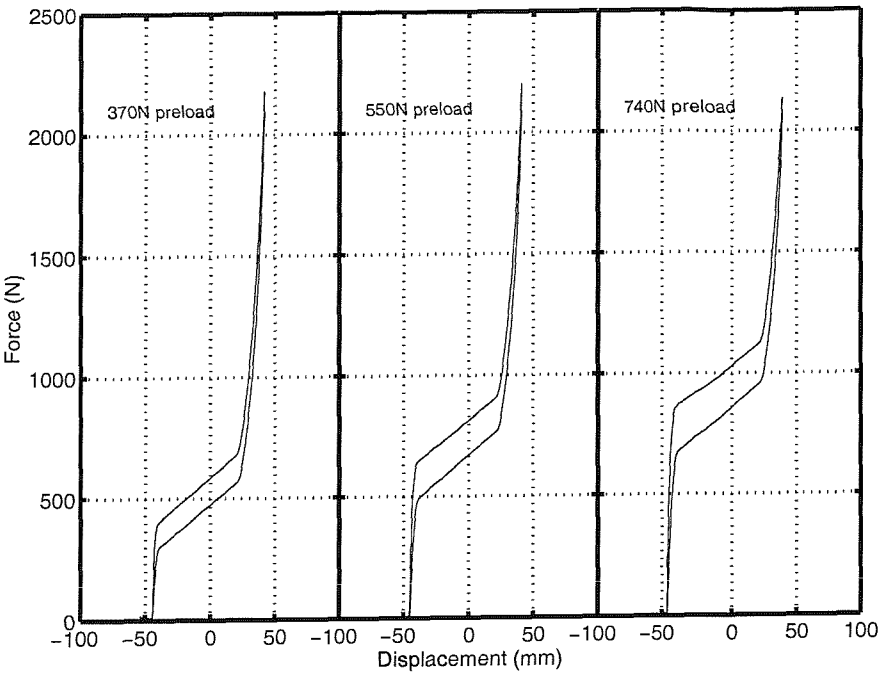

Figure 6-34 The quasi-static force-deflection characteristic of the earthmover seat suspension mechanism

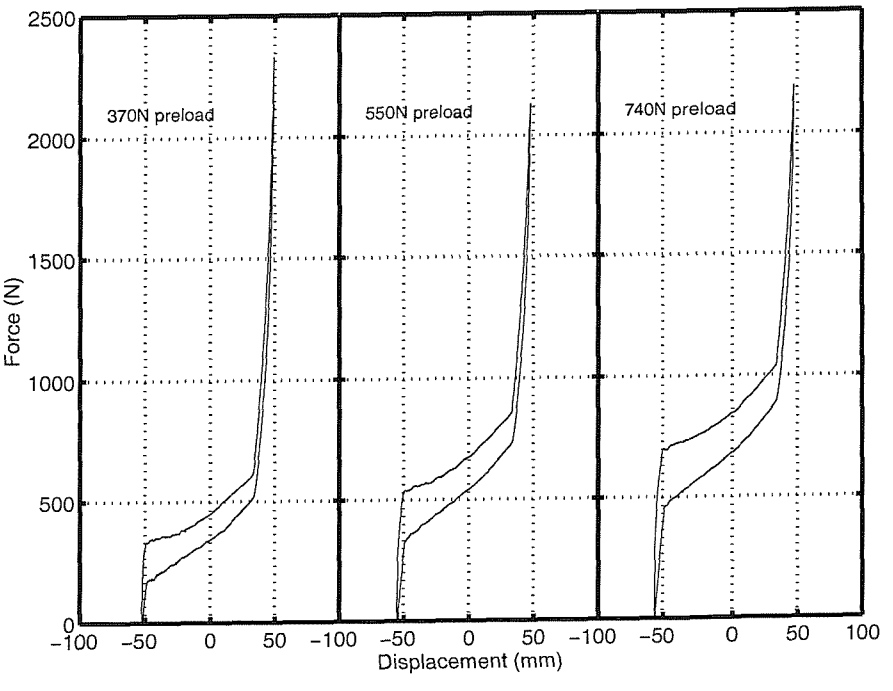

Figure 6-35 The quasi-static force-deflection characteristic of the forwarder seat suspension mechanism

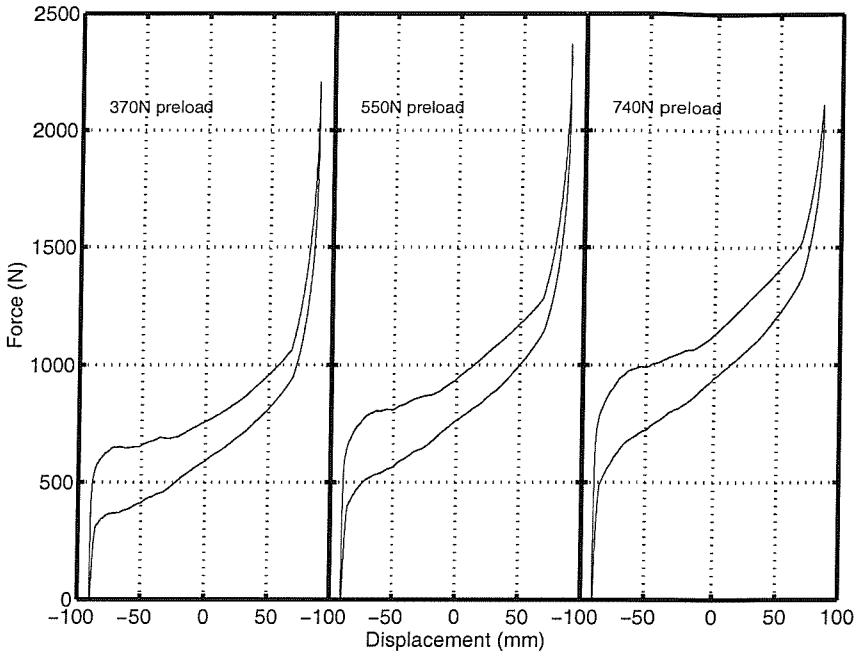

Figure 6-36 The quasi-static force-deflection characteristic of the agricultural tractor seat suspension mechanism

6.4.5 The suspension stiffness

The free travel compression and extension sections of the force-deflection data were extracted for each of the three seats and preload conditions. A least squares linear fit over the suspension free travel was used to estimate a value for the spring rate in compression and extension. Figure 6-37 to Figure 6-39 show the results obtained. The spring rate was taken as the mean rate in extension and compression for each preload as shown in Table 6-10.

These stiffness values were those seen by the suspension moving vertically, not necessarily the stiffnesses of the individual springs. In the case of the earthmover seat the springs were substantially stiffer than the value measured by the force-deflection test and were connected to the suspension via a cam arrangement.

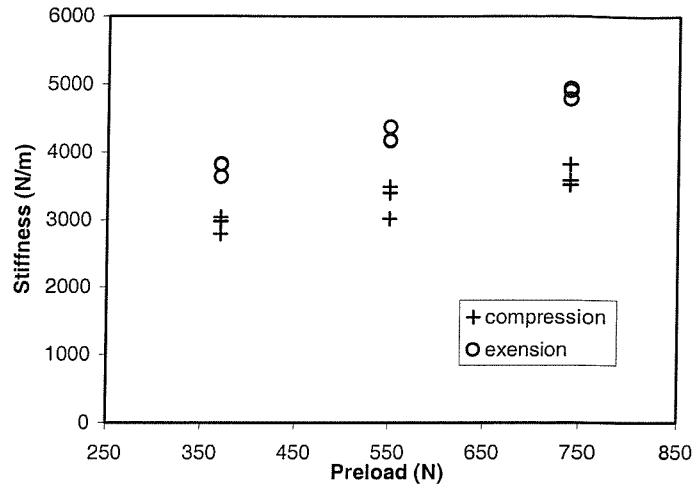

Figure 6-37 The approximate linear spring rate of the agricultural tractor seat suspension

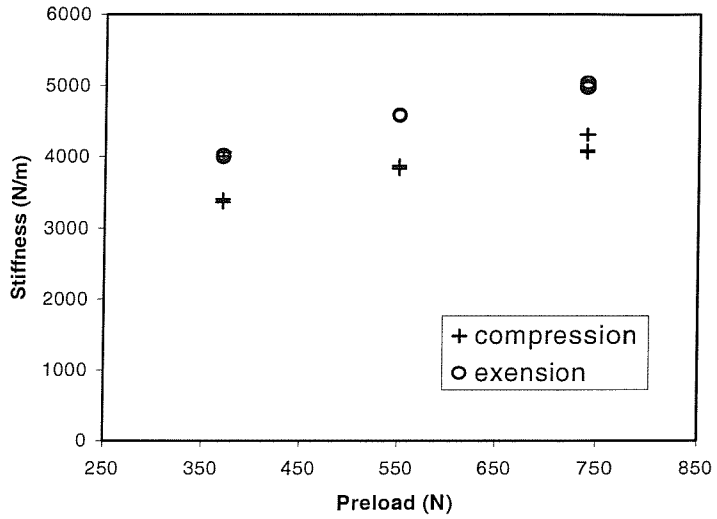

Figure 6-38 The approximate linear spring rate of the forwarder seat suspension

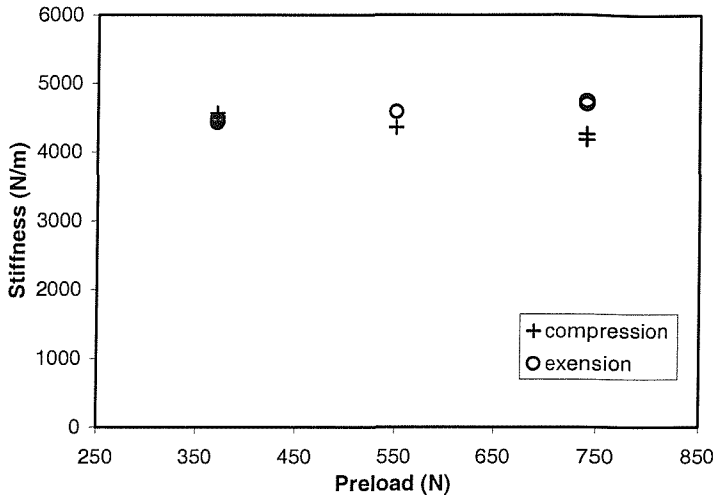

Figure 6-39 The approximate linear spring rate of the earthmover seat suspension

Table 6-10, Estimated linear suspension spring rates, in Nm^{-1}

	370 N preload			550 N preload			740 N preload		
	Comp ⇓	Ext ⇑	Mean	Comp ⇓	Ext ⇑	Mean	Comp ⇓	Ext ⇑	Mean
Tractor	2937	3760	*3349*	3381	4008	*3694*	4543	4450	*4497*
Forwarder	3301	4235	*3768*	3850	4579	*4215*	4356	4586	*4471*
Earthmover	3640	4872	*4256*	4149	4999	*4574*	4234	4717	*4475*

6.4.6 Linkage friction force

The friction force was estimated as half the mean difference between the compression and extension data over the suspension free travel. The extracted compression and extension data were resampled against a constant increment displacement vector and a mean difference was obtained from the average of the differences at each increment. The friction force was taken as half this difference value on the assumption that the friction force acted with the same magnitude with the suspension moving upwards and downwards. Figure 6-40 shows mean estimates for the friction force. The friction forces averaged over 3 repetitions of each measurement are shown in Table 6-11

The friction force increased with increasing preload for all three seats. The agricultural tractor seat had a higher friction force for all preloads, but the increase with preload was less than with the forwarder and earthmover seats. The increase in friction with increasing preload may have been due to the increased loading on the bearings and joints in the seat.

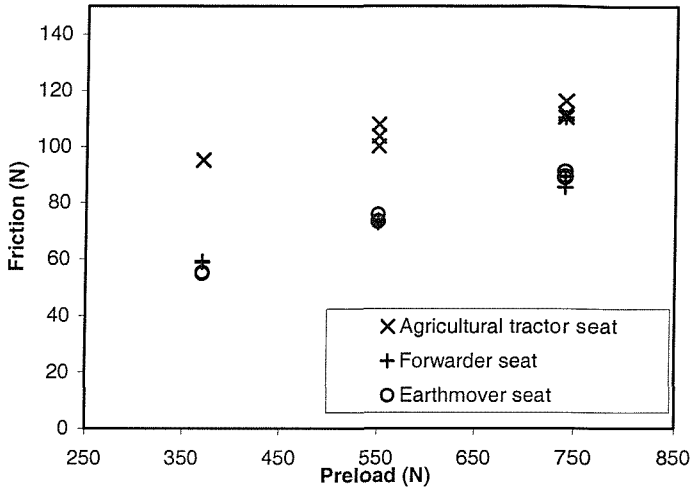

Figure 6-40 The linkage friction force for all suspension mechanisms

Table 6-11, Estimated suspension linkage friction force

	370N preload	550N preload	740N preload
Tractor	95 N	104 N	115 N
Forwarder	59 N	73 N	95 N
Earthmover	55 N	74 N	90 N

6.5 The suspension damper

6.5.1 Measurement of the damper dynamic characteristics

6.5.1.1 Introduction

The approach adopted for this project was initially to use a commercial damper test device that outputted a force-velocity characteristic and a Coulomb friction component. Simulations conducted using the results from this device were disappointing and a global parametric optimisation indicated that the coefficients describing the damper were substantially (between 1.5 and 2 times) greater than optimal.

Further tests on the damper were conducted using a different apparatus in order to examine the dynamic damper behaviour in more detail. Revised values for the force-velocity and Coulomb friction coefficients were obtained using sinusoidal input motions between 1 and 5 Hz. However, the discrepancies between the results from the two sets of test apparatus led to the numerical estimates of the damper dynamic characteristics as described in Chapter 9.

Both sets of apparatus used an actuator to apply sinusoidal motions to the damper and measured the applied velocity and the resulting force.

6.5.1.2 The need to extrapolate

The laboratory seat tests conducted in the laboratory indicated that the highest axial velocity experienced by the suspension dampers during this project were up to 0.38 ms^{-1} for the earthmover and forwarder seats and up to 0.51 ms^{-1} for the agricultural tractor seat. These values were obtained by differentiating the measured relative suspension displacement and allowing for the angled damper mounting for a number of high magnitude test conditions according to the following calculation:

$$\dot{z}_{d\max} = \max\left[\frac{dz_s}{dt}\cdot\cos\left(\arctan\left(\frac{H}{V+z_s}\right)\right)\right] \qquad \text{Equation 6-10}$$

where z_s is the relative vertical displacement and velocity and displacement across the suspension mechanism as measured using the LVDT and H and V are respectively the horizontal and vertical distances between the damper mounting points at mid ride (determined in Section 6.5.3).

This range of velocities was not investigated using the damper test equipment, firstly because the required range of velocities was not known at the time the initial measurements were made and secondly and more significantly because the test apparatus actuators were not capable of a sufficient range of velocities at the frequencies and displacements of interest. It was therefore necessary to extrapolate outside the range of the available data. More powerful damper test equipment would be required to measure the seat dampers over a more complete range of velocities.

6.5.1.3 Tests using a commercial testing device

6.5.1.3.1 Method

The suspension damper units were tested by a member of the TESTOPS consortium using a commercially available damper testing device. The damper was mounted vertically in the device with the same polarity (head up or head down) as it would be mounted in the seat. Depending on the method of construction of each damper, the measured damping forces might not be representative if the damper were tested inverted. The device then applied two swept frequency sinusoids of 30 mm peak-to-peak displacement amplitude to the damper.

The first sinusoid increased from peak velocities of zero to 130 mms^{-1}. The peak velocity was plotted against the corresponding damper force to obtain a force-velocity characteristic for the damper. The damper force in compression and extension were extracted.

The second sinusoid increased from zero to peak velocities of 4 mms^{-1}. This low-velocity force-velocity characteristic of the damper was used to obtain an estimate of the friction force. Again, the compression and extension forces were considered separately. The friction force was estimated as the zero–velocity intercept of a least-squares linear fit to the measured data.

6.5.1.3.2 Results

6.5.1.3.2.1 Force-velocity measurements

Figure 6-41 to Figure 6-43 show the force-velocity characteristics of the damper units fitted to the three seats with the effect of friction removed (i.e. with the force tending towards zero at zero velocity). A two-stage 3rd order polynomial fit was applied to each compression and extension curve according to the following formula:

$$|F| = \left[a_1|\dot{z}| + a_2|\dot{z}|^2 + a_3|\dot{z}|^3\right]_{\dot{z}=0}^{Z} + \left[b_1(|\dot{z}| - Z) + b_2(|\dot{z}| - Z)^2 + b_3(|\dot{z}| - Z)^3 + (a_1 Z + a_2 Z^2 + a_3 Z^3)\right]$$

Equation 6-11

where a_1, a_2 and a_3 are the coefficients of the first stage of the fit for velocities across the damper ($\dot{z}$) between 0 and Z and b_1, b_2 and b_3 are the coefficients for the second stage fit for velocities greater than Z. The coefficients are summarised in Table 6-12

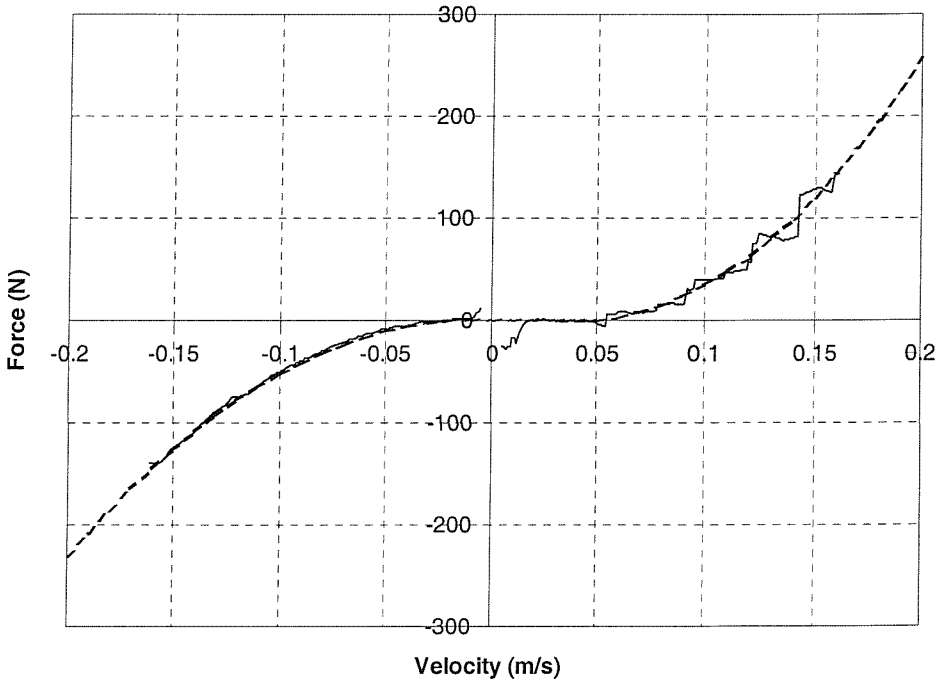

Figure 6-41 Compression and extension force-velocity characteristic of the earthmover seat suspension damper where a positive velocity indicates extension of the damper. The two-stage polynomial curve fit is shown as a dotted line.

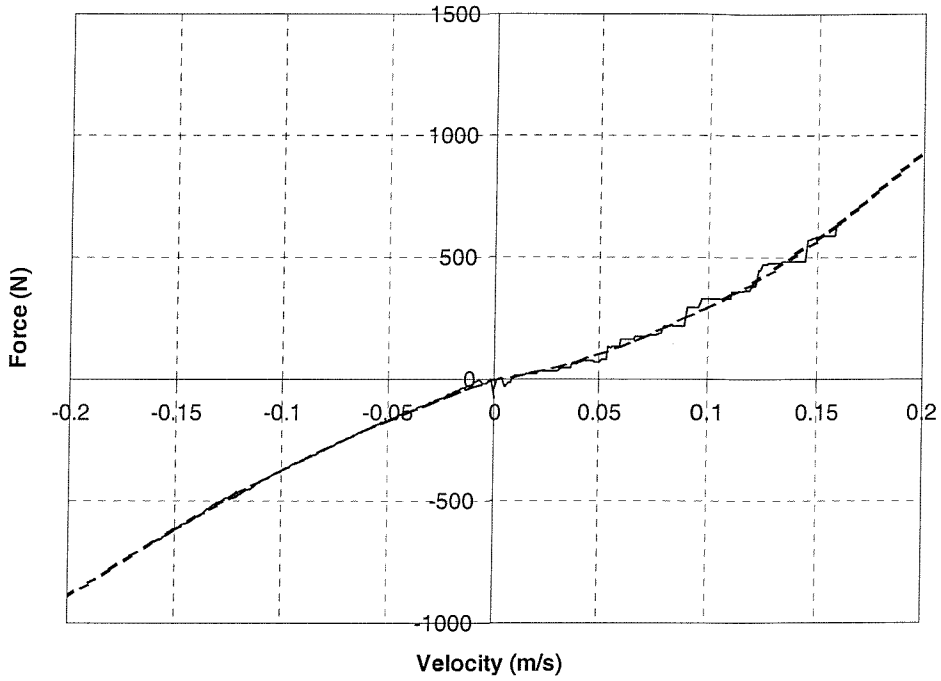

Figure 6-42 Compression and extension force-velocity characteristic of the forwarder seat suspension damper where a positive velocity indicates extension of the damper. The two-stage polynomial curve fit is shown as a dotted line.

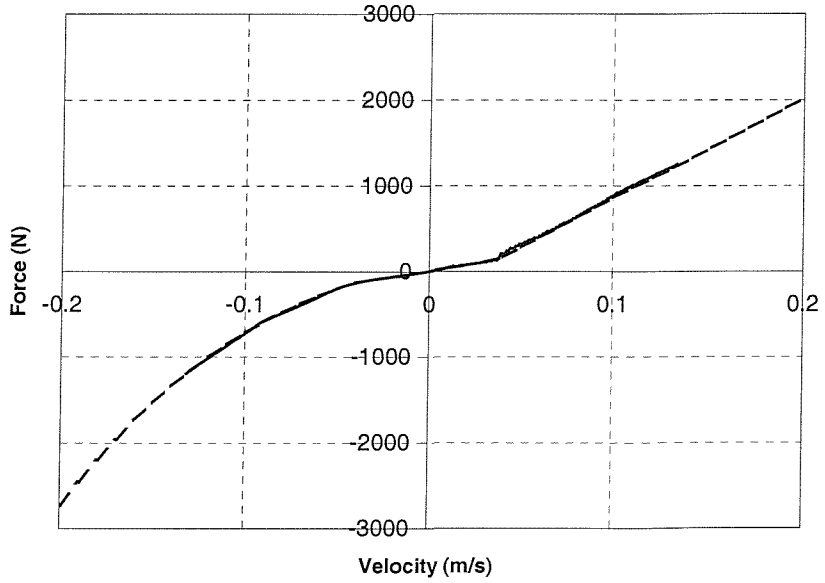

Figure 6-43 Compression and extension force-velocity characteristic of the agricultural tractor seat suspension damper where a positive velocity indicates extension of the damper. The two-stage polynomial curve fit is shown as a dotted line.

Table 6-12 Curve fit coefficients obtained from the force-deflection characteristics obtained using the commercial apparatus

		Earthmover	Forwarder	Agricultural tractor
Compression	a_1	0	0	3220
	a_2	0	0	0
	a_3	0	0	0
	Z	0 ms^{-1}	0 ms^{-1}	0.041 ms^{-1}
	b_1	-107	3020	7370
	b_2	6320	7300	36600
	b_3	0	0	125000
Extension	a_1	0	0	3700
	a_2	0	0	0
	a_3	0	0	0
	Z	0.045 ms^{-1}	0 ms^{-1}	0.038 ms^{-1}
	b_1	61.6	1290	11600
	b_2	10300	16800	0
	b_3	0	0	0

6.5.1.3.2.2 Friction measurements

The friction forces in extension and compression were obtained by extrapolating a series of low-velocity force-velocity measurements to obtain an estimated force at zero velocity. The results are shown in Figure 6-44 to Figure 6-46 and are summarised in Table 6-13.

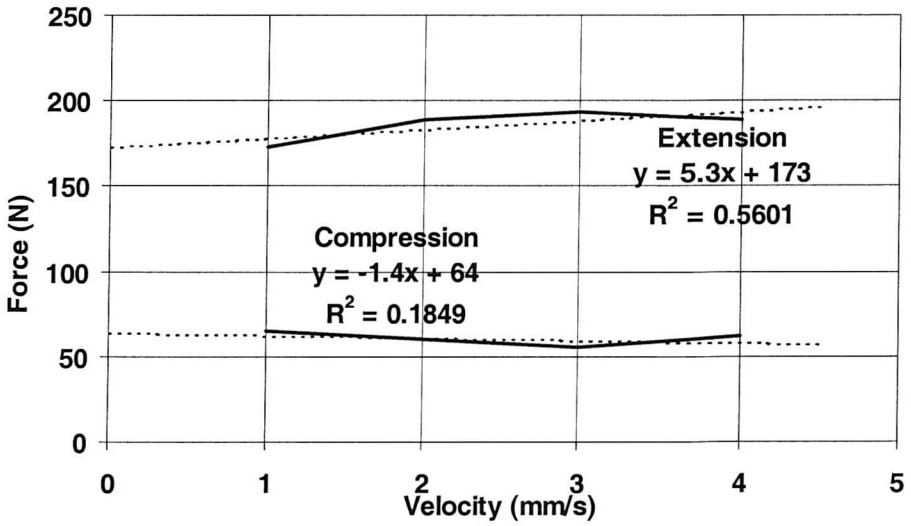

Figure 6-44 Low velocity force-velocity characteristic of the earthmover seat 'light' damper used to determine friction

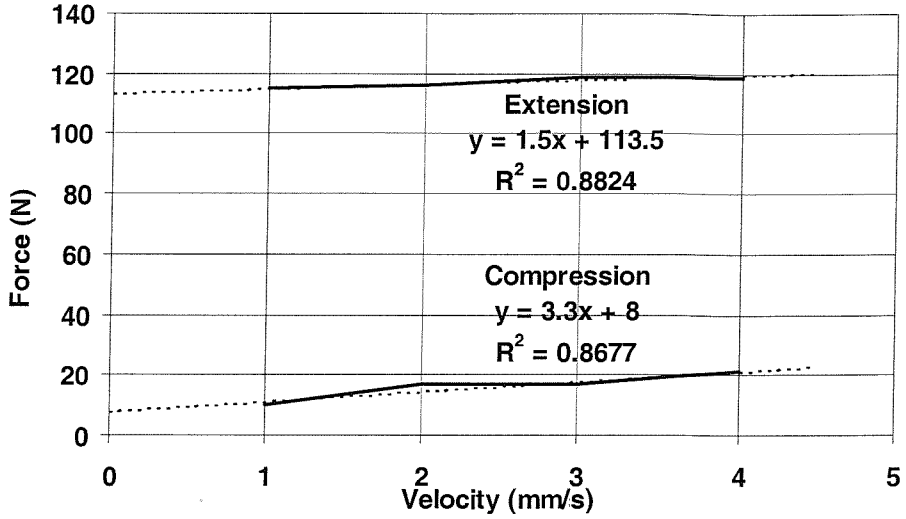

Figure 6-45 Low velocity force-velocity characteristic of the forwarder seat damper used to determine friction

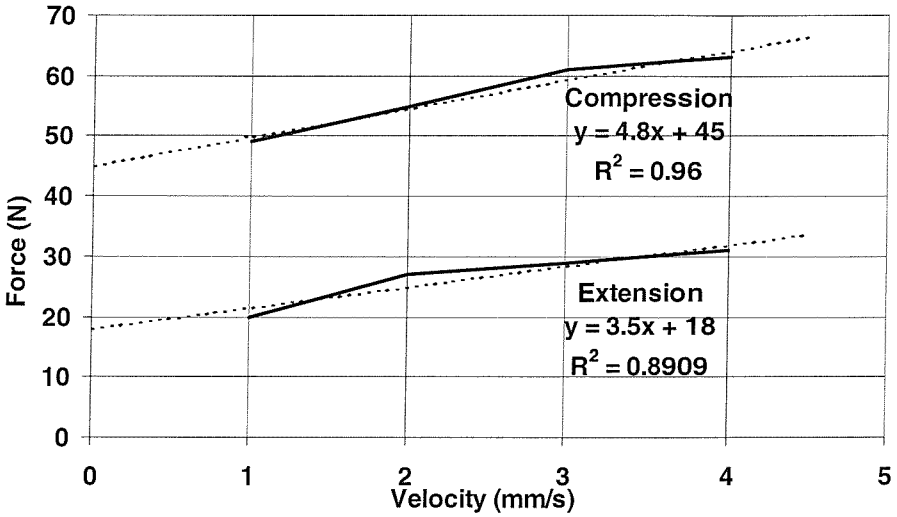

Figure 6-46 Low velocity force-velocity characteristic of the tractor seat damper used to determine friction

Table 6-13 Damper friction measurements from low-velocity tests using the commercial apparatus

Earthmover seat friction (N)		Forwarder seat friction (N)		Agricultural tractor seat friction (N)	
Compression	Extension	Compression	Extension	Compression	Extension
64	173	8	114	45	18

6.5.1.4 Further tests using alternative test apparatus

6.5.1.4.1 Apparatus

The alternative damper test apparatus is shown in Figure 6-47. Each damper was mounted using the same orientation and method of attachment as used in the seat. The damper temperature was monitored using a thermocouple attached to the damper case. A damper case temperature of 30°C ± 2.5°C was maintained for all tests. The dampers were warmed when necessary by cycling with a ± 10 mm 2 Hz sinusoid. This motion was applied for 5 minutes in order to run in the damper on first attaching it to the test apparatus. Cooling was applied to the case during this run in process if the measured case temperature exceeded 35°C.

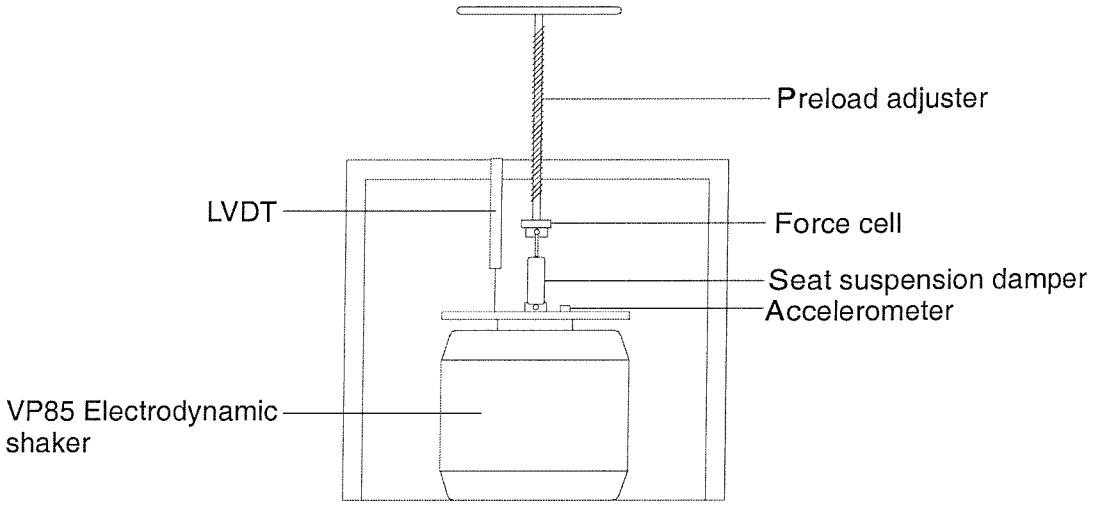

Figure 6-47 The damper test apparatus

The frictional component of the damper was determined from a low velocity force-deflection measurement. Each damper was compressed and extended using the preload adjustment at a rate of 1.5 mms^{-1} with the position of the force cell measured using the LVDT.

The force-velocity characteristics of the dampers were measured using sinusoidal motions at 1.25 Hz, 2 Hz and 3.15 Hz at a displacement amplitude of ± 10 mm. The motions were limited to five seconds duration to reduce the effect of changes in temperature.

The force-displacement-velocity surfaces were determined using an input motion consisting of the sum of ten sinusoids with different phase relationships between 1.25 Hz and 3.15 Hz as listed in Table 6-14. This form of motion was referred to by

Duym (1997) as a 'multisine' but will be referred to here as a quasi-random motion. The phase relationships were chosen to provide an approximately even coverage of the velocity-displacement space as shown in Figure 6-48. The velocity was determined numerically by differentiating the measured displacement after applying a 4^{th} order zero-phase Butterworth bandpass filter between 1 and 10 Hz.

All measurements made with this apparatus use a positive velocity to indicate damper extension. This is the same as the results using the commercial apparatus.

Table 6-14 The components of the quasi-random motion used to obtain the damper force-velocity-displacement surface

	Frequency (Hz)	Phase (degrees relative to an arbitrary reference)
Component 1	1.25	279
Component 2	1.45	248
Component 3	1.65	316
Component 4	1.85	187
Component 5	2.05	27
Component 6	2.25	275
Component 7	2.45	163
Component 8	2.65	285
Component 9	2.85	192
Component 10	3.05	154

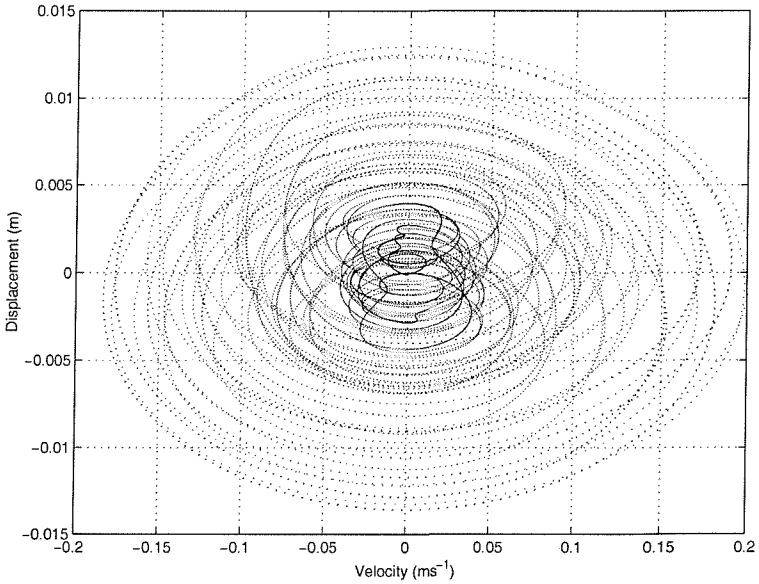

Figure 6-48 The velocity-displacement surface coverage measured using the quasi-random motion input

6.5.1.4.2 Results

6.5.1.4.2.1 Friction measurements

The quasi-static force-deflection characteristics of the three seat dampers are shown in Figure 6-49 to Figure 6-51. Friction forces were extracted as the mean force in compression and extension over the complete damper stroke. These results are summarised in Table 6-15.

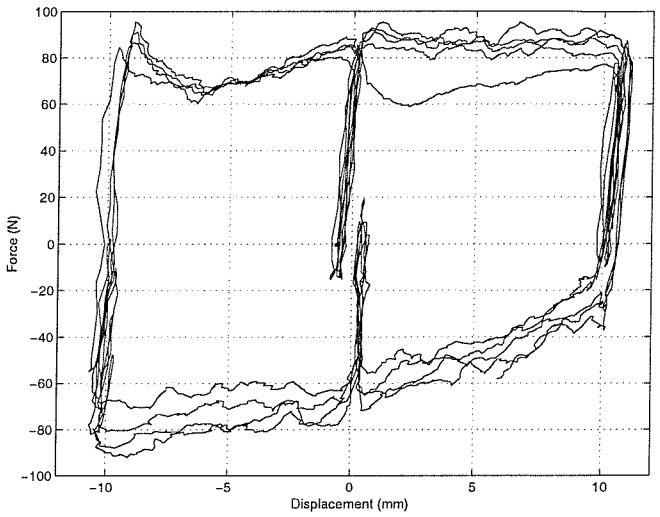

Figure 6-49 Quasi-static force-deflection characteristic of the earthmover seat damper

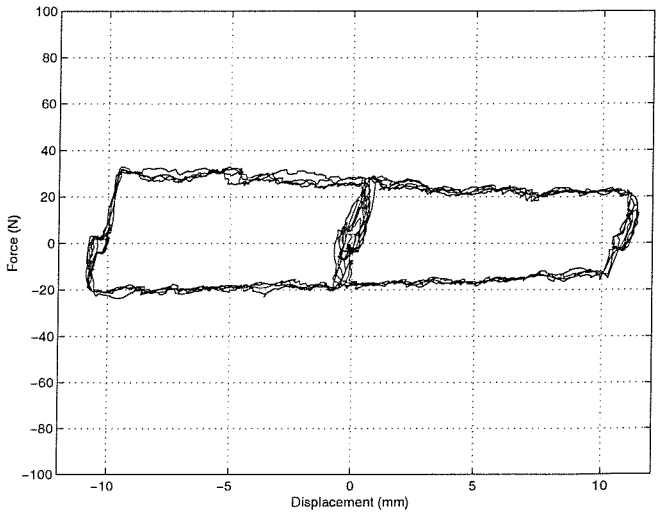

Figure 6-50 Quasi-static force-deflection characteristic of the forwarder seat damper

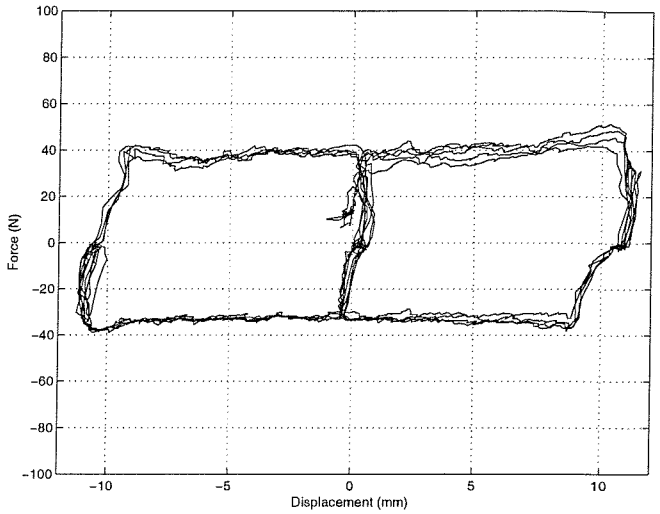

Figure 6-51 Quasi-static force-deflection characteristic of the agricultural tractor seat damper

Table 6-15 Friction values extracted from the low velocity force-deflection measurements using the alternative apparatus

Earthmover seat friction (N)		Forwarder seat friction (N)		Agricultural tractor seat friction (N)	
Compression	**Extension**	**Compression**	**Extension**	**Compression**	**Extension**
80	60	23	18	42	33

6.5.1.4.2.2 Single frequency force-velocity measurements

The force-velocity characteristics of the dampers obtained using sinusoidal input motions are shown in Figure 6-52 to Figure 6-54.

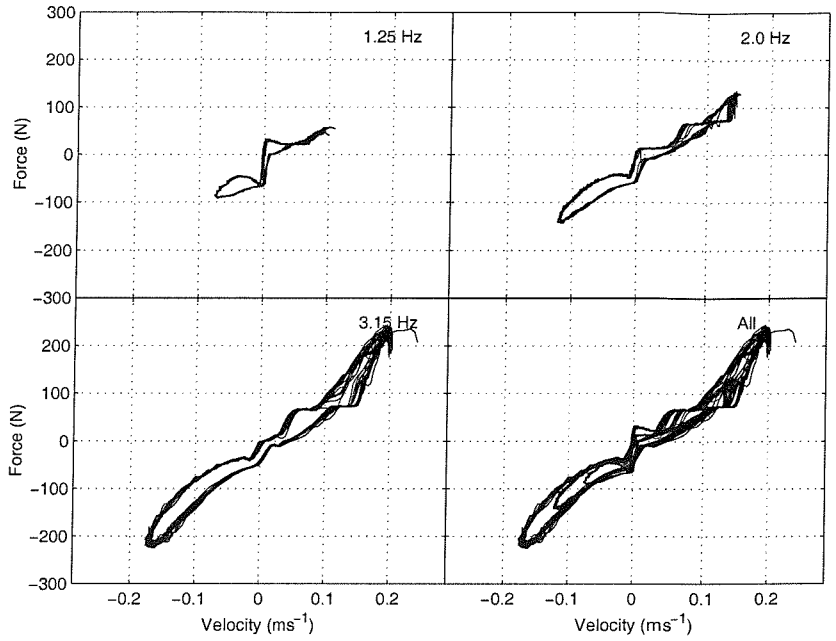

Figure 6-52 The force velocity characteristic of the earthmover seat damper measured using ±10 mm peak-to-peak sinusoidal input motions. Positive velocity corresponds to extension of the damper.

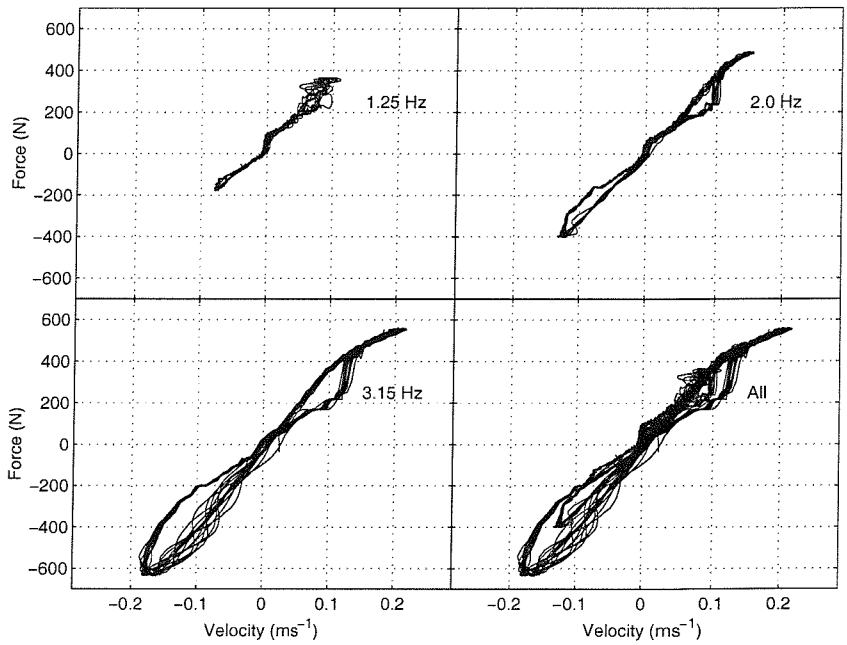

Figure 6-53 The force velocity characteristic of the forwarder seat damper measured using ±10 mm peak-to-peak sinusoidal input motions. Positive velocity corresponds to extension of the damper.

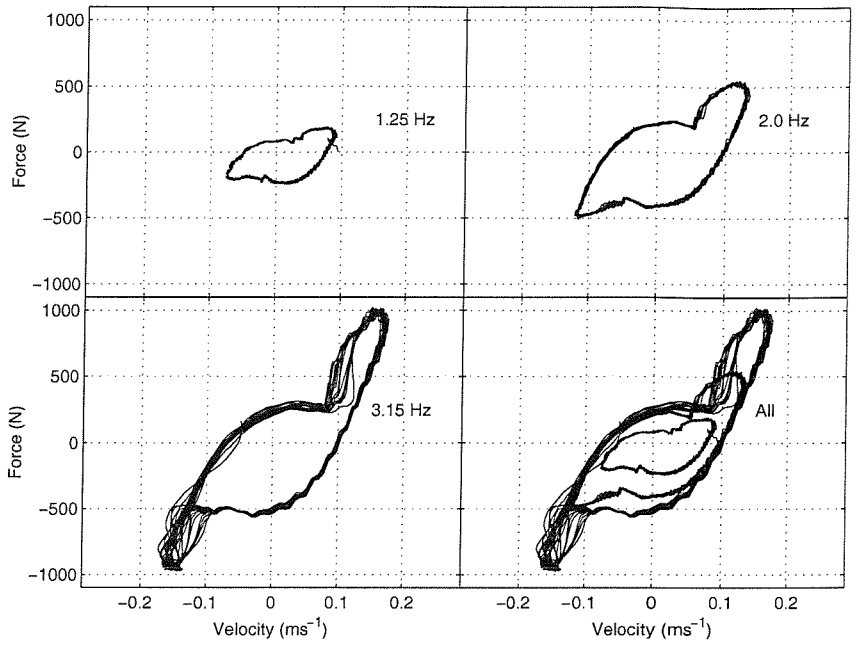

Figure 6-54 The force velocity characteristic of the agricultural tractor seat damper measured using ±10 mm peak-to-peak sinusoidal input motions. Positive velocity corresponds to extension of the damper.

The force-velocity characteristics showed substantial non-linearities. The amount of hysteresis-like behaviour generally increased with increasing magnitude, in particular with the agricultural tractor seat damper. The force-velocity characteristic obtained at all magnitudes, ignoring the hysteresis losses, appeared to follow a similar path. This suggested that for the frequency ranges investigated a single frequency sinusoidal measurement with a suitably high peak velocity might give a reasonable estimate for the non-hysteretic damper force-velocity characteristic.

6.5.1.4.2.3 Force-velocity-displacement surfaces

The force-velocity-displacement surfaces for the three dampers are shown in Figure 6-55 to Figure 6-57. The surface was obtained by binning the measured forces according to the corresponding velocity and displacement and using the mean force within each bin as the force value for that grid node. This was a simpler approach to that adopted by Duym (1997) who obtained coefficients from curve-fits to the data within each bin. The surfaces showed that the damper force with the velocity and displacement in phase was generally greater than with the velocity and displacement out of phase. This suggested that a greater force was required to move the damper

away from the mean position towards a peak displacement than was required to return it to the mean position.

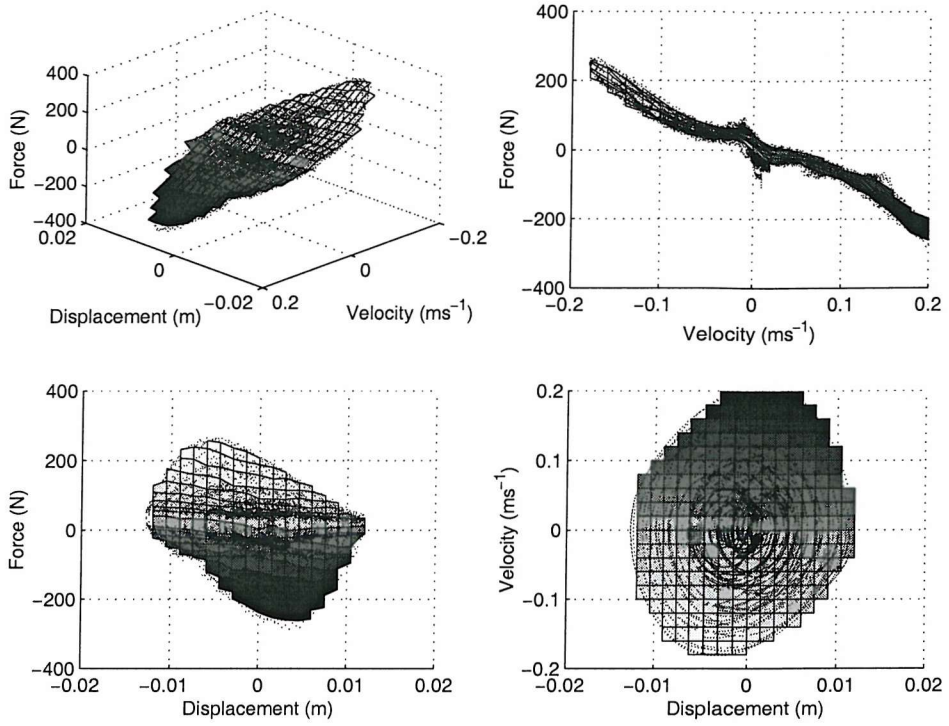

Figure 6-55 Force-velocity-displacement characteristic of the earthmover seat damper

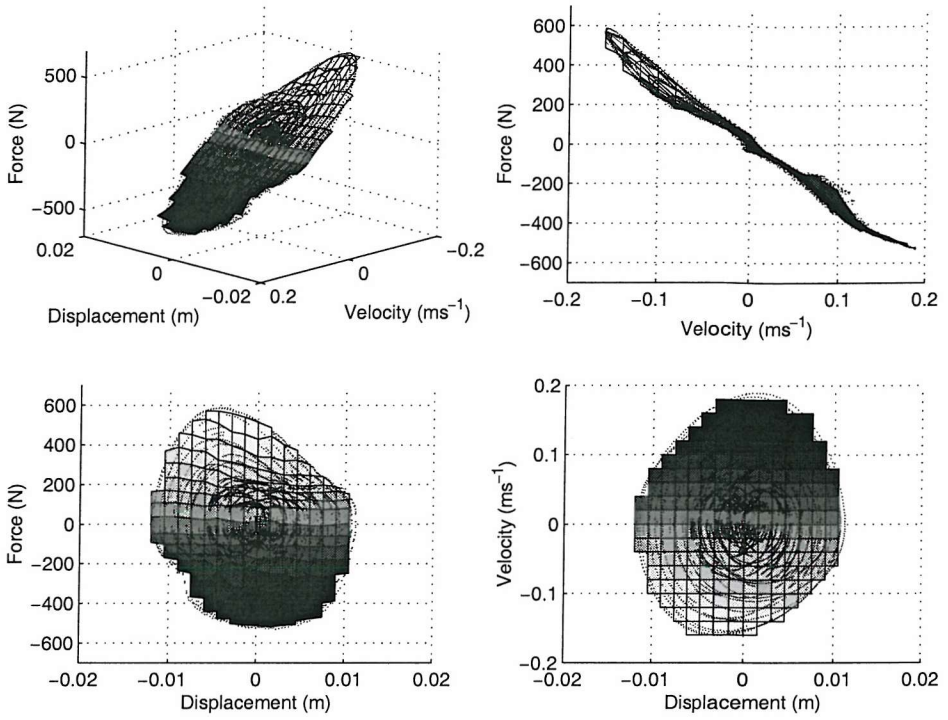

Figure 6-56 Force-velocity-displacement characteristic of the forwarder seat damper

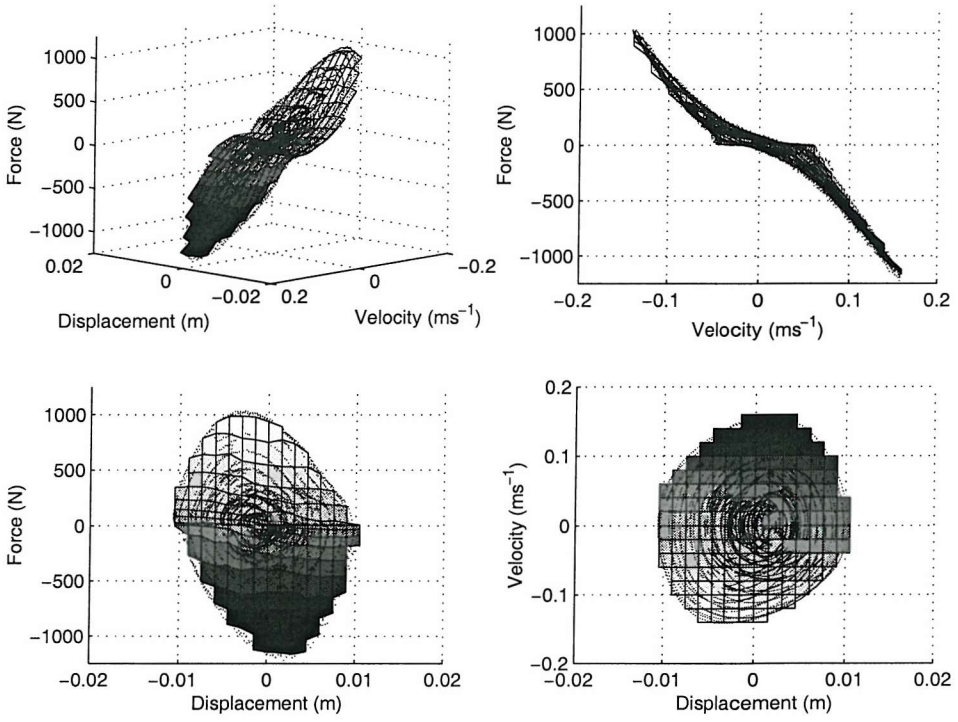

Figure 6-57 Force-velocity-displacement characteristic of the agricultural tractor seat damper

The force-velocity-displacement surfaces include the effects of stiffness, viscous damping and friction. However, Coulomb friction is defined as a constant force opposing the motion, or a force sufficient to prevent movement. An implementation of a damper using such a surface would not exhibit the correct friction-locking behaviour at low magnitudes. It is therefore of interest to extract the friction force and treat this separately.

Figure 6-58 to Figure 6-60 show part of the force-velocity characteristic of the seat dampers measured in response to the quasi-random motion. The effect of friction can be seen as a change in the force as the velocity passes through zero. The friction in compression and extension was extracted from the mean force for all displacements at velocities of between 0 and 0.01 ms^{-1} for the forwarder and agricultural tractor seats and 0.02 and 0.03 ms^{-1} for the earthmover seat. These velocities were sufficiently low to minimise the effect of the velocity-proportional viscous force, but sufficiently high to avoid the discontinuity as the velocities passed through zero for the earthmover seat. These friction forces were extracted to give a force-velocity-displacement surface independent of friction and a value for the friction in compression and extension. The friction forces are shown in Table 6-16.

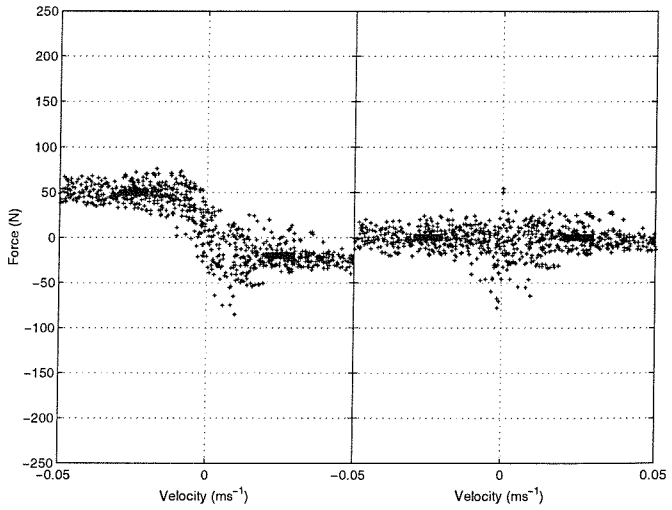

Figure 6-58 Low velocity force-velocity data for the earthmover seat damper as measured (left) and after removing the friction force (right) in response to the quasi-random motion input. Positive velocity corresponds to damper extension.

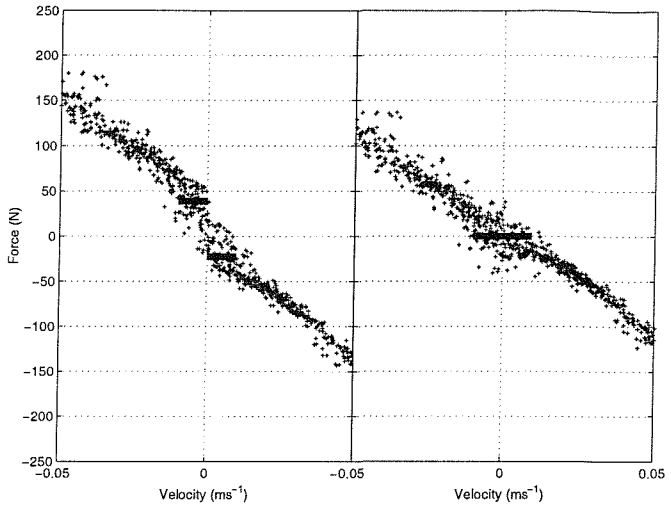

Figure 6-59 Low velocity force-velocity data for the forwarder seat damper as measured (left) and after removing the friction force (right) in response to the quasi-random motion input. Positive velocity corresponds to damper extension.

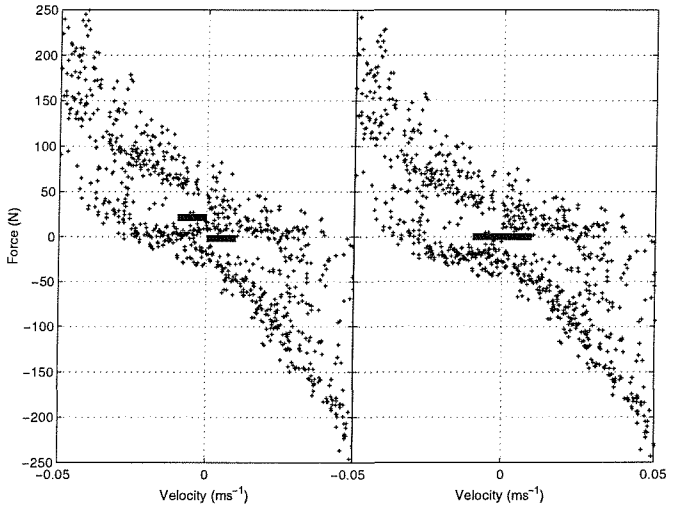

Figure 6-60 Low velocity force-velocity data for the agricultural tractor seat damper as measured (left) and after removing the friction force (right) in response to the quasi-random motion input. Positive velocity corresponds to damper extension.

Table 6-16 Damper friction forces determined from the force-velocity-displacement characteristic in response to the quasi-random motion input

Earthmover seat friction (N)		Forwarder seat friction (N)		Agricultural tractor seat friction (N)	
Compression	**Extension**	**Compression**	**Extension**	**Compression**	**Extension**
47	16	39	22	22	2

6.5.2 Discussion

6.5.2.1 Force-velocity characteristics

The force-velocity characteristics obtained using sinusoidal motions with the commercial and alternative apparatus are shown in Figure 6-61 to Figure 6-63. The results for the alternative apparatus were those obtained using the 3.15 Hz input motion in order to show the greatest range of velocities. The force-velocity characteristic using the alternative apparatus was adjusted to remove the friction force using the friction values obtained from the quasi-random motion test (Table 6-16). The commercial apparatus automatically corrects for the friction force.

The alternative apparatus returned a shallower force-velocity characteristic for the forwarder and agricultural tractor seat dampers but was similar to the result from the commercial apparatus for the earthmover seat damper. A simple force-velocity curve such as that produced by the commercial apparatus does not include the hysteresis-like behaviour of the damper. Discounting this effect could lead to substantial errors in the prediction of the damping force.

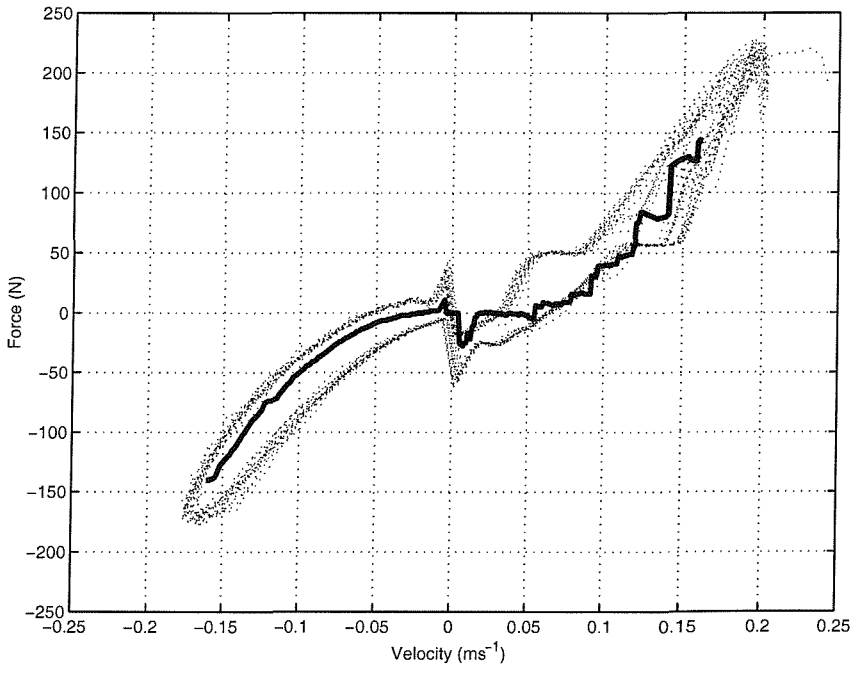

Figure 6-61 The force-velocity characteristics of the earthmover seat damper obtained with sinusoidal inputs using the commercial (solid line) and alternative (dotted line) apparatus with both results adjusted to remove friction. Positive velocity indicates damper extension.

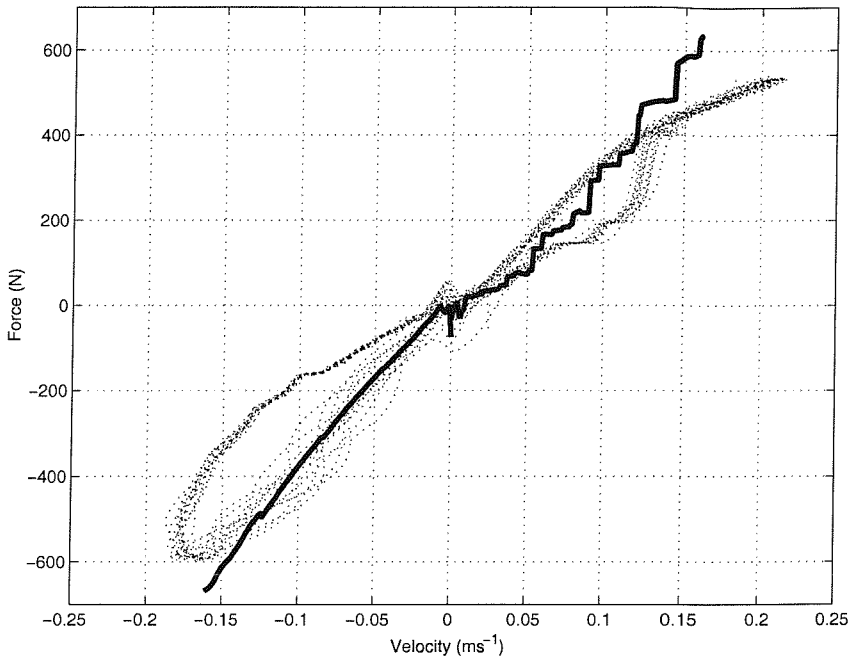

Figure 6-62 The force-velocity characteristics of the forwarder seat damper obtained with sinusoidal inputs using the commercial (solid line) and alternative (dotted line) apparatus with both results adjusted to remove friction. Positive velocity indicates damper extension.

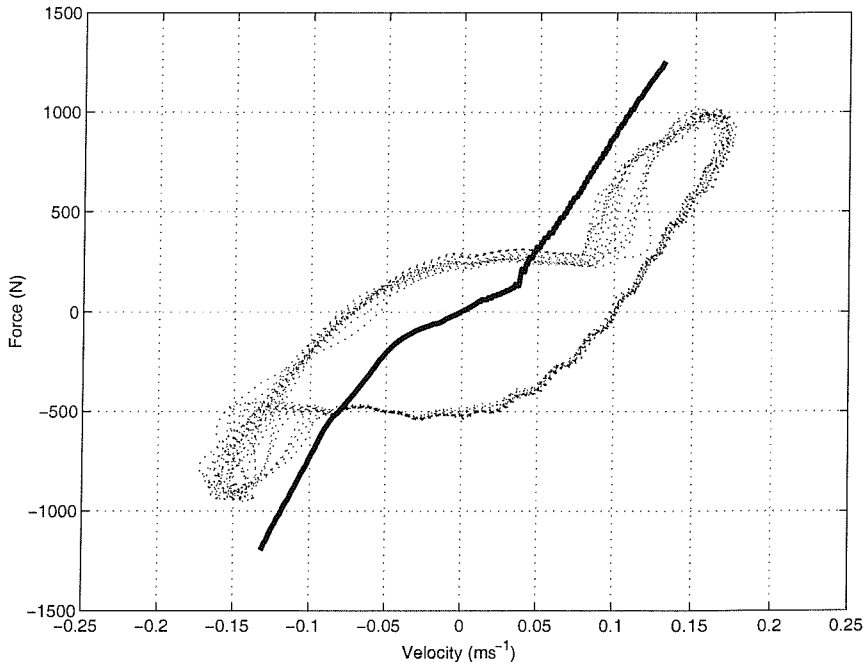

Figure 6-63 The force-velocity characteristics of the agricultural tractor seat damper obtained with sinusoidal inputs using the commercial (solid line) and alternative (dotted line) apparatus with both results adjusted to remove friction. Positive velocity indicates damper extension.

6.5.2.2 Friction measurements

The values measured for the damper friction force are summarised in Table 6-17. It can be seen that there are substantial differences between the values measured using different methods.

Table 6-17 Measurements of the damper friction in compression, extension and the total friction (compression + extension) measured using different apparatus

	Earthmover seat friction (N)			Forwarder seat friction (N)			Agricultural tractor seat friction (N)		
	Com	Ext	Total	Com	Ext	Total	Com	Ext	Total
(A) Low velocity force-deflection, commercial apparatus	64	173	237	8	114	122	45	18	63
(B) Low velocity force/deflection, alternative apparatus	80	60	140						
(C) Derived from the force-velocity-displacement surface	47	16	63						

The differences between the results may have been affected by off-axis loadings due to differences in the geometries of the damper mounting clamps in the test apparatus, or by changes in the damper characteristics over time. The results labelled set A were obtained after the seats were involved in the field trials but before any laboratory experiments while set B and set C were obtained after all laboratory experiments were complete. The damper mounting arrangements in set B and set C were identical and held the damper in place without applying a strong compressive force to the damper itself as illustrated in Figure 6-64. The tests used to obtain set A used a stronger force to hold the damper in place.

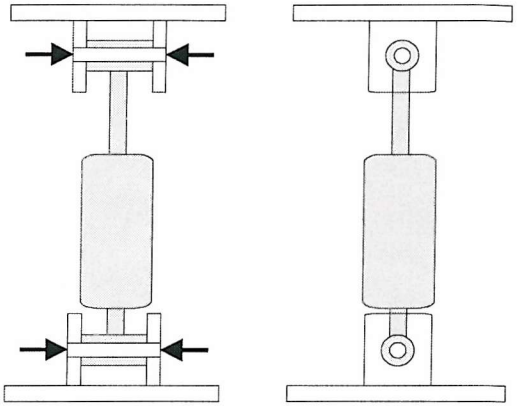

Figure 6-64 Detail of the damper mounting method showing where the clamping force may have been greater for the test conducted with the commercial apparatus to produce the set 'A' results.

The results obtained for the damper friction suggest that methods of measuring the friction present in suspension seat dampers and the manner in which damper friction changes with time both require further investigation if reliable and repeatable damper friction measurements are to be obtained.

6.5.3 Damper mounting geometry

The dampers were all mounted at an angle between the base and top plates of the suspension mechanism so the viscous damping and friction forces due to the damper change with the suspension mechanism displacement. It is necessary to know the relative positions of the damper mounting points at a known suspension position in order to define the relationship between damper force and suspension displacement.

The suspension linkages confine the suspension mechanisms to move in the vertical direction only. The fore and aft suspension present on the agricultural tractor seat was disabled for all measurements and tests. The horizontal distance between the damper mountings therefore remains constant and was measured for all three seats using a tape measure.

The vertical distance between the damper mounting points was measured with the suspension mechanisms just in contact with the top end stop. The free travel, measured previously, was then used to obtain the vertical distance between the mounting points at the midpoint of the free travel.

Table 6-18 The relative location of the damper mounting points (mm)

	Tractor	Forwarder	Earthmover
Horizontal distance	145 mm	128 mm	150 mm
Vertical distance at the midpoint of the free travel	92 mm	83 mm	111 mm

6.6 The end-stop buffers

6.6.1 The geometry of the linkage

Measurements of the linkage geometry were required in order to convert the vertical movement of the suspension mechanism into movement along the axes of the end-stop buffers.

The linkage and buffer positions of the earthmover seat are shown in Figure 6-65. The distance *ll* is the linkage arm length and is constant. The distances *lv* and *lh* are the distances between the linkage arm mounting points at the mid ride position. The distances the suspension must move vertically before contacting the top or bottom stop are known from the measurement of the suspension free travel and the offset of the mean ride position from the mid-point of the free travel.

Two top and bottom buffers were present on the earthmover seat, one of each on each side of the suspension mechanism. The bottom buffers were attached to the base of the suspension and acted against a plate attached to the top of the suspension. The top buffers acted horizontally against one of the suspension linkage cross-members.

The forwarder seat has an equivalent layout with the two bottom buffers mounted on the top of the suspension and acting on a plate attached to the bottom of the suspension. Two top buffers acted horizontally against one of the suspension cross members.

The agricultural tractor seat had the bottom buffer attached to one of the linkage arms acting downward onto the base of the suspension. However, this linkage arm was almost horizontal when the buffer contact began so it was reasonable to approximate the axial compression of the buffer to the vertical movement of the suspension mechanism. A single top buffer acted against the centre of one of the suspension cross members.

The geometric measurements for the three seats are shown in Table 6-19.

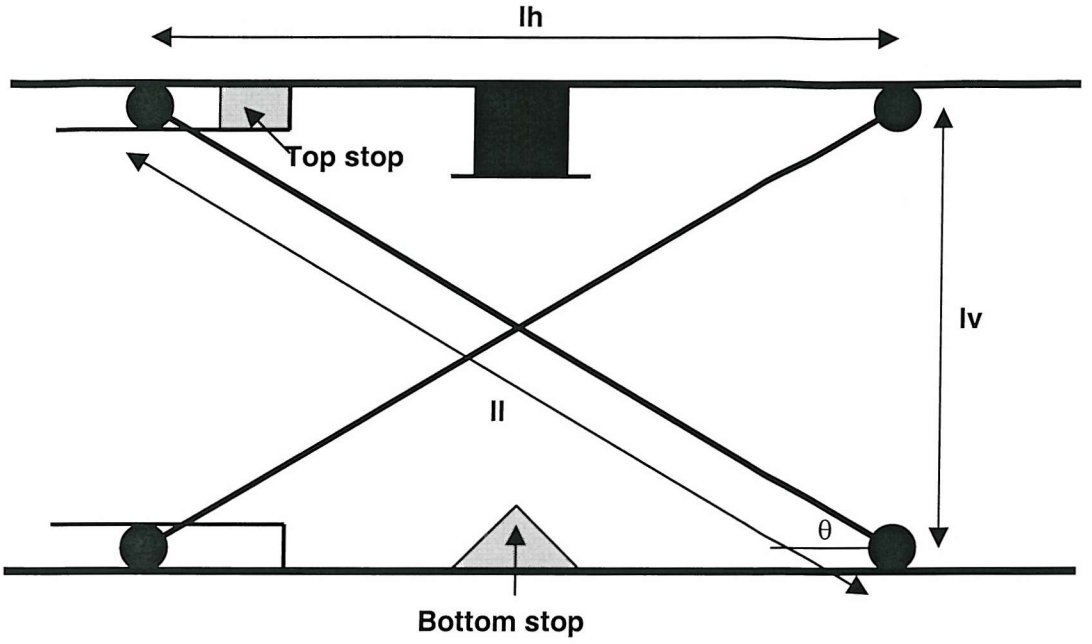

Figure 6-65 Schematic of the Earthmover seat linkage and buffer layout

Table 6-19 Suspension linkage measurements

	lh	lv
Earthmover seat	295 mm	150 mm
Agricultural tractor seat	270 mm	250 mm
Forwarder seat	280 mm	160 mm

6.6.2 The suspension free travel

The free travel of each suspension mechanism was measured on the indenter rig. The displacement of the suspension mechanism was measured using the LVDT while the mechanism was compressed from a position just in contact with the top stop to just in contact with the bottom stop. The results are shown in Table 6-20.

Table 6-20, Suspension free travel (mm)

	Tractor	Forwarder	Earthmover
Suspension free travel	156 mm	85 mm	68 mm

6.6.3 The buffer dynamic characteristics

6.6.3.1 Method

End-stop buffer measurements were carried out by a member of the TESTOPS consortium using commercially available materials testing apparatus. The measurement data was made available to the project. The buffer force-deflection characteristics were obtained by compressing the buffer along its axis. The end-stop

buffers were mounted in jigs to simulating the real environment. Top stop buffers were confined if necessary to simulate the mounting position within the seat guide rails. The buffers were compressed by an indenter with the same geometry as found on the seat. The bottom stop buffers were compressed with a flat plate while top stop buffers were compressed with a rounded indenter to simulate the suspension cross member.

6.6.3.2 Results

6.6.3.2.1 Buffer stiffness

The force-deflection characteristics of individual earthmover seat top and bottom end-stop buffers are shown in Figure 6-66 and Figure 6-67. The characteristics of the bottom buffers from the Forwarder and Agricultural tractor seats are shown in Figure 6-68 and Figure 6-69. The top buffer characteristics of these seats were not supplied. A 5th order least-squares polynomial fit was made to the data in order to quantify the curve for use in the model. A lower order fit appeared sufficient for some of the buffers, but some, such as the top stop, showed a 'two-stage' stiffness. This buffer had an approximately linear stiffness over the first 3 mm, then an increasing stiffness as compression continued. It was considered more versatile to quantify this buffer by a higher (5th) order polynomial fit rather than a composite curve consisting of a linear and exponential regions. The same order fit was applied to the remaining buffers. The curve fit coefficients are shown in Table 6-21 to Table 6-23.

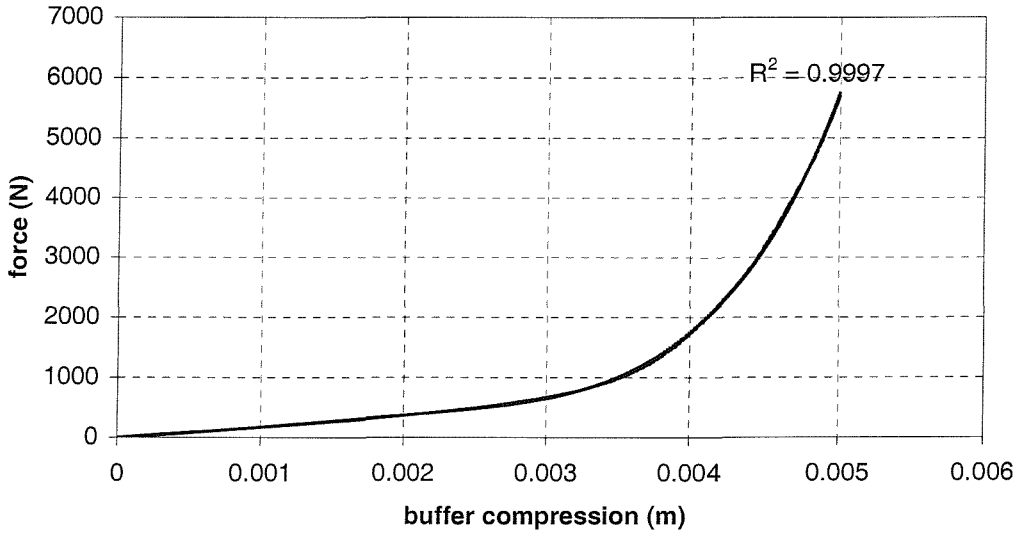

Figure 6-66 Earthmover seat single top end-stop buffer force-deflection characteristic (solid line) with 5th order polynomial fit (dashed line)

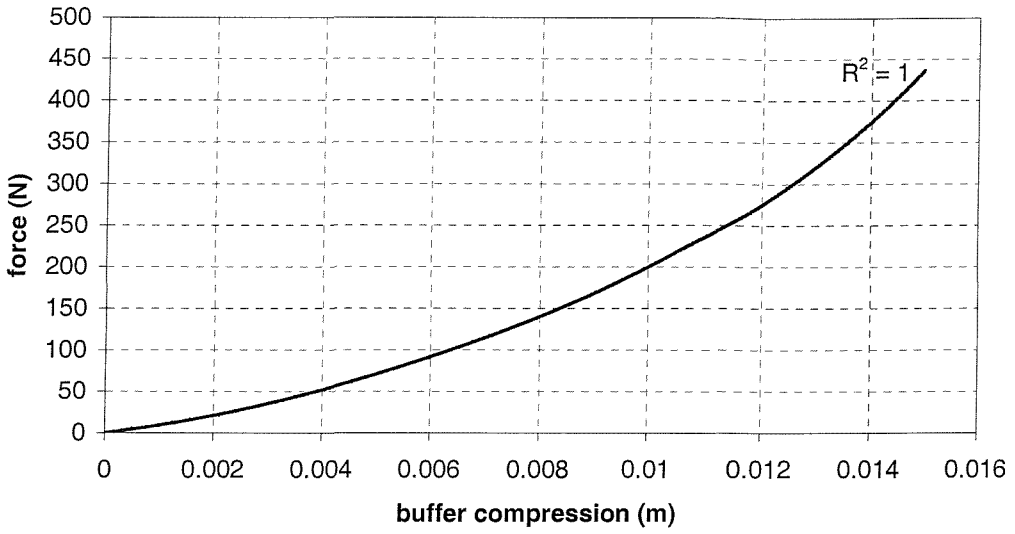

Figure 6-67 Earthmover seat single bottom end-stop buffer force-deflection characteristic (solid line) with 5th order polynomial fit (dashed line)

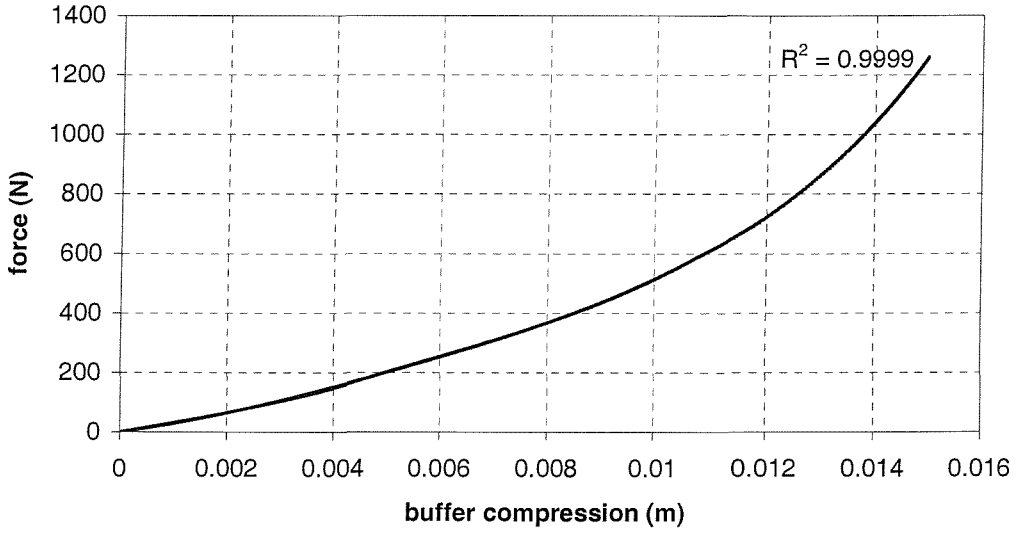

Figure 6-68 Forwarder seat single bottom end-stop buffer force-deflection characteristic (solid line) with 5th order polynomial fit (dashed line)

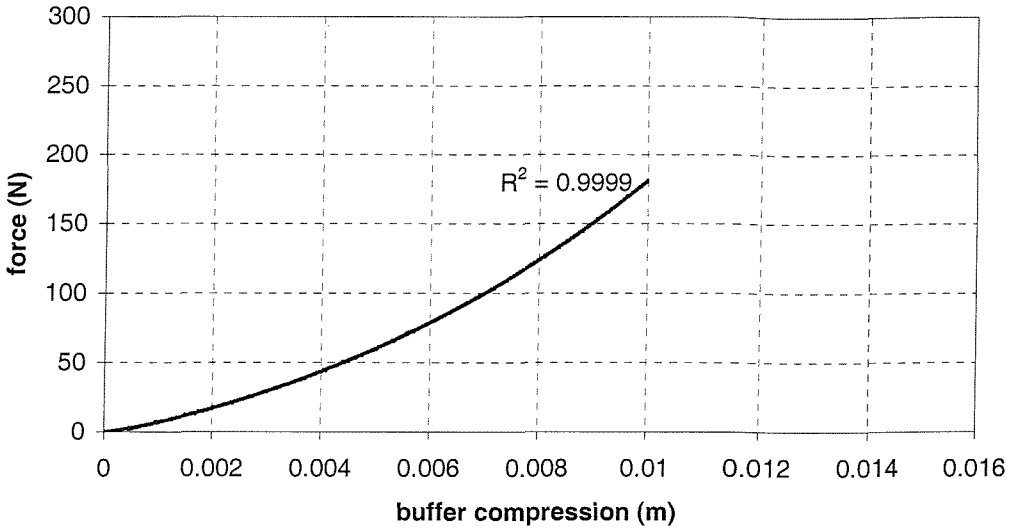

Figure 6-69 Agricultural tractor seat single bottom end-stop buffer force-deflection characteristic (solid line) with 4th order polynomial fit (dashed line)

Table 6-21 Least squares polynomial 5th order fit coefficients to the Earthmover seat buffer force-deflection characteristic

Earthmover seat buffer force/deflection coefficients	Top stop	Bottom stop
$buff^{5}_{compression}$ x	5.4778 x 10^{15}	1.832 x 10^{11}
$+ buff^{4}_{compression}$ x	-2.5734 x 10^{4}	-8.57 x 10^{7}
$+ buff^{3}_{compression}$ x	2.5952 x 10^{3}	-4.45 x 10^{7}
$+ buff^{2}_{compression}$ x	3.2737 x 10^{7}	1.5035 x 10^{6}
$+ buff_{compression}$ x	1.34808 x 10^{5}	7.6245 x 10^{3}
+	0	0

Table 6-22 Least squares polynomial 5th order fit coefficients to the Forwarder seat buffer force-deflection characteristic

Forwarder seat buffer force/deflection coefficients	Top stop	Bottom stop
$buff^{5}_{compression}$ x	-	4.64 x 10^{11}
$+ buff^{4}_{compression}$ x	-	2.21 x 10^{10}
$+ buff^{3}_{compression}$ x	-	-5.23 x 10^{8}
$+ buff^{2}_{compression}$ x	-	5.35 x 10^{6}

$+ buff_{compression}$ x	-	2.34 x 10^4
+	-	0

Table 6-23 Least squares polynomial 5th order fit coefficients to the Agricultural tractor seat buffer force-deflection characteristic

Agricultural tractor seat buffer force/deflection coefficients	Top stop	Bottom stop
$buff^5_{compression}$ x	-	0
$+ buff^4_{compression}$ x	-	5.62 x 10^9
$+ buff^3_{compression}$ x	-	-8.93 x 10^7
$+ buff^2_{compression}$ x	-	1.58 x 10^6
$+ buff_{compression}$ x	-	5.68 x 10^3
+	-	0

The force-deflection polynomial fit was differentiated to obtain an estimated buffer stiffness characteristic. This approach of differentiating the polynomial fit avoids the problems associated with differentiating experimental data, but requires a good fit to the data. In all cases, the R^2 value using a 5th order fit was greater than 0.999.

The curve fit was reduced to a lower order if the first ($\propto x^5$) coefficient was a negative value. The highest order polynomial below 5th for which the first coefficient was positive was selected instead. The end-stop buffer should get progressively stiffer as the compression increases. If the highest order coefficient is negative the force will eventually decrease with increasing compression. It was considered preferable that the function resulted in an incorrectly high value when extrapolating to high compression values rather than a decreasing or negative value.

The estimated buffer stiffnesses are shown in Figure 6-70 Figure 6-71. The coefficients describing this buffer characteristic were obtained by exact differentiation of the force-deflection polynomial and are shown in Table 6-24.

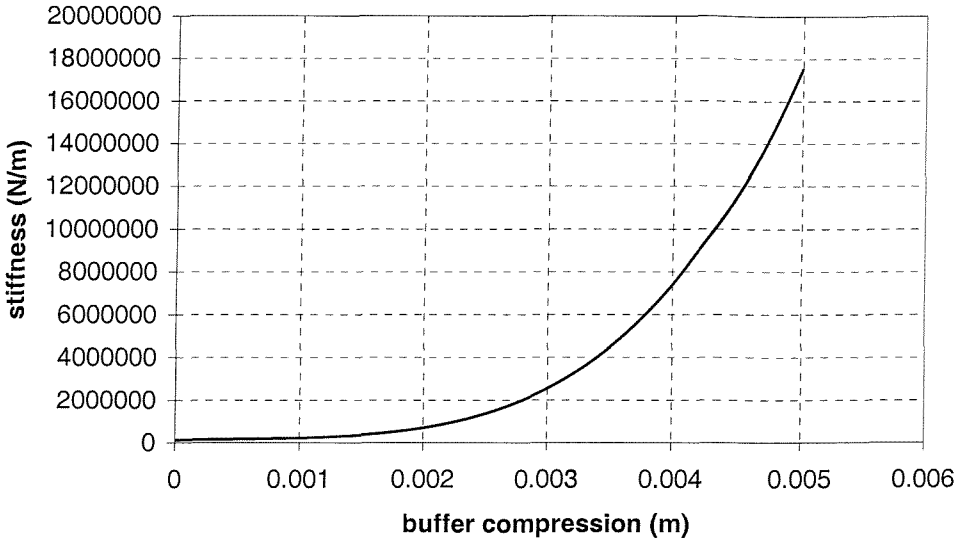

Figure 6-70 Estimated Earthmover seat top buffer stiffness obtained using the differentiated polynomial approximation to the force-deflection characteristic

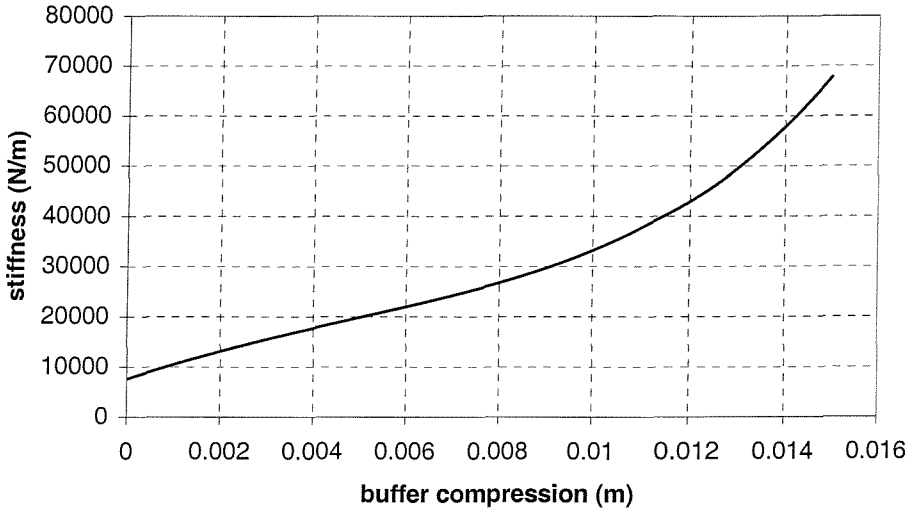

Figure 6-71 Estimated Earthmover seat bottom buffer stiffness obtained using the differentiated polynomial approximation to the force-deflection characteristic

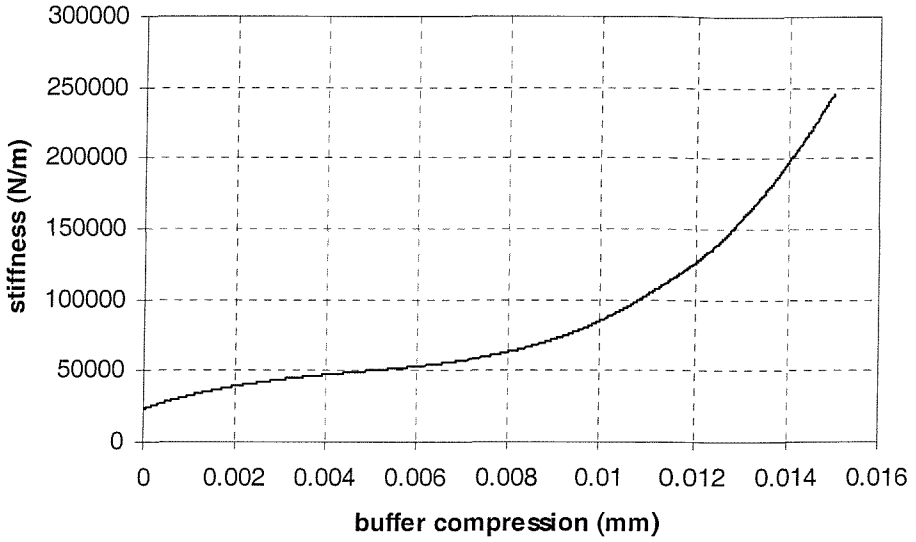

Figure 6-72 Estimated Forwarder seat bottom buffer stiffness obtained using the differentiated polynomial approximation to the force-deflection characteristic

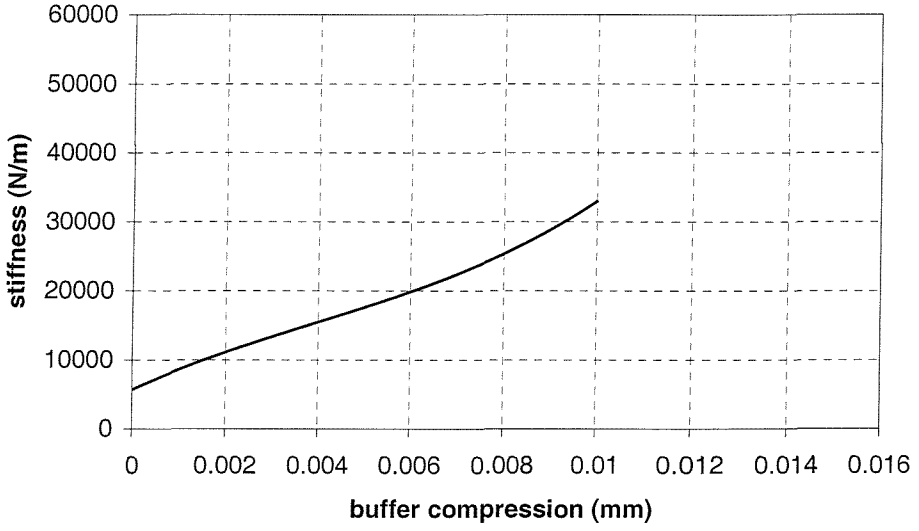

Figure 6-73 Estimated agricultural tractor seat bottom buffer stiffness obtained using the differentiated polynomial approximation to the force-deflection characteristic

Table 6-24 Earthmover seat estimated end-stop buffer stiffness characteristic coefficients

Earthmover seat buffer stiffness	Top stop	Bottom stop
$buff^4_{compression}$ x	2.7389 x 10^{16}	9.16 x 10^{11}
$+ buff^3_{compression}$ x	-1.02936 x 10^5	-3.428 x 10^8
$+ buff^2_{compression}$ x	7.7856 x 10^3	-1.335 x 10^8
$+ buff_{compression}$ x	6.5474 x 10^7	3.007 x 10^6
+	1.34808 x 10^5	7.6245 x 10^3

Table 6-25 Forwarder seat estimated end-stop buffer stiffness characteristic coefficients

Forwarder seat buffer stiffness	Top stop	Bottom stop
$buff^4_{compression}$ x	-	2.32 x 10^{12}
$+ buff^3_{compression}$ x	-	8.84 x 10^{10}
$+ buff^2_{compression}$ x	-	-1.57 x 10^9
$+ buff_{compression}$ x	-	1.07 x 10^7
+	-	2.34 x 10^4

Table 6-26 The agricultural tractor seat estimated end-stop buffer stiffness characteristic coefficients

Agricultural tractor seat buffer stiffness	Top stop	Bottom stop
$buff^4_{compression}$ x	-	0
$+ buff^3_{compression}$ x	-	2.25 x 10^{10}
$+ buff^2_{compression}$ x	-	-2.68 x 10^8
$+ buff_{compression}$ x	-	3.16 x 10^6
+	-	5.68 x 10^3

The stiffness force was doubled within the model to account for the fact that there were two end-stop buffers acting together during an impact, one on each side of the

suspension mechanism. The only exception was the agricultural tractor seat top stop that consisted of a single central buffer only.

The absence of test data for the top stop buffers of two of the seats is unfortunate but not critical. As previously mentioned, a severe top-stop impact involves the suspension coming to a sudden stop and the load mass continuing upwards. All three seats used top-stop buffers of similar thickness so the range of displacements over which the force exerted by the buffer would increase to a value capable of rapidly reducing the velocity of the suspended mass to zero would be similar for all seats. It was anticipated that the sensitivity analysis would show that the exact values of the top-stop buffer coefficients were not critical.

6.6.3.2.2 Buffer damping

The damping characteristics of the end-stop buffers were provided in terms of loss angle values (α). The damping force in terms of the loss angle is defined by

$$F_{cbuff} = \frac{buff_{velocity} \cdot k_{buff}}{\omega \cdot \tan(\alpha)}$$ Equation 6-12

where F_{cbuff} is the damping force, $buff_{velocity}$ is the buffer compression velocity, k_{buff} is the buffer stiffness, ω is the angular frequency and α is the loss angle. The loss angles provided for the Earthmover seat buffers are shown in Table 6-27.

Table 6-27 Earthmover seat end-stop buffer loss angles

	Top buffer	**Bottom buffer**
Loss angle in radians	0.19199	0.05236

This method of describing the buffer damping results in an expression for the damping ratio of a mass in contact with a buffer of:

$$\zeta = \frac{k_{buff}}{2\omega \tan(\alpha)\sqrt{k_{buff} m}}$$ Equation 6-13

where ω is the angular frequency, α is the loss angle, m is the mass *and* k_{buff} is the buffer stiffness. This expression was derived by assuming a damping force linearly proportional to velocity and substituting Equation 6-12 into the expression for the damping ratio of a linear single degree-of-freedom system given by:

$$\zeta = \frac{damping}{2\sqrt{k_{buff} m}}$$ Equation 6-14

A simple test was performed using the earthmover bottom buffer in contact with a 22 kg mass. The system was exited by an impulsive force and the acceleration of the system was acquired as shown in Figure 6-74. This clearly shows as under damped

system with a resonance frequency of approximately 6 Hz implying a stiffness of 30 kNm^{-1}. This stiffness is in agreement with the expected stiffness for this mass loading (see Figure 6-67 and Figure 6-71). The damping ratio can be determined using the logarithmic decrement method by:

$$\frac{4\pi\zeta}{\sqrt{1-\zeta^2}} = \frac{1}{n}\log_e\left(\frac{A_0}{A_n}\right) \qquad \text{Equation 6-15}$$

where ζ is the damping ratio and n is the number of cycles between a measurement of the amplitude A_0 and a second measurement A_n. The damping ratio calculated using this method for the data shown in Figure 6-74 was ζ=0.0015.

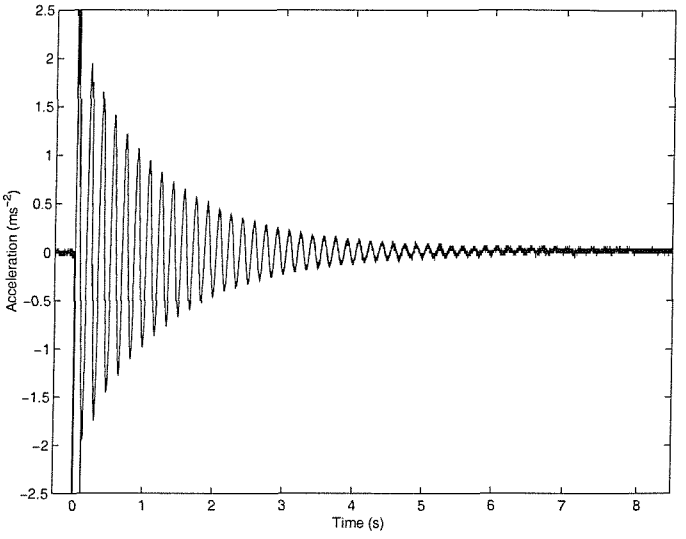

Figure 6-74 The impulse response of a 22 kg mass suspended on an earthmover seat bottom buffer

The damping ratio calculated from the loss angle using the relevant equation above for a 30 kNm^{-1} stiffness and a 22 kg mass at 6 Hz with the relevant loss angle data for the earthmover buffer was ζ=9.35 which is clearly unrealistic for a rubber component.

This loss angle method of quantifying rubber damping is not suitable for this application. The end-stop buffers were implemented in the model as undamped stiffnesses. It was not anticipated that the absence of the buffer damping would be critical to the model performance due to the low damping of the material and the relatively short period of time for which the suspension would contact the buffer.

6.7 Conclusions

Parameter values have been obtained describing the dynamic characteristics of each seat component and measurement techniques not previously applied to suspension seat modelling have been investigated. The cushion and the suspension damper showed complex dynamic behaviour and a range of measurements were obtained to allow component models of varying complexity to be used within the dynamic model of the seat. The only measurement that was not obtained was the value for the friction present within the suspension damper. Different results were obtained for this parameter using equivalent sets of apparatus. Alternative methods for estimating this value are described later in Chapter 9.

7. The suspension seat model structure

7.1 Introduction

Suspension seats lend themselves well to lumped parameter modelling methods. The seat can be divided into a number of discrete components, most of which can be implemented as a small number of idealised elements. All previously published suspension seat models have used this approach (Marsh, 1965, Rakheja *et al*, 1987, Gouw *et al*, 1990, Boileau *et al*, 1993, Rakheja *et al*, 1994, Lewis, 1994, Wu and Griffin, 1995) with the exception of Fairley (1990) who characterised the seat using the measured apparent mass and Rebelle (2000) who optimised the parameters of a Bouc-Wen characteristic to fit the measured seat suspension dynamic behaviour.

Fairley (1990) used linear techniques to describe the seat dynamics. The model parameters were therefore relevant to the specific input motion used to determine the suspension apparent mass but did not result in a general model of the seat. The approach used by Rebelle (2000) accounted for the non-linearities in the seat performance but did not attempt to relate the dynamic behaviour of the seat to the physical properties of the individual component parts.

The intention of the present model was to improve upon the most advanced non-linear lumped parameter suspension seat model as reported by Rakheja *et al* (1994), continuing the approach of describing the seat in terms of non-linear coefficients relevant to the individual component parameters. This chapter describes the equations used for each seat component, the block diagram implementations of these equations, the numerical techniques used to solve the block diagram and the overall structure of the simulation software.

7.2 Software structure

7.2.1 The graphical user interface (GUI)

The model was activated from the *Matlab* command line, opening the graphical user interface (GUI). The GUI, shown in Figure 7-1, allowed the user to enter coefficients describing the component parts of a specific seat. These sets of coefficients can be saved to an ASCII file for later retrieval. The name and location of the desired seat base acceleration time history was specified from the GUI. Parameters relating to the equation solving routines used by *Simulink* also be set and the simulation of the seat could be started. Each of the actions described by the GUI was performed by one or more *Matlab* functions.

The GUI was generated by two *Matlab* functions. The first generated the figure window and the buttons and fields with the exception of the parameter value boxes and their corresponding labels. These latter controls were generated individually with reference to a separate file listing each of the parameter names. Adding a parameter name to this reference file caused a labelled value field to be created in the GUI and generated a global variable for the parameter to allow the current value to be passed from the GUI to the model.

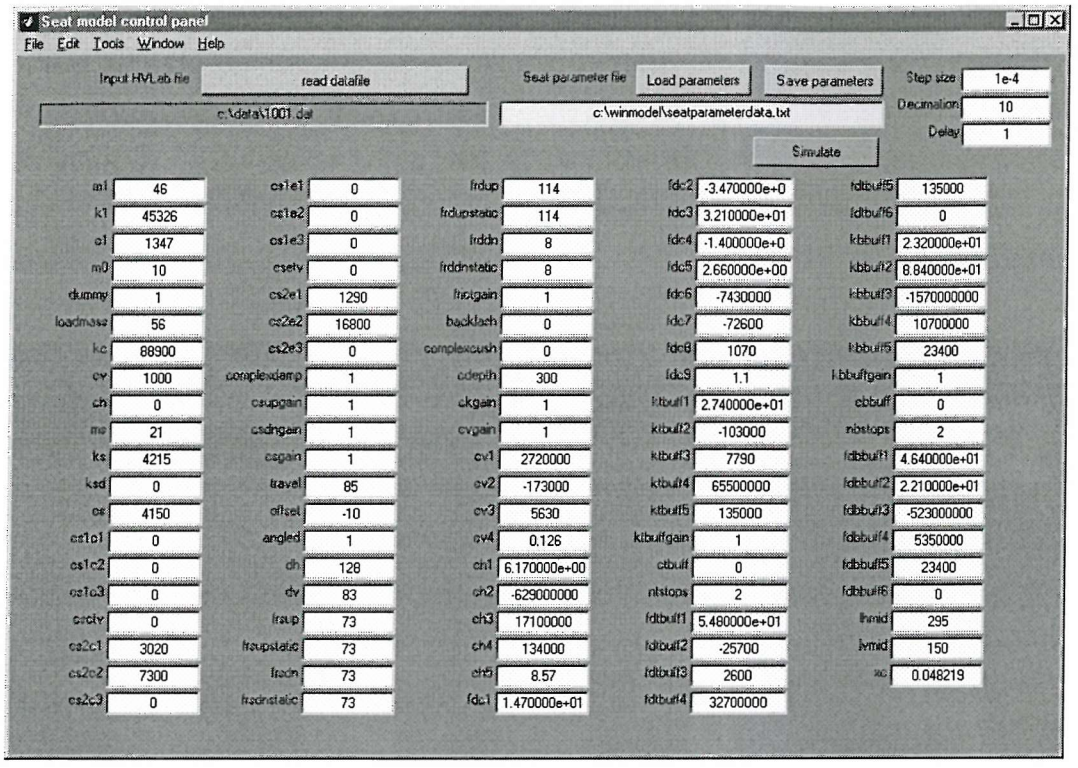

Figure 7-1 The model graphical user interface (GUI)

7.2.2 Passing data to the model

The acceleration time history to be applied to the base of the simulated seat was read from an *HVLab* format data file, any DC offset was removed and a 40 Hz low pass zero phase 8-pole Butterworth filter was applied. The seat base motions found in vehicles using suspension seats are usually dominated by frequency content below 10 Hz. This filter was present to remove predominantly 50 Hz noise introduced by the data acquisition system when using laboratory measurements as the model input. The input time history was interpolated to match the sampling interval to the time step size of the *Simulink* differential equation solver.

The sets of parameter values describing each individual seat were stored in ASCII format. Controls in the GUI allowed the parameter sets to be loaded, modified and saved. On starting a simulation, the current values for each parameter as shown in

the GUI were passed to global workspace variables which could be accessed by the *Simulink* model. The software structure is illustrated in Figure 7-2.

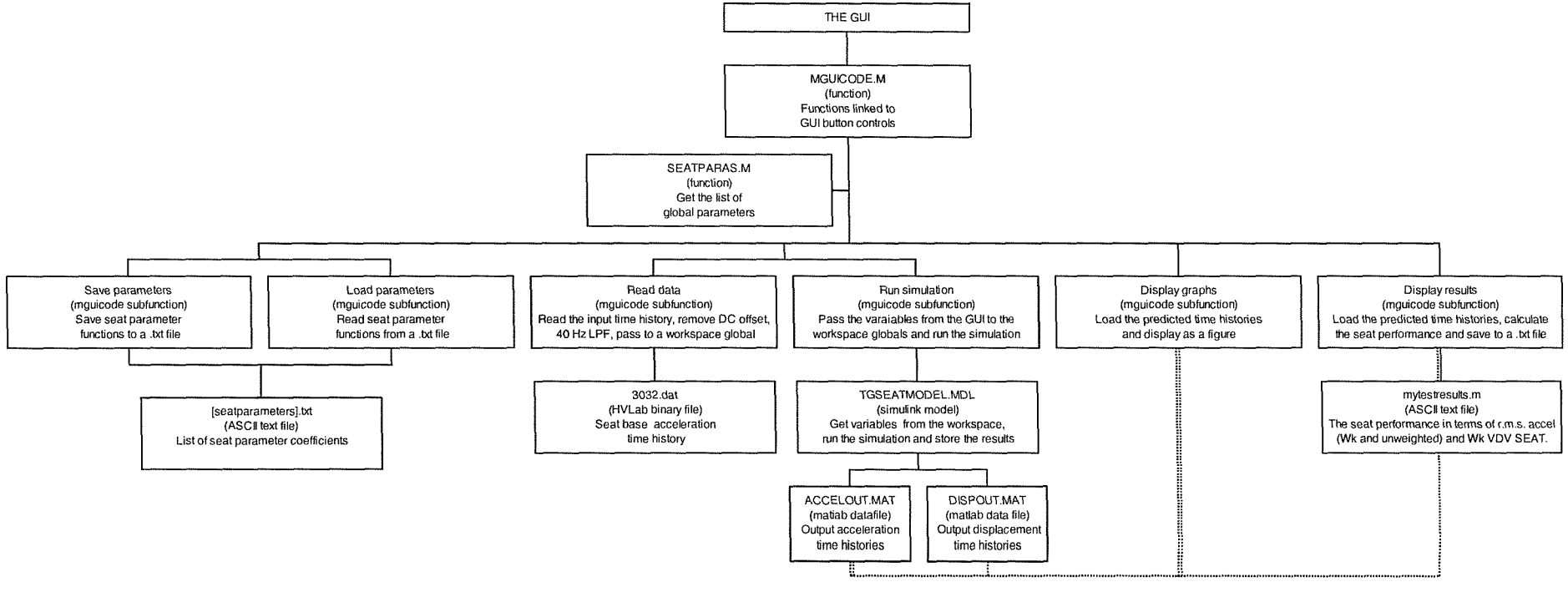

Figure 7-2 The structure of the simulation software

7.3 The model mathematical structure

7.3.1 Overview

Mathematical descriptions of the seat components were implemented as block diagrams and are described in the following sections. A schematic of the model structure is shown in Figure 7-3 and a list of symbols is shown in Table 7-1. The top level of the *Simulink* block diagram is shown in Figure 7-4 and the complete *Simulink* block diagram is included in Appendix 3. The equations shown in this chapter should be assumed to apply to an instantaneous time *t* at which the model was evaluated unless otherwise stated.

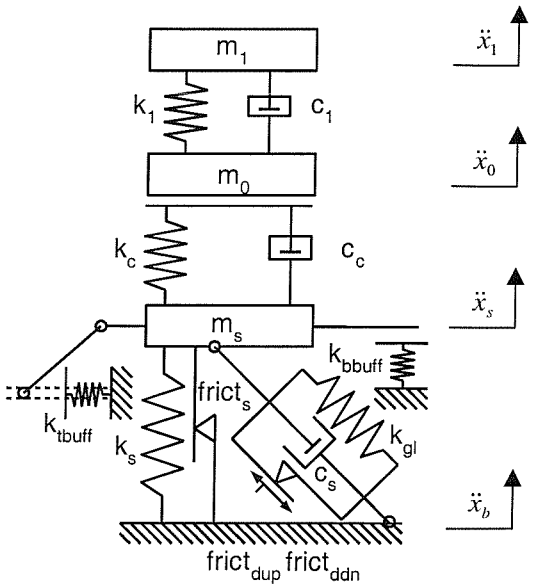

Figure 7-3 A schematic of the suspension seat mathematical model

Table 7-1 List of symbols

Symbol	Units	Description
$a_{1\text{-}5}$	-	Polynomial coefficients for the bottom buffer force-deflection characteristic
ang	-	Multiplier applied to any force generated along the damper axis to obtain the vertical component
$b_{1\text{-}5}$	-	Polynomial coefficients for the top buffer force-deflection characteristic
$bbuff_{compression}$	m	The instantaneous axial compression of the bottom end-stop buffer.
c_1	Nsm^{-1}	The human body model linear damping
c_c	Nsm^{-1}	The linearised cushion damping
c_s	Nsm^{-1}	The damping coefficient of the suspension damper
Δt_{lock}	s	The friction lock-up time constant
dh	m	The horizontal distance between the damper mounting

		points with the suspension at the mid-point of the free travel between the end-stop buffers
dv	m	The vertical distance between the damper mounting points with the suspension at the mid-point of the free travel between the end-stop buffers
F_{lock}	N	Force required to reduce the suspension relative velocity to zero over the time period Δt_{lock}
F_{tbuff}	N	Force due to the top end-stop buffer
F_X	N	The instantaneous force due to the component or combination of components 'X'
$fricti_{ddn}$	N	The magnitude of the friction force from the damper acting in compression
$fricti_{ddn}$	N	The damper friction coefficient acting in compression
$fricti_{dup}$	N	The magnitude of the friction force from the damper acting in extension
$fricti_{dup}$	N	The damper friction coefficient acting in extension
frictgain	-	Gain applied to all friction coefficients, determined in Chapter 9
frictioffset	-	Value between –1 and 1 to defining the proportion of the total friction force acting in compression and extension
$fricti_s$	N	The suspension linkage friction coefficient
$fricti_{total}$	N	The instantaneous total friction magnitude
g	ms^{-2}	The acceleration due to gravity
k_1	Nm^{-1}	The human body model linear stiffness
k_{bbuff}	Nm^{-1}	The (non-linear) bottom buffer stiffness
k_c	Nm^{-1}	The linearised cushion stiffness
k_{gl}	Nm^{-1}	Stiffness caused by the damper gas loading
k_s	Nm^{-1}	The equivalent vertical stiffness of the suspension spring
k_{tbuff}	Nm^{-1}	The (non-linear) top buffer stiffness
lh	m	The instantaneous horizontal distance between the ends of the suspension linkage arm which contacts the top end-stop buffer
lh_{mid}	m	The horizontal distance between the ends of the suspension linkage arm which contacts the top end-stop buffer with the suspension at the mid-point of the free travel
ll	m	The length of the suspension linkage arm which contacts the top end-stop buffer
lv_{mid}	m	The vertical distance between the ends of the suspension linkage arm which contacts the top end-stop buffer with the suspension at the mid-point of the free travel.
m_0	kg	The lower mass of the human body model, or the total load mass if a rigid seat load were used.
m_1	kg	The upper mass of the human body model
m_s	kg	The mass of the suspended part of the seat, including the seat pan, cushion, backrest, armrests and the upper parts of the suspension.
offset	m	The initial position of the suspension mechanism relative to the offset between the mid-point of the free travel.
t	s	The instantaneous time
$tbuff_{compression}$	m	The instantaneous axial compression of the top end-stop buffer
θ	radians	The instantaneous angle between the suspension linkage

		arm which contacts the top end-stop buffer and the horizontal plane
$\theta_{contact}$	radians	The angle between the suspension linkage arm and the horizontal plane at the point of contact with the top stop buffer
θ_{mid}	radians	The angle between the suspension linkage arm which contacts the top end-stop buffer and the horizontal plane with the suspension at the mid-point of the free travel.
travel	m	The vertical free travel displacement between the end-stop buffers
$\ddot{x}_N$	ms^{-2}	The instantaneous vertical acceleration of the mass 'm_N'
$\dot{x}_N$	ms^{-1}	The instantaneous absolute vertical velocity of the mass 'm_N'
x_N	m	The instantaneous absolute vertical displacement of the mass 'm_N'

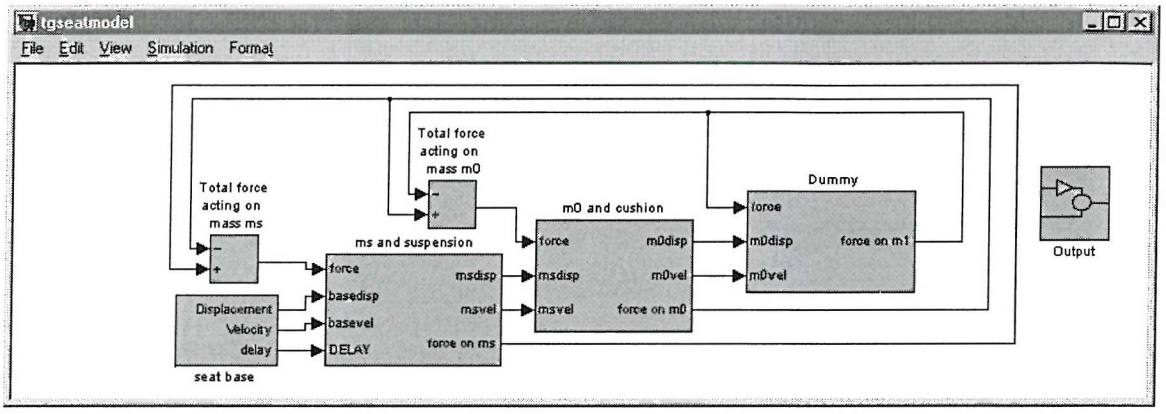

Figure 7-4 The top level of the SIMULINK block diagram

The model calculated the force acting on each mass within the system and determined the acceleration of the mass according to Newton's second law ($F = m.\ddot{x}$). The acceleration was integrated to obtain the instantaneous velocity of each mass and again to obtain the instantaneous displacement. The relative velocity or displacement between each pair of adjacent masses was used to calculate the force generated by the components connecting them and the forces due to each of the connecting components were summed to determine the total force acting on each mass. The model then advanced one time step and repeated the process.

The equations were solved at each time step using a 4th order Runga-Kutta ordinary differential equation (ODE) fixed-step algorithm. *Simulink* had available a number of fixed and variable step ordinary differential equation (ODE) solvers, but preliminary investigations using the various variable step solvers intended for both stiff and non-stiff systems were not productive. The indications were that the solvers could provide efficient and accurate results for an initial condition problem but caused the simulation to fail with a continuously varying base motion in the presence of a friction force.

7.3.2 The load mass

Field studies of off-road vehicles invariably have a human vehicle operator on the seat. Laboratory experiments allow simpler and more consistent loading methods to be used, such as simple masses or anthropodynamic dummies. The model should ideally be able to predict the motion of a suspension seat using any of these loading methods. However, at frequencies below approximately 3 Hz the impedance of the human body approximates that of a rigid mass. The equations describing these loads are shown in Figure 7-5 and Figure 7-6.

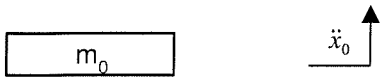

$$F_{m0} = m_0.\ddot{x}_0 \qquad \text{Equation 7-1}$$

Figure 7-5 A simple, rigid load mass

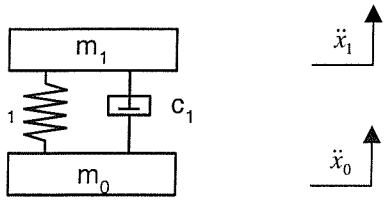

$$F_{m0} = m_0.\ddot{x}_0 \qquad \text{Equation 7-2}$$

$$F_{m1} = m_1.\ddot{x}_1 \qquad \text{Equation 7-3}$$

$$F_{c1} = c_1.(\dot{x}_1 - \dot{x}_0) \qquad \text{Equation 7-4}$$

$$F_{k1} = k_1.(x_1 - x_0) \qquad \text{Equation 7-5}$$

Figure 7-6 The anthropodynamic dummy / human body model

7.3.3 The cushion

A seat cushion as used on a suspension seat is generally foam with a fabric or plastic covering. The modelling of foam cushions is of considerable interest to the automotive industry. Several methods of measuring and modelling foam cushion performance have been suggested (e.g. Wei and Griffin, 1998; Patten *et al.*, 1998). However, few investigations have been concerned with the high accelerations experienced on suspension seats during end-stop impact events. The time domain investigation of seat end-stop impact performance by Wu and Griffin (1998) involved measurement at the suspension top but did not include measurements of the vibration transmitted through the cushion.

The cushion was initially modelled as a parallel linear spring and linear viscous damper with a force-limiting term to prevent the cushion applying a downward acceleration to the load of greater than 1g. This model was known to be a considerable simplification. A more advanced cushion model is investigated in Chapter 11.

The equations describing the cushion used in the model up to Chapter 11 were:

$$F_{cc} = -c_c.(\dot{x}_0 - \dot{x}_s) \qquad \text{Equation 7-6}$$

$$F_{kc} = -k_c.(x_0 - x_s)$$ Equation 7-7

$$F_{cush} = F_{kc} + F_{cc} \quad \text{where} \quad (F_{kc} + F_{cc}) > -(g(m_0 + m_1)),$$ Equation 7-8

otherwise

$$F_{cush} = -(g(m_0 + m_1))$$ Equation 7-9

7.3.4 The suspension linkage

The suspension linkage confined the suspension motion to the vertical direction and provided the basic structure to which the seat components were attached. The linkage was implemented as a mass and a friction element.

The mass of the linkage mechanism was lumped as a single value consisting of the masses of other seat components that move with the linkage. This included the cushion and backrest, a part of the suspension damper, part or all of the suspension spring and any of the seat fore-and-aft, height, rotation and inclination adjustment mechanisms mounted on or above the suspension top plate.

The friction present in the linkage was modelled as a Coulomb friction element acting between the suspension linkage mass and the base of the seat. The friction force was assumed to be constant for all displacements and velocities and no distinction was made between static and dynamic friction. The friction force due to the linkage was implemented as a part of the total friction force, as described below in Section 7.3.8.

7.3.5 The suspension spring

The suspension stiffness is usually provided by a pair of steel coil springs acting in tension, or an air-filled diaphragm acting in compression. The model assumed the spring to be a simple, linear stiffness element. This was likely to be a close approximation in the case of the steel springs, but air springs may change in stiffness with displacement or have other non-linear characteristics. The stiffness element in the model acted in the vertical direction, irrespective of how the spring was mounted in the suspension mechanism. Non-linear effects due to the geometry of the spring mounting were assumed to be small relative to the effect of other uncertainties and were ignored. The suspension stiffness force was described by:

$$F_{ks} = k_s.(x_s - x_b)$$ Equation 7-10

7.3.6 The suspension damper

A damper used in an under-seat suspension mechanism is usually mounted at an angle between the top of the suspension mechanism and the base of the seat. This was the configuration for all three of the seats used in this project. The damping force

is therefore greatest when the damper is closest to the vertical, when the suspension is at the highest point of its travel.

The effect of damper angle was accounted for as shown in Equation 7-11. The damper force-velocity characteristic was initially modelled as a 2-stage 3rd-order polynomial as described in Chapter 6, but discrepancies between damper measurements taken on different apparatus resulted in the development of a revised model of the damper as described in Chapter 9.

$$ang = \sin\left(\arctan\left(\frac{dv + (x_s - x_b)}{dh}\right)\right) \qquad \text{Equation 7-11}$$

7.3.7 The end stop buffers

The end stop buffers were modelled as non-linear stiffness described in terms of 5th order polynomials as described in the following sections.

7.3.7.1 Bottom buffer

The vertical movement of the suspension corresponded directly to the axial compression of the buffer. The compression of the bottom buffer was:

$$bbuff_{compression} = -(x_s - x_b) - \left(\frac{travel}{2} + offset\right) \qquad \text{Equation 7-12}$$

for conditions where $\left(-(x_s - x_b) - \left(\frac{travel}{2} + offset\right)\right) > 0$ and

$bbuff_{compression} = 0$ for all other situations. Equation 7-13

where $(x_s - x_b)$ is the displacement across the suspension mechanism relative to the mean ride position. The mean ride position is described by the free vertical travel of the suspension mechanism ($travel$) plus the offset from the mid point of the free travel ($offset$).

The force generated by the compression of the end-stop buffer was defined by a 5th order polynomial function as shown in Equation 7-14. The coefficients were defined in Chapter 6 from least squares curve-fit to the measured force-deflection characteristic of the end-stop buffer.

$$F_{bbuff} = F = a_1 bbuff_{compression}^{\ 5} + a_2 bbuff_{compression}^{\ 4} + a_3 bbuff_{compression}^{\ 3} + a_4 bbuff_{compression}^{\ 2} + a_5 bbuff_{compression} \qquad \text{Equation 7-14}$$

7.3.7.2 Top buffer

The compression of the top end-stop buffers can be derived trigonometrically from the suspension linkage geometry.

The angle described by the suspension linkage arm from the horizontal (θ) at the mid ride position is

$$\theta_{mid} = \sin^{-1}\left(\frac{lv_{mid}}{ll}\right) \qquad \text{Equation 7-15}$$

where lv_{mid} is the vertical distance between the linkage arm mounting points at mid ride and ll is the length of the linkage arm. ll is calculated from:

$$ll = \sqrt{lv_{mid}^2 + lh_{mid}^2} \qquad \text{Equation 7-16}$$

The angle between the linkage arm and the horizontal at any suspension displacement is:

$$\theta = \sin^{-1}\left(\frac{lv_{mid} + (x_s - x_b) + offset}{ll}\right) \qquad \text{Equation 7-17}$$

where $((x_s - x_b) + offset)$ is the relative displacement of the suspension mechanism from the mean ride position.

The horizontal distance between the suspension mounting points at any suspension displacement is given by:

$$lh = ll \cdot \cos(\theta) \qquad \text{Equation 7-18}$$

The top stop buffer is in compression if:

$$\left(\left(\frac{travel}{2} - offset\right) - (x_s - x_b)\right) > 0 \qquad \text{Equation 7-19}$$

and the angle between the linkage arm and the horizontal at the point of contact with the top stop buffer is:

$$\theta_{contact} = \sin^{-1}\left(\frac{lv_{mid} + \frac{travel}{2}}{ll}\right) \qquad \text{Equation 7-20}$$

So the compression of the top stop buffer is

$$tbuff_{compression} = ll \cdot \cos(\theta) - ll \cdot \cos(\theta_{contact}) \qquad \text{Equation 7-21}$$

where the angles θ and $\theta_{contact}$ are as defined above and the end-stop buffer is in compression. If the buffer is not in compression then

$$tbuff_{compression} = 0 \qquad \text{Equation 7-22}$$

As with the bottom buffer, the force generated by the compression of the top end-stop buffer was defined by a 5th order polynomial function as shown in Equation 7-23. The coefficients were defined in Chapter 6 from least squares curve-fit to the measured buffer force-deflection characteristic.

$$F_{tbuff} = F = b_1 tbuff_{compression}^{5} + b_2 tbuff_{compression}^{4} + b_3 tbuff_{compression}^{3} + b_4 tbuff_{compression}^{2} + b_5 tbuff_{compression} \quad \text{Equation 7-23}$$

7.3.8 Friction

The physical processes leading to the generation of a friction force are due to interactions at the molecular level (Resnick *et al*, 1992) and as such are beyond the scope of a lumped parameter suspension seat model. Some sources of friction within a seat suspension mechanism are the bearings and joints in the linkage mechanism and the oil seals within the damper unit. On a macroscopic level, friction can be approximated by a Coulomb friction force, defined as proportional to the perpendicular force between two sliding surfaces. Coulomb friction is usually defined in terms of two coefficients usually having a greater magnitude when the surfaces are at rest (coefficient of static friction) compared with the surfaces in motion (coefficient of dynamic friction). The Coulomb friction force acts to oppose the motion of a mass unless the forces acting on the mass are insufficient to overcome the friction force, in which case the friction force acts to hold the mass stationary.

The primary difficulty in evaluating a numerical model involving a Coulomb friction component is that the theoretical model of friction described above is discontinuous in terms of acceleration. This discontinuity is illustrated in Figure 7-7 and Figure 7-8, which show the displacement, velocity and acceleration of a moving mass with no forces acting apart from a simple friction force which brings the mass to a halt.

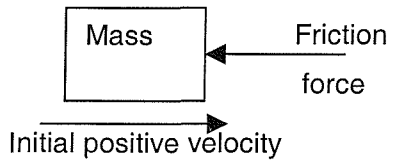

Figure 7-7 A moving mass opposed by a friction force

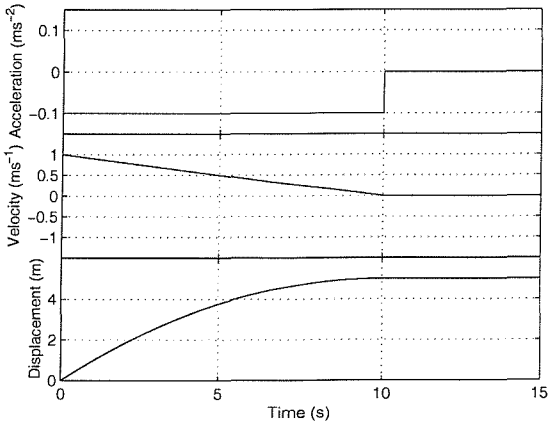

Figure 7-8 The acceleration, velocity and displacement of the system shown in Figure 7-7

The numerical integration model was solved by approximation at discrete time intervals, so the smallest time interval in which an instantaneous event could occur was equal to the time step used by the numerical integration routine, so the performance of the model was affected by the choice of integration time step. Furthermore, discontinuities could interfere with the correct functioning of the differential equating solving routine causing the simulation to fail.

A further complication involved in simulating friction in suspension seating was that the input to the model was applied to the base of the suspension. As the suspension became friction locked then the suspended seat mass must become stationary in the reference frame of the seat base, rather than the gravitational reference frame. The model was defined in the gravitational reference frame and the relative velocity across the suspension was derived from the acceleration of the suspended seat mass. Some method was therefore required to set the acceleration of the seat load mass to a value that caused the relative velocity across the suspension to become zero when the suspension was locked, applied a constant force opposing the motion when the suspension was in motion and was able to switch between these two states.

Previous simulations (e.g. Rakheja *et al.*, 1994) implemented the friction force as a constant magnitude force acting to oppose the relative velocity across the suspension mechanism as follows:

$$F_{friction} = fric t_{total} \cdot \mathrm{sgn}\left(\dot{x}_s - \dot{x}_b\right) \qquad \text{Equation 7-24}$$

This form of friction model did not attempt to explicitly 'friction lock' the suspension for low magnitude motions, but approximated the friction-locked situation by alternating the direction of the friction force as necessary to reduce the velocity towards zero. If the instantaneous velocity were of sufficiently low magnitude, the acceleration due to the friction force ($fric t/m_s$) would cause the velocity to change sign before the next numerical integration time step. The friction force at the next time step would therefore be applied in the opposite direction and could also cause the velocity to change sign by the subsequent time step, causing a further reversal of the friction force. By this process the relative velocity across the suspension, obtained from the integrated acceleration could be maintained at approximately zero.

Two difficulties were encountered with this approach. Firstly, the alternating friction force naturally resulted in the load mass experiencing an alternating acceleration with a magnitude of up to $fric t/m_s$. The acceleration at the seat surface was determined from the velocity and displacement of the suspended seat mass and the integration process used to obtain these values would smooth out the oscillation so evaluations

of the model performance in terms of the acceleration at the seat surface were not expected to be strongly affected. However, it would not be possible to examine the acceleration of the suspended mass without processing this time history in some way to remove the oscillating acceleration artefact. Secondly, the relative displacement across the suspension was observed to 'drift' by a small amount (in the order of 2 mm, but dependant on a wide range of factors) when the suspension was in the friction-locked state. This drift appeared to be proportional to the seat base displacement. It appeared that the motion of the base was creating a condition whereby the rapidly alternating acceleration was integrating to a small but consistently non-zero value, resulting in a gradual motion of the 'locked' suspension. It was found to be possible to reduce, but not eliminate, the drift by using the knowledge of the base velocity at one integration step in the future. By this method, the friction would act to set the relative velocity to zero at the impending time step rather than the current time step where the relative velocity has already been calculated.

In order to eliminate these artefacts, a more advanced friction model was developed, defined in terms of a locked and an unlocked state. In the unlocked state, the friction was implemented as a constant force opposing the motion as defined in Equation 7-24 above. In the locked state, an acceleration was applied to the suspended mass such that the velocity of the suspended seat mass would be equal to the velocity at the seat base when the model was evaluated at the next time step as shown in Equation 7-25. All other forces acting on the suspended seat mass due to the remaining suspension components or the cushion were set to zero. This equation is an approximate derivative of the relative velocity over the time interval Δt_{lock}. If adequate friction coefficient measurements were to be obtained then this time interval could be removed from the model and replaced by a more numerically rigorous derivative function in order to apply the measured friction magnitude coefficients with the correct scale factor.

$$F_{locked} = \frac{-m_s\left(\dot{x}_s(t) - \dot{x}_b(t + \Delta t_{lock})\right)}{\Delta t_{lock}} \qquad \text{Equation 7-25}$$

The locked or unlocked state was chosen by comparing the friction magnitude with the force required to bring the relative velocity between the suspended seat mass and the seat base to zero within an arbitrarily small time period, including the forces due to the cushion and the remainder of the suspension mechanism, according to the following equation:

$$frict_{total} \geq F_{locked} - \left(F_{ks} + F_{cs} + F_{tbuff} + F_{obuff} - F_{cush}\right) \qquad \text{Equation 7-26}$$

If this expression was true, then the friction considered locked and the force acting on the suspended seat mass was defined by:

$$F_{ms} = F_{locked} \qquad \text{Equation 7-27}$$

Otherwise, the force acting on the suspended seat mass was defined by:

$$F_{ms} = F_{ks} + F_{cs} + F_{tbuff} + F_{bbuff} - F_{cush} - frict_{total} \qquad \text{Equation 7-28}$$

The arbitrarily small 'lock-up' time used in the model was 100 μs which for most simulations was equal to the numerical integration step size. The lock up time constant was defined independantly of the integration step size so the friction model would remain consistent for simulations using smaller integration time steps. The assumption implicit in this friction model was that the forces acting on the mass would remain constant until the next integration step. A small lock-up time would require a large friction force, while a large lock-up time would require a small friction force as the force could act for a longer time to negate the relative velocity. This presents a difficulty if a measured friction magnitude value in terms of Newtons were to be used, but in this thesis the friction magnitude was estimated from the model performance as described in Chapter 9.

Discussion with damper manufacturers and experience of the dampers tested in Chapter 6 suggested that the oil-seal within a damper unit can be fitted so as to exert a greater friction force in compression than in extension. The model was therefore designed so that the coefficient of friction could be defined in terms of the components due to the suspension linkage and the damper and could have different magnitudes for the damper friction in compression and in extension. The equations defining the friction force magnitude were as follows:

If $(\dot{x}_s - \dot{x}_b) > 0$, then

$$frict_{total} = frictgain\left(\begin{array}{l} frict_s(1 + frictoffset) + \\ frict_{dup} \cdot ang \cdot (1 + frictoffset) \end{array}\right) \qquad \text{Equation 7-29}$$

Otherwise

$$frict_{total} = frictgain\left(\begin{array}{l} frict_s(1 - frictoffset) + \\ frict_{ddn} \cdot ang \cdot (1 - frictoffset) \end{array}\right) \qquad \text{Equation 7-30}$$

The coefficients *frictgain* and *frictoffset* were defined in Chapter 9, relegating the friction magnitude coefficients that were unsatisfactorily measured in Chapter 6 ($frict_s$, $frict_{dup}$, $frict_{ddn}$) to the status of arbitrary constants. The facility to allow different coefficients of static and dynamic friction was temporarily included, but in the absence

of suitably accurate measurements this was not used in this thesis and is not shown in the model configuration shown in Appendix 3.

7.4 Selection of the step size

The model was implemented to use a fixed step fourth order Runga-Kutta ODE solver. The choice of integrator step size was a key factor influencing the accuracy and stability of the model and the time taken to evaluate the model for a given duration of input signal. The step size must be sufficiently small so that consistent and accurate results are obtained, but a very small step size can require considerable processor power and/or time.

The response of the model was evaluated in response to fifty input motions selected from the measured seat base accelerations reproduced on the shaker platform in Chapter. Conditions involving end-stop impacts and conditions with the suspension in an almost friction-locked condition were included. The simulation was configured to model the earthmover seat. The damper force-velocity characteristic and suspension friction coefficients were not known at this time, so arbitrary but realistic values were used as the intention of this section was to investigate the performance of the simulation software rather than a specific seat. The linear damper force velocity coefficient was set to 900 Nsm^{-1} and the overall suspension friction coefficient was set to 100 N.

The seat response to each test motion was evaluated with integrator step sizes from 50 μs to 10 ms. The root-mean-quad (r.m.q.) acceleration measured at the seat cushion and on the suspension mass was evaluated at each step size. The acceleration on the cushion was of more interest as a model output as this is experienced by the vehicle operator. However the seat cushion acts as a mechanical low-pass filter. The suspension mass acceleration was expected to be a more sensitive measure of the consistency of the model operation. It was anticipated that the results at both locations should converge towards a consistent result for each motion as the step size decreased. The results for each test motion were normalised by the value obtained at the smallest step size to allow the results from different test conditions to be compared.

The results are shown in Figure 7-9. These results indicate that the error inherent in the simulation software would be less than 1% at the seat surface and less than 5% at the suspended seat mass if a step size of 1 ms were used. The simulation was observed to run in approximately real time (1 second to evaluate a 1-second test signal) using the computing facilities available. The sensitivity analysis calculations in

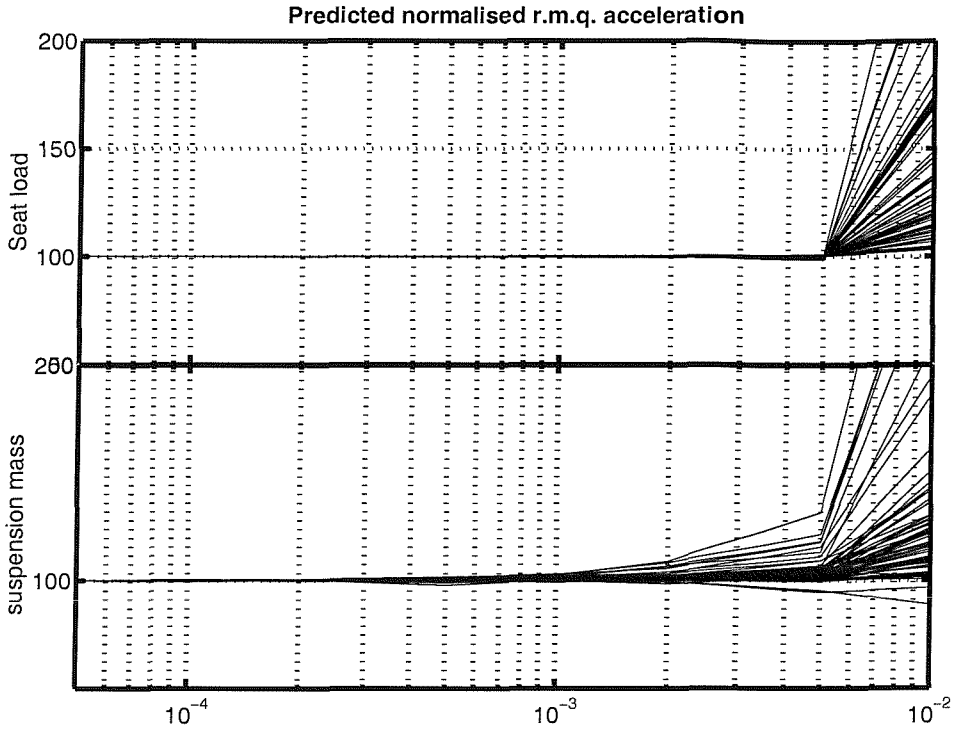

Figure 7-9 Predicted r.m.q. acceleration varying with integrator step size normalized with respect to the r.m.q. acceleration with a step size of $5x10^{-4}$ seconds.

Chapter 12 would require approximately 6 hours to investigate the effect of each suspension coefficient, which was considered acceptable. Reducing the step size further to 100 μs would result in a substantial increase in simulation time for a comparatively small improvement in accuracy.

It should be noted that the effect of including an asymmetric friction force was not considered at this stage. This is discussed later in Chapter 9.

7.5 Conclusions

This chapter described the software and mathematical structure used in this thesis to simulate a suspension seat and determined a suitable integration step size to obtain an error in the r.m.q. acceleration at the seat surface of less than 1% for all results from fifty test conditions. A force-limited cushion to allow the load to lift clear of the seat and a method of explicitly defining the friction-locked state of the suspension were also presented. More advanced methods of mathematical modelling of the damper force-velocity characteristic and the cushion dynamic characteristics are presented later in Chapters 9 and 11 respectively.

8 A method of estimating the suspension damper characteristics

8.1 Introduction

Previous simulation studies discussed in Chapter 2 noted that the suspension damper had a strong influence on the predicted seat performance. Accurate simulations of suspension seat dynamic performance therefore require the suspension damping to be accurately measured and modelled. However, the methods used for quantifying the suspension damper characteristics (Chapter 6) were found to be insufficient for the requirements of this thesis. The test apparatus used was not capable of exercising the dampers over sufficiently high magnitudes and the measurements of the damper friction made before and after the complete seat was tested in the laboratory were found to give different values. Some method of estimating the seat friction and the damper force-velocity characteristics at high magnitudes was therefore required.

An optimisation procedure might be used to estimate the damper characteristic from the dynamic performance of the complete seat. Unknown parameters might be estimated by minimising the difference between the predictions from the simulations and the measured dynamic performance of the complete seat. As mentioned in Chapter 2, the choice of optimisation method is highly dependent on the characteristics of the function to be solved. Algorithms such as the Nelder-Mead simplex (Nelder and Mead, 1965) and the search method used in the current study attempt to locate the minimum of a function of n parameters by attempting to move 'downhill' from a starting point. These methods can fail to locate the global minimum if the function has more than one minima (i.e. is not 'convex'). In such cases alternative approaches such as the genetic algorithms described by Holland (1975) and Goldberg (1989) can be employed, but this can be at the expense of greater processing power requirements (Seo, 2001).

The work reported in this chapter was undertaken to determine if a simple global optimisation procedure could converge to a consistent prediction for the suspension damper force-velocity characteristic and friction value by comparing the predicted seat performance to the measured seat performance obtained in a limited number of test conditions taken from the results presented in Chapter 5. The work reported in the present chapter was also intended to determine if the damper characteristic obtained by this method was similar to that obtained from laboratory tests of the damper in Chapter 6.

Table 8-1 Parameter values used to simulate each seat

Description		Symbol	Parameter values used for each seat		
			Earthmover	Forwarder	Tractor
Load mass (kg)		m_0	56	56	56
Cushion stiffness (kNm^{-1})		k_c	92.1	88.9	91.6
Cushion damping ($kNsm^{-1}$)		c_c	1.37	1.00	1.38
Suspended seat mass (kg)		m_s	27	21	36
Vertical suspension stiffness (kNm^{-1})		k_s	4.57	4.22	3.69
Damper gas loading stiffness (kNm^{-1})		k_{gl}	2.32	0	0
Suspension free travel (mm)		*travel*	64	85	156
Horizontal and vertical distances at mid free travel between the damper mounting points (mm)		*dh*	150	128	145
		dv	111	83	92
Horizontal and vertical distances at mid free travel between the ends of the suspension link arm that contacted the top end-stop buffer (mm)		*lh*	295	280	270
		lv	150	160	250
Coefficients of a 5th order polynomial fit to the end-stop buffer force-deflection characteristic as described by: $F = a_1x^5 + a_2x^4 + a_3x^3 + a_4x^2 + a_5x$ where F is the force corresponding to a deflection x.	Top	b_1	5.48 x10^{15}	5.48 x10^{15}	5.48 x10^{15}
		b_2	-2.58 x10^{4}	-2.58 x10^{4}	-2.58 x10^{4}
		b_3	2.60 x10^{3}	2.60 x10^{3}	2.60 x10^{3}
		b_4	3.27 x10^{7}	3.27 x10^{7}	3.27 x10^{7}
		b_5	1.35 x10^{5}	1.35 x10^{5}	1.35 x10^{5}
	Bottom	a_1	1.83 x10^{11}	4.64 x10^{11}	0
		a_2	-8.57 x10^{7}	2.21 x10^{10}	5.62 x10^{9}
		a_3	-4.45 x10^{7}	-5.23 x10^{8}	-8.93 x10^{7}
		a_4	1.50 x10^{6}	5.35 x10^{6}	1.58 x10^{6}
		a_5	7.62 x10^{3}	2.34 x10^{4}	5.68 x10^{3}

8.2 Method

8.2.1 Overview and seat model coefficients

The predicted seat suspension displacements were obtained from the response to two magnitudes of input motion using theoretical models of all three seats. The input motions were taken from the laboratory study described in Chapter 5. An iterative non-linear optimisation process was devised and used to iteratively minimise the difference between the predicted suspension displacement and that measured in the laboratory with the same test conditions by adjusting the coefficients describing the suspension damper.

The 'optimal' suspension damper models obtained in this manner were compared with the damper force-velocity characteristics measured in Chapter 6. The three seats were simulated using the parameter measurements obtained in Chapter 6 and summarised in Table 8-1.

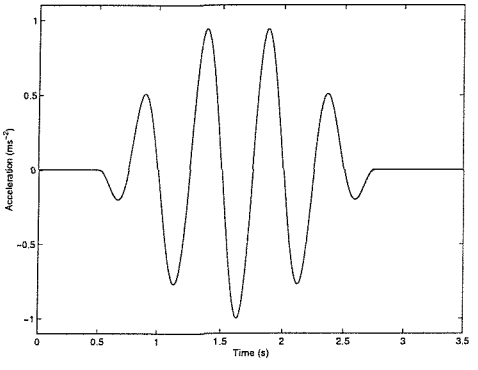

Figure 8-1 The seat base acceleration waveform

8.2.2 Input motion

The damper characteristics were optimised using the measured seat performance in response to two magnitudes of 4.5 cycle 2.0 Hz motion obtained in Chapter 5 and illustrated in Figure 8-1. For the earthmover and forwarder seats, motion number one involved moderate magnitude, 'stage 3' seat motion (see Table 8-2) with the peak seat suspension displacement within 5 mm of the end-stop buffers without striking and motion number two was a high magnitude motion involving 'stage 4/5' seat behaviour with end-stop impacts. In the case of the tractor seat, end-stop impact events were not obtained with the higher magnitude due to the long suspension stroke, so both motions were considered to result in 'stage 3' seat motion.

Table 8-2 A method of characterising suspension seat behaviour with changing input magnitude, summarised from Wu and Griffin (1996)

Stage 1	Low magnitudes with the seat suspension friction locked
Stage 2	'Breaking away' from friction
Stage 3	Moving relatively freely but not contacting the end-stop buffers
Stage 4	Mild to moderate end-stop impacts
Stage 5	Severe end-stop impacts

8.2.3 Theoretical seat model

The structure of the theoretical model used to describe the seats for this chapter was as described in Chapter 8, using the rigid load in place of the two degree-of-freedom human body model. The present study involved strong top stop impacts and the simpler load model allowed the forces acting during a top stop impact as the load becomes disconnected from the cushion to be simulated more simply. Some cases were observed of the model becoming unstable during severe top-stop impacts when using the human body model. The acceleration measured at the base of the seat in the laboratory was used as the input to the model and the load acceleration and relative suspension displacement time histories were returned as the output.

8.2.4 Error function

An optimisation process attempts to locate the minimum value of an objective function. The objective function used for project was the error between the predicted and measured displacement across the suspension mechanism normalised by the root-mean-square of the measured displacement as defined by Equation 8-1. The displacement was chosen as this property was expected to be sensitive to the suspension damping characteristics.

$$e = \frac{\left[\int_{t=0}^{T} \left(z_{predicted}(t) - z_{measured}(t)\right)^2 dt\right]^{1/2}}{\left[\int_{t=0}^{T} \left(z_{measured}(t)\right) dt\right]^{1/2}}$$

Equation 8-1

where the error e for a motion of duration T is in terms of the unweighted relative displacement between the seat base and the top of the seat suspension underneath the cushion obtained from the model ($z_{predicted}$) and from the laboratory measurements ($z_{measured}$). The error e_{acc} for a motion of duration T is in terms of the unweighted acceleration of the seat surface obtained from the model ($a_{predicted}$ and $a_{measured}$).

8.2.5 Friction symmetry

Each evaluation of the error function required the model to simulate the response to a specific input motion. This provided a predicted output that was compared with a target motion measured in the laboratory in order to obtain the error. The model ran on an IBM PC with a 750 MHz CPU and operated in approximately real time (1 second to simulate the response to a 1-second time history) simulation when using a 100 μs integration time step. It was found that asymmetric friction forces (greater friction in compression than in extension or vice-versa) required the model to use a smaller integration time step to obtain consistent results so increasing the time required to run each simulation.

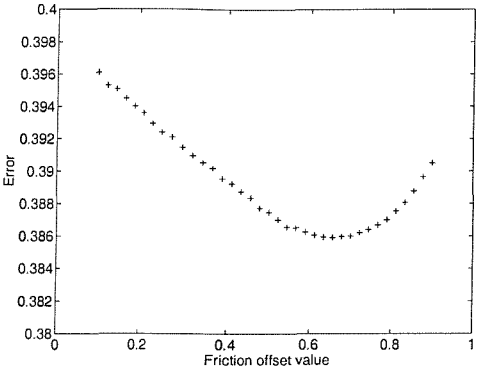

Figure 8-2 The effect of the friction symmetry on the accuracy of the model evaluated in terms of the load mass acceleration for the high magnitude of motion with the earthmover seat. A value of zero indicates 100% of the friction force acting in compression with a zero friction force in compression and a value of one indicates 100% of the force acting in extension.

Figure 8-2 shows the effect of friction on the model accuracy expressed in terms of e_{acc} for the higher magnitude earthmover seat test motion where a coefficient value of 0.5 indicates symmetrical friction. It can be seen that although the optimal friction symmetry coefficient was 0.62 rather than 0.5, the variation in error on over the ±90% range investigated was less than 3% of the minimum and the difference in error between the optimal coefficient value and a value of 0.5 was less than 0.5% of the minimum. Similar results were found in other test conditions, so symmetrical friction forces were used throughout this experiment.

8.2.6 Suspension damper model

The expression shown in Equation 8-2 was used to model the damper force-velocity characteristic in terms of a small number of coefficients. The range of values used for

each coefficient during this experiment is shown in Table 8-3 and the characteristics possible using this expression are illustrated in Figure 8-3.

The suspension linkage and suspension damper friction forces were initially considered independently, but some preliminary tests failed to converge as the two values were components of the overall friction force and the distribution of friction between the linkage and the damper had minimal influence on the performance of the model at some magnitudes. The friction forces were therefore optimised as a combined variable with an arbitrary but not unreasonable distribution of 40% acting as suspension friction and 60 % as damper friction based on the initial friction measurements from Chapter 5.

$$F_c = \left[A_c|\dot{z}|^{B_c} + C_c|\dot{z}|z + (D+E)\right]\cdot sign(\dot{z})\Big|_{\dot{z}<0}$$

$$F_e = \left[A_e|\dot{z}|^{B_e} + C_e|\dot{z}|z + (D+E)\right]\cdot sign(\dot{z})\Big|_{\dot{z}\geq 0} \qquad \text{Equation 8-2}$$

$$F_{damper} = F_c + F_e$$

where F_{damper} is the total force generated by the damper exercised with an axial velocity $\dot{z}$, A and B are coefficients describing an exponential curve in compression and extension, C is a coefficient introducing hysteresis-like behaviour to the force-velocity characteristic and D and E are the magnitudes of the damper and seat suspension friction forces.

Table 8-3 Starting and limiting ranges and optimisation step sizes for each coefficient

Coefficient	Range of initial values (uniform distribution)		Range of permissible values		Step sizes	
	Min.	Max.	Min.	Max.	Coarse	Fine
A_c, A_e (Nsm^{-1})	1000	3000	0	10000	500	100
B_c, B_e	0.5	1.5	0	5	0.25	0.025
C_c, C_e (Nsm^{-2})	5000	15000	0	30000	2500	250
$D+E$ (N)	50	150	0	500	25	2.5

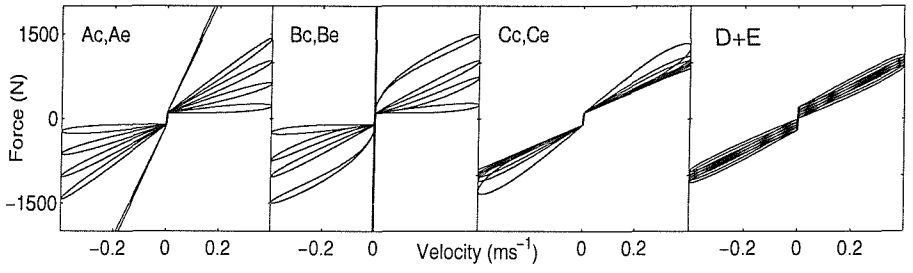

Figure 8-3 The damper model as described by Equation 8-2 showing the force-velocity characteristic described by the median of the range of initial values and the maximum and minimum initial and permissible values for each coefficient.

8.2.7 Optimisation procedure

A convex error in terms of each individual parameter does not necessarily indicate a convex error space in terms of all parameters. The error space was investigated by using the optimisation procedure shown in Table 8-4 (and listed in Appendix 6) repeated 20 times using a range of randomised coefficients. The range of initial starting values was ±50% of a set of coefficients describing an arbitrary damper with a linear force-velocity gradient, a 100 N friction force and a hysteresis loop similar to that observed in laboratory damper measurements (Table 8-3). The starting values for each parameter were selected from independent uniform distributions within this range.

Two variations of the optimisation procedure were investigated. Method one used the higher magnitude input motion to optimise all parameters. Method two used the higher magnitude motion to optimise all the parameters except for the friction magnitude (*D+E*), which was optimised using the lower magnitude motion.

Table 8-4 Summary of the optimisation procedure

1. The order of the coefficients was randomised
2. The model was evaluated in response to one of the two input motions using the first coefficient at its current value and with the current value plus and minus the coarse step size. Error values (*e*) were obtained for each case by comparing the predicted suspension displacement with that measured in the laboratory. The higher magnitude input motion was used in all cases except for the friction coefficient with optimisation method two where the lower magnitude motion was used.
3. If one of the two modified values showed a lower error than the current value then the current value for that coefficient was adjusted to be the modified value assuming that the value was within the permitted bounds and that the change in error was greater than 0.001. Otherwise the coefficient was not modified.
4. The process was repeated from Step 2 using the next coefficient until all coefficients had been tested.
5. If at least one coefficient was modified then the process was repeated from Step 1.
6. The variation in parameter value was reduced to the fine step size and the process was repeated from Step 1. The result of the process was the set of coefficients obtained having reached a solution with this step size.

8.3 Results

The coefficients that resulted in the minimum error (e in Equation 8-1) from 20 repeats of the optimisation procedures (the 'minimum error' result) and the median values obtained for the 20 repeats are shown in Table 8-5. The maximum, minimum and interquartile ranges of the error and the coefficients are shown in Figure 8-4, normalised with respect to the median. The predicted damper characteristics are shown in Figure 8-5 along with the damper characteristics measured in the laboratory. The laboratory friction measurements were adjusted to match the median friction returned by the model to allow the force-velocity characteristic to be directly compared. The time histories for the high magnitude motion measured in the laboratory and predicted using the 'minimum error' characteristics from optimisation method two are shown in Figure 8-6.

Table 8-5 The predicted damper coefficients that resulted in the lowest value for e. The median values for all 20 repeats of the optimisation process are shown in brackets.

Seat and optimisation method	e	A_c	A_e	B_c	B_e	C_c	C_e	D	E
Earthmover seat, method 1	0.11 (0.14)	2030 (1680)	2780 (1900)	1.32 (1.17)	1.74 (1.53)	16600 (13600)	1400 (1350)	56.9 (58.1)	35.5 (36.3)
Earthmover seat, method 2	0.12 (0.13)	2370 (1940)	1680 (1500)	1.49 (1.27)	1.57 (1.47)	21200 (11300)	2360 (1370)	70.2 (64.8)	43.8 (40.5)
Forwarder seat, method 1	0.26 (0.27)	258 (1210)	3690 (3190)	1.58 (1.56)	1.33 (1.24)	2300 (1410)	27800 (28800)	32.3 (30.5)	20.2 (19.0)
Forwarder seat, method 2	0.27 (0.28)	226 (829)	2130 (3090)	0.37 (1.54)	0.98 (1.23)	345 (1050)	29400 (28700)	6.72 (25.7)	4.2 (16.0)
Tractor seat, method 1	0.24 (0.25)	2010 (1980)	1650 (1770)	1.10 (1.06)	0.98 (0.98)	2470 (2280)	24200 (11600)	16.1 (13.9)	10.1 (8.7)
Tractor seat, method 2	0.23 (0.25)	2450 (2080)	1910 (1840)	1.20 (1.09)	1.06 (1.01)	689 (6040)	26800 (11400)	12.5 (12.2)	7.8 (7.6)

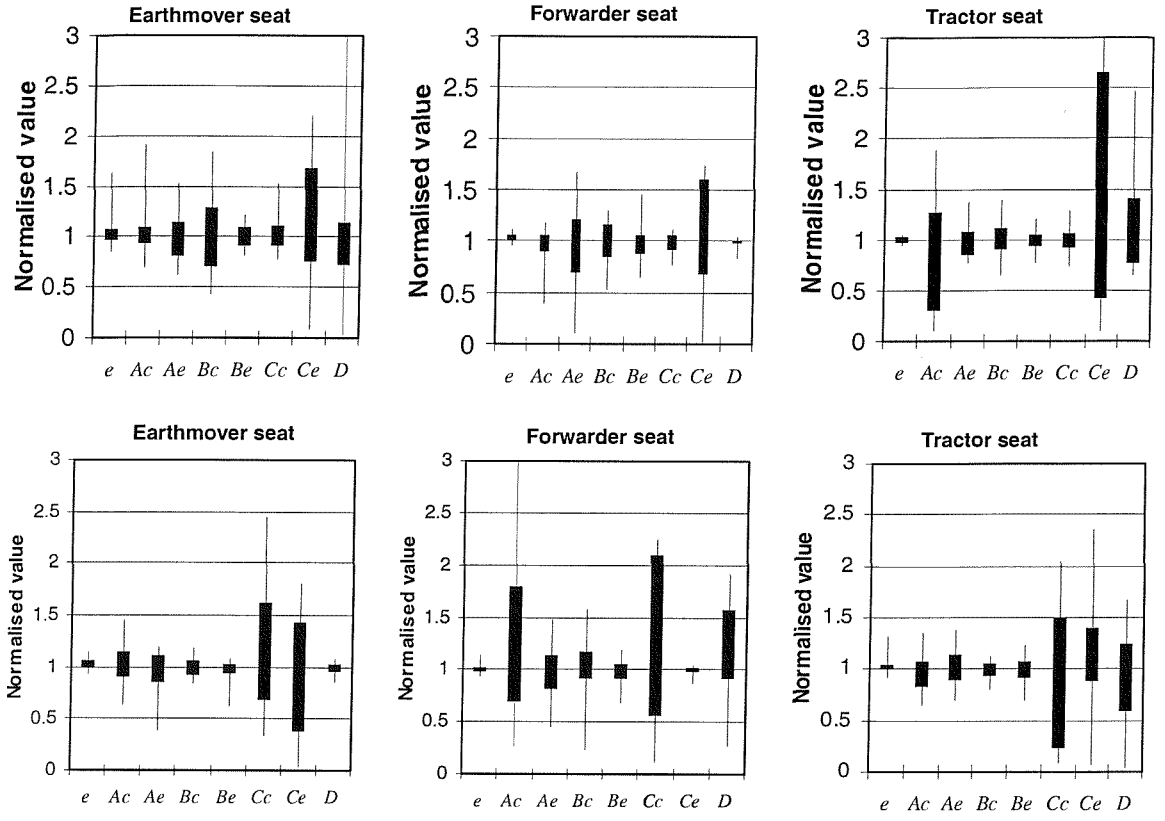

Figure 8-4 The maximum, minimum and inter-quartile error and damper coefficient values obtained from 20 repeats of the optimisation process normalised with respect to the median value using optimisation method one (top row) and method two (bottom row). The results for parameter *E* were identical to those for *D* as they were optimised as a combined value.

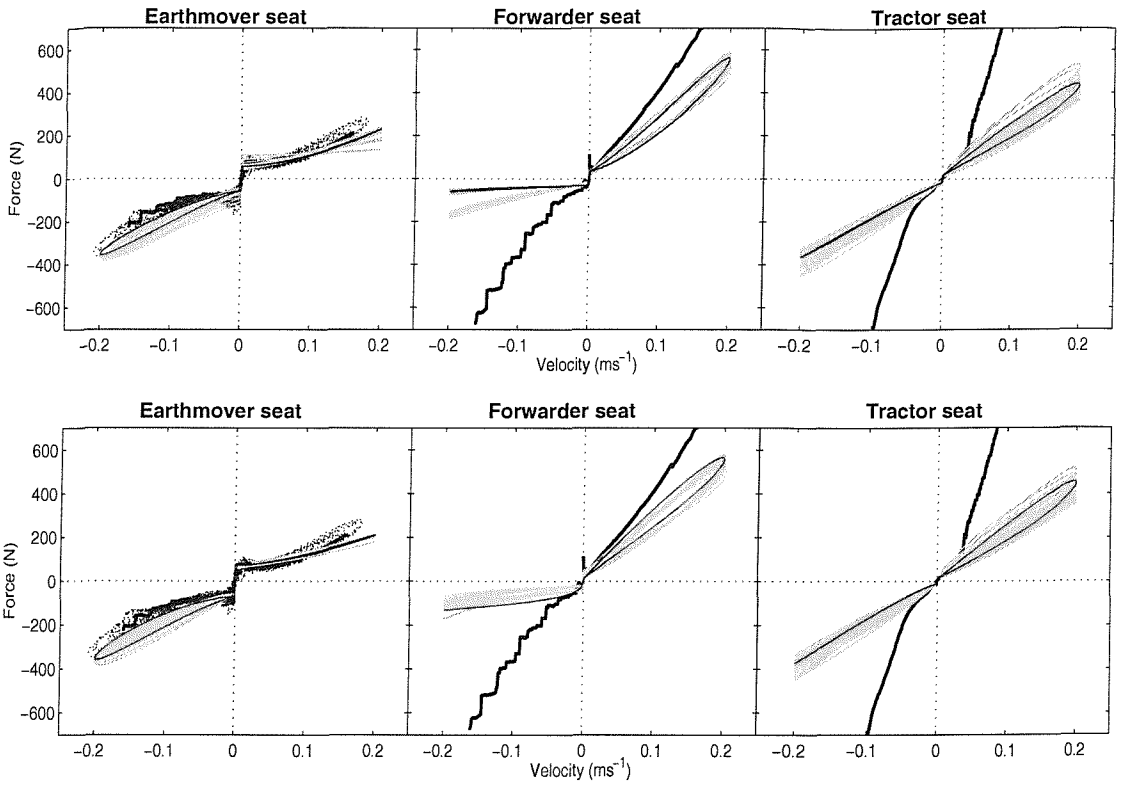

Figure 8-5 The damper characteristics obtained from optimisation method one (top) and method two (bottom) compared with the measured damper characteristic. The thin grey lines are results from the optimisation process, with the characteristic that produced the most accurate model behaviour shown in black. The thick lines are the measurements obtained using the commercial damper test apparatus and the dotted line shows the results of the earthmover damper re-test obtained after the seat tests were complete.

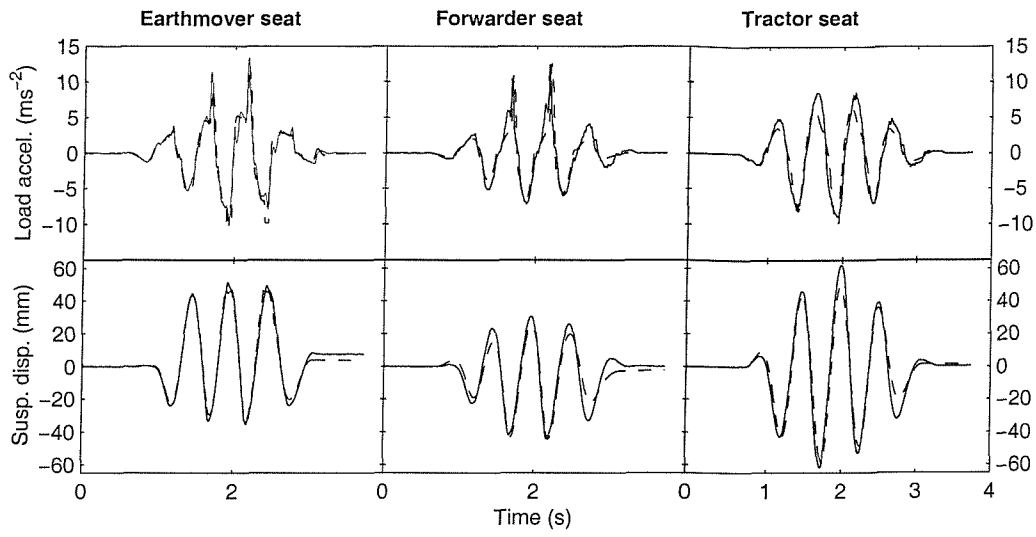

Figure 8-6 The measured time histories (solid lines) using the higher magnitude motion compared with the predicted motions using the damper characteristic that resulted in the smallest error when using optimisation method two (dashed lines).

8.4 Discussion

The damper characteristics obtained from 20 repeats of the optimisation procedures resulted in a distribution of predicted forces for a given velocity of within 20% of the minimum error result over most velocities, except in the case of the earthmover seat damper using optimisation method one and the forwarder seat damper in compression with both methods.

There were significant correlations between some of the damper coefficients obtained for the twenty repeats of each optimisation method, in particular between the pairs *Ac* and *Bc* and *Ae* and *Be* which showed significant positive correlations for all dampers using both optimisation methods except for the seat two damper in compression (Spearman, $p<0.01$). Similar damper characteristics might be obtained over a limited range of velocities using different coefficients, so accounting for some of the variation in coefficient values shown in Table 8-5. The variation in the characteristic shown in Figure 8-5 is a better indication of the ability of the optimisation processes to converge to a consistent result.

The force-velocity characteristic for the earthmover seat damper was within approximately 60 N of the results obtained by testing the damper independently for all velocities when using method two. The optimised characteristics obtained with the other two seats showed more substantial differences. The relatively poor results obtained with the forwarder and tractor seats could have been due to a number of factors. The damper performance may have changed in some way due to a failed oil

seal or other element between the measurements of the damper and the tests of the seat performance with the damper fitted. Alternatively, the mathematical models of the forwarder and tractor seats may have been missing some aspect of the seat dynamic behaviour, such as non-linearities within the air spring, which was capable of influencing the seat performance. Some support for this second hypothesis is provided by the fact that the error in the prediction of the suspension displacement as indicated by *e* in Table 8-5 was lower for seat one that that obtained with the other two seats by a factor of in excess of 1.6.

The use of the additional low magnitude motion in optimisation method two resulted in more consistent predictions for the friction coefficient of the earthmover seat (see Figure 8-4 and Figure 8-5). No improvement was noticeable for the tractor seat and a more consistent result was obtained for the forwarder seat using method one. This latter result was contrary to expectations, but is not inconsistent with the hypothesis that the mathematical model of this seat was lacking some necessary component. Obtaining a consistent solution for two test conditions is more demanding than for a single condition.

8.5 Conclusions

The optimisation process was found to converge to similar but not identical damper characteristics from randomised starting conditions for most situations with all three dampers. Noticeably more accurate predictions of the damper characteristic and of the seat motion were obtained with the earthmover seat as compared with the other two seats. The results suggested that the optimised models of the tractor and forwarder seats might have been using incorrect physical mechanisms to arrive at the predicted load motion. The work reported in the thesis was therefore continued using the results with the earthmover seat only.

This method of determining the suspension damper characteristic from the motion of the complete seat shows potential, as indicated by the results using the earthmover seat. However, the greater error in the simulations and the differences between the predicted and measured damper characteristics with the forwarder and tractor seats indicate the need for further work to determine if improvements to the optimisation method or the theoretical model itself are required for this method to be generally applicable to suspension seating.

9 Quantification of the model performance

9.1 Introduction

This chapter used the model as described in Chapter 8 to simulate the response of the earthmover seat to the input motions measured in the laboratory in Chapter 5. The predictions from the model were compared with the measured seat responses. The differences between the model predictions and the laboratory measurements were quantified in terms of the difference in SEAT value and the root-mean-square error between the predicted and measured load acceleration.

The intention of this chapter was to obtain quantitative measures of the differences between the model performance and the laboratory measurements over a range of frequencies, magnitudes and durations of input motion.

9.2 Choice of the error function

9.2.1 Overview

The requirements of an error function were reviewed and a number of possible functions were considered. The error function was required to:

1. detect some difference between the behaviour of the real and simulated system responding to an identical input stimulus
2. express the difference as a single, real value
3. return a minimum value *only* when the real and simulated model outputs are identical

It was also deemed to be beneficial if the error function:

4. account for the sensitivity of the seated human body
5. could detect if the prediction was an underestimate or an overestimate
6. could be used to directly compare the response to input motions with different frequencies, durations and magnitudes
7. could be selectively biased toward a particular aspect of the model behaviour, for instance the brief, high magnitude shocks produced by end-stop impact

Some of the possible methods for quantifying the difference between the measured and predicted seat performance were considered in the following sections.

9.2.2 Ratio of vibration dose values or SEAT values

The ratio of the VDV at the seat load predicted by the model to that measured in the laboratory as given by:

$$e = \frac{\left[\int_{t=0}^{t=T} a_{w\_predicted}{}^{4}(t)dt\right]^{1/4}}{\left[\int_{t=0}^{t=T} a_{w\_measured}{}^{4}(t)dt\right]^{1/4}} \qquad \text{Equation 9-1}$$

The vibration dose value applies a weighting filter to the acceleration time history and uses a fourth power sum to emphasise the frequencies and magnitudes of vibration to which the human body is most sensitive.

An advantage of the method are that errors produced using signals of different duration can be compared directly as the waveform length does not affect the ratio-based calculation. The function can also discriminate between an over-estimate and an under-estimate in the vibration prediction.

The main disadvantage of this method is that there are an infinite number of acceleration time histories that will produce the same VDV. A perfect result (e=1.0 for Equation 9-1 as shown above) does not necessarily mean that the predicted acceleration time history is similar to the laboratory measurement.

There is no difference to the equation if the SEAT value were used in place of the seat surface VDV as the base motions are identical for the prediction and the measurement and so cancel out.

9.2.3 Difference in vibration dose values or SEAT values

The difference between the predicted and measured vibration dose value at the seat load as given by:

$$e = \left[\int_{t=0}^{t=T} a_{w\_predicted}{}^{4}(t)dt\right]^{1/4} - \left[\int_{t=0}^{t=T} a_{w\_measured}{}^{4}(t)dt\right]^{1/4} \qquad \text{Equation 9-2}$$

This approach shares the advantages of the VDV ratio approach with the added advantage that identical VDVs would result in e=0 rather than e=1.0 and the magnitude of the error for a 10% underestimate would be the same as for a 10% overestimate.

A disadvantage is that the error obtained with a long duration waveform would not be comparable with a short duration waveform. The accumulative nature of the VDV means that if the model time history had a greater magnitude than the measured time history then the error would increase with increasing waveform duration. Also, as with the VDV ratio method there are an infinite number of waveforms that could return a difference in VDV of zero.

The SEAT value could be used in place of the VDV to obtain a result normalised to the input motion. This would allow the result to be compared between different durations and magnitudes of input motion but would still not result in a specific measure.

$$e = \frac{\left[\int_{t=0}^{t=T} a_{w\_predicted}{}^{4}(t)dt\right]^{1/4} - \left[\int_{t=0}^{t=T} a_{w\_measured}{}^{4}(t)dt\right]^{1/4}}{\left[\int_{t=0}^{t=T} a_{w\_seat\_base}{}^{4}(t)dt\right]^{1/4}}$$

Equation 9-3

9.2.4 The root-mean-square error

The square root of the sum of the squared difference between the measured and predicted acceleration time histories at the cushion surface, divided by the duration of the motion as given by:

$$e = \frac{1}{T}\left[\int_{t=0}^{t=T} \left(a_{predicted} - a_{measured}\right)^{2} dt\right]^{1/2}$$

Equation 9-4

The root-mean-square (rms) error is the simplest and most commonly used method of quantifying the differences between two time histories. The function returns a value of zero if the waveforms are identical and a positive value if there are differences. It cannot by itself differentiate between an under- and an over-estimate of the vibration.

Comparison of errors from different duration input motions is possible as the error function includes a division by time so long as the amplitude distribution is similar for the different motions. Zero-padding would cause the error to decrease.

This is a difference method, so will return a higher error for a 10% difference in waveform magnitude at high a magnitudes as compared to a low magnitudes. Also, a phase difference between low frequency components of the predicted and measured

acceleration time histories will tend to result in a high error even if the waveforms are otherwise identical.

9.2.5 Root-mean-quad error

The fourth root of the sum of the fourth power of the difference between the measured and predicted acceleration time histories at the cushion surface, divided by the duration of the motion as given by:

$$e = \frac{1}{T}\left[\int_{t=0}^{t=T}\left(a_{predicted} - a_{measured}\right)^4 dt\right]^{1/4}$$

Equation 9-5

This technique is identical to the rms error function except for the use of a higher power. This exponent is identical to that used by the VDV to account for the disproportionately greater sensitivity of the human body to increasing vibration magnitude.

9.2.6 Difference in Maximum Transient Vibration Value (MTVV)

The error is given by:

$$e = \max\left[\left(\frac{1}{\tau}\int_{\infty}^{t_0} a_{w\_measured}{}^2(t)\exp\frac{[t-t_0]}{\tau}dt\right)^{1/2}\right] - \max\left[\left(\frac{1}{\tau}\int_{\infty}^{t_0} a_{w\_predicted}{}^2(t)\exp\frac{[t-t_0]}{\tau}dt\right)^{1/2}\right]$$

Equation 9-6

using a recommended integration time of 1 second.

An output of 0 indicates there is no difference in MTVV, implying that the highest amplitude event is of similar size in both the predicted and measured acceleration time histories. A negative result indicates that the predicted MTVV is too high and a positive result indicates that the predicted MTVV is too low.

This value is a possible alternative to the VDV for determining the severity of a vibration. The MTVV assumes that the highest magnitude shock is the dominant part of a vibration affecting the human body. It takes a running average of the acceleration time history and extracts the maximum value. The result is entirely dependent on the highest amplitude event. This method provides information on the relative value of the highest amplitudes, such as might be caused by end-stop impacts, but no information on the remainder of the time history. This method can differentiate between a high and a low prediction, but the VDV can emphasise high amplitudes without discounting the rest of the signal. There seems to be no advantage to using the MTVV over the VDV.

9.2.7 Difference or ratio of the peak of the power spectrum

This quantity is non-specific in that an infinite number of waveforms could produce the same spectral peak. It is particularly unsuitable for the present study as the input motions used in the laboratory tests were effectively sinusoidal so providing little frequency domain information.

The power spectrum on the seat surface is dependant on the input motion. The transfer function between the predicted and measured cushion surface accelerations has the potential to provide a more detailed description of the seat performance with less reliance on the input motion and is widely used for comparing the differences between automotive seating.. However this method cannot be used in the present application due to the substantial non-linear components present in suspension seating which result in poor coherence and hence an unreliable transfer function.

9.2.8 Final choice

It was decided to adopt two complementary measures to assess the performance of the model.

The root-mean-square error (Equation 9-4) was selected as a well-understood and specific method for quantifying the difference between waveforms. A normalising element was introduced to express the error as a ratio of the magnitude of the target motion. This permitted the direct comparison of errors due to motions of any duration, frequency or magnitude and could be applied to the suspension displacement just as easily as to the load acceleration.

$$e = \frac{\left[\int_{t=0}^{t=T} \left(a_{predicted} - a_{measured}\right)^2 dt\right]^{1/2}}{\left[\int_{t=0}^{t=T} a^2_{measured}\, dt\right]^{1/2}}$$

Equation 9-7

The second measure chosen for use in this chapter was the difference in SEAT value. This measure quantifies the performance in terms of the reduction (or increase) in discomfort achieved by the seat and was therefore considered to be the most relevant measure of seat performance. As this measure was non-specific (i.e. different waveforms can have the same SEAT value), it was considered to be more informative to overlay the measured and predicted SEAT values (Equation 9-8) graphically rather than to calculate the error as defined in Equation 9-3. The SEAT value was calculated

using Equation 9-8 such that a value of 1.0 indicated that the vibration at the seat base and at the seat surface resulted in the same discomfort, rather than expressing the SEAT result as a percentage value. This approach was adopted in order to avoid potential confusion in the results and discussion arising from discussing the percentage error between SEAT values which were themselves expressed as percentages.

$$SEAT = \frac{\left[\int_{t=0}^{t=T} a_{w\_seat\_surface}{}^{4}(t)dt\right]^{1/4}}{\left[\int_{t=0}^{t=T} a_{w\_seat\_base}{}^{4}(t)dt\right]^{1/4}}$$

Equation 9-8

9.3 Experimental procedure

The seat parameters were determined as described in Chapter 6 and used the damper characteristics determined in Chapter 9. The input motions measured at the base of the seat for each of the earthmover seat tests with the anthropodynamic dummy described in Chapter 5 were used as the input to the model. The tests therefore involved five frequencies, three waveforms and up to 16 magnitudes with five repeat tests for each condition. The parameters used in the model are shown in Appendix 7.

The seat load accelerations predicted by the model and measured in the laboratory were normalised to remove any DC offset and low pass filtered at 40 Hz using a 6th order zero-phase Butterworth filter. The filtered data were used to calculate the predicted and measured W_b-weighted SEAT value and the r.m.s. error between the measured and predicted seat load motion (Equation 9-7and Equation 9-8).

9.4 Results

The figures on the following pages show the measured and predicted SEAT values and the r.m.s. error values (e_{rms}) for five repeat tests of all magnitudes, frequencies and durations of test motion. Also shown are the predicted and measured seat load acceleration and suspension displacement time histories obtained for the third repeat of each test condition.

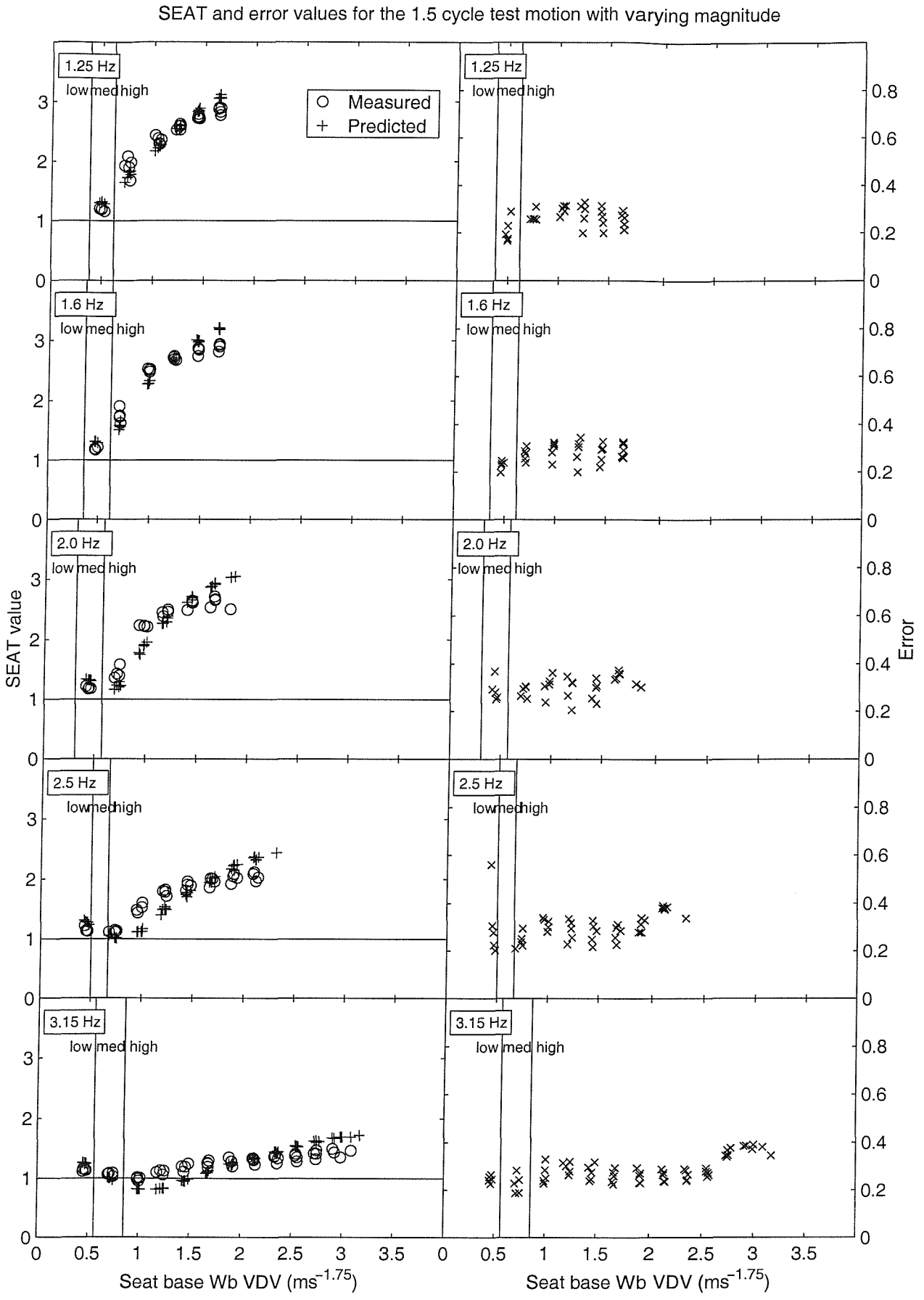

Figure 9-1 The predicted and measured SEAT values and the root-mean-square error between the load acceleration time histories using the **1.5 cycle test motion** for all frequencies and magnitudes and all repeat tests.

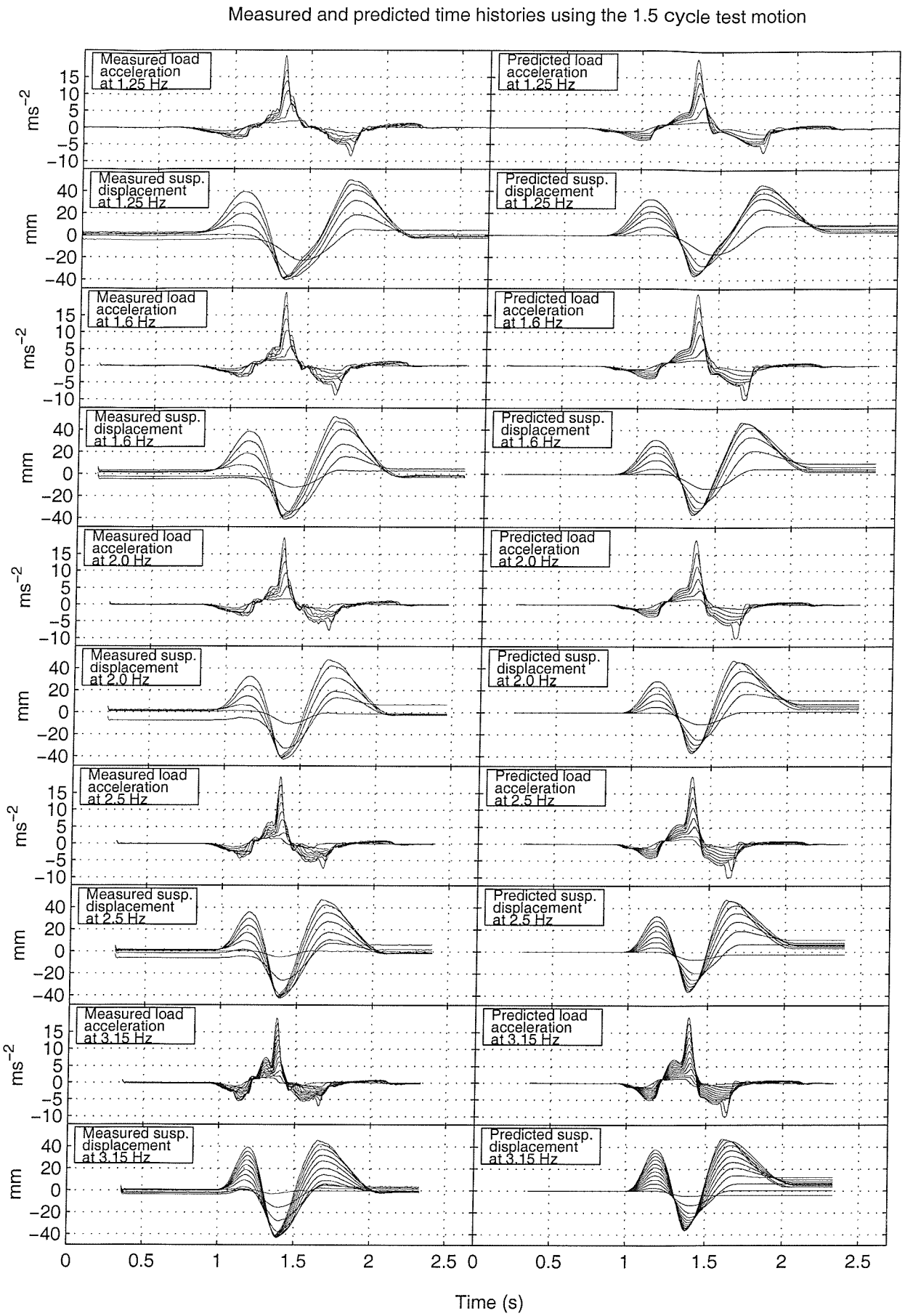

Figure 9-2 The predicted and measured load mass acceleration and relative suspension displacement time histories using the **1.5 cycle test motion** for the third repeat test for all frequencies and magnitudes.

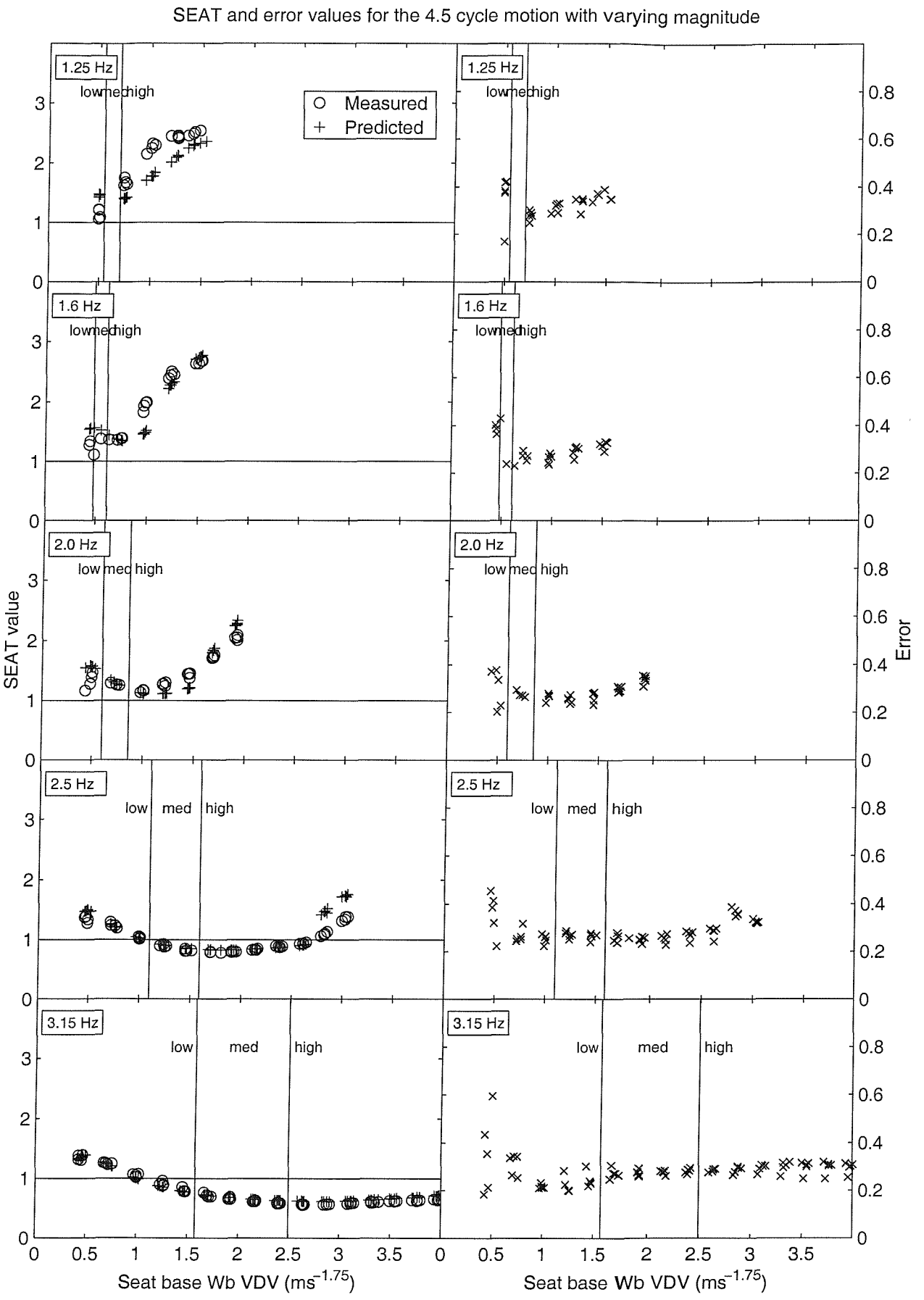

Figure 9-3 The predicted and measured SEAT values and the root-mean-square error between the load acceleration time histories using the **4.5 cycle test motion** for all frequencies and magnitudes and all repeat tests.

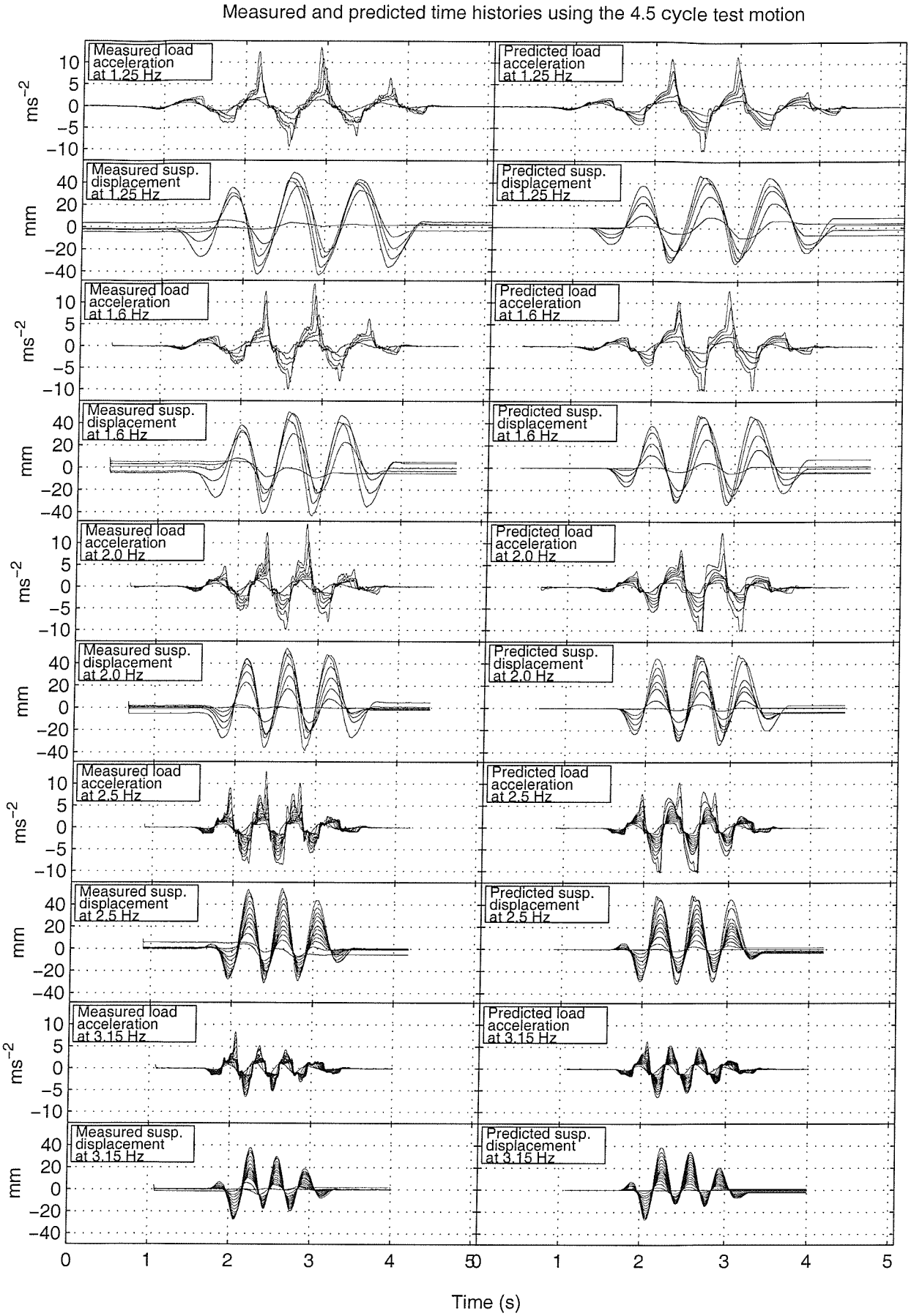

Figure 9-4 The predicted and measured load mass acceleration and relative suspension displacement time histories using the **4.5 cycle test motion** for the third repeat test for all frequencies and magnitudes.

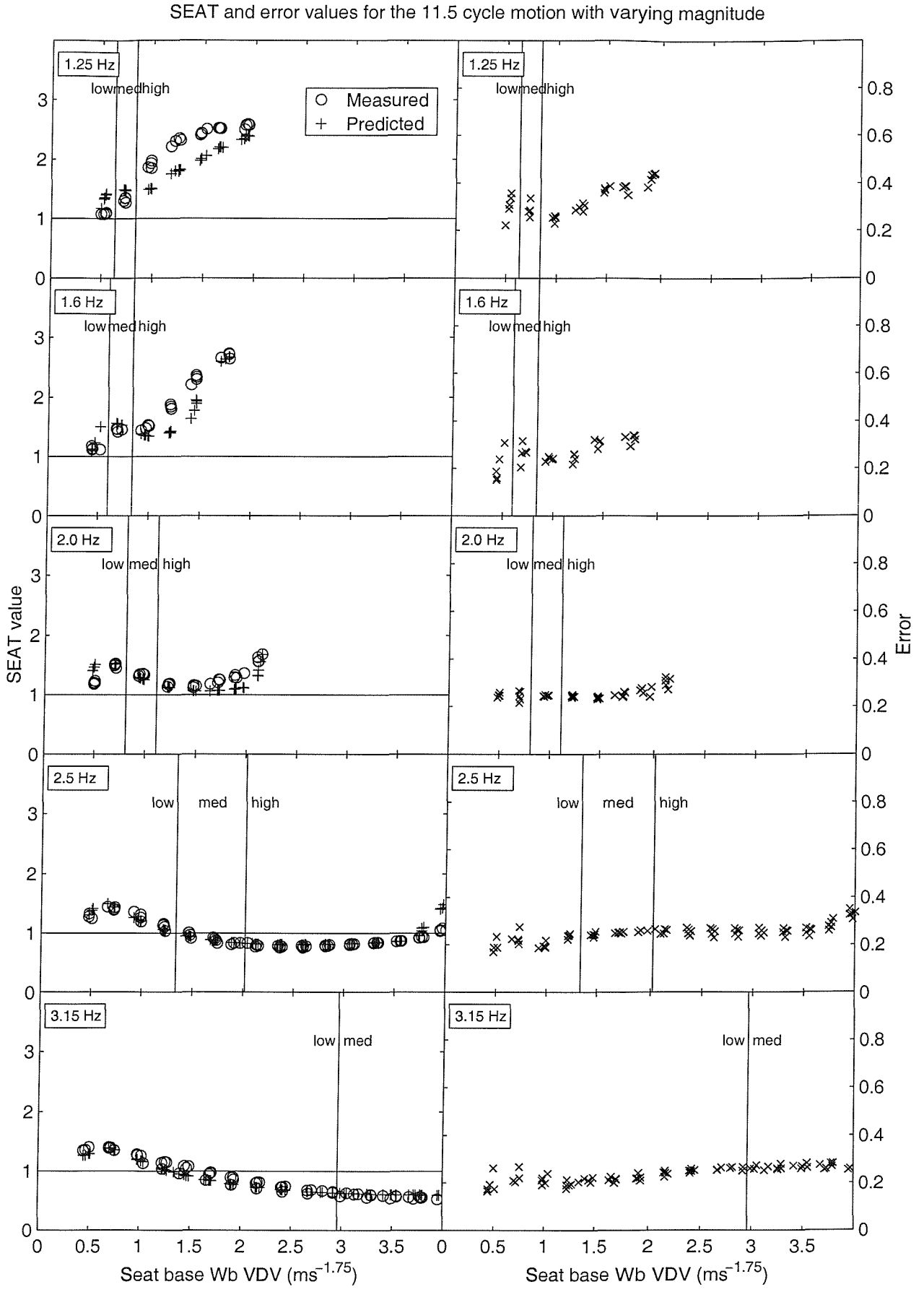

Figure 9-5 The predicted and measured SEAT values and the root-mean-square error between the load acceleration time histories using the **11.5 cycle test motion** for all frequencies and magnitudes and all repeat tests.

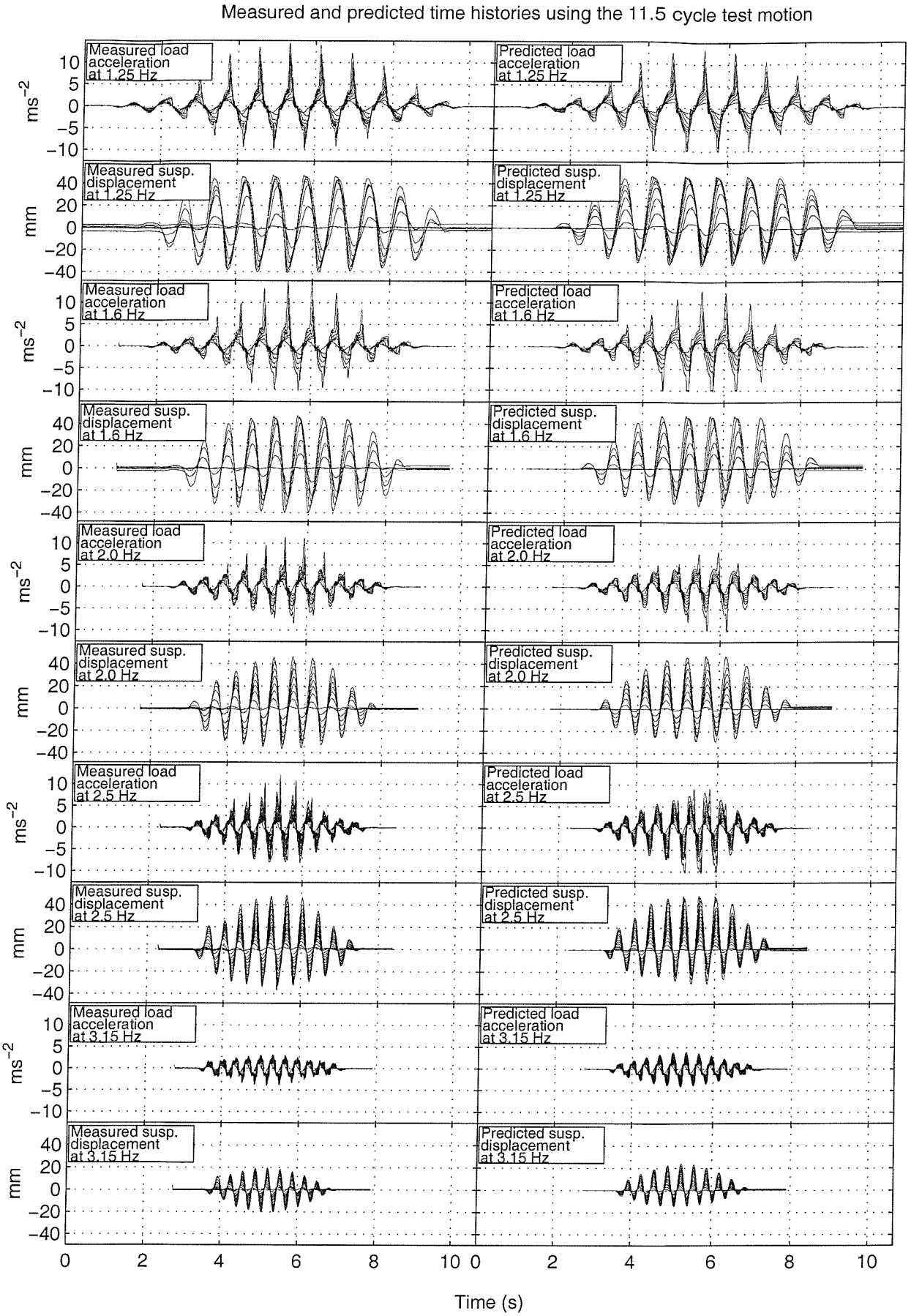

Figure 9-6 The predicted and measured load mass acceleration and relative suspension displacement time histories using the **11.5 cycle test motion** for the third repeat test for all frequencies and magnitudes.

9.5 Discussion

9.5.1 Overall performance

Of the 673 comparisons between the measured and predicted motions, 81% of predictions were found to be within 15% of the measured SEAT value

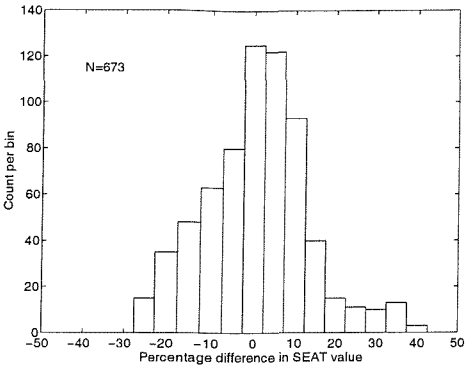

Figure 9-7 The distribution of the between the measured and predicted SEAT value as expressed as a percentage of the measured value

The median difference between the measured and predicted SEAT values was 1.2% of the measured SEAT value with 25th and 75th percentiles of -7.0% and 8.4%. Positive values indicate that the model overestimated the SEAT value and vice-versa. The distribution of differences between the predicted and measured SEAT values is shown in Figure 9-7. The magnitude of the median difference was 7.8% with 25th and 75th percentiles of 3.5% and 13.1%.

The r.m.s. error between the measured and predicted time histories was found to have a median value of 0.27 with an interquartile range of 0.04. The Spearman's correlation coefficient between the r.m.s. error and the difference in SEAT value over all conditions was 0.28 and was significant at $p<0.01$. This relationship is shown in Figure 9-8.

9.5.2 Test conditions that resulted in higher errors

The time histories for all test conditions that returned error values or differences in SEAT value in the upper quartile were visually examined. Some common features were observed and are summarised in the following sections.

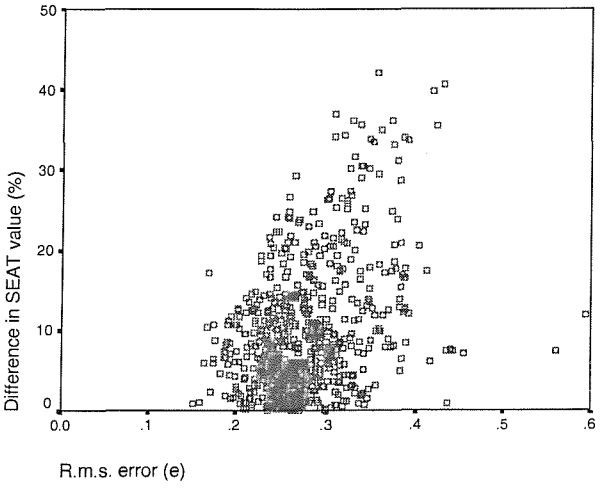

Figure 9-8 The correlation between the r.m.s. error and the difference in SEAT value

9.5.2.1 Low magnitude 4.5 cycle motions

The r.m.s. error (*e*) for the lowest magnitude 4.5 cycle motions

showed substantial variation for the five repeat tests at all frequencies (Figure 9-3). The corresponding SEAT values showed minimal variation for the same test conditions. This effect could also be observed with some other test conditions such as using the 1.5 cycle motion at 2.5 Hz (Figure 9-1). It was found from visual examination of the time histories that although the simulated seat began each motion at the correct ride position for every test, the seat as measured in the laboratory did not. An example of this effect is shown in Figure 9-9. The variation in r.m.s. error was therefore at least partly due to the laboratory test method rather than the model. This problem might be partially alleviated by 'buzzing' the suspension with a comparatively high frequency low magnitude sinusoid (perhaps 5 Hz ±1mm) before each test motion to overcome the suspension friction and allow the suspension to return to the correct position.

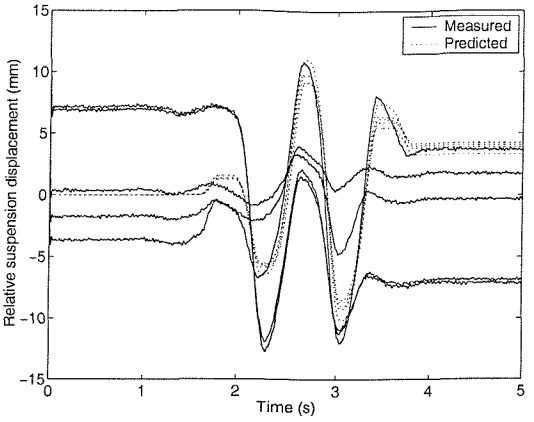

Figure 9-9 Measured and predicted suspension displacements for the five repeat tests at the lowest magnitude of 4.5 cycle 1.25 Hz motion showing the variation in initial suspension position for the seat in the laboratory

9.5.2.2 Low frequency 4.5 and 11.5 cycle motions

The second set of test conditions to be investigated corresponded to conditions with the 4.5 and 11.5 cycle motions that involved end-stop impacts at 1.25 and 1.6 Hz (Figure 9-3 and Figure 9-5). Several of these test conditions showed errors in the upper quartile and the SEAT values were underestimated with a median difference of 12.8% between the measured and predicted SEAT values for these conditions expressed as a percentage of the measured value. The error values and SEAT values were relatively consistent for each test

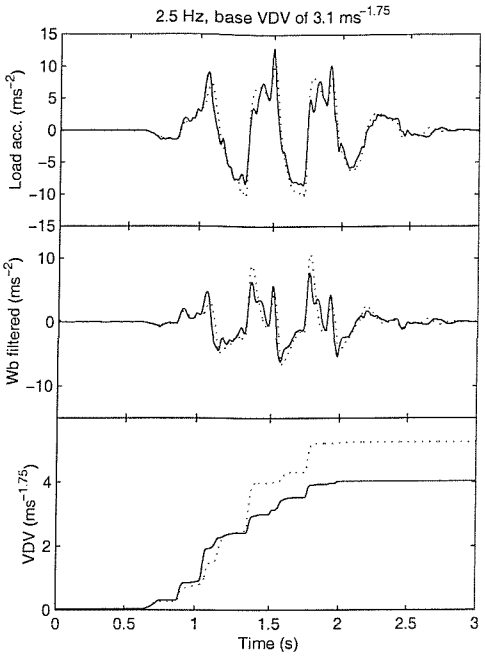

Figure 9-11 The cumulative seat load VDV at the highest magnitude of 4.5 cycle 2.5 Hz motion showing the overestimation of the vibration due to top end-stop impacts

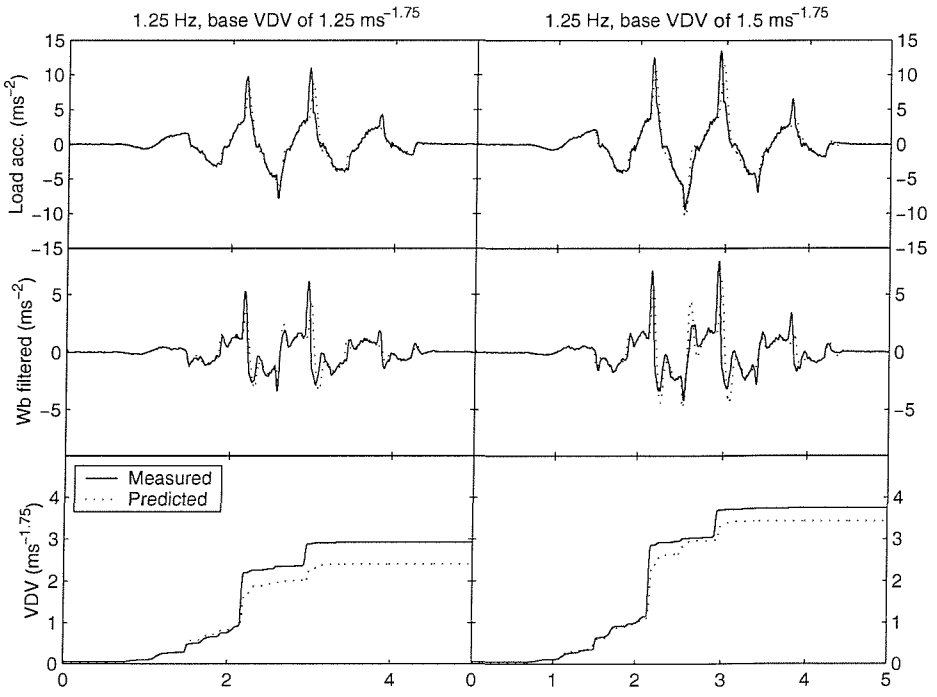

Figure 9-10 The cumulative VDV for two time histories of low frequency 4.5 cycle motion involving end-stop impacts

condition, so the time histories obtained from the third repeat for each test condition were considered representative and examined in more detail.

The measured and predicted load acceleration time histories for two test conditions are shown in Figure 9-10. The effects on the time histories of applying the 'W_b' frequency weighting filter are also shown, along with the cumulative VDV calculated using the frequency-weighted time histories. It can be seen from these results that the model has a tendency to underestimate the severity of the bottom end-stop impacts resulting in a lower predicted VDV. The difference in VDV tended to lessen at the higher magnitude as the model overestimated the severity of the load returning to the seat after the top end-stop impact. The time histories shown are typical of the results obtained with other test conditions of this type.

9.5.2.3 The 4.5 and 11.5 cycle motions at 2.0 and 2.5 Hz

The model overestimated the SEAT value at the highest two magnitudes with the 4.5 and 11.5 cycle motions at 2.0 and 2.5 Hz and an increase in the r.m.s error for these conditions was observed relative to lower magnitudes. Examination of the time histories for these conditions showed that the model was slightly underestimating the severity of the bottom end-stop impact, but was overestimating the vibration due to the top stop impact as shown in Figure 9-11. The measured seat load acceleration showed three positive peaks during each cycle with the third corresponding to the impact with the bottom end-stop. The predicted motion showed this bottom end-stop impact peak but with only one, broader peak preceding it. This difference in motion immediately following the top end-stop impact was responsible for greater increases in predicted VDV as compared with the measured VDV.

It was suspected that the differences in dynamic behaviour might have been due to the non-linear properties of the cushion. In order to investigate this the linear cushion stiffness used in the model was replaced by a simple non-linear stiffness characteristic according to Equation 9-9.

$$F_{kcush} = \frac{\left((0.006 - z_c)^n - 0.006^n\right)}{0.006^n} m_0 g \qquad \text{Equation 9-9}$$

where the stiffness force generated by the cushion (F_{kcush}) was determined from the displacement across the cushion relative to the static equilibrium position (z_c) expressed in metres raised to a power n and multiplied by the static force on the cushion surface m_0g. The compression of the cushion at equilibrium was chosen as 6 mm to give the same linear stiffness as used previously in the model. This model resulted in an increasing stiffness when the cushion was compressed beyond equilibrium and a lessening stiffness as the load on the cushion decreased. The range of cushion characteristics corresponding to values for n from 1 to 3 are shown in Figure 9-12.

The load mass accelerations produced in response to the test condition shown in Figure 9-11 using the cushion stiffness characteristics shown in Figure 9-12 are shown in Figure 9-13. The non-linear cushion stiffness was found to result in the 'three peak' behaviour shown by the seat measured in the laboratory. The magnitudes of the peaks were not identical to the laboratory results, but this was expected using a

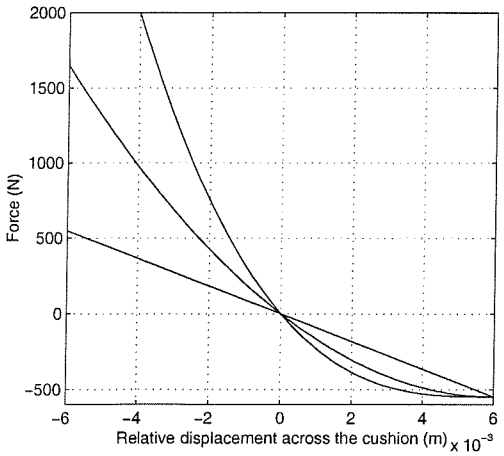

Figure 9-12 The simple non-linear cushion stiffness model with values for n from 1 to 3. Negative relative displacement corresponds to compression of the cushion resulting in an increased upwards force on the load.

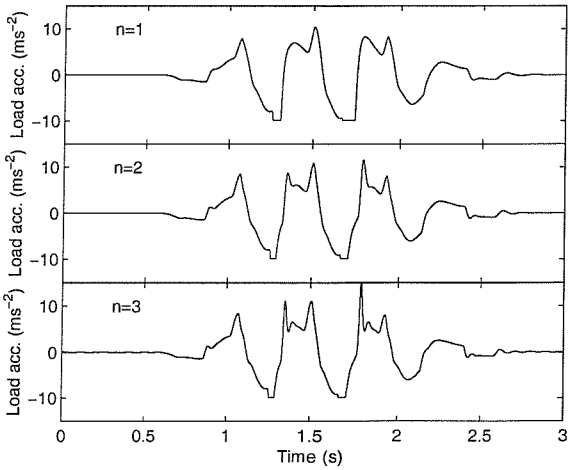

Figure 9-13 The variation in load acceleration using non-linear cushion stiffness exponents (n) of 1, 2 and 3 in response to the 4.5 cycle 2.5 Hz motion with a base VDV of 3.1 $ms^{-1.75}$

simple model with arbitrary coefficient values. The results were sufficient to suggest that improved model performance might be obtained in some situations with a non-linear cushion.

9.6 Conclusions

The predicted SEAT values for all tests were within 15% of the measured SEAT values in 81% of cases with a median r.m.s. error of 0.27. Closer examination of test conditions that resulted in larger errors or differences in SEAT value showed that the model tended to slightly underestimate the severity of bottom end-stop impacts and overestimate the severity of vibration immediately after top stop impacts, but otherwise showed similar dynamic behaviour to the measured system. A simple theoretical investigation suggested that a non-linear cushion stiffness might allow the accuracy of the seat load acceleration predictions to be increased in the vicinity of the top stop impacts. A more advanced non-linear cushion model is investigated in the following chapter.

The difference in SEAT showed a significant, but low, positive correlation with the r.m.s. error. This low correlation, along with examination of the time histories, indicated that a good prediction of the SEAT value does not necessarily correspond to a strong similarity in waveform shape and that similar waveform shapes, especially in situations involving end-stop impacts, may not result in accurate predictions of the SEAT values. The use of the normalised root-mean-square error provides a useful, additional measure to evaluate the performance of seat simulations.

10 The effect of cushion linearity on the model performance

10.1 Introduction

The cushion model was originally implemented using the assumption that the cushion stiffness was so much greater than the suspension stiffness that the cushion displacements would be small enough for equivalent linear coefficients to be used. This approach was similar to that used in previous suspension seat cushion models (e.g. Rakheja *et al*, 1994).

However, it was apparent during the implementation of the cushion model that a mechanism was required to simulate the load lifting off the cushion as observed in the laboratory. This was achieved by limiting the maximum downward force that the cushion could exert on the load mass as described in Chapter 8. The seat model including this force-limited linear cushion was assessed in Chapter 10 and results of a preliminary study described in that chapter suggested that a more complex cushion model might result in improved model performance.

The present chapter describes a cushion model with stiffness and damping coefficients that vary with cushion compression displacement. The intention of this chapter was to quantify any differences in seat-load system performance when using cushion models with and without compression-varying characteristics in comparison with the seat-load performance measured in the laboratory.

10.2 The cushion models

10.2.1 The 'force-limited linear' model

The force limited linear model is the model of the cushion as used in this thesis up to the present point. It consists of a linear spring and damper in parallel with coefficients of 92.1 kNm^{-1} and 1.37 $kNsm^{-1}$ respectively determined from linear measurements of the cushion apparent mass measured at 2 Hz with a

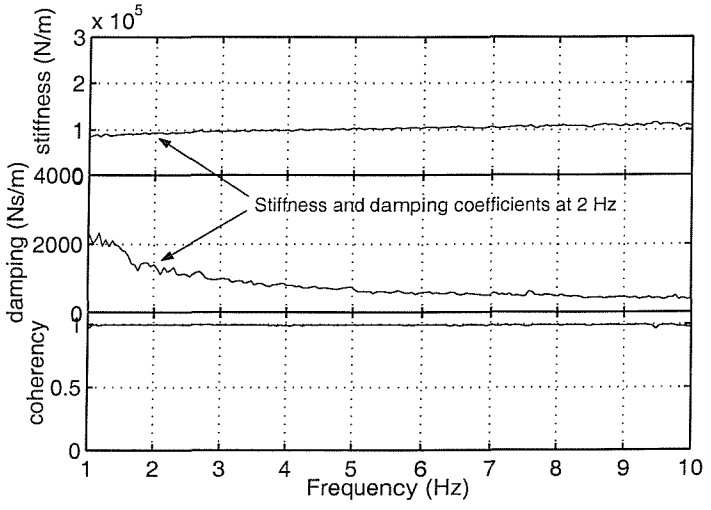

Figure 10-1 Linear cushion stiffness and damping measured from the cushion preloaded with a 500 N force and exposes to a 1 to 10 Hz random motion

500 N preload (Figure 10-1). The maximum downward force that this cushion can exert on the load was limited such that the downward load mass acceleration cannot exceed the acceleration due to gravity. The cushion model was implemented as shown by Equation 10-1 to Equation 10-4.

$$F_{cc} = -c_c.(\dot{x}_0 - \dot{x}_s) \qquad \text{Equation 10-1}$$

$$F_{kc} = -k_c.(x_0 - x_s) \qquad \text{Equation 10-2}$$

$$F_{cush} = F_{kc} + F_{cc} \quad \text{where} \quad (F_{kc} + F_{cc}) > -(g(m_0 + m_1)), \qquad \text{Equation 10-3}$$

otherwise

$$F_{cush} = -(g(m_0 + m_1)) \qquad \text{Equation 10-4}$$

10.2.2 The 'compression-varying' model

10.2.2.1 Overview

The compression-varying cushion model was developed from the measurements of the cushion taken in Chapter 6, including stiffness and damping coefficients that varied with varying cushion compression.

10.2.2.2 The cushion stiffness

The non-linear model stiffness was developed using the following assumptions:

- The cushion was assumed to be loaded with a rigid mass of 56 kg which resulted in a cushion compression of approximately 30 mm, calculated from the quasi-static measurements obtained in Chapter 6 (Figure 10-2). This mass was the same as the total mass of the anthropodynamic dummy used on the seat in the laboratory.
- The maximum cushion compression was assumed to be 60 mm. Precise measurements of the cushion stiffness were complicated by the contouring of the cushion surface, but the value was estimated to be within 3 mm of the actual value at the seat index point (ISO5353, 1999).

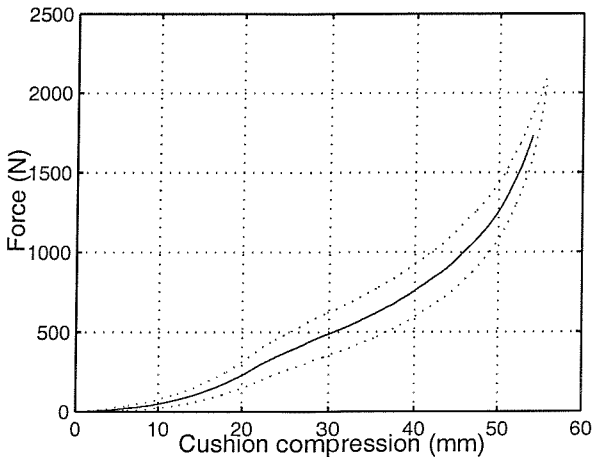

Figure 10-2 Quasi-static force-deflection characteristic of the earthmover seat cushion tested at 1.5 mms^{-1}, showing the measured (dotted) and mean (solid) characteristic

- The maximum permitted downward force between the cushion and the load was equal to the force caused by the acceleration of the load mass due to gravity. The load is not attached to the cushion so the cushion cannot pull the load down.

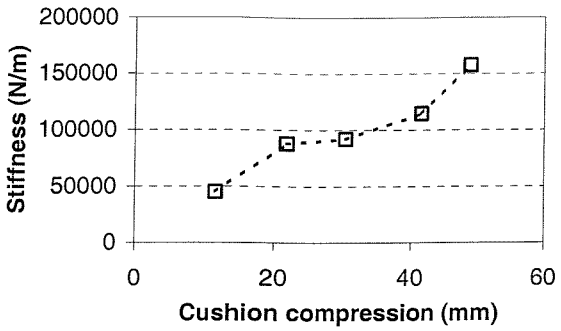

Figure 10-3 The cushion stiffness coefficients measured in the laboratory using dynamic testing methods

- The cushion stiffness coefficient should be as obtained using dynamic rather than quasi-static measurements. The cushion stiffness coefficients calculated in Chapter 6 from the apparent mass of the cushion when exposed to random vibration with a range of preload forces is shown in Figure 10-3.

The cushion stiffness was modelled by curve fitting to the measured cushion stiffness characteristic obtained dynamically. A 5th order polynomial combined with a *tan* function used as shown in Equation 10-5 and Equation 10-7. This form of equation results in an infinite cushion stiffness at maximum compression.

$$k_c(z_c) = \mathrm{Re}\left(K_1 \cdot \tan\left(\frac{\beta - \chi - z_c}{\delta - \chi} \cdot \frac{\pi}{2} \right) \right) + K_2 \cdot (-z_c) + K_3(-z_c)^2 + K_4(-z_c)^3 + K_5(-z_c)^4 + K_6(-z_c)^5 \quad \text{Equation 10-5}$$

for values of z_c where $z_c \le (\beta - \chi)$. Otherwise:

$$k_c(z_c) = 0 \quad \text{Equation 10-6}$$

$$F_k(z_c) = z_c \cdot k_c(z_c) \quad \text{Equation 10-7}$$

where k_c is the cushion stiffness as a function of the displacement z_c about the equilibrium cushion compression displacement magnitude β, expressed relative to the cushion surface, with an initial compression distance χ where the cushion stiffness was approximated to zero. The total cushion thickness was δ . All displacements were in metres and were absolute values with the exception of z_c, where positive displacements indicated movement towards the cushion surface.

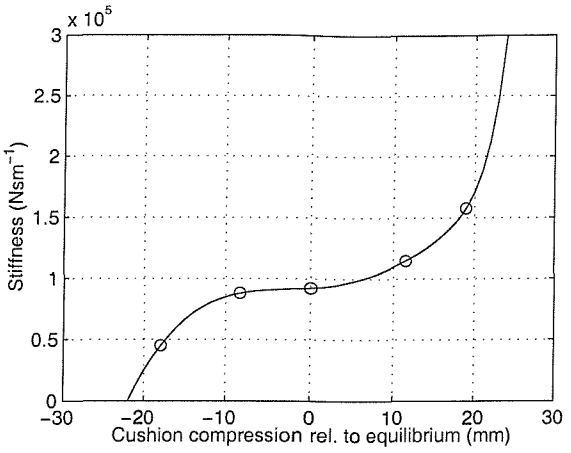

Figure 10-4 The measured cushion stiffness coefficient measured dynamically compared with the non-linear stiffness model where zero displacement is the equilibrium condition with the cushion loaded with a 56 kg load and positive values indicate increased compression

The coefficients were obtained by a least squares fit to the measured cushion dynamic stiffness values and are shown in Table 10-1. The sum of the squared difference between the measured stiffness and the model at the five measurement points was negligible ($<1x10^{-15}$ N^2m^{-2}). The coefficients describe the compression-varying stiffness of a 60 mm deep cushion with negligible forces over the first 8 mm and an equilibrium compression of 50% when loaded with 56 kg. The model is compared with the dynamic stiffness measurements from Chapter 6 in Figure 10-4.

The coefficient χ was introduced to describe the initial part of the cushion compression where the cushion forces were comparatively small. An accurate curve-fit to the available data was obtained by allowing the cushion stiffness to be approximated to zero over this range. Higher order (6^{th} and 7^{th} order) polynomials were able to offer an accurate fit to the data including the origin only at the expense of uneven behaviour between the known data points. As discussed in the

Table 10-1 Cushion stiffness coefficients

Symbol	Characteristic	Value
β	Compression at equilibrium	30 mm
χ	First stage of compression at the cushion surface	8 mm
δ	Maximum compression	60 mm
K_1	Stiffness coefficient	1.18×10^5
K_2		-5.19×10^6
K_3		-5.65×10^7
K_4		2.10×10^9
K_5		-4.43×10^{11}
K_6		-7.85×10^{12}

following paragraphs, this approximation for low-stiffness forces is irrelevant to the model performance.

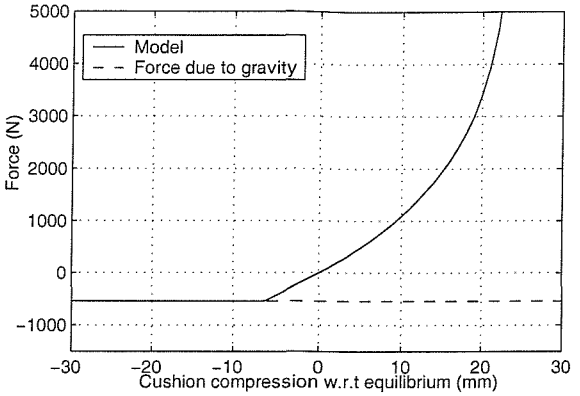

Figure 10-5 The modelled cushion stiffness force including the effect of gravity and normalised to the loaded, equilibrium position

Two difficulties remained in using this cushion model as part of the suspension seat model. Firstly, the model is at an equilibrium situation with the cushion preloaded and the stiffness force tends to zero as the load lifts up off the seat. There is no independent gravitational force present in the seat model so there is no force present to bring the load mass back down again. The second problem is that the measurements in Chapter 6 showed a factor of four difference between the cushion stiffness measured dynamically and quasi-statically with the dynamic measurement being the greater. The measured cushion compression is a product of the load mass and the quasi-static stiffness, not the dynamic stiffness. This results in the cushion producing a downwards force greater than that due to gravity as the load moves. This is unrealistic as it describes the cushion pulling the load back down onto the seat.

In situations where the cushion stiffness exceeded the force on the load due to gravity the cushion force was set to equal the gravitational force. The cushion was assumed to remain in contact with the load as the load moves upward without exerting any additional stiffness force until the cushion became completely uncompressed. A critical displacement could be calculated from the cushion stiffness model at which the cushion stiffness force equalled the gravitational force on the load. The model was adjusted such that the force remained constant at the gravitational force for all values of the relative displacement access the cushion greater than this critical value as shown Equation 10-8 and Equation 10-9.

$z_{contact}$ is the value of z_c such that $m_0 \cdot g = k_c(z_c) \cdot z_c$ Equation 10-8

where m_0 is the load mass, g is the acceleration due to gravity and the other terms are described above.

$$F_{kc} = k_c(z_c) \cdot z_c$$ Equation 10-9

for values of z_c less than $z_{contact}$. Otherwise:

$$F_{kc} = k_c(z_{contact}) \cdot z_{contact}$$ Equation 10-10

where F_{kc} is the force due to the cushion stiffness and also generates the force due to gravity with the load out of contact with the cushion.

A value for the critical displacement $z_{contact}$ of 6.1 mm was obtained. The cushion model including limitation of the stiffness characteristics for displacements greater than this critical value resulted in the force-displacement characteristic shown in Figure 10-5. This was the force-deflection characteristic used to simulate the cushion stiffness in the compression-varying cushion model.

10.2.2.3 The cushion damping

It is not necessary for the cushion damping expression to tend to infinity at the maximum cushion compression, as the damping model will be used in parallel with the cushion stiffness model, which already displays this characteristic. The variation in cushion damping with cushion compression was described in terms of a 4th order polynomial fit to the cushion damping characteristics measured dynamically in Chapter 6 using Figure 10-12 to Figure 10-14.

$$c_v(z_c) = d_1(\beta - z_c)^4 + d_2(\beta - z_c)^3 + d_3(\beta - z_c)^2 + d_4(\beta - z_c) + d_5$$ Equation 10-11

for values of z_c less than β, otherwise

$$c_v(z_c) = 0$$ Equation 10-12

where d_n are the curve fit coefficients and c_v is the velocity-proportional damping coefficient varying with cushion compression z_c. The cushion damping force is therefore:

$$F_{cv}(z_c, \dot{z}_c) = -\dot{z}_c \cdot c_v(z_c)$$ Equation 10-13

The curve fit coefficients d_n are shown in Table 10-2 and this model is compared with the measured coefficient values in Figure 10-6.

10.2.3 Summary of the compression-varying model

The complete compression-varying cushion model was described by Equation 10-14 and assumes that the cushion will expand up to its uncompressed state as the load lifts off and then compress as the load

Table 10-2 Cushion velocity proportional damping polynomial curve fit coefficients to least-squares optimisation results

Symbol	Value
d_1	2.66×10^9
d_2	-2.39×10^8
d_3	6.10×10^6
d_4	1.83×10^3
d_5	-1.90

returns. The cushion forces can act as long as the load is in contact with the cushion surface as long as the total downward force generated by the cushion does not exceed that due to gravity acting on the load mass.

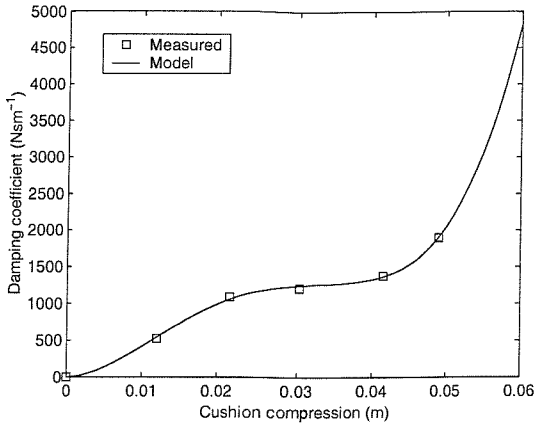

Figure 10-6 The cushion damping coefficient least squares fit to the measured damping coefficients determined from dynamic tests of the cushion with a 1 to 10 Hz random motion and preloads from 100 to 900 N.

$$F_c(z_c, \dot{z}_c) = F_{kc}(z_c) + F_{cv}(z_c, \dot{z}_c)$$

Equation 10-14

The damping was modelled as resulting in a force proportional to the velocity across the cushion multiplied by a coefficient which increased with increasing cushion compression. The damping coefficient at the equilibrium compression position with a 56 kg load was as used in the force-limited linear model.

The model stiffness characteristic was limited to prevent the cushion preventing the load lifting off and increased so as to cause an infinite force when the cushion was completely compressed. The stiffness coefficient at the equilibrium compression position with a 56 kg load was as used in the force-limited linear model.

Results obtained with this model are compared to the measured results for a randomly selected 5-second sample of 4 mm peak-to-peak random motion in Figure 10-7.

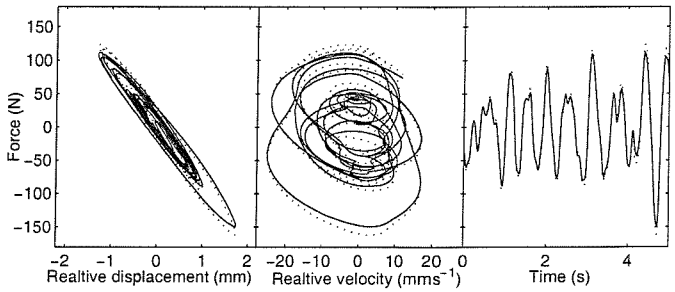

Figure 10-7 The force transmitted through the cushion as measured in the laboratory (solid lines) and as simulated by the compression-varying model (dotted lines) for a randomly selected 5 second sample of 1 to 10 Hz band-limited random motion.

10.3 Comparing simulation results using both cushion models with measured results

10.3.1 Method

The methodology used to quantify the seat model performance was the same as used in Chapter 10. The suspensions seat model was configured to use a rigid mass on the seat surface for comparison with the laboratory measurements of the seat-load performance obtained as described in Chapter 5. Simulations were conducted using all magnitudes and frequencies of the 1.5, 4.5 and 11.5 cycle windowed sinusoidal test motions as used in the laboratory tests. The predictions of the load mass motion from of each of the two seat models were compared in the time domain with laboratory measurements using the anthropodynamic dummy as the seat load in terms of the SEAT value and the r.m.s. error as shown in Equation 10-15 and Equation 10-16 respectively. Results were obtained for each frequency, magnitude and duration of test motion.

$$SEAT = \frac{\left[\int_{t=0}^{t=T} a_{w\_seat\_surface}{}^{4}(t)dt\right]^{1/4}}{\left[\int_{t=0}^{t=T} a_{w\_seat\_base}{}^{4}(t)dt\right]^{1/4}} \qquad \text{Equation 10-15}$$

which describes the vibration dose value (VDV) of the W_b-weighted vertical acceleration on the load mass ($a_{w\_seat\_surface}$), divided by the VDV of the W_b-weighted vertical acceleration at the base of the seat ($a_{w\_seat\_base}$). SEAT values were calculated for the laboratory measurements and for the seat model simulation results using both cushion models.

$$e = \frac{\left[\int_{t=0}^{t=T} \left(a_{predicted} - a_{measured}\right)^2 dt\right]^{1/2}}{\left[\int_{t=0}^{t=T} a^2_{measured}\, dt\right]^{1/2}} \qquad \text{Equation 10-16}$$

which describes the root-mean-square difference between the acceleration of the load as predicted by the model ($a_{predicted}$) and as measured in the laboratory ($a_{measured}$), normalised by the r.m.s. acceleration recorded in the laboratory.

10.3.2 Results and Discussion

The SEAT values and the r.m.s. errors obtained for each test condition with each model are shown in Appendix 8. Figure 10-8 shows a sample of these results for the 4.5-cycle test motion.

It was observed that, for test conditions without end-stop impacts, the inclusion of the non-linear cushion model had negligible effect on the seat performance in terms of the SEAT value and in terms of the r.m.s. error between the measured and predicted load mass acceleration as can be seen in Figure 10-9.

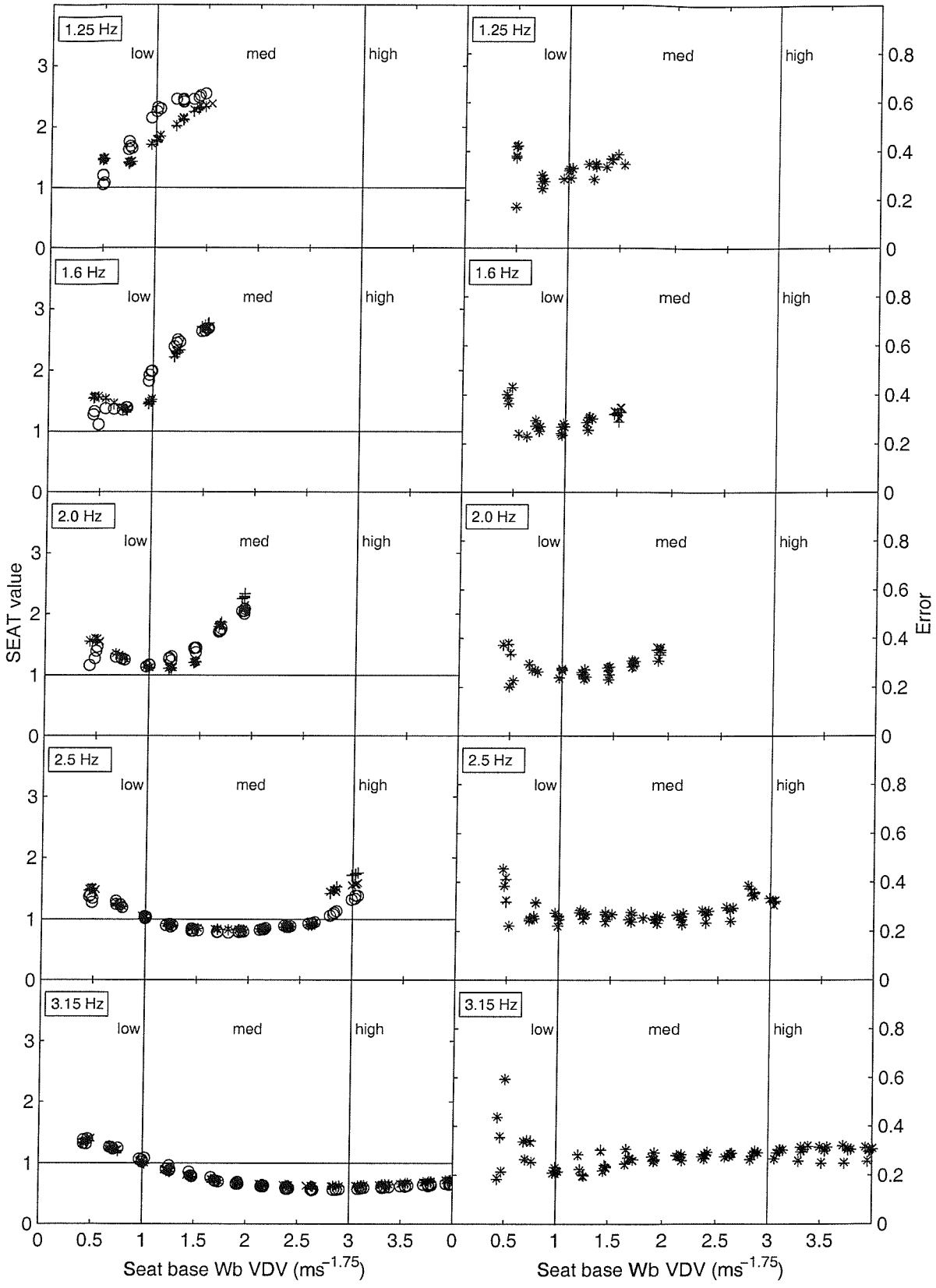

Figure 10-8 The left-hand column shows the SEAT values obtained using the 4.5 cycle input motion in the laboratory (o) and using the seat model with the force-limited linear (+) and compression-varying (x) cushions. The right-hand column shows the r.m.s. error between the measured load acceleration and the seat model with the force-limited linear (+) and compression-varying (x) cushions.

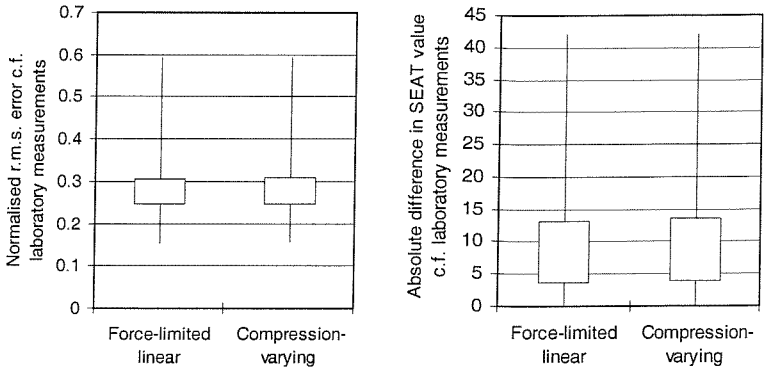

Figure 10-9 The interquartile, maximum and minimum r.m.s. error and difference in SEAT value compared to laboratory measurements for all test conditions using the force-limited linear and non-linear cushion models

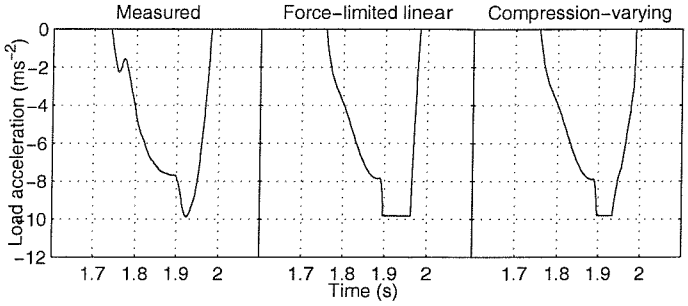

Figure 10-10 The downward load acceleration in the vicinity of a top-stop impact as measured in the laboratory and simulated using the force-limited linear and non-linear cushions

The waveform shape as the load returned to the seat after a top-stop impact varied with different cushion models. This was due to the non-linear cushion including a specific displacement at which the damping force was permitted to act as the load returned to the seat. The force-limited linear model did not specify the displacement at which the damping force could act and was restricted only by the requirement that the total downward cushion force must not exceed the gravitational force on the load. The variation in waveform shape around the top-stop impact for both cushion models compared with laboratory measurements for a 2 Hz 4.5 cycle motion is shown in Figure 10-10. The load acceleration waveform appears closer in shape to the measured result than the force-limited linear cushion result.

The non-linear model applied a damping force over a greater displacement range in this test condition as can be seen from the forces generated by the simulated cushions shown in Figure 10-11. The forces acting close to the bottom end-stop impact resulted in peak negative cushion displacements approximately 8 mm from the equilibrium position for both models. The cushion force and the resulting load acceleration for cushion compressions at or below the equilibrium position was similar for both models.

At higher magnitudes where the load was out of contact with the cushion for 200 ms or longer, the force-limited linear and non-linear cushion models showed almost identical acceleration waveforms near the top stop impact (the 'clipped' downward accelerations in Figure 10-12), but the force-limited linear cushion force was observed to act over a greater displacement range then the non-linear model in this situation (Figure 10-13). The non-linear cushion can be observed to produce greater forces for cushion compression situations (negative displacements in Figure 10-13). These resulted in greater peak upward load accelerations than the force-limited linear model as can be seen in Figure 10-12. The SEAT values obtained with the two cushion models for 2 Hz 4.5 cycle motions with VDVs of up to 5 $ms^{-1.75}$ are shown in Figure 10-14. It can be seen that the two cushion models result in similar SEAT values at low and moderate magnitudes, but the non-linear model predicts

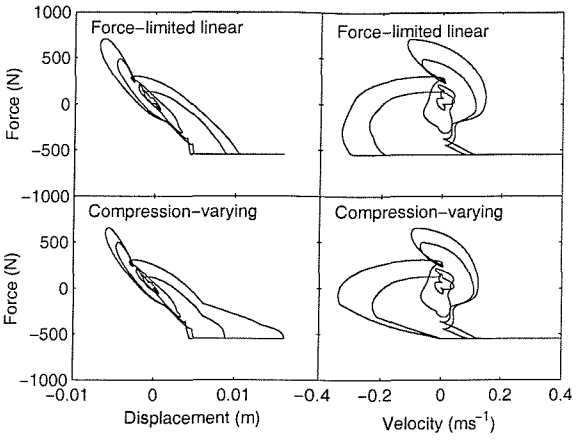

Figure 10-11 The forces generated by the cushion models for a 2 Hz 4.5 cycle input motion with a VDV of 2 $ms^{-1.75}$ in terms of the displacement across the cushion relative to the equilibrium position and the relative velocity across the cushion.

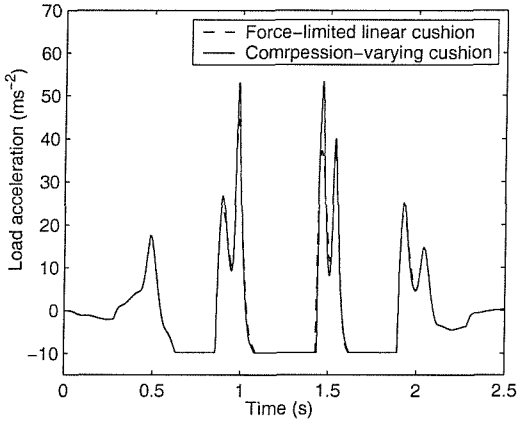

Figure 10-12 The simulated load acceleration resulting from a 2 Hz 4.5 cycle input motion with a VDV of 4 ms^{-2} using the force-limited linear and non-linear cushion models

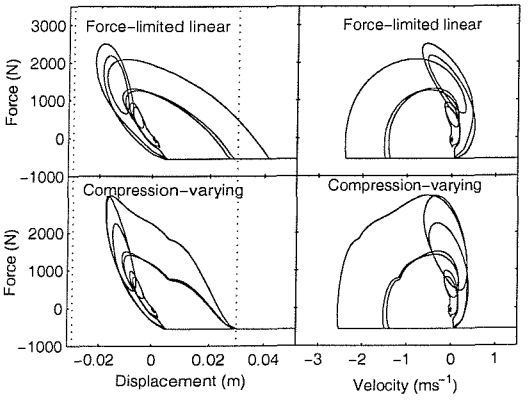

Figure 10-13 The forces generated by the cushion models for a 2 Hz 4.5 cycle input motion with a VDV 4 $ms^{-1.75}$ in terms of the displacement across the cushion relative to the equilibrium position and the relative velocity across the cushion. The measured extent of the cushion is shown by dotted lines.

greater SEAT values at high magnitudes. The differences in SEAT values between the two cushion models became more pronounced at magnitudes where seat load VDVs were in excess of 10 $ms^{-1.75}$ for a single test motion. A vehicle operator might be expected to avoid exposure to such violent motions where possible by adjustment of the vehicle speed or avoidance of obstacles. In applications where this form of control may be undesirable, for instance in military or emergency services vehicles where high speeds are necessary, alternative methods to protect the operator appear to be essential.

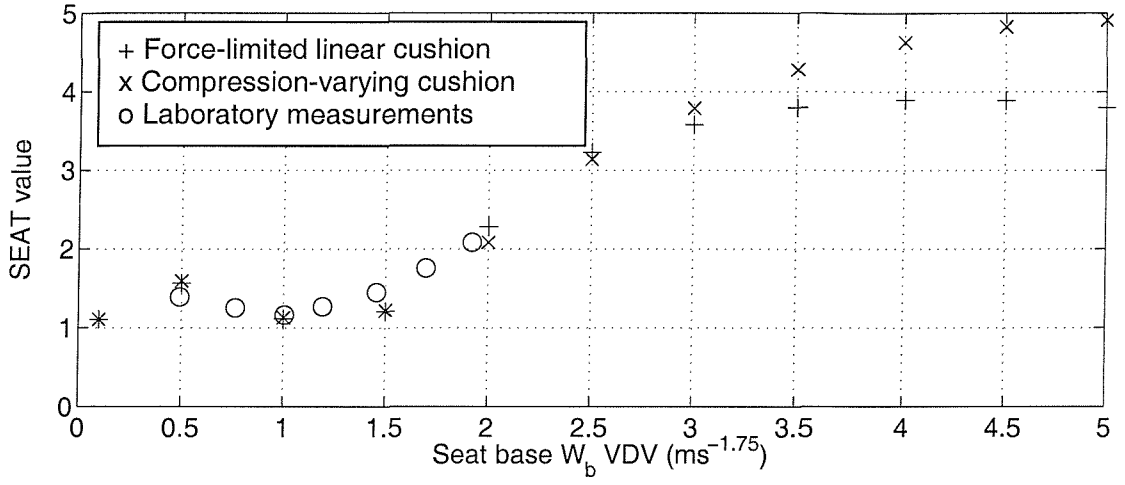

Figure 10-14 The SEAT values predicted by the suspension seat model for different magnitudes of 2 Hz 4.5 cycle test motion. Also shown are the results obtained from the laboratory seat tests which were conducted over a more limited range of magnitudes.

10.4 Conclusions

The inclusion of compression-varying cushion coefficient was found to have minimal influence on the suspension seat dynamic performance for all frequencies and magnitudes of motion up to the occurrence of end-stop impacts. The models showed minimal differences for magnitudes of end-stop impact investigated in the laboratory, but further increases in input magnitude resulted in greater SEAT values using the non-linear cushion model.

This study indicated that a linear cushion with a limiting force to prevent the load experiencing a downwards acceleration greater than gravity may be sufficient to model the performance of a suspension seat cushion in most situations with and without end-stop impacts in response to narrow-band low-frequency motions of the form used in this thesis.

11 Parametric sensitivity analysis

11.1 Introduction

Previous studies have conducted parameter sensitivity analyses using fixed magnitude input motions, fixed displacement amplitude frequency sweeps or standardised motions reproduced at two or three magnitudes as discussed in Section 2.7 of Chapter 2. However, in order obtain a better general understanding of the seat dynamic behaviour as opposed to the seat response to a particular vehicle motion, the seat performance should be investigated over a systematic range of frequencies and magnitudes.

The work described in this chapter was undertaken to quantify how proportional changes in the values of the seat component coefficients affected the predicted performance of a suspension seat over a range of frequencies, magnitudes and durations of motion. The results are then examined to suggest how the earthmover seat might be modified to improve performance.

11.2 Method

The model of the earthmover seat had the mathematical structure as defined in Chapter 8 with the suspension damper characteristics as determined in Chapter 9 and the non-linear cushion as described in Chapter 11. An exception to this arrangement was the investigation of the influence of the cushion stiffness and damping. These two parameters

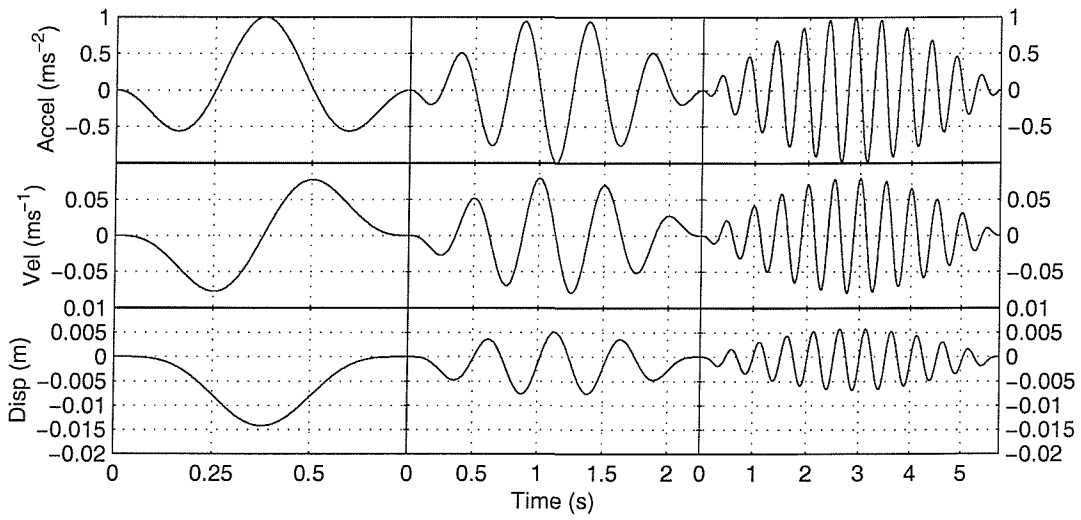

Figure 11-1 The time histories of the 1.5, 4.5 and 11.5 cycle duration input motions shown in terms of acceleration, velocity and displacement with an arbitrary 1 ms^{-2} peak acceleration at 2 Hz.

Table 11-1 The seat components investigated showing the form of cushion model used in each case.

Seat component	Dynamic characteristic varied	Cushion model
Cushion stiffness	Linear stiffness	Force-limited linear
Cushion damping	Linear damping	Force-limited linear
Suspended mass	Mass	Non-linear
Suspension stiffness	Linear stiffness	Non-linear
Suspension friction	Force opposing the suspended mass motion with a lock-up mode.	Non-linear
Suspension friction symmetry	Proportion of the friction force acting in compression as opposed to extension.	Non-linear
Suspension damping	Non-frictional damping force generated by the suspension mechanism	Non-linear
Suspension damping symmetry	Proportion of the damping force acting in compression as opposed to extension.	Non-linear
Free travel	The displacement between the end-stop buffers	Non-linear
Mean ride offset position	The equilibrium position of the suspension relative to the mid-point between the end-stop buffers.	Non-linear
End-stop buffer stiffness	The stiffness force generated by the top and bottom end-stop buffers.	Non-linear

were investigated using the force-limited linear cushion to avoid making assumptions regarding the relationship between the static and dynamic and dynamic cushion stiffness. The remaining component characteristics for all tests were as measured in Chapter 6 and the model parameters are summarised in Appendix 7.

The simulated earthmover seat was set to a mean ride position at the centre of the free travel between the end-stop buffers rather that the centre of the total available travel used in previous chapters. This adjustment was made in order to allow the effect of the suspension offset and total travel to be investigated over a wide range of values without requiring the seat suspension to begin the motion in contact with the lower bump stop.

All three motions defined in Chapter 4 were used in order to provide a shock-like 1.5 cycle motion, a quasi-steady state 11.5 cycle motion and an intermediate 4.5 cycle condition (Figure 11-1). The waveforms were generated at five frequencies from 1.25 Hz to 3.15 Hz. The range of amplitudes was extended beyond that investigated in Chapter 10 with the knowledge that the results from these regions should be treated with caution. Base motions with W_b-weighted VDVs varying from 0.1 $ms^{-1.75}$ to 5 $ms^{-1.75}$ in fifteen steps

were used at all frequencies. Longer motions therefore had lower peak accelerations than shorter motions at the same VDV.

Table 11-2 A method of characterising suspension seat behaviour with changing input magnitude, summarised from Wu and Griffin (1996)

Stage 1	Low magnitudes with the seat suspension friction locked
Stage 2	'Breaking away' from friction
Stage 3	Moving relatively freely but not contacting the end-stop buffers
Stage 4	Mild to moderate end-stop impacts
Stage 5	Severe end-stop impacts

The seat component parameters were grouped as shown in Table 11-1 and varied over an eight to one range unless it was not meaningful to do so, as in the case of the suspension offset from the mid ride position. The model was evaluated with 19 coefficient values for each test condition. A total of 4560 simulations were performed, corresponding to tests for 3 waveforms, 5 frequencies, 16 magnitudes and 19 coefficient values. Each test produced time histories of the accelerations of each mass and the relative velocity and displacement between each mass.

The seat base and load mass acceleration time histories obtained from each simulation were used to calculate the SEAT values using the W_b frequency weighting. The effect of each parameter on the SEAT value was considered taking into account the frequency and duration of the test motion and the seat behaviour stage as shown in Table 11-2.

11.3 Results

11.3.1 Overview of results

The effect of each parameter on the seat performance for all test conditions is shown in Appendix 9 and the effect of each component is summarised in the following sections. Unless otherwise stated, the discussion of the seat performance in the following sections refers to test conditions with frequencies of 2.0 Hz and greater where the seat was capable of some useful vibration isolation performance. The effect of the seat parameters on the seat performance in response to vibration at frequencies closer to the main seat-load resonance frequency can be seen from examination of the results for tests at 1.25 and 1.6 Hz as shown in Appendix 9 but are of less practical relevance as the seat used in this study would be unsuitable for use in a vehicle with substantial vibrations at these frequencies.

The highest input magnitudes used in this study were greater than those investigated when quantifying the model performance in Chapter 10 as there were no ethical or safety

constraints limiting the amount of vibration experienced by the load. The results from the most severe test conditions must therefore be examined with some caution.

Unless otherwise stated, any effects on the seat performance for an increase in parameter value showed the opposite result with similar magnitude for a decrease in parameter value.

11.3.2 The effect of the cushion

The cushion stiffness and damping were investigated using the force-limited linear cushion as used in Chapters 8 to 11. The cushion stiffness and damping parameters were varied over a range of plus and minus a factor of eight either side of the values obtained in Chapter 6. This range of values is believed to be greater than can currently be achieved in practice.

11.3.2.1 Cushion stiffness

The effect of the linearised cushion stiffness on the seat performance in shown in Appendix 9 Figures 1 to 3 and summarised in Table 11-3.

Table 11-3 The effect of changing the linearised cushion stiffness:	
On the seat performance during stage 1 seat motions	The seat performance improved with increased cushion stiffness at all frequencies for all durations of motion. Higher frequencies showed greater improvements, with a doubling of cushion stiffness producing a 5% improvement at 2 Hz and a 15% improvement at 3.15 Hz with the 4.5 cycle motion. This is illustrated in Figure 11-2 and Figure 11-3. This might be explained using linear theory. The resonance frequency of the mode of vibration involving the rigid load vibrating on the cushion was determined using linear modal analysis as being at approximately 11 Hz. This placed this cushion resonance above the input frequencies used in the present study. An increase in cushion stiffness would be expected to move this resonance to a higher frequency so increases in cushion stiffness would be expected to result in a seat transmissibility (with the suspension friction locked)

	asymptotically decreasing towards unity. Decreasing the cushion stiffness would result in poorer performance as the cushion-load resonance moved to lower frequencies closer to the input frequency range.
On the friction breakaway magnitude	Negligible effect.
On the seat performance during stage 3 seat motions	A stiffer cushion resulted in poorer performance, but a factor of two change in cushion stiffness showed a change in seat performance of less than 4% for all frequencies and magnitudes. This effect can be seen in Figure 11-3.
On the magnitude of onset of end-stop impacts	Negligible effect.
On the seat performance during stage 4/5 seat motion	Increasing the cushion stiffness resulted in poorer seat performance for all frequencies and waveforms. Examples of this can be seen in Figure 11-2 and Figure 11-3.

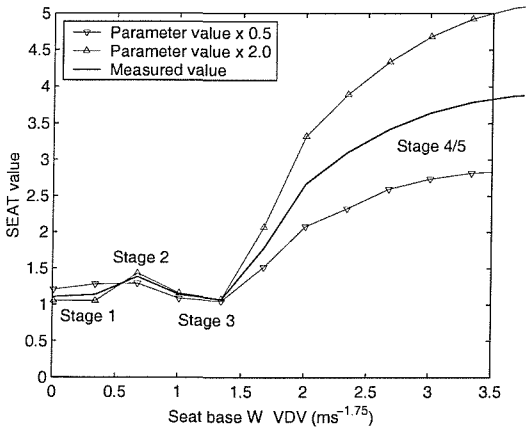

Figure 11-2 The effect on the seat performance of plus and minus a factor of two change in linearised cushion stiffness using the 4.5 cycle 2.5 Hz motion

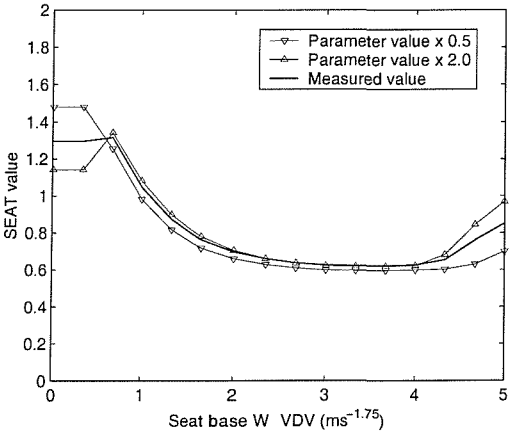

Figure 11-3 The effect on the seat performance of plus and minus a factor of two change in linearised cushion stiffness using the 4.5 cycle 3.15 Hz motion

11.3.2.2 Cushion damping

The effect of a plus and minus a factor of eight in the linearised cushion damping on the seat performance in shown in Appendix 9 Figures 4 to 6 and summarised in Table 11-4.

Table 11-4 The effect of changing the linearised cushion damping:	
On the seat performance during stage 1 seat motions	Increased damping resulted in better seat performance for most frequencies and waveforms. This effect was more pronounced for the short duration motion compared to the long motion and was more pronounced at higher frequencies. Doubling the cushion damping coefficient showed a decrease in SEAT value of 7% and 15% for the long and short duration motions respectively at 3.15 Hz. An example at this frequency using the 4.5 cycle motion is shown in Figure 11-4.
On the friction breakaway magnitude	Negligible effect.
On the seat performance during stage 3 seat motions	Increased damping resulted in better seat performance. This effect decreased with increasing magnitude as can be seen in Figure 11-4. Similar results were observed with all frequencies and durations of input motion with a doubling of the in damping coefficient resulting in an improvement of approximately 10%, decreasing to less than 2% with increasing input vibration magnitude if end-stop impacts did not occur first.
On the magnitude of onset of end-stop impacts	Negligible effect.
On the seat performance during stage 4/5 seat motion	The results suggested that there was an optimal cushion damping resulting in a minimum SEAT value for a given input motion. The shortest motion showed this minimum to be at approximately the measured damping value, while the increased durations showed this minimum to be substantially higher (greater than eight times the

	measured value). A doubling of the cushion damping coefficient resulted in an improvement in seat performance with the 4.5 and 11.5 cycle motions of up to 28% by approaching this minimum. The short duration motion showed either a negligible improvement (<2%) or a worsening in performance of up to 8% for either an increase or decrease in cushion damping. These results are illustrated in Figure 11-6 and Figure 11-7 using the 1.5 and 4.5 cycle input motions at 2.0 Hz.

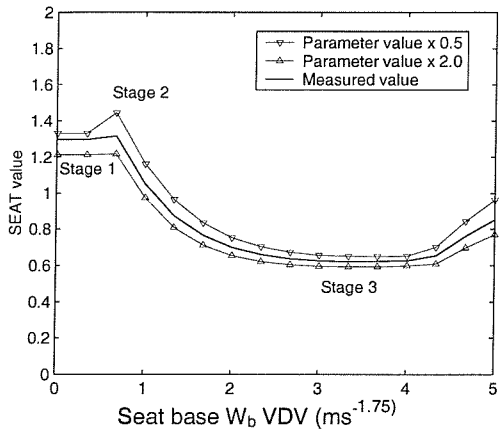

Figure 11-4 The effect on the seat performance of plus and minus a factor of two change in linearised cushion damping using the 4.5 cycle 3.15 Hz motion

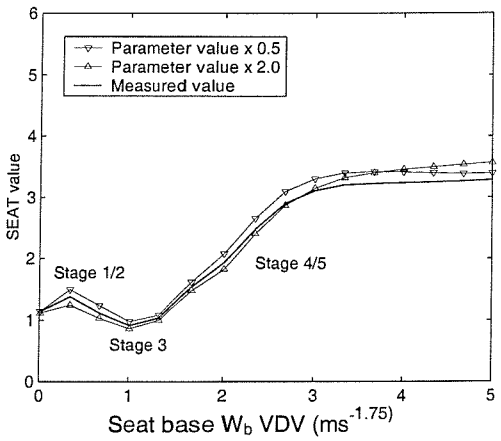

Figure 11-5 The effect on the seat performance of plus and minus a factor of two change in linearised cushion damping using the 1.5 cycle 2.0 Hz motion

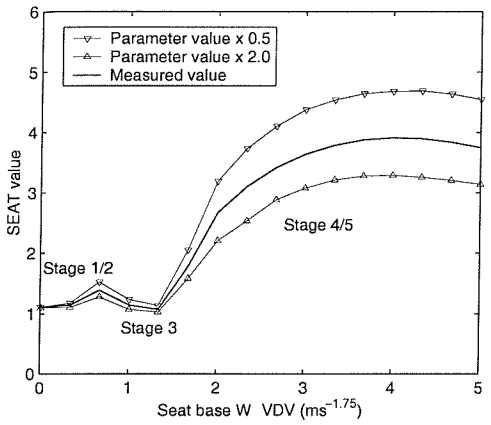

Figure 11-6 The effect on the seat performance of plus and minus a factor of two change in linearised cushion damping using the 4.5 cycle 2.0 Hz motion

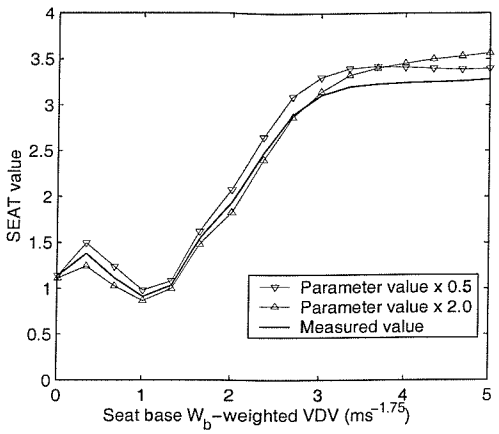

Figure 11-7 The effect on the seat performance of plus and minus a factor of two change in linearised cushion damping using the 1.5 cycle 2.0 Hz motion

11.3.3 The effect of the suspended seat mass

The suspended seat mass was varied over a range of plus and minus a factor of eight relative to the measured value. The seat load mass remained unchanged at 56 kg. The results are shown in Appendix 9 Figures 7 to 9 and summarised in Table 11-5.

Table 11-5 The effect of changing the suspended seat mass:	
On the seat performance during stage 1/2 seat motions	Greater seat masses caused the seat to break away from friction at lower magnitudes, as described below. Because of this effect it was difficult to evaluate the effect on the seat performance in the Stage 1/2 region.
On the friction breakaway magnitude	The friction breakaway magnitude decreased with increasing seat mass. The quantizing effect caused by the limited number of magnitudes at which the model was evaluated confounded accurate quantifications of this effect, but examination of Figures 7 to 9 in Appendix 9 suggest that a doubling of the seat mass from the measured value resulted in a decrease in breakaway magnitude of

	between 30 and 50%.
On the seat performance during stage 3 seat motions	The seat performance improved with increased suspended seat mass at all magnitudes, frequencies and waveforms of stage 3 motion. The reduction in SEAT value for a doubling of the suspended seat mass from the measured value was highly consistent with a median of 16.3% and an inter-quartile range of 3.7% for all Stage 3 conditions (55 conditions). An example using the 2.5 Hz 4.5-cycle motion is shown in Figure 11-8.
On the magnitude of onset of end-stop impacts	End-stop impacts occurred at lower magnitudes with greater suspended seat masses. A doubling of the suspended seat mass from the measured value resulted in a decrease in the magnitude at which end-stop impacts occurred of approximately 10% at 2.5 Hz, increasing with increasing frequency as shown in Appendix 9 Figures 7 to 9.
On the seat performance during stage 4/5 seat motion	An increase in the suspended mass resulted in a loss of seat performance. A doubling in the suspended mass resulted in an increase in the SEAT value of up to 120%. The example shown in Figure 11-8 is typical of the results with other frequencies and waveforms. A halving of the suspended seat mass improves the seat performance for a constant input magnitude in the Stage 4/5 region, but by only up to 45%.

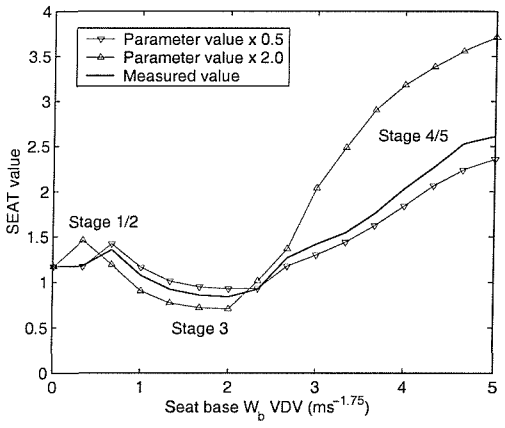

Figure 11-8 The effect of a change of plus and minus a factor of two in the suspended seat mass on the seat performance at 2.5 Hz using the 4.5 cycle motion.

11.3.4 The effect of the suspension stiffness

The suspension stiffness was varied over a range of plus and minus a factor of eight relative to the measured value. The results are shown in Appendix 9 Figures 10 to 12 and are summarised in Table 11-6.

Table 11-6 The effect of changing the suspension stiffness:	
On the seat performance during stage 1/2 seat motions	Negligible effect.
On the friction breakaway magnitude	Negligible effect.
On the seat performance during stage 3 seat motions	Increasing the suspension stiffness resulted in poorer seat performance in the Stage 3 region. Reducing the suspension stiffness by a similar factor was beneficial, but the effect was smaller. Results at 3.15 Hz showed an increase in SEAT value of up to 35% for a doubling of the suspension stiffness. This effect decreased with decreasing magnitude and frequency. Halving the suspension stiffness decreased the SEAT

	value by a maximum of 7%. These effects can be seen for the example at 2.5 Hz using the 11.5 cycle input motion shown in Figure 11-9.
On the magnitude of onset of end-stop impacts	Increasing the suspension stiffness resulted in end-stop impacts at lower magnitudes as the seat-load resonance frequency approached the vehicle vibration frequency. Further increases in suspension stiffness would tend towards a situation where the seat would provide amplification due to the cushion dynamics with no beneficial effect from the suspension in response to the low frequency vehicle vibration. These trends are clearly visible in Appendix 9 Figures 10 to 12. A doubling of the seat suspension stiffness resulted in a reduction of the end-stop impact onset magnitude by up to 80%.
On the seat performance during stage 4/5 seat motion	Doubling the suspension stiffness was found to be detrimental to seat performance in the Stage 4/5 region (up to 45%), except at high (Stage 5) magnitudes with the 1.5 cycle motion, where beneficial result (up to 15%) was observed. The results shown in Figure 11-9 and Figure 11-10are for the 11.5 cycle motion at 2.5 Hz and 2 Hz respectively. The 4.5 cycle results were similar. The results for the 1.5 cycle motion at these frequencies are shown in Figure 11-11 and Figure 11-12.

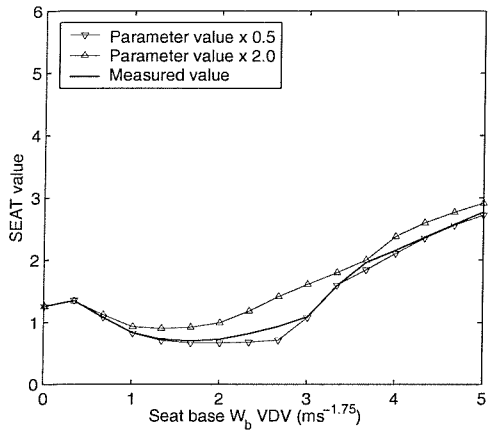

Figure 11-9 The effect of a change of plus and minus a factor of two in suspension stiffness on the seat performance at 2.5 Hz using the 11.5 cycle input motion.

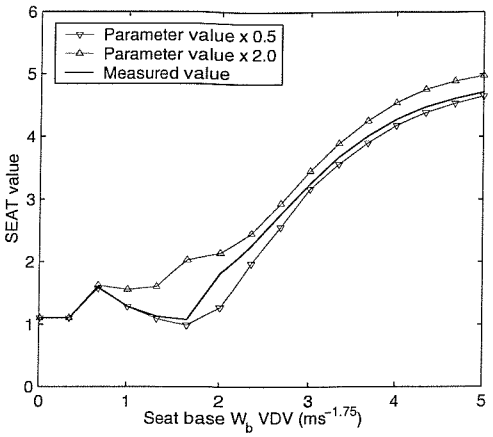

Figure 11-10 The effect of a change of plus and minus a factor of two in suspension stiffness on the seat performance at 2 Hz using the 11.5 cycle input motion.

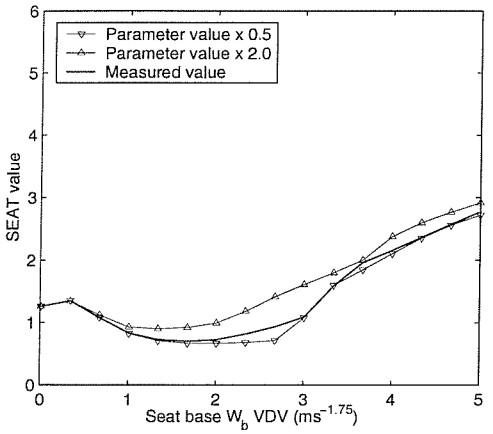

Figure 11-11 The effect of a change of plus and minus a factor of two in suspension stiffness on the seat performance at 2.5 Hz using the 1.5 cycle input motion.

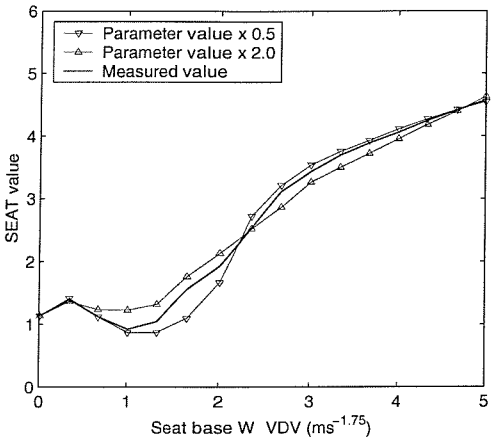

Figure 11-12 The effect of a change of plus and minus a factor of two in suspension stiffness on the seat performance at 2 Hz using the 1.5 cycle input motion.

11.3.5 The effect of the suspension friction

11.3.5.1 Friction magnitude

The effect of the suspension friction magnitude was investigated using symmetrical friction forces varying in magnitude by plus and minus a factor of eight compared to the value determined in Chapter 9 The results are shown in Appendix 9 Figures 13 to 15 and are summarised in Table 11-7.

Table 11-7 The effect of changing the suspension friction magnitude:	
On the seat performance during stage 1/2 seat motions	There was no obvious change in seat behaviour during Stage 1 and 2 motions for different friction values, but the magnitude range of this region varied due to the change in friction breakaway magnitude as described below.
On the friction breakaway magnitude	The magnitude at which the suspension began to break away from friction increased with increasing friction magnitude. This breakaway point was characterised by peak in the SEAT value as the jolts caused by the locking and unlocking of the suspension mechanism were transmitted to the load through the cushion as illustrated in Figure 11-13. The movement of this peak in the amplitude domain can be seen in Appendix 9 Figures 13 to 15 to be similar for all frequencies and waveforms. An example using the 4.5 cycle 2 Hz motions is shown in Figure 11-14. The variation in suspension breakaway magnitude with varying friction was observed to be approximately linear as shown in Figure 11-15.
On the seat performance during stage 3 seat motions	The Stage 3 region was shifted to higher magnitudes with increasing friction by the increase in the friction breakaway and end-stop occurrence magnitudes as described above and below. This effect occurred with all frequencies and waveform durations and can be clearly seen in the example of 2.5 Hz 1.5 cycle motion shown in

	Figure 11-16. The amount of vibration isolation provided across the Stage 3 region decreased with increasing friction. Substantial increases in friction resulted in the seat providing no effective vibration isolation at any magnitude. The minimum SEAT value at any amplitude was found to increase by between 19 and 26% (with one exception at 13%) for a doubling of the friction magnitude from the measured value. The rate of change of minimum SEAT value in the Stage 3 region for the 11.5 cycle 2.5 Hz motion was non-linear and is shown in Figure 11-17. This trend, with differing gradients, was typical of the other frequencies and waveforms.
On the magnitude of onset of end-stop impacts	The onset of end-stop impacts occurred at higher magnitudes for greater suspension friction values as can be seen in Figure 11-14 and Figure 11-16. An increase of between 5 and 50% was observed for a factor of 2 increase in friction magnitude. The relationship between the rate of change of the end-stop impact occurrence magnitude and the friction magnitude can be seen in Figure 11-18 for the 11.5 cycle 2 Hz motion. This was typical of other frequencies and waveforms. A doubling of the friction from the measured value resulted in an increase in the end-stop impact occurrence magnitude of between 25 and 50%.
On the seat performance during stage 4/5 seat motion	The increase in the end-stop impact occurrence magnitude resulted in better seat performance for the same input magnitude in the Stage 4/5 region. A doubling in the friction resulted in reductions in the SEAT value of up to 35%. This effect can be seen in Figure 11-14 and Figure 11-16.

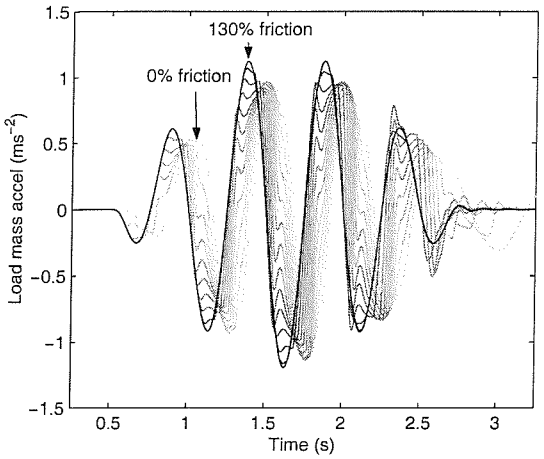

Figure 11-13 The seat load acceleration in response to a 4.5 cycle 2 Hz seat base motion with a $W_b$weighted VDV of 0.35 ms$^{-1.75}$ using suspension friction values fro m 0 to 130% of the measured value in 10% increments illustrating the transition from Stage 1 to Stage 3 seat motion. The load acceleration with the friction at 130% is almost identical in magnitude and phase to the input motion.

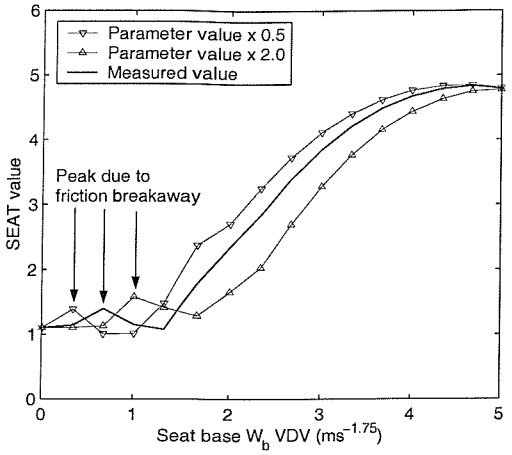

Figure 11-14 The effect of a factor of two change in the suspension friction magnitude using the 4.5 cycle input motion at 2 Hz. The movement of the peak due to the initial breakaway from friction is indicated.

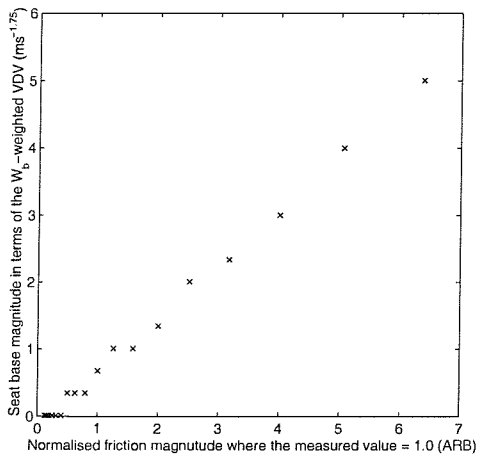

Figure 11-15 The relationship between the friction force magnitude and the input vibration magnitude at the transition through Stage 2 (as defined by the SEAT value passing through unity) with the 1.5 cycle motion at 3.15 Hz.

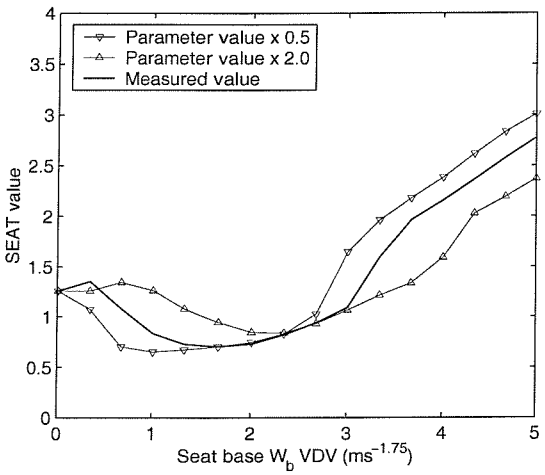

Figure 11-16 The effect of a factor of two change in friction magnitude on the seat performance using the 1.5 cycle input motion at 2.5 Hz, showing the magnitude shift of the Stage 3 region.

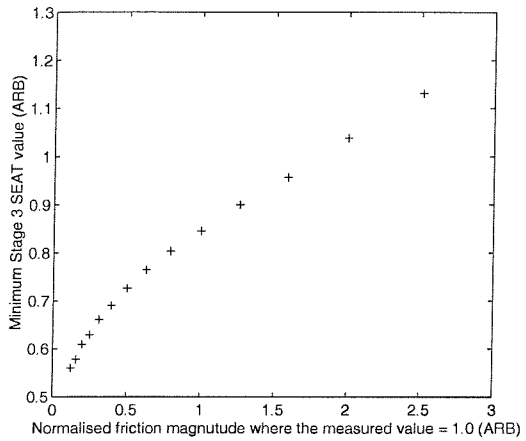

Figure 11-17 The relationship between the friction force magnitude and the minimum SEAT value in the Stage 3 region at 2.5 Hz using the 11.5 cycle motion.

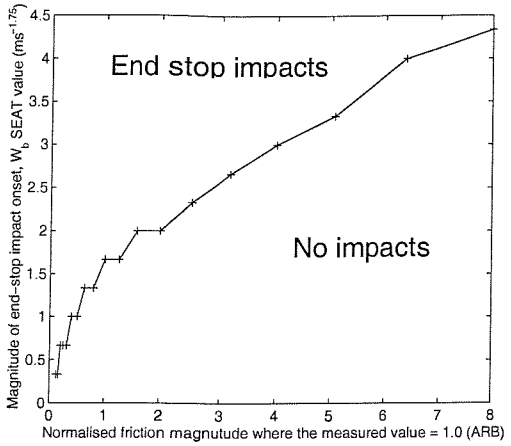

Figure 11-18 The relationship between the friction force magnitude and the minimum magnitude of occurrence of end stop impacts at 2 Hz using the 11.5 cycle motion.

11.3.5.2 Friction symmetry

Preliminary investigations of the effect of the symmetry of the suspension friction force were conducted in Chapter 9 and indicated that the effect on the seat performance was minimal. A more extensive study was conducted in this chapter by maintaining the same total suspension friction force but varying the proportion acting in compression and extension from 10% to 90% of the total. As mentioned in Chapter 9, the model was found to require smaller integration time steps to remain stable with substantial frictional asymmetry, so the simulations were conducted with an integration time step of 100 μs in place of the 1 ms step used for the remainder of the simulations in this chapter.

The results for the short and medium duration motions can be found in Appendix 9 Figures 16 and 17. Some instances of instability in the model can be seen as diamond-shaped 'spikes' on the SEAT value contour plot where a value was substantially greater than the four immediately adjacent points. Results with the long duration motion were not obtained. The results are summarised in Table 11-8.

Table 11-8 The effect of changing the suspension friction symmetry:	
On the seat performance during stage 1/2 seat motions	The lowest magnitude at which the suspension was fully friction locked showed no change in seat performance as the friction force changed from acting mostly against upward motion of the suspension to acting mostly against the downward motion (Figure 11-19 and Figure 11-20). The SEAT values obtained during friction breakaway showed a minimum value at 2 and 2.5 Hz for both durations of test motion. This minimum occurred with approximately 40% of the force acting in compression for the short duration motion and 50% (symmetric friction forces) with the medium duration motion. The effect of the friction symmetry on the time histories can be seen in Figure 11-21 and Figure 11-22. It can be seen that the displacement during the motion and the final lock-up displacement both move upwards as more of the force acts in compression.
On the friction breakaway magnitude	Negligible effect
On the seat performance during stage 3 seat motions	Negligible effect
On the magnitude of onset of end-stop impacts	With the short duration motion, the magnitude of onset of end-stop impacts decreased as the friction force was altered to act more in compression than in extension (Figure 11-19). The reverse was observed with the medium duration motion (Figure 11-20). This occurred at all frequencies. Time histories showing the effect of the friction symmetry with moth durations of input motion with VDVs of

	2.6 $ms^{-1.75}$ are shown in Figure 11-23 and Figure 11-24. It can be seen that asymmetric friction discourages motion towards one end-stop and encourages motion towards the other. The short motion has a more severe bottom stop impact, so more friction in compression is beneficial. The medium duration motion has more severe top-stop impacts so more friction in extension results in better seat performance. The final lock-up position is affected by the friction symmetry for both motions.
On the seat performance during stage 4/5 seat motion	The seat variation in seat performance with varying friction symmetry was greatest during the occurrence of end-stop impacts. Friction symmetry had less effect at high magnitudes with the short duration motion and negligible effect with the medium duration motion (Figure 11-19 and Figure 11-20).

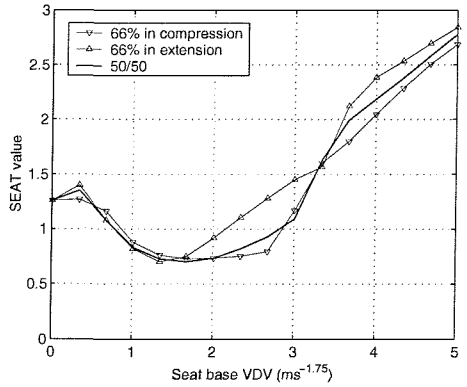

Figure 11-19 The effect of the friction symmetry on the seat performance in response to the short duration (1.5 cycle) 2.5 Hz input motion.

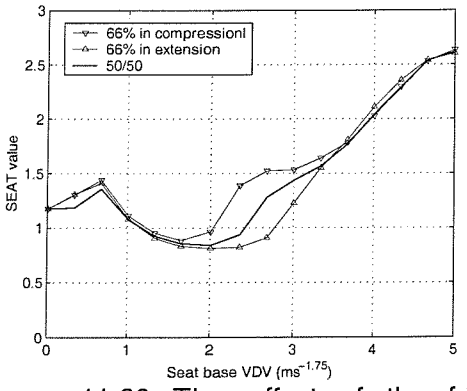

Figure 11-20 The effect of the friction symmetry on the seat performance in response to the medium duration (4.5 cycle) 2.5 Hz input motion.

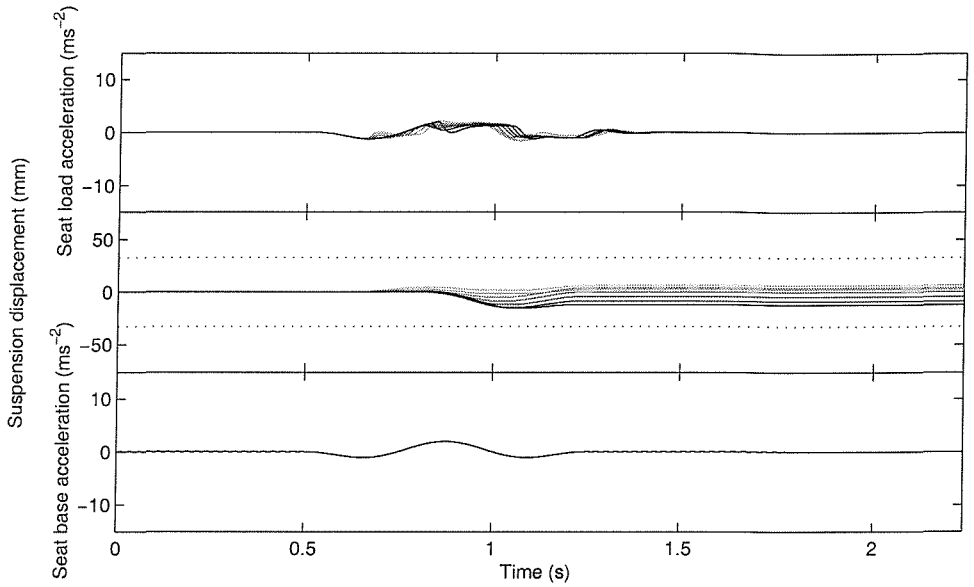

Figure 11-21 The simulated seat response to the short duration, 0.45 ms$^{-1.75}$ VDV, 2 Hz input motion, varying the proportion of the friction force acting in compression from 10% to 90% in seven steps. The lightest line indicates 90% acting in compression and the dotted lines indicate the end-stop buffer locations.

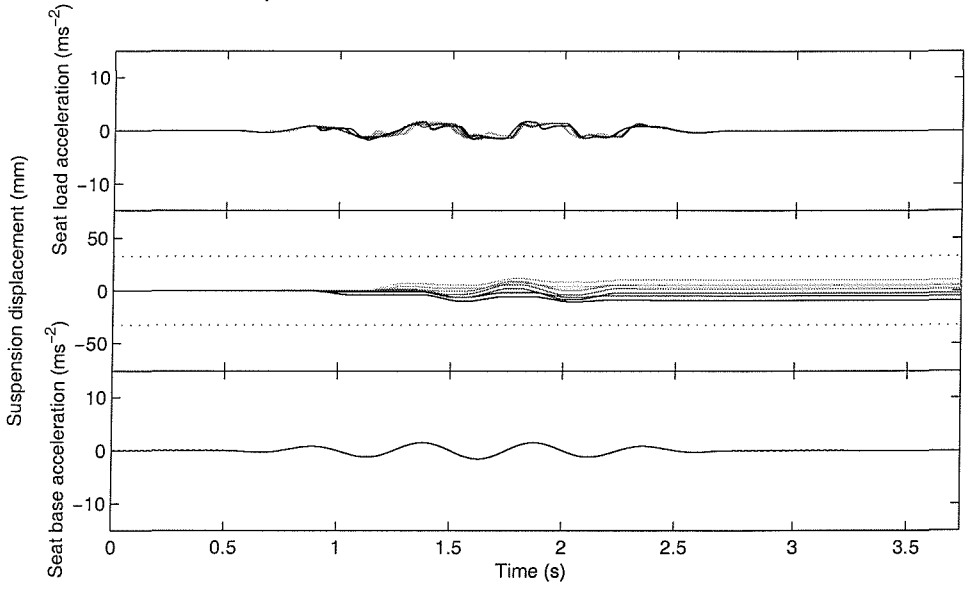

Figure 11-22 The simulated seat response to the medium duration, 0.45 ms$^{-1.75}$ VDV, 2 Hz motion, varying the proportion of the friction force acting in compression from 10% to 90% in seven steps. The lightest line indicates 90% acting in compression and the dotted lines indicate the end-stop buffer locations.

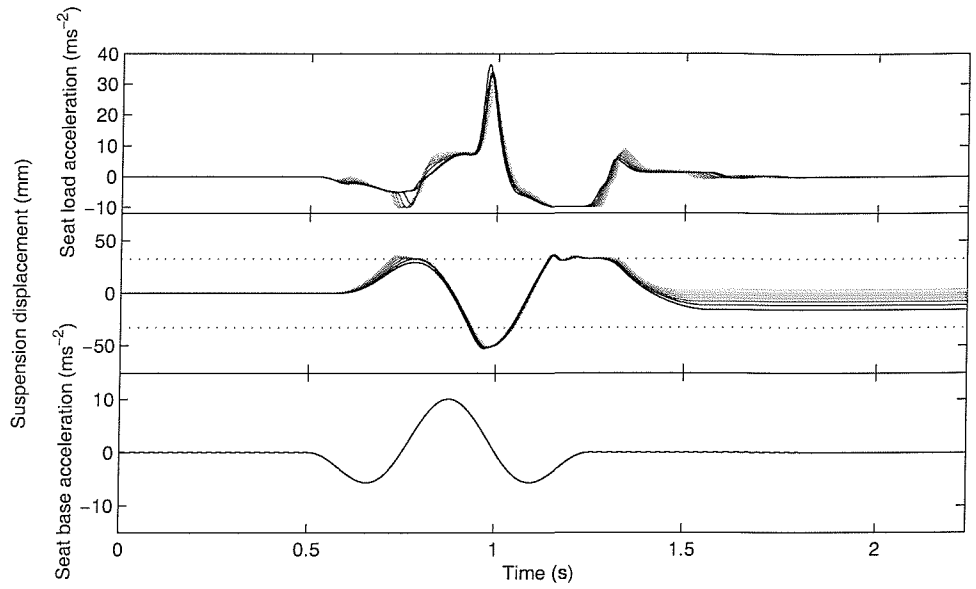

Figure 11-23 The simulated seat response to the medium duration, 2.6 $ms^{-1.75}$ VDV, 2 Hz motion, varying the proportion of the friction force acting in compression from 10% to 90% in seven steps. The lightest line indicates 90% acting in compression and the dotted lines indicate the end-stop buffer locations.

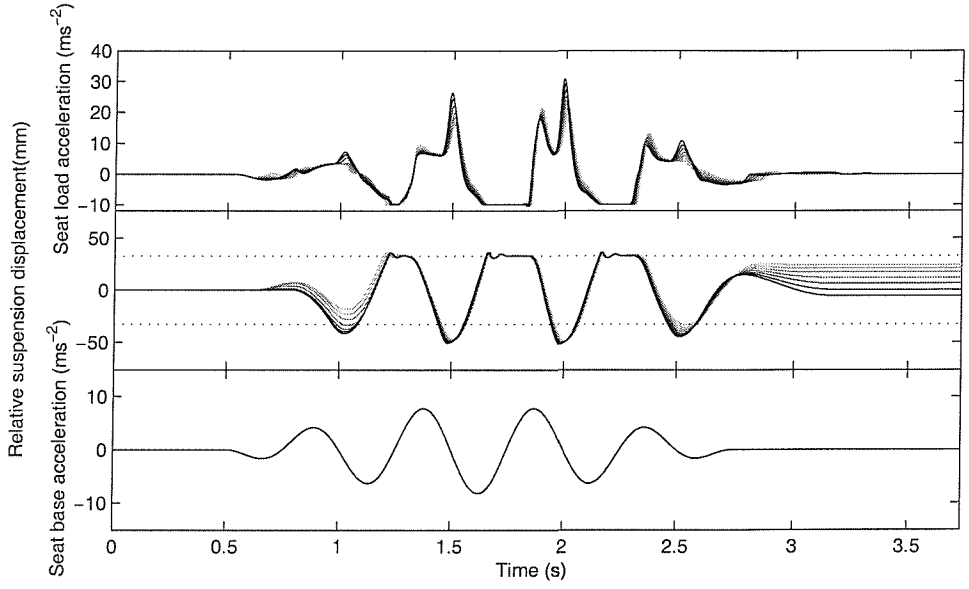

Figure 11-24 The effect on the simulated seat response to the medium duration, 2.6 $ms^{-1.75}$ VDV, 2 Hz motion, varying the proportion of the friction force acting in compression from 10% to 90% in seven steps. The lightest line indicates 90% acting in compression and the dotted lines indicate the end-stop buffer locations.

11.3.6 The effect of the suspension non-frictional damping

11.3.6.1 Suspension damping magnitude

The non-frictional (i.e. nominally velocity proportional) damping magnitude was varied by adjusting the linear damping term (*A* in Equation 11-1) over a factor of plus and minus eight. The effect of this variation is shown in Appendix 9 Figures 18 to 20 and summarised in Table 11-9.

$$F_c = \left(A_c|\dot{z}|^{B_c} + C_c|\dot{z}|z + (D+E)\right)sign(\dot{z})\Big|_{\dot{z}<0}$$

$$F_e = \left(A_e|\dot{z}|^{B_e} + C_e|\dot{z}|z + (D+E)\right)sign(\dot{z})\Big|_{\dot{z}\geq 0} \qquad \text{Equation 11-1}$$

$$F_{damper} = F_c + F_e$$

where F_{damper} is the total force generated by the damper, *A* and *B* are coefficients describing an exponential curve in compression and extension, *C* is a coefficient introducing hysteresis-like behaviour to the force-velocity characteristic and *(D+E)* is the magnitude of the damper friction force and suspension linkage force.

Table 11-9 The effect of changing the suspension non-frictional damping magnitude:	
On the seat performance during stage 1 seat motions	Negligible effect
On the friction breakaway magnitude	Negligible effect
On the seat performance during stage 3 seat motions	The seat performance improved with decreased damping magnitude approximately according to an inverse power relationship as shown in the example in Figure 11-25. A change in SEAT value of up to 20% was observed for a factor of 2 increase or decrease in the damping magnitude for the 4.5 cycle motion with a seat base VDV of 2 $ms^{-1.75}$ as illustrated in Figure 11-26. At 3.15 Hz a factor of 2 decrease in damping had a similar effect as at 2.5 Hz, while a factor of 2 increase in damping resulted in an increase in SEAT value of up to 30%. These values

	were typical of the results with the other waveform durations and input magnitudes as can be seen from the figures in Appendix 9.
On the magnitude of onset of end-stop impacts	Decreased damping resulted in end-stop impacts occurring at lower input magnitudes, so reducing the range of magnitudes over which the seat showed Stage 3 behaviour. Increased damping extended the magnitude range of Stage 3 seat behaviour. Increases in end-stop impact magnitude resulting from a factor of 2 increase in damping from the measured value varied from 10% at 2 Hz with the 1.5 cycle motion up to 75% at 2.5 Hz, again with the 1.5 cycle motion. The range of values with the other two motions was less extreme and the median increase in onset magnitude for all three motions at 2, 2.5 and 3.15 Hz where end-stop impacts were observed was 23 %.
On the seat performance during stage 4/5 seat motion	Increased damping resulted in reduced SEAT values (and vice versa) as can be seen in the 2.5 Hz 4.5 cycle example shown in Figure 11-26. Changes in SEAT value in excess of 100% for a factor of 2 change in damping were observed at 2 Hz for all waveform durations.

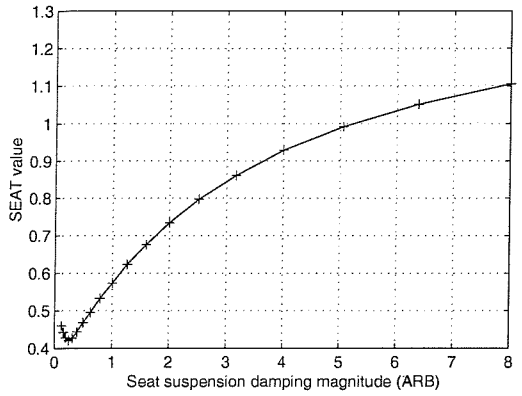

Figure 11-25 The effect of the damping magnitude on the seat performance at 3.15 Hz with a 1.5 cycle Stage 3 seat motion with a 2.3 $ms^{-1.75}$ seat base VDV.

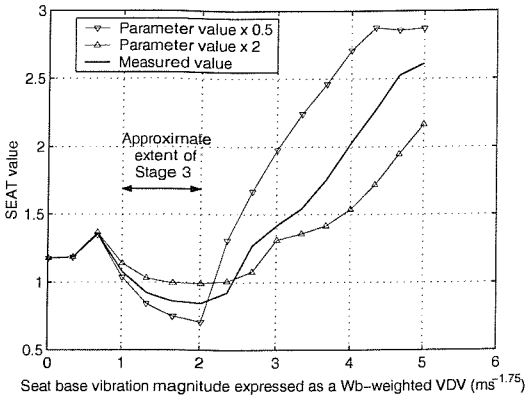

Figure 11-26 the effect of a factor of 2 change in the damping magnitude on the seat performance at all magnitudes of 2.5 Hz 4.5 cycle motion.

11.3.6.2 Suspension damping symmetry

The effect of varying the damping symmetry was investigated by applying multipliers to the total non-frictional damping force acting in compression and in extension. The sum of the two multipliers was always equal to 2.0 and varied linearly from 2.0 in compression and zero in extension to zero in compression and 2.0 in extension.

Equation 11-2, adapted from the damper model described in Chapter 9, describe the theoretical damper model used during this investigation:

$$F_c = \left(M_c\left[A_c|\dot{z}|^{B_c} + C_c|\dot{z}|z\right] + D\right)sign(\dot{z})\Big|_{\dot{z}<0}$$

$$F_e = \left(M_e\left[A_e|\dot{z}|^{B_e} + C_e|\dot{z}|z\right] + D\right)sign(\dot{z})\Big|_{\dot{z}\geq 0}$$

Equation 11-2

$$F_{damper} = F_c + F_e$$

where F_{damper} is the total force generated by the damper, A and B are coefficients describing an exponential curve in compression and extension, C is a coefficient introducing hysteresis-like behaviour to the force-velocity characteristic, D is the magnitude of the damper friction force and M_c and M_e are the multipliers used to vary the symmetry of the damping force. The results are shown in Appendix 9 Figures 21 to 23 and are summarised in Table 11-10.

Table 11-10 The effect of changing the suspension non-frictional damping symmetry:	
On the seat performance during stage 1/2 seat motions	Negligible effect.
On the friction breakaway magnitude	Negligible effect.
On the seat performance during stage 3 seat motions	Some change in waveform shape, but minimal effect on the SEAT value. Time histories predicted for the load mass using a 3.15 Hz 4.5 cycle input motion with a seat base W_b-weighted VDV of 2 $ms^{-1.75}$ are shown in Figure 11-27.
On the magnitude of onset of end-stop impacts and the seat performance during stage 4/5 seat motion	The time histories of the suspension displacement showed that adjusting the damping symmetry caused the mean seat displacement throughout the duration of the motion to become offset from the mid-free-travel location. This effect is illustrated in Figure 11-28. The short duration motion was naturally biased towards bottom stop impacts as observed in Chapter 4, so adjusting the damping to act more in compression than extension improved the seat performance as shown in Figure 11-29. The longer duration motions showed better seat performance with a more symmetrical damping characteristic, but showed poor results with extension-biased damping with less severe end-stop impacts and poor results with compression-biased damping for more severe impacts. An example of this is shown in Figure 11-30.

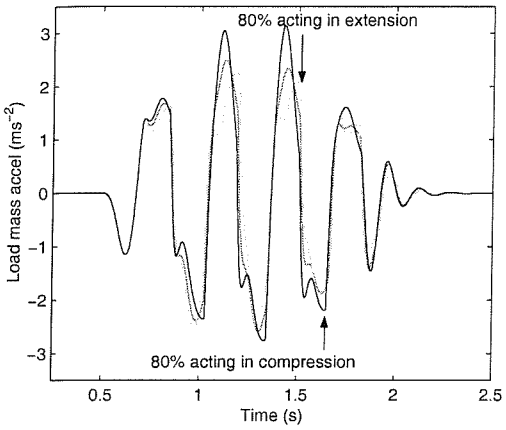

Figure 11-27 the effect of altering the suspension damping symmetry from 80% acting downwards to 80% acting upwards, also showing the measured 50/50 distribution, using a 3.15 Hz 4.5 cycle input motion with a seat base W_b-weighted VDV of 2 $ms^{-1.75}$

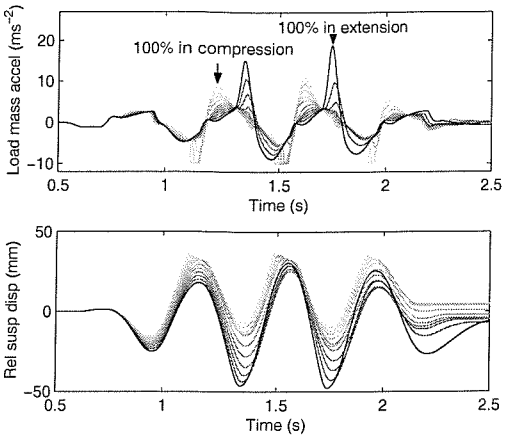

Figure 11-28 The effect of adjusting the suspension damping offset on the seat response to a 4.5 cycle 2.5 Hz input motion with a seat base VDV of 2.34 $ms^{-1.75}$.

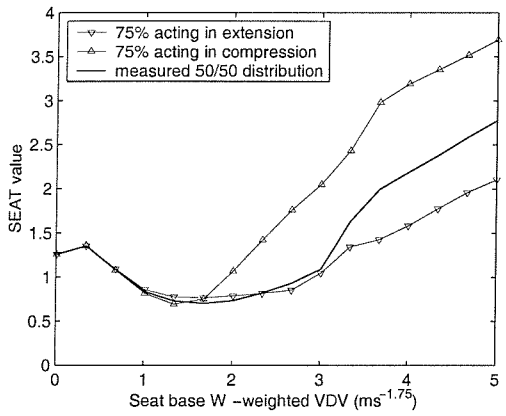

Figure 11-29 The effect of the suspension damper characteristic symmetry on the seat performance in response to the short duration (1.5 cycle) 2 Hz input motion.

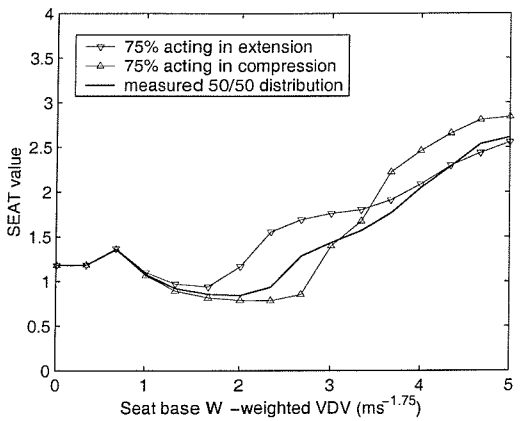

Figure 11-30 The effect of the suspension damper characteristic symmetry on the seat performance in response to the medium duration (4.5 cycle) 2 Hz input motion.

11.3.7 The effect of the suspension free travel displacement

The suspension free travel displacement was varied over a range of plus and minus a factor of five relative to the measured value. The results are shown in Appendix 9 Figures 24 to 26 and are summarised in Table 11-11.

Table 11-11 The effect of changing the suspension free travel displacement:	
On the seat performance during stage 1/2 seat motions	Negligible effect.
On the friction breakaway magnitude	Negligible effect.
On the seat performance during stage 3 seat motions	At 2 and 2.5 Hz, the seat performance degrades with increasing magnitude. This may be due to the non-linearly increasing suspension damping. This effect is illustrated in Figure 11-31.
On the magnitude of onset of end-stop impacts	Increasing the free travel causes the magnitude at which end-stop impacts occur to increase. The relationship between the magnitude at which end-stop impacts occur and the suspension free travel at 2.5 Hz using the 4.5 cycle motion is shown in Figure 11-32. This result is typical of the other frequencies and magnitudes shown in Appendix 9 Figures 25 to 27. A doubling of the free travel was observed to eliminate the occurrence of end-stop impacts for the 4.5 and 11.5 cycle motions. This suggests that increasing the suspension free travel approaches an asymptote where end-top impacts will not occur at any realistic magnitude.
On the seat performance during stage 4/5 seat motion	At 2 and 2.5 Hz, the SEAT value varying with increasing suspension free travel increases rapidly and then decreases as shown in Figure 11-33. At small free travel values the relative velocities between the seat and the base do not have time to increase substantially before encountering an end-stop buffer, so the impacts are less severe. At sufficiently high free travel values, no end-stop impacts occur. The seat load acceleration time histories varying with free travel with a 4.5 cycle, 2.5 Hz, 2 $ms^{-1.75}$ base VDV motion are shown in Figure 11-34.

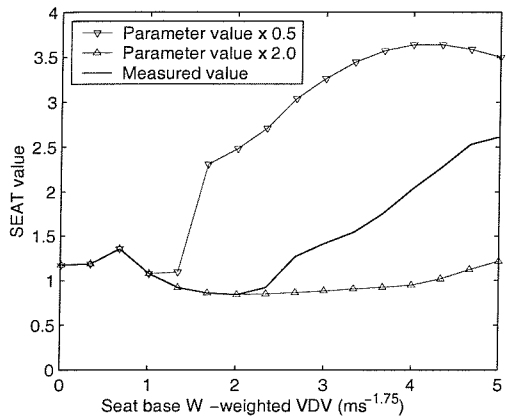

Figure 11-31 The effect of the suspension free travel on the magnitude of end-stop impact occurrence at 2.5 Hz using the 4.5 cycle motion.

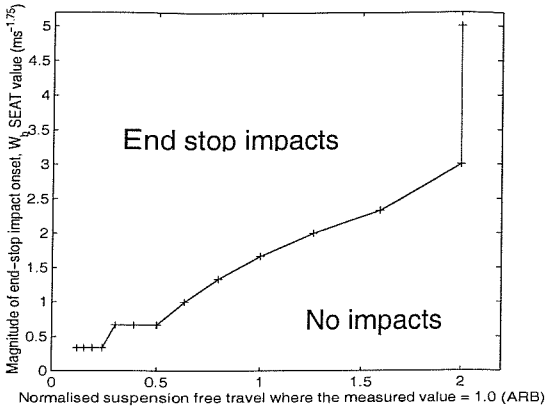

Figure 11-32 The effect of the suspension free travel on the magnitude of end-stop impact occurrence at 2.5 Hz using the 4.5 cycle motion.

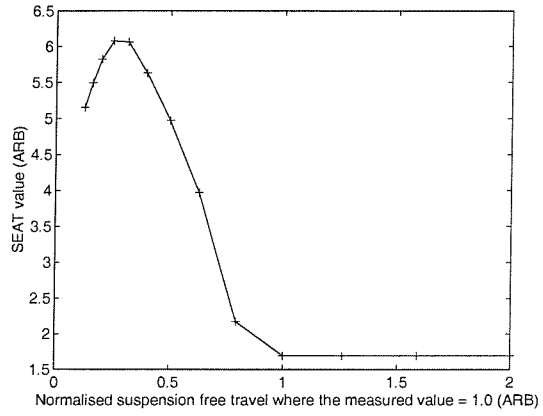

Figure 11-33 The variation in SEAT value with varying suspension free travel at 2.5 Hz with the 4.5 cycle motion.

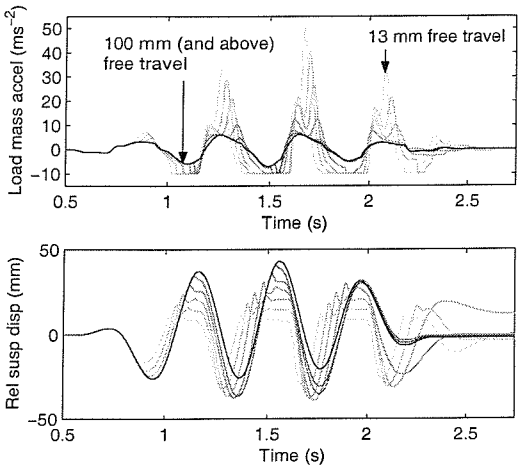

Figure 11-34 The seat load accelerations varying with free travel with a 4.5 cycle, 2.5 Hz, 3 $ms^{-1.75}$ base VDV motion.

11.3.8 The effect of the suspension offset displacement

The offset of the suspension mechanism from the mid-point of the free travel was investigated over a linear range from just in contact with the bottom stop to just in contact with the top stop. The results are shown in Appendix 9 Figures 27 to 29 and summarised in Table 11-12.

Table 11-12 The effect of changing the suspension offset displacement:	
On the seat performance during stage 1 seat motions	Negligible effect.
On the friction breakaway magnitude	Negligible effect.
On the seat performance during stage 3 seat motions	Offsetting the suspension towards the bottom stop was found to result in a small improvement in the seat performance (a 10 mm adjustment, corresponding to 17% of the total travel resulted in an improvement of up to 3%). This was probably due to the suspension offset causing the damper angle to vary, so modifying the effective damping force. An example is shown in Figure 11-35.
On the magnitude of onset of end-stop impacts	A 10 mm change in suspension offset displacement was found to adjust the magnitude at which end-stop impacts occurred by up to 40%, with this effect increasing with increasing frequency. An optimal offset to avoid the onset of end-stop impacts was visible. This position was +3 mm for the short motion and –11 mm for the longer motions.
On the seat performance during stage 4/5 seat motion	With the exception of magnitudes close to the occurrence of end-stop impacts where comparatively large differences in SEAT were observed, the suspension offset had a relatively small effect on the SEAT value in end-stop impact situations. A 10 mm change in offset position resulted in a change in SEAT value of up to 140% due to the change in end-stop impact magnitude, but less than 10% for all situations involving more severe end-stop impacts. An example of this trend is shown in Figure 11-36.

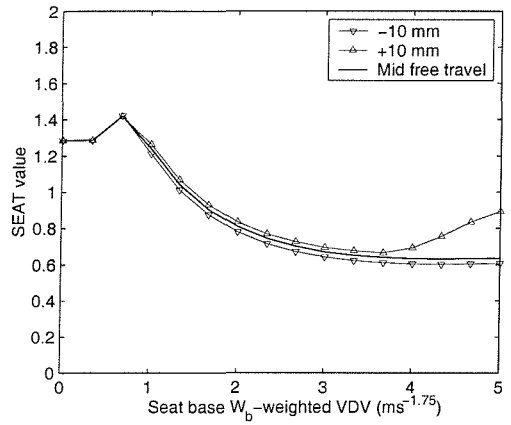

Figure 11-35 The effect on the seat response of changing the suspension offset position relative to the mid-free-travel point using an 11.5 cycle, 3.15 Hz input motion.

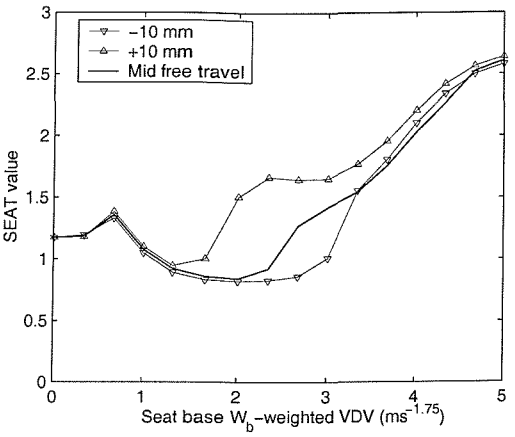

Figure 11-36 The effect on the seat response of changing the suspension offset position relative to the mid-free-travel point using a 4.5 cycle, 2.5 Hz input motion.

11.3.9 The effect of the end-stop buffer stiffness

The stiffness of the top and bottom end-stop buffers were varied independently over a range of plus and minus a factor of five. The stiffness of each buffer was non-linear and was defined in the model in the form of a 5th order polynomial as described in Chapter 6. A decrease in stiffness therefore leads to an effective increase in the available overall suspension travel. The results for both buffers are shown in Appendix 9 Figures 30 to 35 and summarised in Table 11-12.

Table 11-13 The effect of changing the end-stop buffer stiffness	
On the seat performance during stage 1 seat motions	The end-stop buffers cannot affect the seat performance until they are contacted, so the buffers had no effect for these conditions.
On the friction breakaway magnitude	
On the seat performance during stage 3 seat motions	
On the magnitude of onset of end-stop impacts	

On the seat performance during stage 4/5 seat motion	Increasing the top-stop buffers stiffness showed worsening in seat performance, but this effect was less than 3% for a doubling in stiffness. This effect is shown in Figure 11-37 and Figure 11-38. Smaller differences were observed with shorter motions. Increasing the bottom buffer stiffness resulted in poorer seat performance as shown in Figure 11-39, with a doubling in stiffness resulting in a 15% increase in SEAT value. Example histories are shown in Figure 11-40.

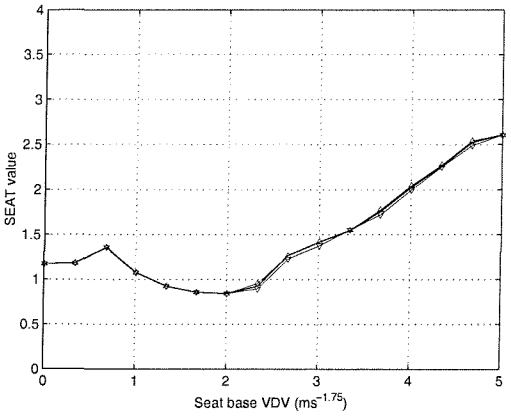

Figure 11-37 The effect on the SEAT value of changing the top buffer stiffness using a 4.5 cycle, 2.5 Hz input motion.

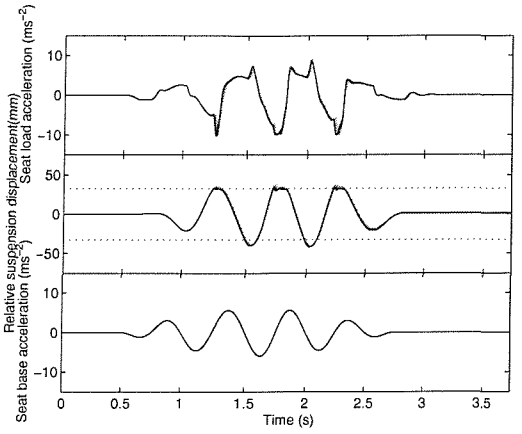

Figure 11-38 The effect on the time domain seat response of changing the top buffer stiffness logarithmically from 1/8 to 8 times the measured stiffness using a 4.5 cycle, 2.5 Hz input motion. Darker lines indicate higher stiffness values.

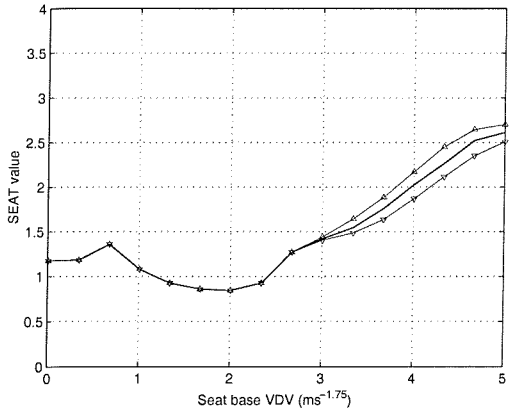

Figure 11-39 The effect on the seat response of changing the bottom buffer stiffness using a 4.5 cycle, 2.5 Hz input motion.

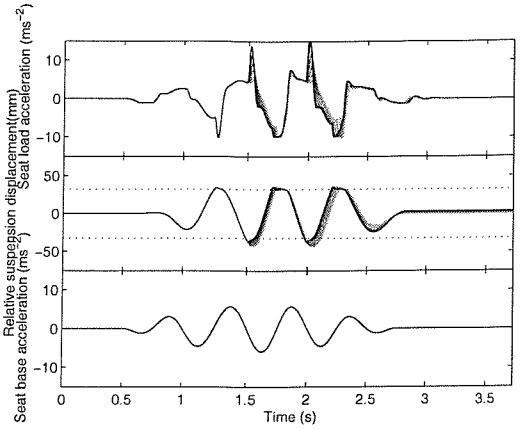

Figure 11-40 The effect on the time domain seat response of changing the bottom buffer stiffness logarithmically from 1/8 to 8 times the measured stiffness using a 4.5 cycle, 2.5 Hz input motion. Darker lines indicate higher stiffness values.

11.3.10 Summary

A summary of the results described above is shown in Table 11-14. Example quantities are shown but the figures in Appendix 9 should be carefully studied to obtain a more complete understanding of the influence of each parameter. The cases where the frequency, magnitude or waveform had an obvious effect are indicated. Otherwise, these summaries refer to all results using the input frequencies of 2.0, 2.5 and 3.15 Hz.

Table 11-14 Effect of a factor of four increase in the parameter value from half to double the measured value. Beneficial effects are shown in bold and detrimental effects in italics.

Parameter (and range of values if different from a factor of four).	**Stage 1/2 SEAT value (decrease is beneficial)**	**Friction breakaway magnitude (decrease is beneficial)**	**Stage 3 SEAT value (decrease is beneficial)**	**End-stop impact onset magnitude (increase is beneficial.**	**Stage 4/5 SEAT value (decrease is beneficial)**
Cushion stiffness	**Decreased; between 10 and 30%.**	Negligible effect.	*Increased; Up to 10%.*	Negligible effect.	*Increased; up to 75%.*
Cushion damping	**Decreased; 30% at 3.15Hz with the short motion, less with longer motions and lower frequencies.**	Negligible effect.	**Decreased; Approx. 15% at low magnitudes for all conditions, decreasing with increasing magnitude.**	Negligible effect.	**Decreased; up to 50%.** *5% increase with the short motion.*
Suspended seat mass	No clear effect.	**Decreased; between 50% and 100%.**	**Decreased; consistent change, median 24%, IQR 6%.**	*Decreased; approximately 20% at 2.5Hz.*	*Increased; up to 140%.*
Suspension stiffness	Negligible effect.	Negligible effect.	*Increased; up to 45% at 3.15Hz. Decreasing the stiffness showed progressively smaller changes.*	*Decreased; up to 80%.*	*Generally increased; up to 55%* **(1.5 cycle Stage 5 results showed a decrease of up to 20%)**
Suspension friction magnitude	No clear effect.	*Linear increase; between 200% and 300%.*	*Increased; between 26% and 52%*	**Increased; between 60% and 133%.**	**Decreased; up to 90% at 2Hz.**
Suspension friction symmetry (35% to 65% of the total acting in compression)	Optimal value within 10% of 50/50 split, motion dependant. Changes up to 30% observed.	Negligible effect.	Negligible effect.	Changes of up to 50% observed, decreasing at higher magnitudes. Direction was motion dependant.	Changes of up to 100% observed, decreasing at higher magnitudes. Direction was motion dependant.

Suspension non-frictional damping magnitude	Negligible effect.	Negligible effect.	*Increased; up to 50% at 3.15Hz.*	**Increased; up to 175% with the shortest duration motion.**	**Decreased; in excess of 300% at 2Hz.**
Suspension non-frictional damping symmetry (30% in compression to 30% in extension)	Negligible effect.	Negligible effect.	Minimal effect despite changes in waveform shape.	**The short motion benefited from an extension-biased damping characteristic (75% improvement).** The longer motions benefited from a more symmetrical characteristic.	
Suspension free travel	No effect.	No effect.	Negligible effect at comparable magnitudes. *Seat performance becomes poorer at high magnitudes.*	**Increased; possibly infinite, certainly in excess of 250%.**	**Decreased; in excess of 250%.**
Mean ride offset (-10 mm to +10mm)	Negligible effect.	Negligible effect.	*Increased; <5% due to changing damper angle.*	Up to 75% difference in onset magnitude for a 20 mm change in offset, but the absolute values varied with the motion duration.	Up to 150% due to the change in impact onset magnitude. Up to 25% change at more severe magnitudes, Different trends with duration and frequency.
Top end-stop stiffness	No effect.	No effect.	No effect.	No effect.	*Less than 5% increase in SEAT value.*
Bottom end-stop stiffness	No effect.	No effect.	No effect.	No effect.	*Approximate 15% increase in SEAT value.*

11.4 Discussion

The results provide a description of the effect of the individual seat components on the seat performance. In the majority of cases, component changes could result in an improvement in performance at some magnitudes, but a loss in performance at others. Exceptions to this rule were the suspension stiffness and the suspension travel. Both of these parameters could be modified (decreased stiffness and increased travel) without a detrimental effect at any frequency or magnitude.

Reductions in the stiffness were found to be beneficial in most conditions, but below a stiffness of around 2 kNm^{-1}, reductions in stiffness were found to have little effect on the seat performance. Increasing the suspension travel was found to be beneficial in reducing end-stop impact occurrence and a free travel of 210 mm was found to prevent the occurrence of end-stop impacts for any of the conditions investigated.

The seat performance at very low magnitudes, where the suspension remained friction locked, was only influenced by the cushion, as would be expected.

Improved friction breakaway performance could be obtained by increasing the seat mass or reducing the friction in order to reduce the magnitude at which the seat broke away from friction. Friction had a much greater effect than mass for the same proportional change in value. Both of these changes would also improve the seat performance for moderate (Stage 3) motions, but would lead to the occurrence of end-stop impacts at lower magnitudes. No other components affected the breakaway magnitude.

The seat performance at Stage 3 magnitudes could be improved by increasing the seat mass, reducing the suspension stiffness (subject to a law of diminishing returns), reducing the cushion stiffness, increasing the cushion damping, reducing the suspension damping, reducing the suspension friction, or adjusting the seat towards toward the lower buffer causing an effective reduction in suspension damping. The largest effects were observed for changes in the suspension damping (frictional and force-velocity), the suspension stiffness and the seat mass. These results were as expected, as the seat most closely approximates a linear system at these magnitudes.

The stiffness of the top end-stop buffer was observed to have minimal effect on the vibration experienced by the seat load. The bottom end-stop buffer was observed to have a greater effect. It should be noted that a softer buffer effectively results in a greater

stroke and the stroke was observed to have a substantial effect on the performance of the seat.

The magnitude required for the onset of end-stop impacts would be increased by reducing the seat mass, reducing the suspension stiffness (again with diminishing benefit), reducing the friction, reducing the suspension non-frictional damping, increasing the free travel, reducing the bottom end-stop buffer stiffness or biasing the suspension friction, non-frictional damping or offset position according to the characteristics of the input motion.

The suspension non-frictional damping symmetry was observed to adjust the effective offset of the suspension when the seat was in motion, so allowing the suspension to impact one or other of the end-stop buffers. The symmetry of the suspension friction force was found to affect the seat displacement at the start and end of the motion and the severity of end-stop impacts but did not have such a strong effect on the suspension mean ride displacement.

Examination of time histories (e.g. Figure 11-24 and Figure 11-28) indicated that a top stop impact could cause a substantial positive acceleration peak (>10 ms^{-2}) due to the load returning to the seat after being thrown clear of the seat surface. This peak occurred independently of any peak due to the seat impacting the bottom buffer.

The results obtained by varying the suspension stroke suggested that long stroke (up to 300 mm) suspension seats could be designed with suitable damper units in such a way that end-stop impacts would not occur for any magnitude steady state or shock-like input motion. The seat would be expected to have a SEAT value in excess of unity for high magnitudes, but would not generate the shocks typical of end-stop impact events. The manufacture of long-stroke suspension seats is limited by the space within vehicles and the discomfort experienced by the driver by the relative movement of the controls. The former factor would require the modification of some vehicle cab designs to include more headroom. The latter factor could be overcome by including the vehicle controls relevant to the vehicle travel, as opposed to relatively stationary operations such as loading or excavating, on the armrests and footrests attached to the suspended part of the seat. Further research into damper designs to ensure that the damping force continued to increase with velocity and did not overheat would also be required. However, the investment may be more economical than suspending the vehicle or the cab with sufficient stroke to prevent overtravel in these suspension systems.

The severity of the end-stop impacts for a given input magnitude could be reduced by increasing the suspension travel and the suspension non-frictional damping. Increased suspension friction, reduced cushion stiffness and reduced seat mass were also observed to be beneficial. The cushion damping, suspension stiffness, suspension non-frictional damping symmetry and suspension offset position were found to affect the results, but showed different trends with the short, highly asymmetrical 1.5 cycle motion as compared with the longer, more symmetrical 4.5 and 11.5 cycle input motions.

11.5 Conclusions

Only the seat mass and the friction affected the friction breakaway magnitude and only the cushion affected the seat performance at lower magnitudes where the suspension was friction-locked. The suspension stiffness, damping, friction and suspended mass (and a small effect of cushion stiffness and damping) all had a clear effect on the performance at moderate magnitudes and all of these parameters except the cushion affected the magnitude at which end-stop impacts occurred.

The seat performance in response to motions that caused end-stop impacts was affected by all the seat components, with the available free travel and the suspension damping having the greatest effect for a similar proportional change in value. It was observed that top end-stop impacts could result in substantial (>10 ms^{-2}) peak upwards accelerations as the load returned to the seat and that the top end-stop buffer had minimal effect on the seat performance.

Only the suspension stiffness and the free travel could be adjusted without having a detrimental effect on the seat performance. Reduced stiffness resulted in better seat performance, but the proportional benefit of reducing the suspension stiffness progressively decreased. Increasing the free travel up to (and in excess of) 210 mm resulted in no end-stop impacts for any test condition.

12 Conclusions and Further Work

12.1 Key findings

The first objective of this thesis was to develop a theoretical model capable of simulating the dynamic performance of production suspension seats in response to input motions with a range of frequencies, magnitudes and waveform shapes representative of those observed in the field on wheeled off-road vehicles.

The general model was developed and used to simulate a steel-sprung suspension seat with a manner of construction similar to a substantial number of seats currently in use in vehicles. The model was found to predict the SEAT values to within 15% of the measured results in 81% of the 673 conditions tested, with a median absolute difference between the measurements and the predictions of 7.8% of the measured value.

The second objective of the thesis was to use this model to understand and quantify the influence of the individual seat components on the seat performance over this range of test conditions.

The sensitivity analysis was conducted over frequencies from 1.25 Hz to 3.15 Hz and at magnitudes that resulted in minimal or friction-locked suspension motion up to strong end-stop impacts using three durations of input motion. The seat parameters were investigated over an 8 to 1 range about their measured value for each frequency, magnitude and duration of motion.

Only the seat mass and the friction affected the friction breakaway magnitude and only the cushion affected the seat performance at lower magnitudes where the suspension was friction-locked. The suspension stiffness, damping, friction and suspended mass (and a small effect of cushion stiffness and damping) all had a clear effect on the performance at moderate magnitudes and all of these parameters except the cushion affected the magnitude at which end-stop impacts occurred.

The seat performance in response to motions that caused end-stop impacts was affected by all the seat components, with the available free travel and the suspension damping having the greatest effect for a similar proportional change in value. It was observed that top end-stop impacts could result in substantial (>10 ms^{-2}) peak upwards accelerations as the load returned to the seat and that the top end-stop buffer had minimal effect on the seat performance.

Only the suspension stiffness and the free travel could be adjusted without having a detrimental effect on the seat performance. Reduced stiffness resulted in better seat

performance, but the proportional benefit of reducing the suspension stiffness progressively decreased. Increasing the free travel up to (and in excess of) 210 mm resulted in no end-stop impacts for any test condition.

12.2 Additional findings

A form of test motion suitable for use in the laboratory for testing suspension seat response to high magnitude motions was defined from examination of the characteristics of the cab floor motion recorded on three off-road wheeled vehicles using acceleration time history data provided by field test laboratories. The test motion was observed to produce similar seat suspension end-stop impact occurrences in the laboratory as observed in the field.

Tests in the laboratory to compare the performance of suspension seats using human subjects and alternative loads did not find consistent differences in the seat performance at most magnitudes for the range of frequencies investigated (1.25 to 3.15 Hz) but identified a problem with the accepted procedure for measuring seat surface vibration in that suspension seat upper end-stop impacts can cause the subject to leave the seat and return, resulting in artefactual transients in the seat surface accelerometer measurement. Comparisons between the mathematical model and laboratory measurements were made using results obtained with an anthropodynamic dummy with an accelerometer attached rigidly to the lower part of the dummy.

The mathematical model described in this thesis improved on previous work in the field by including an explicit friction-locked state. The possibility of determining the non-linear suspension damping characteristics by minimising the difference between simulated and measured seat performance in response to a specific test motion was demonstrated. A non-linear model of the seat cushion incorporating compression-varying stiffness and damping was also investigated but found to have minimal effect on the predicted seat performance except for severe magnitudes of input vibration.

12.3 Further work

Further work following on from the model developed in this thesis might be grouped into four categories as discussed below:

The first category might be described as 'refinement'. This thesis developed a model of an earthmover suspension seat, built confidence in the model by comparison with laboratory measurements and then investigated the effect of the seat components on the predicted seat performance. Simulations of other vertical suspension seats should be carried out and compared with laboratory measurements. Comparisons between simulated and measured dynamic performance with other seats is likely to identify dynamic characteristics that are not currently accounted for in the model. Some of these characteristics were identified during this thesis, such as the self-levelling mechanism in the forwarder seat, the variable height adjustment mechanism in the agricultural tractor seat and the discrepancies between the simulations and measurements using the air-sprung seats in Chapter 9, where the air spring was suspected of contributing to the poor performance. The process of incorporating these and other elements into the model would aid in the understanding of the dynamic performance of the existing seats and build confidence in the general usefulness of the theoretical model. Active or semi-active components, the effect of temperature and the effect of component wear could also be considered as part of the refinement process.

The second category of further work might be called 'improvements' to the model. This group is distinct from the first category in that it involves more major expansions of the model capabilities. Examples of this might be expanding the model to account for two or more axes of motion or implementing simulations of the vehicle and terrain as additional model components between the input and the vibration experienced by the operator.

The third category of further work relates to the seat occupant. The dynamic behaviour and comfort of the operator have not been widely investigated for suspension seat situations by this thesis or other authors. The relative displacement amplitude between the operator and the controls has been suggested as one of the practical limits on the suspension seat stroke (the other being the available space in the vehicle cab) but this factor has not been scientifically investigated. Also, accepted methods do not currently exist for assessing the vibration on the seat surface of a vehicle where the operator may leave the seat during severe motions. This has implications for the accurate

assessment of driver vibration exposure in the field. Other factors directly relevant to the simulation of a seated person on a suspension seat relate to methods of restraint (e.g. seat belts), posture, especially for some agricultural operations where the driver may be twisted in the seat for substantial periods, and muscle tension and active control, for instance in the case of a vehicle operator anticipating an obstacle and choosing to stand up out of the seat and absorb the shock in the legs rather than attempt to adjust the vehicle speed or direction. Finally, a rigid human body model was used during the majority of this thesis to simplify the calculations during top-stop impacts where the load leaves the seat. The use of this body model in response to higher frequency input motions, such as those found in smaller off-road vehicles or tracked machines, would be expected to be insufficient as the seated apparent mass would be expected to deviate from the static mass at these frequencies.

The fourth category of further work might be classified as 'industrial applications' and relates to the practicalities of transferring the model from a theoretical study to a design tool that could be used by engineers involved in the design, manufacture and selection of suspension seats for specific vehicles. This might involve working with interested parties to modify the graphical interface to the satisfaction of the intended users and simplifying the methods of supplying data to the model and analysing the results. As an example of this, one manufacturer expressed an interest in relating the methods of defining the component parameters used in the model to their database of component performance data and including a simple method of running simulations of seats using these stock components in response to the test motions defined in existing standards for testing suspension seats for use in earthmoving and agricultural machines and industrial trucks. The model could also be used in a manufacturing context to suggest the influence of manufacturing tolerance on the dynamic performance of specific seats.

References

Allen, G.R. (1977) Human tolerance to repeated shocks. Proceedings of the European Symposium of Life Sciences Research in Space, Cologne, ESA SP-130, 343-349.

Anton, D.J. (1986), The incidence of spinal fracture on Royal Air Force ejections 1968 – 1983 Report No. 529, Aircrew Equipment Group, Royal Air Force, Institute of Aviation Medicine, Farnborough.

Barak, P. (1992) Passive versus active and semi - active suspension from theory to application in North American Industry World - wide Passenger Car Conference and Exposition, Dearborn, Michigan, September 28 - October 1.

Barlow (1989) Statistics, a guide to the use of statistical methods in the physical sciences. John Wiley and Sons.

Bies, D.A. and Hansen, C.H. (1996) Engineering noise control, theory and practice, second edition. E & FN SPON, London.

Boileau P-É. and Rakheja S. (1999) Whole-body vertical biodynamic response characteristics of the seated vehicle driver. Measurement and model development. Occupational Health and Industrial Medicine, 1999, vol. 40, no. 1, pp. 3-3(1).

Boileau, P-É. and Rakheja, S. (1990), Vibration Attenuation Performance Of Suspension Seats For Off-Road Forestry Vehicles International Journal of Industrial Ergonomics, 5 (1990) 275-291.

Boileau, P-É. and Rakheja, S. (1997) Whole-body vertical biodynamic response characteristics of the seated vehicle driver, measurement and model development. International Journal of Industrial Ergonomics, Accepted for publication 20 February 1997.

Boileau, P-É., Rakheja, S. and Feng, J. (1993), Response of seat - driver system to shock excitation. Proceedings of the United Kingdom Informal Group Meeting on Human Response to Vibration held at the Army Personnel Research Establishment, Ministry of Defence, Farnborough, 20 - 22 September, 1993.

Boileau, P-É., Wu, X., and Rakheja, S. (1998) Definition of a range of idealised values to characterize seat body biodynamic response under vertical vibration. Journal of Sound and Vibration 215 (4), 841-862.

Boshuizen, H.C., Bogers, P.M., and Hulshof, C.T.J. (1992) Self-reported back pain in fork-lift and freight-container tractor drivers exposed to whole-body vibration. Spine, 17 (1) 59-65.

Bovenzi, M. and Betta, A. (1994) Low-back disorders in agricultural tractor drivers exposed to whole-body vibration and postural stress. Applied Ergonomics, 25 (4) 231-241.

Bovenzi, M. and Hulsoff, C.T.J. (1998) An updated review of epidemiological studies on the relationship between exposure to whole-body vibration and low back pain. Journal of Sound and Vibration, 215 (4) 595-611.

Box, M.J. (1965). A new method of constrained optimization and a comparison with other methods. Computer Journal, 8:42--52.

Brinckmann, P., Biggemann, M., and Hilweg, D. (1998) Fatigue fracture of human lumbar vertebrae. Clinical Biomechanics, Supplement No. 1, 1998.

Brinckmann, P., Frobin, W., Biggemann, M., Burton, K., Tillotson, M., and Burton, K. (1998) Quantification of overload injuries to thoracolumbular vertebrae and disks in persons exposed

to heavy physical exertions or vibration at the work place - Part 2. Clinical Biomechanics 13, Supplement No. 2, S(2)1-S(2)36.

Brinckmann, P., Frobin, W., Biggemann, M., Hilweg, D., Seidel, S., Burton, K., Tillotson, M., Sandover, J., Atha, J., and Quinnell, R. (1994) Quantification of overload injuries to thoracolumbular vertebrae and disks in persons exposed to heavy physical exertions or vibration at the work place - Part 1. Clinical Biomechanics 9, Supplement No. 1, S4-S83.

Brown, J.D. (1997) Skewness and Kurtosis. JALT Testing & Evaluation SIG Newsletter, Vol. 1 No. 1 Apr. 1997. (p. 16 - 18)

BS 6841 (1987), British Standard Guide to Measurement and evaluation of human exposure to whole body mechanical vibration and repeated shock British Standards Institution.

Cafferty, S. and Tomlinson, G.R. (1996). Characterization of automotive dampers using higher order frequency response functions. Proceedings of the Institution of Mechanical Engineers, Vol. 211 Part D, 181-203.

Callister, W.D. (1994) Materials science and engineering: An introduction, 3rd ed., Wiley.

Chen, C.Y. and Griffin, M.J. (1989) The application of non-linear least squares methods to predicting seat transmissibility. Technical Report No. 173, Institute of Sound and Vibration Research, The University of Southampton.

Chisholm, C.J. (1970) The techniques of driver protection by suspension seating. Paper No. 7, United Kingdom Informal Group Meeting on the Human Response to Vibration, held at Loughborough University of Technology, September 1970.

Christ, W. and Dupuis, H. (1968) Investigation of the possibility of injury to health in the region of the spine in tractor drives, Part 1. Medizinische Welt 19 (1919-1920).

Christ, W. and Dupuis, H. (1968) Investigation of the possibility of injury to health in the region of the spine in tractor drives, Part 2. Medizinische Welt 19 (1967-1972).

Clark, M.J. and Oborne, D.J. (1975) Reaction of passengers to public service vehicle ride. National Aeronautics and Space Administration, NASA TM X-3295, DOT-TSC-OST-75-40, Ride Quality Symposium, Williamsburg, Virginia, 11-12 August 1975, pp 437-470.

Coermann, R.R. (1962), The mechanical impedance of the human body in sitting and standing position at low frequencies Human Factors 4: 227 – 253.

Coermann, R.R., and Whittwer, A.L. (1960), The Passive Dynamic Mechanical Properties of the Human Abdomen Thorax System and of the Whole-body System Aerospace Medicine, Vol. 31, No. 6, pp. 443.

Comite De Pilotage Charge De La Mise Au Point De Guides Par Le Choix De Sieges Suspendus De Chariots Elevateurs / Steering committee charged with developing guides for choosing suspension seats for lift trucks (1992) Les sieges a suspension pour chariots elevateurs (Suspension seats for fork lift trucks) HSE translation no. 92/95B, July 1992, Health and Safety Executive Language Services.

Corbridge, C. (1984), A comparison of the vertical and fore - and - aft performance of six suspension seats Proceedings of the United Kingdom Informal Group Meeting on Human Response to Vibration, Heriot-Watt Univeristy, Edinburgh, 9 - 11 September 1981, pp 78 – 91.

Corbridge, C. and Griffin, M.J. (1986) Vibration and comfort: vertical and lateral motions in the range 0.5 to 50 Hz. Ergonomics 29: 249-272.

Corbridge, C., Griffin, M.J., and Harborough, P. (1989) Seat dynamics and passanger comfort. Institute of Mechanical Engineers, Part F: Journal of Rail and Rapid Transit 203: 57-64.

Corbridge, C., Morten, J., Messenger, A., Paddan, G., Skene, P., Whitham, E. and Woodgate, R. (1990) 1 metre vertical vibrator manual: operating instructions, performance measures and maintenance. Human Factors Research Unit, Institute of Sound and Vibration Research, University of Southampton, Southampton.

Donati, P.M. and Bonthoux, C. (1983) Biodynamic response of the human body in the sitting position when subjected to vertical vibration. Journal of Sound and Vibration 89, 312-331.

Donati, P.M. and Patel, J.A. (1999). Subjective assessment of fork-lift truck seats under laboratory conditions. Applied Ergonomics, 30 (4), pp. 295-309.

Donati, P.M., Boldero, A.G. and Stayner, R.M. (1982) Simulation of the tractor driver's task for ergonomics experiments. Objective measures to compare tractor seats National Institute of Agricultural Engineering, Wrest Park, Silsoe, Bedford.

Donati, P.M., Grosjean, A., Mistrot, P. and Roure, L. (1983) The subjective equivalence of sinusoidal and random whole-body vibration in the sitting position (an experimental study using the 'floating reference vibration' method). Ergonomics 26, pp. 251-273.

Dove, R.A., Turner, D.M. and Martin, T. (1977), Model for uncured rubber behaviour Plastics and Rubber: Processing, December 1977.

Dupuis H. and Christ W. (1966) Untersuchung der Mo-glichkeit von Gesundheitsschädigungen im Bereich der Wirbelsäule bej Schlepperfahrern. Research report. Max Planck Institute für Landarbeit und Landtechnik.

Dupuis, H., Hartung, E. and Louda, L. (1972) Random vibrations of a limited frequency range compares with sinusoidal vibrations with regard to its effect on man. SAM TT G-115, School of Aerospace Medicine, Brooks Air Force Base, Texas.

Duym, S. (1997) An alternative force state map for shock absorbers. Proceedings of the Institution of Mechanical Engineers, Vol 211, Part D, 175-179.

Ebe, K. and Griffin, M.J. (2000a) Qualitative models of seat discomfort including static and dynamic factors. Ergonomics, 1 June, vol. 43, no. 6, pp. 771-790(20).

Ebe, K. and Griffin, M.J. (2000b) Quantitative prediction of overall seat discomfort. Ergonomics, 1 June, vol. 43, no. 6, pp. 791-806(16).

Edwards, M. (1997) Anthropometric measurements and ejection injuries. Occupational Health and Industrial Medicine, vol. 36, no. 3, pp. 125-125(1).

Eklund, G. (1969) Influence of muscle vibration on balance in man. A preliminary report. Acta Societatis Medicorum Upsaliensis 74: 113-117.

European Economic Community (1999). Council Directive 78/764/EEC Driver's seat on agricultural wheeled vehicles, as amended by Directives 82/890/EEC, 83/190/EEC, 87/354/EEC, 88/465/EEC and 97/54/EEC.

Fairley, T.E. (1988), Predicting seat transmissibilities: the effect of the legs Proceedings of the joint French - English meeting, Groupe Francais des Etudes des Effets des Vibrations sur l'Homme and U.K. Informal Group on Human Response to Vibration, INRS, Vandoeuvre, France, 26 - 28 September 1988.

Fairley, T.E. (1990), Predicting the transmissibility of a suspension seat. Ergonomics, 1990, VOL. 33, NO. 2, 121-135.

Fairley, T.E. and Griffin M.J. (1983) Application of mechanical impedance methods to seat transmissibility. International Conference on Noise Control Engineering, Edinburgh, 422-425.

Fairley, T.E. and Griffin, M.J. (1986) A test method for the prediction of seat transmissibility. Society of Automotive Engineers International Congress and Exposition, Detroit, 24-18 February 1986. SAE paper 860047.

Fairley, T.E. and Griffin, M.J. (1989) The apparent mass of the seated human body: vertical vibration Journal of Biomechanics 22: 81 – 94.

Feeny, B.F. and Liang, J.W. (1996). A decrement method for the simultaneous estimation of Coulomb and viscous friction. Journal of Sound and Vibration 195 (1) 149-154.

Gent, A.N. and Rusch, K.C. (1966), Viscoelastic behaviour of open cell foams. Rubber Chemical Technology 39: 380-396.

Gibson, L.J. and Ashby, M.F. (1988) Cellular Solids Structure & Properties. New York: Pergamon.

Goldberg, D.E. (1989) Genetic Algorithms in Search, Optimization and Machine Learning. Reading, Massachusetts: Addison-Wesley.

Goodwin, G.M., McCloskey, D.I., and Matthews, P.B.C. (1972) The contribution of muscle effects to kinaesthesia shown by vibration induced illusions of movement and by the effects of paralysing joint afferents. Brain 95: 705-748.

Gouw, G.J., Rakheja, S., Sankar, S. and Afework, Y. (1990) Increased comfort and safety of drivers of off-highway vehicles with optimal seat suspension. SAE Trans., J. Commercial Vehicles, 1990, 99(2), 541-548.

Griffin, M.J. (1975) Vertical vibration of seated subjects: effects of posture, vibration level and frequency. Aviation, Space and Environmental Medicine 46: 1033-1040.

Griffin, M.J. (1976) Subjective equivalence of sinusoidal and random whole-body vibration. The Journal of the Acoustical Society of America 60:1140-1145.

Griffin, M.J. (1978) The evaluation of vehicle vibration and seats. Applied Ergonomics 9: 15-21.

Griffin, M.J. (1990) Handbook of human vibration. London: Academic Press.

Griffin, M.J. and Lewis, C.H. (1978) A review of the effects of vibration on visual acuity and continuous manual control, Part 1 - Visual acuity Journal of Sound and Vibration 56: 383 – 413.

Griffin, M.J. and Witham, E.M. (1977), Studies of discomfort produced by impulsive whole body vibration Proceedings of the United Kingdom Informal Group Meeting on Human Response to Vibration, UOP Bostrom, Northampton, 7 - 9 September 1977.

Griffin, M.J. and Witham, E.M. (1980), Discomfort produced by impulsive whole body vibration Journal of the Acoustical Society of America 68: 1277 – 1284.

Griffin, M.J., Parsons, K.C. and Witham, E.M. (1982) Vibration and comfort IV. Application of experimental results. Ergonomics 25:603-630.

Guignard, J.C., and Irving, A. (1960), Effects of low frequency vibration on man Engineering, 9th September, 364-367

Guingard, J.C. (1965) Vibration. In: A textbook of Aviation Physiology. Ed.: Giles, .G.A., Chap. 29, 813-894. New York: Pergamon.

Guingard, J.C. (1985) Vibration. In: Patty's Industrial Hygene and Toxicology Vol. 3b: Biological Responses, 2nd Edition (Eds: Cralley and Cralley). 653-724. New York: Wiley.

Gyi D.E. and Porter J.M. (1999) Interface pressure and the prediction of car seat discomfort. Applied Ergonomics, April 1999, vol. 30, no. 2, pp. 99-107(9).

Hansson, T.H., Keller, T.S. and Spengler, D.M. (1987) Mechanical behaviour of the human lumbar spine. II Fatigue strength during dynamic compressive loading. Journal of Orthopaedic Research, 5, 479-487.

Hertzberg, H.T.E. (1972) The human buttocks in sitting: pressures, patterns, and palliatives. Society of Automotive Engineers Paper 720005.

Hilyard, N.C. (1982) Mechanics of cellular plastics, Chapters 1, 2B and 4. Applied Science Publishers, London.

Hilyard, N.C. and Kanakkanatt, S.V. (1970) The dynamic properties of liquid filled foams. Journal of Physics D (3) 906.

Hilyard, N.C., Collier, P., and Care, C.M. (1983) Dynamic behaviour of flexible foam cushion materials and its influence on ride comfort.

Himmelblau D M (1972) Applied non-linear programming. Mcgraw-Hill, New York.

Hinz, B. and Seidel, H. (1983) The nonlinearity of the human body's dynamic response during sinusoidal whole body vibration. Industrial Health 25, 169-181.

Hinz, B., Blüthner, R., Gericke, L., Menzel, G. and Seidel, H. (1998) Vergleichende Untersuchungen and Versuchspersonen und mechanischen Modellen bei Einwirkung von Ganzkörperschwingungen (Abschlussbericht). Schritenreihe der Bundesanstalt für Arbeitsschultz und Arbeitsmedizin, Forshung Fb 801, ISBN: 3-89701-149-2.

Holland, J.H. (1975) Adaptation in Natural and Artificial Systems, The University of Michigan Press.

Holmlund, P., Lundström, R.M. and Lindberg, L. (1995) Mechanical impedance of human body in the vertical direction. Proceedings of the UK Informal Group Meeting on Human Response to Vibration, Silsoe, United Kingdom. Whole-body vibration.

Howarth, H.V.C. and Griffin, M.J. (1988) The frequency dependence of subjective reaction to vertical and horizontal whole-body vibration at low magnitudes. The Journal of the Acoustical Society of America, 83, (4), 1406-1413.

Howarth, H.V.C. and Griffin, M.J. (1991) Subjective reaction to vertical mechanical shocks of various waveforms. Journal of Sound and Vibration 147(3) 395-408.

Hulsof, C. and Veldhuijzen van Zanten, B. (1987) Whole-body vibration and low-back pain. A review of epidemiologic studies. International Archive of Occupational Environmental Health, 59: 205-220.

Huston, D.R., Johnson, C.C. and Zhao, X.D. (1998) A human analog for testing vibration attenuating seating (letter). Journal of Sound and Vibration, 214, (1), 195-200.

Ifeachor, E.C. and Jervis, B.W. (1993) Digital signal processing, a practical approach. Addison-Wesley.

INRS (1992), La conduite sans les secousses. Comment choisir et entretenir un siege a suspension pour chariot elevateur (Driving smoothly. Choosing and mentaining suspension seats for fork - lift trucks) INRS ED 1373, Paris, July 1992. HSE translation no. 92/101A, February 1993, Health and Safety Executive Language Services.

International Organisation for Standardisation (1974, 1985, 1997) ISO 2631-1 - Mechanical vibration and shock – Evaluation of human exposure to whole body vibration – Part 1: General requirements. International Standards Organisation.

International Organisation for Standardisation (1978) ISO 5353 - Earth-moving machinery – seat index point.

International Organisation for Standardisation (1982, 2000) ISO 7096 - Earth moving machinery – Laboratory evaluation of operator seat vibration. International Standards Organisation.

International Organisation for Standardisation (1990) ISO 5007 - Agricultural wheeled tractors – Operator's seat – Laboratory evaluation of transmitted vibration. International Standards Organisation.

International Organisation for Standardisation (1992) ISO 10326-1 - Mechanical vibration – Laboratory method for evaluating vehicle seat vibration – Part 1: Basic requirements. International Standards Organisation.

International Organisation for Standardisation (1993) COMMITTEE DRAFT CD 5982 - Mechanical Driving Point Impedance and Transmissibility of the Human Body. ISO:TC 108:SC 4 N226.

International Organisation for Standardisation (1993) ISO 5347-5 - Calibration of vibration and shock pick-ups – Part 5 Method of calibration by Earth's gravitation.

International Organisation for Standardisation (1999) ISO 5353 - Earth-moving machinery, and tractors and machinery for agriculture and forestry – seat index point. International Standards Organisation.

Jansson, A., Krus, P. and Palmberg, J-O. (1995) Optimisation of fluid power systems with two alternative non-derivative methods. Division of Fluid Power Technology, Department of Mechanical Engineering, Linköping Univeristy, S-58183, Linköping, Sweden. Published online at http://hydra.ikp.liu.se/~arnja/ga/ga.html.

Jones, A.J. and Saunders, D.J. (1972) Equal comfort contours for whole body vertical, pulsed sinusoidal vibration. Journal of Sound and Vibration 23:1-14.

Jones, A.J. and Saunders, D.J. (1974) A scale of human reaction to whole body, vertical, sinusoidal vibration. Journal of Sound and vibration, 35, (4), 503-520.

Karnopp, D. (1979) Are active suspensions really necessary? ASME Paper No. 78WA:DE01.

Kelsey, J.L. and Hardy, R.J. (1975) Driving of motor vehicles as a risk factor for acute herniated lumbar intervertebral disks. International Journal of Epidemiology 102: 63-75.

Kinkelaar, M.R. and Cavender K.D. (1998) Vibrational characteristics of various polyurethane foams employed in automotive seating applications. Journal of Cellular Plastics, 34, 155-173.

Kitazaki, S. and Griffin, M.J. (1997) A modal analysis of whole-body vertical vibration, using a finite element model of the human body. Journal of Sound and Vibration, 200(1) 83-103.

Kitazaki, S. and Griffin, M.J. (1998) A modal analysis of whole-body vertical vibration, using a finite element model of the human body. Journal of Sound and Vibration, 200, (1), 83-103.

Kjellberg, A. and Wikstrom B-O. (1985) Whole-body vibration: exposure time and acute affects- a review. Ergonomics 28: 535-544.

Kjellberg, A., Wikström, B-O., and Landström, U. (1994) Injuries and other adverse effects of occupational exposure to whole-body vibration, a review for criteria documentation. Arbete och Hälsa vetenskaplig skriftserie, 1994:41.

Krasnicki. E.J. 1981 Shock and Vibration Bulletin, 51 May. The experimental performance of an on-off active damper.

Lang, H.H. (1977) A study of the characteristics of automotive hydraulic dampers at high stroking frequencies. PhD thesis, University of Michigan.

Latham, F. (1957) A study in body ballistics, seat ejection. Proceedings of the Royal Society B-147, 121-139.

Leatherwood, J.D. and Dempsey, T.K. (1976) Psycophysical relationships characterising human response to whole-body sinusoidal vertical vibration. NASA TN D-8188. National Aeronautics and Space Administration.

Lewis C.H. (1994) Simple procedures for estimating the occurrence of suspension seat end-stop impacts. Paper presented at the UK Informal Group Meeting on Human Response to Vibration held that the Institute of Naval Medicine, Alverstoke, Gosport, Hants, PO12 2DL, 29th – 21st September.

Lewis C.H. and Griffin M.J. (2000) An active anthropodynamic dummy for the evaluation of the dynamic performance of seats. Paper presented at the 2nd International Conference on Whole-body Vibration Injuries, 7-9 November, in Siena, Italy.

Lewis, C.H. (1998) The implementation of an improved anthropodynamic dummy for testing the vibration isolation of vehicle seats. Paper presented at the United Kingdom Group on Human Response to Vibration, held at the Health and Safety Executive, Buxton, Derbyshire, 16-18 September.

Lewis, C.H. and Griffin, M.J. (1978) A review of the effects of vibration on visual acuity and continuous manual control, Part 2 - Continuous manual control. Journal of Sound and Vibration, 56, (3), 415-457.

Lines, J., Stiles, M. and Whyte, R. (1995) Whole body vibration during tractor driving. Journal of Low Frequency Noise and Vibration, 14, (2), 87-104.

Lines, J., Whyte, R. and Stayner, R.M. (1989) Suspensions for tractor cabs. Vibration at Work, Proceedings of the 3rd International Symposium of the International Section of the ISSA for Research on Prevention of Occupational Risks, Vienna, 19-21 April, ISBN: 3-9000608-07-5, 148-150.

Lorentz, H. (1924) Lehrbuch der Technischen Physik, Erster Band. Technische Mechanik starrer Gebilde. Berlin: Verlag von Julius Springer.

Lowe, F.G., (1972) Practical aspects of suspension seat design Paper presented at the Vibration Isolation Symposium, Jan 1972, SEE London.

Magid, E.B., Coermann, R.R., and Ziegenruecker G.H. (1960) Human tolerance to whole body sinusoidal vibration: short-time, one-minute and three-minute studies. Aerospace Medicine 31: 915-924.

Malchaire, J., Piette, A. and Mullier, I. (1995) Vibration exposure on fork-lift trucks. Annals of Occupational Hygene, 40(1) pp. 79-91.

Mansfield, N. J. (1997), A consideration of alternative non-linear lumped parameter models of the apparent mass of a seated person Proceedings of the United Kingdom Informal Group Meeting on Human Response to Vibration held at the Institute of Sound and Vibration Research, University of Southampton, 17 - 19 September 1997, 221 – 233.

Mansfield, N.J. and Griffin, M.J. (1996) Vehicle seat dynamics measured with an anthropodynamic dummy and human subjects Inter - noise '96, Proceedings of the 25th Anniversary Congress, Liverpool, Book 4, Pub: IOA, ISBN 1-873082 91 6 1725-1730

Marieb, E.N. (1995) Human anatomy and physiology. The Benjamin/Cummings Publishing Company Inc, California.

Marsh, J.A. (1965), A case for engineered vehicle suspension seating and a review of current developments Report of a paper presented by the Author at Ordinary General Meetings of the Institution of Body Engineers in Oxford on 13th January and in London on 9th March, 1965. Reprinted from the July Issue of the Institute Bulletin Vol. 29, No. 607.

Matsumoto, Y. and Griffin, M.J. (1998) movement of the upper-body of seated subjects exposed to vertical whole-body vibration at the principal resonance frequency. Journal of Sound and Vibration 215(4) 743-762.

Matthews J. (1973) The measurement of tractor ride comfort. SAE paper no. 730795.

Miwa, T. (1967) Evaluation methods for vibration effect. Part 1. Measurements of the threshold and equal sensation contours of whole body vibration for vertical and horizontal motions. Industrial Health 5, 183-205.

Miwa, T. (1967) Evaluation methods for vibration effect. Part 2. Measurement of equal sensation level for whole body between vertical and horizontal sinusoidal vibrations. Industrial Health 5: 206-212.

Miwa, T. (1968), Evaluation methods for vibration effect. Part 4. Measurements of vibration greatness level on compound vibrations Industrial Health 6: 11 – 17.

Morishata, S. and Mitsui, J. (1991) Controllable shock absorber system "An application of electro-Rheological fluid. Society of Automotive Engineers Paper 910744.

Nelder, J.A. and Mead, R. (1965) A Simplex Method for Function Minimization. Computing Journal, 7, 308-313.

Nell, S. and Steyn, J.L. (1994) Experimental evaluation of an unsophisticated two state semi-active damper. Journal of Terramechanics 31, 116-127.

Oborne, D.J. and Boarer, P. (1982) Subjective response to whole body vibration, the effects of posture. Ergonomics 25:673-681.

Oborne, D.J., Boarer, P. and Heath, T.O. (1981), Variations in response to whole body vibration, intensity effects Ergonomics 24: 301 – 313.

Parsons, K.C., Griffin, M.J. and Witham, E.M. (1982) Vibration and comfort III Translational vibration of the feet and back. Ergonomics 25:705-719.

Patten, W.N., Sha, S. and Mo, C. (1998) A vibration model of open celled polyurethane foam automotive seat cushions. Journal of Sound and Vibration 217 (1), 145-161.

Payne P.R. (1965) Personnel restraint and support system dynamics. Aerospace Medical Research Laboratory, Wright-Patterson Air Force Base, Ohio, Report No. AMRL-TR-65-127.

Payne P.R. (1969) Injury potential of ejection seat cushions. Journal of Aircraft 6: 273-278.

Payne P.R. and Band, E.G.U. (1971) A four-Degree-Of-Freedom lumped parameter model of the seated human body. Aerospace Medal Research Laboratory, Wright-Patterson airforce Base, Ohio, Report No. AMRL-TR-70-35.

Perkio-Makela M.; Riihimaki H. (1997) Intervention on seat adjustment among drivers of forest tractors. International Journal of Industrial Ergonomics, March 1997, vol. 19, no. 3, pp. 231-237(7).

Petek, N.K. (1992) An electronically controlled shock absorber using electro-rheological fluid. Society of Automotive Engineers 920275.

Pope, M.H., Wilder, D.G. and Magnusson, M.L. (1999) A review of studies on seated whole body vibration and low back pain. Proceedings of the Institution of Mechanical Engineers, Vol. 213 Part H 435-446.

prEN 13490 (2002) Mechanical vibration – industrial trucks – laboratory evaluation and specification of operator seat vibration. European draft standard.

Rakheja S. and Sankar S. (1983) An optimum seat suspension for off-road vehicles. The shock and vibration bulletin 53 (part 3 of 4).

Rakheja S. and Sankar S. (1984) Improved off-road tractor ride via passive cab and seat suspensions. Journal of vibration, acoustics stress and reliability in design. Vol 106 pp 305-313.

Rakheja S. and Sankar S. (1995). Vibration and shock isolation performance of a semi-Active on-off damper. Transactions of the ASME, Journal of Vibration, Acoustics and Reliability in Design 107.

Rakheja S., Afework Y. and Sankar S. (1994) An analytical and experimental investigation of the driver-seat-suspension system. Vehicle System Dynamics, 23 pp 501-524.

Rakheja S., Sankar S., Ahmed A.K.W. and Bhat R.B. (1987) Ride vibration at the driver seat interface. Report prepared by the Concave Research Centre, Department of Mechanical Engineering, Concordia University, Montreal, Quebec for the Transportation Research Centre.

Ranganathan R. and Sriram K. (1994) Development of a PC-based software for analysis of off-road vehicle seat suspensions. SAE technical paper 941677.

Rayleigh, Lord (John William Strutt) (1877) The theory of sound, Volume 1. New York: reprinted by Dover, 1945, 46-51.

Rebelle, J. (2000) Development of a numerical model of a seat suspension to optimise the end-stop buffers. Presented at the 35th UK Group Meeting on Human Response to Vibration, 13-15th Septemberm held at the Institute of Sound and Vibration Research, University of Southampton, UK.

Resnick, R., Halliday, D. and Krane, K. (1992) Physics. New York: Wiley.

Robertson, C.D. and Griffin M.J. (1989) Laboratory studies of electromyographic response to whole body vibration. Technical report No. 184, Institute of Sound and Vibration Research, The University of Southampton.

Rosegger, R. and Rosegger, S. (1960) Health effects of tractor driving. Journal of Agricultural Engineering Research 5(3) 242.

Saint-Eve, P. and Donati, P.M. (1992) The prevention of dorso-lumbar risks associated with the driving of lift-trucks, seat and lift manufacturers, users. (Prevention des risques dorso-

lumbaires lies a la conduite de chariots elevateurs). Lorraine Assoc. Of Oct. Med. Services (ALSMT) National Institute for Research and Safety (INRS).

Sandover, J. (1981) Vibration, posture amd low back disorders of professional drivers. Report DHS 402. Department of Human Sciences, Loughborough University.

Sandover, J. (1982) Measurements of the frequency response characteristics of man exposed to vibration. Ph.D. Thesis, Loughborough University of Technology.

Sandover, J. (1988) Behaviour of the spine under shock and vibration: a review. Clinical Biomechanics, 3, 249-256.

Sandover, J. and Dupuis, H. (1987) A reanalysis of spinal motion during vibration. Ergonomics 30, 975-985.

Seidel, H. (1988) Myoelectric reactions to ultra-low frequency and low-frequency whole-body vibration. European Journal of Applied Physiology 57: 558-562.

Seidel, H. (1996) A contribution to the revision of ISO 5982 .Mechanical driving point impedance and transmissibility of the human body. Personal communications to A. J. Brammer.

Seidel, H. and Heide R. (1986) Long-term effects of whole-body vibration: a critical survey of the literature. International Archives of Occupational and Environmental Health 58: 1-26.

Seidel, H.; Blüthner, R.; Hinz, B. and Schust, M. (1998) On the health risk of the lumbar spine due to whole-body vibration—theoretical approach, experimental data and evaluation of whole-body vibration. Journal of Sound and Vibration, vol. 215, no. 4, pp. 723-741(19).

Seo (2001) Masters dissertation. Institute of Sound and Vibration Research, University of Southampton, UK.

Shoenberger, R.W. (1975), Subjective response to very low-frequency vibration Aviation, Space and Environmental Medicine 46: 785 – 790.

Shoenberger, R.W. and Harris, C.S. (1971), Psycophysical assessment of whole body vibration Human Factors 13: 41 – 50.

Siegel (1956) Non-parametric statistics for the behavioural sciences. McGraw-Hill.

Sinha, S.; Pope, M.; Broman, H. and Hansson T. (1996) A mathematical model of the impact response of the seated subject. Medical Engineering and Physics, July 1996, vol. 18, no. 5, pp. 410-419(10).

Society of Automotive Engineers (1980) Deflection of seat cushions for off-road work machines. SAE J1051, Jan 80, 327-328.

Society of Automotive Engineers (1983) Vibration performance evaluation of operator seats. SAE J1384, May 83, 334-335.

Society of Automotive Engineers (1986) Classificaion of agricultural wheeled tractors for vibration tests of operator seat. SAE J1386, Jan86, 40.391-394

Sorainen, E.; Penttinen, J. and Kallio, M. (1999) Whole-body vibration of tractor drivers during harrowing. Occupational Health and Industrial Medicine, 1999, vol. 40, no. 1, pp. 33-33(1).

Stayner, R.M. (1971) Aspects of the development of a test code for tractor suspension seats. Journal of Sound and Vibration 20(2), 247-252.

Stayner, R.M. (1972), Aspects Of The Development Of A Test Code For Tractor Suspension Seats Journal of Sound and Vibration, 1972, 20 (2), 247 – 252.

Stayner, R.M. (2001) Whole-body vibration and sock – a literature review (extension of a study of overtravel of seat suspensions). Report prepared for the Health and Safety Executive by RMS Vibration Test Laboratory, 26 Coder Road, Ludlow Business Park, Ludlow, Shropshire, SY8 1XE.

Stayner, R.M. and Bean, A. (1971) Review Of Measurements Of Tractor Suspension Seats 1970/1971 Tractor and Machine Division, National Institute Of Agricultural Engineering, Wrest Park, Silsoe, Bedford. DN/TE/214/1443.

Stein, G.J. (1995a) An electro-pneumatic active suspension for driver's seat for agricultural tractors. Proceedings of 10th International Conference on Noise Control '95, Warsaw, June 20-22.

Stein, G.J. (1995b) Results of investigation of an electro-pneumatic active vibration control system for a driver's seat. Proceedings of the Institution of Mechanical Engineers, Part D, 209, 227-234.

Stein, G.J. (1995c) Review of the investigation of an electro-pneumatic active suspension for driver's seat. Proceedings of the 30th International Acoustics Conference, Slovak Acoustics Association, High Tatras Mountains, Slovakia, June 6-8, 145-150.

Stein, G.J. (1997) A driver's seat with active suspension of electro-pneumatic type. Transactions of the ASME, Vol. 119, 230-235.

Stein, G.J. (1998a) Active electro-pneumatic suspension system. Proceedings of ISMA23, Volume 3, 1311-1317.

Stein, G.J. (1998b) Preliminary investigations of a new active electro-pneumatic suspension system. Vehicle Systems Dynamics Supplement 28, 479-484.

Stein, G.J. and Ballo, I. (1991) Active vibration control system for the driver's seat for off-road vehicles. Vehicle System Dynamics 20, 57-78.

Stein, G.J., Ballo, I. and Gajarsky, M. (1992) Active vibration control system for the driver's seat. Proceedings of the 25th ISATA Silver Jubilee International Symposium of Automotive Technology and Automation Conference on Mechatronics, Florence, 1-5 June, 183-190.

Stevens, S.S. (1975), Psychophysics, New York: Wiley.

Stiles, M.A. (1994) A farmer's daily dose-Part II: Result of the tractor ride vibration survey. UK Informal Group Meeting on Human Response to Vibration, Institute of Naval Medicine, Gosport, 19-21 September.

Suggs, C. W., Stikeleather, L.F. and Abrams, C.F. (1970), Field tests of an active - seat suspension for off - road vehicles Transactions of the ASEA 13 (5) pp 608 – 611.

Suggs, C.W., Abrams, C.F. and Stikeleather, L.F. (1969) Application of a damped spring-mass human vibration simulator in vibration testing of vehicle seats. Ergonomics 01, 68-89.

Suggs, C.W., Stikeleather, L.F., Harrison, J.Y. and Young, R.E, (1969), Application of a dynamic simulator in seat testing Annual meeting of the American Society of Agricultural Engineers, Paper No. 69 - 172, Perdue University, June 22 - 25, 1969.

Surace, C., Storer, D. and Tomlinson, G.R. (1992) Characterising an automotive shock absorber and the dependency on the temperature. 10th International Conference on Modal Analysis, San Diego, California.

Tomlinson, R.W. and Kyle, D.J. (1970), The development of a dynamic model of the seated human operator Departmental note DN/TE/037/1445, Tractor and Machine Performance Division, National Institute Of Agricultural Engineering, Wrest Park, Silsoe, Bedford.

Turner, D. M. (1988), A triboelastic model for the mechanical behaviour of rubber Plastics and Rubber Processing and Applications, Vol 9, No. 4, 1988, pp. 197 – 2011.

Umehara, H., Hikida, R., Kuno, H., Sawa, M., and Uchiyamada, K. (1971) Measurement and display of the load distribution on a vehicle seat. Society of Automotive Engineers, Automotive Engineering Congress, Detroit, 11-15 Janurary 1971. SAE Paper 710042.

van Deursen, D.L.; Lengsfeld, M.; Snijders, C.J.; Evers, J.J.M. and Goossens R.H.M. Mechanical effects of continuous passive motion on the lumbar spine in seating. Journal of Biomechanics, June 2000, vol. 33, no. 6, pp. 695-699(5)

Volterra, V. (1959) Theory of functionals and of integral and integro-differential equations. New Your: Dover Publications Inc.

Wei, L. and Griffin, M.J. (1998) The prediction of seat transmissibility from measured of seat impedance. Journal of Sound and Vibration 214(1), 121-137.

Whitham, E.M. and Griffin, M.J. (1977) Measuring vibration on soft seats. Society of Automotive Engineers Paper No. SAE 770253. International Automotive Engineering Congress and Exposition, Detroit, 28 February - 4 March. Society of Automotive Engineers, Detroit, Michigan.

Worden, K. and Tomlinson, G.R. (1992) Parametric and nonparametric identification of automotive shock absorbers. 10th International Conference on Modal Analysis, San Diego, California.

Wu and Griffin (1995) Simulation study of factors influencing the severity of suspension seat end-stop impacts. Paper presented at the UK Informal Group Meeting on Human Response to Vibration held at t he Silsoe Research Institute, Wrest Park, Silsoe, Bedford MK45 4HS, 18th 20th September.

Wu, X, Rakheja, S. and Boileau, P-É. (1999) Study of human-seat interactions for dynamic comfort analysis. SAE Paper 1999-01-1303, 137-146.

Wu, X. and Griffin, M. J. (1997) A semi-active control policy to reduce the occurrence and severity of end-stop impacts in a suspension seat with an electrorheological fluid damper Journal of Sound and Vibration, 1997, 203 (5) 781 – 793.

Wu, X. and Griffin, M.J. (1996) Towards the standardisation of a testing method for the end-stop impacts of suspension seats. Journal of Sound and Vibration 192(1) 307-319.

Wu, X. and Griffin, M.J. (1998) The influence of end-stop buffer characteristics on the severity of suspension seat end-stop impacts. Journal of Sound and Vibration 215(4) 989-996.

Wu, X., Rakheja, S. and Boileau, P-É. (1996) Distribution of human-seat interface pressure under vertical vibration. Proceedings of the United Kingdom Informal Group Meeting on Human Response to Vibration, held at MIRA, Watling Street, Nuneaton, Warwickshire, 18-20 September.

Wu, X., Wong J.Y., Sturk, M. and Russell, D.L. (1994) Simulation and experimental study of a semi-Active suspension with an electrorheological damper. International Journal of Modern Physics B 7, 2987-3003.

Yao G. Z., Meng, G. and Fang, T. (1995) The characteristics research of electro-rheological fluid and its application for vibration control. Journal of Machine Vibration 3, 121-139.

Yokenawa, Y. and Miwa, T. (1972) Sensational responses of sinusoidal whole-body vibrations with ultra-low frequencies. Industrial Health 10:63-76.

Zach, D.J. (1971) The development of a seat suspension for mobile construction equipment SAE Paper 710515, ER-715-3

Ziegenruecker, G.H. and Magid, E.B. (1959) Short time human tolerance to sinusoidal vibration. WADC Technical Report 59-391. United States Air Force Wright Air Development Center, Wright-Patterson Air Force Base, Ohio.

APPENDIX 1 THE HUMAN SUBJECT CONSENT FORM REQUIRED FOR PARTICIPATION IN A VIBRATION EXPERIMENT

Consent form to be completed by adult subjects who are being paid for their participation in an experiment
(Adults are 18 years of age or older).

Exposure Number: .....

Vibration Experiment Exposure and Consent Form

Before completing this form, please read the 'Information for Subjects' on the reverse side of this sheet.

(i) Name ..... (Mr/Mrs/Miss/)

(ii) Do you have any of the conditions listed on the reverse side of this form?.....

(iii) Have you ever suffered any serious illness or injury? .....

(iv) Are you under medical treatment or suffering disability affecting your daily life? .....

.....

If your answer is 'YES' to questions (ii), (iii) or (iv), please give details to Experimenter.

I understand that for my participation in this experiment I am to be paid the sum of £.....

for my attendance on ..... occasion(s).

DECLARATION

I volunteer to be a subject in a vibration experiment. My replies to the above questions are correct to the best of my belief, and I understand that they will be treated by the experimenter as confidential. I understand that I may at any time withdraw from the experiment and that I am under no obligation to give reasons for withdrawal or to attend again for experimentation.

I undertake to obey the regulations of the laboratory and instructions of the Experimenter regarding safety, subject only to my right to withdraw declared above. The purpose and methods of the research have been explained to me and I have had the opportunity to ask questions.

Signature of Subject ..... Date .....

I confirm that I have explained to the subject the purpose and nature of the investigation which has been approved by the Human Experimentation Safety and Ethics Committee.

Signature of Experimenter ..... Date .....

Medical assistance is available if required.

Cont/...

This form must be submitted to the Secretary of the Human Experimentation Safety and Ethics Committee on completion of the experiment.

Information for Subjects

Persons with any of the following conditions are usually considered unfit for vibration experiments

Active disease of respiratory system: including recent history of coughing-up blood or chest pain.

Active disease of the gastro-intestinal tract: including internal or external hernia, peptic ulcer, recent gall-bladder disease, rectal prolapse, anal fissure, haemorrhoids or pilonidal sinus.

Active disease of the genito-urinary system: including kidney stones, urinary incontinence or retention or difficulty in micturition.

Active disease of the cardiovascular system: including hypertension requiring treatment, angina of effort, valvular disease of the heart, or haemophilia.

Active disease of the musculo-skeletal system: including degenerative or inflammatory disease of the spine, long bones, or major joints or a history of repeated injury with minor trauma.

Active or chronic disease or disorders of the nervous system: including eye and ear disorders and any disorder involving motor control, wasting of muscles, epilepsy or retinal detachment.

Pregnancy: any woman known to be pregnant should not participate as a subject in a vibration experiment.

Mental Health: subjects must be of sound mind and understanding and not suffering from any mental disorder that would raise doubt as to whether their consent to participate in the experiment was true and informed.

Recent trauma and surgical procedures: persons under medical supervision following surgery or traumatic lesions (e.g. fractures) should not participate in vibration experiments.

Prosthesis: persons with internal or external prosthetic devices normally should not participate in vibration experiments (although dentures need not exclude participation in experiments with low magnitudes of vibration).

Other: .....

(For completion by experimenter)

To be completed by the Experimenter:

VIBRATOR:

DESCRIPTION OF VIBRATION: State levels, frequencies, axes, durations etc. (If subject is in direct or indirect control of the vibration level, also state maximum vibration level for each condition.) Indicate subject posture, seat type, etc. and any other factors affecting subject exposure. Description must be sufficient to enable reader to reproduce a similar exposure pattern.

COMMENTS: (If more space is required, please attach a continuation sheet.)

APPENDIX 2 GRAPHS OF SEAT VALUE AND SUSPENSION DISPLACEMENT

Figure 2-2 to Figure 2-10 show the SEAT value (vibration transmitted to the vehicle operator) in the left column of graphs and the positive and negative peak displacements of the suspension mechanism relative to the seat base on the right. Increasing input magnitude expressed in terms of the VDV at the seat base is shown on the x-axis of each graph. The frequency of the input motion (1.25, 1.6 , 2.0, 2.5 and 3.15 Hz) increases down the page.

The 'low', 'med' and 'high' groupings shown on each graph correspond to the seat displacement amplitude defined as follows: 'Low' indicates peak suspension displacement of less than 15mm as indicated by the horizontal dashed lines on the displacement graphs. 'Med' corresponds to higher amplitude suspension displacements without end-stop buffer contact and 'high' corresponds to motions with at least one end-stop buffer contact, with the buffers indicated by the solid horizontal lines on the suspension displacement graphs.

The layout of results is shown in Figure 2-1. Each combination of seat and input waveform is shown on a separate page.

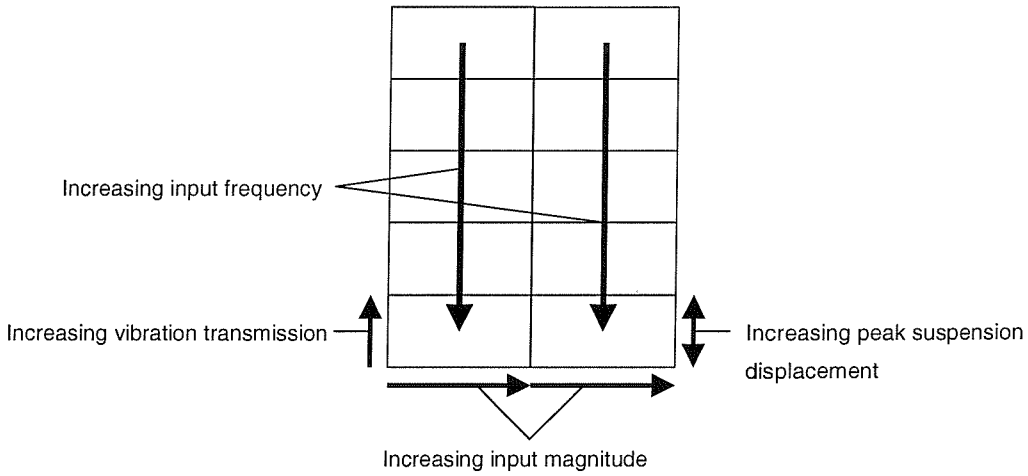

Figure 2-1 Illustration of the layout of results

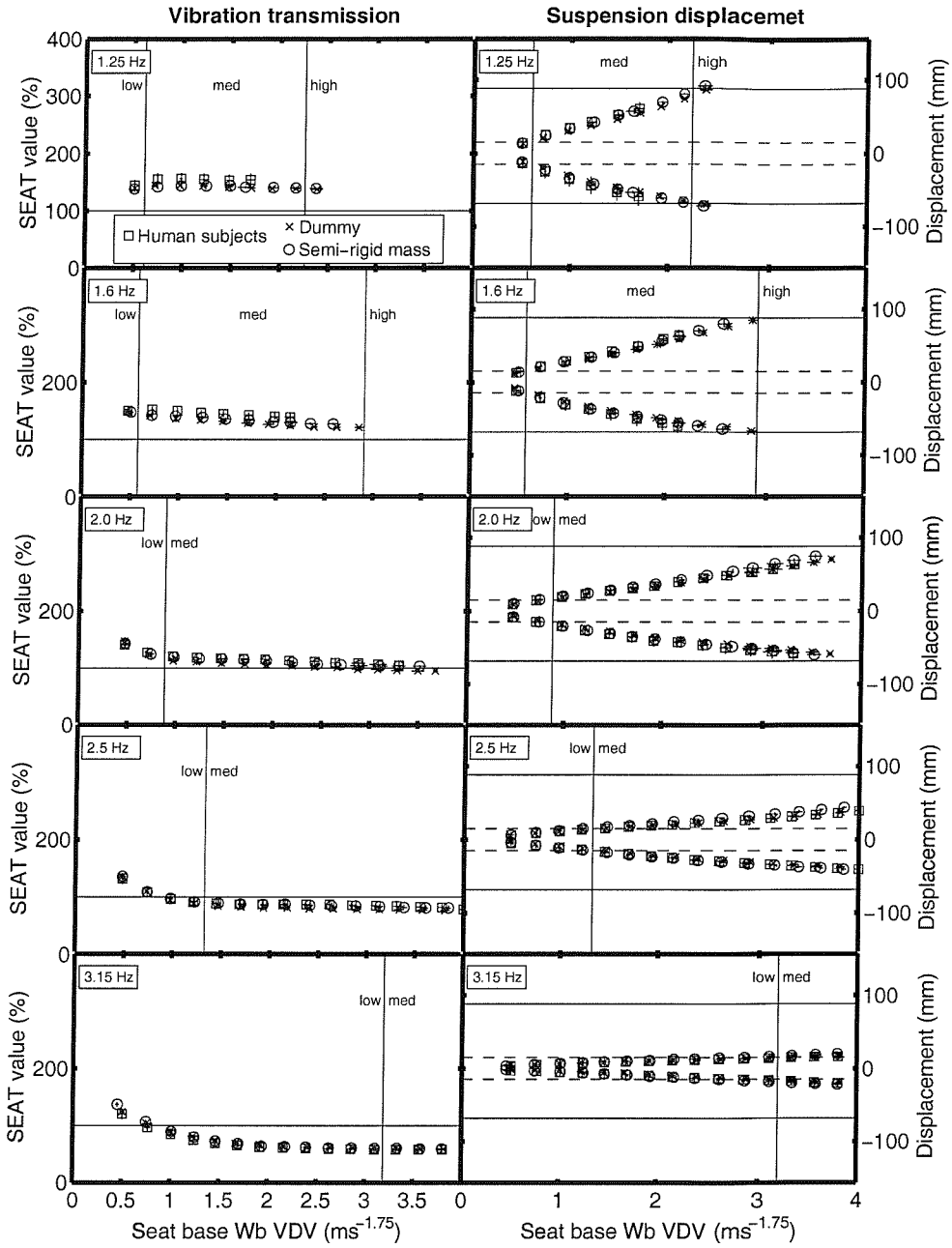

Figure 2-2 Mean SEAT values obtained with 12 subjects and 5 repeat tests with the anthropodynamic dummy and the semi-rigid mass for the **agricultural tractor seat with the 11.5 cycle input motion**. The error bars indicate the inter-quartile range in the x and y axes.

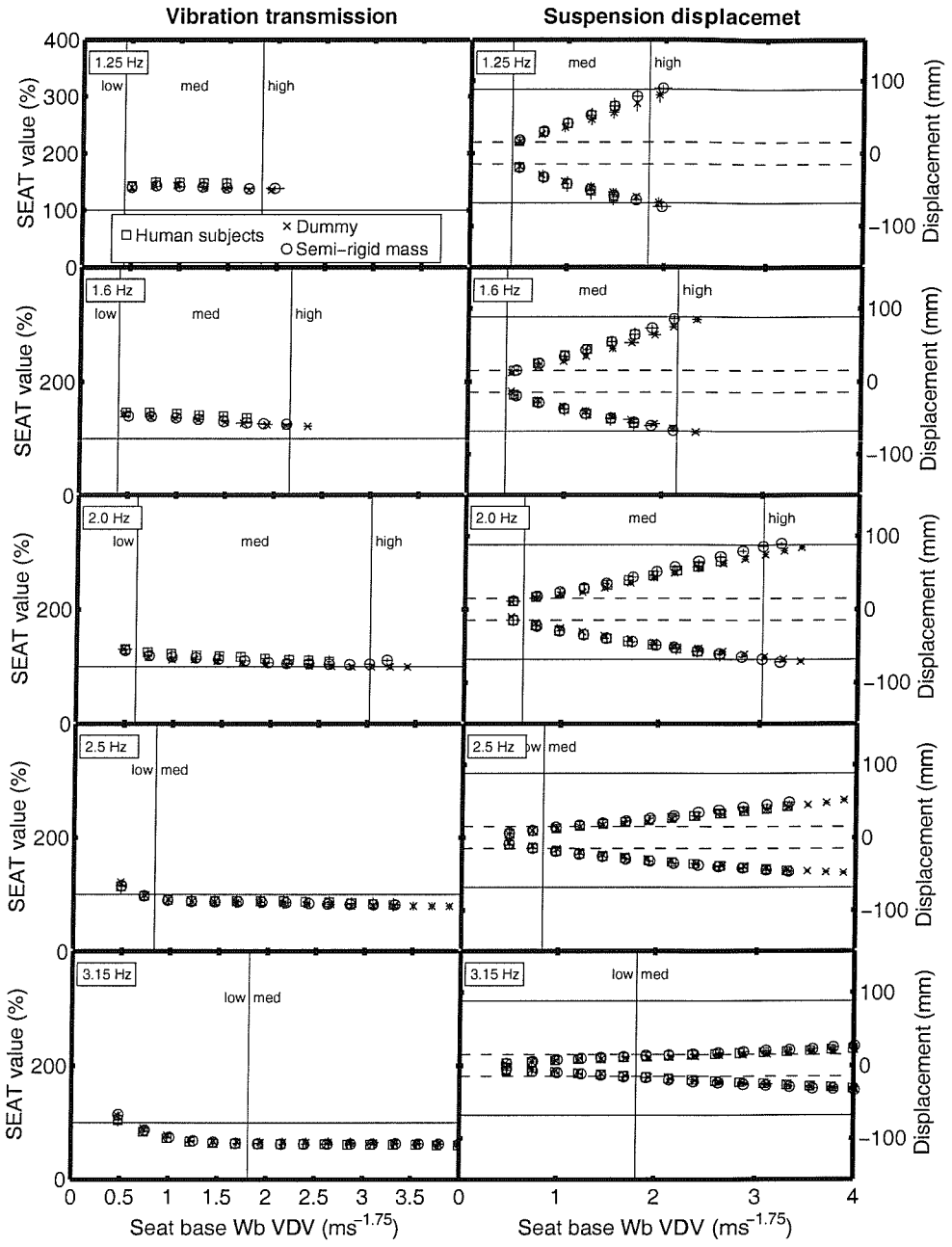

Figure 2-3 Mean SEAT values obtained with 12 subjects and 5 repeat tests with the anthropodynamic dummy and the semi-rigid mass for the **agricultural tractor seat with the 4.5 cycle input motion**. The error bars indicate the inter-quartile range in the x and y axes.

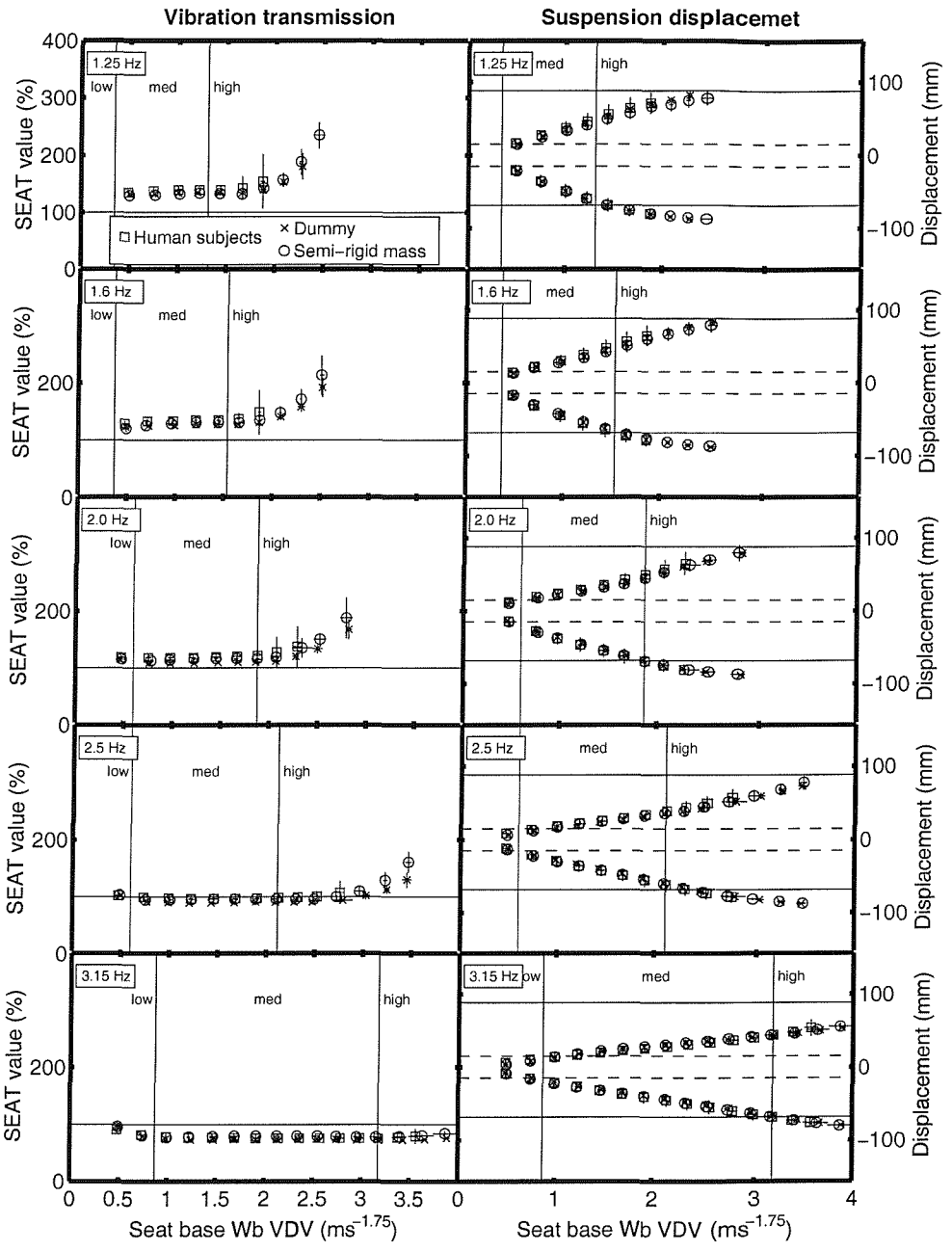

Figure 2-4 Mean SEAT values obtained with 12 subjects and 5 repeat tests with the anthropodynamic dummy and the semi-rigid mass for the **agricultural tractor seat with the 1.5 cycle input motion**. The error bars indicate the inter-quartile range in the x and y axes.

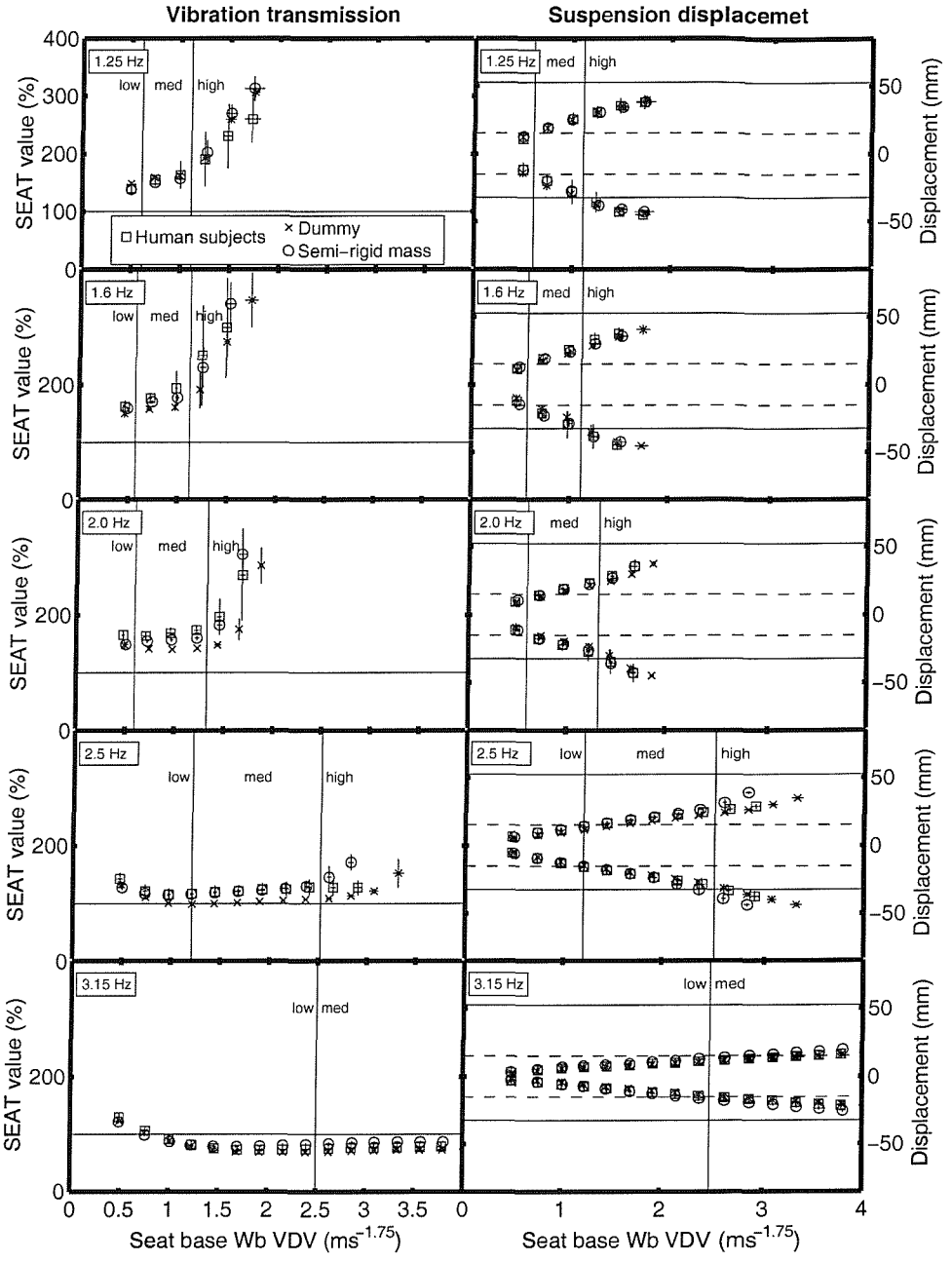

Figure 2-5 Mean SEAT values obtained with 12 subjects and 5 repeat tests with the anthropodynamic dummy and the semi-rigid mass for the **forestry forwarder seat with the 11.5 cycle input motion**. The error bars indicate the inter-quartiie range in the x and y axes.

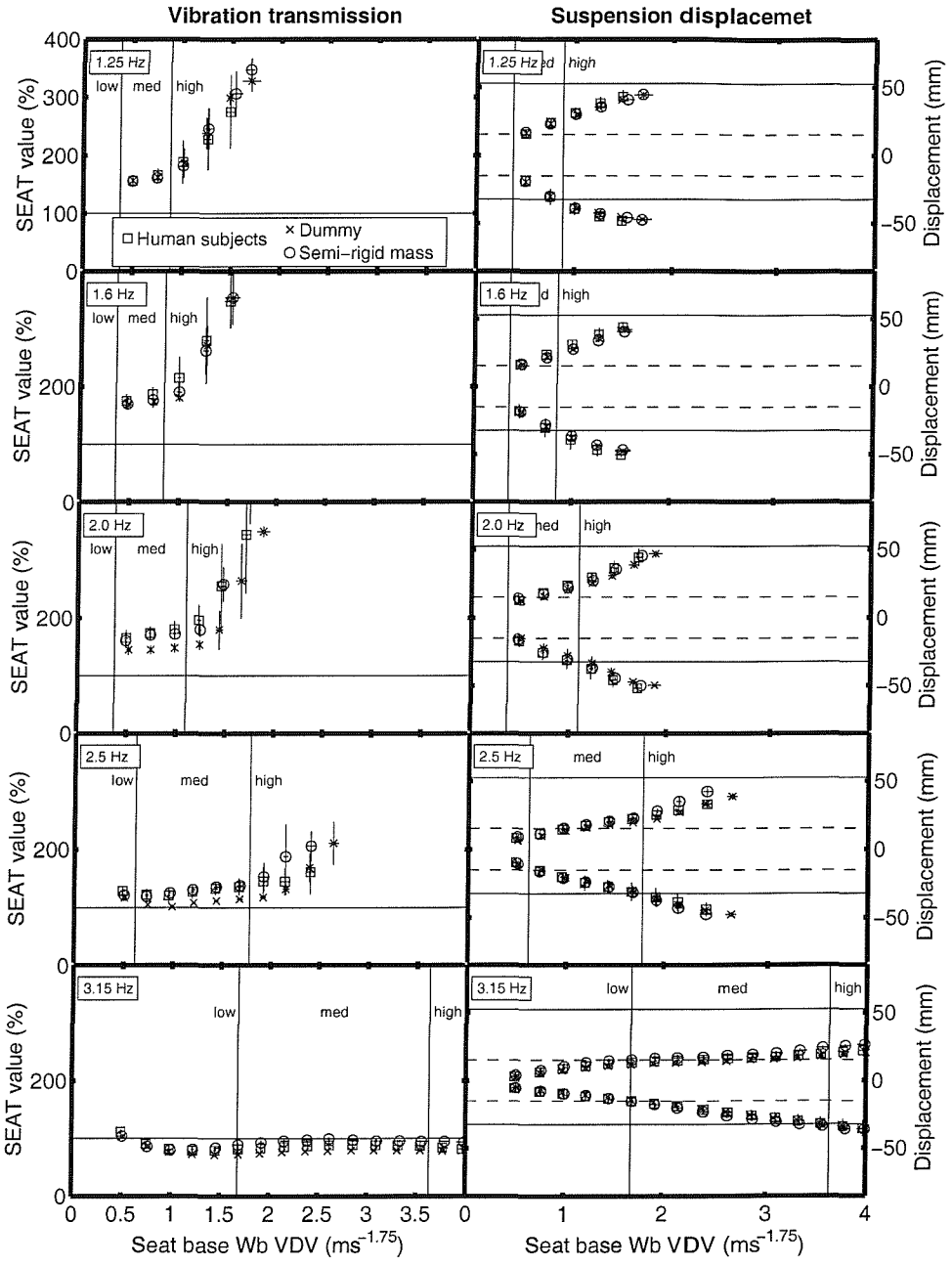

Figure 2-6 Mean SEAT values obtained with 12 subjects and 5 repeat tests with the anthropodynamic dummy and the semi-rigid mass for the **forestry forwarder seat with the 4.5 cycle input motion**. The error bars indicate the inter-quartile range in the x and y axes.

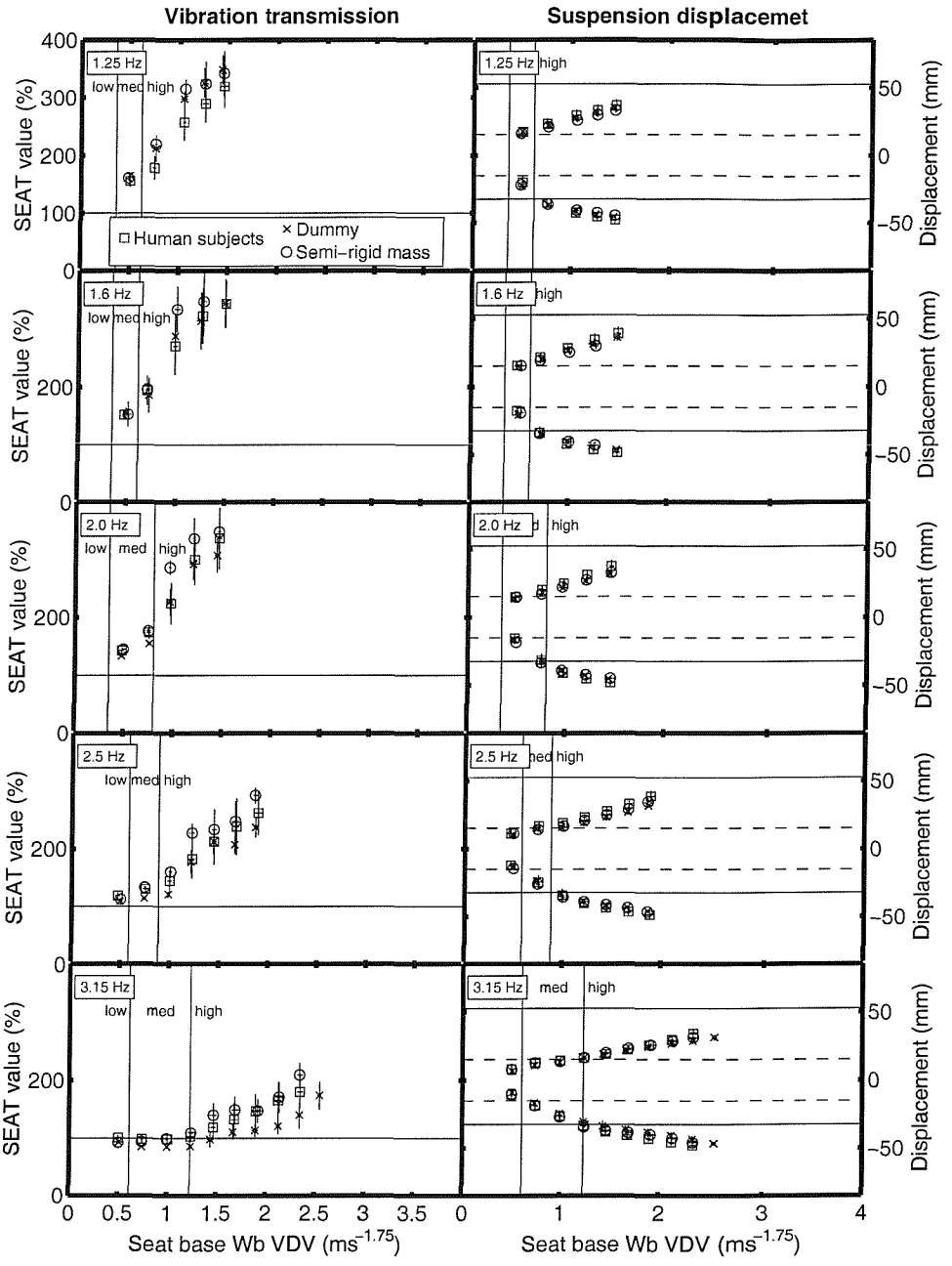

Figure 2-7 Mean SEAT values obtained with 12 subjects and 5 repeat tests with the anthropodynamic dummy and the semi-rigid mass for the **forestry forwarder seat with the 1.5 cycle input motion.** The error bars indicate the inter-quartile range in the x and y axes.

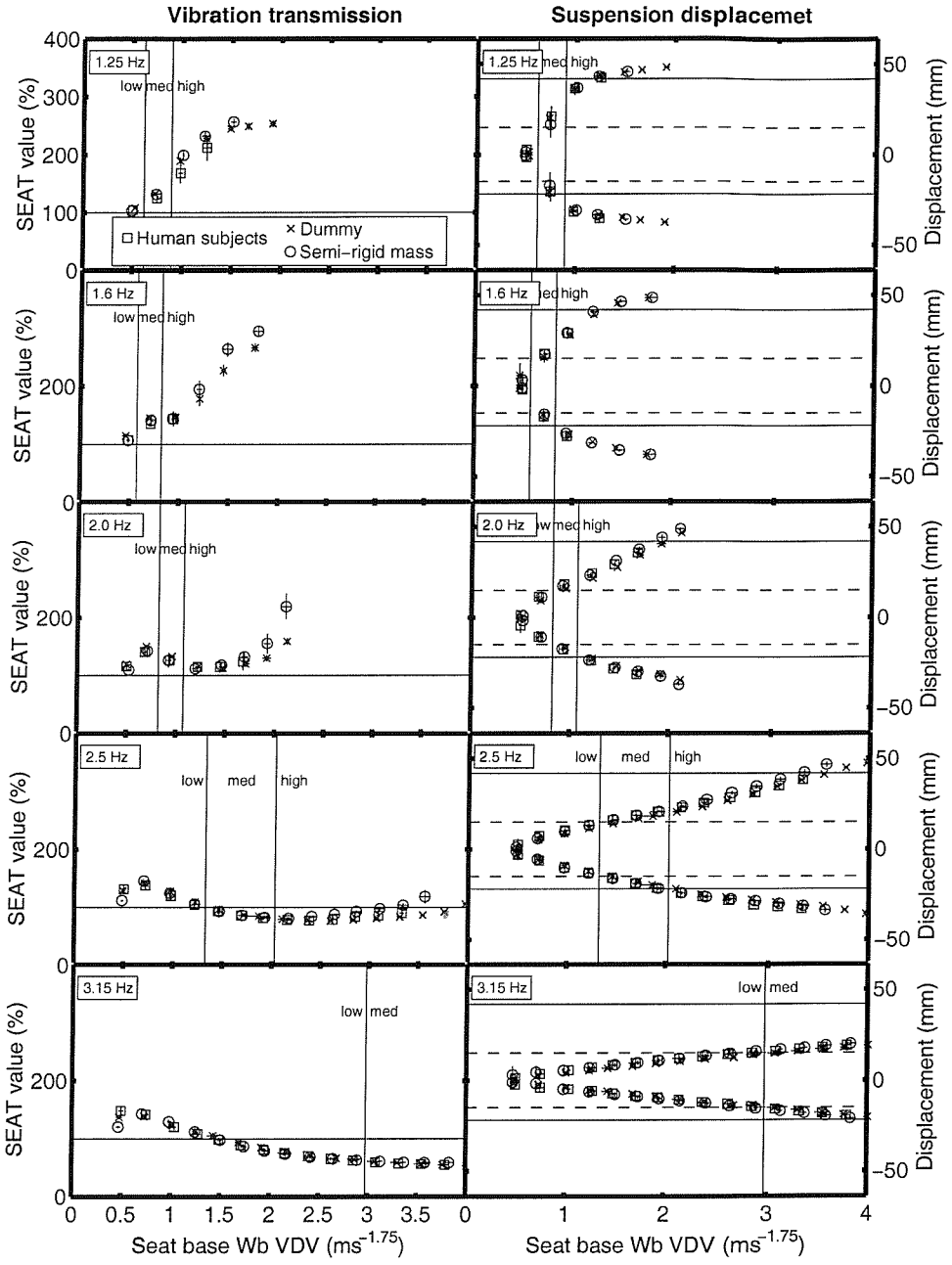

Figure 2-8 Mean SEAT values obtained with 12 subjects and 5 repeat tests with the anthropodynamic dummy and the semi-rigid mass for the **earthmover seat with the 11.5 cycle input motion**. The error bars indicate the inter-quartile range in the x and y axes.

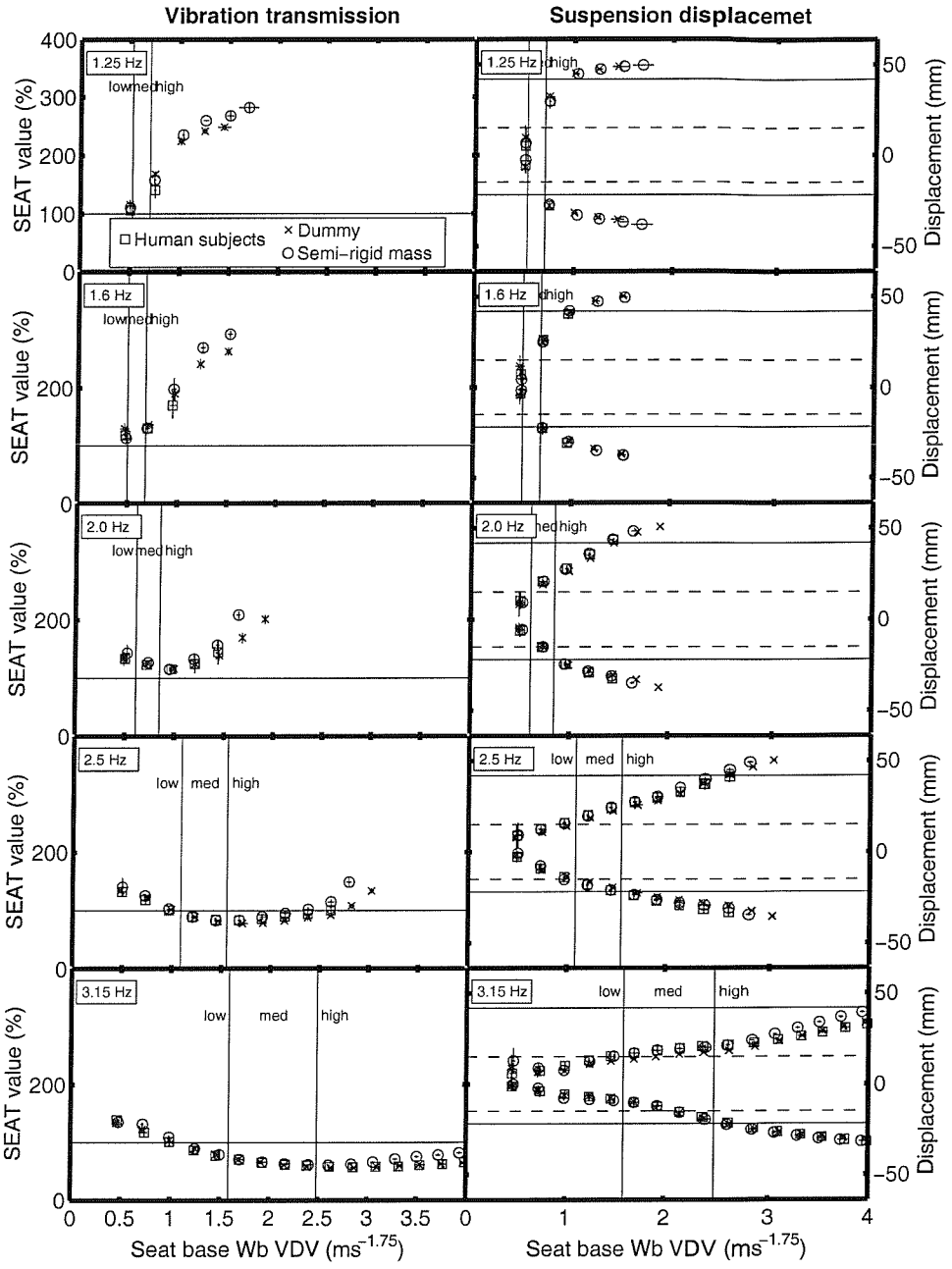

Figure 2-9 Mean SEAT values obtained with 12 subjects and 5 repeat tests with the anthropodynamic dummy and the semi-rigid mass for the earthmover **seat with the 4.5 cycle input motion**. The error bars indicate the inter-quartile range in the x and y axes.

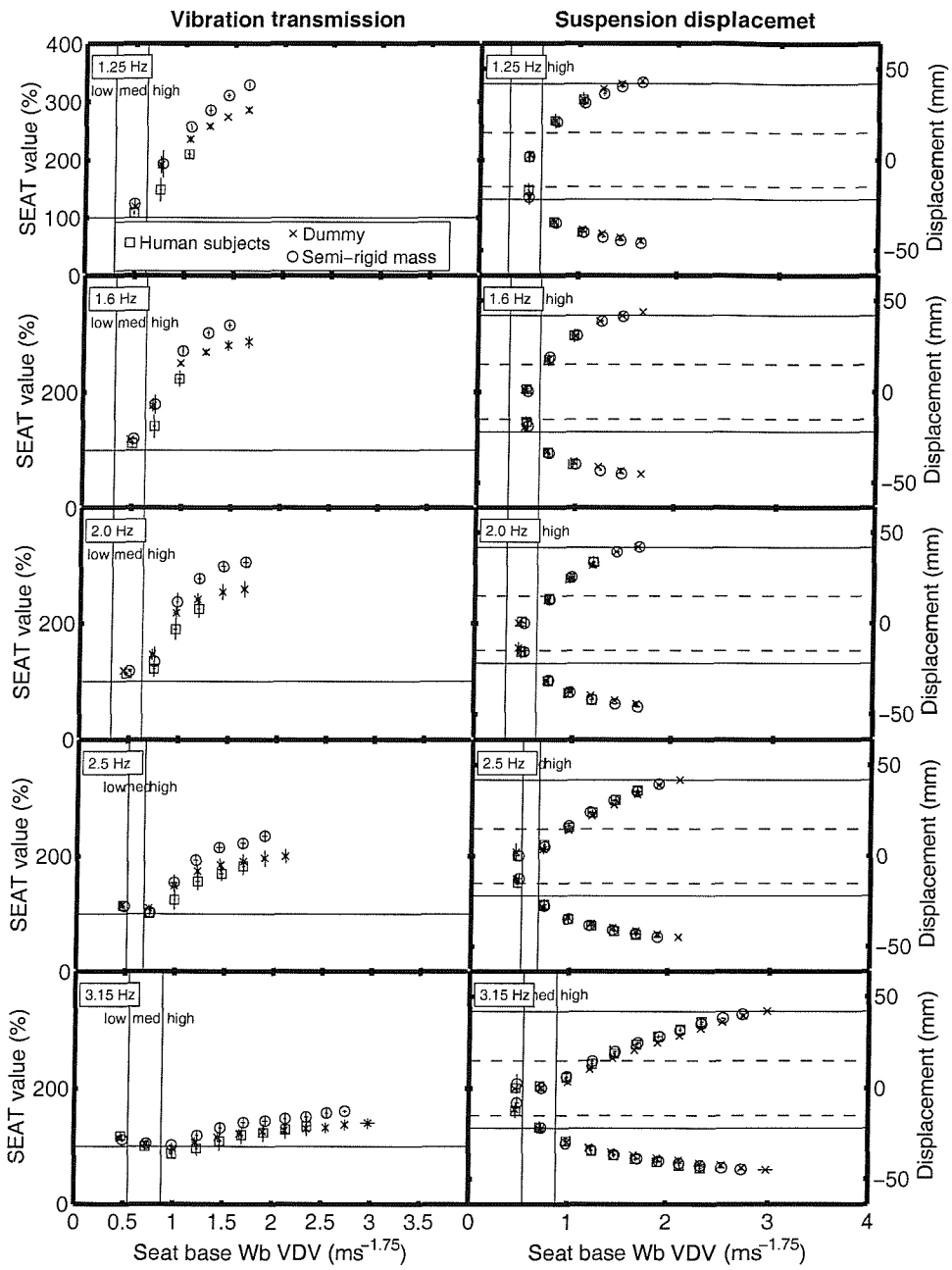

Figure 2-10 Mean SEAT values obtained with 12 subjects and 5 repeat tests with the anthropodynamic dummy and the semi-rigid mass for the **earthmover seat with the 1.5 cycle input motion**. The error bars indicate the inter-quartile range in the x and y axes.

APPENDIX 3 RESULTS OF THE SPEARMAN'S CORRELATION BETWEEN SUBJECT MASS AND SEAT VALUE

A3.1 Overview

The following tables show Spearman's correlation coefficient and the significance (in brackets) testing for correlation between the subject mass and the SEAT value measured in the laboratory for all tests with human subjects.

A3.2 The agricultural tractor seat

Table 3-1 The agricultural tractor seat with the long (11.5 cycle) waveform

Seat base Wb VDV (ms-1.75)	1.25 Hz	1.6 Hz	2.0 Hz	2.5 Hz	3.15 Hz
0.5	0.868 ** (0.001)	0.105 (0.745)	-0.519 (0.084)	-0.611 * (0.035)	-0.565 (0.056)
0.73	0.795 ** (0.003)	-0.039 (0.905)	-0.776 ** (0.005)	-0.653 * (0.021)	-0.719 ** (0.008)
0.97	0.737 ** (0.006)	-0.128 (0.709)	-0.772 ** (0.003)	-0.776 ** (0.005)	-0.758 ** (0.007)
1.20	0.688 * (0.013)	-0.196 (0.540)	-0.761 ** (0.004)	-0.509 (0.091)	-0.642 * (0.024)
1.43	0.526 (0.079)	-0.313 (0.322)	-0.839 ** (0.001)	-0.467 (0.126)	-0.726 ** (0.007)
1.67	0.603 (0.050)	-0.616 * (0.043)	-0.835 ** (0.001)	-0.393 (0.232)	-0.730 ** (0.007)
1.90	. .	-0.698 * (0.012)	-0.934 ** (0.000)	-0.449 (0.143)	-0.674 * (0.016)
2.13	. .	-0.705 * (0.010)	-0.923 ** (0.000)	-0.360 (0.277)	-0.674 * (0.016)
2.37	. .	. .	-0.917 ** (0.000)	-0.396 (0.202)	-0.670 * (0.017)
2.60	. .	. .	-0.863 ** (0.000)	-0.498 (0.119)	-0.688 * (0.013)
2.83	. .	. .	-0.905 ** (0.000)	-0.475 (0.119)	-0.653 * (0.021)
3.07	. .	. .	-0.926 ** (0.000)	-0.635 * (0.026)	-0.639 * (0.025)
3.30	. .	. .	-0.788 ** (0.004)	-0.488 (0.108)	-0.649 * (0.022)
3.53	. .	. .		-0.516 (0.086)	-0.639 * (0.025)
3.77	. .	. .		-0.632 * (0.028)	-0.604 * (0.038)
4.00	. .	. .	. .	-0.638 * (0.047)	-0.614 * (0.034)

*significant at p<0.05, **significant at p<0.01

Table 3-2 The agricultural tractor seat with the medium duration (4.5 cycle) waveform

Seat base Wb VDV (ms-1.75)	1.25 Hz	1.6 Hz	2.0 Hz	2.5 Hz	3.15 Hz
0.5	0.740 ** (0.006)	0.393 (0.206)	-0.835 ** (0.001)	-0.868 ** (0.001)	-0.720 * (0.013)
0.73	0.695 * (0.012)	0.253 (0.428)	-0.874 ** (0.000)	-0.904 ** (0.000)	-0.811 ** (0.001)
0.97	0.589 (0.057)	0.078 (0.821)	-0.951 ** (0.000)	-0.886 ** (0.000)	-0.947 ** (0.000)
1.20	0.579 * (0.049)	0.053 (0.871)	-0.856 ** (0.000)	-0.831 ** (0.002)	-0.888 ** (0.000)
1.43	0.558 (0.059)	0.087 (0.800)	-0.919 ** (0.000)	-0.808 ** (0.003)	-0.916 ** (0.000)
1.67	. .	-0.161 (0.616)	-0.898 ** (0.000)	-0.790 ** (0.004)	-0.849 ** (0.000)
1.90	. .	. .	-0.930 ** (0.000)	-0.831 ** (0.002)	-0.839 ** (0.001)
2.13	. .	. .	-0.867 ** (0.000)	-0.904 ** (0.000)	-0.804 ** (0.002)
2.37	. .	. .	-0.817 ** (0.002)	-0.900 ** (0.000)	-0.807 ** (0.002)
2.60	. .	. .	-0.789 ** (0.002)	-0.900 ** (0.000)	-0.856 ** (0.000)
2.83	. .	. .	. .	-0.909 ** (0.000)	-0.853 ** (0.000)
3.07	. .	. .	. .	-0.918 ** (0.000)	-0.842 ** (0.001)
3.30	. .	. .	. .	-0.932 ** (0.000)	-0.846 ** (0.001)
3.53	. .	. .	. .	. .	-0.839 ** (0.001)
3.77	. .	. .	. .	. .	-0.877 ** (0.000)
4.00	. .	. .	. .	. .	-0.905 ** (0.000)

*significant at p<0.05, **significant at p<0.01

Table 3-3 The agricultural tractor seat with the short (1.5 cycle) waveform

Seat base Wb VDV (ms-1.75)	1.25 Hz	1.6 Hz	2.0 Hz	2.5 Hz	3.15 Hz
0.5	0.544 (0.068)	-0.116 (0.720)	-0.358 (0.253)	-0.765 ** (0.004)	-0.726 ** (0.007)
0.73	0.600 * (0.039)	0.284 (0.371)	-0.263 (0.409)	-0.526 (0.079)	-0.712 ** (0.009)
0.97	0.491 (0.105)	0.372 (0.234)	-0.207 (0.519)	-0.558 (0.059)	-0.825 ** (0.001)
1.20	0.449 (0.143)	0.302 (0.340)	-0.330 (0.295)	-0.642 * (0.024)	-0.846 ** (0.001)
1.43	0.554 (0.061)	0.211 (0.511)	-0.375 (0.229)	-0.600 * (0.039)	-0.870 ** (0.000)
1.67	0.688 * (0.013)	0.262 (0.411)	-0.326 (0.301)	-0.653 * (0.021)	-0.849 ** (0.000)
1.90	0.807 ** (0.002)	0.600 * (0.039)	-0.253 (0.428)	-0.663 * (0.019)	-0.870 ** (0.000)
2.13	. .	. .	-0.049 (0.879)	-0.596 * (0.041)	-0.884 ** (0.000)
2.37	. .	. .	0.463 (0.129)	-0.396 (0.202)	-0.884 ** (0.000)
2.60	. .	. .	. .	-0.354 (0.258)	-0.916 ** (0.000)
2.83	. .	. .	. .	-0.067 (0.837)	-0.870 ** (0.000)
3.07	. .	. .	. .	. .	-0.796 ** (0.002)
3.30	. .	. .	. .	. .	-0.470 (0.123)
3.53	. .	. .	. .	. .	-0.393 (0.206)
3.77	. .	. .	. .	. .	-0.312 (0.323)
4.00	. .	. .	. .	. .	. .

*significant at p<0.05, **significant at p<0.01

A3.3 The forestry forwarder seat

Table 3-4 The forestry forwarder seat with the long (11.5 cycle) waveform

Seat base Wb VDV (ms-1.75)	1.25 Hz	1.6 Hz	2.0 Hz	2.5 Hz	3.15 Hz
0.5	0.446 (0.147)	0.919 ** (0.000)	-0.092 (0.813)	-0.618 * (0.032)	-0.716 ** (0.009)
0.73	0.579 * (0.049)	0.849 ** (0.000)	-0.670 * (0.017)	-0.937 ** (0.000)	-0.667 * (0.018)
0.97	0.507 (0.112)	0.845 ** (0.001)	-0.639 * (0.025)	-0.904 ** (0.000)	-0.660 * (0.020)
1.20	0.598 (0.052)	0.877 ** (0.000)	-0.502 (0.096)	-0.884 ** (0.000)	-0.632 * (0.028)
1.43	0.621 * (0.031)	0.470 (0.171)	0.477 (0.117)	-0.905 ** (0.000)	-0.737 ** (0.006)
1.67	0.177 (0.625)		0.537 (0.072)	-0.958 ** (0.000)	-0.774 ** (0.005)
1.90		. .		-0.926 ** (0.000)	-0.761 ** (0.004)
2.13	. .	. .		-0.932 ** (0.000)	-0.877 ** (0.000)
2.37	. .	. .	. .	-0.922 ** (0.000)	-0.893 ** (0.000)
2.60	. .	. .	. .	-0.937 ** (0.000)	-0.867 ** (0.000)
2.83	. .	. .	. .	-0.875 ** (0.000)	-0.800 ** (0.002)
3.07	. .	. .	. .		-0.768 ** (0.004)
3.30	. .	. .	. .		-0.807 ** (0.002)
3.53	. .	. .	. .	. .	-0.818 ** (0.001)
3.77	. .	. .	. .	. .	-0.758 ** (0.004)
4.00	. .	. .	. .	. .	-0.836 ** (0.001)

*significant at p<0.05, **significant at p<0.01

Table 3-5 The forestry forwarder seat with the medium duration (4.5 cycle) waveform

Seat base Wb VDV (ms-1.75)	1.25 Hz	1.6 Hz	2.0 Hz	2.5 Hz	3.15 Hz
0.5	0.884 ** (0.000)	0.553 (0.078)	-0.330 (0.295)	-0.744 ** (0.006)	-0.477 (0.117)
0.73	0.649 * (0.022)	0.323 (0.306)	-0.661 * (0.027)	-0.836 ** (0.001)	-0.905 ** (0.000)
0.97	0.684 * (0.014)	0.512 (0.089)	-0.333 (0.290)	-0.947 ** (0.000)	-0.937 ** (0.000)
1.20	0.646 * (0.023)	0.628 * (0.029)	0.088 (0.786)	-0.916 ** (0.000)	-0.961 ** (0.000)
1.43	0.663 * (0.019)	0.476 (0.165)	0.407 (0.189)	-0.789 ** (0.002)	-0.940 ** (0.000)
1.67			0.409 (0.241)	-0.702 * (0.011)	-0.944 ** (0.000)
1.90		. .		-0.340 (0.279)	-0.905 ** (0.000)
2.13	. .	. .	. .	0.134 (0.712)	-0.888 ** (0.000)
2.37	. .	. .	. .	-0.032 (0.926)	-0.793 ** (0.004)
2.60	. .	. .	. .	. .	-0.811 ** (0.001)
2.83	. .	. .	. .	. .	-0.926 ** (0.000)
3.07	. .	. .	. .	. .	-0.937 ** (0.000)
3.30	. .	. .	. .	. .	-0.916 ** (0.000)
3.53	. .	. .	. .	. .	-0.891 ** (0.000)
3.77	. .	. .	. .	. .	-0.834 ** (0.001)
4.00	. .	. .	. .	. .	-0.839 ** (0.002)

*significant at p<0.05, **significant at p<0.01

Table 3-6 The forestry forwarder seat with the short (1.5 cycle) waveform

Seat base Wb VDV (ms-1.75)	1.25 Hz	1.6 Hz	2.0 Hz	2.5 Hz	3.15 Hz
0.5	0.681 * (0.015)	0.084 (0.795)	-0.225 (0.483)	-0.646 * (0.023)	-0.519 (0.084)
0.73	0.397 (0.226)	0.007 (0.983)	-0.242 (0.448)	-0.698 * (0.012)	-0.737 ** (0.006)
0.97	0.642 * (0.033)	0.161 (0.616)	0.354 (0.258)	-0.021 (0.948)	-0.870 ** (0.000)
1.20	0.551 (0.063)	0.074 (0.820)	0.165 (0.609)	0.186 (0.563)	-0.425 (0.169)
1.43	0.284 (0.371)	0.009 (0.979)	0.372 (0.234)	0.239 (0.455)	-0.161 (0.616)
1.67		. .		0.372 (0.234)	-0.123 (0.704)
1.90	. .	. .	. .	-0.006 (0.987)	0.018 (0.957)
2.13	. .	. .	. .		0.165 (0.609)
2.37	. .	. .	. .	. .	0.534 (0.090)
2.60	. .	. .	. .	. .	
2.83	. .	. .	. .	. .	
3.07	. .	. .	. .	. .	. .
3.30	. .	. .	. .	. .	. .
3.53	. .	. .	. .	. .	. .
3.77	. .	. .	. .	. .	. .
4.00	. .	. .	. .	. .	. .

*significant at p<0.05, **significant at p<0.01

A3.4 The earthmover seat

Table 3-7 The earthmover seat with the long (11.5 cycle) waveform

Seat base Wb VDV (ms-1.75)	1.25 Hz		1.6 Hz		2.0 Hz		2.5 Hz		3.15 Hz	
0.5	-0.130	(0.687)	0.028	(0.931)	0.027	(0.936)	0.397	(0.226)	0.588	(0.057)
0.73	0.494	(0.103)	-0.583	(0.060)	-0.478	(0.137)	-0.762 *	(0.010)	-0.516	(0.086)
0.97	0.372	(0.234)	-0.611 *	(0.035)	-0.679 *	(0.022)	-0.575	(0.064)	-0.281	(0.377)
1.20	0.827 **	(0.003)	.	.	-0.850 **	(0.004)	-0.320	(0.338)	-0.225	(0.483)
1.43	.	.	.	.	-0.897 **	(0.000)	-0.575	(0.064)	-0.011	(0.974)
1.67	.	.	.	.	-0.856 **	(0.001)	-0.475	(0.140)	0.025	(0.940)
1.90	.	.	.	.	.	.	-0.447	(0.168)	0.000	(1.000)
2.13	.	.	.	.	.	.	-0.822 **	(0.002)	-0.193	(0.548)
2.37	.	.	.	.	.	.	-0.930 **	(0.000)	-0.018	(0.957)
2.60	.	.	.	.	.	.	-0.950 **	(0.000)	-0.279	(0.407)
2.83	.	.	.	.	.	.	-0.909 **	(0.000)	-0.260	(0.415)
3.07	.	.	.	.	.	.	-0.904 **	(0.000)	-0.538	(0.088)
3.30	.	.	.	.	.	.	-0.922 **	(0.000)	-0.509	(0.091)
3.53	.	.	.	.	.	.	.	.	-0.667 *	(0.025)
3.77	.	.	.	.	.	.	.	.	-0.695 *	(0.012)
4.00	.	.	.	.	.	.	.	.	-0.703 *	(0.016)

*significant at p<0.05, **significant at p<0.01

Table 3-8 The earthmover seat with the medium duration (4.5 cycle) waveform

Seat base Wb VDV (ms-1.75)	1.25 Hz		1.6 Hz		2.0 Hz		2.5 Hz		3.15 Hz	
0.5	0.347	(0.269)	-0.147	(0.648)	-0.098	(0.761)	-0.298	(0.346)	0.081	(0.803)
0.73	-0.011	(0.974)	-0.847 **	(0.001)	-0.551	(0.063)	-0.400	(0.198)	-0.337	(0.284)
0.97	.	.	-0.175	(0.585)	-0.860 **	(0.000)	-0.312	(0.323)	-0.393	(0.206)
1.20	.	.	.	.	-0.705 *	(0.010)	-0.288	(0.364)	-0.393	(0.206)
1.43	.	.	.	.	-0.730 **	(0.007)	-0.375	(0.229)	-0.137	(0.672)
1.67	.	.	.	.	.	.	-0.614 *	(0.034)	-0.130	(0.688)
1.90	.	.	.	.	.	.	-0.698 *	(0.012)	-0.168	(0.601)
2.13	.	.	.	.	.	.	-0.839 **	(0.001)	-0.547	(0.065)
2.37	.	.	.	.	.	.	-0.884 **	(0.000)	-0.625 *	(0.030)
2.60	.	.	.	.	.	.	-0.860 **	(0.000)	-0.449	(0.143)
2.83	.	.	.	.	.	.	.	.	-0.923 **	(0.000)
3.07	.	.	.	.	.	.	.	.	-0.926 **	(0.000)
3.30	.	.	.	.	.	.	.	.	-0.842 **	(0.001)
3.53	.	.	.	.	.	.	.	.	-0.888 **	(0.000)
3.77	.	.	.	.	.	.	.	.	-0.888 **	(0.000)
4.00	.	.	.	.	.	.	.	.	-0.868 **	(0.001)

*significant at p<0.05, **significant at p<0.01

Table 3-9 The earthmover seat with the short (1.5 cycle) waveform

Seat base Wb VDV (ms-1.75)	1.25 Hz		1.6 Hz		2.0 Hz		2.5 Hz		3.15 Hz	
0.5	0.326	(0.301)	-0.218	(0.497)	-0.214	(0.504)	-0.621 *	(0.041)	-0.214	(0.504)
0.73	0.428	(0.165)	0.284	(0.371)	0.133	(0.680)	-0.626 *	(0.040)	-0.698 *	(0.012)
0.97	0.656 *	(0.020)	0.491	(0.105)	0.207	(0.519)	0.119	(0.728)	-0.733 **	(0.007)
1.20	.	.	.	.	-0.319	(0.312)	0.066	(0.846)	-0.214	(0.504)
1.43	.	.	.	.	.	.	-0.462	(0.179)	-0.572	(0.052)
1.67	.	.	.	.	.	.	-0.470	(0.144)	-0.598	(0.052)
1.90	.	.	.	.	.	.	.	.	-0.691 *	(0.013)
2.13	.	.	.	.	.	.	.	.	-0.811 **	(0.001)
2.37	.	.	.	.	.	.	.	.	-0.821 **	(0.001)
2.60	.	.	.	.	.	.	.	.	.	.
2.83	.	.	.	.	.	.	.	.	.	.
3.07	.	.	.	.	.	.	.	.	.	.
3.30	.	.	.	.	.	.	.	.	.	.
3.53	.	.	.	.	.	.	.	.	.	.
3.77	.	.	.	.	.	.	.	.	.	.
4.00	.	.	.	.	.	.	.	.	.	.

*significant at p<0.05, **significant at p<0.01

APPENDIX 4: RESULTS OF THE MANN-WHITNEY U-TEST BETWEEN THE SUBJECTS, DUMMY AND SEMI-RIGID MASS

A4.1 Overview

The following tables show the significance of the Mann-Whitney U-test for each combination of loading condition. Bold type indicates no significant difference at the 1% significance level. It should be noted that at the 1% significant level a number of false results were expected due to the large number of tests performed. A reduction in significance level (i.e. using p/N where N is the total number of tests performed) was not possible due to the small number of samples available for each individual comparison, so it should be remembered that on average there will be one false significance for each 100 measurements. The intention of these tests was to identify trends rather than to confirm differences for each individual condition so the presence of a small number of false results was not considered to be important. The results are shown in the following tables for each frequency and magnitude as follows:

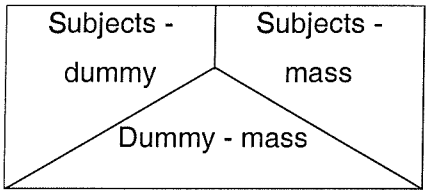

A4.2 The agricultural tractor seat

Table 4-1 The agricultural tractor seat with the long (11.5 cycle) waveform

Base W_b VDV ($ms^{-1.75}$)	Frequency				
	1.25 Hz	1.6 Hz	2.0 Hz	2.5 Hz	3.15 Hz
0.50	.361 .282 .806	.833 .461 .347	.171 .673 .251	.343 .248 .754	.343 *.006*** *.008***
0.73	.047* .019* .142	*.002*** *.006*** .754	.396 .533 .754	.754 .673 .465	.073 .011* .175
0.97	*.008*** .021* 1.000	*.003*** .011* .047*	.029* .598 .014*	.777 .462 .754	.234 .126 .465
1.20	*.008*** .035* .601	*.002*** *.006*** .028*	.058 .628 .142	.598 .833 .465	.126 .140 .347
1.43	*.008*** .052 .221	*.004*** .011* .083*	.045* .833 .016*	.461 1.000 .175	.206 .171 .465
1.67	*.002*** .011* .600	*.002*** *.004*** *.009***	.035* .833 *.009***	.335 .955 .175	.275 .316 .624
1.90	.602	*.002*** *.004*** *.009***	.020* .692 .028*	.171 .916 .117	.292 .430 .327
2.13	.286	*.002*** .011* .014*	.035* .399 .028*	.157 1.000 .086	.343 .461 .602
2.37	.095	*.009***	.020* .342 .047*	.092 .673 .175	.399 .461 .754
2.60		*.009***	.052 .399 .050*	.079 .692 .175	.292 .343 .917
2.83			.035* .399 .012*	.035* .598 .175	.399 .399 .917
3.07			.027* .598 *.009***	.058 .673 .347	.292 .343 .917
3.30			.036* .036* *.009***	.114 .598 .347	.292 .461 .917
3.53			*.009***	.114 .673 .251	.527 .399 .917
3.77				.206 .874 .175	.808 .598 .806
4.0				.624 .391 .076	.396 .399 1.000

* difference is significant at 5%
** difference is significant at 1%

Table 4-2 The agricultural tractor seat with the medium duration (4.5 cycle) waveform

Base W_b VDV ($ms^{-1.75}$)	Frequency				
	1.25 Hz	1.6 Hz	2.0 Hz	2.5 Hz	3.15 Hz
0.50	.399 .461 .917	.527 .058 .347	.916 .527 .347	.234 .692 .175	.100 .126 .917
0.73	.206 .206 .917	.058 .045* .917	.020* .206 .175	.692 .777 .917	.058 .246 .251
0.97	.433 .157 .462	.047* .062 .602	.027* .461 .117	.955 .692 .602	.092 .343 .175
1.20	.027* .092 .465	.020* .020* .754	.090 .268 .327	1.000 .692 .465	.171 .461 .465
1.43	.045* .073 .754	*.003*** *.002*** .602	.045* .246 .465	.692 .777 .602	.206 .343 .917
1.67	.462	*.004*** *.008*** .917	.035* .171 .465	.396 .777 .602	.343 .461 .917
1.90	.251	.465	.045* .206 .602	.396 .955 .602	.343 .467 .806
2.13		.050*	.073 .399 .602	.282 .865 .602	.399 .461 .917
2.37			.047* .234 .465	.396 .865 .602	.399 .527 .917
2.60			.092 .673 .465	.777 .777 .602	.527 .673 .754
2.83			.117	.586 .865 .456	.527 .493 .602
3.07			.117	.865 .865 .602	.461 .461 .602
3.30			.016*	.777 .777 .463	.461 .461 .602
3.53					.527 .396 .624
3.77					.628 .206 .221
4.0					.292 .225 .624

* difference is significant at 5%
** difference is significant at 1%

Table 4-3 The agricultural tractor seat with the short (1.5 cycle) waveform

Base W_b VDV ($ms^{-1.75}$)	Frequency				
	1.25 Hz	1.6 Hz	2.0 Hz	2.5 Hz	3.15 Hz
0.50	**.343** | .035* / .047*	**.058** | .027* / **.754**	**.343** | **.399** / **.347**	**.916** | **.544** / **.624**	**.092** | **.171** / **.754**
0.73	**.058** | .011* / **.175**	*.008*** | .011* / **.347**	*.002*** | **.058** / .016*	*.004*** | **.073** / *.009***	**.140** | **.752** / **175**
0.97	**.092** | .020* / **.465**	*.006*** | .045* / .028*	*.003*** | **.206** / *.009***	.015* | **.292** / *.009***	**.092** | **.461** / .016*
1.20	**.082** | **.073** / **.754**	*.004*** | **.058** / *.009***	*.003*** | **.399** / *.009***	.015* | **.598** / *.009***	**.058** | **.292** / *.009***
1.43	**.073** | .035* / **.602**	.018* | **.092** / *.009***	*.006*** | **.399** / *.009***	.035* | **.752** / *.009***	**.092** | **.140** / *.009***
1.67	**.171** | .045* / **.347**	*.006*** | **.114** / .028*	*.006*** | **.246** / *.009***	.035* | **.598** / *.009***	**.114** | .045* / *.009***
1.90	**.673** | **.628** / **.462**	**.058** | **.527** / **.347**	.015* | **.268** / *.009***	.035* | **.527** / *.009***	**.246** | .045* / *.009***
2.13	**.754**	**.465**	*.008*** | **.399** / .047*	.045* | **.247** / *.009***	**.343** | .045* / *.009***
2.37	**.465**	**.175**	**.114** | **.527** / **.075**	.035* | **.332** / .014*	**.292** | .045* / *.009***
2.60		**.347**	.028*	.020* | **.339** / .016*	**.462** | **.100** / *.009***
2.83			**.462**	.015* | **.527** / *.009***	**.140** | **.092** / *.009***
3.07				**.076**	**.140** | **.206** / .016*
3.30				.028*	**.146** | **.206** / .027*
3.53				.050*	**.092** | **.225** / .014*
3.77					**.171** | **.114** / .016*
4.0					.028*

* difference is significant at 5%
** difference is significant at 1%

A4.3 The forestry forwarder seat

Table 4-4 The forestry forwarder seat with the long (11.5 cycle) waveform

Base W_b VDV ($ms^{-1.75}$)	Frequency				
	1.25 Hz	1.6 Hz	2.0 Hz	2.5 Hz	3.15 Hz
0.50	.058 .916 .047*	.058 1.000 .009**	.021* .004** .806	.045* .011* .117	.018* .008** .347
0.73	.140 .246 .016*	.003** .171 .009**	.002** .035* .009**	.073 .598 .009**	.140 .011* .047*
0.97	.234 .610 .047*	.004** .336 .009**	.002** .027* .009**	.006** .777 .009**	.275 .171 .389
1.20	.282 .126 .465	.079 .777 .117	.002** .006** .009**	.002** 1.000 .009**	.527 .916 .251
1.43	.114 .114 .251	.462 .462 .028*	.002** .343 .009**	.002** .673 .009**	.461 .292 .009**
1.67	.020* .020* .754		.006** .275 .014*	.002** .752 .009**	.336 .100 .009**
1.90				.002** .673 .009**	.292 .058 .009**
2.13				.004** .955 .009**	.399 .058 .009**
2.37				.008** .695 .014*	.399 .020* .009**
2.60				.011* .092 .014*	.399 .020* .009**
2.83				.011* .004** .014*	.343 .073 .009**
3.07					.527 .045* .009**
3.30					.292 .035* .009**
3.53					.246 .058 .009**
3.77					.206 .027* .009**
4.0					.240 .100 .014*

* difference is significant at 5%
** difference is significant at 1%

Table 4-5 The forestry forwarder seat with the medium duration (4.5 cycle) waveform

Base W_b VDV ($ms^{-1.75}$)	Frequency				
	1.25 Hz	1.6 Hz	2.0 Hz	2.5 Hz	3.15 Hz
0.50	**.673** **.292** **.917**	.047* **.282** **.917**	*.008*** **.598** .028*	.011* .045* .050*	*.006*** *.006*** **.754**
0.73	**.598** **.598** **.917**	.045* **.140** **.917**	*.002*** **.533** *.009***	*.002*** **.462** *.009***	.027* .018* **.917**
0.97	**.833** **.833** **.754**	.027* **.171** **.602**	*.002*** **.171** *.009***	.011* **.140** *.009***	.045* **.461** .047*
1.20	**.598** **.527** **.754**	**.752** **.833** **.917**	*.003*** **.171** *.009***	*.008*** **.399** *.009***	**.058** **.399** *.009***
1.43	**.343** **.343** **.754**	**.806** **.713** **.754**	.020* **.598** .016*	*.002*** **.833** *.009***	**.058** **.206** *.009***
1.67			**.142** **.462** .016*	*.006*** **.752** *.009***	.035* **.114** *.009***
1.90				.011* **.527** *.009***	.020* .020* *.009***
2.13				**.540** **.111** .016*	*.004*** .011* *.009***
2.37				**.533** **.073** **.101**	.011* .036* *.009***
2.60					.011* **.052** .014*
2.83					.020* .045* *.009***
3.07					.045* .045* *.009***
3.30					**.073** .035* *.009***
3.53					**.140** .035* *.009***
3.77					**.282** .011* *.009***
4.0					**.462** .011* .025*

* difference is significant at 5%
** difference is significant at 1%

Table 4-6 The forestry forwarder seat with the short (1.5 cycle) waveform

Base W_b VDV ($ms^{-1.75}$)	Frequency				
	1.25 Hz	1.6 Hz	2.0 Hz	2.5 Hz	3.15 Hz
0.50	**.140** **.292** **.117**	**.833** **.527** **.917**	*.002*** **.343** *.009***	*.003*** .020* .028*	.011* *.006*** **.602**
0.73	.015* *.006*** **.347**	**.461** **.752** **.602**	*.002*** **.461** *.009***	*.002*** **.140** *.009***	*.002*** **.092** *.009***
0.97	.036* *.006*** **.117**	**.673** .035* **.076**	**.673** *.006*** *.009***	*.002*** .035* *.009***	*.002*** **.527** *.009***
1.20	.027* **.114** **.754**	**.752** **.292** **.175**	**.752** **.092** .047*	**.916** .015* *.009***	*.002*** **.140** *.009***
1.43	**.140** **.246** **.917**	**.777**	**.140** **.527** .047*	**.598** **.246** **.209**	.035* **.114** .016*
1.67				**.078** **.598** .028*	**.114** **.246** .028*
1.90				**.221** **.157** .014*	.035* **.916** .028*
2.13					.011* **.752** .016*
2.37					.020* **.090** .014*
2.60					
2.83					
3.07					
3.30					
3.53					
3.77					
4.0					

* difference is significant at 5%
** difference is significant at 1%

A4.4 The earthmover seat

Table 4-7 The earthmover seat with the long (11.5 cycle) waveform

Base W_b VDV ($ms^{-1.75}$)	Frequency				
	1.25 Hz	1.6 Hz	2.0 Hz	2.5 Hz	3.15 Hz
0.50	.002** .015* .009**	.002** .140 .009**	.100 .036* .009**	.433 .002** .014*	.036* .002** .009**
0.73	.058 .027* .675	.004** .047* .251	.003** .396 .047*	.178 .027* .175	.527 .292 .117
0.97	.045* .015* .086	.461 .673 .602	.027* .692 .917	.062 .336 .754	.045* .003** .117
1.20	.111 .066 .602	.221	.739 .463 .175	.062 .692 .251	.045* .246 .602
1.43	.027*	.009**	.610 .610 .251	.079 .777 .251	.035* .598 .047*
1.67		.009**	.610 .282 .059	.794 .610 1.000	.058 .343 .047*
1.90			.027*	.151 .396 1.000	.100 .308 .076
2.13			.009**	.336 .027* .251	.206 .292 .117
2.37				.713 .020* .009**	.206 .246 .175
2.60				.533 .015* .009**	.697 .734 .881
2.83				.327 .037* .009**	.052 .833 .086
3.07				.610 .027* .009**	.157 .610 .465
3.30				.336 .047* .009**	.429 .246 .602
3.53				.009**	.777 .036* .028*
3.77					1.000 .015* .009**
4.0					.692 .011** .009*

* difference is significant at 5%
** difference is significant at 1%

Table 4-8 The earthmover seat with the medium duration (4.5 cycle) waveform

Base W_b VDV ($ms^{-1.75}$)	Frequency				
	1.25 Hz	1.6 Hz	2.0 Hz	2.5 Hz	3.15 Hz
0.50	.027* .461 .117	.027* .206 .047*	.598 .058 .076	.673 .073 .175	.171 .343 .602
0.73	*.006*** .027* .076	.027* .193 .047*	.396 .275 .564	.206 .027* .347	.140 *.003*** *.009***
0.97	.076	.092 .035* .347	.903 1.000 1.000	.343 .246 .602	.461 .035* .117
1.20	.014*	*.009***	.916 .292 .175	.833 .752 .917	.399 .246 .917
1.43	*.009***	.014*	.833 .171 *.009***	.206 .916 .076	.673 .628 .806
1.67			*.009***	.045* .399 *.009***	.833 .916 .917
1.90				.073 .292 *.009***	.598 .833 .754
2.13				.206 .140 *.009***	.752 .171 .094
2.37				.206 .146 .014*	.092 .092 *.009***
2.60				.399 .027* *.009***	.114 .035* *.009***
2.83				.014*	.916 *.004*** *.009***
3.07					.292 *.005*** .014*
3.30					.399 *.002*** *.009***
3.53					.527 *.002*** *.009***
3.77					.673 *.002*** *.009***
4.0					.610 *.002*** *.009***

* difference is significant at 5%
** difference is significant at 1%

Table 4-9 The earthmover seat with the short (1.5 cycle) waveform

Base W_b VDV ($ms^{-1.75}$)	Frequency				
	1.25 Hz	1.6 Hz	2.0 Hz	2.5 Hz	3.15 Hz
0.50	.002** .002** .117	.011* .008** .347	.020* .020* .602	.777 .533 .754	.114 .045* .602
0.73	.004** .002** .917	.004** .004** .754	.006** .171 .175	.011* .514 .086	.073 .140 .917
0.97	.002** .002** .009**	.004** .002** .009**	.015* .002** .076	.020* .011* .602	.020* .002** .076
1.20	.009**	.009**	.045* .002** .009**	.036* .002** .028*	.092 .008** .117
1.43	.014*	.009**	.009**	.050* .002** .009**	.399 .011* .016*
1.67	.025*		.009**	.193 .002** .009**	.955 .006** .009**
1.90				.009**	.833 .008** .009**
2.13					.673 .020* .009**
2.37					.460 .045* .009**
2.60					.009**
2.83					.025*
3.07					
3.30					
3.53					
3.77					
4.0					

* difference is significant at 5%
** difference is significant at 1%

APPENDIX 5: THE THEORETICAL MODEL BLOCK DIAGRAM

The following pages contain the SIMULINK block diagram of the seat model as used for the sensitivity analysis in Chapter 12. The model structure is as described in Chapter 8 with the additional elements introduced in Chapter 9 and Chapter 11. Some additional elements that were investigated but not validated and therefore not used in the final model version, such as non-linear end-stop buffer damping, are shown in the block diagram but are disconnected from or switched out of the model.

The block diagram expects to find the seat component coefficients (shown in the GUI in Chapter 9) as capitalized global variables. These values and other constants used by the model are shown in the light colored square blocks. The top level is the first window shown (Page 1/102) named 'tgseatmodel. The name of each sub-diagram is shown at the top of each window.

The model accepts the input time history "c:\winmodel\run\inputaccel.mat" in two column Matlab format (time and acceleration). The model outputs two files named 'accelout.mat' and 'dispout.mat' (page 11/102). Each contains a matrix in Matlab format and contains time as the first column. The 'dispout.mat' file contains the relative displacement across the suspension, the cushion, and the human body model as a further three columns. The 'accelout.mat' matrix contains the acceleration of the base and of each mass in a further four columns.

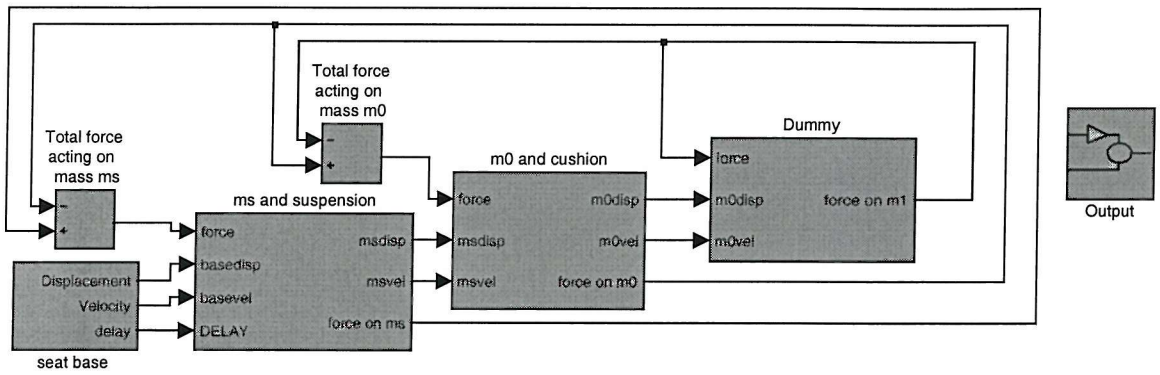
Total force
acting on
mass ms
Total force
acting on
mass m0
ms and suspension
m0 and cushion
Dummy
force
basedisp
basevel
DELAY
msdisp
msvel
force on ms
force
msdisp
msvel
m0disp
m0vel
force on m0
force
m0disp
m0vel
force on m1
Displacement
Velocity
delay
seat base
Output

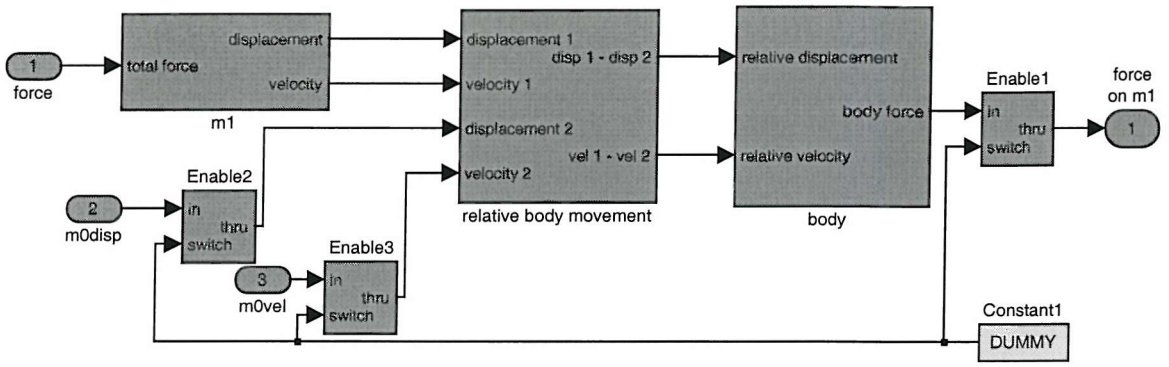
1
force
total force
displacement
velocity
m1
displacement 1
disp 1 - disp 2
velocity 1
displacement 2
vel 1 - vel 2
velocity 2
relative body movement
relative displacement
body force
relative velocity
body
Enable1
in
thru
switch
force
on m1
1
2
m0disp
Enable2
in
thru
switch
3
m0vel
Enable3
in
thru
switch
Constant1
DUMMY

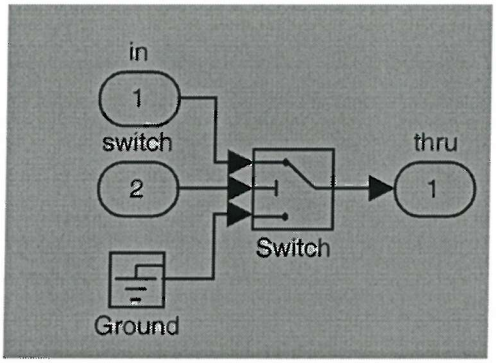
in
1
switch
2
Switch
thru
1
Ground

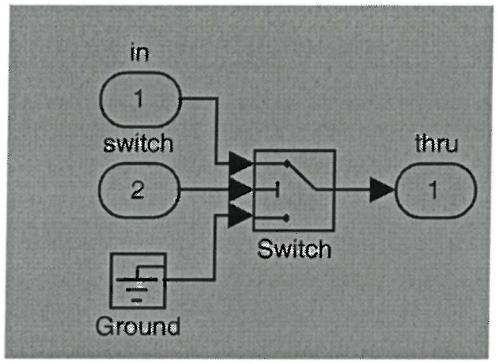
in
1
switch
2
Switch
thru
1
Ground

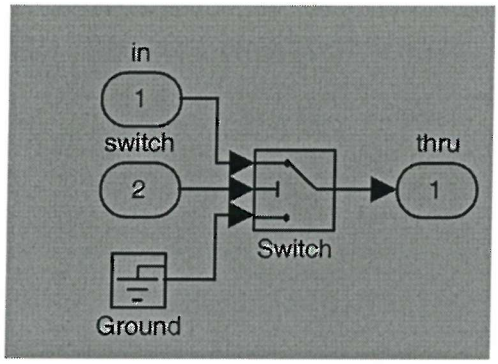
in
1
switch
2
Switch
thru
1
Ground

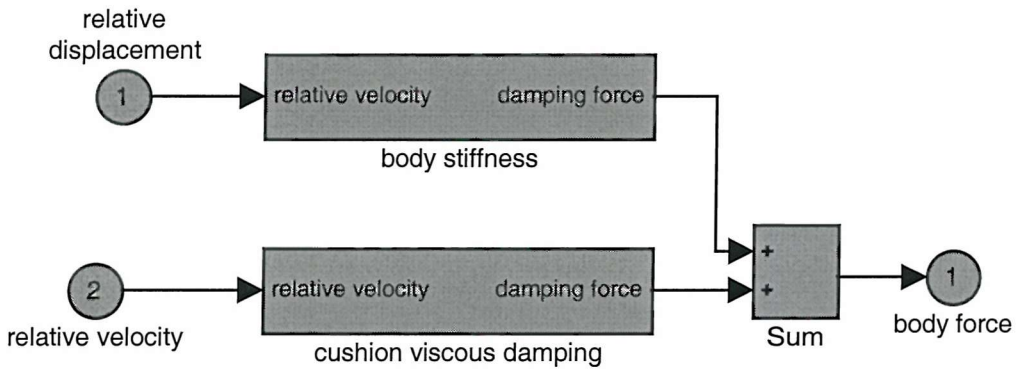
relative
displacement
1
relative velocity
damping force
body stiffness
2
relative velocity
relative velocity
damping force
cushion viscous damping
+
+
Sum
1
body force

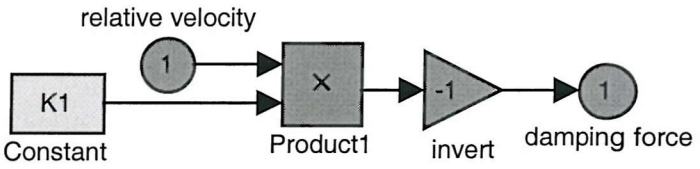
relative velocity
1
K1
Constant
X
Product1
-1
invert
1
damping force

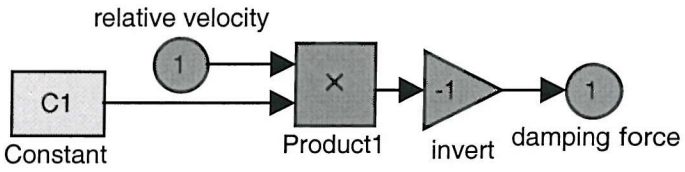
relative velocity
1
C1
Constant
×
Product1
-1
invert
1
damping force

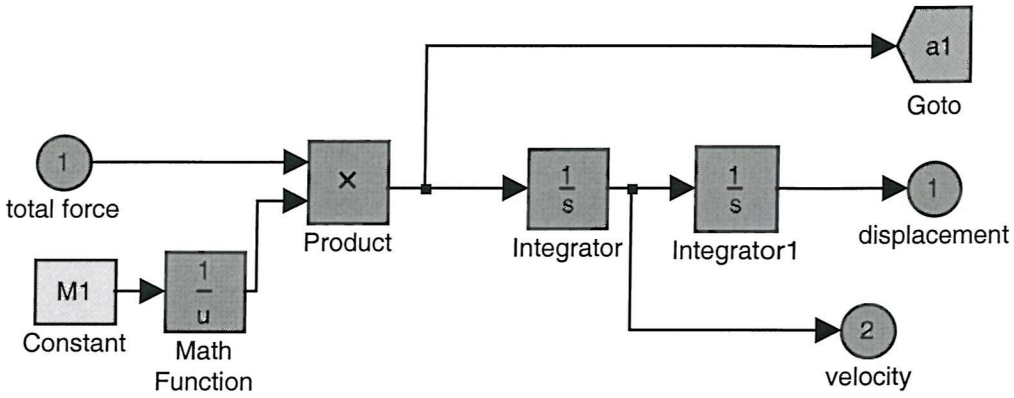
a1
Goto
1
total force
×
Product
1
s
Integrator
1
s
Integrator1
1
displacement
M1
Constant
1
u
Math
Function
2
velocity

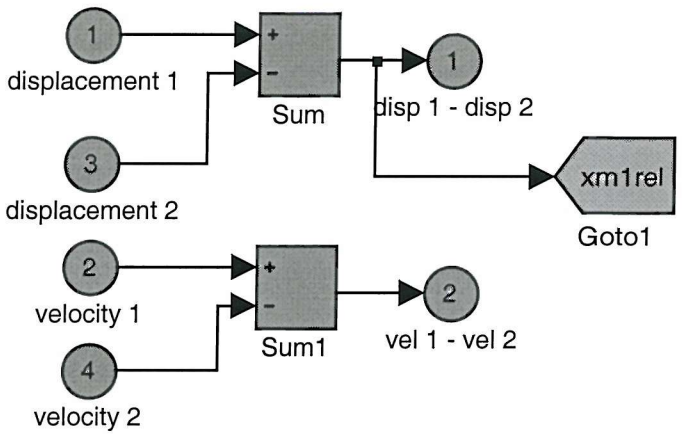
1
displacement 1
3
displacement 2
+
-
Sum
1
disp 1 - disp 2
xm1rel
Goto1
2
velocity 1
4
velocity 2
+
-
Sum1
2
vel 1 - vel 2

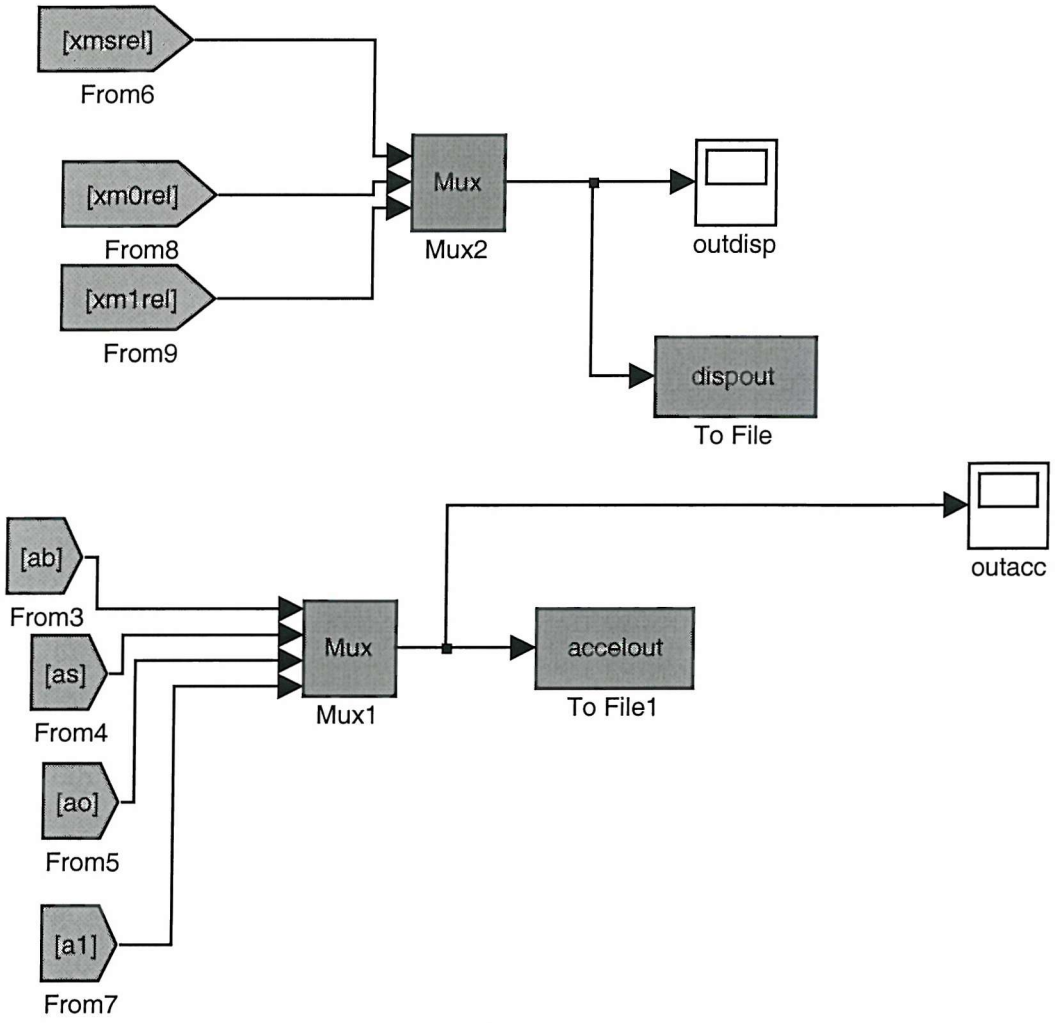
[xmsrel]
From6
[xm0rel]
From8
[xm1rel]
From9
Mux
Mux2
outdisp
dispout
To File
[ab]
From3
[as]
From4
[ao]
From5
[a1]
From7
Mux
Mux1
accelout
To File1
outacc

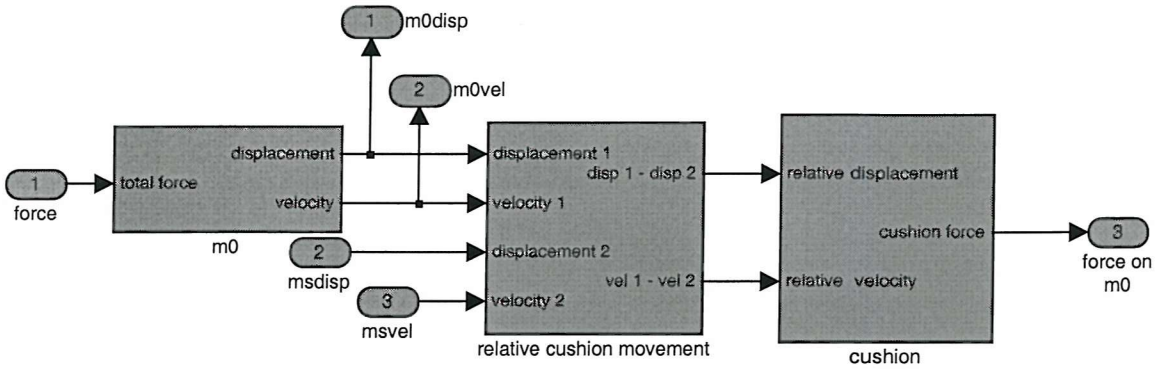
1
m0disp
2
m0vel
1
force
total force
displacement
velocity
m0
2
msdisp
3
msvel
displacement 1
disp 1 - disp 2
velocity 1
displacement 2
vel 1 - vel 2
velocity 2
relative cushion movement
relative displacement
cushion force
relative velocity
cushion
3
force on
m0

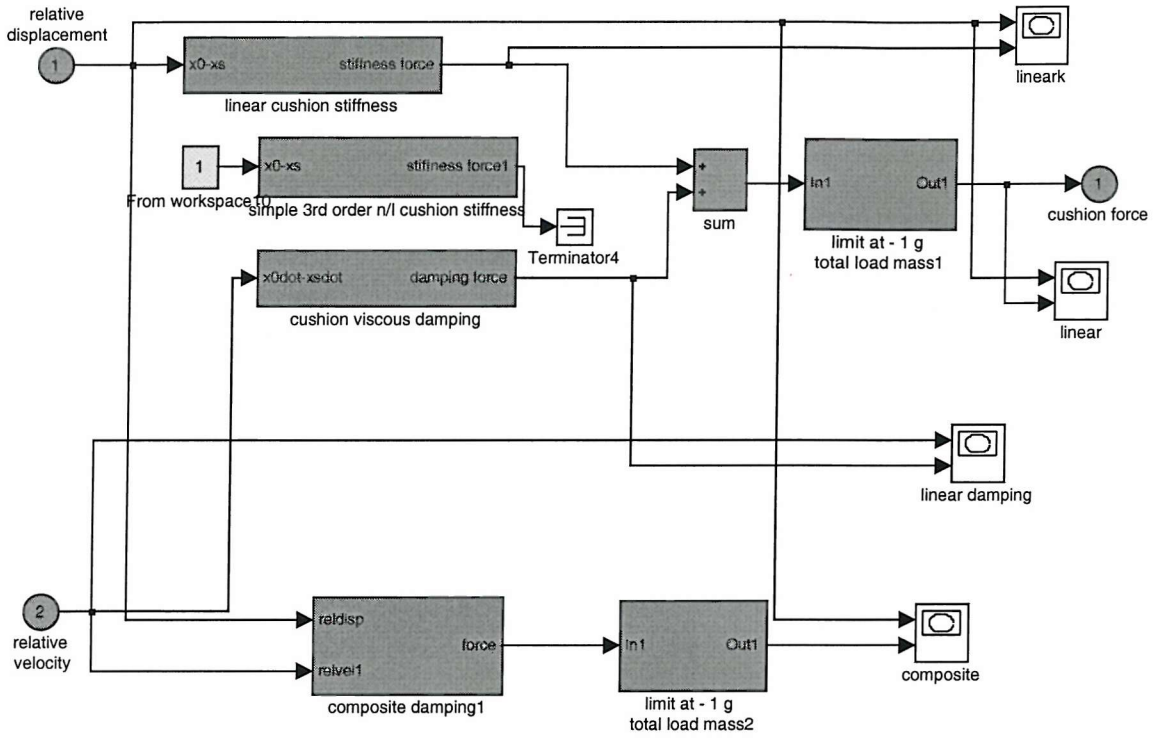
relative
displacement
1
x0-xs
stiffness force
linear cushion stiffness
lineark
1
From workspace10
x0-xs
stiffness force1
simple 3rd order n/l cushion stiffness
Terminator4
sum
In1
Out1
limit at - 1 g
total load mass1
1
cushion force
x0dot-xsdot
damping force
cushion viscous damping
linear
linear damping
2
relative
velocity
reldisp
relvel1
force
composite damping1
In1
Out1
limit at - 1 g
total load mass2
composite

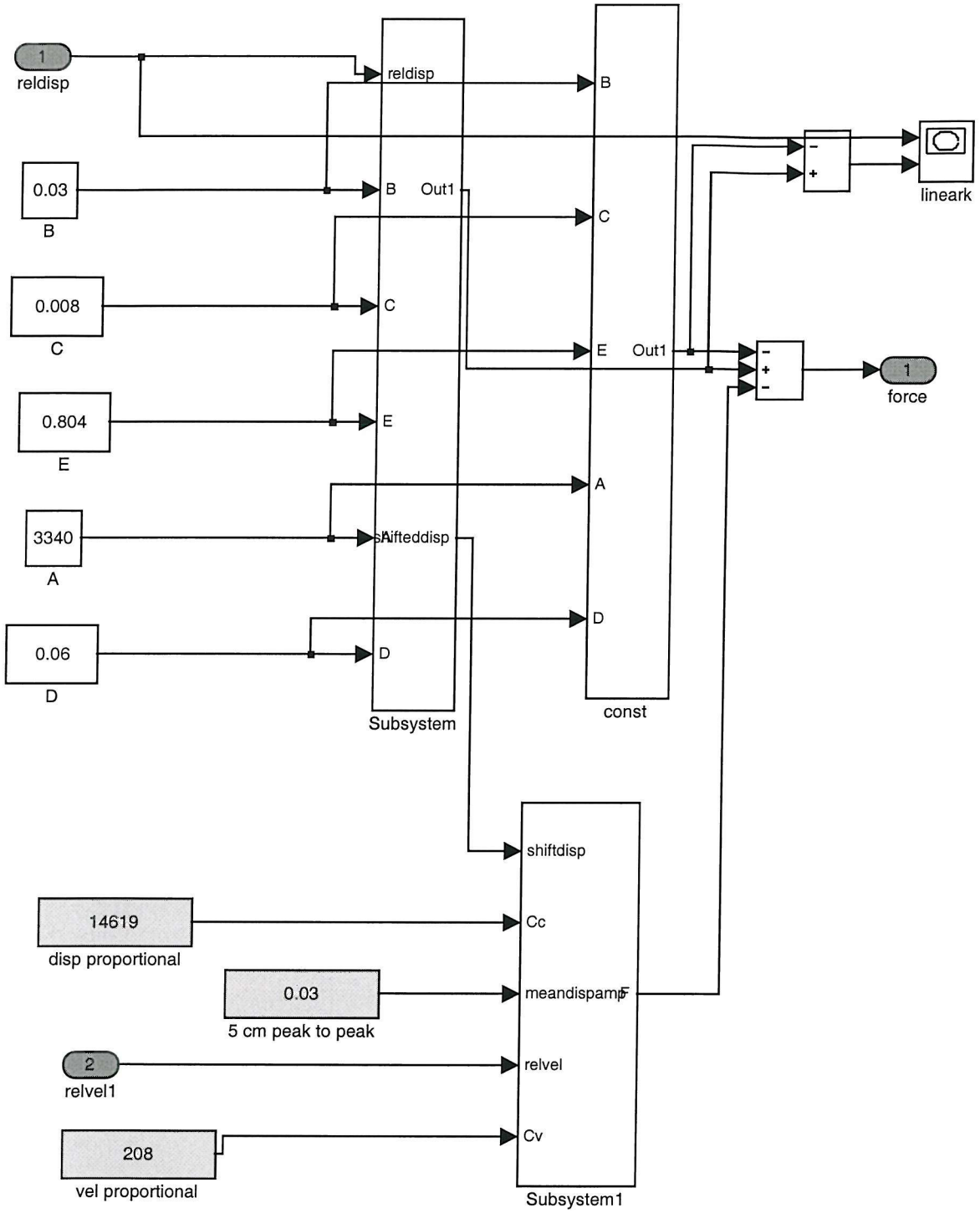
1
reldisp
reldisp
B
0.03
B
B
Out1
C
0.008
C
C
E
Out1
0.804
E
E
A
3340
A
shiftedisp
D
0.06
D
D
Subsystem
const
lineark
1
force
shiftdisp
14619
disp proportional
Cc
0.03
5 cm peak to peak
meandispamp
2
relvel1
relvel
208
vel proportional
Cv
Subsystem1

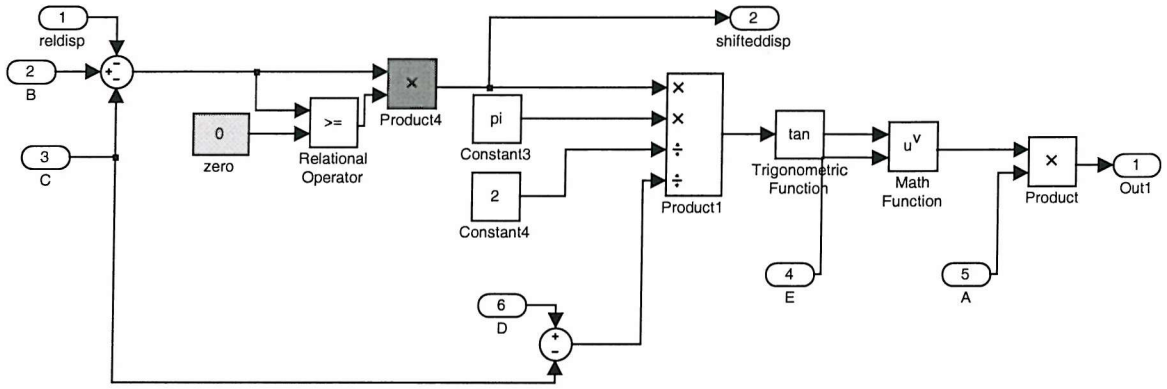
1
reldisp
2
B
3
C
0
zero
>=
Relational
Operator
Product4
pi
Constant3
2
Constant4
2
shifteddisp
Product1
tan
Trigonometric
Function
u^v
Math
Function
Product
1
Out1
4
E
5
A
6
D

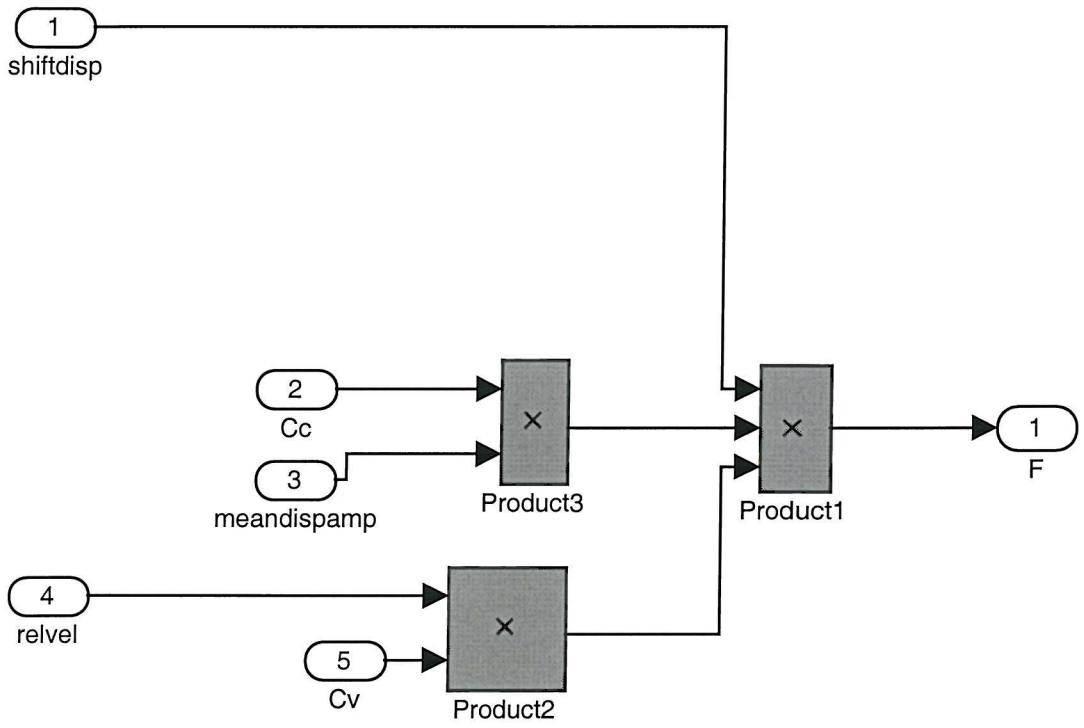
1
shiftdisp
2
Cc
3
meandispamp
Product3
Product1
1
F
4
relvel
5
Cv
Product2

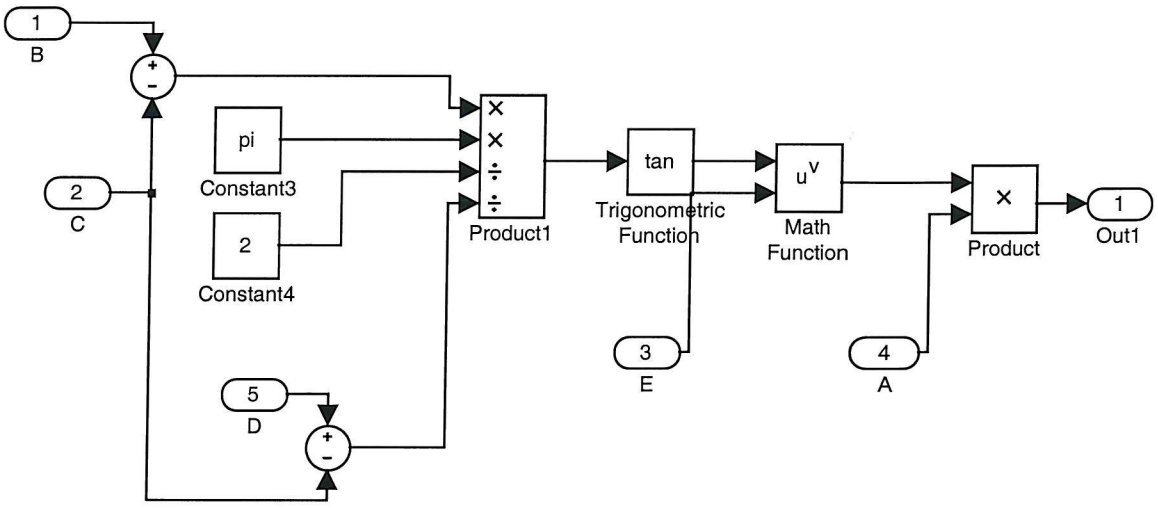
1
B
2
C
pi
Constant3
2
Constant4
5
D
Product1
tan
Trigonometric Function
u^v
Math Function
3
E
4
A
Product
1
Out1

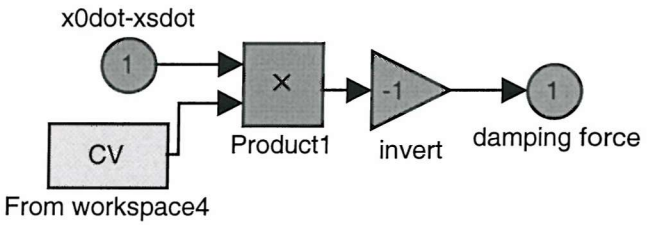
x0dot-xsdot
1
X
Product1
-1
invert
1
damping force
CV
From workspace4

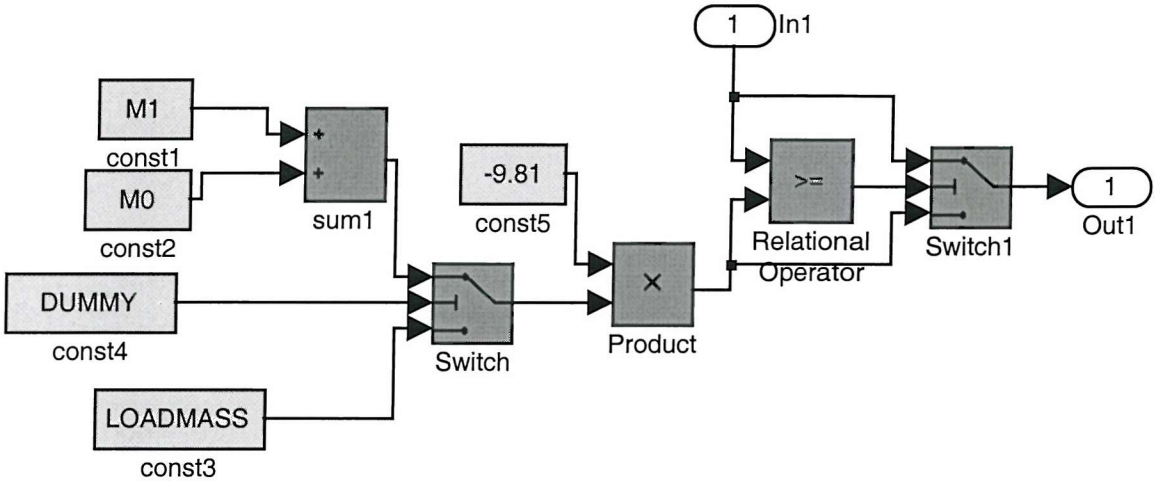
1
In1
M1
const1
M0
const2
sum1
-9.81
const5
>=
Relational
Operator
Switch1
1
Out1
DUMMY
const4
Switch
Product
LOADMASS
const3

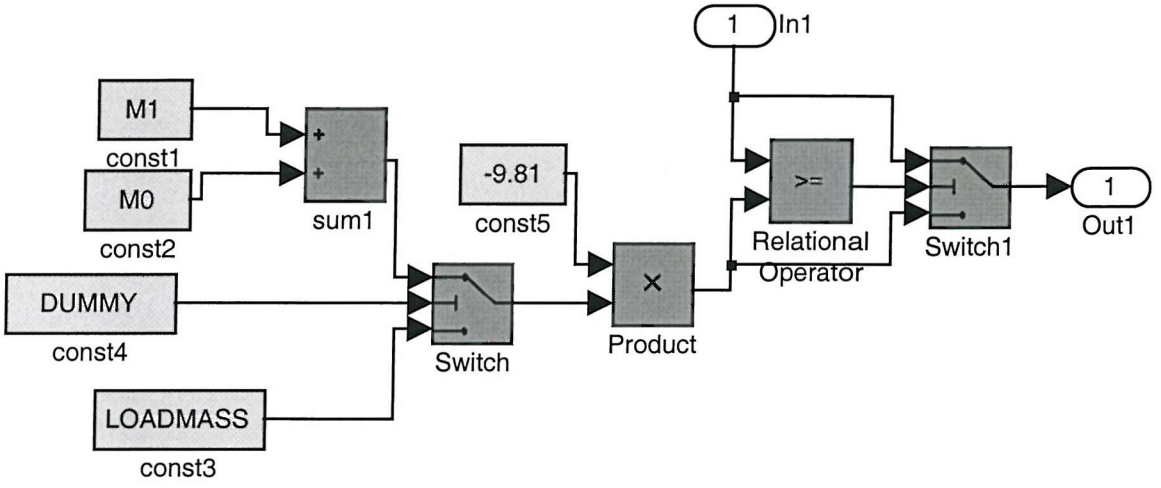
1
In1
M1
const1
M0
const2
sum1
-9.81
const5
>=
Relational
Operator
Switch1
1
Out1
DUMMY
const4
Switch
Product
LOADMASS
const3

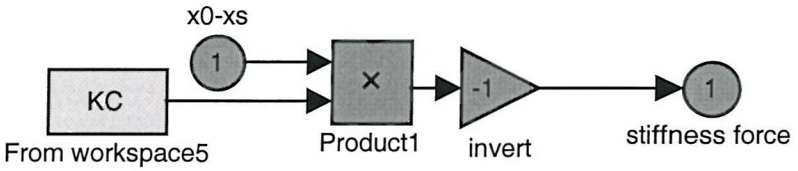
x0-xs
1
KC
From workspace5
×
Product1
-1
invert
1
stiffness force

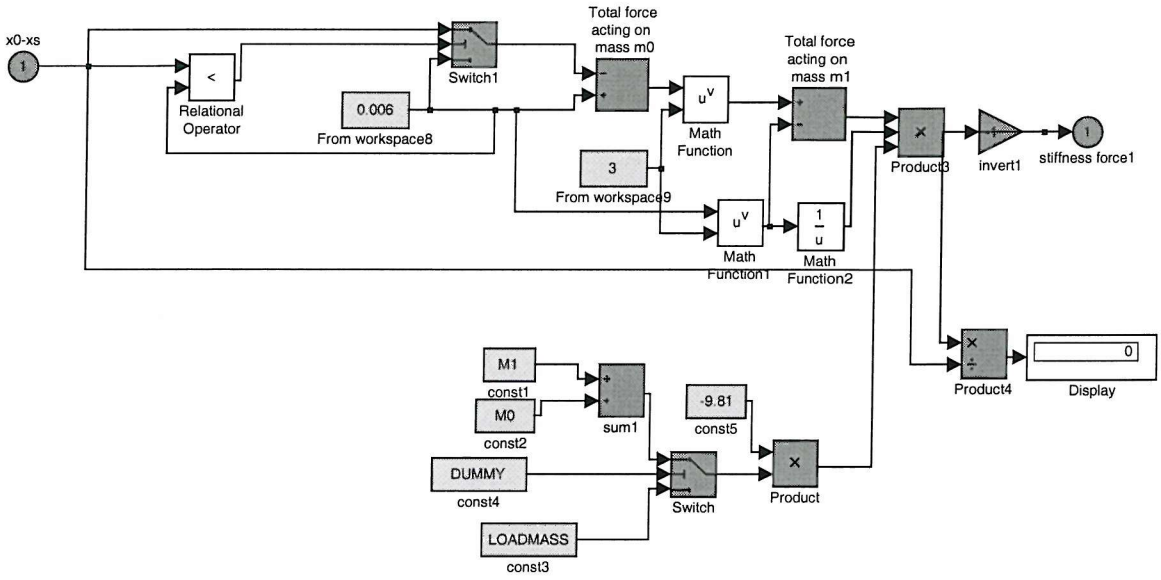
x0-xs
1
<
Relational Operator
0.006
From workspace8
Switch1
Total force acting on mass m0
u^v
Math Function
Total force acting on mass m1
3
From workspace9
u^v
Math Function1
1/u
Math Function2
Product3
invert1
1
stiffness force1
Product4
0
Display
M1
const1
M0
const2
sum1
-9.81
const5
DUMMY
const4
Switch
Product
LOADMASS
const3

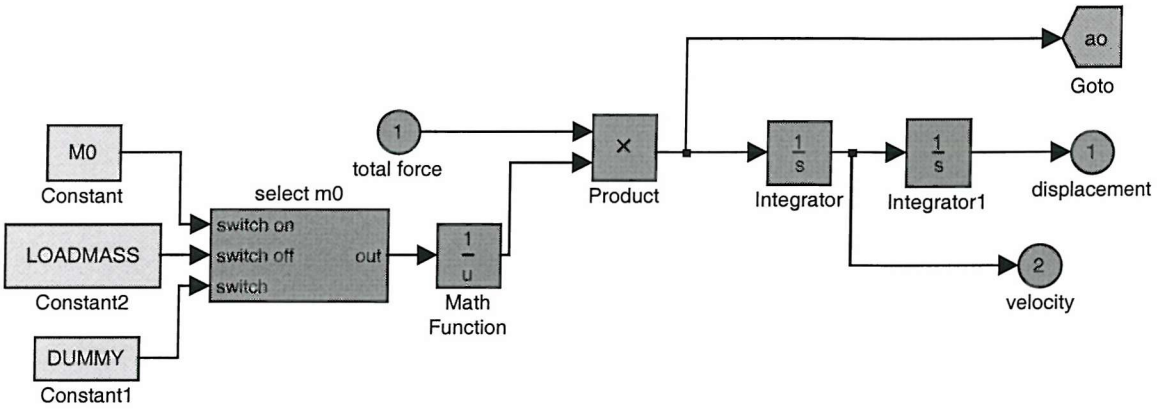
M0
Constant
LOADMASS
Constant2
DUMMY
Constant1
select m0
switch on
switch off
switch
out
1
total force
1
u
Math
Function
×
Product
1
s
Integrator
1
s
Integrator1
ao
Goto
1
displacement
2
velocity

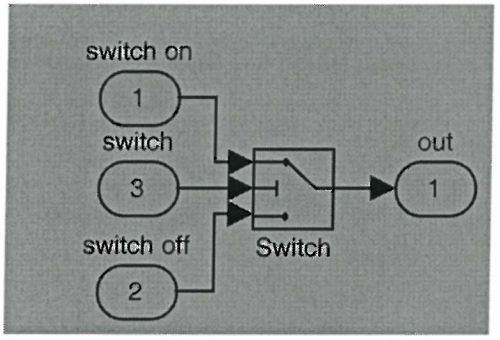
switch on
1
switch
3
switch off
2
Switch
out
1

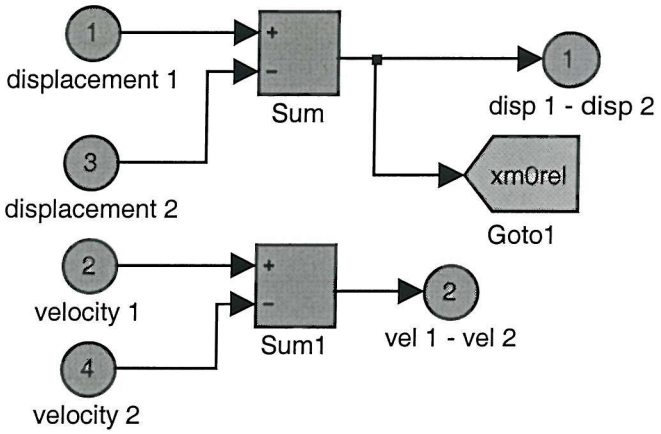
1
displacement 1
3
displacement 2
+
-
Sum
1
disp 1 - disp 2
xm0rel
Goto1
2
velocity 1
4
velocity 2
+
-
Sum1
2
vel 1 - vel 2

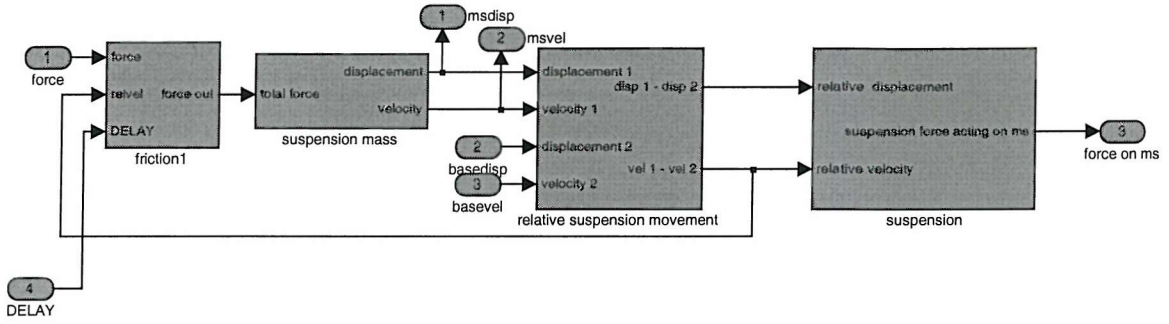
1
force
force
relvel
force out
DELAY
friction1
displacement
total force
velocity
suspension mass
1
msdisp
2
msvel
displacement 1
disp 1 - disp 2
velocity 1
2
basedisp
displacement 2
vel 1 - vel 2
3
basevel
velocity 2
relative suspension movement
relative displacement
suspension force acting on ms
relative velocity
suspension
3
force on ms
4
DELAY

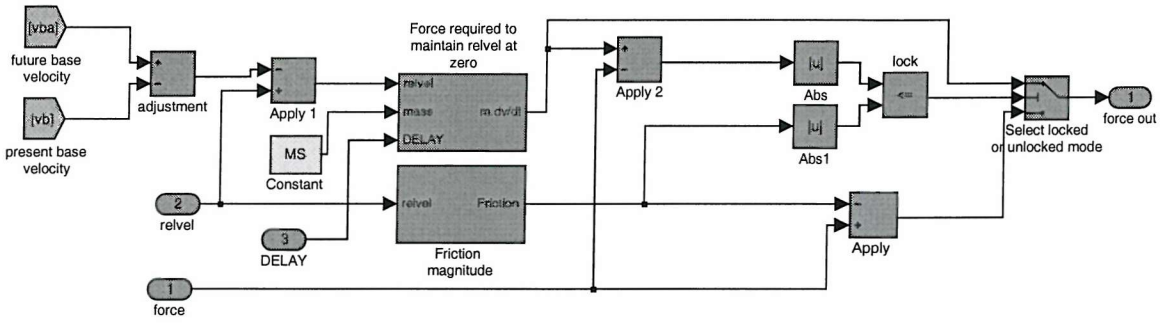
[vba]
future base velocity
[vb]
present base velocity
adjustment
Apply 1
MS
Constant
2
relvel
3
DELAY
Force required to maintain relvel at zero
relvel
mass
m dv/dt
DELAY
relvel
Friction
Friction magnitude
1
force
Apply 2
|u|
Abs
|u|
Abs1
lock
<=
Select locked or unlocked mode
1
force out
Apply

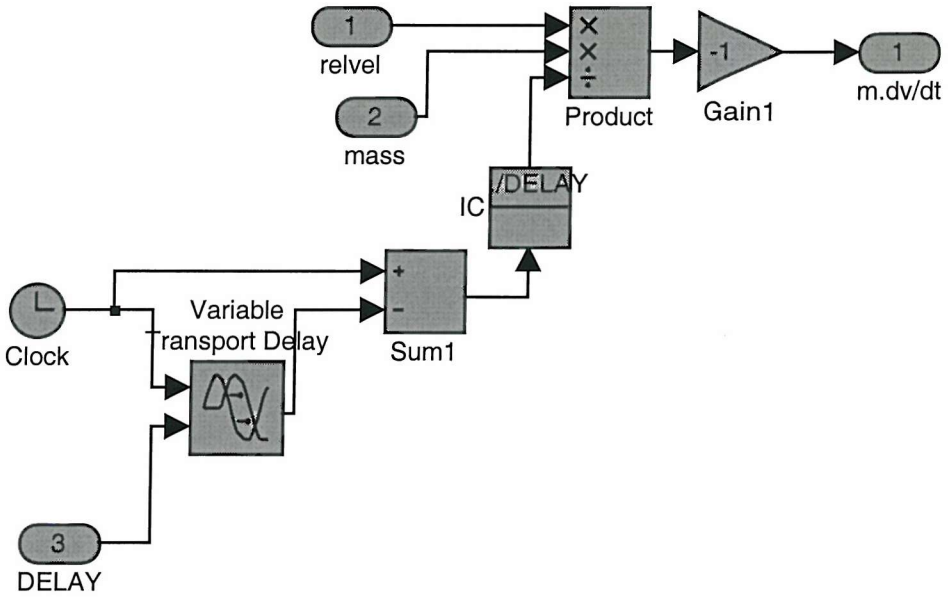
1
relvel
2
mass
Product
-1
Gain1
1
m.dv/dt
IC
/DELAY
Clock
Variable
ransport Delay
Sum1
3
DELAY

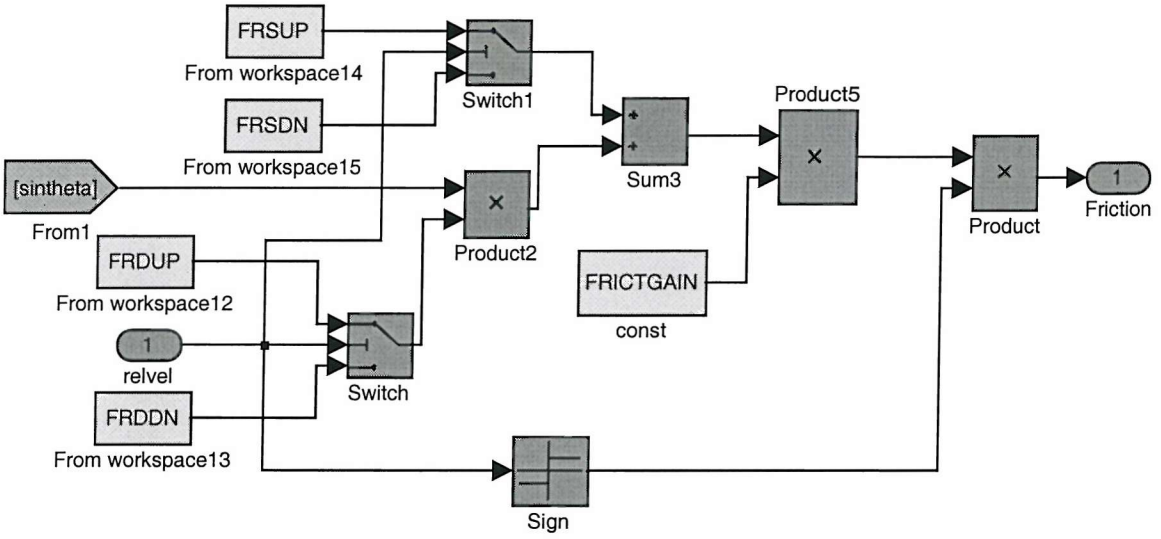
FRSUP
From workspace14
Switch1
FRSDN
From workspace15
Sum3
Product5
[sintheta]
From1
Product2
Product
1
Friction
FRDUP
From workspace12
FRICTGAIN
const
1
relvel
Switch
FRDDN
From workspace13
Sign

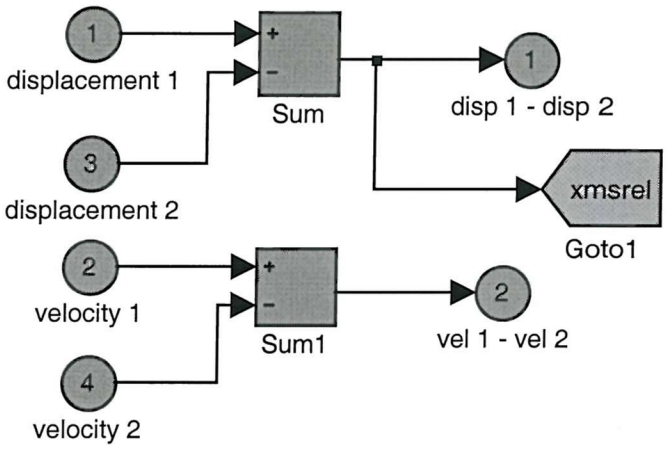
1
displacement 1
3
displacement 2
+
-
Sum
1
disp 1 - disp 2
xmsrel
Goto1
2
velocity 1
4
velocity 2
+
-
Sum1
2
vel 1 - vel 2

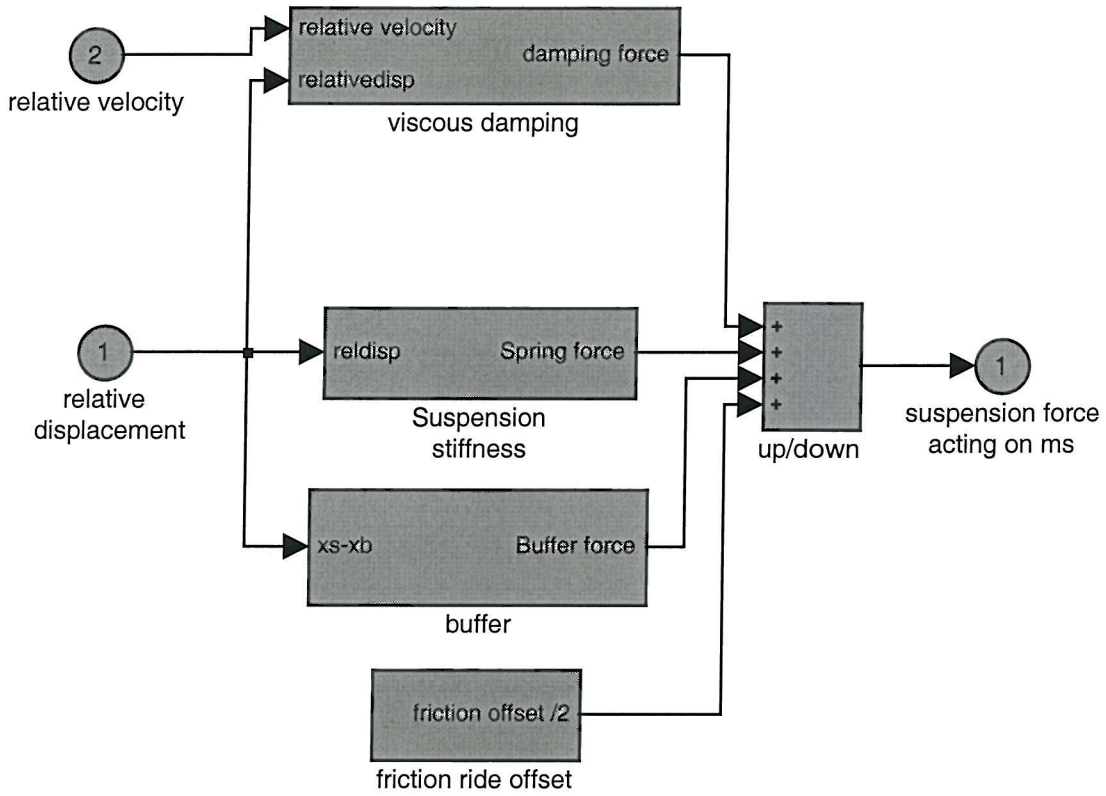
2
relative velocity
relative velocity
relativedisp
damping force
viscous damping
1
relative
displacement
reldisp
Spring force
Suspension
stiffness
xs-xb
Buffer force
buffer
friction offset /2
friction ride offset
+
+
+
+
up/down
1
suspension force
acting on ms

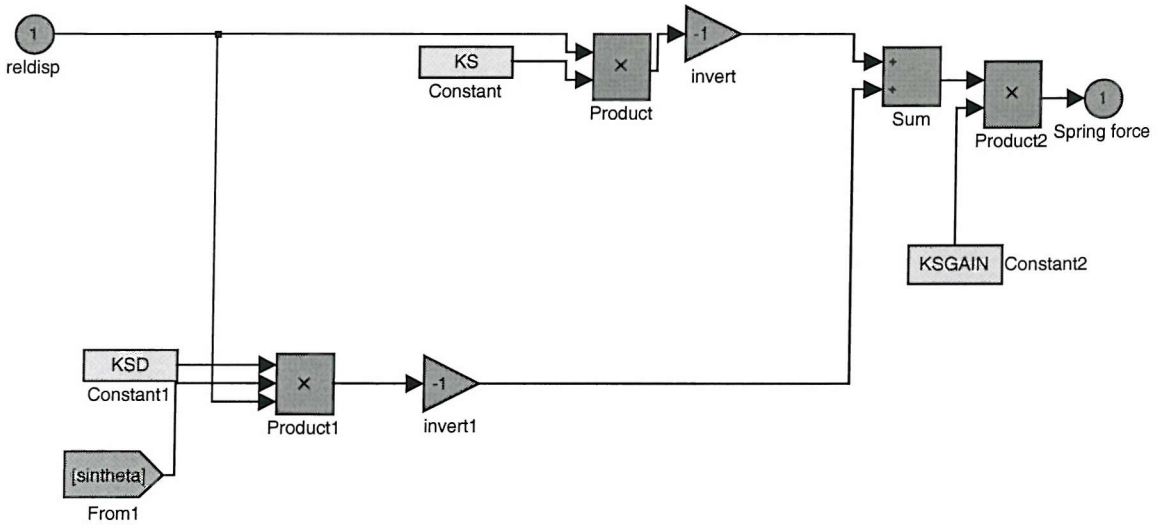
1
reldisp
KS
Constant
Product
-1
invert
Sum
Product2
1
Spring force
KSGAIN
Constant2
KSD
Constant1
Product1
-1
invert1
[sintheta]
From1

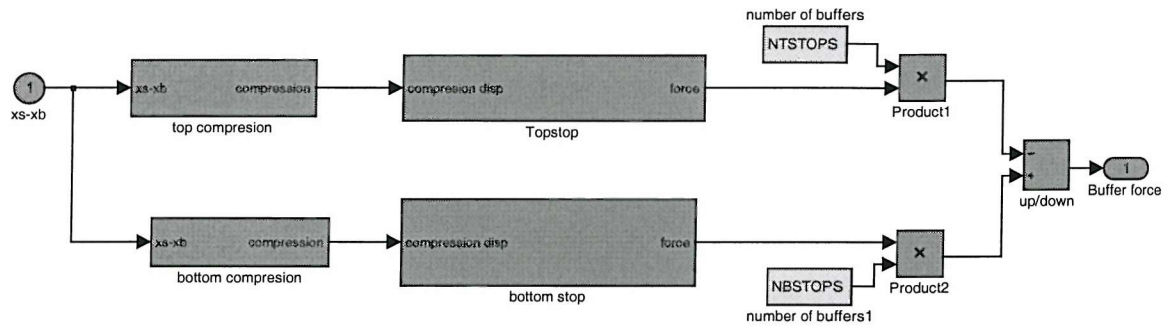
1
xs-xb
xs-xb
compression
top compression
compression disp
force
Topstop
number of buffers
NTSTOPS
Product1
xs-xb
compression
bottom compression
compression disp
force
bottom stop
NBSTOPS
number of buffers1
Product2
up/down
1
Buffer force

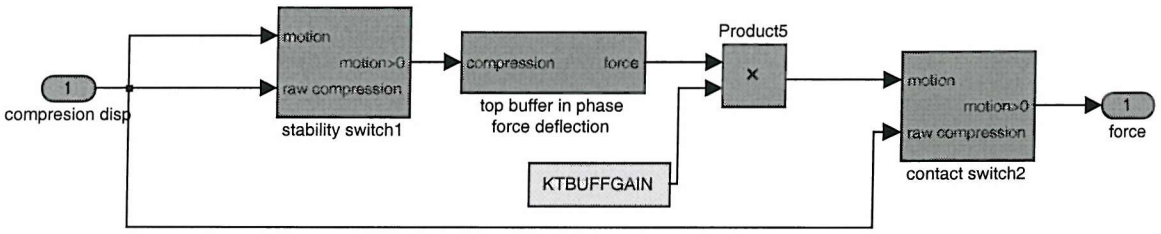
1
compresion disp
motion
motion>0
raw compression
stability switch1
compression
force
top buffer in phase
force deflection
Product5
×
KTBUFFGAIN
motion
motion>0
raw compression
contact switch2
1
force

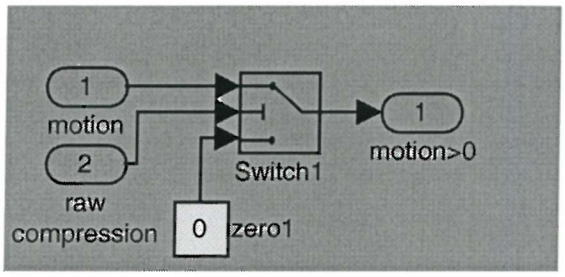
1
motion
2
raw
compression
0
zero1
Switch1
1
motion>0

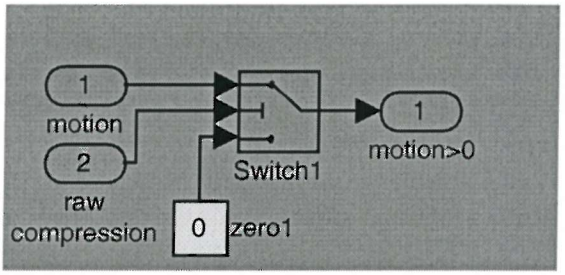
1
motion
2
raw
compression
Switch1
0
zero1
1
motion>0

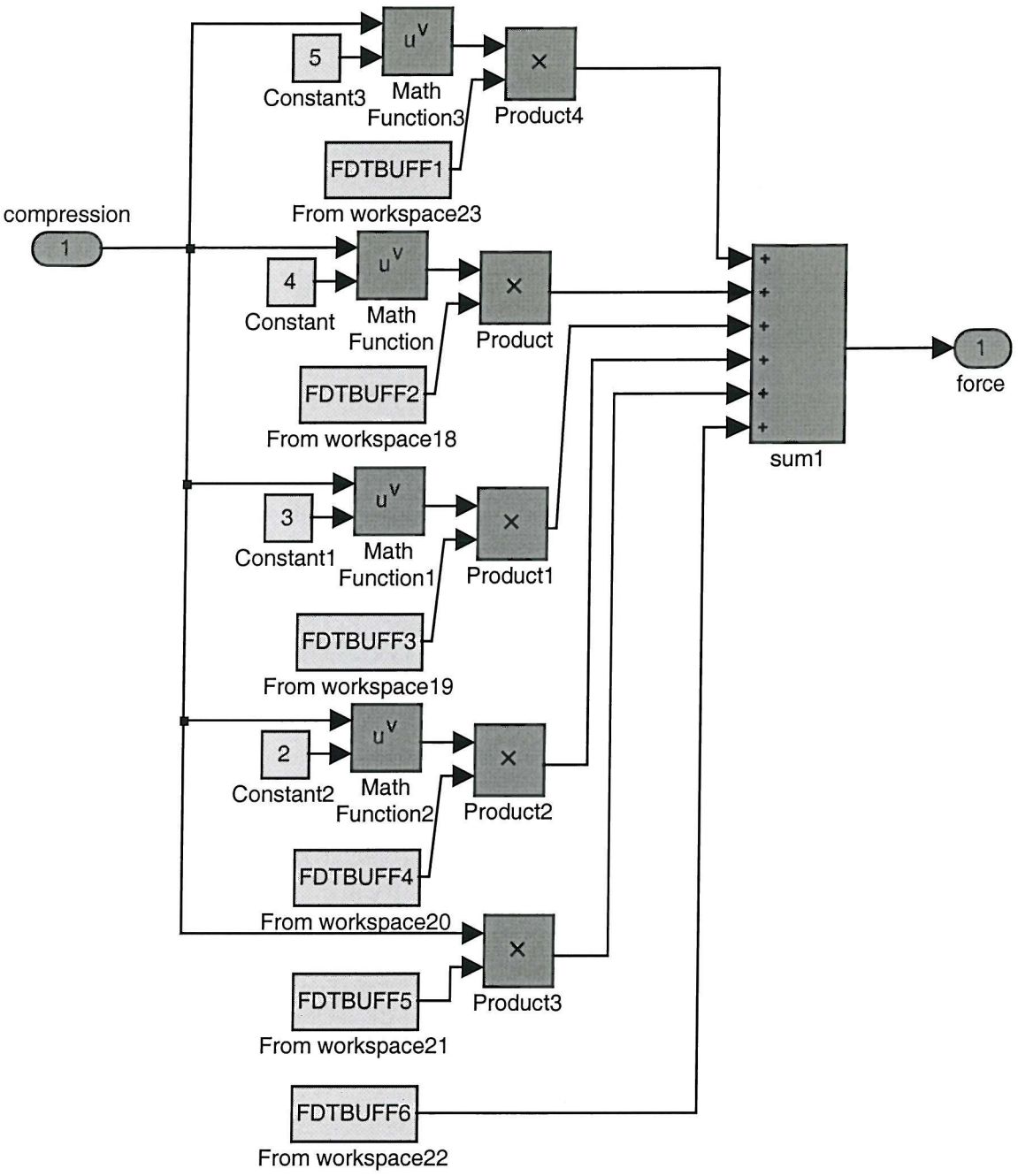
compression
1
5
Constant3
u^v
Math Function3
Product4
FDTBUFF1
From workspace23
4
Constant
Math Function
Product
FDTBUFF2
From workspace18
3
Constant1
Math Function1
Product1
FDTBUFF3
From workspace19
2
Constant2
Math Function2
Product2
FDTBUFF4
From workspace20
Product3
FDTBUFF5
From workspace21
FDTBUFF6
From workspace22
sum1
1
force

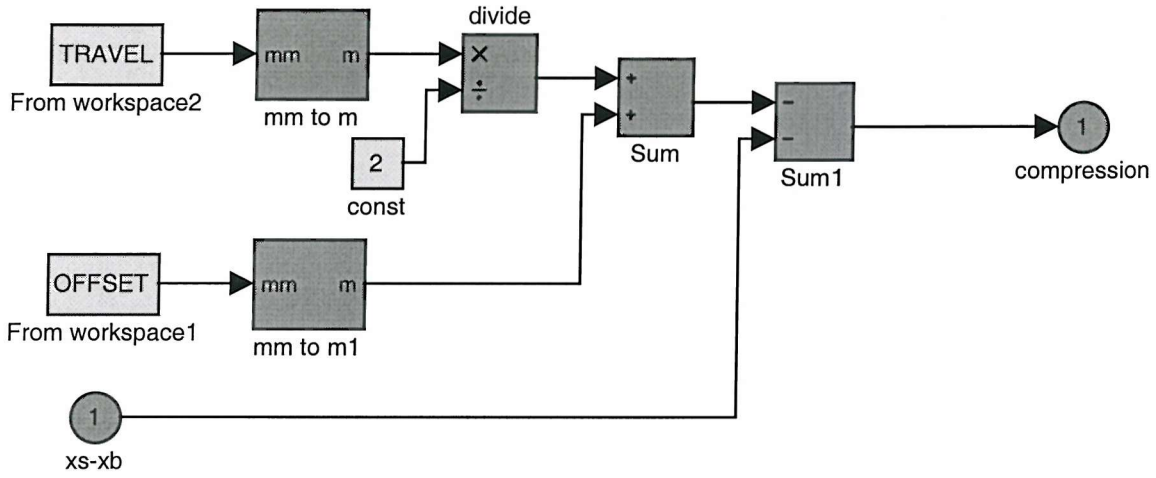
TRAVEL
From workspace2
mm
m
mm to m
divide
2
const
Sum
Sum1
1
compression
OFFSET
From workspace1
mm
m
mm to m1
1
xs-xb

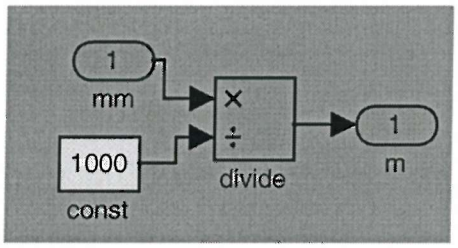
1
mm
1000
const
divide
1
m

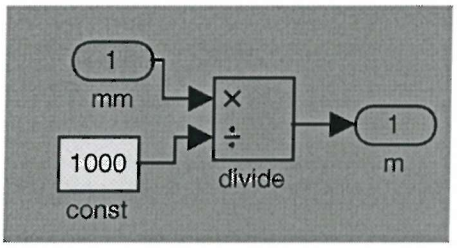
1
mm
1000
const
×
÷
divide
1
m

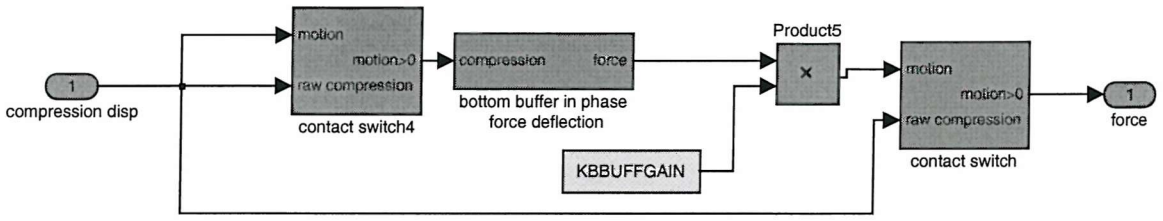
1
compression disp
motion
motion>0
raw compression
contact switch4
compression
force
bottom buffer in phase
force deflection
Product5
×
KBBUFFGAIN
motion
motion>0
raw compression
contact switch
1
force

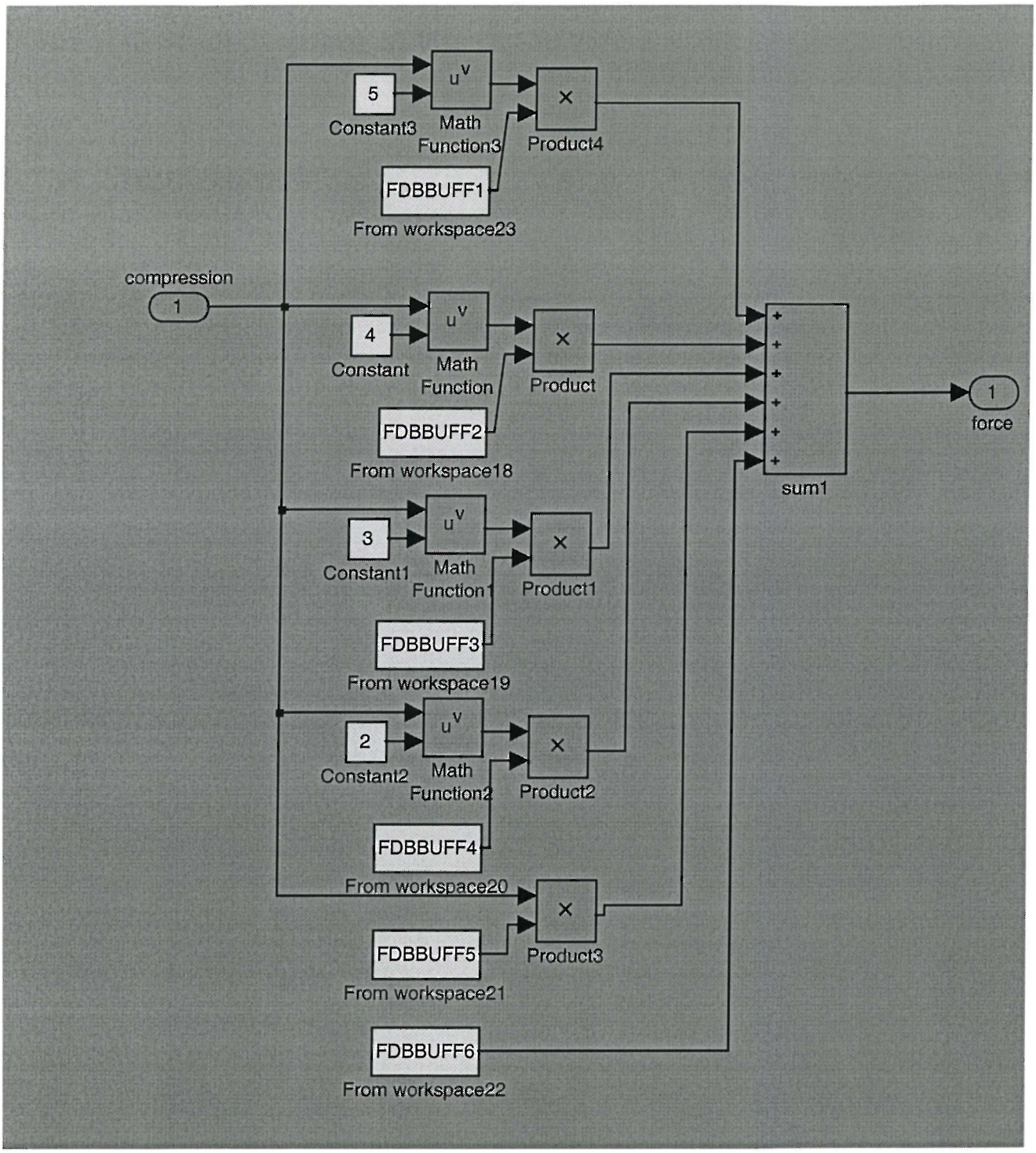
compression
1
5
Constant3
u^v
Math Function3
×
Product4
FDBBUFF1
From workspace23
4
Constant
Math Function
Product
FDBBUFF2
From workspace18
3
Constant1
Math Function1
Product1
FDBBUFF3
From workspace19
2
Constant2
Math Function2
Product2
FDBBUFF4
From workspace20
Product3
FDBBUFF5
From workspace21
FDBBUFF6
From workspace22
sum1
1
force

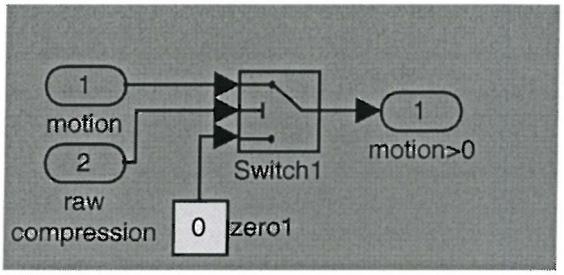
1
motion
2
raw
compression
0
zero1
Switch1
1
motion>0

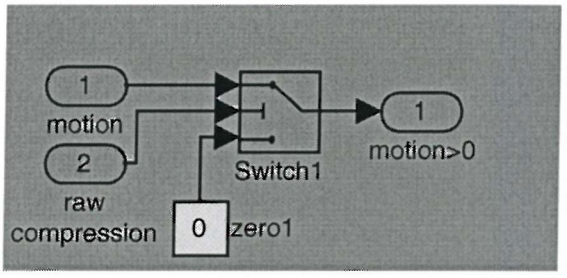
1
motion
2
raw
compression
Switch1
0
zero1
1
motion>0

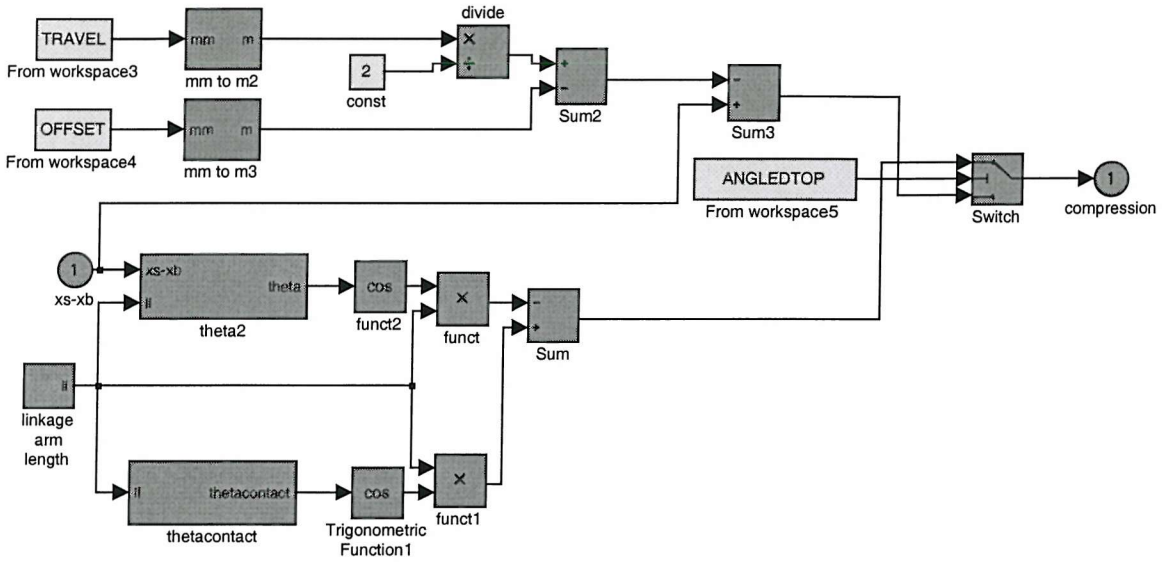
TRAVEL
From workspace3
mm
m
mm to m2
divide
2
const
Sum2
Sum3
OFFSET
From workspace4
mm to m3
ANGLEDTOP
From workspace5
Switch
1
compression
1
xs-xb
xs-xb
theta
theta2
cos
funct2
funct
Sum
linkage arm length
thetacontact
thetacontact
cos
Trigonometric Function1
funct1

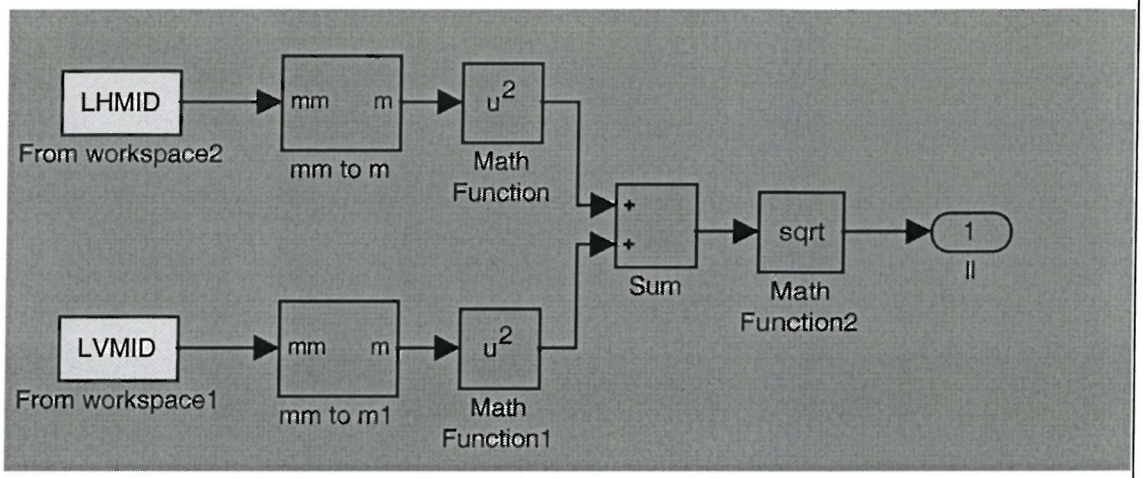
LHMID
From workspace2
mm
m
mm to m
u2
Math
Function
LVMID
From workspace1
mm
m
mm to m1
u2
Math
Function1
+
+
Sum
sqrt
Math
Function2
1
ll

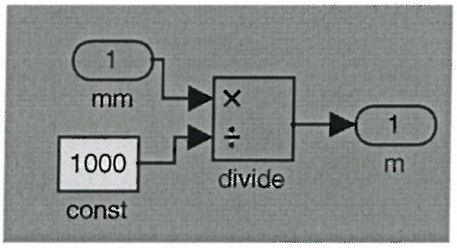
1
mm
1000
const
divide
1
m

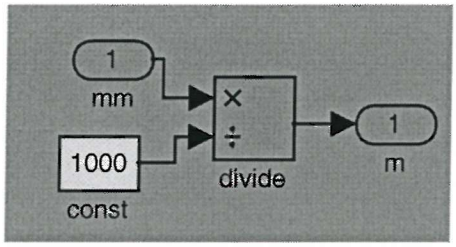
1
mm
1000
const
divide
1
m

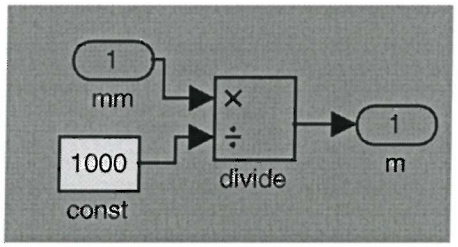
1
mm
1000
const
×
÷
divide
1
m

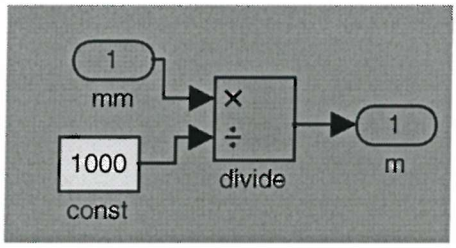
1
mm
1000
const
×
÷
divide
1
m

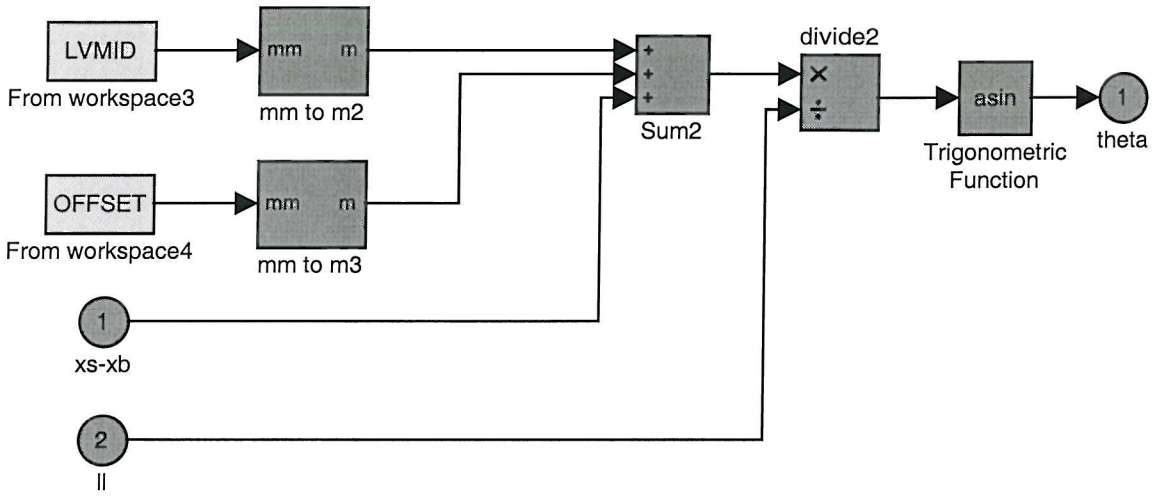
LVMID
From workspace3
mm m
mm to m2
OFFSET
From workspace4
mm m
mm to m3
1
xs-xb
2
ll
Sum2
divide2
asin
Trigonometric
Function
1
theta

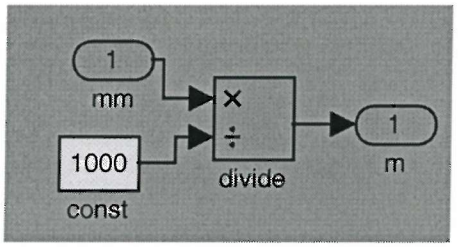
1
mm
1000
const
×
÷
divide
1
m

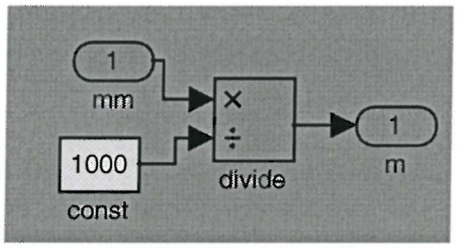
1
mm
1000
const
×
÷
divide
1
m

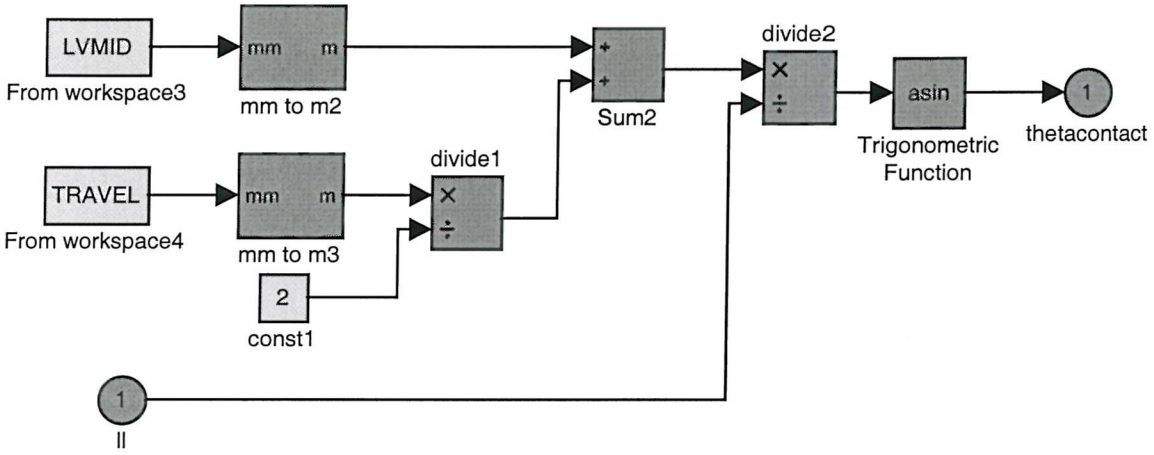
LVMID
From workspace3
mm
m
mm to m2
TRAVEL
From workspace4
mm
m
mm to m3
divide1
2
const1
Sum2
divide2
asin
Trigonometric
Function
1
thetacontact
1
ll

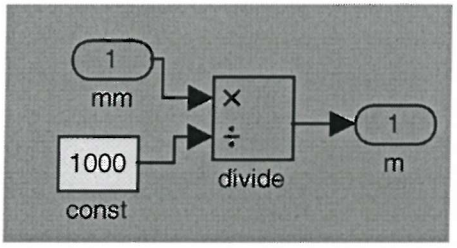
1
mm
1000
const
divide
1
m

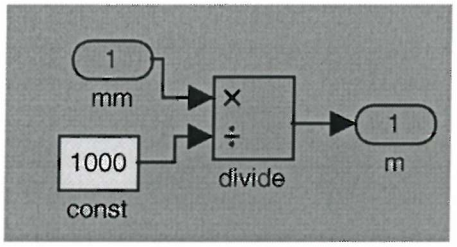
1
mm
1000
const
divide
1
m

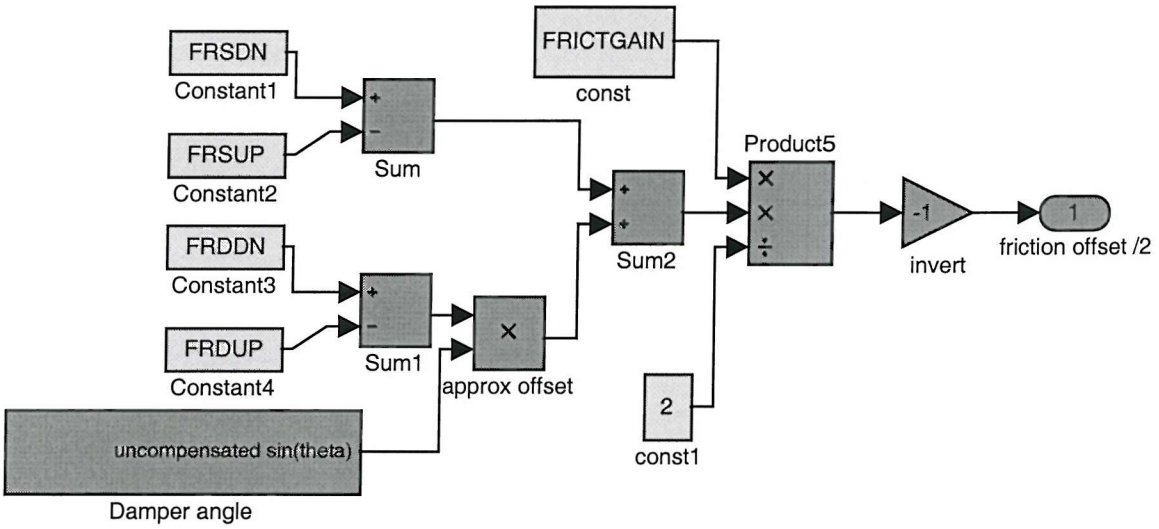
FRSDN
Constant1
FRSUP
Constant2
Sum
FRICTGAIN
const
Sum2
Product5
-1
invert
1
friction offset /2
FRDDN
Constant3
FRDUP
Constant4
Sum1
approx offset
2
const1
uncompensated sin(theta)
Damper angle

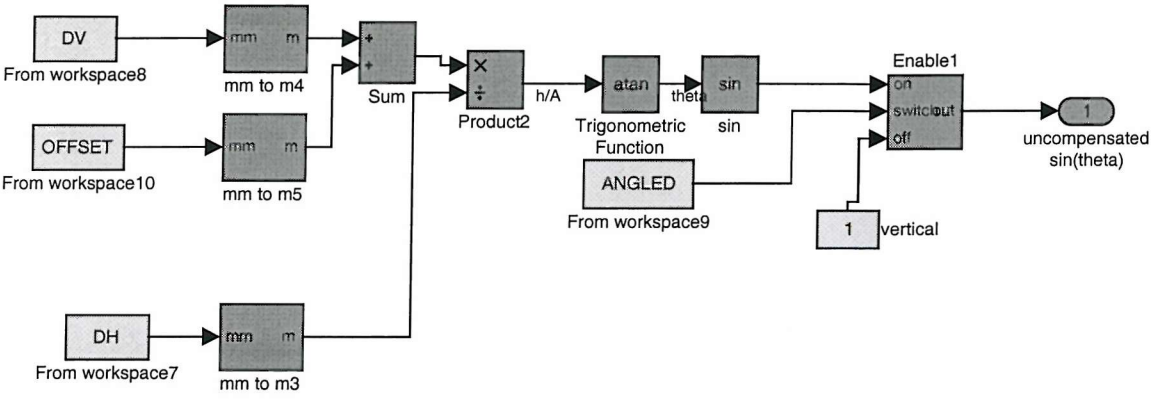
DV
From workspace8
mm m
mm to m4
OFFSET
From workspace10
mm m
mm to m5
DH
From workspace7
mm m
mm to m3
Sum
Product2
h/A
atan
Trigonometric Function
theta
sin
sin
ANGLED
From workspace9
Enable1
on
switch out
off
1
vertical
1
uncompensated sin(theta)

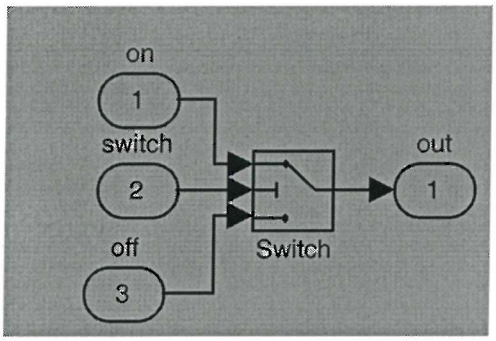
on
1
switch
2
off
3
Switch
out
1

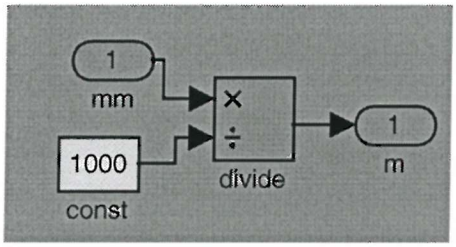
1
mm
1000
const
divide
1
m

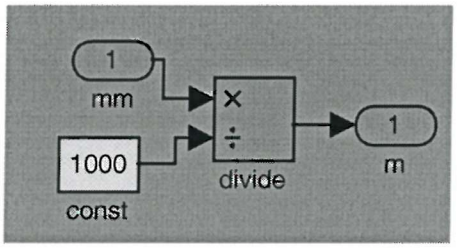
1
mm
1000
const
×
÷
divide
1
m

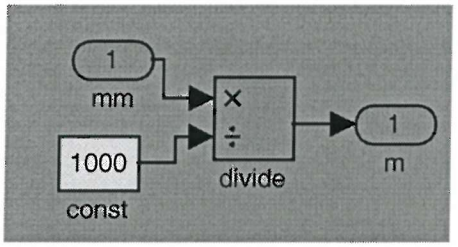
1
mm
1000
const
×
÷
divide
1
m

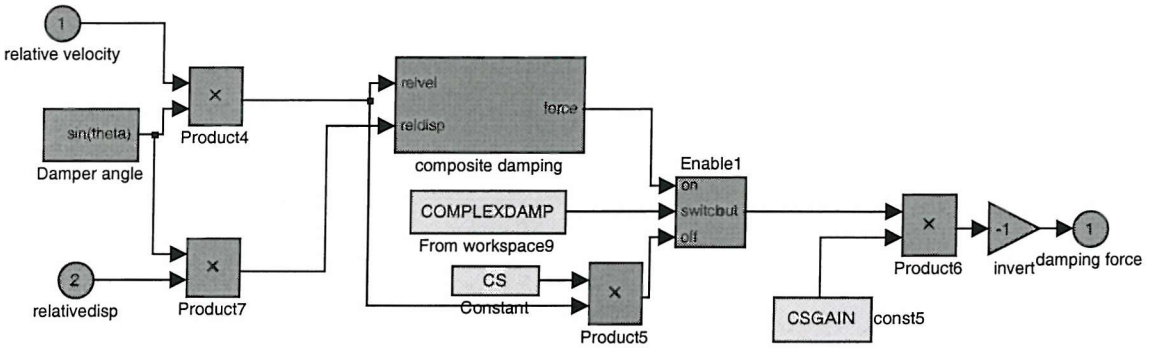
1
relative velocity
sin(theta)
Damper angle
Product4
relvel
reldisp
force
composite damping
COMPLEXDAMP
From workspace9
Enable1
on
switchbut
off
Product6
-1
invert
1
damping force
2
relativedisp
Product7
CS
Constant
Product5
CSGAIN
const5

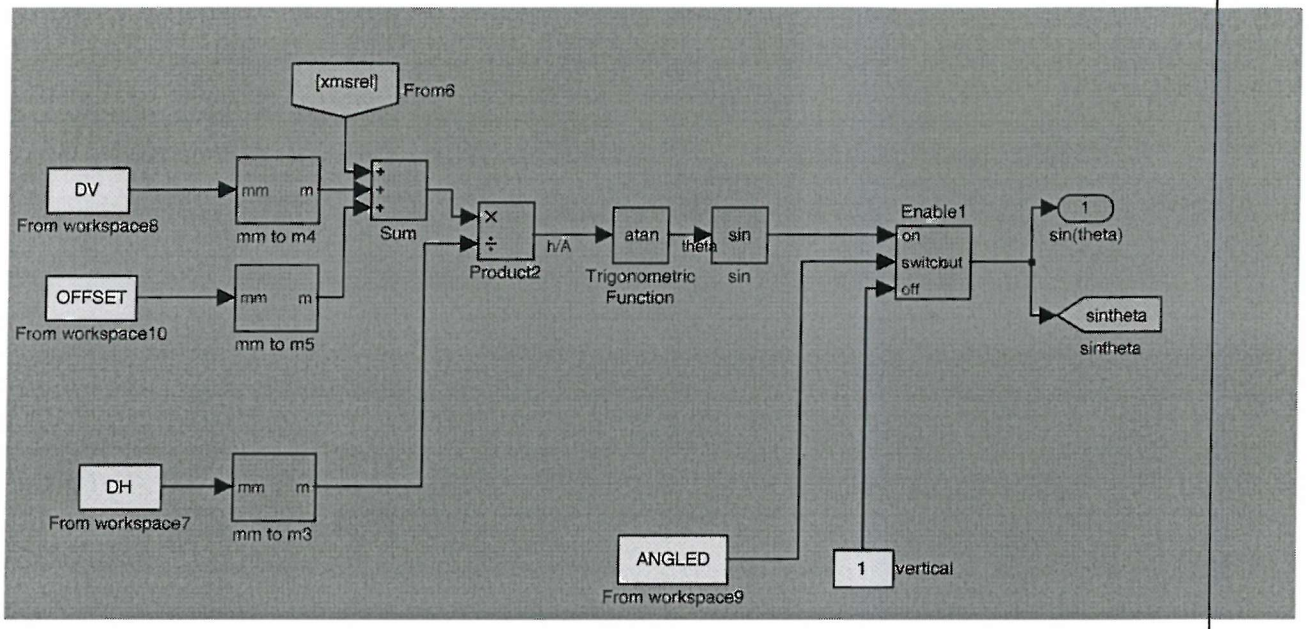
[xmsrel]
From6
DV
From workspace8
mm
m
mm to m4
Sum
OFFSET
From workspace10
mm to m5
Product2
h/A
atan
theta
sin
Trigonometric Function
sin
Enable1
on
switchout
off
1
sin(theta)
sintheta
sintheta
DH
From workspace7
mm to m3
ANGLED
From workspace9
1
vertical

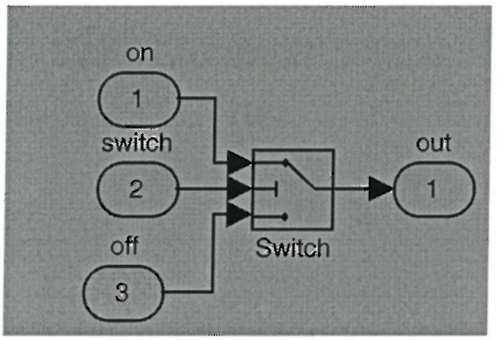
on
1
switch
2
off
3
Switch
out
1

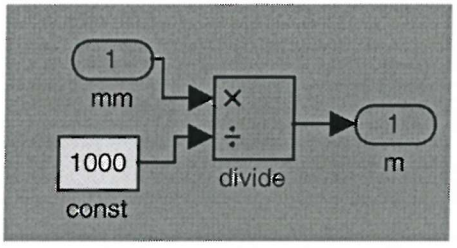
1
mm
1000
const
×
÷
divide
1
m

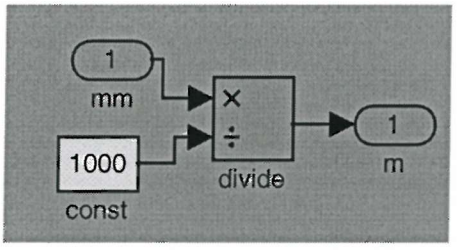
1
mm
1000
const
×
÷
divide
1
m

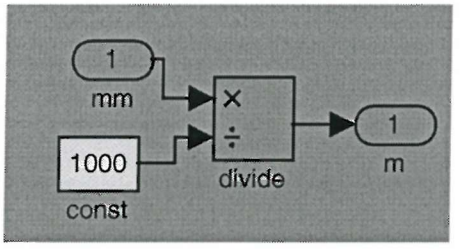
1
mm
1000
const
×
÷
divide
1
m

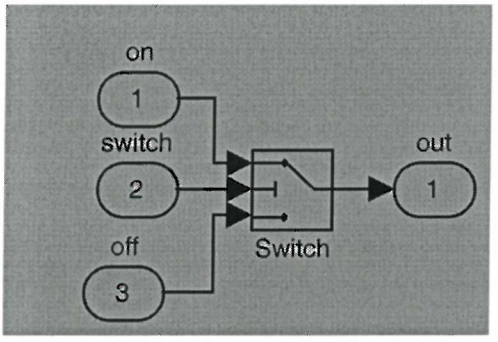
on
1
switch
2
off
3
Switch
out
1

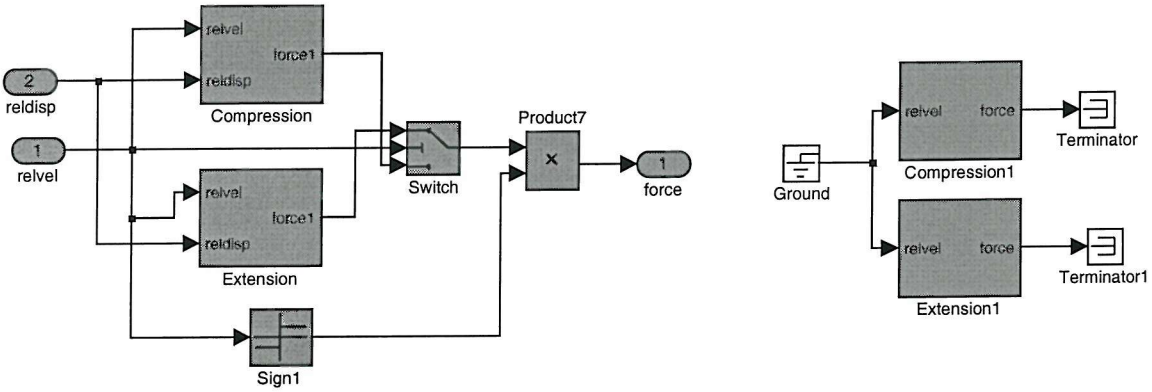
2
reldisp
1
relvel
relvel
reldisp
force1
Compression
relvel
reldisp
force1
Extension
Switch
Product7
×
1
force
Sign1
Ground
relvel
force
Compression1
Terminator
relvel
force
Extension1
Terminator1

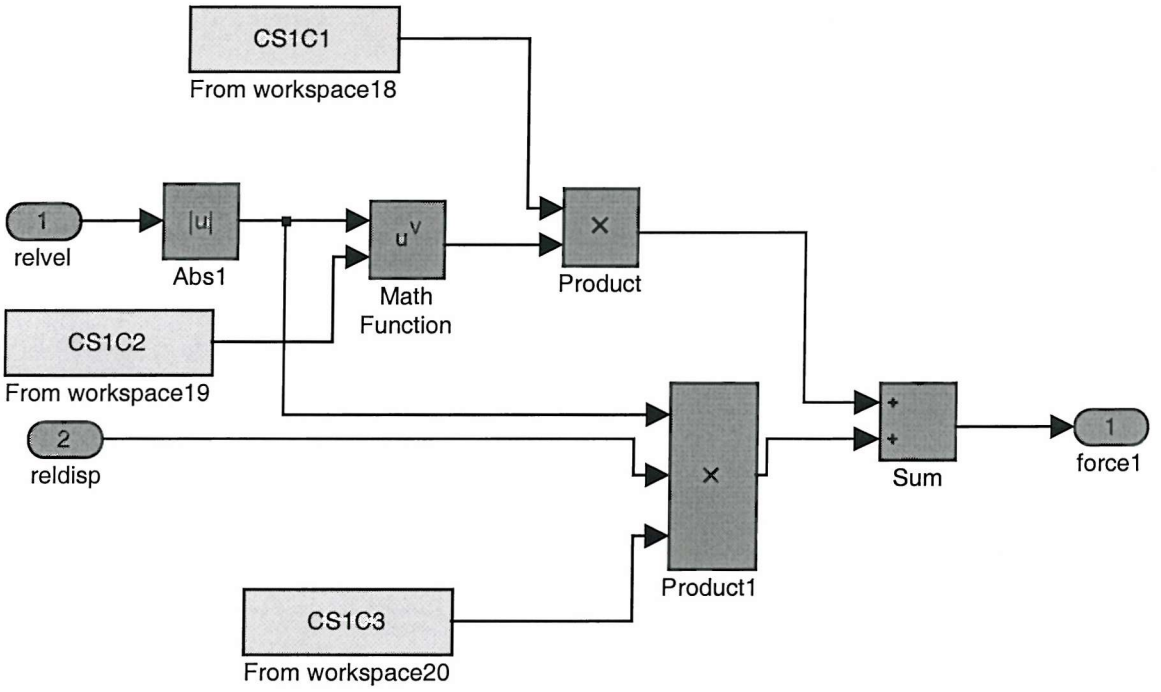
CS1C1
From workspace18
1
relvel
|u|
Abs1
u^v
Math
Function
×
Product
CS1C2
From workspace19
2
reldisp
×
Product1
+
+
Sum
1
force1
CS1C3
From workspace20

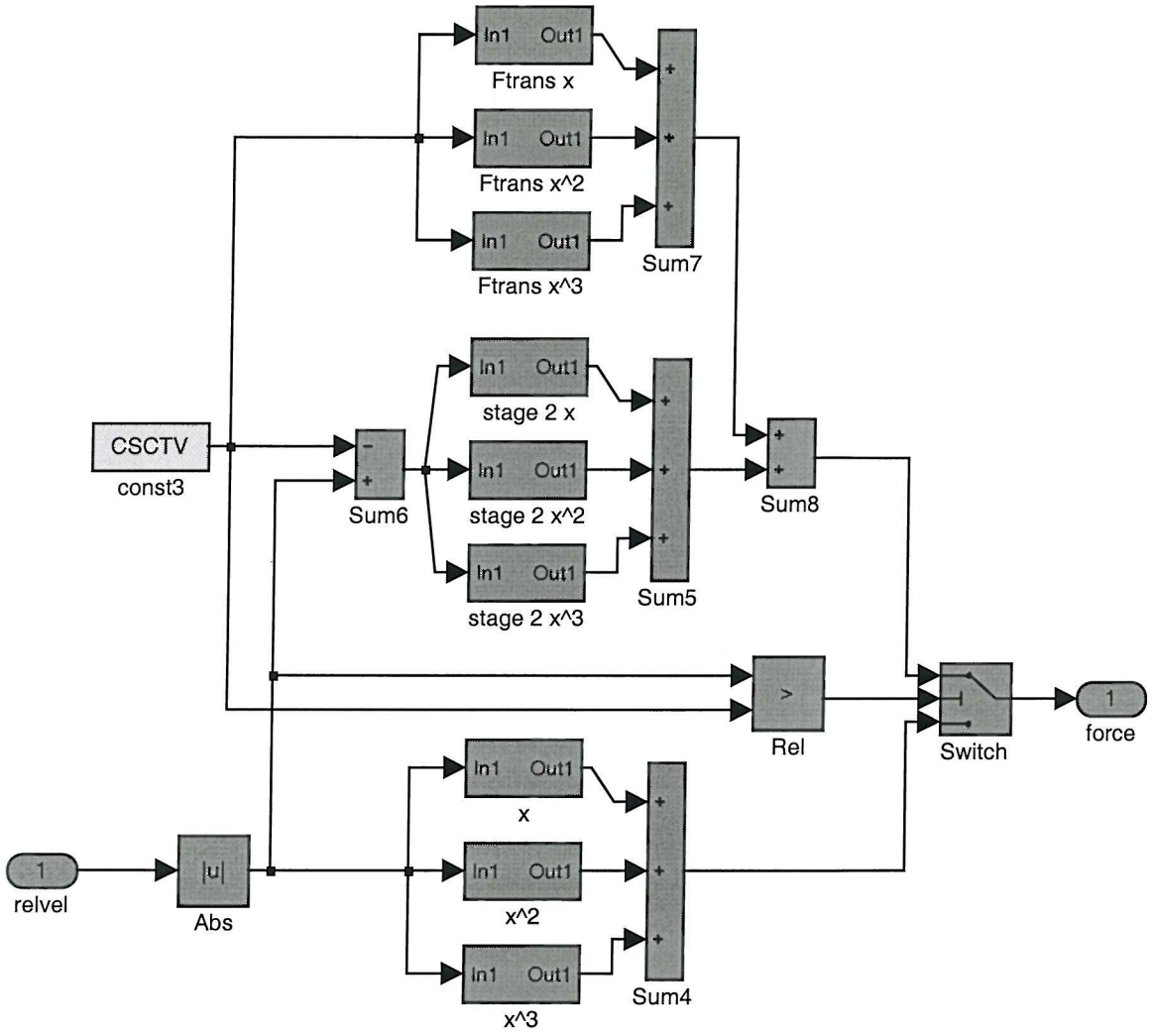
In1 Out1
Ftrans x
In1 Out1
Ftrans x^2
In1 Out1
Ftrans x^3
Sum7
In1 Out1
stage 2 x
In1 Out1
stage 2 x^2
In1 Out1
stage 2 x^3
Sum5
CSCTV
const3
Sum6
Sum8
>
Rel
Switch
1
force
1
relvel
|u|
Abs
In1 Out1
x
In1 Out1
x^2
In1 Out1
x^3
Sum4

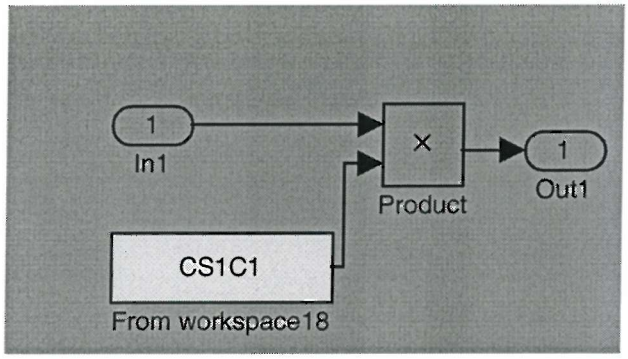
1
In1
×
Product
1
Out1
CS1C1
From workspace18

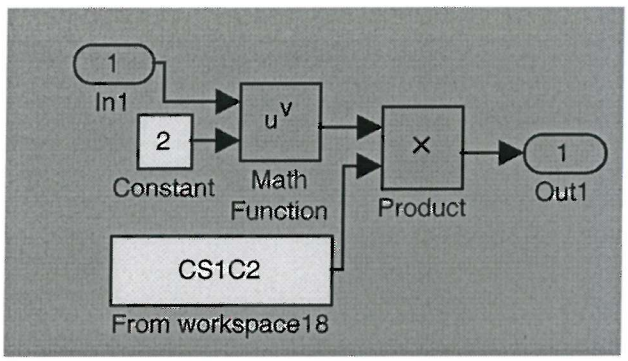
1
In1
2
Constant
u^v
Math
Function
×
Product
1
Out1
CS1C2
From workspace18

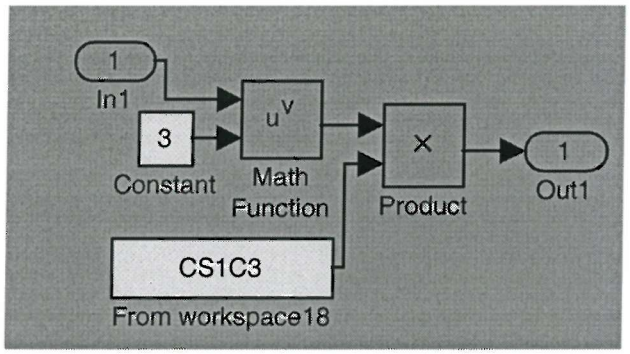
1
In1
3
Constant
u^v
Math
Function
×
Product
1
Out1
CS1C3
From workspace18

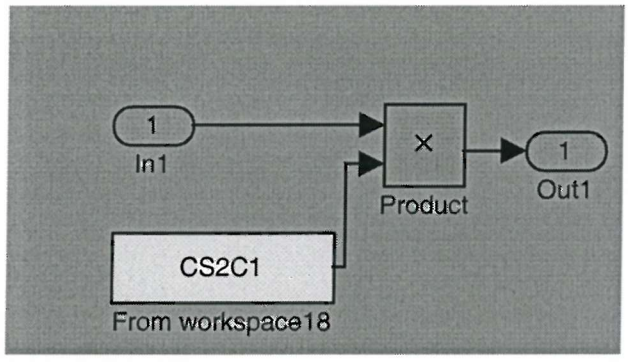
1
In1
×
Product
1
Out1
CS2C1
From workspace18

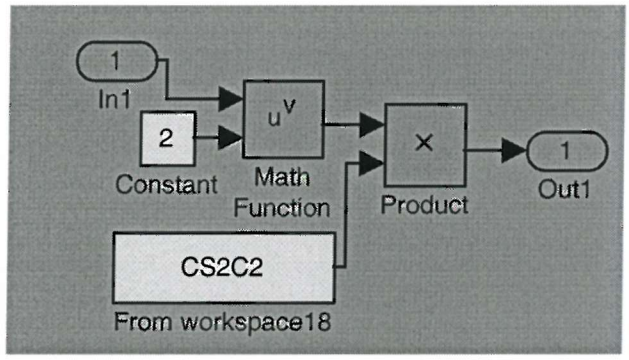
1
In1
2
Constant
u^v
Math
Function
×
Product
1
Out1
CS2C2
From workspace18

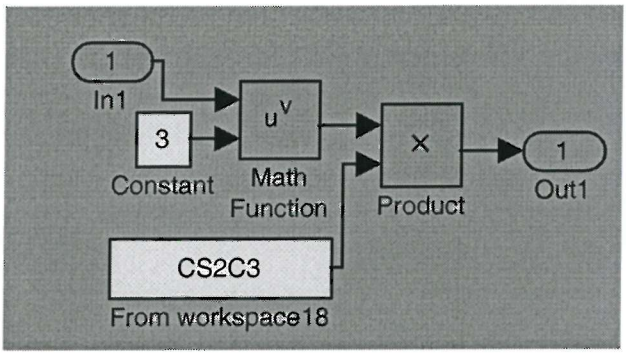
1
In1
3
Constant
u^v
Math
Function
X
Product
1
Out1
CS2C3
From workspace18

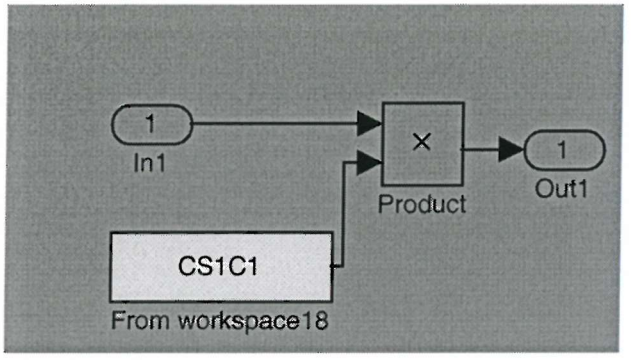
1
In1
×
Product
1
Out1
CS1C1
From workspace18

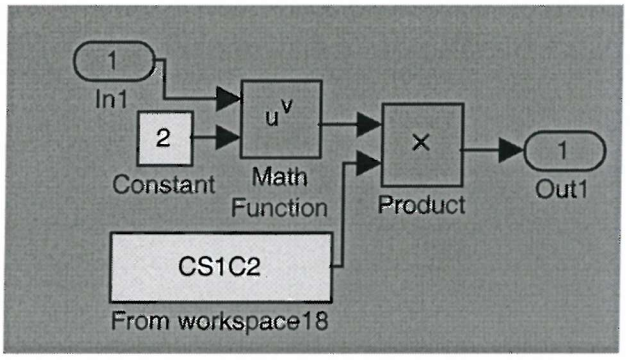
1
In1
2
Constant
u^v
Math
Function
×
Product
1
Out1
CS1C2
From workspace18

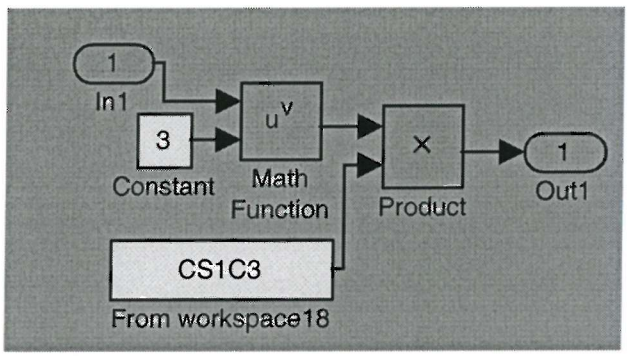
1
In1
3
Constant
u^v
Math
Function
×
Product
1
Out1
CS1C3
From workspace18

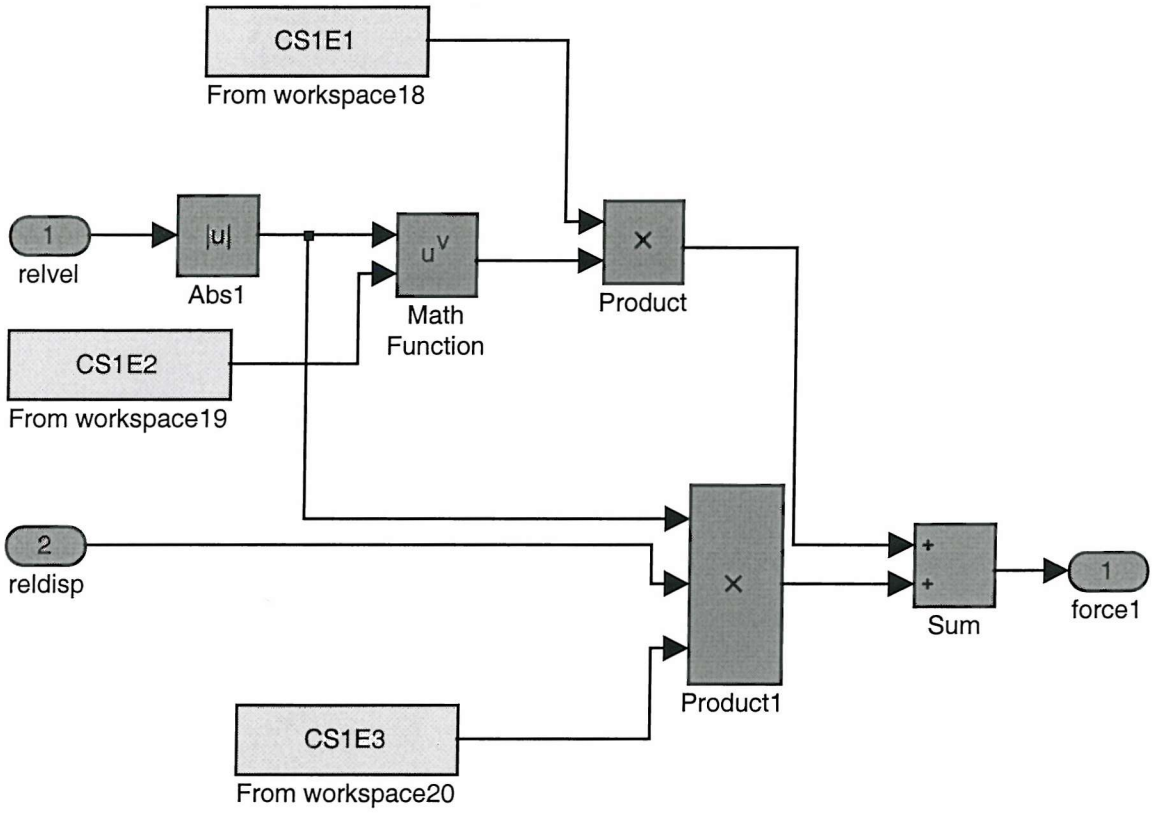
CS1E1
From workspace18
1
relvel
|u|
Abs1
u^v
Math
Function
×
Product
CS1E2
From workspace19
2
reldisp
×
Product1
+
+
Sum
1
force1
CS1E3
From workspace20

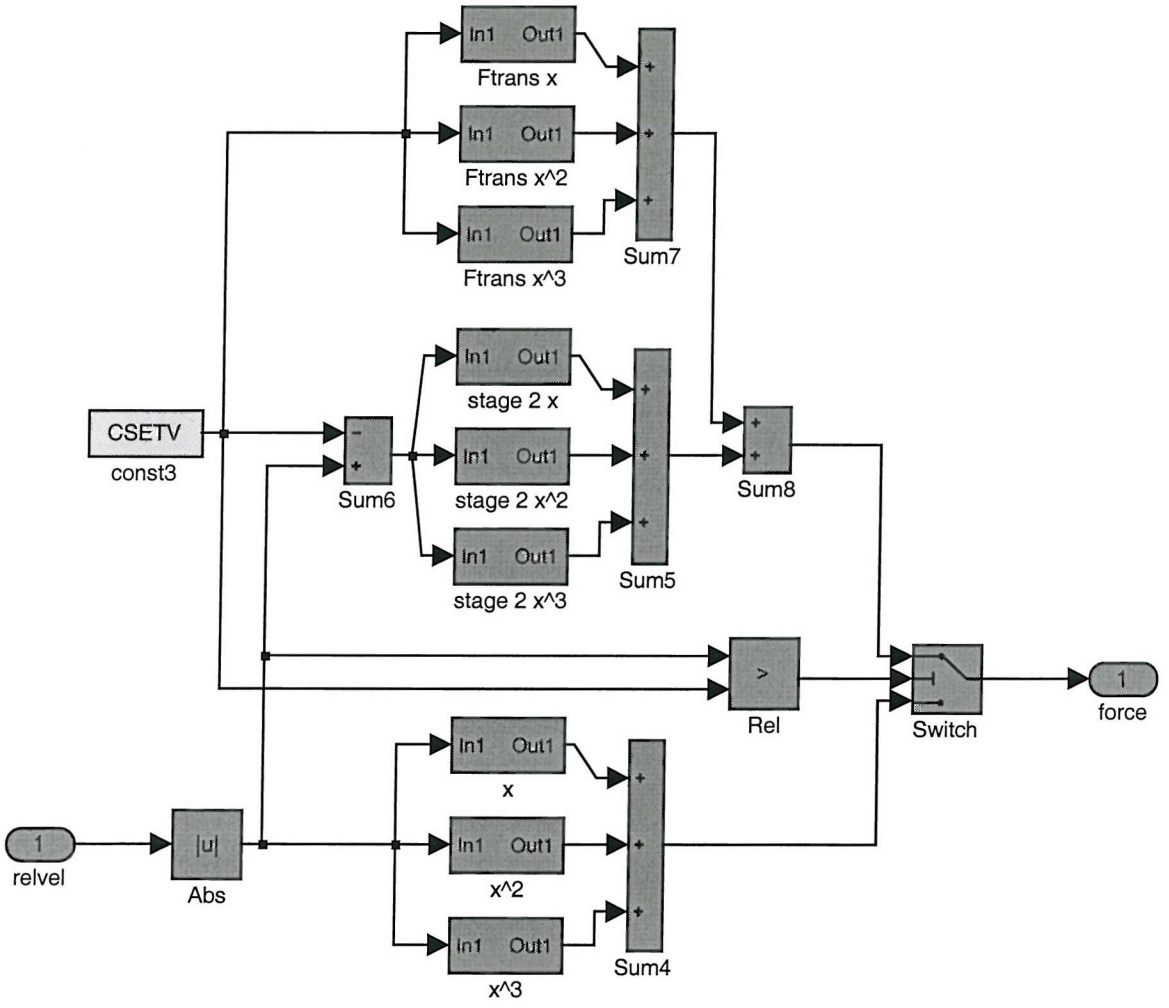
In1 Out1
Ftrans x
In1 Out1
Ftrans x^2
In1 Out1
Ftrans x^3
Sum7
In1 Out1
stage 2 x
In1 Out1
stage 2 x^2
In1 Out1
stage 2 x^3
Sum5
CSETV
const3
Sum6
Sum8
>
Rel
Switch
1
force
1
relvel
|u|
Abs
In1 Out1
x
In1 Out1
x^2
In1 Out1
x^3
Sum4

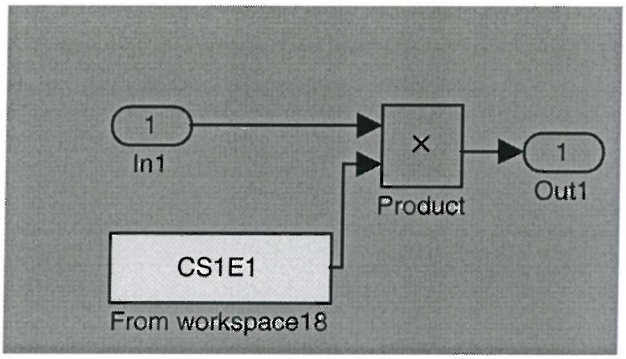
1
In1
×
Product
1
Out1
CS1E1
From workspace18

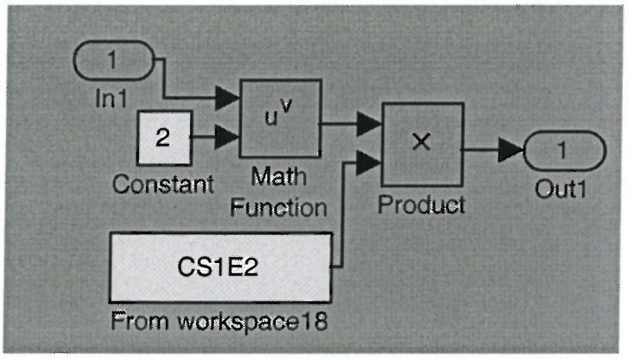
1
In1
2
Constant
u^v
Math
Function
×
Product
1
Out1
CS1E2
From workspace18

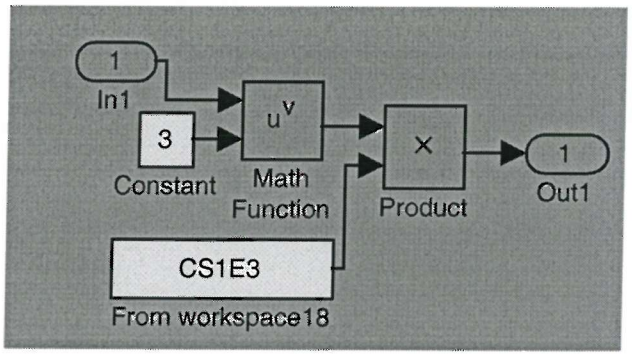
1
In1
3
Constant
u^v
Math
Function
×
Product
1
Out1
CS1E3
From workspace18

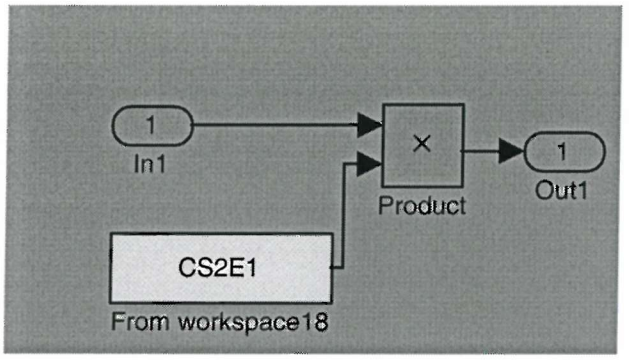
1
In1
×
Product
1
Out1
CS2E1
From workspace18

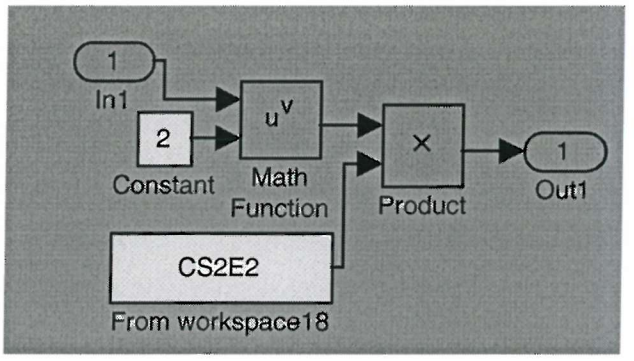
1
In1
2
Constant
u^v
Math
Function
×
Product
1
Out1
CS2E2
From workspace18

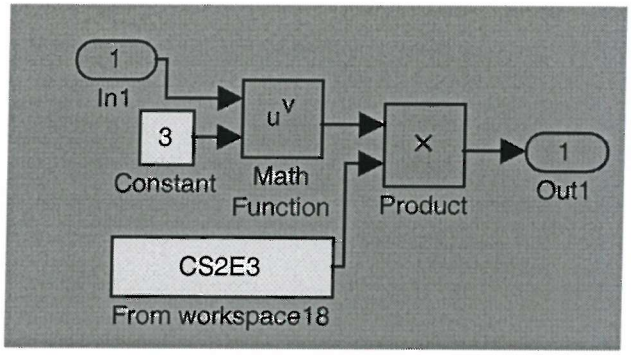
1
In1
3
Constant
u^v
Math
Function
×
Product
1
Out1
CS2E3
From workspace18

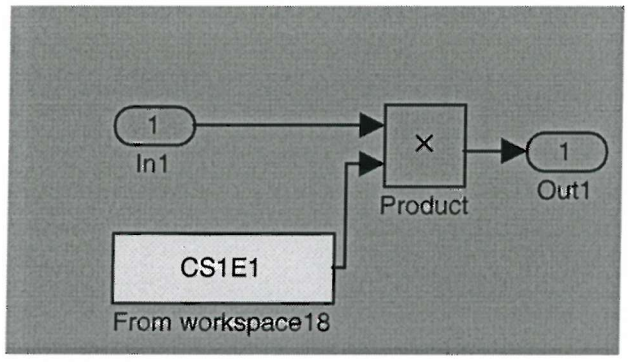
1
In1
×
Product
1
Out1
CS1E1
From workspace18

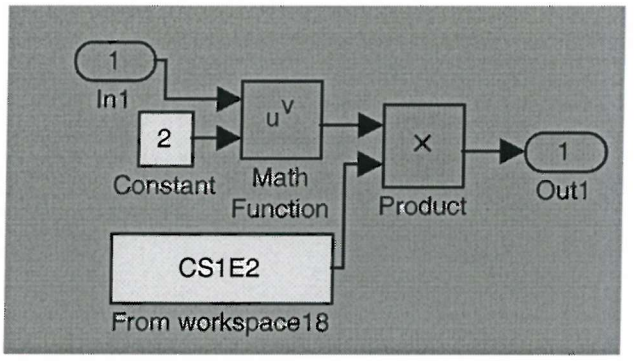
1
In1
2
Constant
u^v
Math
Function
×
Product
1
Out1
CS1E2
From workspace18

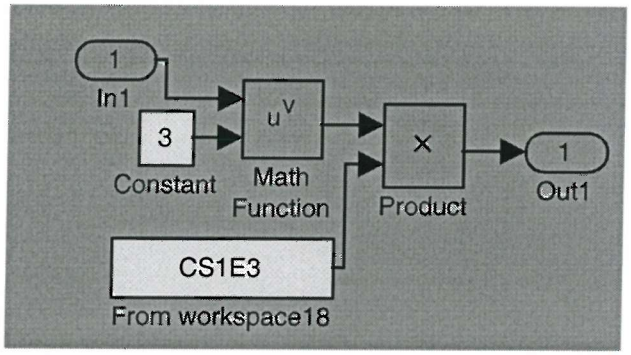
1
In1
3
Constant
u^v
Math
Function
×
Product
1
Out1
CS1E3
From workspace18

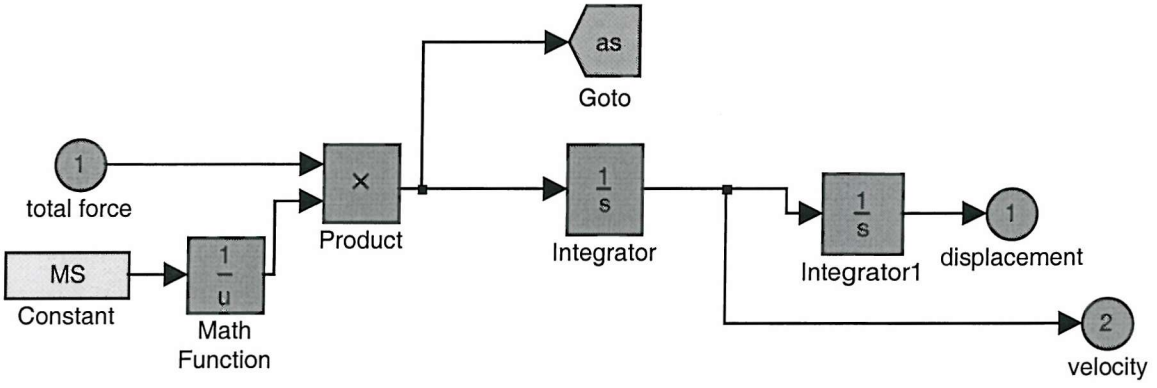
as
Goto
1
total force
×
Product
1
s
Integrator
1
s
Integrator1
1
displacement
MS
Constant
1
u
Math
Function
2
velocity

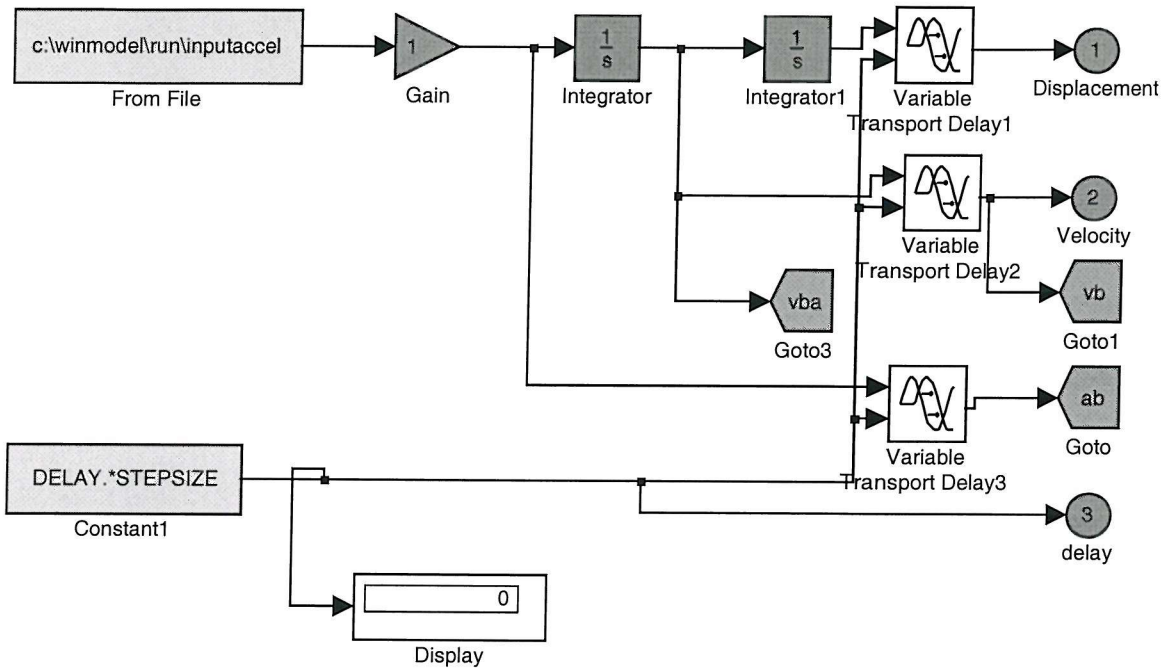
c:\winmodel\run\inputaccel
From File
1
Gain
1/s
Integrator
1/s
Integrator1
Variable Transport Delay1
1
Displacement
Variable Transport Delay2
2
Velocity
vba
Goto3
vb
Goto1
Variable Transport Delay3
ab
Goto
DELAY.*STEPSIZE
Constant1
3
delay
0
Display

APPENDIX 6: THE PARAMETER OPTIMISATION ROUTINE

The following pages contain the MATLAB code used for the parameter optimization process described in Chapter 9. The code requires the SIMULINK seat model and the associated GUI.

```
% script written TPG 18/4/2001 to optimise two (or more) seat model coefficients using separate input motions
%
% updated TPG 9-5-2001 to use PhD data for chapter 9a.
%
%  tgmultioptimisephd.m

OPTseattype='gra';%'kab','isr','gra'

%parameter set
switch OPTseattype

case 'kab'
   OPTmeasured_parameter_file='c:\winmodel\kabmessymmetric.txt';

   %low
   OPTparameters(1).datapath='E:\pexpt1datafromcd\d\d05k\EART\';
   OPTparameters(1).basenum=3022;
   OPTparameters(1).loadnum=3024;

   %high
   OPTparameters(2).datapath='E:\pexpt1datafromcd\d\d01k\EART\';
   OPTparameters(2).basenum=3072;
   OPTparameters(2).loadnum=3074;

case 'isr'
   OPTmeasured_parameter_file='c:\winmodel\isrimessymmetric.txt';

   %low
   OPTparameters(1).datapath='E:\pexpt1datafromcd\d\d01i\EART\';
   OPTparameters(1).basenum=3032;
   OPTparameters(1).loadnum=3034;

   %high
   OPTparameters(2).datapath='E:\pexpt1datafromcd\d\d0
```

```
1i\EART\';
    OPTparameters(2).basenum=3052;
    OPTparameters(2).loadnum=3054;

case 'gra'
    OPTmeasured_parameter_file='c:\winmodel\grammessymm↙
etric.txt';

    %low
    OPTparameters(1).datapath='E:\pexpt1datafromcd\d\d0↙
1g\FORW\';
    OPTparameters(1).basenum=3072;
    OPTparameters(1).loadnum=3074;

    %high
    OPTparameters(2).datapath='E:\pexpt1datafromcd\d\d0↙
1g\FORW\';
    OPTparameters(2).basenum=3112;
    OPTparameters(2).loadnum=3114;



end

% set the maximum number of simulations
OPTmaxsims=1000;

% solver parameters
OPTstepsize=1e-3;
OPTdecfact=1;

% the first parameter name, range of acceptable values↙
, and input motion to use when optimising
OPTparameters(1).name='frictgain';
OPTparameters(1).min=0;
OPTparameters(1).max=2;
OPTparameters(1).coarse=0.1;
OPTparameters(1).fine=0.01;


% the second parameter
```

```
OPTparameters(2).name='csgain';
OPTparameters(2).min=0;
OPTparameters(2).max=2;
OPTparameters(2).coarse=0.1;
OPTparameters(2).fine=0.01;

%%%%%%%%%%%%%%%%%%%%%%%%%%%%%%%%%%%%%%%%%%%%%%%%%%%%%%%%%%%%%%%%%%%%%%%%%%%%%%%
%%%%


% open the model
seatmodel

% load the model GUI handle list
OPThandlist=allchild(1);

% load the measured parameter set
set(findobj(OPThandlist,'Tag','seatdata'),'string',OPT
measured_parameter_file);
mguicode(7);

% set the sampling rate and output decimation factor
set(findobj(OPThandlist,'Tag','stepsize'),'string',num
2str(OPTstepsize));
set(findobj(OPThandlist,'Tag','decfact'),'string',num2
str(OPTdecfact));


%%%%%%%%%%%%%%%%%%%%%%%%%%%%%%%%%%%%%%%%%%%%%%%%%%%%%%%%%%%%%%%%%%%%%%%%%%%%%%%
%%%%%%%%%%%%%%

OPTsuccessflag=0;
OPTstepsize=0; % coarse step size (fine=1)
OPTnsim=0; % counter of simulations
OPTnparas=length(OPTparameters); % get the number of p
arameters to optimise

% set arbitrarily high initial error values
for cc=1:OPTnparas
   OPTparameters(cc).OPTolderr=100;
end
```

```
%%%%%%%%%%%%%%%%%%%%%%%%%%%%%%%%%%%%%%%%%%%%%%%%%%%%%%%%%%%%%%%%%%%%%%%
%%%%

% loop through up to OPTmaxiter iterations

tic; % start clock
while OPTsuccessflag==0

   % randomise the order of the parameters
   OPTparaord=randperm(OPTnparas);

   % loop through parameters
   for r=1:OPTnparas


      % get current parameter value, name and step size.
      %(OPTparaval(2) is the middle of the three values to be investigated)

      eval(['OPTparaval(2)=',upper(OPTparameters(OPTparaord(r)).name),';'])

      OPTcurrpara=upper(OPTparameters(OPTparaord(r)).name);

      % select coarse or fine step size
      if OPTstepsize==0
         OPTcurrstep=OPTparameters(OPTparaord(r)).coarse;
      else
         OPTcurrstep=OPTparameters(OPTparaord(r)).fine;
      end


      % get the target acceleration time history and low pass filter at 40 Hz
      % load, invert and filter the data
```

```
      eval(['cd ',OPTparameters(OPTparaord(r)).datapat↙
h]);
      [OPTmcush, OPTt0, OPTmfs, OPTmode, OPTother] = r↙
eadf(OPTparameters(OPTparaord(r)).loadnum);
      OPTmcush=(OPTmcush-mean(OPTmcush(round(0.1.*OPTm↙
fs):round(0.4.*OPTmfs))));
      OPTmtime=OPTt0(1:length(OPTmcush));
      [OPTb,OPTa]=butter(6,40./(OPTmfs./2));
      OPTmcush=filtfilt(OPTb,OPTa,OPTmcush);

      [OPTmdisp, OPTt0, OPTmfs, OPTmode, OPTother] = r↙
eadf(OPTparameters(OPTparaord(r)).loadnum+1);
       OPTmdisp=(OPTmdisp-mean(OPTmdisp(round(0.1.*OPT↙
mfs):round(0.4.*OPTmfs))));

      % set the seat base (model input) motion
      set(findobj(OPThandlist,'Tag','pathnam'),'string↙
',[OPTparameters(OPTparaord(r)).datapath,...
            num2str(OPTparameters(OPTparaord(r)).basen↙
um),'.dat']);
      mguicode(9)



      % evaluate the model at the two values either si↙
de of the currnet value
      %%%%%%%%%%%%%%%%%%%%%%%%%%%%%%%%%%%%%%%%%%%%%%%↙
%%%%%%%%%%%%%%%%%%%



      % update the GUI
      drawnow
      OPTparaval(2)=str2num(get(findobj(OPThandlist,'T↙
ag',[lower(OPTcurrpara),'val']),'string'));

      % run the simulation
      mguicode(3)

      % load model acceleration results
      load c:\winmodel\run\accelout
```

```
      OPTnsim=OPTnsim+1; % counter of successful simul↙
ations

      % check sample rates and interpolate the predice↙
td time history if necessary
      OPTmfs=round(1./(OPTmtime(2)-OPTmtime(1)));
      OPTpfs=round(1./(accelout(1,2)-accelout(1,1)));
      if OPTmfs~=OPTpfs
         OPTaccelout4 = interp1(accelout(1,:),accelout↙
(4,:),OPTmtime,'spline');
      else
         OPTaccelout4=accelout(4,:)';
      end



      load c:\winmodel\run\dispout
      figure(6)
      subplot(2,1,1)
      plot(OPTmcush,'k-')
      hold on
      plot(OPTaccelout4,'g:')
      hold on
      subplot(2,1,2)
      plot(OPTmdisp,'k-')
      hold on
      plot(dispout(2,:).*1000,'g:')
      hold on



      % calculate the error
      OPTerror(2)=tgrmserr(OPTmcush,OPTaccelout4);


      %%%%%%%%%%%%%%%%%%%%%%%%%%%%%%%%%%%%%%%%%%%%%%%↙
%%%%%%%%%%%%%%%%%%

      OPTparaval(1)=OPTparaval(2)-OPTcurrstep;

      % set the parameter value in the GUI and update ↙
```

```
it
      set(findobj(OPThandlist,'Tag',[lower(OPTcurrpara↙
),'val']),'string',num2str(OPTparaval(1)))
      drawnow

      % run the simulation
      mguicode(3)

      % load model acceleration results
      load c:\winmodel\run\accelout

      OPTnsim=OPTnsim+1; % counter of successful simul↙
ations

      % check sample rates and interpolate the predice↙
td time history if necessary
      OPTmfs=round(1./(OPTmtime(2)-OPTmtime(1)));
      OPTpfs=round(1./(accelout(1,2)-accelout(1,1)));
      if OPTmfs~=OPTpfs
         OPTaccelout4 = interp1(accelout(1,:),accelout↙
(4,:),OPTmtime,'spline');
      else
         OPTaccelout4=accelout(4,:)';
      end


            load c:\winmodel\run\dispout
      figure(6)
      subplot(2,1,1)
      hold on
      plot(OPTaccelout4,'b:')
      hold on
      subplot(2,1,2)
      hold on
      plot(dispout(2,:).*1000,'b:')
      hold on




      % calculate the error
```

```
      OPTerror(1)=tgrmserr(OPTmcush,OPTaccelout4);


      %%%%%%%%%%%%%%%%%%%%%%%%%%%%%%%%%%%%%%%%%%%%%%%%%%%%%%%%%%%%%%%%%%%%%%%%%%%%%%%%%

      OPTparaval(3)=OPTparaval(2)+OPTcurrstep;

      % set the parameter value in the GUI
      set(findobj(OPThandlist,'Tag',[lower(OPTcurrpara),'val']),'string',num2str(OPTparaval(3)))
      drawnow

      % run the simulation
      mguicode(3)

      % load model acceleration results
      load c:\winmodel\run\accelout

      OPTnsim=OPTnsim+1; % counter of successful simulations

      % check sample rates and interpolate the predicted time history if necessary
      OPTmfs=round(1./(OPTmtime(2)-OPTmtime(1)));
      OPTpfs=round(1./(accelout(1,2)-accelout(1,1)));
      if OPTmfs~=OPTpfs
         OPTaccelout4 = interp1(accelout(1,:),accelout(4,:),OPTmtime,'spline');
      else
         OPTaccelout4=accelout(4,:)';
      end


            load c:\winmodel\run\dispout
      figure(6)
      subplot(2,1,1)
      plot(OPTaccelout4,'r:')
      hold off
      subplot(2,1,2)
      plot(dispout(2,:).*1000,'r:')
```

```
        hold off

        %  calculate the error
        OPTerror(3)=tgrmserr(OPTmcush, OPTaccelout4);


        %%%%%%%%%%%%%%%%%%%%%%%%%%%%%%%%%%%%%%%%%%%%%%%%%%%%%%%%%%%%%%%%%%%%%%

        % set the present error to be the old error
        OPTparameters(OPTparaord(r)).OPTolderr=OPTerror(2);


        % check for any variation in error between the three values. If all are identical, stay with the current one
        if OPTerror(1)==OPTerror(2)==OPTerror(3)
           OPTnewval=OPTparaval(2);
           % set the initial parameter for the next step
           OPTerror(2)=OPTminerrval;
           % set minima location flag ON
           OPTparameters(OPTparaord(r)).minloc=1;

        else
           % find the lower error
           [OPTminerrval,OPTminerrind]=min(OPTerror);


           if OPTminerrind==2;
              % set minima location flag ON
              OPTparameters(OPTparaord(r)).minloc=1;
              % keep error(2) and parameter(2) as the staring error for next time
              OPTnewval=OPTparaval(2);

              % check if the parameter has exceeded the allowable bounds
           elseif OPTparaval(OPTminerrind)>OPTparameters(OPTparaord(r)).max
              OPTnewval=OPTparaval(2);
```

```
            % set minima location flag ON
            OPTparameters(OPTparaord(r)).minloc=1;
            % keep error(2) as the staring error for n↙
ext time

         elseif OPTparaval(OPTminerrind)<OPTparameters↙
(OPTparaord(r)).min
            OPTnewval=OPTparaval(2);

            % set minima location flag ON
            OPTparameters(OPTparaord(r)).minloc=1;
            % keep error(2) as the staring error for n↙
ext time


         else
            % set minima location flag OFF
            OPTparameters(OPTparaord(r)).minloc=0;
            % keep error(2) as the staring error for n↙
ext time
            OPTerror(2)=OPTminerrval;
            OPTnewval=OPTparaval(OPTminerrind);

         end

      end % end of if statement looking for difference↙
s in error value

      % set new parameter value in the GUI
      set(findobj(OPThandlist,'Tag',[OPTparameters(OPT↙
paraord(r)).name,'val']),'string',num2str(OPTnewval));
      drawnow

      % calculate number of parameters at their optima↙
l value
      OPTnoptimal=0;
      for q=1:OPTnparas;
         OPTnoptimal=OPTnoptimal+OPTparameters(q).minl↙
oc;
      end
```

```
      OPTpercentoptimal=OPTnoptimal./OPTnparas.*100;

      % chalculate relative change in error
      OPTerrchange=(OPTerror(2)-OPTparameters(OPTparao↙
rd(r)).OPTolderr)./OPTparameters(OPTparaord(r)).OPTold↙
err.*100;



      fprintf(['\nParameter ',OPTcurrpara,' was ',num2↙
str(OPTparaval(2)),' and is now ',...
            num2str(OPTnewval),' with error ', num2str↙
(OPTerror(2)),'\n']);
      fprintf(['Values ',num2str(OPTparaval),', ', num↙
2str(OPTpercentoptimal),'%% optimal\n']);
      fprintf(['Errors ',num2str(OPTerror(1)),' ',num2↙
str(OPTparameters(OPTparaord(r)).OPTolderr),' ',num2st↙
r(OPTerror(3)),', ', num2str(OPTerrchange),'%% change\↙
n']);



   end % end of parameter loop

   % check for success
   if OPTpercentoptimal==100
      if OPTstepsize==0;

         fprintf(['\nSWITCHING TO FINE STEP SIZE\n']);
         OPTnoptimal=0;
         for q=1:OPTnparas
            OPTparameters(q).minloc=0;
         end
         % use the fine step size
         OPTstepsize=1;
      else
         fprintf(['\nCOMPLETE\n']);
         OPTsuccessflag=1; % end WHILE statement
      end
```

```
    end % end of success check

    % store result

       res1=(get(findobj(OPThandlist,'Tag',[lower(OPTpa↙
rameters(1).name),'val']),'string'));
     res2=(get(findobj(OPThandlist,'Tag',[lower(OPTpara↙
meters(2).name),'val']),'string'));

    fid=fopen('D:\PHD\Final documents new\09a-Parameter↙
 optimisation\multiopt\multioptlog.txt','a');
    fprintf(fid,['\n',OPTseattype,',',res1,',',res2]);
    fclose(fid)


end % end of iteration WHILE loop
```

APPENDIX 7 : THE SEAT PARAMETER VALUES

The following page shows the seat parameter values used in the model for Chapter 10 and Chapter 12.

Dummy top mass acceleration	$\ddot{x}_1$	initially 0 ms^{-2}
Dummy case mass or semi-rigid load mass acceleration	$\ddot{x}_0$	initially 0 ms^{-2}
Suspension moving mass acceleration	$\ddot{x}_s$	initially 0 ms^{-2}
Seat base acceleration	$\ddot{x}_b$	INPUT
Dummy top mass	m_1	46 kg
Dummy stiffness	k_1	45.3 kNm^{-1}
Dummy damping	c_1	1.35 $kNsm^{-1}$
Dummy case mass	m_0	10 kg
Semi-rigid load mass		56 kg
Cushion stiffness	k_c	92.1 kNm^{-1}
Cushion damping	c_c	1.37 $kNsm^{-1}$
Suspended seat mass	m_s	27 kg
Suspension stiffness	k_s	4.57 kNm^{-1}
Suspension damper gas loading stiffness	k_d	2.32 kNm^{-1}
Horizontal distance between damper mounting points at mid ride	d_h	150 mm
Vertical distance between damper mounting points at mid ride	d_v	111 mm
Suspension damping and friction coefficients (from Chapter 9)	A_c	$2.37x10^3$
	A_e	$1.68x10^3$
	B_c	1.49
	B_e	1.57
	C_c	$2.12x10^4$
	C_e	$2.36x10^3$
	D	70 N
	E	44 N
Free travel between end-stops	*travel*	64 mm
Offset of the mean ride position from the mid point of the free suspension travel	*offset*	-10 mm
Bottom buffer axial force-deflection characteristic fit coefficients	a_1	$1.83x10^{11}$
	a_2	$-8.57x10^7$
	a_3	-4.45x10
	a_4	$1.50x10^6$
	a_5	$7.63x10^3$
Number of bottom buffers	n_{bb}	2
Horizontal distance at mid ride between the ends of the linkage arm which contacts the top buffer	lh_{mid}	295 mm
Vertical distance at mid ride between the ends of the linkage arm which contacts the top buffer	lv_{mid}	150 mm
Top buffer axial force-deflection characteristic fit coefficients	b_1	$5.48x10^{15}$
	b_2	$-2.57x10^4$
	b_3	$2.60x10^3$
	b_4	$3.27x10^7$
	b_5	$1.35x10^5$
Number of top buffers	n_{tb}	2
Present time	t	initially 0 s
Integration time step	Δt	$1x10^{-3}$ s
Acceleration due to gravity	g	9.81 ms^{-2}

APPENDIX 8 : RESULTS OF THE COMPARISON OF THE PERFORMANCE OF THE FORCE-LIMITED LINEAR CUSHION MODEL AND THE COMPRESSION-VARYING CUSHION MODEL

The following pages show the predicted SEAT values and r.m.s. errors obtained with the earthmover seat model as used in Chapter 10 with the force-limited linear cushion and with the earthmover seat model using the compression-varying cushion as described in Chapter 11. Both sets of predictions are compared with the laboratory measurements of the earthmover seat performance obtained in Chapter 5.

The three pages show the results for each waveform (1.5 cycle, 4.5 cycle and 11.5 cycle). The motions corresponding to measured seat behavior classified as stage 1/2 (friction locked or breaking away from friction, defined by less than 15mm peak suspension displacement), stage 3 (greater than 15mm peak suspension displacement but no end-stop impacts) and stage 4/5 (end-stop impacts) are labeled as 'low', 'med' and 'high' respectively.

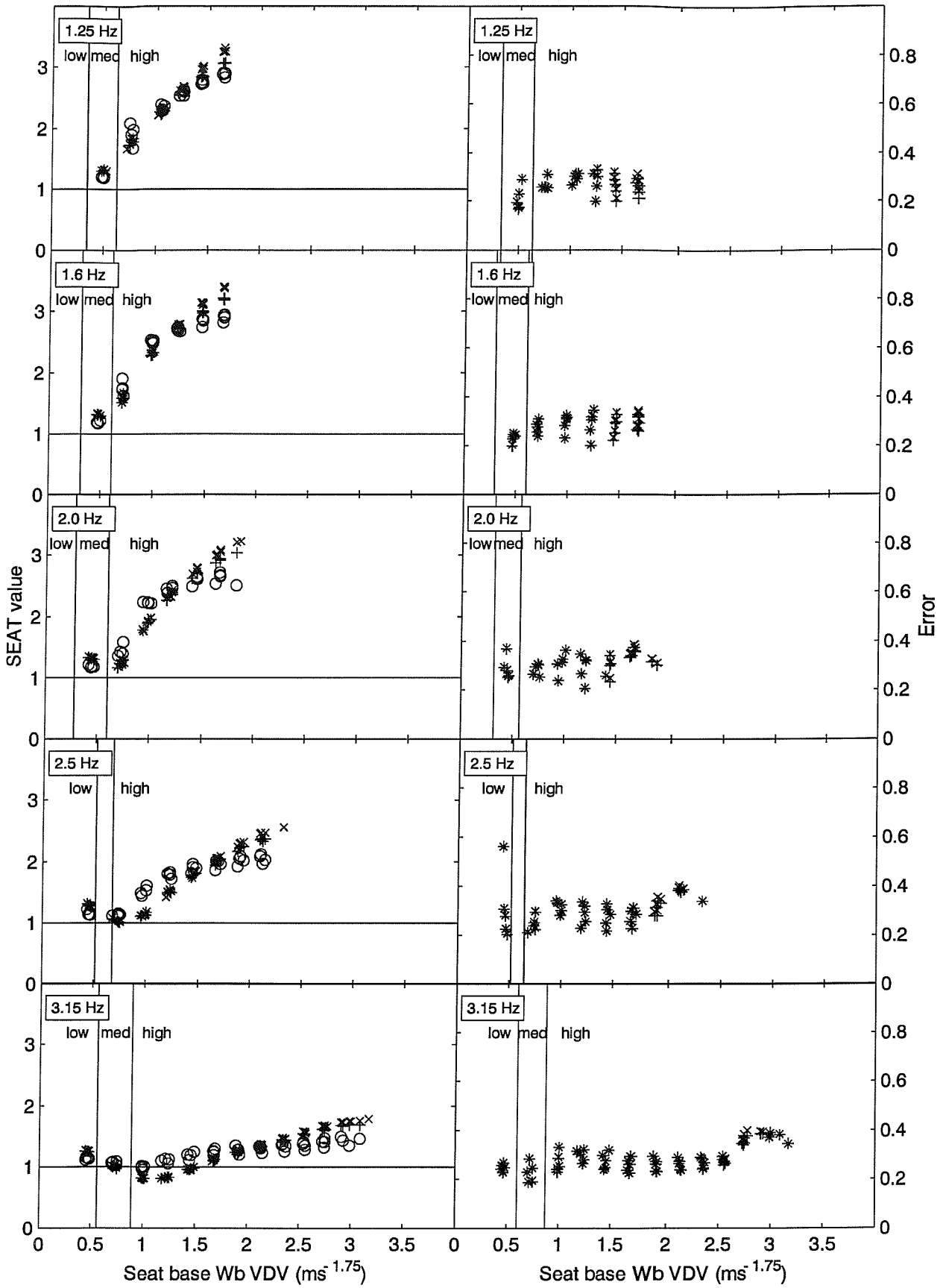

Figure 8:1 The left-hand column shows the SEAT values obtained using the 1.5 cycle input motion in the laboratory (o) and using the seat model with the force-limited linear (+) and compression-varying (x) cushions. The right-hand column shows the r.m.s. error between the measured load acceleration and the seat model with the force-limited linear (+) and compression-varying (x) cushions.

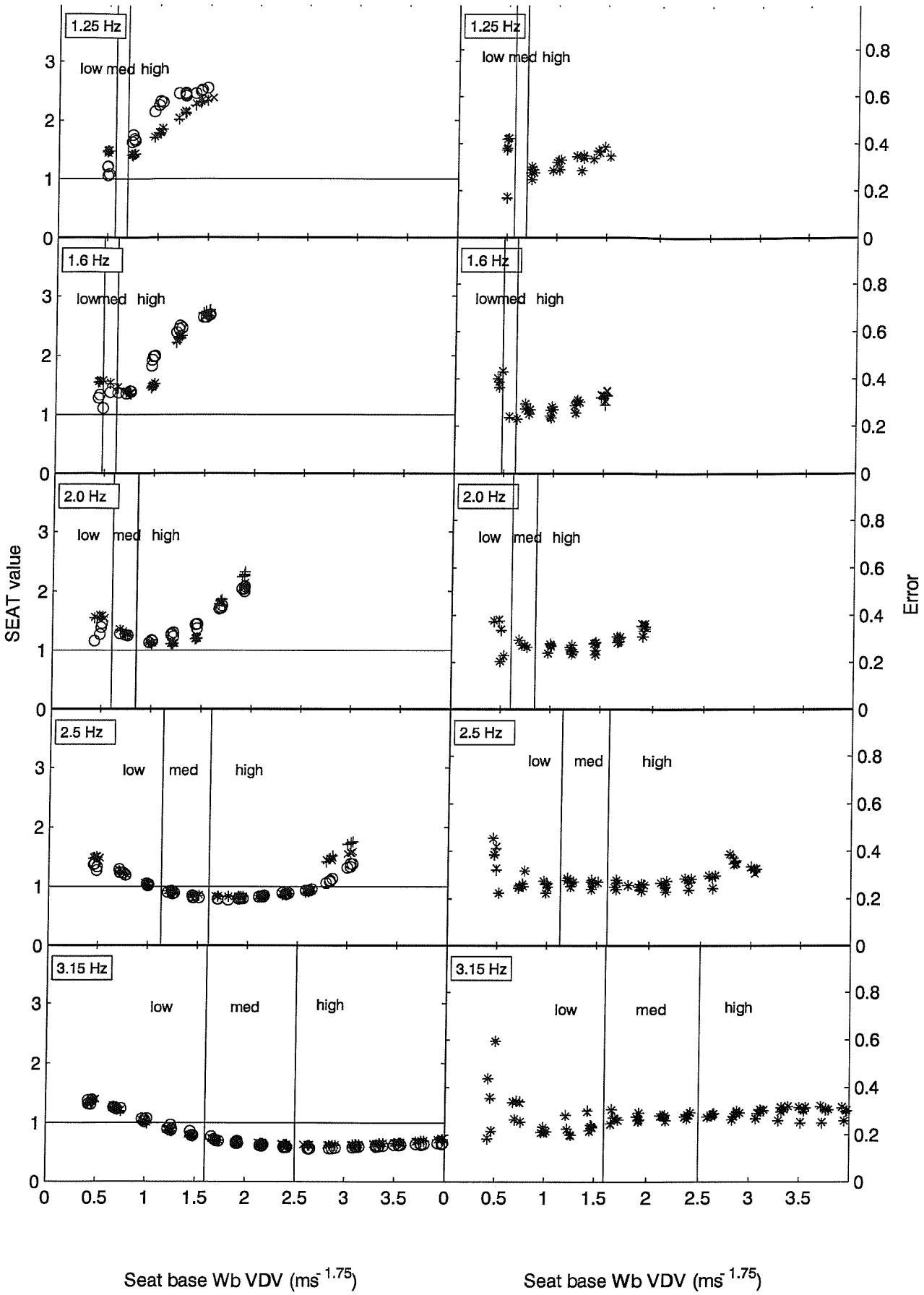

Figure 8:2 The left-hand column shows the SEAT values obtained using the 4.5 cycle input motion in the laboratory (o) and using the seat model with the force-limited linear (+) and compression-varying (x) cushions. The right-hand column shows the r.m.s. error between the measured load acceleration and the seat model with the force-limited linear (+) and compression-varying (x) cushions..

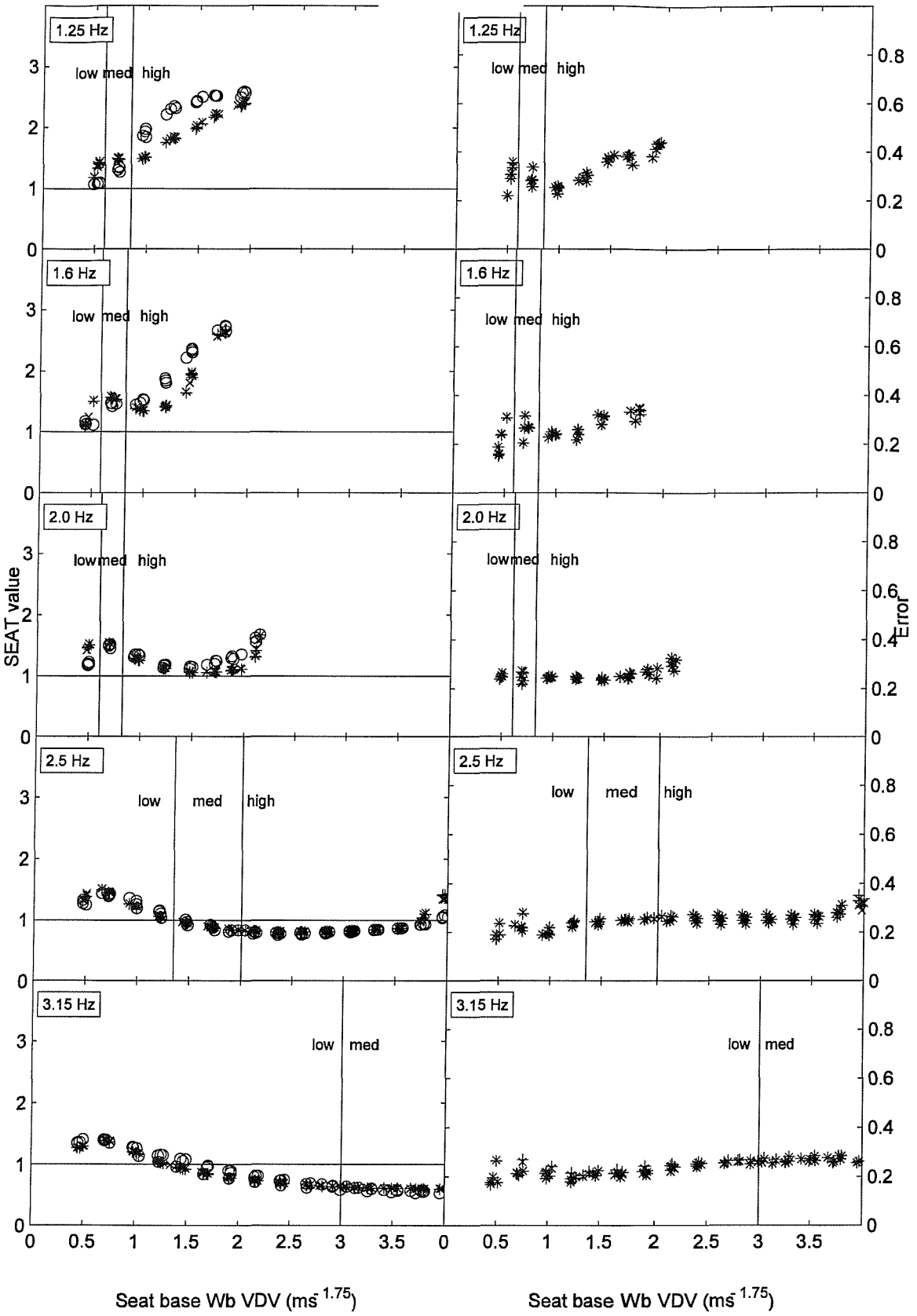

Figure 8:3 The left-hand column shows the SEAT values obtained using the 11.5 cycle input motion in the laboratory (o) and using the seat model with the force-limited linear (+) and compression-varying (x) cushions. The right-hand column shows the r.m.s. error between the measured load acceleration and the seat model with the force-limited linear (+) and compression-varying (x) cushions.

APPENDIX 9 PARAMETRIC SENSITIVITY ANALYSIS RESULTS

This appendix shows the effect of changes in seat component parameters on the performance of the earthmover seat as quantified by the W_b-weighted SEAT value.

Each page shows the SEAT values obtained when varying one seat component parameter value in response to one duration of input motion. There were three durations of motion (1.5, 4.5 and 11.5 cycles) so there are three pages of results for each component parameter.

There are five pairs of graphs down each page corresponding to the five input frequencies used in this study (1.25 Hz, 1.6 Hz, 2.0 Hz, 2.5 Hz and 3.15 Hz). Each graph shows the SEAT value varying with input magnitude. The input magnitude is on the x-axis in each case and is shown in terms of the W_b-weighted VDV at the seat base.

The contour plots on the left of each page show the parameter value (e.g. the cushion stiffness) varying on the y-axis, and show the SEAT value as shaded contours. Minor contours are shown at intervals of 0.1, and major contours at intervals of 1. The SEAT values are expressed such that a value of 1.0 indicates the same VDV on the seat surface as at the seat base. This notation was used in place of the more conventional percentages to avoid confusion between a percentage absolute SEAT value and a percentage change in SEAT value when discussing the results. Each contour plot is based on a 16 x 19 grid of results (sixteen magnitudes and nineteen parameter values) and uses linear interpolation between these points to determine the contours locations.

The line graphs on the right of each page show the SEAT value using the measured component parameter value and half and double this value.

The influence of the linear cushion stiffness on the seat performance
using the shortduration (1.5 cycle) input motion

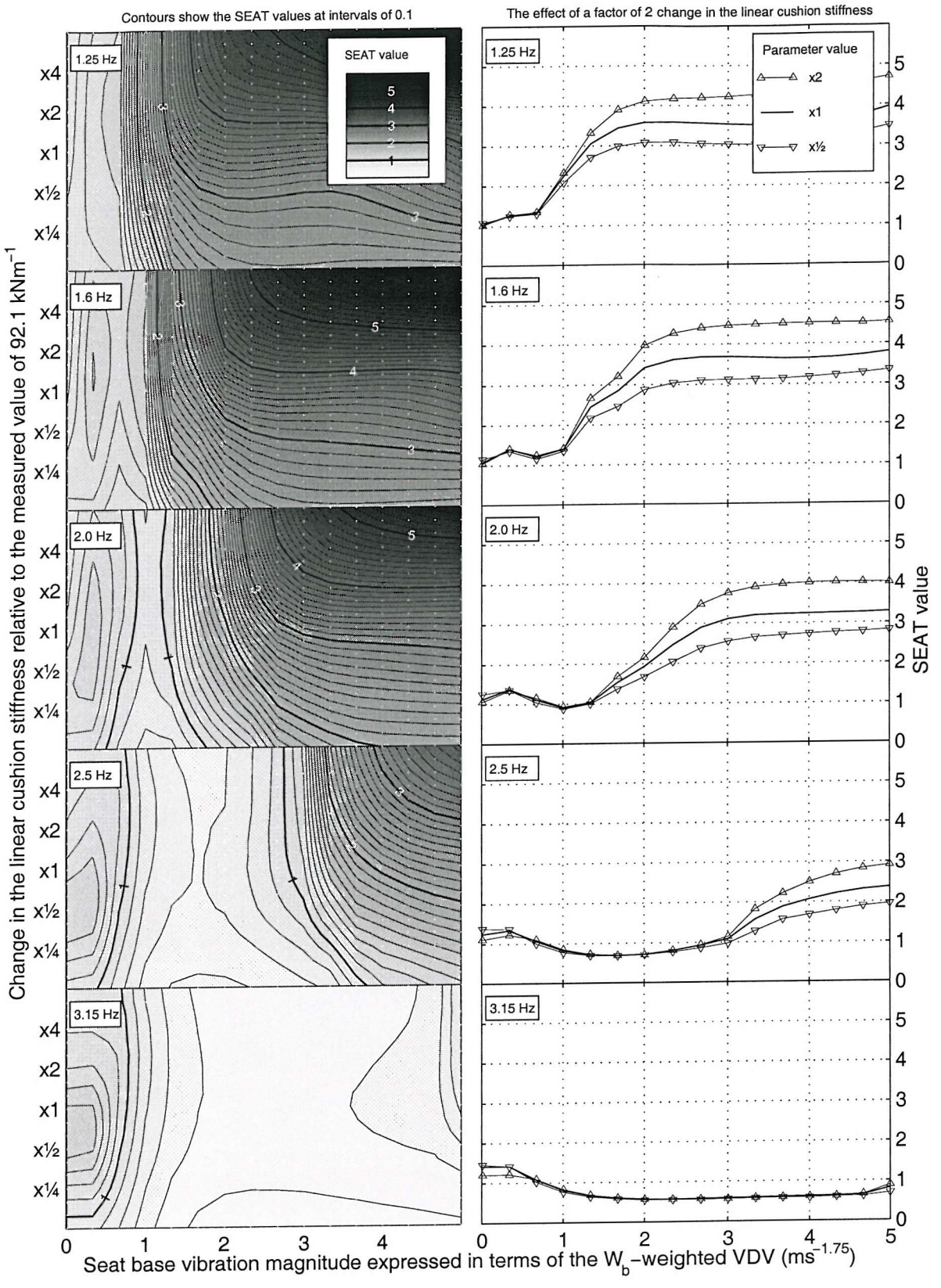

Figure 9:1 The effect of the linear cushion stiffness on the predicted SEAT value using the short duration (1.5 cycle) input motion

The influence of the linear cushion stiffness on the seat performance using the medium duration (4.5 cycle) input motion

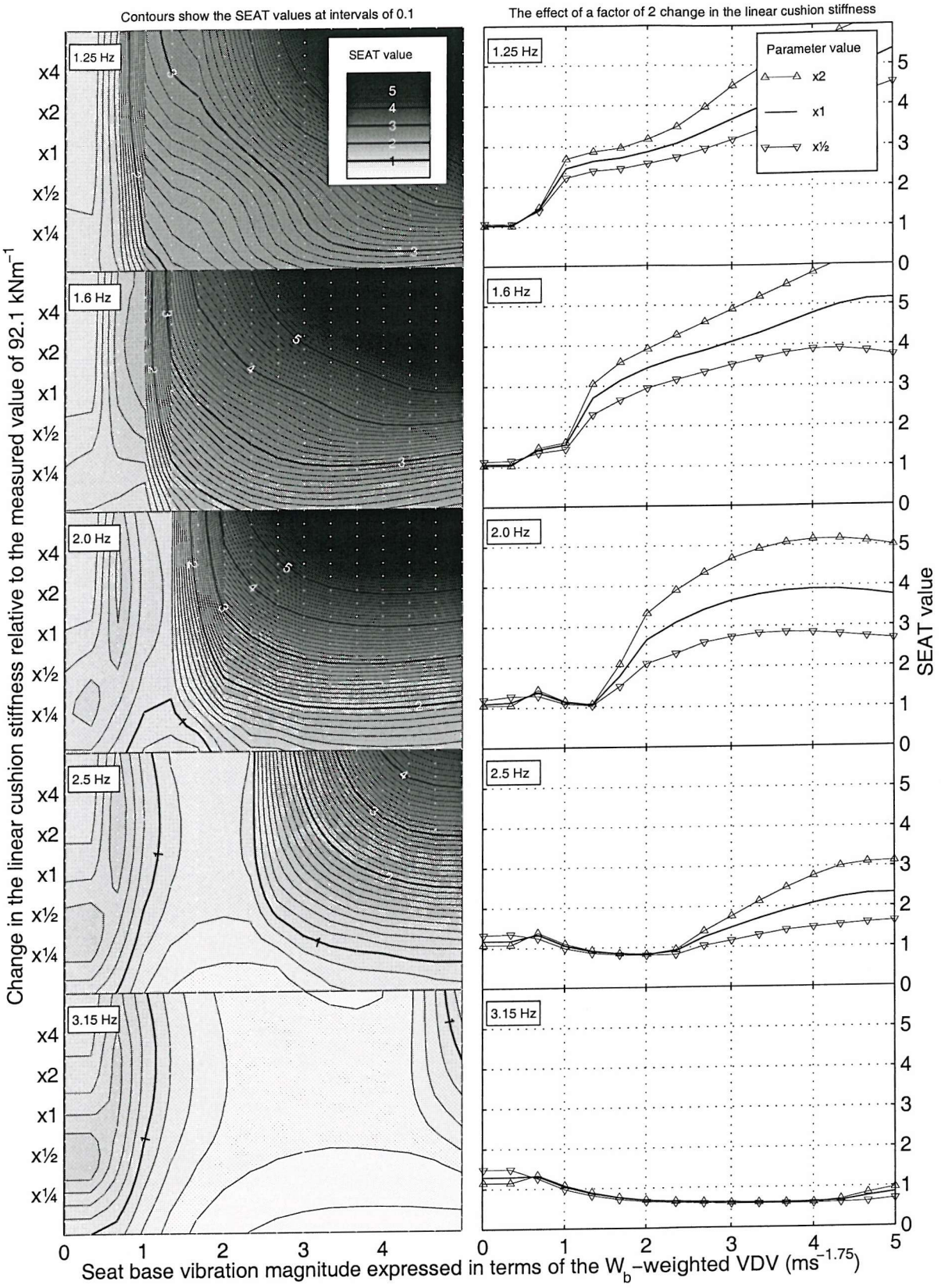

Figure 9:2 The effect of the linear cushion stiffness on the predicted SEAT value using the medium duration (4.5 cycle) input motion

The influence of the linear cushion stiffness on the seat performance using the longduration (11.5 cycle) input motion

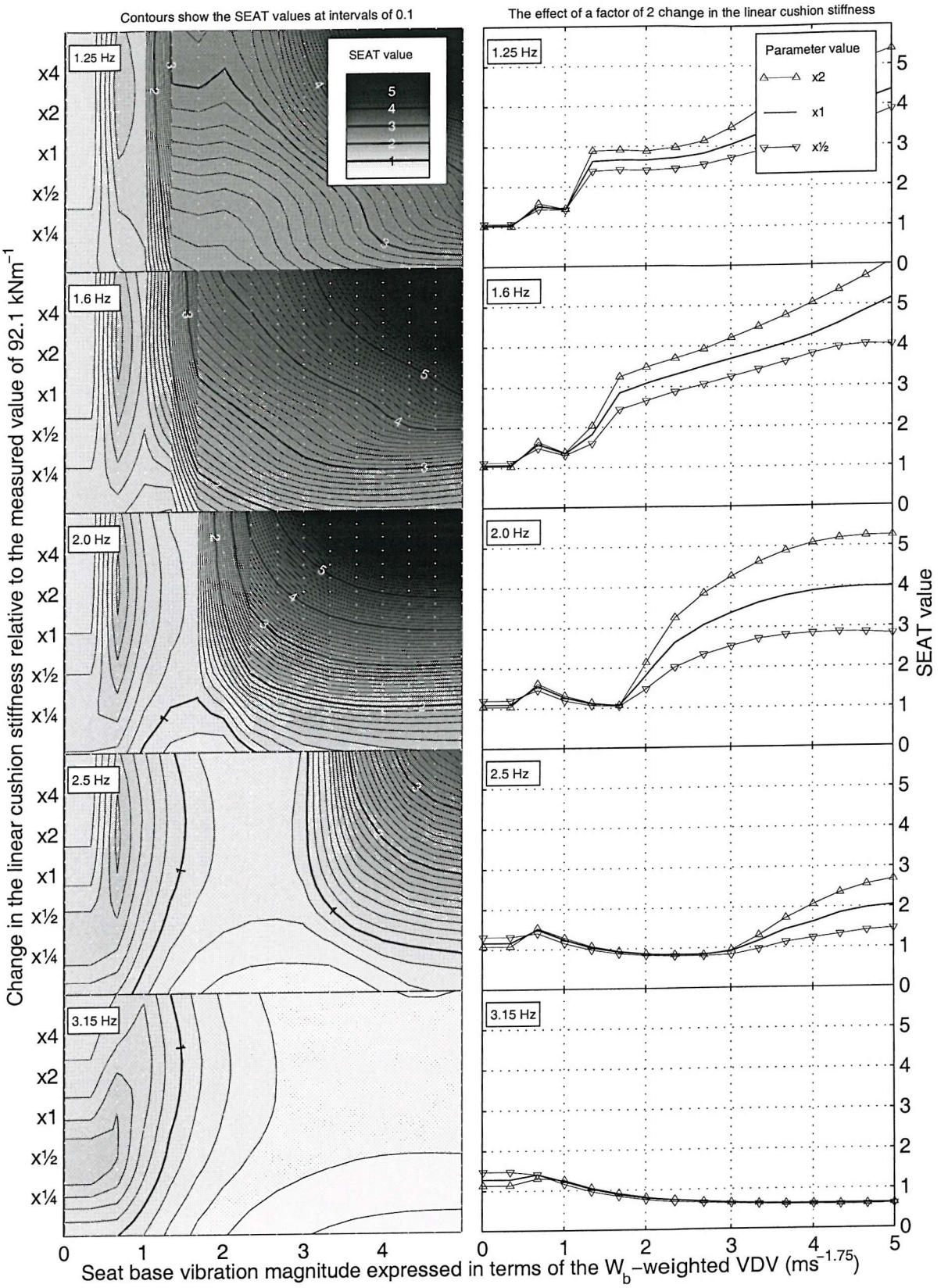

Figure 9:3 The effect of the linear cushion stiffness on the predicted SEAT value using the long duration (11.5 cycle) input motion

The influence of the linear cushion damping on the seat performance
using the short duration (1.5 cycle) input motion

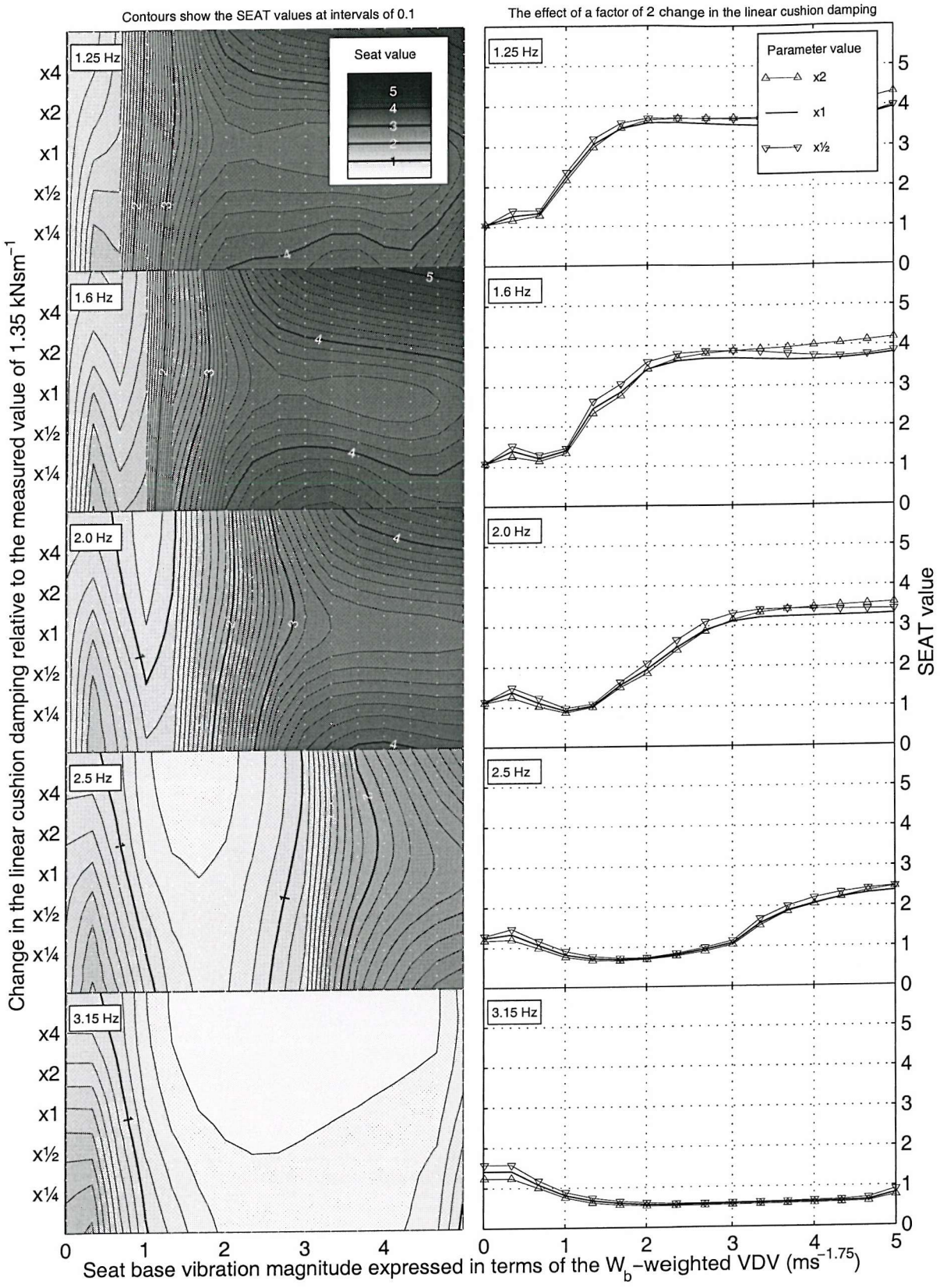

Figure 9:4 The effect of the linear cushion damping on the predicted SEAT value using the short duration (1.5 cycle) input motion

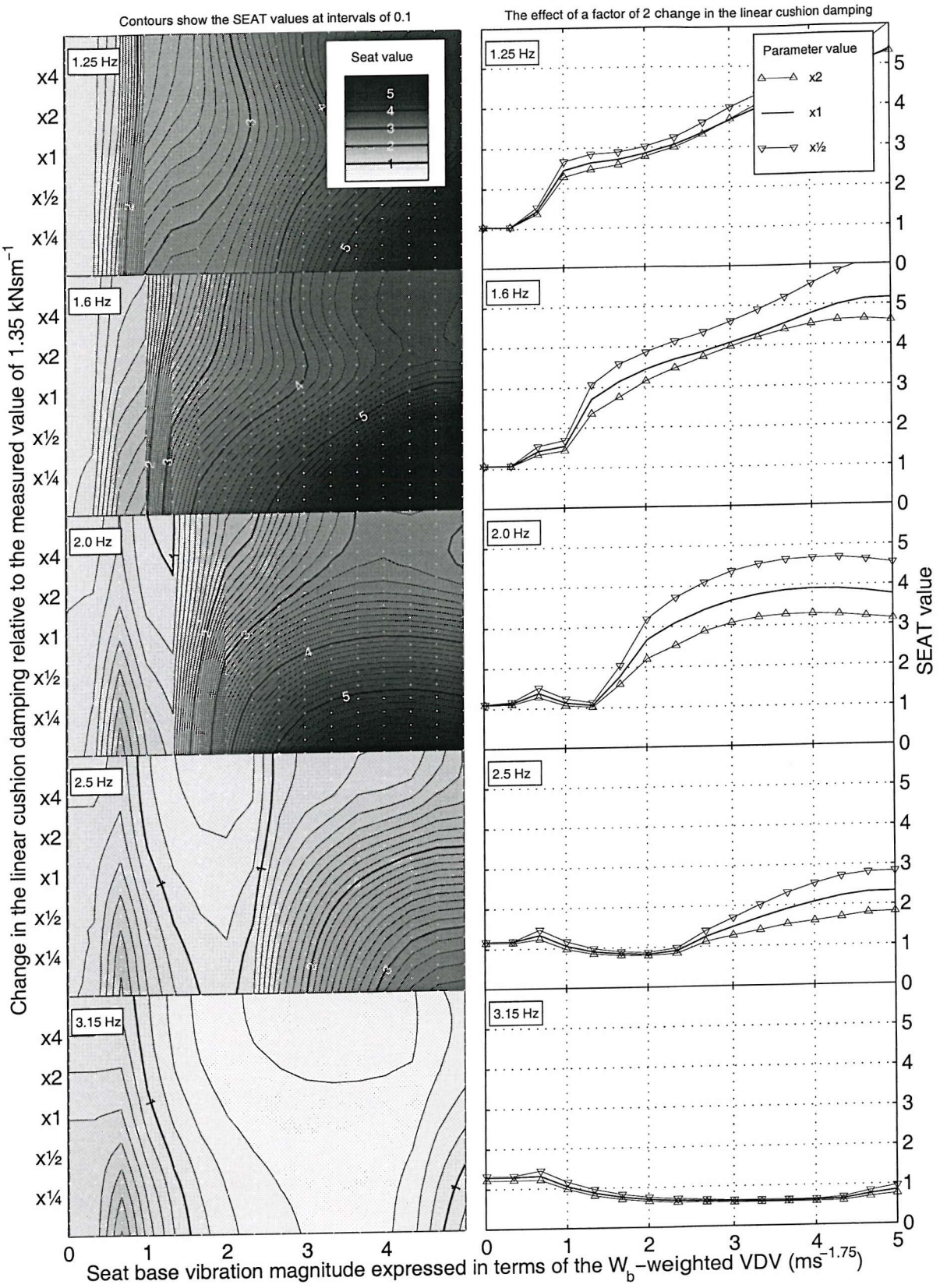

Figure 9:5 The effect of the linear cushion damping on the predicted SEAT value using the medium duration (4.5 cycle) input motion

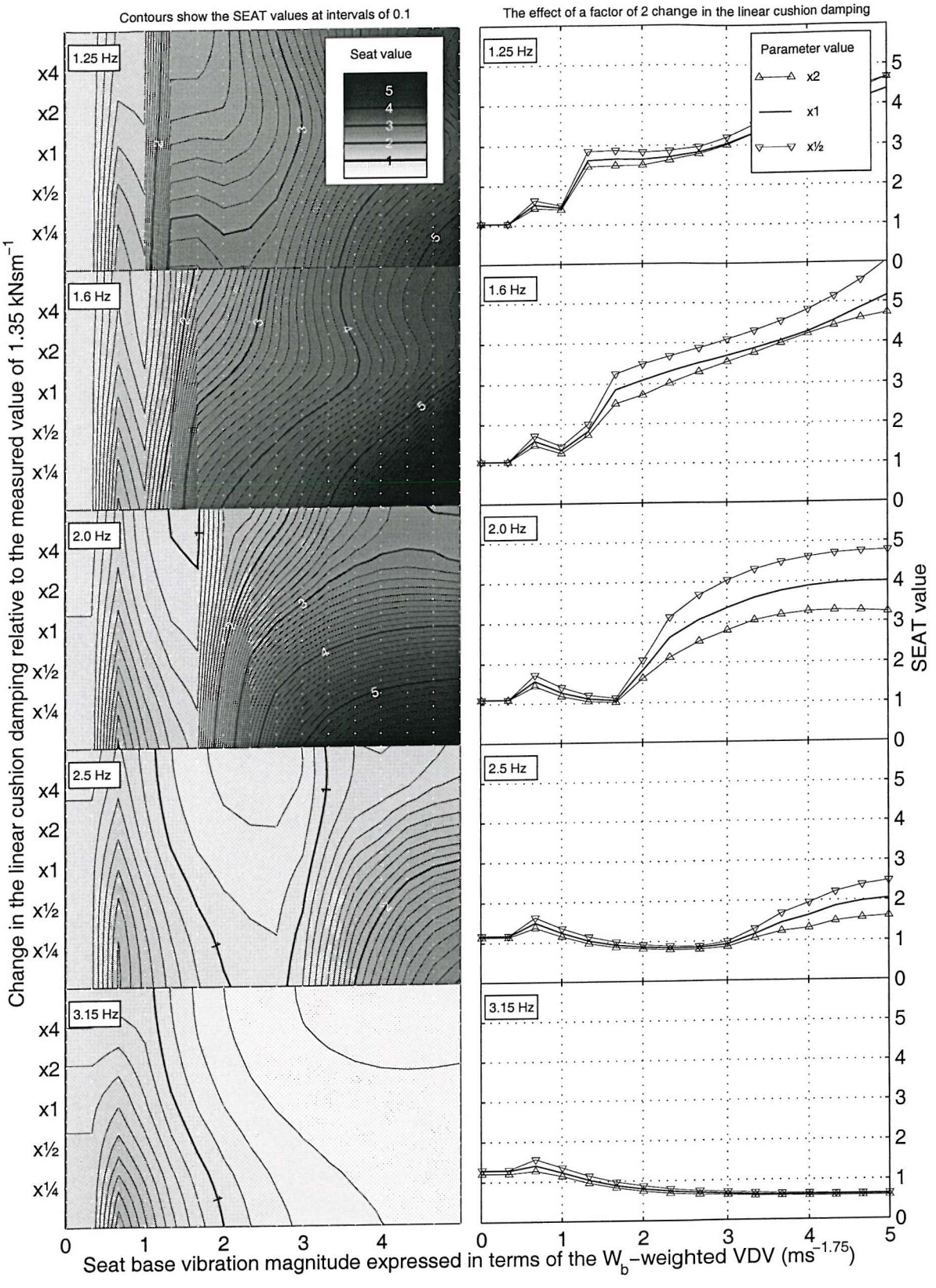

Figure 9:6 The effect of the linear cushion damping on the predicted SEAT value using the long duration (11.5 cycle) input motion

The influence of the suspended seat mass on the seat performance
using the short duration (1.5 cycle) input motion

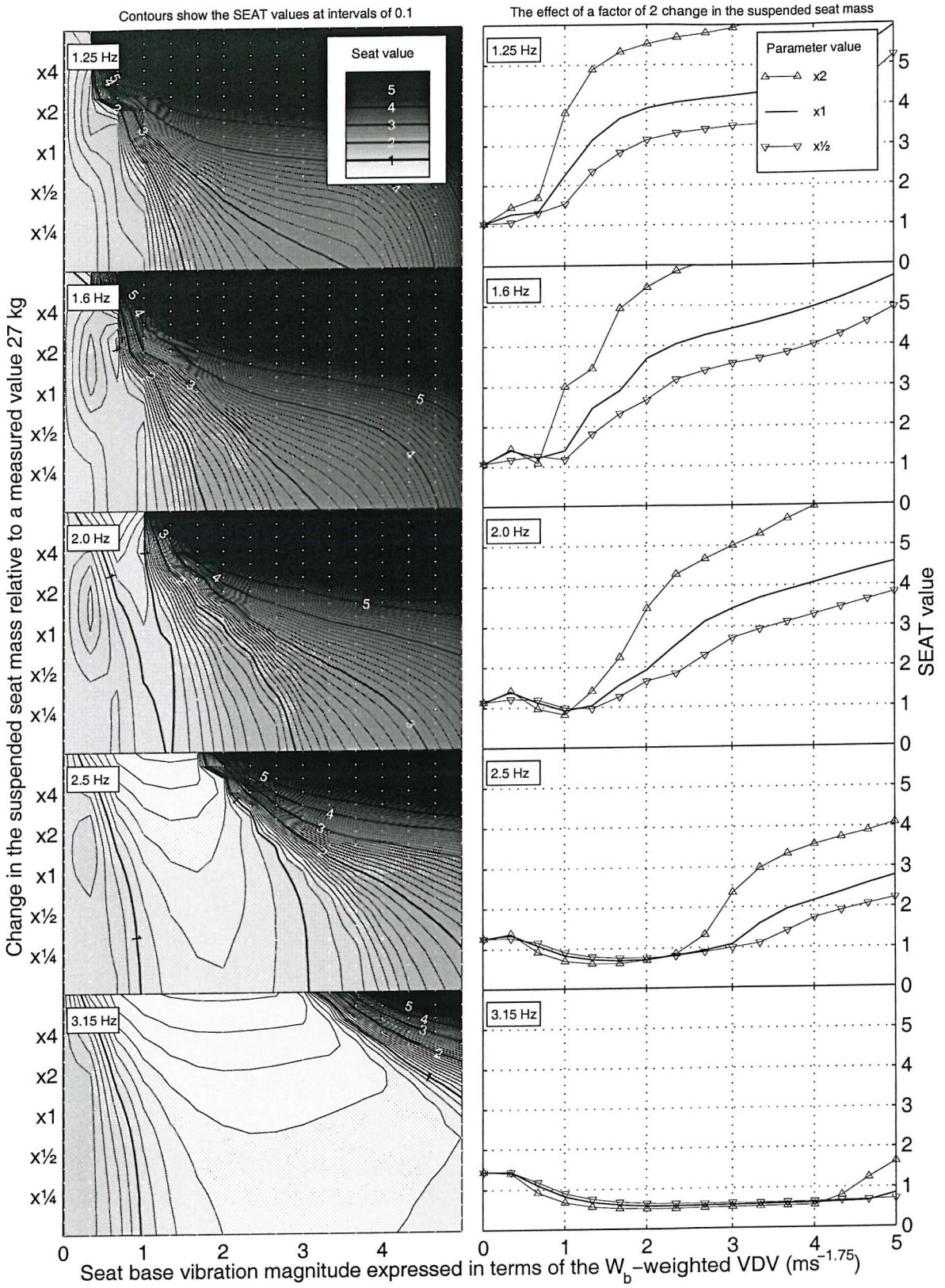

Figure 9:7 The effect of the suspended seat mass on the predicted SEAT value using the short duration (1.5 cycle) input motion

The influence of the suspended seat mass on the seat performance
using the medium duration (4.5 cycle) input motion

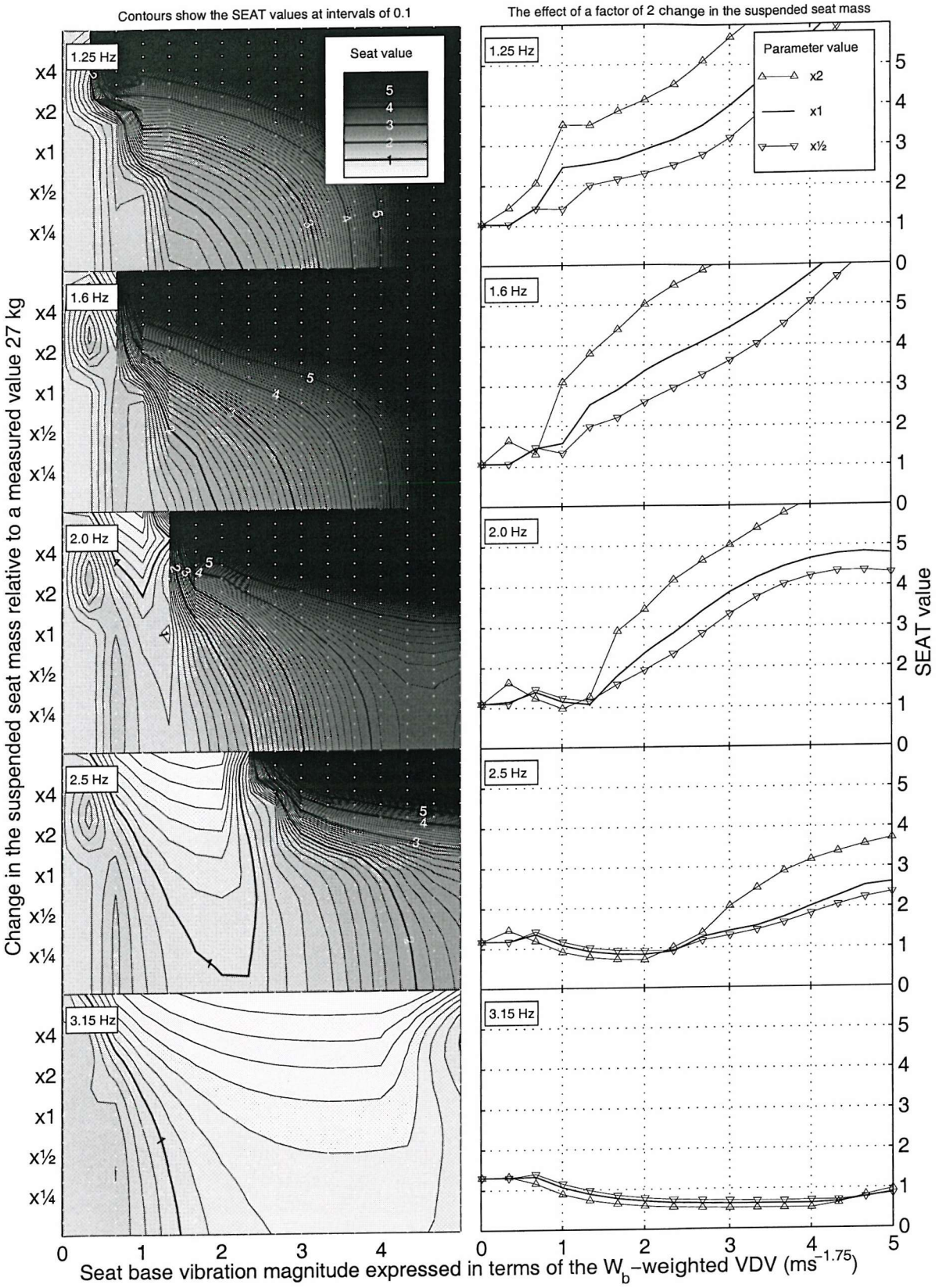

Figure 9:8 The effect of the suspended seat mass on the predicted SEAT value using the medium duration (4.5 cycle) input motion

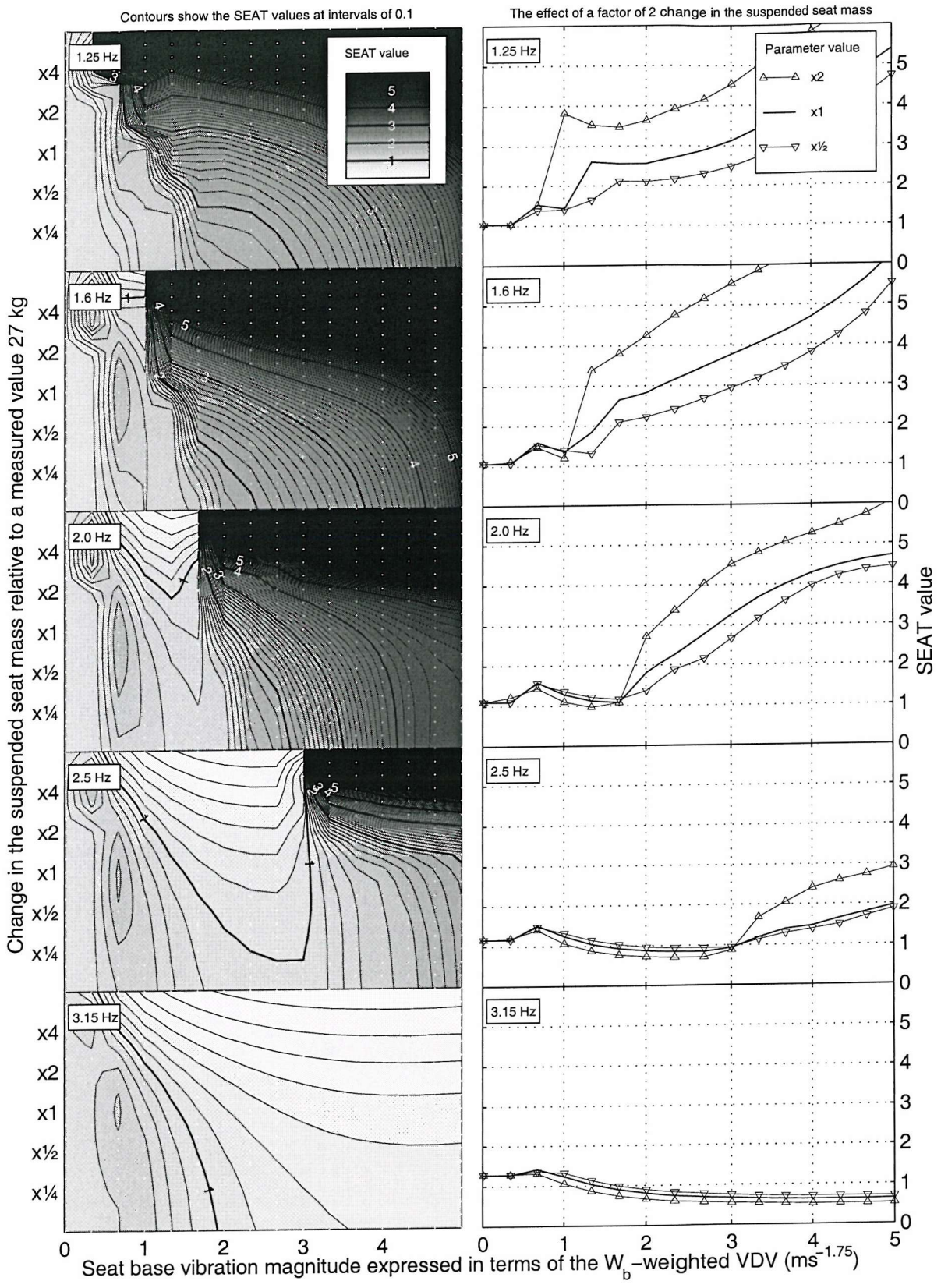

Figure 9:9 The effect of the suspended seat mass on the predicted SEAT value using the long duration (11.5 cycle) input motion

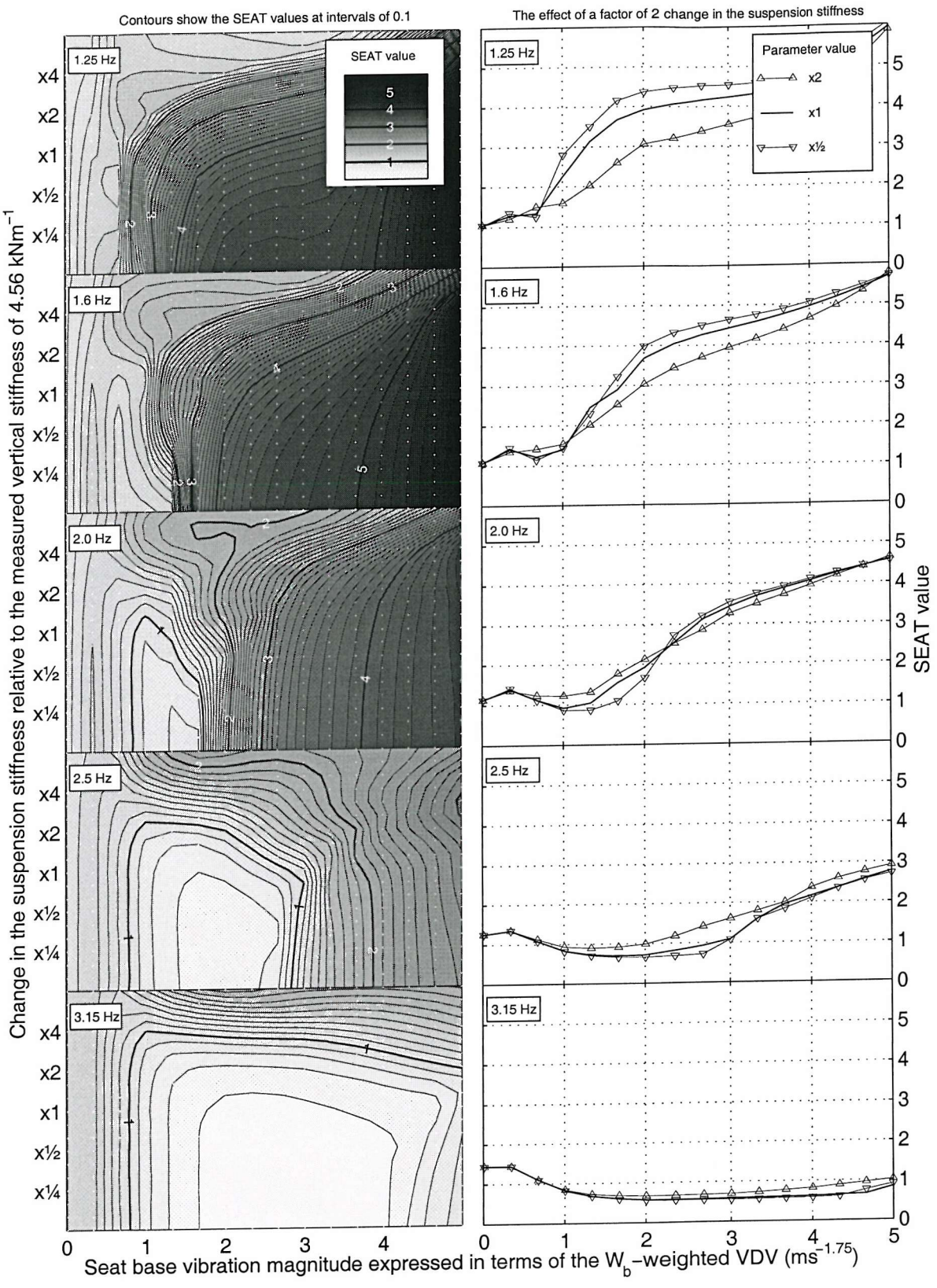

Figure 9:10 The effect of the suspension stiffness on the predicted SEAT value using the short duration (1.5 cycle) input motion

The influence of the suspension stiffness on the seat performance using the medium duration (4.5 cycle) input motion

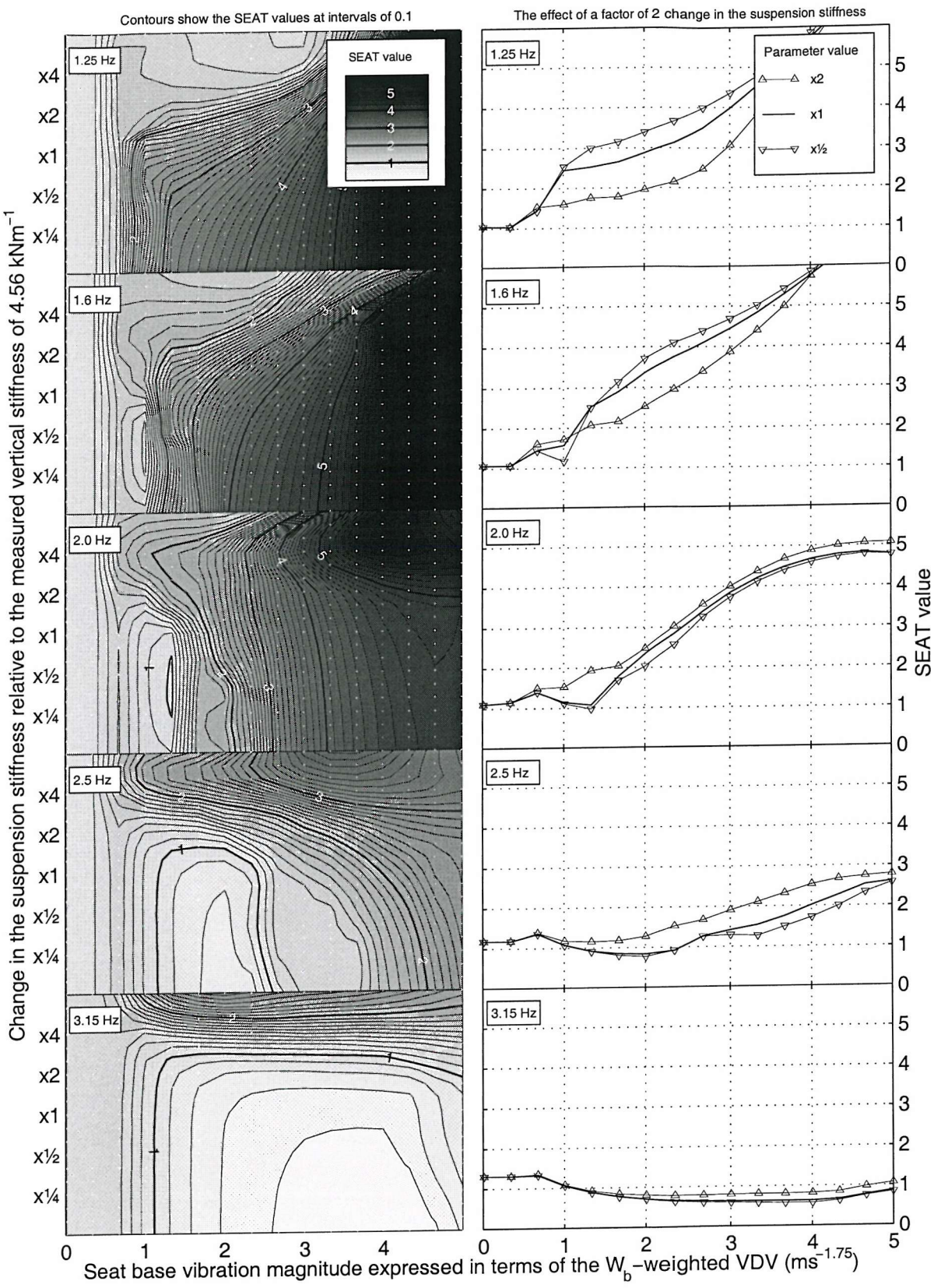

Figure 9:11 The effect of the suspension stiffness on the predicted SEAT value using the medium duration (4.5 cycle) input motion

The influence of the suspension stiffness on the seat performance using the long duration (11.5 cycle) input motion

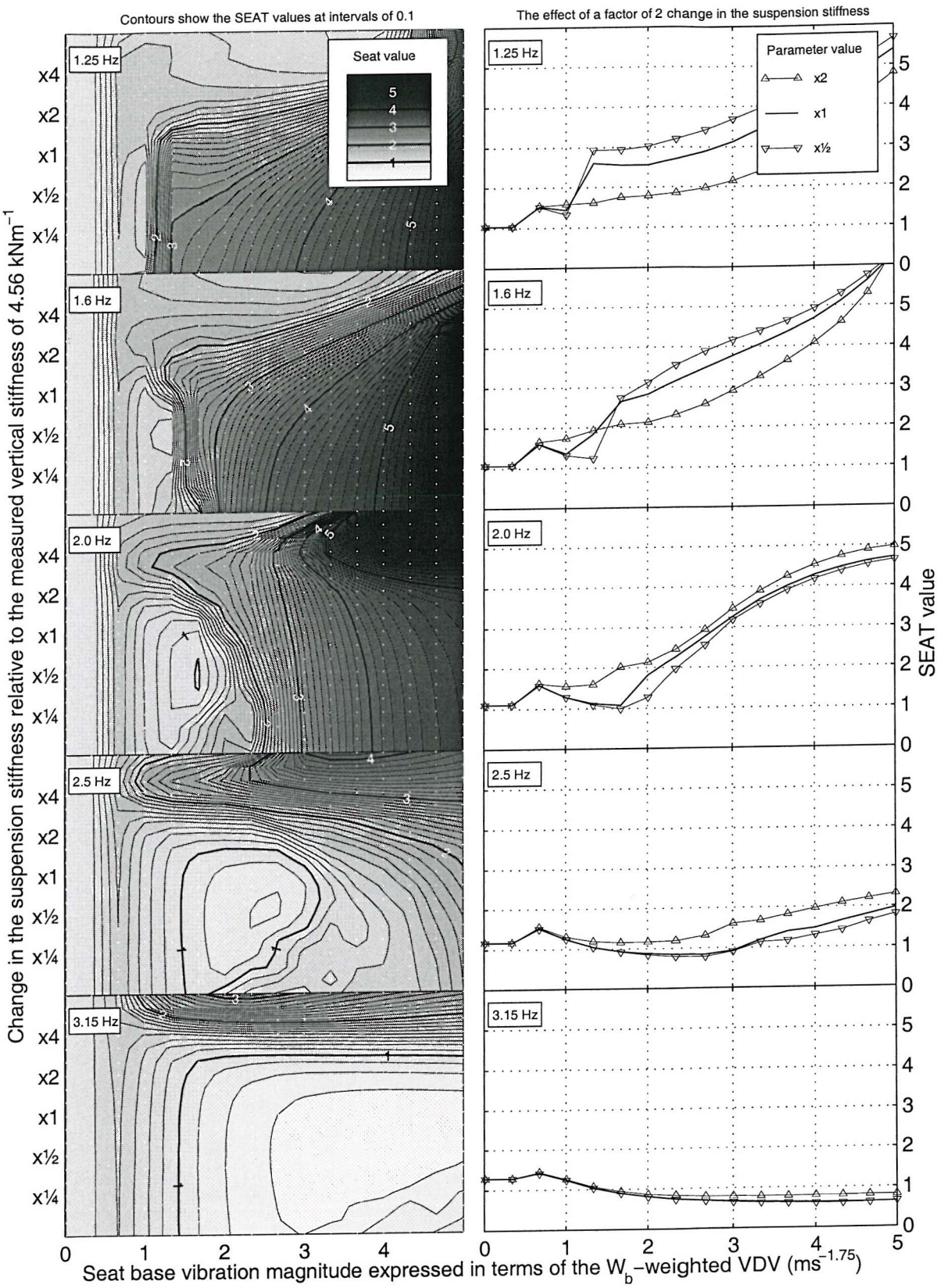

Figure 9:12 The effect of the suspension stiffness on the predicted SEAT value using the long duration (11.5 cycle) input motion

The influence of the suspension friction on the seat performance
using the short duration (1.5 cycle) input motion

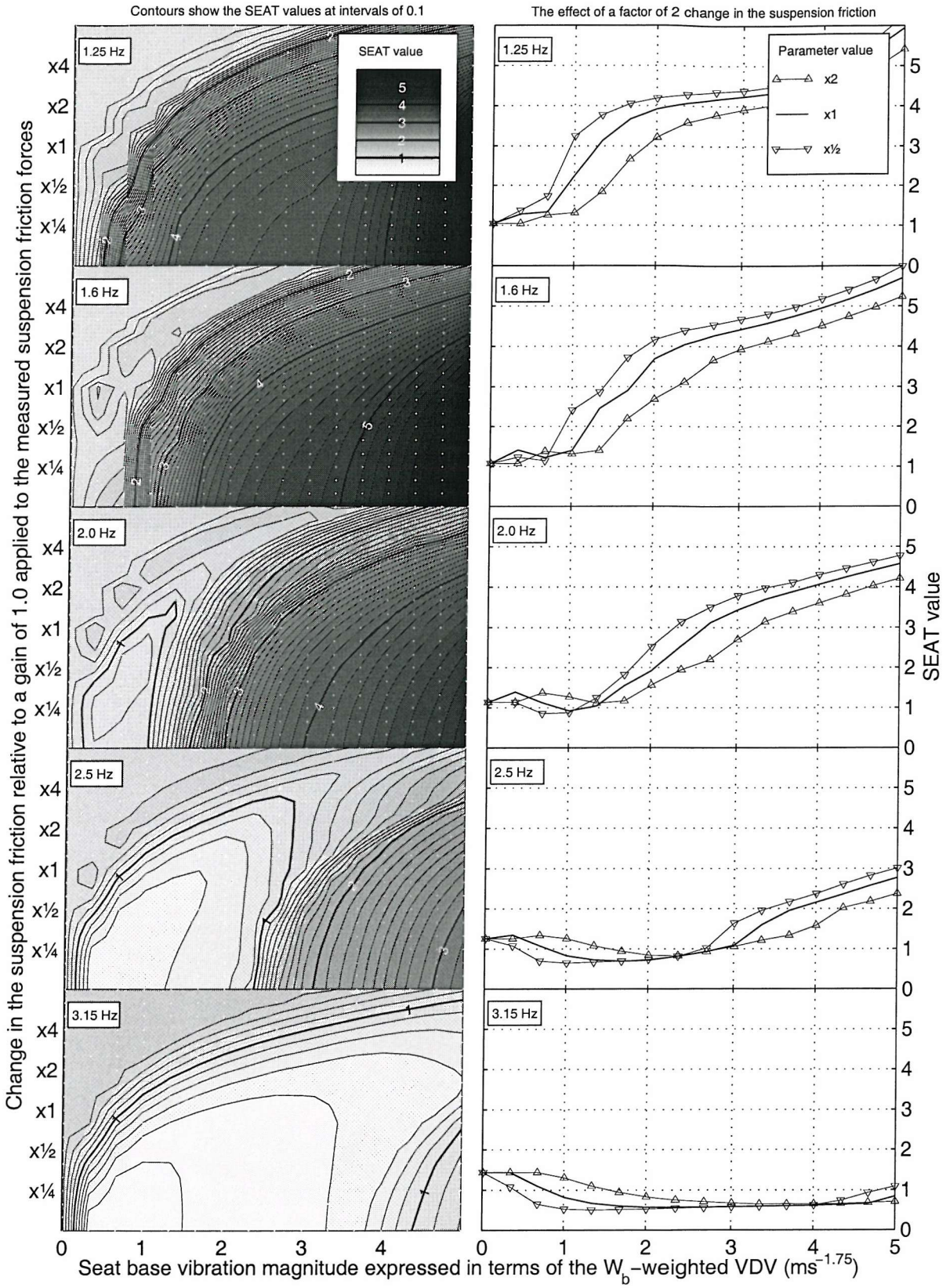

Figure 9:13 The effect of the symmetrical suspension friction magnitude on the predicted SEAT value using the short duration (1.5 cycle) input motion

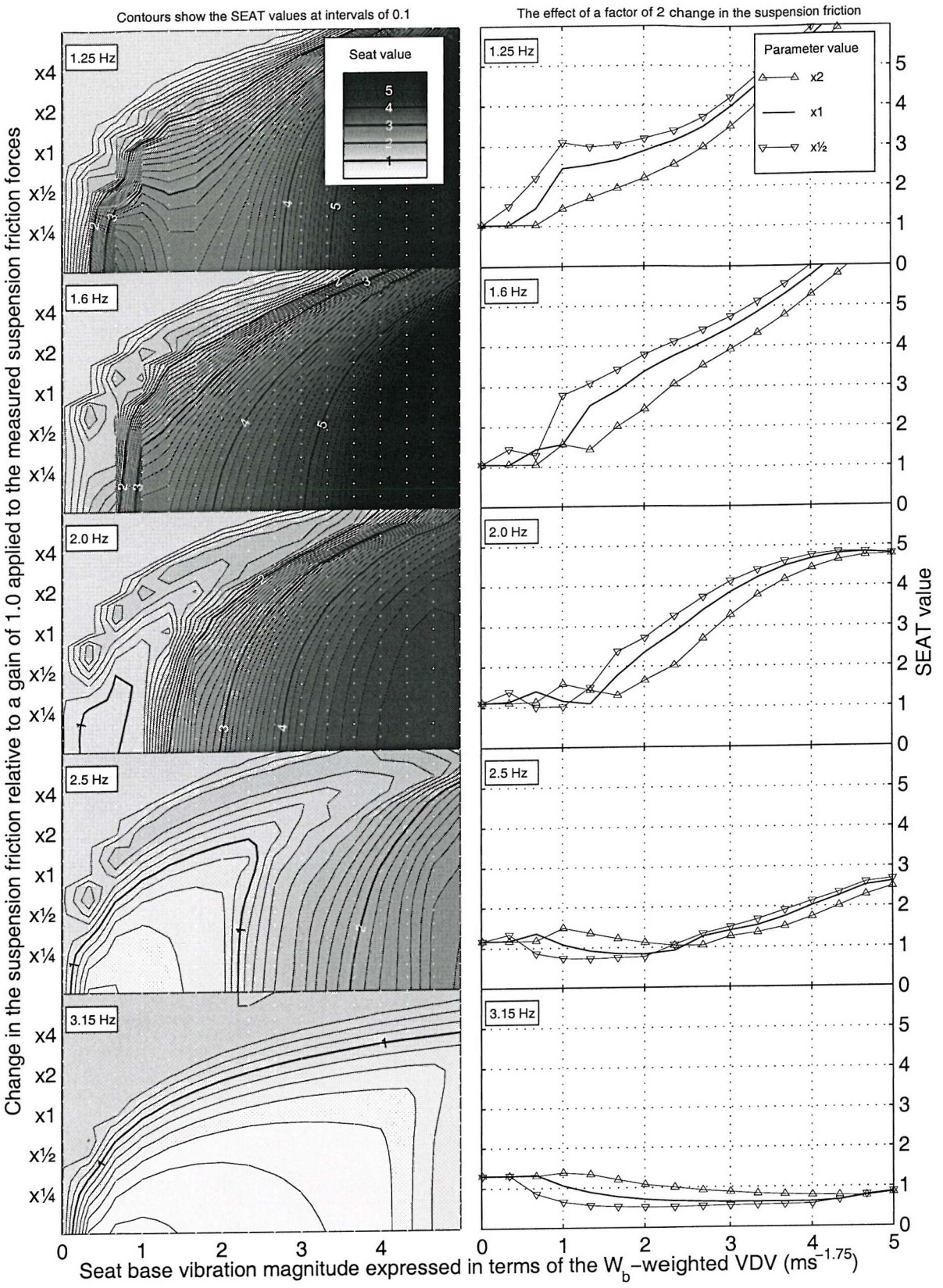

Figure 9:14 The effect of the symmetrical suspension friction magnitude on the predicted SEAT value using the medium duration (4.5 cycle) input motion

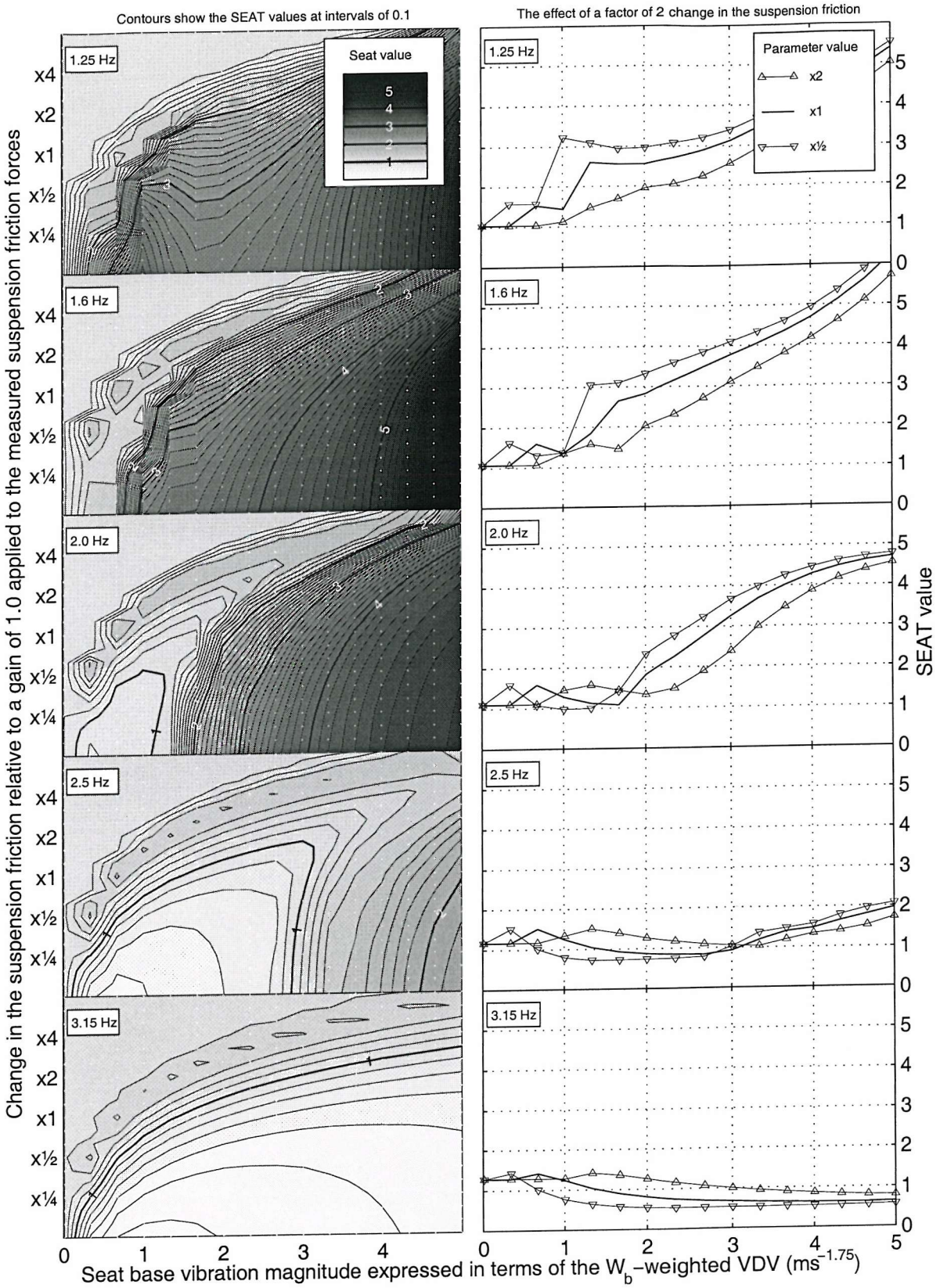

Figure 9:15 The effect of the symmetrical suspension friction magnitude on the predicted SEAT value using the long duration (11.5 cycle) input motion

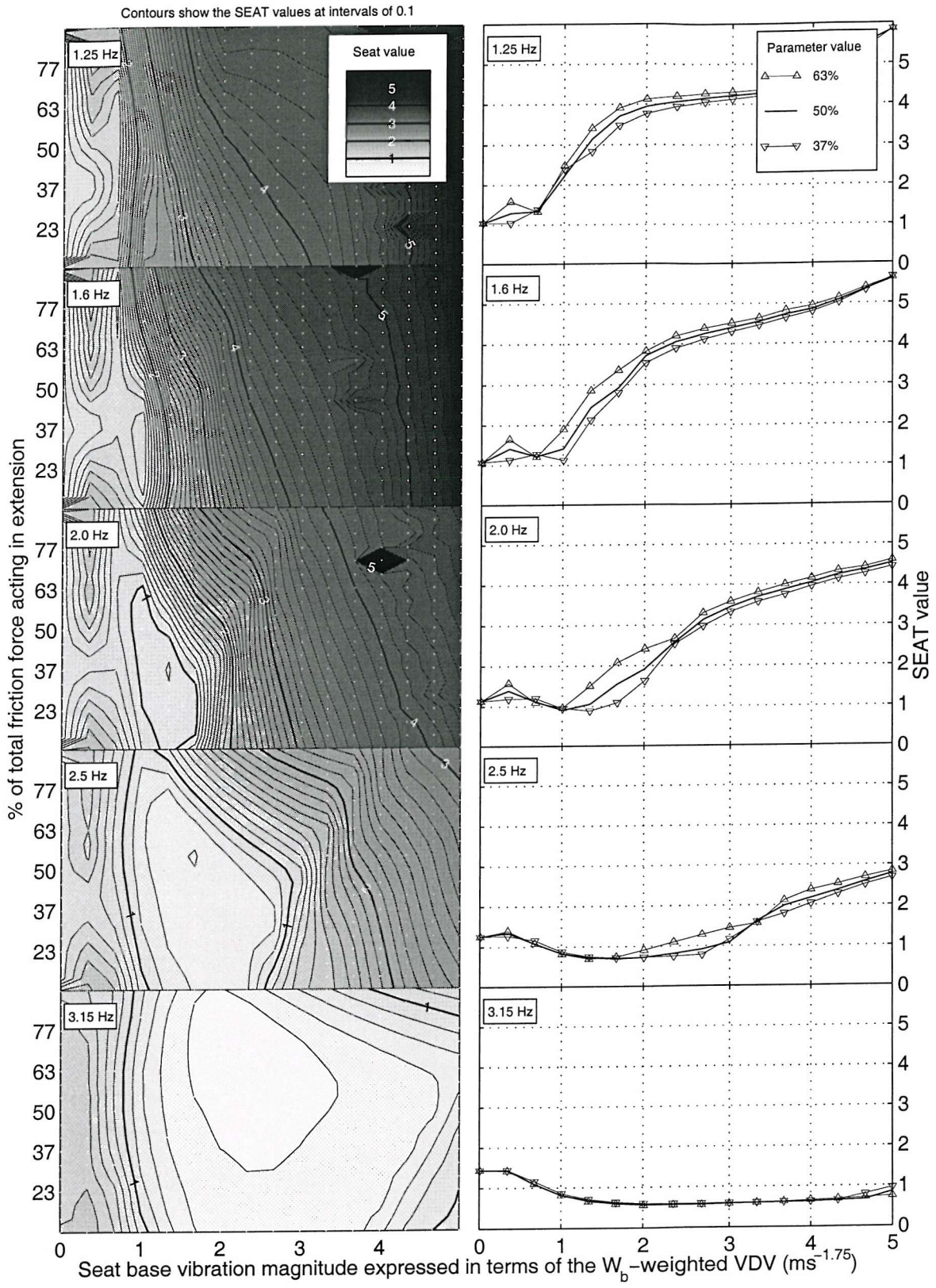

Figure 9:16 The effect of the suspension friction symmetry on the predicted SEAT value using the short duration (1.5 cycle) input motion

The influence of the suspension friction symmetry on the seat performance using the medium duration (4.5 cycle) input motion

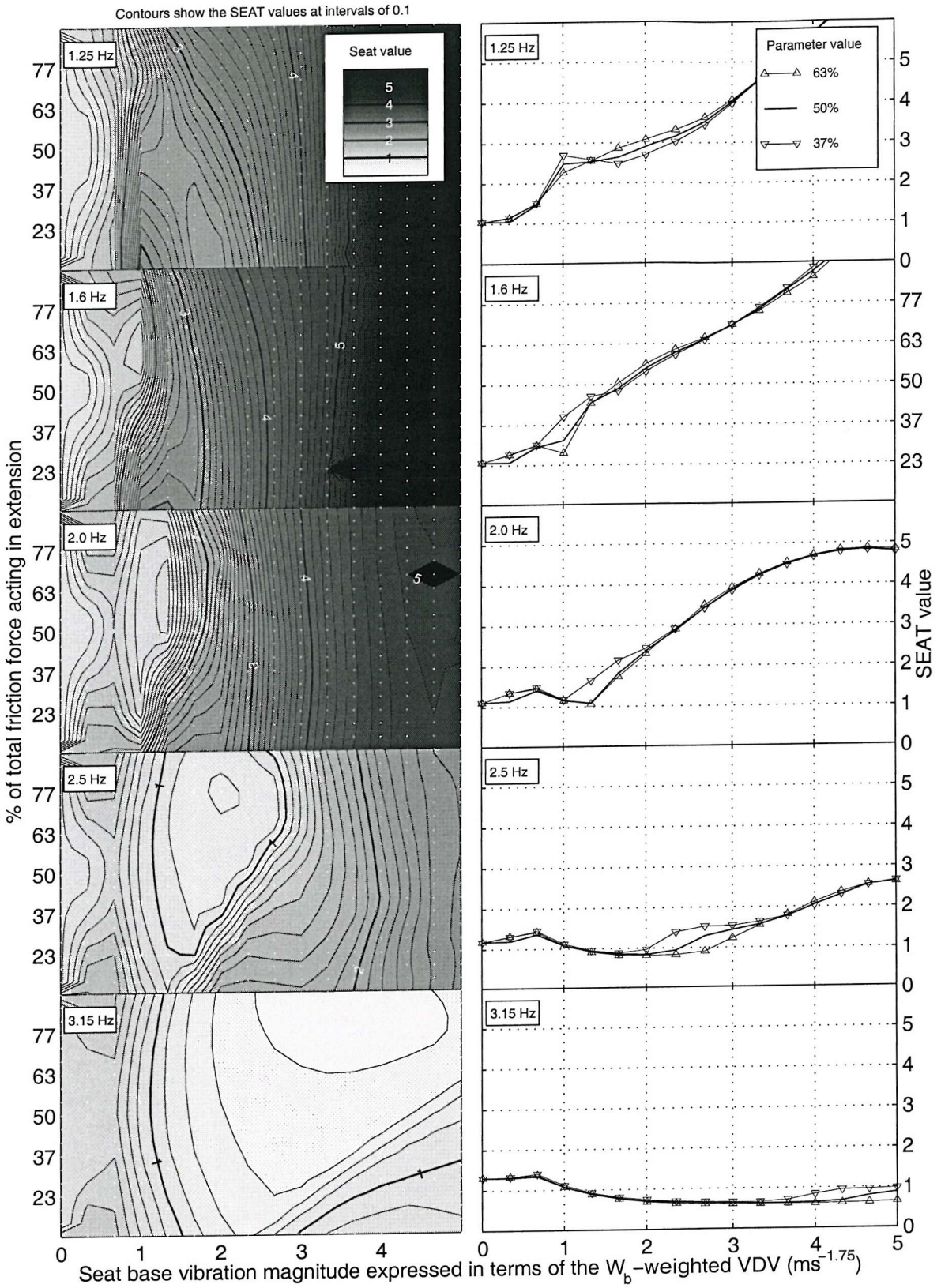

Figure 9:17 The effect of the suspension friction symmetry on the predicted SEAT value using the medium duration (4.5 cycle) input motion

The influence of the suspension force–velocity damping on the seat performance using the short duration (1.5 cycle) input motion

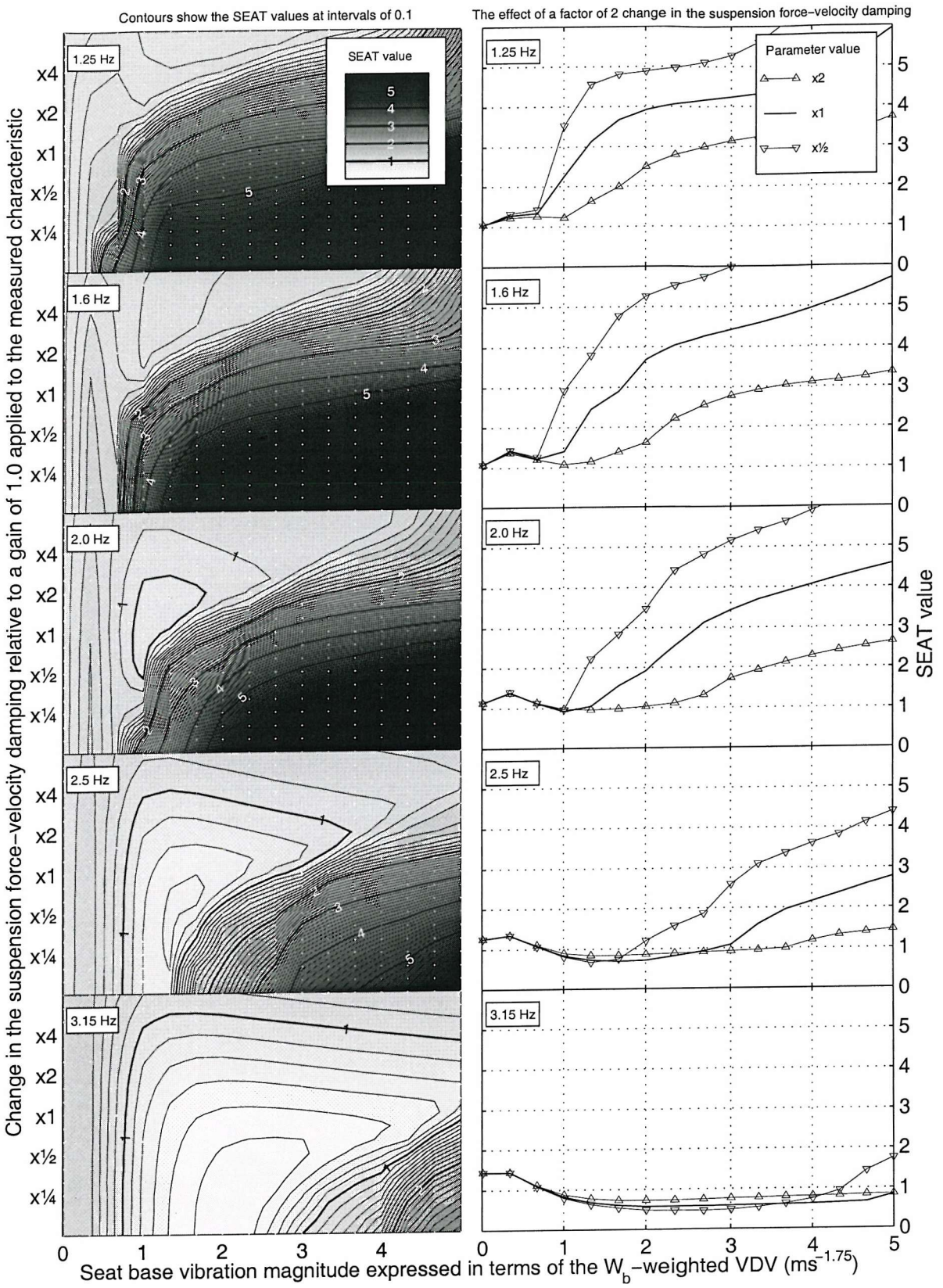

Figure 9:18 The effect of the suspension (non-frictional) damping magnitude on the predicted SEAT value using the short duration (1.5 cycle) input motion

The influence of the suspension force–velocity damping on the seat performance using the medium duration (4.5 cycle) input motion

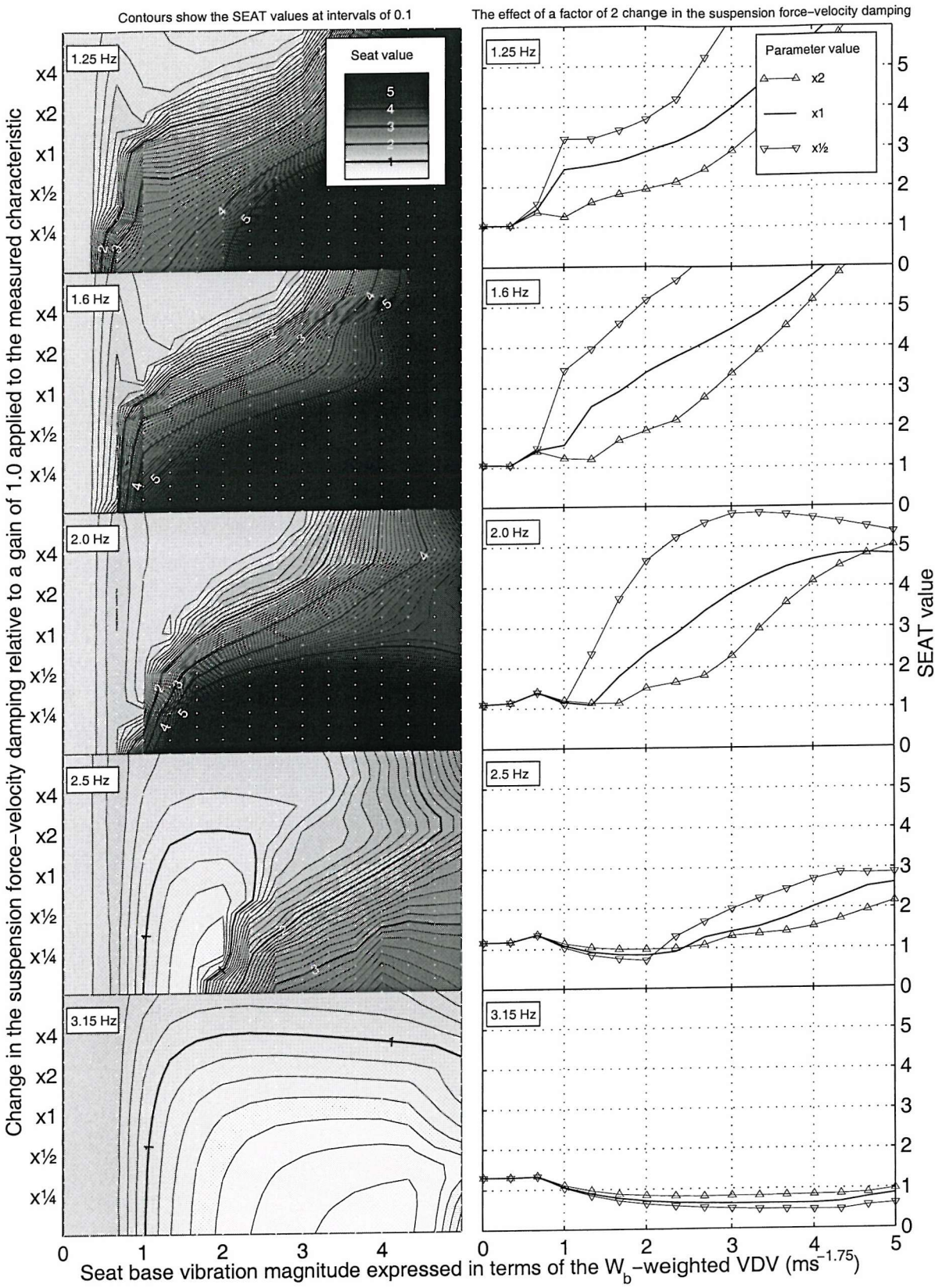

Figure 9:19 The effect of the suspension (non-frictional) damping magnitude on the predicted SEAT value using the medium duration (4.5 cycle) input motion

The influence of the suspension force–velocity damping on the seat performance using the long duration (11.5 cycle) input motion

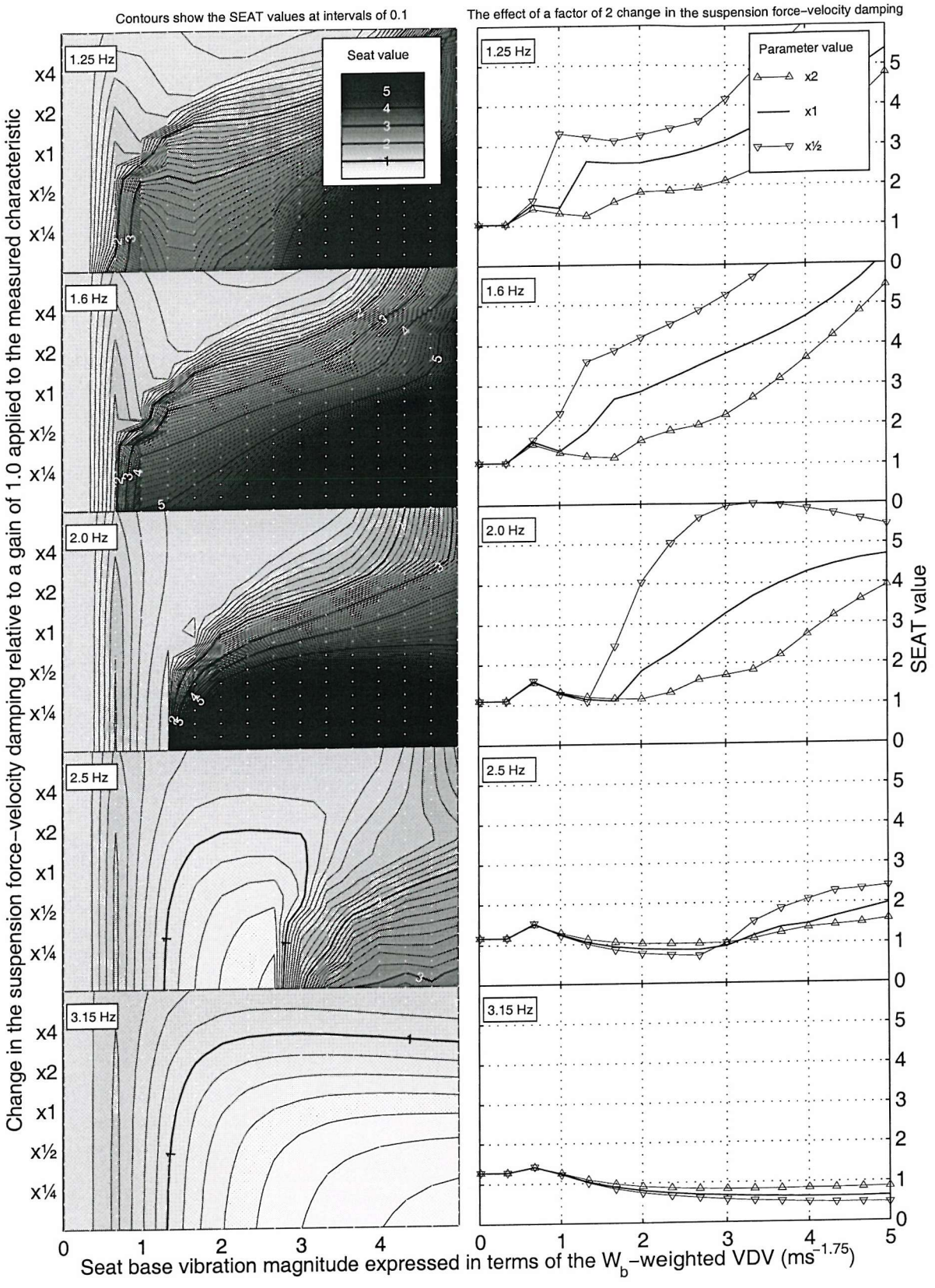

Figure 9:20 The effect of the suspension (non-frictional) damping magnitude on the predicted SEAT value using the long duration (11.5 cycle) input motion

The influence of the suspension damping symmetry on the seat performance using the short duration (1.5 cycle) input motion

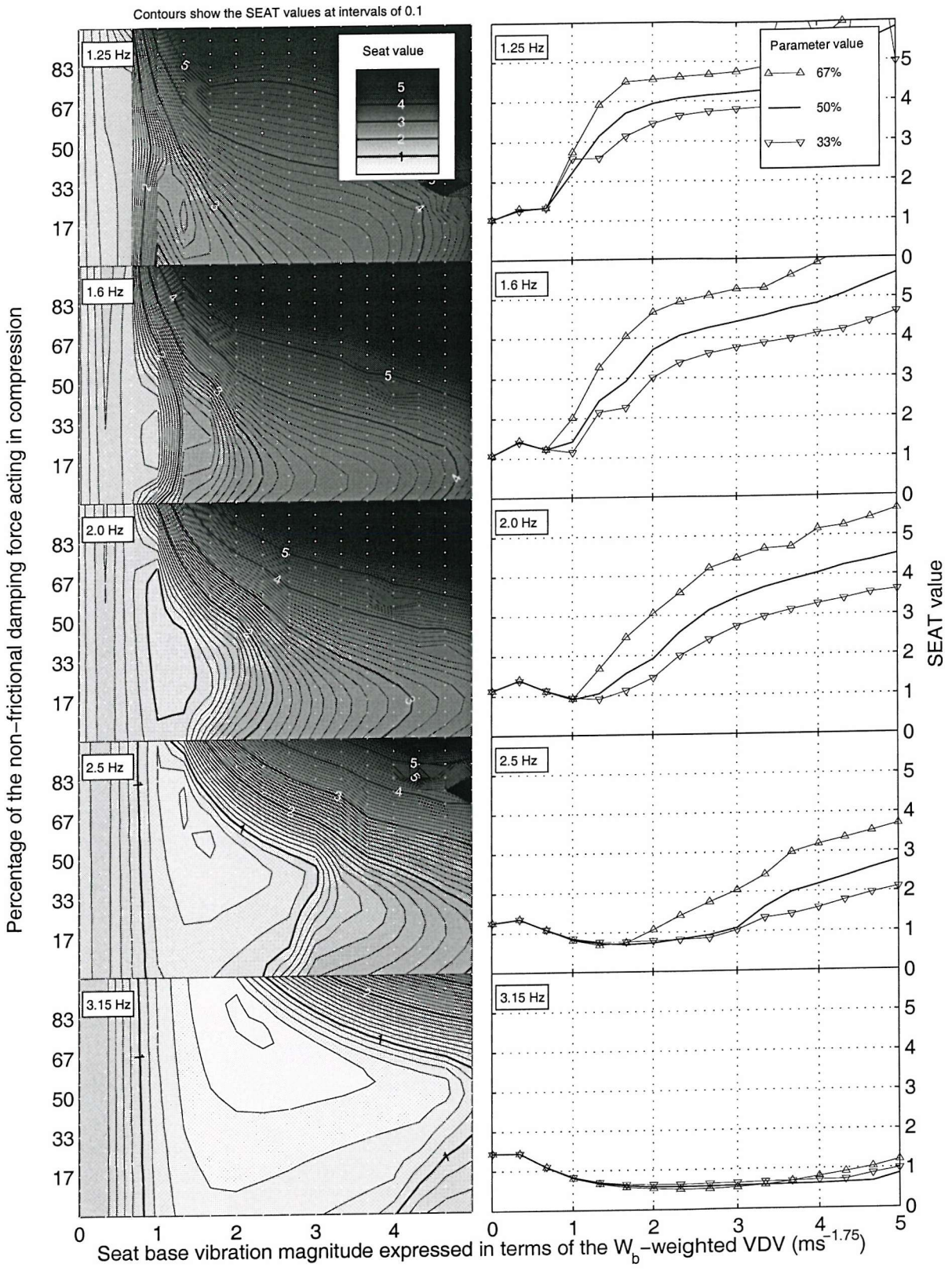

Figure 9:21 The effect of the suspension (non-frictional) damping symmetry on the predicted SEAT value using the short duration (1.5 cycle) input motion

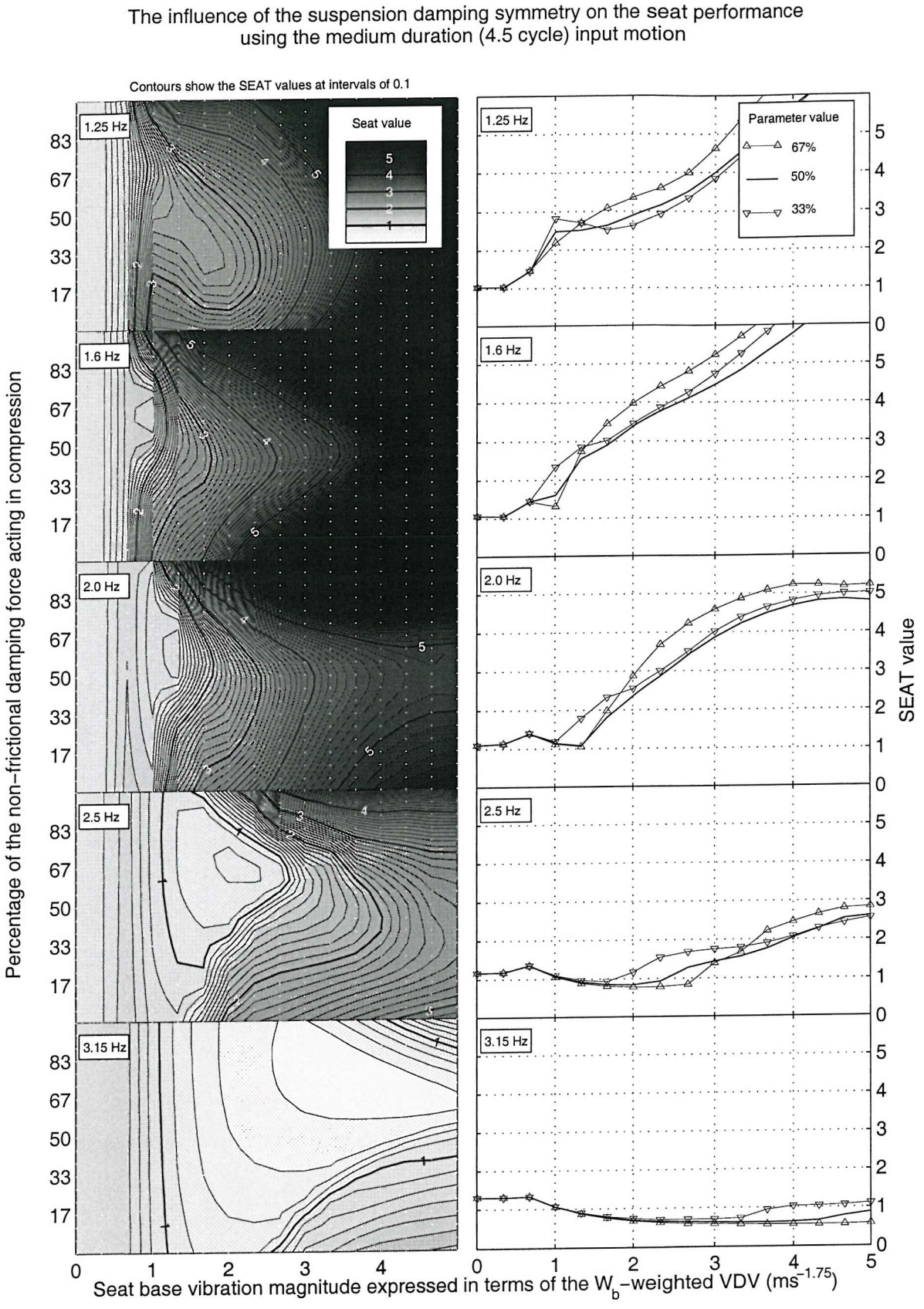

Figure 9:22 The effect of the suspension (non-frictional) damping symmetry on the predicted SEAT value using the medium duration (4.5 cycle) input motion

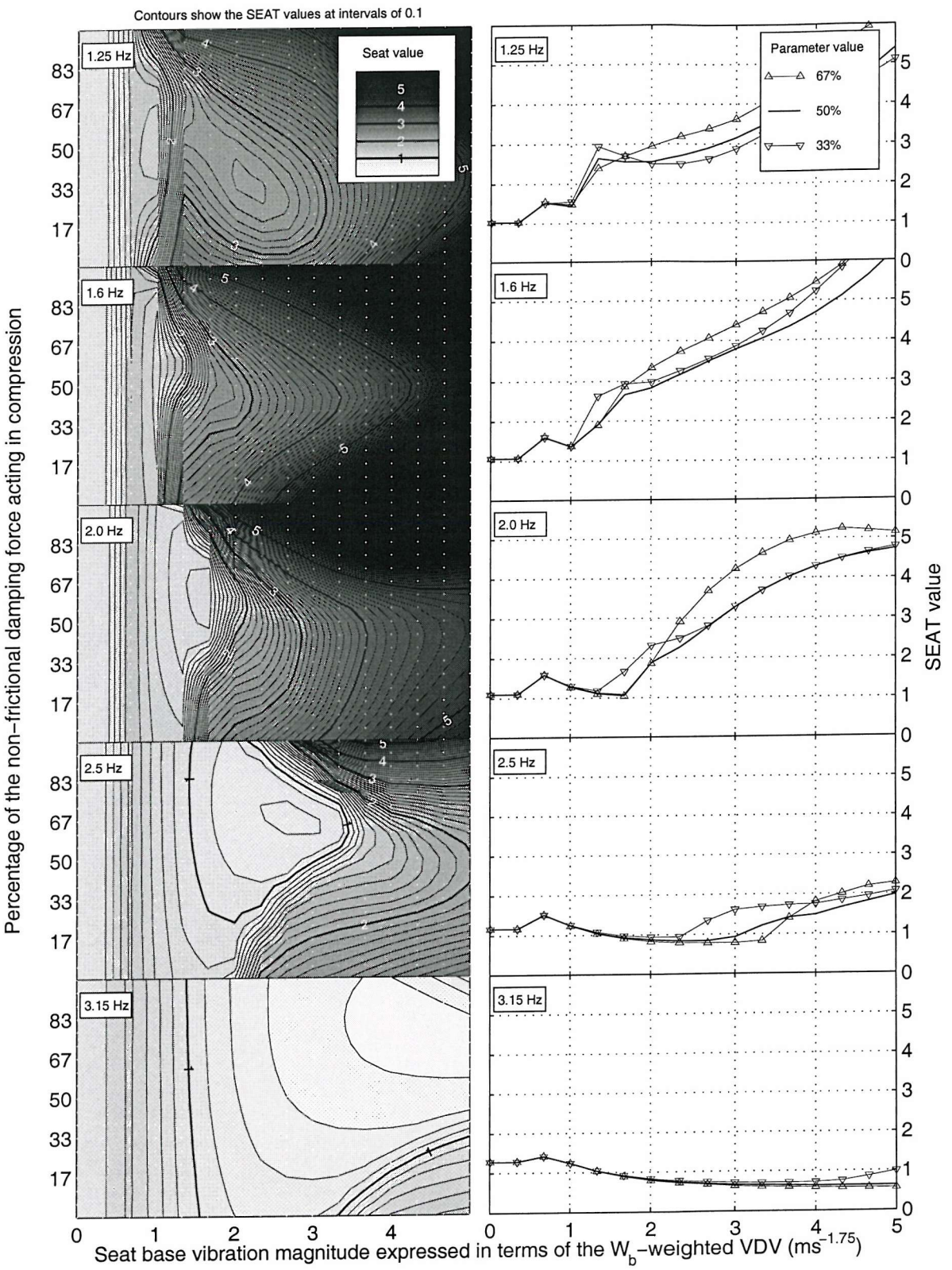

Figure 9:23 The effect of the suspension (non-frictional) damping symmetry on the predicted SEAT value using the long duration (11.5 cycle) input motion

The influence of the suspension free travel on the seat performance
using the short duration (1.5 cycle) input motion

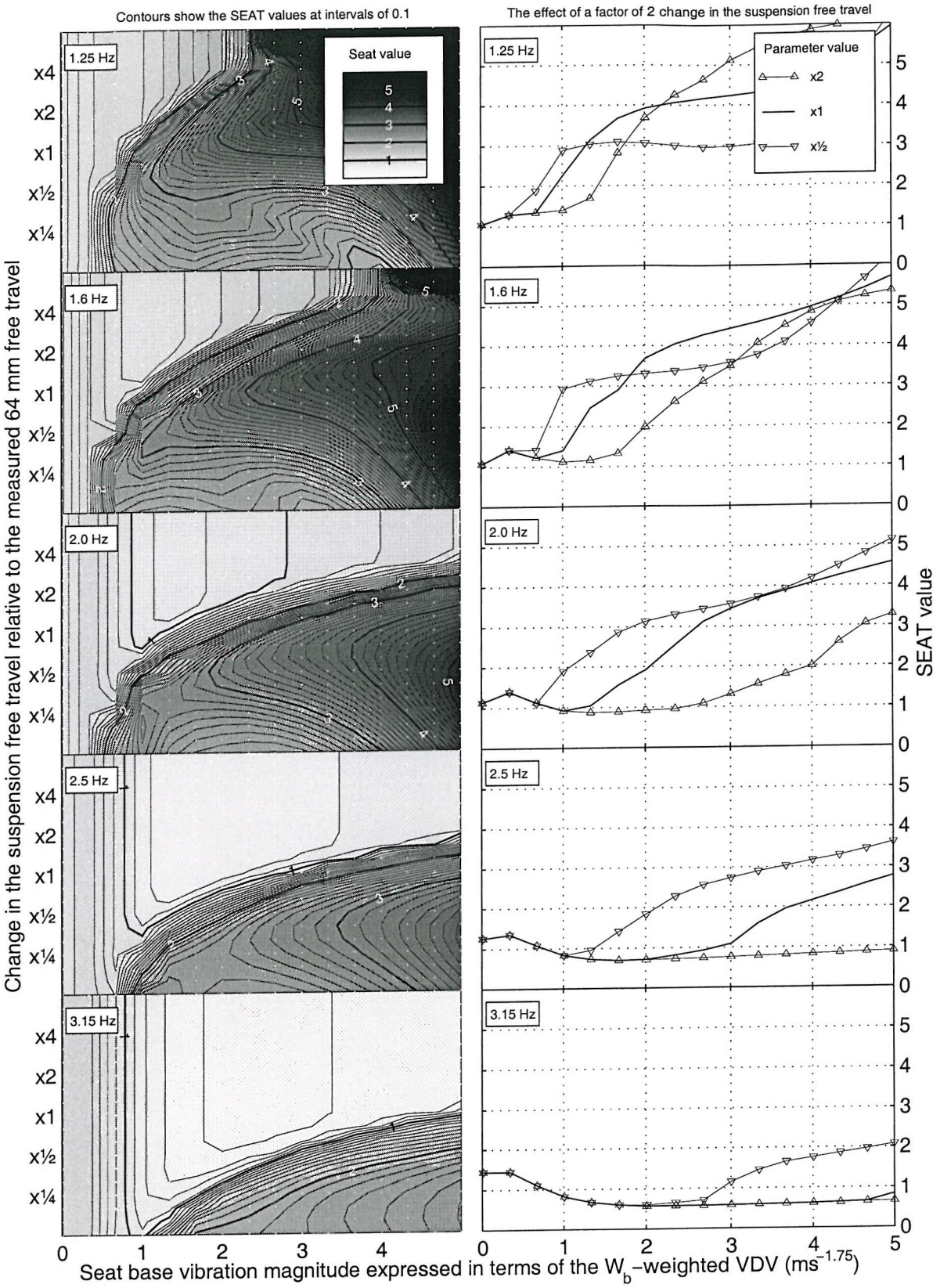

Figure 9:24 The effect of the suspension free travel displacement on the predicted SEAT value using the short duration (1.5 cycle) input motion

The influence of the suspension free travel on the seat performance
using the medium duration (4.5 cycle) input motion

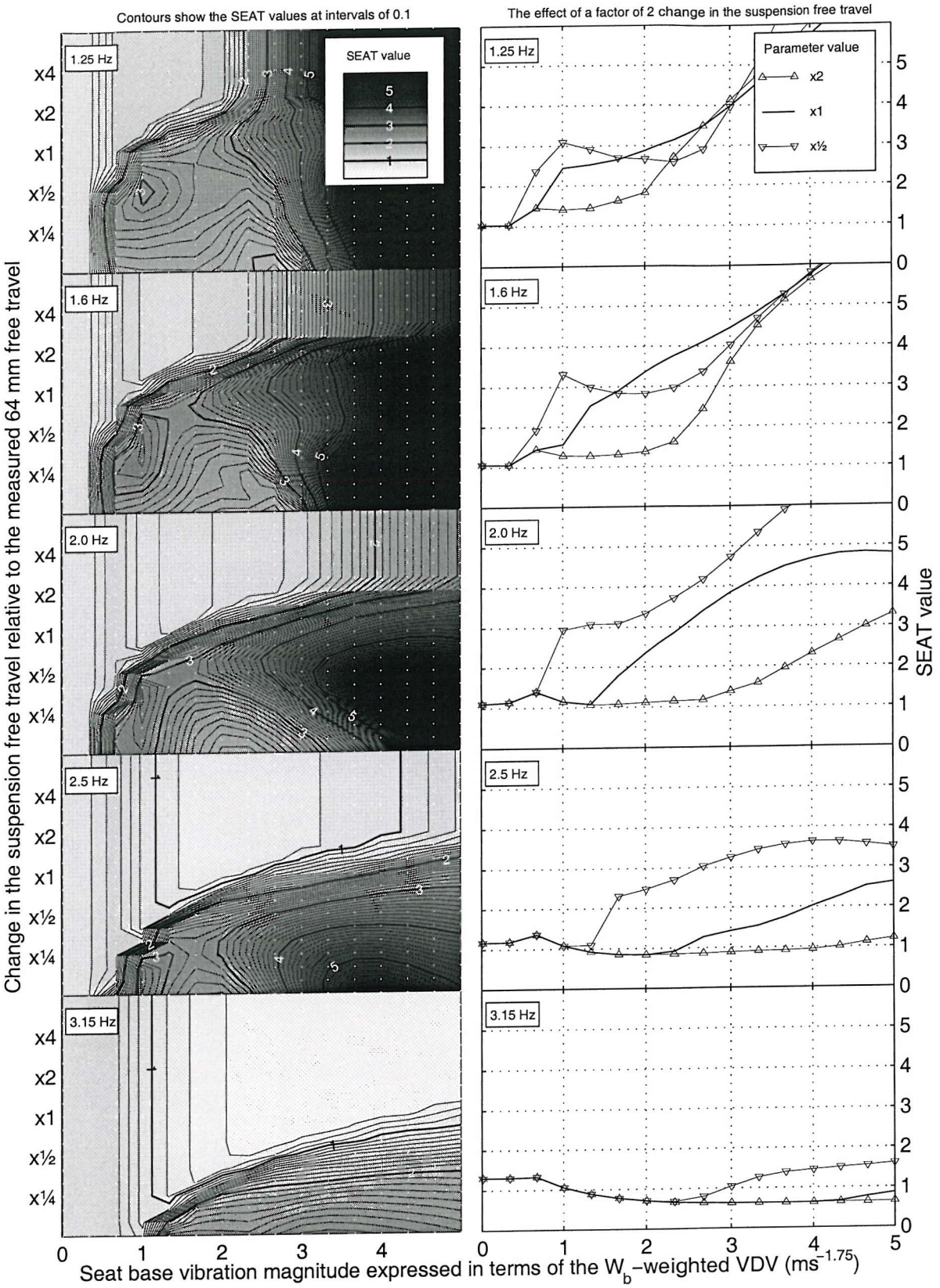

Figure 9:25 The effect of the suspension free travel displacement on the predicted SEAT value using the medium duration (4.5 cycle) input motion

The influence of the suspension free travel on the seat performance
using the long duration (11.5 cycle) input motion

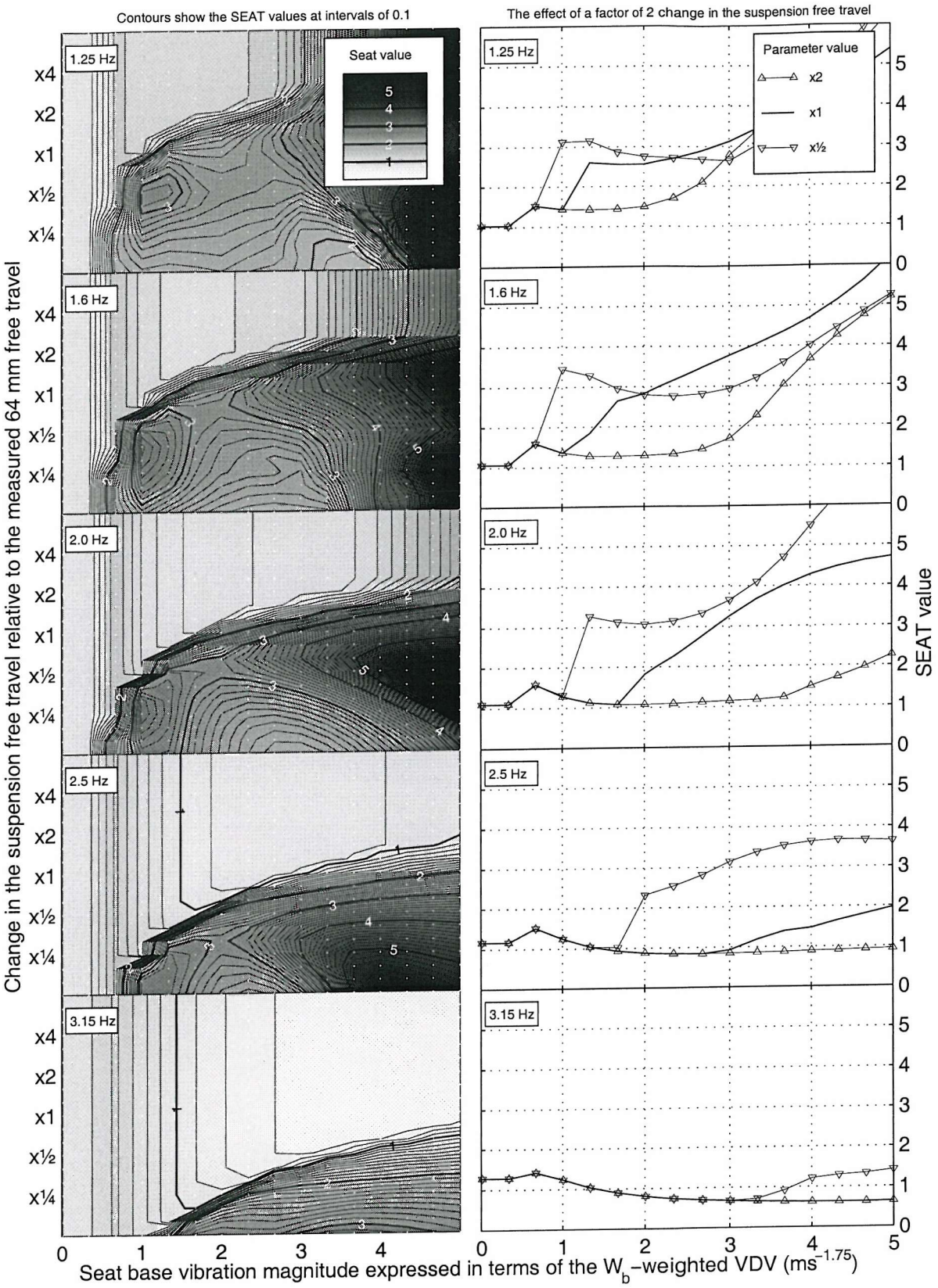

Figure 9:26 The effect of the suspension free travel displacement on the predicted SEAT value using the long duration (11.5 cycle) input motion

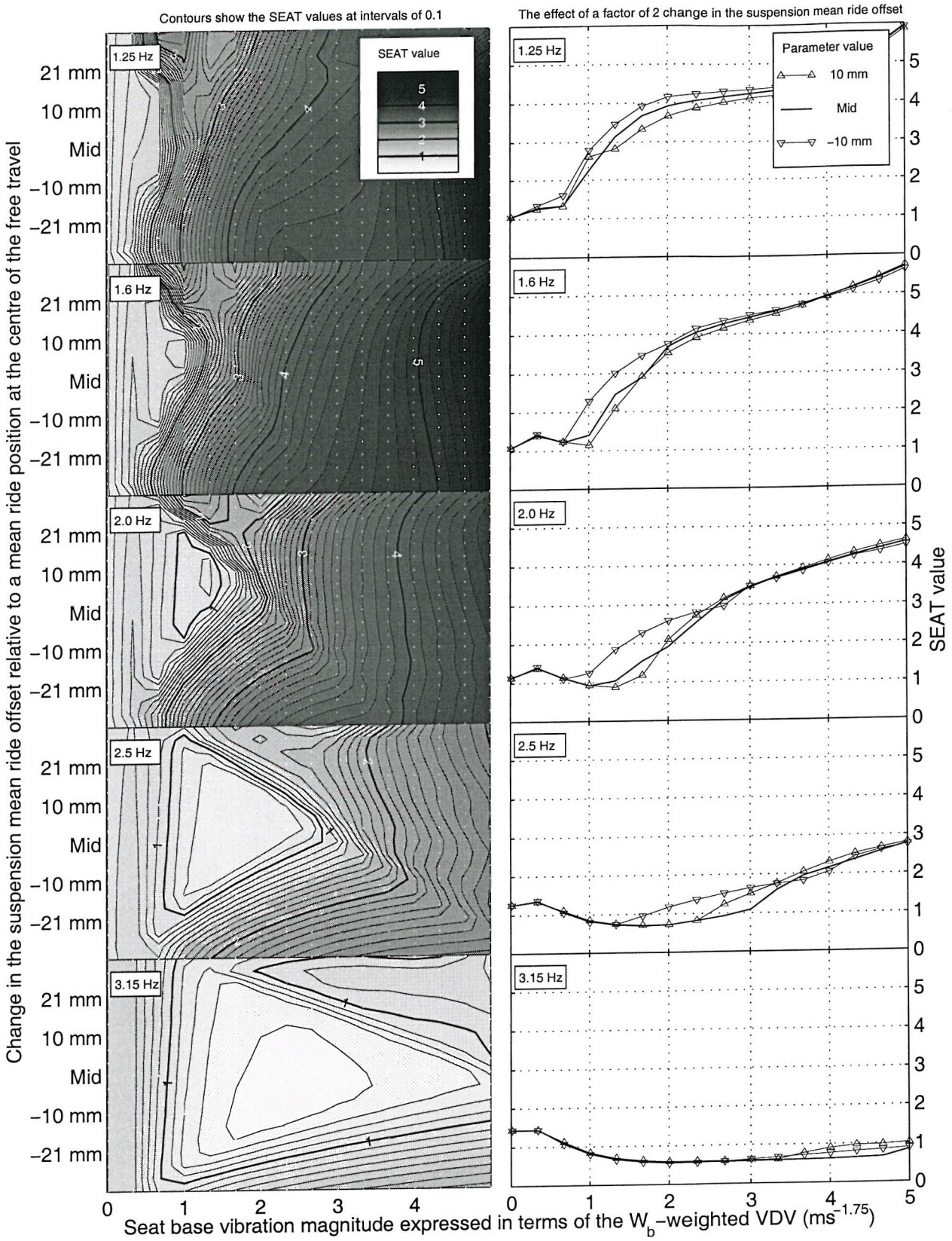

Figure 9:27 The effect of the suspension mean ride offset displacement on the predicted SEAT value using the short duration (1.5 cycle) input motion

The influence of the suspension mean ride offset on the seat performance using the medium duration (4.5 cycle) input motion

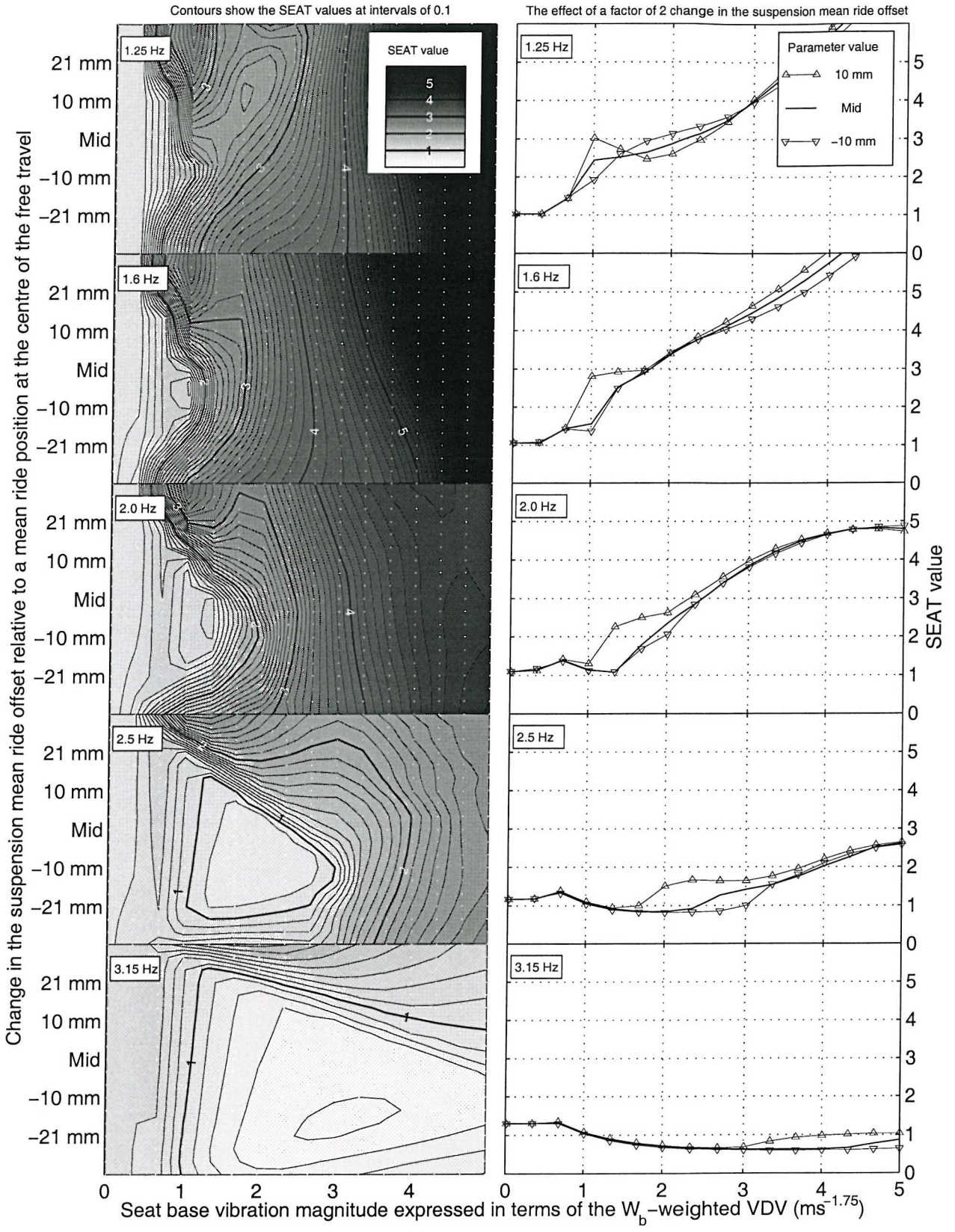

Figure 9:28 The effect of the suspension mean ride offset displacement on the predicted SEAT value using the medium duration (4.5 cycle) input motion

The influence of the suspension mean ride offset on the seat performance using the long duration (11.5 cycle) input motion

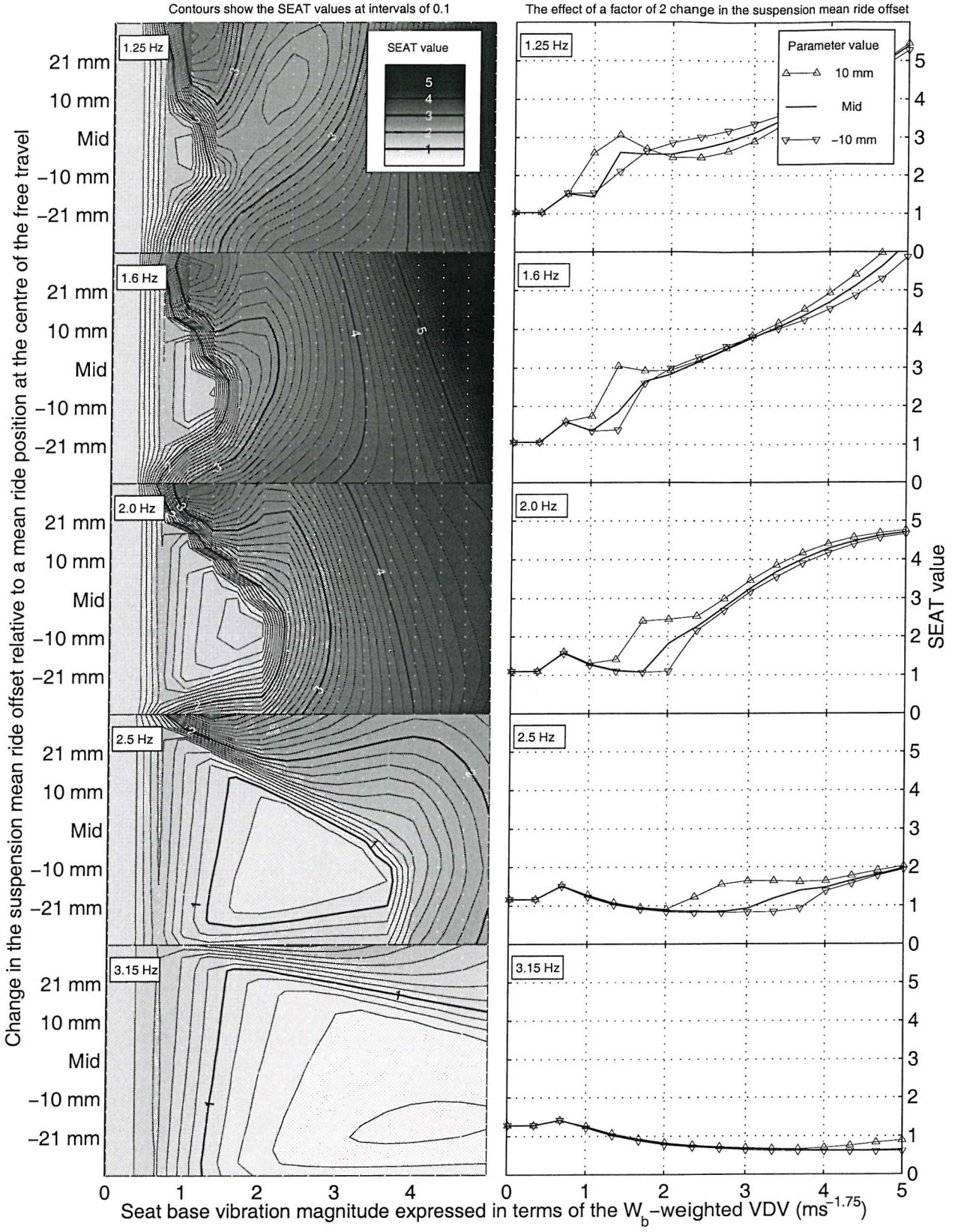

Figure 9:29 The effect of the suspension mean ride offset displacement on the predicted SEAT value using the long duration (11.5 cycle) input motion

The influence of the top end-stop buffer stiffness on the seat performance using the short duration (1.5 cycle) input motion

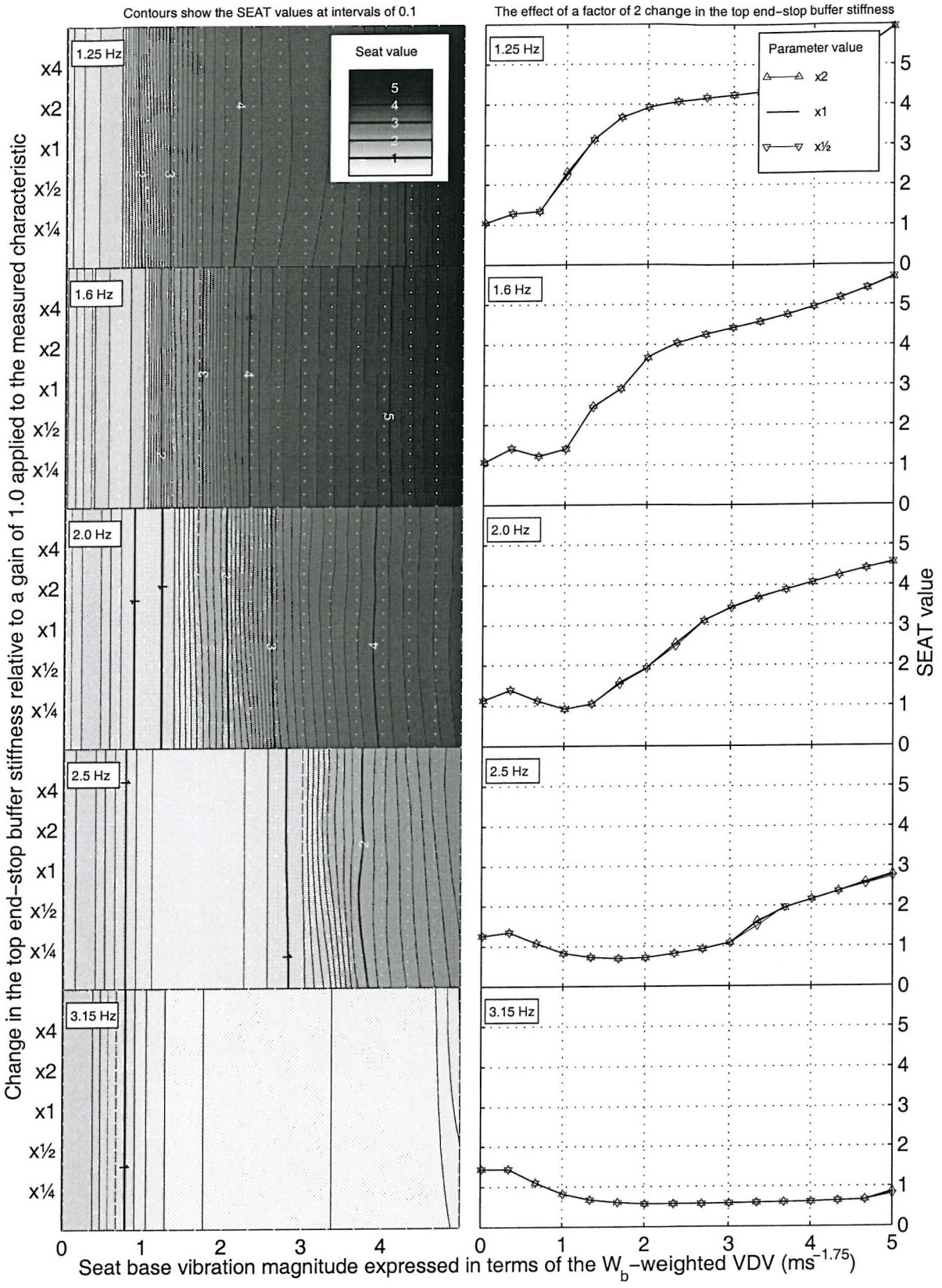

Figure 9:30 The effect of the suspension top buffer stiffness on the predicted SEAT value using the short duration (1.5 cycle) input motion

The influence of the top end–stop buffer stiffness on the seat performance using the medium duration (4.5 cycle) input motion

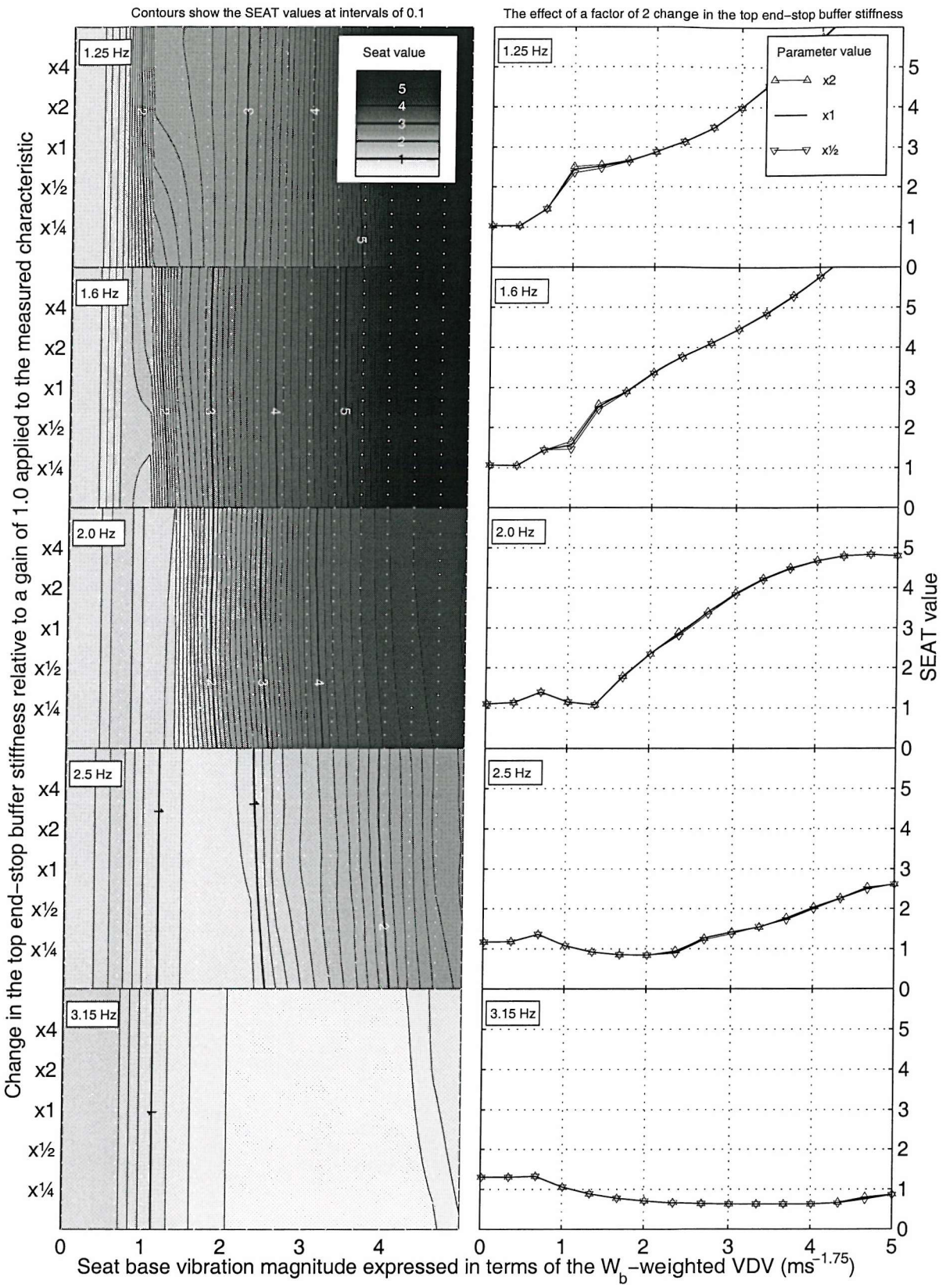

Figure 9:31 The effect of the suspension top buffer stiffness on the predicted SEAT value using the medium duration (4.5 cycle) input motion

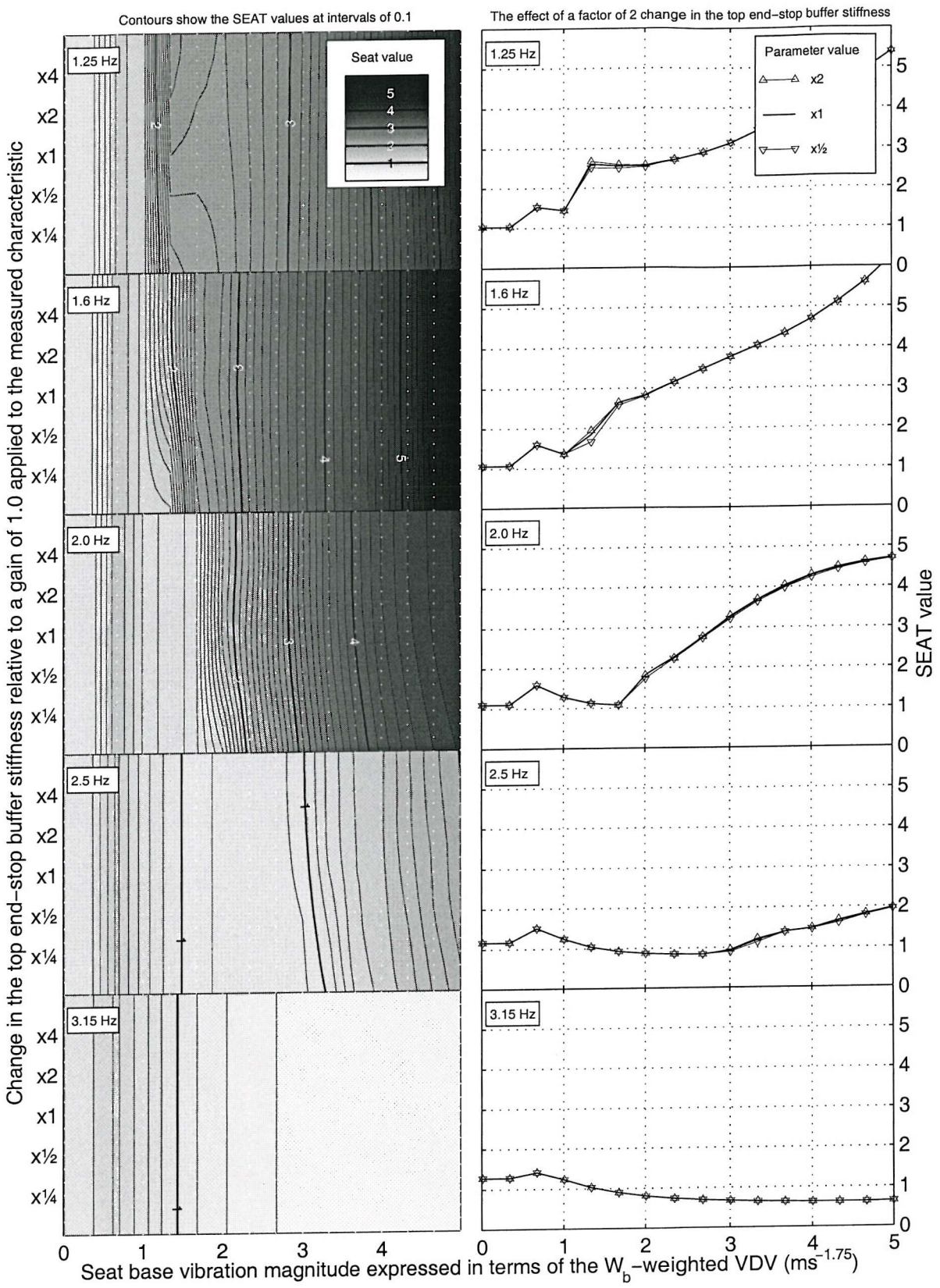

Figure 9:32 The effect of the suspension top buffer stiffness on the predicted SEAT value using the long duration (11.5 cycle) input motion

The influence of the bottom end–stop buffer stiffness on the seat performance using the short duration (1.5 cycle) input motion

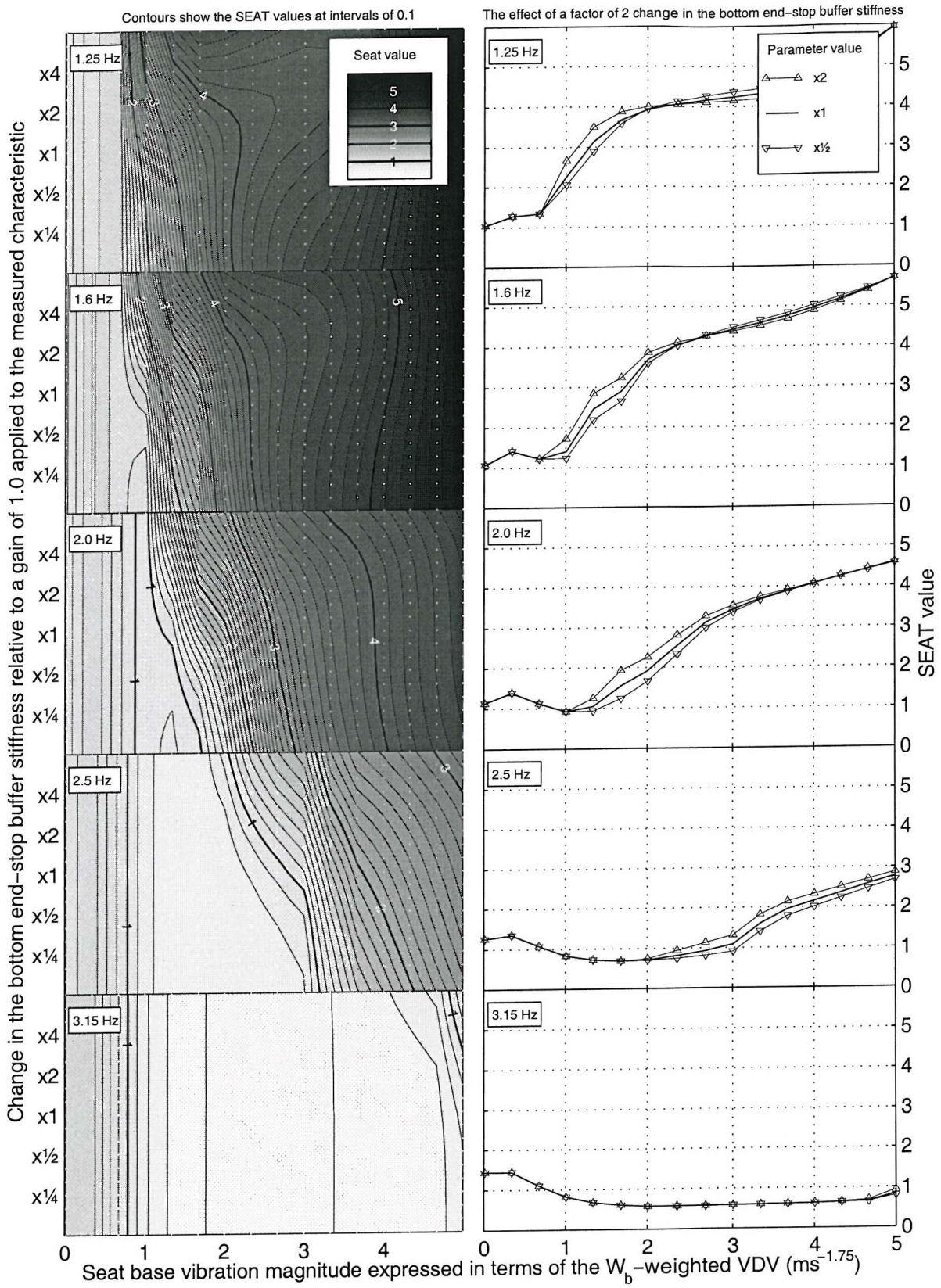

Figure 9:33 The effect of the suspension bottom buffer stiffness on the predicted SEAT value using the short duration (1.5 cycle) input motion

The influence of the bottom end-stop buffer stiffness on the seat performance using the medium duration (4.5 cycle) input motion

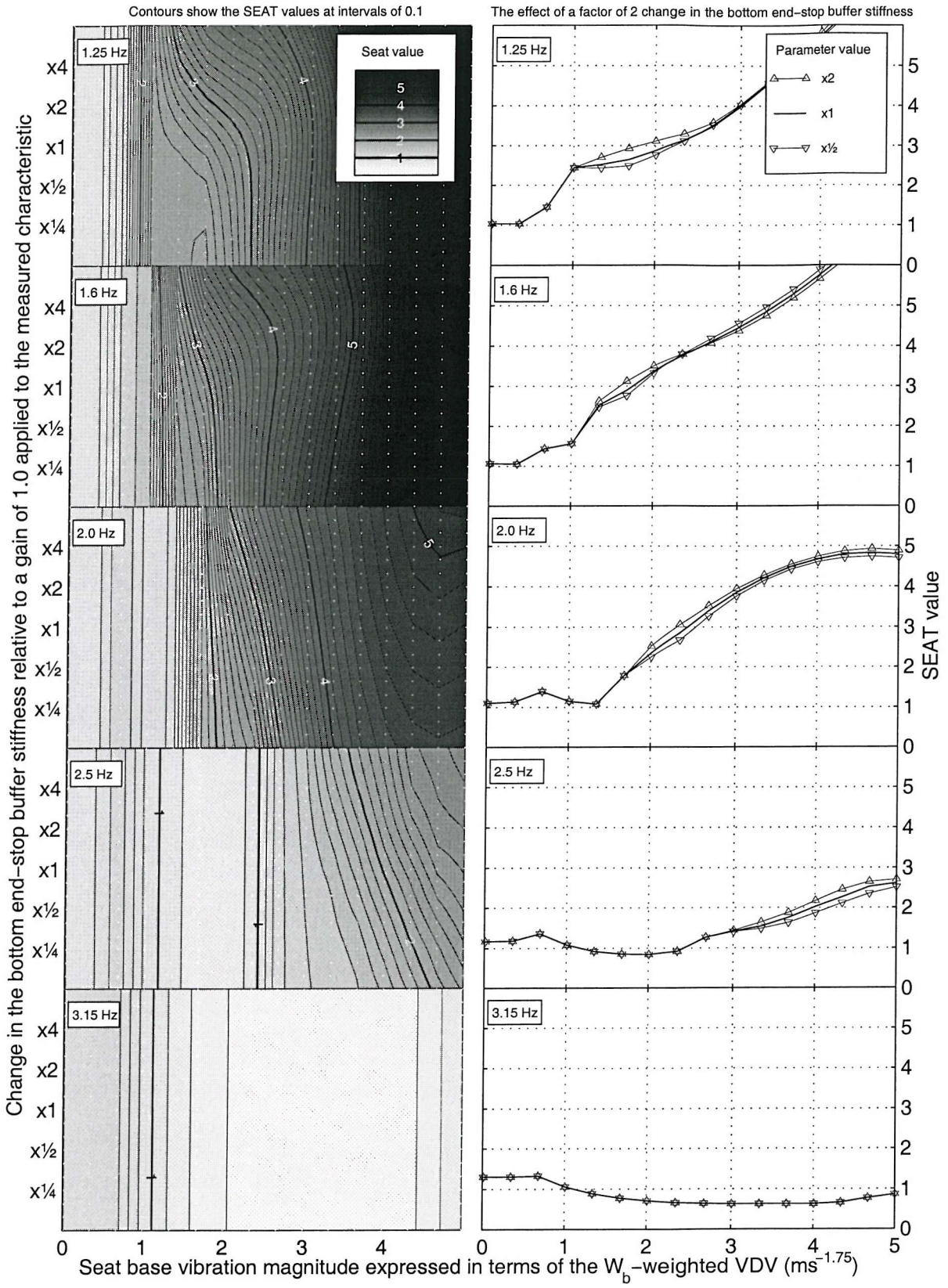

Figure 9:34 The effect of the suspension bottom buffer stiffness on the predicted SEAT value using the medium duration (4.5 cycle) input motion

The influence of the bottom end-stop buffer stiffness on the seat performance using the long duration (11.5 cycle) input motion

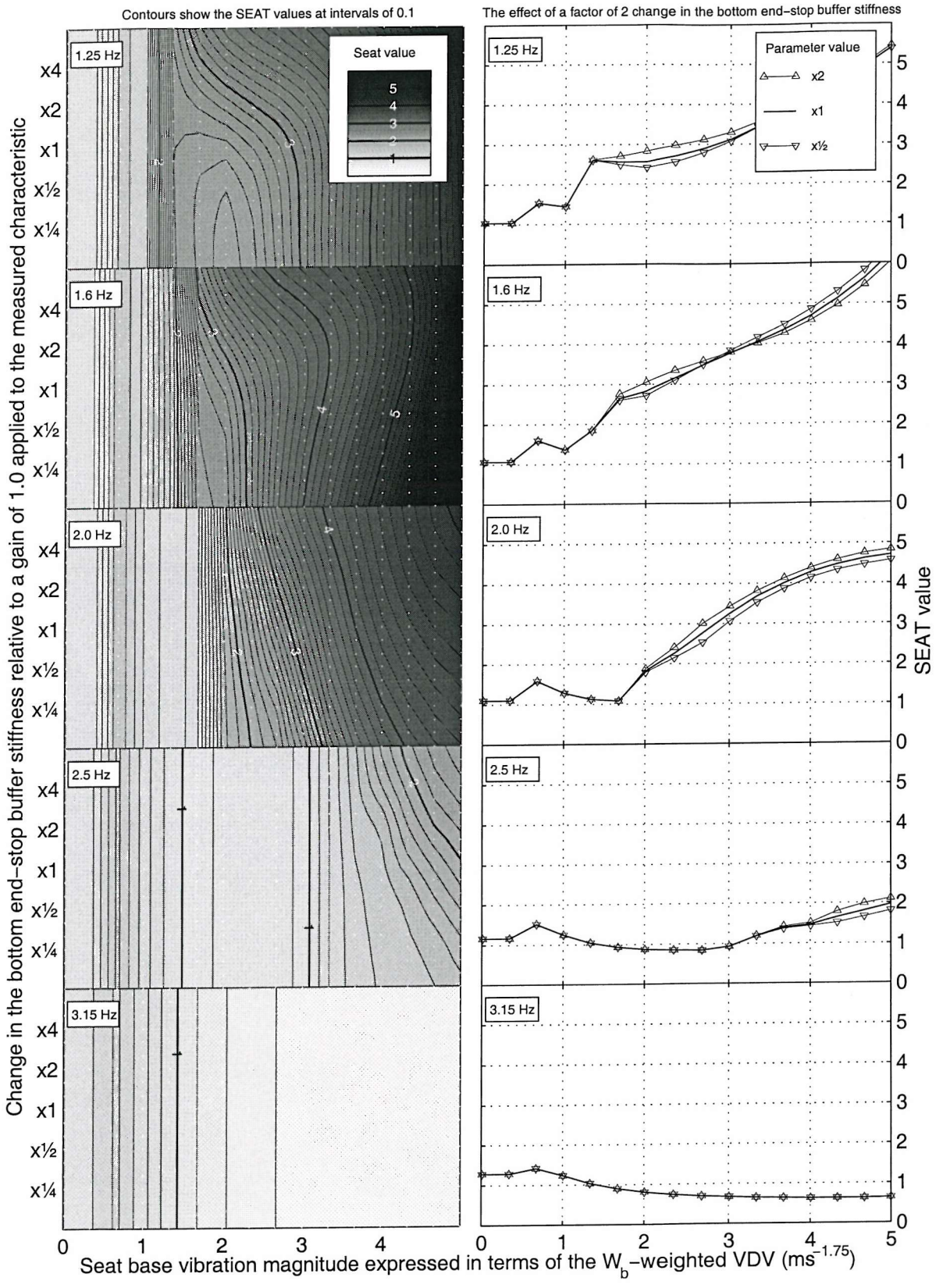

Figure 9:35 The effect of the suspension bottom buffer stiffness on the predicted SEAT value using the long duration (11.5 cycle) input motion